An Investigation of the Structure-Property Relationships for High Performance Thermoplastic Matrix, Carbon Fiber Composites with a Tailored Polyimide Interphase

by

Slade Havelock Gardner

Dissertation submitted to the Faculty of the Virginia Polytechnic Institute and State University in partial fulfillment of the requirements for the degree of

Doctor of Philosophy

in

Chemical Engineering

Approved by:

Richey M. Davis, Chairman	**Garth L. Wilkes**
Eva Marand	**Kenneth L. Reifsnider**
Judy S. Riffle	**J. Jack Lesko**

August 17, 1998
Blacksburg, Virginia

Keywords: polyamic acid, polyimide, interphase, composite

An Investigation of the Structure-Property Relationships for High Performance Thermoplastic Matrix, Carbon Fiber Composites with a Tailored Polyimide Interphase

Slade Havelock Gardner

(Abstract)

The aqueous suspension prepregging technique was used to fabricate PEEK and PPS matrix composites with polyimide interphases of tailored properties. The structure-property relationships of Ultem-type polyimide and BisP-BTDA polyimide which were made from various water soluble polyamic acid salts were studied. The molecular weight of the polyimides was shown to be dependant upon the selection of the base used for making the polyamic acid salt. The development of an Ultem-type polyimide with controlled molecular weight and properties similar to commercial Ultem 1000 was accomplished with the Ultem-type TPA^+ polyamic acid salt. Both the Ultem-type polyimides and the BisP-BTDA polyimides derived from the NH_4^+ salt and the TMA^+ salt were shown to crosslink at elevated temperatures.

Blends of Ultem-type polyimide with PEEK and BisP-BTDA polyimide with PEEK were prepared to study the structure-property relationships of model composite matrices. Since both polyimides are miscible with PEEK, interdiffusion of the polyimides with PEEK is expected, however, the interdiffusion behavior is complicated by the crosslinking mechanism of the polyimides.

Ultem-type polyimide interphase, PEEK matrix composites and BisP-BTDA polyimide interphase, PEEK matrix composites were fabricated using the aqueous suspension prepregging technique and evaluated to determine the effects of the interphase properties on the bulk

composite performance and durability. Three different Ultem-type polyimides from the NH_4^+, TMA^+ and TPA^+ polyamic acid salts were used and two different BisP-BTDA polyimides from the NH_4^+ and TMA^+ polyamic acid salts were used. The transverse flexure strength was used to qualitatively rank the composites by level of interfacial shear strength. The longitudinal tensile strength of the composites was shown to vary with relative interfacial shear strength. The trend of these data qualitatively support the existence of a maximum longitudinal tensile strength at an optimum interfacial shear strength. Notched fatigue testing of the Ultem-type polyimide interphase, PEEK matrix composites showed that the initial split growth rate increased with decreasing relative interfacial shear strength.

Ultem-type polyimide interphase, PPS matrix composites were fabricated using the aqueous suspension prepregging technique and evaluated to determine the effects of the interphase properties on the bulk composite performance. Three different Ultem-type polyimides from the NH_4^+, TMA^+ and TPA^+ polyamic acid salts were used. The transverse flexure strength was used to qualitatively rank the composites by level of interfacial shear strength. The longitudinal tensile strength of the composites was shown to vary with relative interfacial shear strength. The trend of these data qualitatively support the existence of a maximum longitudinal tensile strength at an optimum interfacial shear strength.

Grant Information

The work for this thesis was supported by the National Science Foundation Science and Technology Center for High Performance Adhesives and Composites under Grant # DMR 91-20004.

Acknowledgments

The author would like to gratefully acknowledge the support and contributions of the following people:

◦ Professor Richey Davis, my Advisor, who began with intense guidance, endless patience and supportive direction and then allowed me to find my own way when I was ready.

◦ The members of my Graduate Committee for guidance and discussion.

◦ Dr. John Facinelli for enormous collaborative work regarding the synthesis of polyamic acids, formation of aqueous polyamic acid salts, and the imidization of these materials. John also generously provided the pyrolysis GC data in Chapter 3. Many helpful discussions with John guided my research. Every Chemical Engineer needs a good friend who is a Synthetic Chemist, John was mine.

◦ Dr. Scott Case who is a genius of composite mechanics and who's calm, reserved interpretations of results did not let me get too carried away. Scott invested many days of work on my behalf performing the R=1.0 notched fatigue experiments and coordinating the R=0.1 notched fatigue experiments among other work. Scott always made his time available for extremely valuable discussions of composite mechanics.

◦ Dr. Srivatsan Srinivas for many things however the most important is as an example of how an outstanding scientist should work. More specific items include thermal analysis, loaning of equipment and supplies, and discussions of important topics such as polymer crystallization, melt rheology and the complex science of drinking whiskey.

◦ Dr. Biao Tan for synthesis of an extra-ordinary quantity of Ultem-type polyamic acid and for synthesis of BisP-BTDA polyamic acid.

◦ Kurt Jordens for little things like thermal analysis and Friday afternoon coffee breaks, and big things like a solid friendship.

◦ Dr. Venkat Venkatessan for development of the formation and precipitation procedures for the Ultem-type TPA^+ polyamic acid salt.

◦ Steve McCartney who is the wizard of microscopy who trained me in SEM operation and for performing the XPS experiment and analyzing the data for the sized fibers in Chapter 4.

◦ Christelle Laot for conducting the FTIR-ATR experiments in Chapter 3.

◦ Christy Sensenich for assistance in synthesis of polyamic acids, formation of aqueous polyamic acid salts, and the imidization of these materials.

◦ Brady Walther for assistance in longitudinal tension testing in Chapter 4 and Chapter 6.

◦ Sneha Patel for conducting the R=0.1 notched fatigue experiments.

◦ Chris Robertson for DSC analysis of polyimides in Chapter 3 and Chapter 5.

◦ Professor Al Loos for use of his laboratory and equipment for suspension prepregging.

◦ Dr. Anand Rau for his assistance in training me to operate the prepregger and the programmable hot press.

◦ Hans DeSmidt for repeated loading longitudinal tension testing in Chapter 4.

◦ Mike Weber for optimizing and operating the air classifier to separate the PPS powder into a narrow particle size distribution.

◦ Dr. Mark Muggli and Robert Jensen for assistance with the DuPont TGA.

◦ Dr. Wilson Tsang for conducting the Iosipescu shear testing and coordinating the repeated loading longitudinal tension testing in Chapter 4.

◦ Dr. Limin Dong and Dr. Q. Ji for conducting the GPC experiments in Chapter 3.

◦ Dr. Jon Geibel of Phillips Chemicals for helpful discussions regarding PPS composites.

◦ Danny Reed for his efforts in installing, modifying and repairing the Wabash vacuum hot press as well as managing the Fab Lab in a clean and organized manner that allowed the concentration of composite fabrication.

◦ Dr. James Miller and Dr. Gerry Zajac of Amoco Chemicals for VC-XPS measurements

◦ Professor James Schaffer of the Lafayette College Chemical Engineering Department who introduced me with brilliance to polymeric composite materials.

◦ members of Professor Richey Davis' research group for all the unmentionable things that contributed to my graduate studies.

◦ My beautiful wife Tara, whose continual loving support made the difficult times manageable and the impossible times bearable.

◦ All the members of the NBA (Noontime Basketball Association) at War Memorial Gym to whom I owe my sanity and many fouls.

Table of Contents

Abstract i
Grant Information ii
Acknowledgments iii
Table of Contents v
List of Tables xiii
List of Figures xvi

Chapter One: Introduction 1
Problems Addressed by This Thesis 3
Research Objectives 6
References 11

Chapter Two: Literature Review 14
Research Objectives 17
Polyimides: Importance 19
Commercial Polyimides 20
Typical Synthesis 22
Chemical Imidization of Polyamic Acids 23
Solution Imidization of Polyamic Acids 23
Bulk Thermal Imidization of Polyamic Acids 24
Polyamic Acid Salts 26
Use in Composites 29
Melt Processing of Polyimides 31
Solvent Processing of Polyamic Acids and Polyimides 31
Aqueous Processing of Polyimide Precursors 34
Effect of Processing on Properties (Characterization of Polyimides) 38
Characterization of Polyamic acids/ Polyamic acid salts and polyimides 40
Spectroscopic Investigation of Chemical Structure 41
Thermal Properties 43
Effect of Chemical Structure and End Groups on Thermal Stability 44
Effect of Polyimide Physical State on Thermal Stability 45
Environmental Effects on Thermal Stability 47
Mechanisms for Degradation 48
Molecular Weight Determination 49
Melt Rheology 52
Mechanical Properties 54
Microstructure 56
Polyether ether ketone 57
Commercial Availability 57
Characterization 58

Thermal properties 59
Bulk mechanical properties 62
Melt Rheology 63
Crystallization/Microstructure 63
Benefits and Limitations as Composite Matrix 64
Composite Applications 66
Characterization of PEEK Matrix Composites in Literature 66
Polyphenylene Sulfide 70
Commercial Availability 70
Applications 70
Characterization 71
Thermal Properties 72
Bulk Mechanical Properties 73
Melt Rheology 74
Crystallization/Microstructure 75
Benefits and Limitations as a Composite Matrix: 77
Composite Matrix Applications 77
Characterization of PPS Matrix Composites 78
Blends of Polyimide and PEEK 82
Background 82
Characterization 84
Ultem Polyimide/PEEK 85
Microstructure 86
Properties 88
Interdiffusion 92
Blends of Polyimide/PPS 95
Background 95
Blends of Ultem Polyimide and PPS 96
Characterization 96
Microstructure 97
Properties 98
Interphase Composites 100
Importance of Interphase 100
Uses, Benefits and Limitations 101
Manufacturing Techniques for Construction of Interphase 102
Characterization of Structure 104
Characterization of Properties 105
Mechanical Models 113
Rule of Mixtures 115
Single Fiber in Continuous Matrix 118
Multiple Fibers in Continuous Matrix 121
Concentric Cylinders Model 123
Figures 127

References 161

Chapter Three: Structure-Property Relationships of Model Interphase
Ultem-type Polyimides Made from Water Soluble Precursors and
Model Matrix PEEK/Polyimide Blends Made From Aqueous Suspension 168
Introduction 168
Materials 170
Procedure 171
Calibration of Bases 171
Polyamic Acid Preparation 172
Model Interphase Ultem-type Polyimide Characterization 174
Preparation of Test Samples 174
Melt Rheology of Ultem-type Polyimides 178
Differential Scanning Calorimetry of Ultem-type Polyimides 179
Gel Permeation Chromatography 180
Solubility Test With Gel Fraction Measurement 180
Fourier Transform Infrared Spectroscopy 181
Thermal Gravimetric Analysis 182
Pyrolysis Gas Chromatography 183
Model Matrix Ultem-type polyimide/PEEK Blend Characterization 184
Preparation of Test Samples 184
Melt Rheology 185
Tensile Testing 186
Differential Scanning Calorimetry 187
Results and Discussion 188
Model Interphase Characterization 188
FTIR ATR 188
Gel Permeation Chromotography 190
Thermal Gravimetric Analysis 191
Solubility Test with Gel Fraction Measurement 193
Differential Scanning Calorimetry 195
Melt Rheology 196
Pyrolysis Gas Chromotography 198
Model Matrix Blend Characterization 199
Tensile Testing of Ultem-type Polyimide/PEEK Blends 199
Melt Rheology 207
Differential Scanning Calorimetry 211
Diffusion Calculations 218
Conclusions 220
Figures 223
References 243

Chapter Four: Fabrication and Characterization of Carbon Fiber PEEK matrix composites with Ultem-type Polyimide Interphases of Tailored Properties for Studying the Effect of Interphase Modifications 247
Introduction 247
Experimental 251
Materials 251
Procedure 252
Calibration of bases 252
Polyamic acid preparation 253
Polyamic Acid Salt Preparation 253
Suspension Preparation 253
Prepregging 254
Composite Layup and Consolidation 255
Panel Evaluation 256
C-Scan 256
Fiber Volume Fraction 256
Image Analysis 257
Surface Chemistry by X-ray Photoelectron Spectroscopy 258
Composite Characterization 260
Iosipescu Shear Testing 260
Transverse Flexure Testing 261
Voltage Contrast X-ray Photoelectron Spectroscopy 262
Notched Fatigue Testing 262
Unidirectional Tension 264
Results and Discussion 266
Estimation of Interphase Thickness 266
Panel Quality 268
Sized Fiber Surface Chemistry by XPS 270
Composite Properties 272
Shear Properties 273
Transverse Flexure Properties 279
Voltage Contrast X-ray Photoelectron Spectroscopy 285
Notched Fatigue Properties (R=1.0) 286
Notched Fatigue Properties (R=0.1) 288
Longitudinal Tension 296
Longitudinal Tension (repeated loading scheme) 310
Conclusions 315
Figures 319
Appendix A 352
References 354

Chapter Five: Structure-Property Relationships of Model Interphase
BisP-BTDA Polyimides Made from Water Soluble Precursors and
Model Matrix Polyimide/PEEK Blends Made From Aqueous Suspension 356
Introduction 356
Materials 359
Calibration of Bases 360
Model Interphase BisP-BTDA Polyimide Characterization 360
Preparation of Test Samples 360
Melt Rheology 362
Differential Scanning Calorimetry 363
Thermal Gravimetric Analysis 364
Model Matrix Blend Characterization 365
Preparation of Test Samples 365
Melt Rheology 367
Tensile Testing 368
Differential Scanning Calorimetry 368
Results and Discussion 369
Model Interphase Characterization 369
Solubility Test with Gel Fraction Measurement 370
Differential Scanning Calorimetry 371
Thermal Gravimetric Analysis 372
Melt Rheology 374
Model Matrix Blend Characterization 376
Tensile Testing 376
Melt Rheology 381
Differential Scanning Calorimetry 383
Conclusions 385
Figures 388
References 398

Chapter Six: Fabrication and Characterization of Carbon Fiber PEEK matrix composites with BisP-BTDA Polyimide Interphases of Tailored Properties for Studying the Effect of Interphase Modifications 400
Introduction 400
Experimental 403
Materials 403
Procedure 404
Calibration of Bases 404
Polyamic Acid Salt Preparation 404
Hydroxypropyl Celulose Fugitive Binder Preparation 405
Suspension Preparation 405
Prepregging 406
Composite Layup and Consolidation 406
Panel Evaluation 407
C-Scan 407
Fiber Volume Fraction 408
Image Analysis 408
Composite Characterization 409
Transverse Flexure Testing and Longitudinal Flexure Testing 409
Unidirectional Tension 410
Results and Discussion 411
Panel Quality 411
Composite Properties 412
Longitudinal Flexure 413
Transverse Flexure Properties 417
Longitudinal Tension 422
Tensile Strength and Interfacial Shear Strength 429
Conclusions 430
Figures 433
References 445

Chapter Seven: Fabrication and Characterization of Carbon Fiber PPS matrix composites with Ultem-type Polyimide Interphases of Tailored Properties for Studying the Effect of Interphase Modifications 447
Introduction 447
Experimental 450
Materials 450
Procedure 451
Calibration of bases 451
Polyamic acid preparation 452
Polyamic Acid Salt Preparation 452
Suspension Preparation 453
Prepregging 453
Composite Layup and Consolidation 454
Panel Evaluation 455
C-Scan 455
Fiber Volume Fraction 455
Image Analysis 457
Composite Characterization 458
Transverse Flexure Testing and Longitudinal Flexure Testing 458
Short Beam Shear 459
Unidirectional Tension 459
Results and Discussion 460
Interphase Microstructure 460
Panel Quality 463
Composite Properties 464
Short Beam Shear 465
Longitudinal Flexure 468
Transverse Flexure 467
Longitudinal Tension 473
Conclusions 492
Figures 495
References 518

Chapter Eight: Summary of Conclusions and Recommended Future Work 521
Summary of Conclusions 521
Structure-Property Relationships of Model Interphase Ultem-type Polyimides Made from Water Soluble Precursors 521
Model Matrix Ultem-type Polyimide/PEEK Blends Made From Aqueous Suspension 522
Fabrication and Characterization of Carbon Fiber PEEK matrix composites with Ultem-type Polyimide Interphases of Tailored Properties for Studying the Effect of Interphase Modifications 523
Structure-Property Relationships of Model Interphase BisP-BTDA Polyimides Made from Water Soluble Precursors 526

Model Matrix BisP-BTDA Polyimide/PEEK Blends Made From Aqueous Suspension 527
Fabrication and Characterization of Carbon Fiber PEEK matrix composites with BisP-BTDA Polyimide Interphases of Tailored Properties for Studying the Effect of Interphase Modifications 528
Fabrication and Characterization of Carbon Fiber PPS matrix composites with Ultem-type Polyimide Interphases of Tailored Properties for Studying the Effect of Interphase Modifications 530
Recommendations For Future Work 532
Polyimides From Water Soluble Polyamic Acid Salts 532
Polyimide/PEEK blends 533
Polyimide Interphase Composites 534

Vita 538

List of Tables

Chapter Two

Table 2-I. Some mechanical properties of commercial polyimides. 21
Table 2-II. Hydrated diameters for aqueous, solvated ammonium ions. 37
Table 2-III. Some properties of two different grades of PEEK supplied by Victrex. 57
Table 2-IV. Measured composite properties from Drzal and Madhukar [162] 106
Table 2-V. Measured composite properties from Chang et al. [171] 108
Table 2-VI. Measured composite properties from Subramanian et al.[169] 110
Table 2-VII. Mechanical testing results from Gonzalez [35]. 111

Chapter Three

Table 3-I. GPC, DSC and solubility test results for Ultem-type polyimides and Ultem-type polyamic acid. 192
Table 3-II. Nomenclature of binary Ultem-type polyimide/PEEK blends. 201
Table 3-III. Tensile properties of 5 wt% Ultem-type polyimide/PEEK binary blends. 202
Table 3-IV. Unpaired *t*-test results comparing each set of model matrix and neat PEEK tensile data. 204
Table 3-V. Parameters of polyimides for discussion of molecular weight changes. 211
Table 3-VI. DSC results and calculated crystalline fractions for Ultem-type polyimide/PEEK blends and neat PEEK samples. 215
Table 3-VII. Ranking of model 5 wt% Ultem-type polyimide/PEEK blends and neat 380 Grade PEEK by complex melt viscosity and temperature of maximum crystallinity. . . 216

Chapter Four

Table 4-I. Polishing schedule of PEEK matrix composite surfaces for image analysis. 257
Table 4-II. Quality of consolidation, fiber volume fraction, panel layup, void volume fraction, and mechanical test for which panel was used. 269
Table 4-III. Surface chemical compositions of carbon fiber tow. 270
Table 4-IV. Mechanical Testing Schedule 273
Table 4-V. Iosipescu (90°) shear test results for PEEK composites. 274
Table 4-VI. Transverse flexure results for PEEK composites. 280
Table 4-VII. Unpaired *t*-test results comparing each set of PEEK matrix composite transverse flexure data. 282
Table 4-VIII. Loading level and number of fatigue cycles before failure for R=1.0 notched fatigue testing. 288
Table 4-IX. R=0.1 Notched fatigue results for 80% UTS 290
Table 4-X. R=0.1 Notched fatigue results for 87.5% UTS. 291
Table 4-XI. Constants for equation 4-10 from second order fit. 292
Table 4-XII. Longitudinal tension test results for PEEK matrix composites 297
Table 4-XIII. Unpaired *t*-test results comparing each set of PEEK matrix composite longitudinal tensile data. 298
Table 4-XIV. Rule of mixture predictions for strength, ratios of measured strength

to predicted strength by the rule of mixtures, and strength reduction factor. 303
Table 4-XV. Unpaired *t*-test results comparing each set of PEEK matrix composite strength reduction factor data. 308
Table 4-XVI. Longitudinal tensile modulus, rule of mixture predictions for modulus and ratios of measured modulus to predicted modulus by the rule of mixtures. 310
Table 4-XVII. Tensile test results with a repeated loading scheme for Ultem-type polyimide interphase/PEEK composites. 311
Table 4-XVIII. Rule of mixture predictions for strength, ratios of experimental strength to rule of mixture predictions, calculated composite ultimate strength and strength reduction factor. 313

Chapter Five

Table 5-I. DSC and solubility test results for BisP-BTDA polyimides and BisP-BTDA polyamic acid. 370
Table 5-II. Tensile properties of model matrix blends and neat PEEK. 377
Table 5-III. Unpaired *t*-test results for comparisons of tensile data for model matrix blends. 379
Table 5-IV. Heats of melting, heats of crystallization, glass transition temperatures and calculated crystalline fractions of PEEK component for model matrix blends and neat PEEK. 385

Chapter Six

Table 6-I. Polishing schedule of PEEK matrix composite surfaces for image analysis. 409
Table 6-II. Quality of consolidation, fiber volume fraction, panel layup, void volume fraction, and mechanical test for which panel was used. 412
Table 6-III. Mechanical Testing Schedule 413
Table 6-IV. Longitudinal flexure properties of Ultem-type interphase/PEEK matrix composites. 415
Table 6-V. Unpaired *t*-test results comparing each set of PEEK matrix composite longitudinal flexure data. 417
Table 6-VI. Transverse flexure results for PEEK composites. 418
Table 6-VII. Unpaired *t*-test results comparing each set of PEEK matrix composite transverse flexure data. 419
Table 6-VIII. Longitudinal tension test results for PEEK matrix composites. 423
Table 6-IX. Unpaired *t*-test results comparing each set of PEEK matrix composite longitudinal tensile data. 423
Table 6-X. Rule of mixture predictions for strength, ratios of measured strength to predicted strength by the rule of mixtures, and strength reduction factor. 426
Table 6-XI. Longitudinal tensile modulus, rule of mixture predictions for modulus and ratios of measured modulus to predicted modulus by the rule of mixtures. 428

Chapter Seven

Table 7-I. Polishing schedule of PPS matrix composite surfaces for image analysis. 457

Table 7-II. Quality of consolidation, fiber volume fraction and panel layup 464
Table 7-III. Mechanical testing schedule for PPS matrix composites 465
Table 7-IV. Short beam shear strengths for Ultem-type interphase/PPS matrix composites. 466
Table 7-V. Longitudinal flexure properties of Ultem-type interphase/PPS matrix composites 469
Table 7-VI. Unpaired *t*-test results comparing each set of PPS matrix composite longitudinal flexure data. 471
Table 7-VII. Transverse flexure results for Ultem-type interphase/PPS matrix composites. 474
Table 7-VIII. Unpaired *t*-test results comparing each set of PPS matrix composite transverse flexure data. 475
Table 7-IX. Longitudinal tension test results for PPS matrix composites. 477
Table 7-X. Unpaired *t*-test results comparing each set of PPS matrix composite longitudinal tension data. 479
Table 7-XI. Rule of mixture predictions for tensile strength compared to experimental data. . 481
Table 7-XII. Rule of mixture predictions for tensile modulus compared to experimental data. 483
Table 7-XIII. Tensile moduli and tensile strength of Ultem-type polyimide interphase/PPS matrix composites corrected to 61% fiber volume fraction using Eq. 7-11 and Eq. 7-12. 485
Table 7-XIV. Ultimate composite tensile strength and strength reduction factor for Ultem-type polyimide interphase/PPS matrix composites. 486
Table 7-XV. Unpaired *t*-test results comparing each set of PPS matrix composite strength reduction factors and tensile data corrected to 61% fiber volume fraction. . . . 491

List of Figures

Chapter Two

Figure 2-1. Generalized polyimide structure. 126
Figure 2-2. Chemical structure for BisP-BTDA polyimide. 127
Figure 2-3. Synthesis of controlled molecular weight Ultem-type polyimide. 128
Figure 2-4. Possible side reactions during thermal imidization. 129
Figure 2-5. Viscosity change of 2 wt% solutions of TEA polyamic acid salts in DMAC. 130
Figure 2-6. Isothermal viscosity sweeps for TPER polyimide with different endgroups. 131
Figure 2-7. Effect of film thickness on polyimide thermal stability. 132
Figure 2-8. Reduced viscosity vs. concentration for solutions of polyamic acid in NMP. 133
Figure 2-9. Melt viscosity vs. shear rate for a typical molten polymer. 134
Figure 2-10. Molecular weight dependance of the zero shear viscosity for polymers. 135
Figure 2-11. Percentage insoluble PEEK gel and intrinsic viscosities after heating in air. . . . 136
Figure 2-12. Steady shear melt viscosity vs. temperature for several thermoplastic polymers. 137
Figure 2-13. Schematic representation of a PEEK spherulite with cylindrical symmetry. 138
Figure 2-14. Subsequent melt flow as a function of solid state curing time for PPS. 139
Figure 2-15. Flexural moduli of thermoplastic polymers and glass filled thermoplastic polymers. 140
Figure 2-16. Glass transition temperature vs. composition for BisP-BTDA/PEEK blends. . . . 141
Figure 2-17. Phase morphologies for blends of crystallizable and noncrystallizable polymers. 142
Figure 2-18. Microstructure morphology of Ultem polyimide/PEEK blends. 143
Figure 2-19. Glass transition temperature vs. concentration of Ultem/PEEK blends. 144
Figure 2-20. Tensile strength and tensile modulus vs. composition for Ultem/PEEK blends. . 145
Figure 2-21. Tensile impact strength vs. composition for Ultem/PEEK blends. 146
Figure 2-22. Heat deflection temperature vs. concentration of Ultem/PEEK blends. 147
Figure 2-23. Estimated diffusion time for complete interdiffusion of Ultem and PEEK. 148
Figure 2-24. Morphology of Ultem/PPS blends. 149
Figure 2-25. Heat deflection temperature vs. composition of Ultem/PPS blends. 150
Figure 2-26. Izod impact strengths vs. composition of Ultem/PPS blends. 150
Figure 2-27. Izod impact strength and tensile modulus vs. composition for Ultem/PPS blends. 151
Figure 2-28. Tensile strength and failure strain vs. composition for Ultem/PPS blends. 151
Figure 2-29. Tensile strengths and strains vs. composition for Ultem/PPS blends. 152
Figure 2-30. Flexure strength and modulus vs. composition for Ultem/PPS blends. 152
Figure 2-31. Geometry for model composite compared to actual composite cross section. . . . 153
Figure 2-32. Rule of mixtures predicted strength vs. fiber volume fraction. 154
Figure 2-33. Single broken fiber in a continuous matrix surrounded by average composite. . . 155
Figure 2-34. Ineffective length ratio vs. ratio of fiber modulus to matrix shear modulus. 156
Figure 2-35. Failure stress vs. ineffective length ratio for several fiber volume fractions. . . . 157
Figure 2-36. Single broken fiber with neighboring unbroken fibers in a continuous matrix. . . 158
Figure 2-37. Hexagonally packed composite fibers represented as an annular ring. 159

Figure 2-38. Predicted variation of composite tensile strength vs. interfacial shear strength. . 160

Chapter Three

Figure 3-1. Chemical structures of monomers and the synthesis of Ultem-type polyamic acid. 225
Figure 3-2. Formation of Ultem-type polyamic acid salts using different bases. 226
Figure 3-3(a-c). FTIR spectra for Ultem-type polyamic acid salts and the resulting polyimides. 227
Figure 3-3(d-e). FTIR spectra comparing Ultem-type polyamic acid salts and polyimides. . . 228
Figure 3-4. TGA scans for Ultem-type polyamic acid salts and neat Ultem-type polyamic acid. 229
Figure 3-5. TGA scans for Ultem-type polyimides during simulated consolidation thermal cycle. 230
Figure 3-6. Imidization and 5% weight loss temperatures for Ultem-type polyimides. 231
Figure 3-7. DSC scans for Ultem-type polyimides and Ultem 1000. 232
Figure 3-8. T_g vs. $1/<M_n>$ compared to Fox-Flory relationship for Ultem-type polyimides. . . 233
Figure 3-9. Complex viscosity of Ultem-type polyimides during simulated consolidation cycle. 234
Figure 3-10. Gas chromatograph spectra after pyrolysis of Ultem-type polyimides. 235
Figure 3-11. Structures of Ultem-type polyimide and molecules detected by pyrolysis GC. . . 236
Figure 3-12. Complex viscosity vs. frequency for 5 wt% Ultem-type polyimide/PEEK blends. 237
Figure 3-13. Hydrolysis and ketimine formation for Ultem-type polyimide and PEEK. 238
Figure 3-14. DSC heating scans for 5 wt% Ultem-type polyimide/PEEK blends. 239
Figure 3-15. DSC cooling scans for 5 wt% Ultem-type polyimide/PEEK blends. 240
Figure 3-16. DSC traces for 50 wt% Ultem-type polyimide/PEEK blends. 241
Figure 3-17. T_g vs. composition for Ultem-type polyimide/PEEK blends. 242
Figure 3-18. Calculated diffusion coefficient vs. temperature for Ultem polyimide/PEEK blends. 243
Figure 3-19. Calculated diffusion distance vs. temperature for Ultem polyimide/PEEK blends. 244

Chapter Four

Figure 4-1. Chemical structure of PEEK. 319
Figure 4-2. Chemical structure of Ultem-type polyamic acid. 320
Figure 4-3. Formation of Ultem-type polyamic acid salts using different bases. 321
Figure 4-4. Schematic drawing of modified Research Tool Corporation drumwinder prepregger 322
Figure 4-5. Temperature and pressure schedule for consolidation of PEEK composites. 323
Figure 4-6. Iosipescu shear loading geometry. 324
Figure 4-7. Notched fatigue specimen loading geometry for R=1.0 and R=0.1 experiments. . 325
Figure 4-8. Transverse flexure specimen loading geometry. 326

Figure 4-9. Unidirectional tension test geometry. 327
Figure 4-10. Repeated loading scheme unidirectional tension test geometry and loading scheme. 328
Figure 4-11. Diagram of fibers with interphase layer in hexagonal packing. 329
Figure 4-12(a-c). C-scan images of panels showing “poor”, “fair”, and “good” consolidation. 330
Figure 4-13. N/C ratios of atomic concentration on fiber surfaces. 333
Figure 4-14. Iosipescu shear failure surfaces for 10 series and 30 series composites. 334
Figure 4-15. Iosipescu shear modulus and calculated shear moduli. 335
Figure 4-16. Shear modulus corrected to a fiber volume fraction of 61%. 336
Figure 4-17. Transverse flexure modulus vs. fiber volume fraction. 337
Figure 4-18. Normalized ISS vs. normalized transverse flexure strength data. 338
Figure 4-19(a-d). Transverse flexure failure surfaces. 339
Figure 4-20. Normalized strength vs. log N for R=1.0 notched fatigue experiments. 341
Figure 4-21. Longitudinal split growth for relief of stress concentrations. 342
Figure 4-22(a-d). Split length vs. number of cycles for R=0.1 notched fatigue testing. 343
Figure 4-23. Split growth rates for R=0.1 notched fatigue experiments. 345
Figure 4-24. Residual tensile strength after R=0.1 notched fatigue loading cycles. 346
Figure 4-25. Initial split growth rate from R=0.1 notched fatigue experiments. 347
Figure 4-26. Longitudinal tensile strength vs. normalized transverse flexure strength. 348
Figure 4-27. Comparison of relative ineffective lengths. 349
Figure 4-28. Tensile modulus for PEEK composites compared to the rule of mixtures. 350
Figure 4-29. Photographs of failed repeated loading tensile specimens. 351

Chapter Five

Figure 5-1. Formation of BisP-BTDA polyamic acid salts using different bases. 388
Figure 5-2. DSC traces for BisP-BTDA polyimides. 389
Figure 5-3(a-b). TGA scans of BisP-BTDA polyamic acid salts and polyamic acid. 390
Figure 5-4. TGA scans of BisP-BTDA polyimides. 391
Figure 5-5. Imidization and 5% weight loss temperatures for BisP-BTDA polyamic acid salts. 392
Figure 5-6. TGA scan for HPC fugitive binder during pyrolysis thermal cycle. 393
Figure 5-7. Complex viscosity of BisP-BTDA polyimides during simulated consolidation cycle. 394
Figure 5-8. Complex viscosity vs. frequency for 5 wt% BisP-BTDA/PEEK blends. 395
Figure 5-9. DSC heating traces for 5 wt% BisP-BTDA/PEEK blends. 396
Figure 5-10. DSC cooling traces for 5 wt% BisP-BTDA/PEEK blends. 397

Chapter Six

Figure 6-1. Chemical structure of PEEK. 433
Figure 6-2. Chemical structure of BisP-BTDA polyimide. 434

Figure 6-3. Formation of BisP-BTDA polyamic acid salts using different bases. 435
Figure 6-4. Schematic drawing of modified Research Tool Corporation drumwinder prepregger 436
Figure 6-5. Temperature and pressure schedule for consolidation of PEEK composites 437
Figure 6-6(a-b). Longitudinal and transverse flexure testing geometry. 438
Figure 6-7. Unidirectional tension test geometry. 440
Figure 6-8. C-scan image of panel representative of “good” consolidation. 441
Figure 6-9(a-c). Transverse flexure failure surfaces. 442
Figure 6-10. Experimental tensile strength vs. normalized transverse flexure strength. 444

Chapter Seven

Figure 7-1. Chemical structure of Ultem-type polyimide. 495
Figure 7-2. Chemical structure of PPS. 496
Figure 7-3. Schematic of air classifier used to separate size distributions of PPS powder. . . . 497
Figure 7-4. Formation of Ultem-type polyamic acid salts using different bases. 498
Figure 7-5. Schematic drawing of modified Research Tool Corporation drumwinder prepregger 499
Figure 7-6. Temperature and pressure schedule for consolidation of PPS composites 500
Figure 7-7(a-b). Longitudinal and transverse flexure testing geometry. 501
Figure 7-8. Composite short beam shear test geometry. 503
Figure 7-9. Unidirectional tension test geometry. 504
Figure 7-10. C-scan image of panel representative of “good” consolidation. 505
Figure 7-11. Photographs of failed short beam shear test samples. 506
Figure 7-12. Longitudinal flexure shear failure mode. 507
Figure 7-13. Normalized longitudinal tensile strengths vs. normalized interfacial shear strength. 508
Figure 7-14. Normalized ISS vs. normalized transverse flexure strength. 509
Figure 7-15(a-c). Photographs of failed longitudinal tension test coupons. 510
Figure 7-16. Longitudinal tensile modulus vs. fiber volume fraction. 512
Figure 7-17. Comparison of relative ineffective lengths. 513
Figure 7-18. Strength reduction factor vs. normalized transverse flexure strength. 514
Figure 7-19. Normalized transverse flexure strength vs. normalized tensile and flexure strengths. 515
Figure 7-20. Predicted variation of composite tensile strength vs. interfacial shear strength. . 516
Figure 7-21. Longitudinal tensile strength corrected to 61% fiber volume fraction vs. normalized transverse flexure strength. 517

Chapter One: Introduction

An important way to improve composite performance and durability is by modifying the interphase. The interphase region is defined as the transition zone between the reinforcing fiber and the bulk matrix in a composite. An interphase typically accounts for less than 2% of the total mass of material in a composite [1]. However, carefully modified interphases have been shown to improve composite longitudinal tensile strength by as much as 29% [2], compressive strength by as much as 50% and notched fatigue lifetime cycles by as many as two orders of magnitude [1]. Therefore, the benefits of implementing a carefully constructed interphase are obvious.

Many models based on the micro-mechanics of failure have been proposed for prediction of composite strength and lifetime. The most recent models proposed by Reifsnider et al. incorporate an interphase region with significantly different material properties from the matrix polymer [1,3-7]. These models have been used to formulate hypotheses regarding further improvements of composite performance and durability based on interphase modifications.

The most intriguing hypothesis is that a maximum composite tensile strength can be attained for an optimal interfacial shear strength between the fiber and the bulk matrix. The most direct method of altering the interfacial shear strength without changing any of the other constituent properties is by modifying the interphase properties. The work of this thesis concerned the fabrication of interphase composites with thermoplastic matrices and systematically controlled interphase properties to test the hypothesis of Reifsnider et al.

The aqueous suspension prepregging technique combines the matrix polymer with the fiber at the same time that the interphase polymer is deposited on the fiber [8-13]. Aqueous suspension prepregging has been done by many researchers using a polyimide precursor, a water

soluble polyamic acid salt neutralized with a base [8-13]. The matrix polymer powder is dispersed in the aqueous polyamic acid salt solution. The polyamic acid salt behaves as a dispersant, adsorbing to the surface of the matrix powder particles, and electrostatically stabilizing the suspension. The fiber tow is then coated with the polyimide precursor and the matrix powder in a single prepregging step. The polyamic acid salt also serves as a binder, adhering the matrix powder to the carbon tow. After drying the water from the prepreg, a heating cycle is used to convert the polyamic acid to the polyimide by way of thermal imidization. The molecular weight of the final polyimide can be controlled by selection of the base and the method used for making the polyamic acid salt [14].

Quite plainly, the main questions that this thesis addresses are:

Can we make thermoplastic matrix composites using the aqueous suspension prepregging technique with a variety of interphases with controlled properties?

Can we then begin to optimize the performance and durability of the thermoplastic matrix composites?

To address these questions, polyether ether ketone (PEEK) matrix composites were fabricated with three different Ultem-type polyimide interphases and two different BisP-BTDA polyimide interphases.

Some of the required information for the micro-mechanical models are material properties of the interphase region and of the bulk matrix. Since techniques have not yet been developed for measuring the properties of the actual interphase region of a composite, model

interphase samples were prepared and characterized. One of the model interphase Ultem-type polyimides from the aqueous process is shown to have physical properties and a controlled molecular weight that are comparable to commercial Ultem 1000.

Since PEEK is miscible with Ultem polyimide [15-17] and also with BisP-BTDA polyimide [36], interdiffusion of the interphase polyimide and the bulk PEEK matrix was expected for both cases. Thus, thermal, mechanical, and rheological properties of model matrix samples with varying compositions were measured.

Another series of composites fabricated by the aqueous suspension prepregging technique, had three different Ultem-type polyimide interphases and a polyphenylene sulfide (PPS) matrix.

All the composites were tested using a variety of techniques to probe the effects of the interphase properties on the overall composite performance and durability of thermoplastic matrix composites.

There were many problems regarding the research project described above. Fabrication of a series of composites containing an interphase with controlled properties, while maintaining similarity of all other properties was a difficult task. Some of the most difficult problems that were addressed by this thesis are described next.

One of the largest complications involved the aqueous suspension prepregging process using polyamic acid salts. Prior to the beginning of this work it was widely believed that molecular weight control of polyamic acid salts dissolved in water was not possible. Hydrolytic degradation of polyamic acids typically occurs when they are dissolved in water [18-21].

Hydrolysis results in decreased molecular weight of the polyamic acid and ultimately the polyimide. Through efforts of the initial work of this thesis and collaborative studies with Riffle et al. [14,22-23], molecular weight control of polyimides processed from an aqueous polyamic acid salt precursor has been demonstrated.

Many studies have been reported in the literature regarding the thermal, mechanical, and physical properties of binary blends composed of Ultem polyimide and PEEK [15-17,24-27]. These studies typically examine the morphology and properties of blends of Ultem 1000 and a commercially available PEEK. In this thesis Ultem-type polyimide interphases were made with three quite different molecular weights, two of which were much lower than the molecular weight of Ultem 1000. Thus, the thermal, mechanical and physical properties of binary blends of these polyimides and PEEK were examined. The issue was complicated, however, by the propensity of the low molecular weight Ultem-type polyimides to branch and crosslink at elevated temperatures.

The aqueous suspension prepregging technique has been used successfully to fabricate PEEK matrix [8-12] and LaRC TPI matrix [9,11-13,28-33] composites. One criticism of this prepregging technique was the potential difficulty in extending it to other polymers which requires powdered polymer particles and the difficulty in controlling powder pickup on the fiber. The aqueous suspension prepregging technique was applied for the fabrication of Ultem-type polyimide interphase/PPS matrix composites.

Work has been done previously by Davis et al. [8,13] to asses the effects of systematically varied polyimide interphases that demonstrate a miscible interphase/matrix system and an immiscible interphase/matrix system. These are believed to be the first studies to specifically

address such a concern for interphase composites. It has been reported in the literature that PPS is immiscible with Ultem 1000 [34]. The work of this thesis extends the studies of Davis et al. to consider two series of systematically modified interphase composites that demonstrate interphase/matrix miscibility (Ultem-type polyimide/PEEK and BisP-BTDA polyimide/PEEK) and another series of composites that demonstrates interphase/matrix immiscibility (Ultem-type polyimide/PPS).

The bulk of the investigations of interphase composites have been on thermosetting matrix systems. Due to the many advantages of engineering thermoplastic polymers, there is increasing interest in thermoplastic matrix, carbon fiber, interphase composites. The work of this thesis addressed polyimide interphase composites that were fabricated with PEEK and PPS, two high performance thermoplastics.

Furthermore, the investigations of interphase composites reported in the literature usually contain the same matrix, but with interphase modifications ranging from an unsized, unsurface-treated fiber to different fiber surface treatments and/or fiber with a polymeric sizing. This can result in differences of fiber/matrix adhesion or alteration of fiber properties rather than modification of the interphase material properties. The systematically modified interphase composites fabricated for the work of this thesis were unique because the same fiber and matrix were maintained throughout each composite series, and the same interphase polyimide was used, but interphase properties and characteristics were a result of variances in interphase molecular weight. This minimized speculation regarding the effects of system chemistry when interpreting the composite performance results.

The hypothesis of Reifsnider et al. indicating that a maximum in composite tensile

strength can be attained for an optimal interfacial shear strength challenges many of the heuristics of composite mechanics. It has been previously accepted that composite tensile strength increases with increasing interfacial shear strength [36]. It has been shown recently by Reifsnider et al. that this notion is not always correct [1,3-7]. The fabrication and evaluation of systematically modified interphase composites in this thesis provides a critical test of the hypothesis of an optimal interfacial shear strength and critical data for further development of micro-mechanical models for composite performance and durability.

Now that the general issues that this thesis will address and the associated problems have been identified, the specific research objectives will next be specified. The research objectives of this work were:

① Processing and characterization of controlled molecular weight polyimides from aqueous polyamic acid salts including assessment of chemical analysis, molecular weight distribution, melt rheology, and thermal analysis.
② Characterization of model interphase/PEEK matrix blends
③ PEEK matrix composite manufacture with tailored, polyimide interphases of controlled properties.
④ PPS matrix composite manufacture with tailored, polyimide interphases of controlled properties.
⑤ Characterization of interphase composite durability and performance with a focus on composite failure mechanics.

Chapter Two of this thesis is a detailed review of the pertinent literature with regard to the objectives of this thesis. The literature review is organized in sequential order of the research

objectives ① -⑤. Chapter Three focuses on objectives ① and ② with regard to Ultem-type polyimide and blends of Ultem-type polyimide with PEEK. Chapter Four focuses on objectives ③ and ⑤ with regard to Ultem-type polyimide interphase composites. Chapter Five focuses on objectives ① and ② with regard to BisP-BTDA polyimide and blends of BisP-BTDA polyimide with PEEK. Chapter Six focuses on objectives ③ and ⑤ with regard to BisP-BTDA polyimide interphase composites. Chapter Seven focuses on objectives ④ and ⑤ with regard to BisP-BTDA polyimide interphase composites.

As described above, the content of this thesis is separated as detailed in the following list:

Chapter 3. Fabrication and characterization of model interphase Ultem-type polyimides and model matrix Ultem-type polyimide/PEEK blends.

Chapter 4. Fabrication of Ultem-type polyimide interphase/PEEK matrix composites with systematically modified interphase properties

Chapter 5. Fabrication and characterization of model interphase BisP-BTDA polyimides and model matrix BisP-BTDA polyimide/PEEK blends.

Chapter 6. Fabrication of BisP-BTDA polyimide interphase/PEEK matrix composites with systematically modified interphase properties

Chapter 7. Fabrication of Ultem-type polyimide interphase/PPS matrix composites with systematically modified interphase properties

Chapters 3-7 are written in the form of separate manuscripts that will be individually condensed for publication. Since similar techniques and procedures are used in many of the chapters, some redundancy will occur in this thesis. This redundancy is necessary so that each chapter can stand alone as a complete study.

Chapter Three concerns model interphase Ultem-type polyimides prepared with simulation of the processing steps required for the aqueous suspension prepregging technique. Three different aqueous Ultem-type polyamic acid salts were made: the ammonium (NH_4^+) salt, the tetramethyl ammonium (TMA^+) salt and the tripropyl ammonium (TPA^+) salt. The aqueous salts were dried and imidized to simulate the processing conditions of comparable composite interphases. The imidization behavior was studied using thermogravimetric analysis.

The resulting polyimides were characterized by universal calibration gel permeation chromatography (GPC), dynamic scanning calorimetry (DSC), melt rheology, Fourier transform infrared spectroscopy (FTIR), a solubility test, and pyrolysis gas chromatography. Using these tests, some of the structure-property relationships were developed for Ultem-type polyimides made from aqueous polyamic acid salts.

Polymer samples which replicated the matrix of Ultem-type polyimide interphase/PEEK matrix composites were prepared and analyzed. Since Ultem polyimide is miscible with PEEK [15-17], interdiffusion of the composite interphase and the PEEK matrix was expected. The possible extreme case of complete interdiffusion of the interphase and matrix was considered. It was important to substantiate that the effects on composite performance were attributed to the properties of the interphase and not modification of the bulk matrix.

Therefore, aqueous suspensions of PEEK powder dispersed in aqueous solutions of Ultem-type polyamic acid salts that replicate the actual suspensions used for prepregging were prepared, dried and pressed into films using identical thermal processing conditions to comparable composites. The films were then characterized using tensile testing, DSC, and melt rheology.

In Chapter Four the aqueous suspension prepregging technique was used to fabricate Ultem-type polyimide interphase/PEEK matrix composites with three different molecular weights of Ultem-type polyimide. The composites were characterized using Iosipescu shear testing, unidirectional tensile testing, transverse flexure testing and notched fatigue testing. The failure surfaces from the transverse flexure test were characterized using voltage contrast x-ray photoelectron spectroscopy (VC-XPS)

In Chapter Five model interphase BisP-BTDA polyimides were prepared with simulation of the processing steps required for the aqueous suspension prepregging technique. Two different aqueous BisP-BTDA polyamic acid salts were made: the ammonium (NH_4^+) salt and the tetramethyl ammonium (TMA^+) salt. The aqueous salts were dried and imidized to simulate the processing conditions of comparable composite interphases. The imidization behavior was studied using thermogravimetric analysis.

The resulting polyimides were characterized by a solubility test, DSC, and melt rheology. Using these tests, some of the structure-property relationships were developed for BisP-BTDA polyimides made from aqueous polyamic acid salts.

Polymer samples which replicate the matrix of BisP-BTDA polyimide interphase/PEEK matrix composites were prepared and analyzed. Since BisP-BTDA polyimide is miscible with PEEK [35], interdiffusion of the composite interphase and the PEEK matrix was expected. As mentioned above, the possible extreme case of complete interdiffusion of the interphase and matrix was considered. Aqueous suspensions of BisP-BTDA polyamic acid salts and PEEK that replicate the actual suspensions used for prepregging were prepared, dried and pressed into films using identical thermal processing conditions as for comparable composites. The films were then

characterized using tensile testing, DSC, and melt rheology.

In Chapter Six the aqueous suspension prepregging technique was used to fabricate BisP-BTDA polyimide interphase/PEEK matrix composites with two different BisP-BTDA polyamic acid salts. The composites were characterized using transverse flexure testing, longitudinal flexure testing and unidirectional tensile testing.

In Chapter Seven the aqueous suspension prepregging technique was applied to fabricate Ultem-type polyimide interphase/PPS matrix composites with three different controlled molecular weights of Ultem-type polyimide. The composites were characterized using transverse flexure testing, short beam shear testing, longitudinal flexure testing, and unidirectional tensile testing.

To summarize, the main goal of the proposed work of this thesis was to fabricate interphase composites and provide sufficient information regarding the properties of the constituent materials so that Reifsnider's hypothesis of an optimum interfacial shear strength could be addressed. The composites must be fabricated with a systematically modified interphase, and the properties of the interphase and the matrix must be characterized.

References

1 Reifsnider, K.L., *Composites*, **25**, 461 (1994).

2 Drzal, L.T. and Madhukar, M., *Journal of Material Science*, **28**, 569 (1993).

3 Subramanian, S., Lesko, J.J., Reifsnider, K.L., and Stinchcomb, W.W., *J. Compos. Mater.*, **30**, 309 (1996).

4 Chang, Y.S, Lesko, J.J., Case, S.W., Dillard, D.D., and Reifsnider, K.L., *Journal of Thermoplastic Composite Materials*, **7**, 311 (1994).

5 Gao, Z., Reifsnider, K.L., and Carman, G., *J. Compos. Mater.*, **26**, 1678 (1992).

6 Carman, G.P., Lesko, J.J., and Reifsnider, K.L., *Composite Materials: Fatigue and Fracture, Fourth Volume, ASTM STP 1156,* W.W. Stinchcomb and N.E. Ashbaugh, Eds., American Society for Testing and Materials, Philadelphia, PA, p. 430, 1993.

7 Case, S.W., Carman, G.P., Lesko, J.J., Fajardo, A.B., and Reifsnider, K.L., *J. Compos. Mater.*, **29**, 208 (1995).

8 The Effect of Polyimide Interphases on Properties of PEEK-Carbon Fiber Composites. S. Gardner, A. Gonzalez, R.M. Davis, J.V. Facinelli, J.S. Riffle, S. Case, J.J. Lesko, K.L. Reifsnider, *AIChE 1995 Annual Meeting.* November 12-17, 1995. Miami Beach, FL.

9 Yu, T.H. and Davis, R.M., *J. Thermoplast.Comp. Mater.*, **6**, 62 (1993).

10 Texier, A., Davis R.M., Lyon, K.R., Gungor, A., McGrath, J.E., Marand, H., and Riffle, J.S., Polymer, **34**, 896 (1993).

11 Gonzalez, A-I, M.S. Dissertation (Virginia Polytechnic Institute and State University, Blacksburg, VA, November 1992)

12 Davis, R.M., and Texier, A., *ANTEC '91 Confer. Proceed.*, **37**, 2018 (1991).

13 Gonzalez-Ibarra, A., Davis, R.M., Heisey, C.L., Wightman, J.P., and Lesko, J.J., *Journal of Thermoplastic Composite Materials*, **10**, 85 (1997).

14 Facinelli, J.V., Gardner, S., Dong, L., Sensenich, C.L., Davis, R.M., and Riffle, J.S., *Macromolecules*, **29**, 7342 (1996).

15 Harris, J.M, and Robeson, L.M., *J. Polym. Sci.: Part B: Polym. Phys.*, **25**, 311 (1987).

16 Harris, J.M., and Robeson, L.M., *J. Appl. Polym. Sci.*, **35**, 1877 (1988).

17 Harris, J.M., *ACS Polymer Preprint*, **28**, 56 (1987).

18 Kochi, M. Yokota, R., Iizuka, T., and Mita, I., *Journal of Polymer Science: Part B: Polymer Physics*, **28**, 2463 (1990).

19 Cotts, P.M., Polyimides: Synthesis, Characterization and Applications, K.L. Mittal, Ed., Plenum, New York, 1984, p. 223.

20 Dine-Hart, R.A., and Wright, W.W., *J. Appl. Polym. Sci.*, **11**, 309 (1967).

21 Sroog, C.E., Endrey, A.L., Abramo, s.V., Berr, C.E., Edwards, W.M., and Olivier, K.L., *J. Polym. Sci.:Part A: Polym. Chem.*, **3**, 1373 (1965).

22 J.V. Facinelli, A.E. Brink, S. Liu, H. Li, S. Gardner, R.M. Davis, J.S. Riffle, M. Marrocco, S. Harding. *J. Appl. Polym. Sci.*, **63,** 1571 (1997).

23 Sensenich, C.L., Facinelli, J.V., Dong, L., Gardner, S., R.M. Davis, Riffle, J.S.,*Polymer Preprints, Division of Polymer Chemistry, American Chemical Society*,**37**, 400 (1997).

24 Hsaio, B.S., Sauer, B.B., *Journal of Polymer Science: Part B: Polymer Physics*, **31**, 901

(1993).
25 Hsaio, B.S., Sauer, B.B., *Journal of Polymer Science: Part B: Polymer Physics*, **31**, 917 (1993).
26 Hudson, S.D., Davis, D.D., Lovinger, A.J., *Macromolecules*, **25**, 1759 (1992).
27 Crevecoeur, G., and Groeninckx, G., *Macromolecules*, **24**, 1190 (1991).
28 Pratt, J.R. and St. Clair, T.L., *SAMPE Journal*, **26**, 29 (1990).
29 Johnston, N.J., St. Clair, T.L., and Baucom, R.M., Polyimide Matrix Composites: Polyimidesulfone/:aRC-TPI (1:1) Blend, *24th International SAMPE Symposium and Exhibition*, Reno, NV, May 8-11, 1989.
30 Johnston, N.J. and St. Clair, T.L., *SAMPE Journal*, **23**, 12 (1987).
31 Johnston, N.J. and St. Clair, T.L., *SAMPE Preprints*, **18**, 53 (1986).
32 Texier, A., Davis R.M., Lyon, K.R., Gungor, A., McGrath, J.E., Marand, H., and Riffle, J.S., *Polymer*, **34**, 896 (1993).
33 Varughese, B., Muzzy, J., and Baucom, R.M., *21st Intern. SAMPE Tech. Confer.*, Sept. 25-28, 1989.
34 Akhtar, S., and White, J.L., *Polymer Engineering and Science*, **31**, 84 (1991).
35 McGrath, J.E., Rogers, M.E., Arnold, C.A., Kim, Y.J. and Hedrick, J.C., *Makromol. Chem., Macromol. Symp*., **51**, 103 (1991).
36 Rosen, B.W. *AIAA Journal*, **2** (1964) 1985.

(This page intentionally left blank)

Chapter Two: Literature Review

A major unsolved problem in composite technology is the role of the interphase in composite performance. If relationships can be developed for interphase composites that can correlate the constitutive material properties, composite geometry, composite composition, interactions between constitutive materials, and interphase microstructure to composite performance, then it will be possible to fabricate composites with tailored, optimal lifetimes. This ambitious undertaking has been the focus of much research in recent years. The requirements for such a task are considerable, and begin with the construction of composites with carefully designed interphase regions. The interphase region is defined as the transition zone between the reinforcing fiber and the bulk matrix in a composite. Much effort in recent years has focused on carbon fibers as the reinforcement.

The interphase region can be constructed with the deposition of a thin polymer layer on a fiber [32-39,164] or can develop spontaneously due to the interactions of the matrix material with the surface of the carbon fiber [165-168]. The bulk of the investigations of interphase composites have been on thermosetting matrix systems. Due to the many advantages of engineering thermoplastic polymers, there is increasing interest in thermoplastic matrix, carbon fiber, interphase composites.

Two high performance, engineering, thermoplastic polymers which have unique and desirable properties for high performance composites are polyether ether ketone (PEEK) and polyphenylene sulfide (PPS). Both of these polymers have found increasing use as composite matrix materials and they are the matrix materials that will be addressed in this thesis.

High performance thermoplastic polyimides represent an important class of materials that

are finding use in many applications that take advantage of the high strength, high temperature stability and solvent resistance of these polymers. Fiber reinforced composites are one of the material systems in which polyimides are finding use. Polyimides can be used as a matrix polymer in a fiber reinforced composite [33,35-37,49,52-54,62-66], and, more recently, as a composite interphase material [32-39]. This thesis focuses on the fabrication and performance of polyimide interphase composites.

The formation of a well defined polyimide interphase can be accomplished with a variety of manufacturing techniques. A simple technique for interphase formation is the application of the interphase polymer as a sizing to the carbon fiber [38-39]. Typically this is executed by passing a carbon fiber tow through a solution of the sizing polymer. A drying step is then used to remove the solvent. The matrix polymer is then applied to the sized fiber in a subsequent step.

The combination of reinforcing fiber and matrix polymer in a form which can be laid up to create a composite structure results in a material intermediate known as prepreg. The manufacture of this intermediate material is called prepregging. Prepregging can be accomplished by many different methods. The method chosen for a particular application reflects the processing conditions that are possible for the matrix polymer. Prepregging of matrix polymers can be done with hot-melt prepregging, solvent prepregging, commingled yarn and powder prepregging techniques.

A method which provides the application of the interphase polymer at the same time as the matrix polymer is the aqueous suspension prepregging technique [32-37]. With aqueous suspension prepregging, a stabilized slurry of polymer matrix powder is suspended in an aqueous solution. The fiber tow is then drawn through the suspension and coated with the matrix powder.

The matrix powder in suspension must be well dispersed in homogeneous manner and the powder particles must adhere to the carbon tow. A surfactant or a polymeric dispersant can be used to disperse the powder and polymeric binders dissolved in the solvent can be used to adhere the powder particles to the fiber tow.

Aqueous suspension prepregging has been done by many researchers using a polyimide precursor, a polyamic acid salt, which is dissolved in water, an neutralized with a base [32-37]. The polyamic acid salt is water processable which leads to an environmentally friendly alternative to organic solvent techniques. The matrix polymer powder is dispersed in the aqueous polyamic acid salt solution. The polyamic acid salt behaves as a surfactant, adsorbing to the surface of the matrix powder particles, and electrostatically stabilizing the suspension. The fiber tow is then coated with the polyimide precursor and the matrix powder in a single prepregging step. The polyamic acid salt also serves as a binder, adhering the matrix powder to the carbon tow. After drying the water from the prepreg, a heating cycle is used to convert the polyamic acid to the polyimide by way of thermal imidization. The aqueous suspension prepregging method is used for the manufacture of interphase composites in this thesis, and will be described in detail in the following chapters.

Hydrolytic degradation of polyamic acids is a problem when they are subjected to aqueous conditions [5-8]. Hydrolysis results in decreased molecular weight of the polyamic acid and ultimately the polyimide. Molecular weight control is an important problem for processing polyimides from aqueous precursors [6-12]. The characterization of the polyimide interphase polymer is extremely important for relating the interphase microstructure to the composite performance.

Characterization of the composite performance is also very important. The mechanical testing strategy must be planned such that the tests probe the effects of the interphase and permit testing of micro-mechanical models. As the fabrication of interphase composites has been of great recent interest, so has the evaluation of interphase composite performance. Durability issues have been of special interest for interphase composites such as composite fatigue, creep, impact, high temperature loading, and hygrothermal loading conditions. Typical composite performance tests, such as tensile, flexure, and shear testing are important in developing micro-mechanical models.

Many mechanical models have been proposed for prediction of composite strength [173-178]. Significant advances have been made in evaluation of mechanical models with finite element methods [163], parametric studies [181], and computer codes [163,176-179] which compensate for the statistical nature of local composite properties.

A review of the pertinent literature is a necessary first step for understanding a research project of this caliber. This chapter concerns a review of the literature, structured in order of the research objectives identified in Chapter One. The research objectives of this work are:

① Processing and characterization of controlled molecular weight polyimides from aqueous polyamic acid salts including assessment of chemical analysis, molecular weight distribution, melt rheology, and thermal analysis.
② Characterization of model interphase/PEEK matrix blends
③ PEEK matrix composite manufacture with tailored, polyimide interphases of controlled properties.
④ PPS matrix composite manufacture with tailored, polyimide interphases of controlled properties.
⑤ Characterization of interphase composite durability and performance with a focus on composite failure mechanics.

Before discussing the details of the processing of controlled molecular weight polyimides from aqueous polyamic acid salts, it is first useful to review the importance and synthesis of polyimides. Some typical processing techniques are next examined for background information which will demonstrate the benefits and limitations of processing of controlled molecular weight polyimides from aqueous polyamic acid salts. Polyamic acid, polyamic acid salt, and polyimide characterization techniques that are pertinent to the goals of this thesis are then presented which will provide background information necessary for a comprehensive discussion.

Because the degree of compatibility of the polyimide interphase with the polymer matrix is important to the microstructure of the composite, a discussion of the important characteristics of model matrix blends will follow. Special consideration will be given to the implications of a thin polyimide interphase region on a carbon fiber surface surrounded by PEEK or PPS matrix polymer.

Some composite manufacturing techniques will be briefly reviewed as well as typical techniques for interphase formation. A review of studies conducted on composites with specially designed interphases will follow as well as a review of interphase characterization techniques. Some important composite characterization methods will be reviewed with an emphasis on techniques that provide information that can be related to the composite interphase. The final topic reviewed will be the development of mechanics used to explain the composite failure modes and models based on these mechanics that can be used to predict the performance of interphase composites.

Polyimides: Importance

The rapid development of polyimides has resulted in great improvements in their properties and new applications. Properties which are typically identified with polyimides are heat resistance, solvent resistance, good mechanical strength, good toughness, excellent dimensional stability, low coefficient of friction, outstanding radiation resistance, high dielectric strength, low outgassing, and resistance to creep and wear [6-8,13-17]. Some polyimides can be processed into structures with typical thermoplastic melt processing techniques such as injection molding and thermoforming [6-7,13-17]. Other polyimides do not display a definite glass transition temperature and behave as a pseudo-thermoset which complicates or prohibits melt processing [16]. These polyimides must be processed using powder sintering techniques or machined into final form. Polyimides can also be applied as a thin film coating from an appropriate solution. The final form of polyimides for commercial applications includes films, molding powders, wire-coating enamels, adhesives, laminating resins, fibers, and foams [13-17].

Some of the important structural applications of polyimides are surgical instruments, aircraft and automotive components, microwave oven hardware, pressure vessels, sleeve bearings, and electric switches [13-17]. The dielectric constant of polyimides makes them useful for semiconductor processing equipment, circuit boards, and electrical switches [69].

Polyimides: Commercial Polyimides

The generalized chemical structure for polyimides is shown in Figure 2-1. Performance characteristics can be tailored to enhance specific applications. It is often found that one area of performance is enhanced at the cost of another.

For example Kapton® film sold by E.I. DuPont has excellent high temperature properties, but the pseudo-thermoset behavior of the polymer limits the shape to films. Vespel® sold by E.I. DuPont also has a pseudo-thermoset behavior, but structures can be machined from bulk polyimide [16]. Torlon® polyamide-imide sold by Amoco is more processable with melt processing techniques, but the yield strength and ultra-high temperature performance is sacrificed [14]. Ultem® polyetherimide sold by General Electric has outstanding melt processing characteristics but is not resistant to many organic solvents [15]. Aurum® polyimide sold by Mitsui Toatsu has good strength in structural parts and it is melt processable. However, thermal degradation issues have been of concern [17].

Table 2-I. Some mechanical properties of commercial polyimides.

	comments	Heat Deflection Temperature	shear strength (MPa)	tensile strength (MPa)	tensile modulus (GPa)	tensile yield strain (%)	tensile failure strain (%)
Ultem 1000[1]	amorphous thermoplastic	200°C	100	105	---	7.0	60
Aurum[2]	amorphous thermoplastic	238°C	83	94	---	---	90
Torlon[3]	amorphous thermoplastic	274°C	---	190.0	---	---	12
Vespel[4]	amorphous pseudo-thermoset	288°C	89.6	86.2	2.76	---	7.5
Kapton[5]	7.6 µm-127 µm film thickness	320°C	---	70-165	2-3	---	8-70
	thermoset						

1. Ultem Resin Design Guide, General Electric [15].
2. Aurum Properties Edition, Mitsui Toatsu Chemicals, Inc. [17].
3. Torlon , Amoco Specialty Polymers [14].
4. Vespel , DuPont [16].
5. Goodfellow material catalog

The most common synthetic route for polyimides involves the production of a polyamic acid using a step growth polymerization scheme of an aromatic dianhydride and an aromatic diamine [6-8,18]. The polyamic acid is then converted to a polyimide using a chemical, thermal, or solution imidization technique [6-8,18]. The most common imidization technique is bulk thermal imidization of a solution cast film of the polyamic acid [6-7]. Due to the vast availability of many aromatic dianhydride and aromatic diamine monomers, and the relative simplicity of the

reaction scheme, proprietary polyimides may be synthesized by an end user to tailor properties for a specific application.

One such polyimide which was synthesized for research purposes by Professor J.E. McGrath in the Virginia Tech chemistry department is BisP-BTDA polyimide [80]. The dianhydride used for this polyimide is benzophenone tetracarboxylic dianhydride and the diamine is 4,4'-[1,4-phenylene-bis-(1-methy ethyidene)] bisaniline. The chemical structure of BisP-BTDA is shown in Figure 2-2. This polyimide has good strength, thermal resistance and is compatible with several ether containing aromatic thermoplastics [80].

Polyimides: Typical Synthesis

High performance polyimides can be made by a variety of synthetic routes. Typically the most widely used synthetic route is a two step method, first producing the polyamic acid from a step-growth polymerization of an aromatic dianhydride and an aromatic diamine [6-7,21-24]. The conversion of the polyamic acid to the polyimide is by a condensation reaction. The condensation reaction which dehydrates the polyamic acid to form the polyimide can be done chemically, in solution or as a bulk thermal imidization [6-7,21-24]. The final polyimide molecular weight distribution will be effected by the imidization method [6,25,80-81].

The synthesis of Ultem polyetherimide is shown in Figure 2-3. Ultem polyimide is cyclized from the polyamic acid made from 2,2'-bis-[4-(3,4-dicarboxyphenoxy)phenyl}propane dianhydride and m-phenylenediamine [28].

Polyimides: Chemical Imidization of Polyamic Acids

Chemical imidization is often done at room temperature in solution utilizing dehydrating agents in conjunction with a basic catalyst. Anhydrides are typical dehydrating agents and typical basic catalysts include pyridine, triethylamine and isoquinoline [7,10,18]. Incomplete imidization and isoimide formation are two disadvantages of the chemical imidization technique. Incomplete imidization will yield a material that is not completely stable and upon *further* melt processing techniques, will continue the imidization reaction. Since the imidization reaction is a condensation reaction, the products are imide moieties and water. The water produced will serve to form voids in the material and could hydrolytically degrade the polyimide. Isoimide formation can produce a more flexible polymer backbone, thereby reducing the bulk polymer melt viscosity, however, at higher temperatures, the isoimide has a tendency to rearrange to form the imide.

Polyimides: Solution Imidization of Polyamic Acids

The polyamic acid can be dissolved in an appropriate, high boiling solvent, and thermally imidized at an elevated temperature. These temperatures are typically lower than the glass transition temperature of the resulting polyimide and in the range of 150° to 200°C [11,84].

As mentioned above, Grenier-Loustalot et al. and Dine-Hart and Wright showed that the solution imidization of polyamic acids was catalyzed by the addition of a base such as a tertiary amine and acetic anhydride [7,10].

Cotts has shown that polyamic acids display polyelectrolytic effects in “as received” NMP [6,12]. At low solute concentrations, the polyelectrolyte effect can reduce the intramolecular forces of the polyamic acid by greatly increasing the hydrodynamic size. The cyclic dehydration reaction of each individual reacting species is more isolated. Thus, undesired side reactions are reduced [6,12].

Kim et al. examined the solution imidization reaction kinetics of several polyamic acids and demonstrated that controlled molecular weight polyimides could be attained when proper polymer chain endcaps are used [81]. The solution imidization reaction was shown to be acid catalyzed and follow second-order kinetic behavior.

Polyimides produced from solution imidization techniques have been shown to possess a more uniform molecular weight distribution and lower melt viscosities than bulk thermally imidized counterparts [6,25,80-81].

Polyimides: Bulk Thermal Imidization of Polyamic Acids

The most common method of polyamic acid imidization is a bulk thermal imidization technique where the polyamic acid is cast into a film and then heated to an imidization temperature [6,20-21,25]. The imidization can be done in air or an inert atmosphere. An inert atmosphere tends to minimize thermal oxidation [20-21]. It is typical to follow a multi-stage heating program incorporating several isothermal holds at successively higher temperatures, such as one hour at 100°C, one hour at 200°C and one hour at 300°C [20-21,25]. This is effective in removing any residual solvent.

Palmese and Gillham demonstrated that a stepwise imidization scheme- which allows partial cyclization to occur, followed by vitrification, as the glass transition temperature of the polyamic acid/polyimide increases above the hold temperature- aids in the formation of linear species [71]. With repeated steps of steadily increasing isothermal hold temperatures which allows sufficient time for vitrification to occur before proceeding to the next isothermal hold temperature, side reactions which result in crosslinking are minimized.

It has been shown by Facinelli et al. that Ultem-type polyamic acids form chemical complexes with some solvents, increasing the difficulty in solvent removal. Thus a multi-stage imidization cycle would provide sufficient conditions for complete imidization and removal of residual solvent [28].

The chemical mechanism of thermal imidization is not fully understood. However several studies have been done on thermal imidization reactions [8,10,85]. There are some proposed mechanisms for this reaction that include complex, multi-step reactions.

Hermans and Streef studied the bulk thermal imidization reaction of polyimides based on hexamethylene diamine and pyromellitic acid and noted brittle, obviously branched or crosslinked products [85]. A proposed mechanism for imidization assumed that a side reaction which forms an amide will occur along with imide formation. This side reaction could lead to branching and crosslinking. The schemes for side reactions during thermal imidization published by Hermans and Streef are shown in Figure 2-4 [85]. The equilibrium reactions show that a diamidation reaction will always occur as a side reaction in imide formation and is probably the main cause of branching and crosslinking. The diamidation reaction is promoted by a slight excess of basic groups and suppressed by a slight excess of acid groups.

Removal of the water produced from the condensation reaction is important, as the presence of water can hydrolytically degrade the polyimide [5-8]. Water removal can be difficult for thick structures. Because of this reason bulk thermal imidization is best suited for thin films or dispersed powders.

Linear, high molecular weight, thermoplastic polyimides are usually desired, thus, intramolecular imidization is an important possible side reaction to consider during bulk thermal imidization. As seen in Figure 2-4, intramolecular imidization is the formation of an imide linkage from an amide moiety and carboxylic acid moiety that are on adjacent polymer chains. This effectively creates a crosslink, which in high concentration, can form a polymeric network.

Solvent retention by a polyimide is important because the presence of NMP has been attributed with participation in the formation of intermolecular bonds during thermal imidization [9]. This results in chain branching or crosslinking and more importantly, does not allow the cyclodehydration reaction to occur which converts the polyamic acid to the thermally stable polyimide [8-10].

Polyimides: Polyamic Acid Salts

The use of polyamic acid salts for polyimide formation has been described by many researchers [6-8,10,12,26-36,40-51]. The benefits of polyamic acid salts include accelerated imidization kinetics, water processability, and orientation of polyimide monolayers.

Studies on the imidization kinetics of polyamic acids in solution have considered the addition of tertiary amines and acetic anhydride to the solution [7,10]. Dine-Hart and Wright [7]

and Grenier-Loustalot et al. [10] have each shown a catalytic effect on solution imidization kinetics with the addition of pyridine, β-picoline, or triethylamine with acetic anhydride. The polyamic acid salt has been shown to imidize more rapidly due to the increased reactivity of the amide group as a result of the base, and the acetic anhydride reacts with the water evolved from the condensation reaction of imidization to form acetic acid, thus removing the water and driving the reaction [10].

A US Patent issued to Endrey in 1966 describes the formation of polyamic acid ammonium salts using tertiary amines for the purpose of making polyimide structures [26]. An interesting possibility noted in the patent is that the base can be added during the polymerization of the polyamic acid or after polymerization is complete. Thus, in some circumstances, the base could be used as part or all of the solvent during polymerization. This would ensure conversion of all amic acid groups to the amic acid salt species without the presence of water and the undesirable side reaction of hydrolysis. The patent issued to Endrey does not describe the processing of polyamic acid ammonium salts from aqueous solution.

Reynolds and Seddon studied the stability of polyamic acid salts in aqueous solution [184]. In their work, polyamic acids made from pyromellitic dianhydride and 4,4'-diaminodiphenyl ether were synthesized in dimethylacetamide and recovered in powder form. The dry polyamic acids were dissolved in aqueous solutions of triethylamine, TEA, to make a 2 wt% solution. The amount of TEA was varied from 90% to 150% of the stoichiometric equivalent to carboxylic acid groups on the polyamic acid and the intrinsic viscosity was measured with time. Results from this study are shown in Figure 2-5. As seen in Figure 2-5, the intrinsic viscosity of the solution with 90% stoichiometric TEA drops rapidly indicating a loss of

molecular weight of the polyamic acid salt. The solution with a stoichiometric equivalent (100%) of TEA has a slowly decreasing intrinsic viscosity, also indicating a loss of molecular weight. The solutions with 110%, 130% and 150% stoichiometric TEA have a constant intrinsic viscosity for at least 250 hours. It is proposed by Reynolds that the TEA protects the polyamic acid from hydrolysis by prohibiting a proton transfer to the amide group [184]. The results show conclusively that an excess of base is required to maintain viscosity stability of an aqueous polyamic acid salt solution.

Considerable work has been done on the processing of polyamic acid salts from aqueous solutions [6,8,12,27-29,32-36,40-51]. The formation of polyamic acid salts by addition of an appropriate base can be done in an organic solvent, recovered and then dissolved in water [28-29]. The polyamic acid salt can also be formed by adding the polyamic acid to an appropriate aqueous basic solution [6,8,12,27-29,32-36,40-51]. Much of the work reported in the literature for aqueous processing of polyamic acid salts is associated with the aqueous suspension prepregging technique for composite manufacture [6,8,12,27-29,32-36,40-51].

The formation of ultrathin polyimide films with controlled thickness and molecular orientation using a Langmuir-Blodgett technique has been reported making use of polyamic acid salts [30-31]. This technique makes use of a organic solvents and very bulky, basic amines. Tamada et al. used an ammonium ion with a long alkyl chain to ensure that a pendant dye moiety attached to the polyamic acid was oriented along the surface of a substrate [30]. Hirano et al. used a tertiary amine with long alkyl chains to provide a well defined periodic structure to the molecular orientation of polyimide films made from a Langmuir-Blodgett technique [31].

Polyimides: Use in Composites

Polyimides have found use in composite materials as a matrix polymer and as an interphase polymer. Some polyimides commonly used as a matrix polymer for manufacture of fiber reinforced composites are PMR-15, LaRC-TPI and Ultem 1000. PMR-15 is a thermosetting polyimide made from three monomers: 5-norbene-2,3-dicarboxylic acid; 4,4'-methylenedianiline; and 3,3',4,4'-benzophenone tetracarboxylic dianhydride [52]. Composites made with PMR-15 matrix have a service temperature up to 260-316°C, are relatively brittle and suffer from interlaminar matrix cracking [52-60]. This addition-cure polyimide has a limited shelf life, a toxic monomer, and difficult handling procedures resulting in matrices with inconsistent properties [53-54]. PMR-15 is available for prepregging in unreacted oligomer form, as well as impregnated unidirectional tape and fabrics [61].

LaRC-TPI polyimide has been reported in the literature as a matrix polymer for high performance composites [33,35-37,49,62-66]. Of particular importance to this work was the development of aqueous suspension prepregging by Texier, Gonzalez, and Davis et al. [35-36] using LaRC-TPI polyamic acid binder with LaRC-TPI polyimide powder. The benefits of LaRC-TPI polyimide matrix include good strength, stiffness, and service temperature up to 256°C [17]. Complications limiting the use of LaRC-TPI polyimide as a matrix material arise because impregnated prepreg is not commercially available. Prepregging must be done by the end-user before composite layup. Although improvements have been made to the processability of LaRC-TPI polyimide, the melt viscosity is still relatively high. Thus, the prepregging processes reported in the literature for LaRC-TPI have been powder based prepregging techniques. LaRC-TPI is commercially available under the recently trademarked name Aurum.

Prepreg tapes and fabrics with Ultem polyimide matrices are available from several manufacturers [61]. The ease of processing this polyimide facilitate melt prepregging and solvent prepregging techniques. While this prepreg yields composites with moderate strength and stiffness, the susceptibility of damage by chlorinated solvents limits this matrix polymer from many applications [15,61].

The use of polyimides as a composite interphase polymer has been reported in the literature [32-39]. Composites with LaRC-TPI polyimide interphases have been made with a PEEK matrix [32-35,37] using an aqueous suspension prepregging technique. Similar PEEK matrix composites were also fabricated with a BisP-BTDA polyimide interphase [35]. The interfacial adhesion of carbon fibers sized with polyamic acid was examined by Chuang et al. for matrix polymers including polyphenyl sulfide, polyether ether ketone, Ultem polyimide, polyethersulfone, and polysulfone [38]. Polyamic acids based on (1) benzophenone tetracarboxylic dianhydride (BTDA) and 4,4'-diaminodiphenyl ether (ODA), (2) BTDA and 4,4'-diaminodiphenyl sulfone, and (3) BTDA and ODA modified with bisaminopropyldisilane were applied as a sizing from NMP, and subsequently imidized. Of all the thermoplastic matrix polymers considered, the best interfacial adhesion was found for PEEK matrix samples and the worst interfacial adhesion was found for the PPS matrix samples [38-39].

Polyimides: Melt Processing of Polyimides

Polyimide processing can be accomplished by a variety of methods. If the polyimide is a linear thermoplastic polymer, melt processing may be a reasonable method. Polyimides typically have high melt viscosities. However, recent advances have included synthesis of polyimides with flexible linkages in the polymer backbone, which have a suitable melt viscosity for conventional melt processing techniques. The development of polyimides with processing melt viscosities (in the range of 100-1,000 Pa·s) which are suitable for melt processing has increased the commercial use of polyimides. Ultem polyimide is manufactured in many grades that are processable with typical polymer melt processing equipment. The molecular weight of many polyimides are just above critical entanglement molecular weight to obtain acceptable mechanical properties while retaining acceptable processability by keeping the molecular weight low.

Since the imidization reaction mechanism is often described as an equilibrium reaction, where the polyamic acid may be formed from the polyimide in the presence of water, the melt processing conditions must remain controlled to minimize the back reaction.

Polyimides: Solvent Processing of Polyamic Acids and Polyimides

Some polyimides are insoluble or the solvents needed for processing are undesirable [8,81]. These polyimides can sometimes be processed by a solvent technique using the polyamic acid. Conditions must be carefully controlled since polyamic acids have been shown to be unstable in solid form and in solution [7-8,67-68]. It is recommended that polyamic acids be used immediately after synthesis and then converted to polyimide or stored below 0°C [7].

For the production of thin films, the polyamic acid can be cast from a solvent, and the film can be thermally imidized [7-9,11-12,30-31,69-71]. This method is not practical for thick, structural parts, because the water released during the condensation reaction must diffuse completely out of the polyimide structure. The diffusion and removal of the water produced is attainable with thin films, but not with thicker pieces.

A complication of solvent processing is that polyimides are not usually soluble in many solvents. The solvents which are typically used are hazardous including NMP, THF, cresols and phenols [7-9,12,70]. There is little desire to work with these solvents routinely on a large scale in industrial operations for health reasons and environmental regulatory reasons.

If a suitable solvent is found, the solvent must be removed after processing the polyimide. This becomes a difficult task with a high boiling solvent. There are further complications since dry solvent conditions are very important because of the possible reverse reaction of polyimide to polyamic acid in the presence of water and solvent purity is important to minimize side reactions.

The effects of specific solvents on the conversion of polyamic acids to polyimides has been studied by several researchers [6,9-12,30-31,70-71]. A polyelectrolyte effect has been observed for polyamic acids with aprotic solvents such as N-methylpyrrolidone, NMP, and dimethylformamide, DMF [6,9,11-12]. The presence of water or basic impurities, such as methylamine in commercial grades of NMP, create ionic polyamic acid salts. The polyelectrolyte effect results in an increased hydrodynamic volume due to electrostatic repulsion of ionic charges on the polymer backbone. The polyelectrolyte effect can be minimized by adding LiBr to serve as a scavenging electrolyte, or eliminated by distilling the NMP [6,12].

Another interaction of aprotic solvents with polyamic acids is complex formation of the

solvent molecule with the polyamic acid. This mechanism has been attributed to hydrogen bonding of the solvent with the amide hydrogen and the carboxylic group of the polyamic acid [9,11]. The solvent becomes difficult to remove completely during oven drying steps and is retained by a cast film of polyamic acid which has implications on the imidization process. The presence of NMP has been attributed with participation in the formation of intermolecular covalent bonds during thermal imidization [9]. This results in chain branching or crosslinking and more importantly, does not allow the cyclodehydration reaction to occur which converts the polyamic acid to the thermally stable polyimide [8-10]. It has been shown by Facinelli et al. that Ultem-type polyamic acids form chemical complexes with NMP and tetrahydrofuran, THF, increasing the difficulty for solvent removal [28-29].

Solvent processing of fully formed polyimides can be accomplished in some uncommon cases. Ultem polyimide is soluble in chloroform and methylene chloride, which can be removed at moderately low temperatures [15].

Unique and remarkable properties of polyimide film processed from cold drawn polyamic acid film has been reported by Kochi et al.[5]. Several polyamic acids were synthesized and solvent cast onto a glass substrate. The films were removed from the substrate and drawn at room temperature. The drawn films were mounted in a metal frame and thermally imidized. One of the polyimides examined, synthesized from biphenyltetracarboxylic dianhydride and paraphenylenediamine, displayed remarkable tensile properties in the draw direction. A tensile modulus of 59.1 GPa and a tensile strength of 1.2 GPa was attained [5].

Polyimides: Aqueous Processing of Polyimide Precursors

The technology for processing polyimides using water based techniques is very new. One such technique makes use of a water soluble form of the polyimide precursor, the polyamic acid salt. Polyamic acids can be made soluble in water with the addition of a base. The polyamic acid combines with a basic counterion to form a polyamic acid salt. Although this chemistry has been known for many years, it has not been used on a large scale due to the belief that thermoplastic polyimides with controlled and high molecular weights could not be produced by this means. This belief was held because, in the presence of water, polyamic acid is hydrolyzed, reducing the molecular weight of the polymer, and creating many reactive end groups [5-8]. Upon water removal and thermal imidization, the reactive end groups can recombine. If the concentration of these reactive end groups is high, then intramolecular imidization can occur, resulting in a crosslinked product [85].

In 1972 a patent was granted to Vincent and Anderson for water dispersible polyimide coatings [86]. The polyamic acid was first synthesized from an unsaturated polycarboxylic monoanhydride and a diamine in organic solvent, then it was heated to 150°C for 2 hours. The extent of imidization was not qualified in the patent at this stage. Maleic anhydride was then added to the solution to "generate carboxyl groups on the polymer". The polymer is always referred to as a "polyimide" in the patent, however, strictly speaking, it is most likely at least partially a polyamic acid at this stage. The polymer was recovered from the organic solvent and dispersed in water with the aid of triethylamine. The backbone structure of these polyimide molecules was partially aliphatic, which limits the high performance characteristics expected from modern polyimides. These polyimide coatings could be applied to a metal substrate by an

aqueous electrodeposition technique which resulted in the formation of films with a controlled thickness even on substrates with a detailed surface topography.

Water soluble polyamic acids with a pendant sulfonic acid group attached to polymer backbone were synthesized by Clemenson et al.[72]. Two different dianhydrides were used, 3,3',4,4'--benzophenone tetracarboxylic dianhydride and 1,2,4,5-benzenetetracarboxylic dianhydride, as well as two different diamines, 4,4'-diaminostilbene-2,2'disulfonic acid and 2,5-diaminobenzenesulfonic acid to synthesize four different polyamic acids. The molecular weights of the polyamic acids were characterized using GPC, revealing very low number average molecular weights (1870-2900) which corresponded to 2.54-5.02 polyamic acid repeat units. Due to the ionization of the sulfonic acid group and the very low molecular weights, all four of the polyamic acids were shown to be soluble in water and methanol. The polyamic acids were all shown to be insoluble in THF, m-cresol and NMP. The polyamic acids were imidized using a staged imidization cycle of 100°C/1 hour, 200°C/1 hour, 300°C/1 hour and 365°C/30 minutes and the resulting polyimides were characterized. Clemenson et al. claim that after the staged imidization cycle, one of the polyimides crystallizes at 292°C, as seen by DSC, and then undergoes melting/decomposition at 370°C. They also show the glass transition temperature is taken as the shoulder of a steep endotherm that peaks at about 225°C. It is evident that further characterization is necessary of these polyimides.

Progar made LaRC-TPI polyimides from aqueous solutions of the polyamic acid ammonium salt [83]. Characterization of the LaRC-TPI polyimide showed good strength and modulus for films cast from aqueous solution and then imidized.

Progar and Pike investigated the possibilities of a water soluble precursor to LaRC-TPI

polyimide for use as an adhesive [84]. The quaternary N,N-dimethylehtanol amine salt of the polyamic acid was made in water at 50-60°C. The resulting solution was applied to E-glass cloth which was then heated in an oven to imidize the polyamic acid salt. The impregnated E-glass was used as an adhesive tape to bond titanium adherends for a lap shear test. Similar samples were made with LaRC-TPI polyamic acid from a diglyme solution for comparison. The lap shear strengths were measured at room temperature, 177°C, 204°C and 232°C. The lap shear strengths of the adhesive prepared from the water soluble polyamic acid salt compared very favorably with the polyamic acid applied from diglyme solution.

Molecular weight control of water soluble polyimide precursors has been demonstrated by Facinelli et al. with Ultem-type polyamic acid salt [28]. A systematic increase in ultimate polyimide molecular weight was developed using several different bases for synthesis of different polyamic acid salts. Molecular weight control was demonstrated with a particularly important polyimide having a glass transition temperature of 218°C and a number average molecular weight of 13,400 made from the Ultem-type polyamic acid triethylammonium salt. The Fox-Flory relationship of molecular weight to glass transition temperature was employed to yield a value for T_g^{∞} of 237°C.

By selection of an appropriate basic counterion, it is possible to produce a linear, thermoplastic polyimide with controlled molecular weight using an aqueous processing route. Several factors will influence the rate at which the counterion binds to the carboxylic acid groups on the polyamic acid chain and the strength of the association. Some of these factors are counterion charge, counterion size, counterion concentration, polyamic acid concentration, and solution temperature. Gregor and Gregor developed a mathematical model for

counterion/polyelectrolyte interactions based on a charged rod model which considers the counterion size, charge density and dielectric constant of the solution [73-74]. Results from the model show that, in general, binding energy increases with counterion charge, but decreases with counterion size. Kielland published ion hydrodynamic radii for many tertiary and quaternary ammonium ions in aqueous solution in 1937 [75].

Table 2-II. Hydrated diameters for aqueous, solvated ammonium ions.

	solvated ion	Hydrated diameter (Å)
ammonium hydroxide	NH_4^+	2.5
tetramethylammonium hydroxide (TMAH)	$(CH_3)_4N^+$	4.5
triethylamine (TEA)	$(C_2H_5)_3NH^+$	5
tetraethylammonium hydroxide (TEAH)	$(C_2H_5)_4N^+$	6
tripropylamine (TPA)	$(C_3H_7)_3NH^+$	7
tetrapropylammonium hydroxide (TPAH)	$(C_3H_7)_4N^+$	8

Polyimides: Effect of Processing on Properties (Characterization of Polyimides)

To achieve high molecular weight, linear, thermoplastic polyimides, molecular weight stability is of paramount importance. For this criteria, the polyimides must be synthesized with a suitable nonreactive endcap that is stable at melt processing conditions [20-21,25,80-81]. Polyamic acids synthesized by a step reaction can be terminated with an amine or an anhydride, simply by adding an excess of either appropriate monomer. However, these species do not form

polymer chain endcaps which are stable at high temperatures. Thus, an additional, monofunctional endcapping monomer must be added. Some typical endcapping monomers are phthalic anhydride, and aniline to create nonreactive phthalimide endgroups.

Srinivas et al. showed the importance of synthesizing polyimides with nonreactive endcapping functionalities for polyimides based on 1,3-bis(4-aminophenoxy) benzene (TPER) and 3,3',4,4'-biphenyltetracarboxylic dianhydride (BPDA) endcapped with phthalic anhydride [21]. Three TPER-BPDA polyimides were synthesized: one with all polyimide chains endcapped with phthalic anhydride, one with half of the chains endcapped and one with no endcap which was amine terminated from an excess of diamine. The isothermal melt viscosity was measured at a processing temperature of 430°C. As seen in Figure 2-6, the TPER-BPDA polyimides that were half-endcapped and amine terminated show a dramatic increase in melt viscosity. The TPER-BPDA polyimide that was fully endcapped maintained a relatively low melt viscosity during the isothermal hold, indicating much better molecular weight control.

Proper endcap selection imparts high temperature thermal stability which is important in maintaining mechanical properties after thermal processing. Polyimide degradation has been investigated in the literature. Heuristic data comparing many monomers guiding monomer selection and the relative effect on thermal stability are available [76].

Without proper endcapping, molecular weight control is unlikely. Thus, crosslinking occurs, increasing melt viscosity and modulus. Crosslinking eliminates the possibility of processing the polyimide from solution and an increased melt viscosity will lead to more difficult melt processing. An increased modulus corresponds to a proportional decrease in ductility which could effect the mechanical properties and decrease the toughness.

One of the purposes of this thesis is to examine the effect of the polyimide interphase properties on the bulk composite properties. Therefore it is very important to understand how the composite processing thermal cycle affects the interphase properties. For interphase composite manufacture with a PEEK matrix, the processing temperature is 380°C for thirty minutes. The thermal stability of the polyimide interphase material at this temperature is important when considering an interphase region that is primarily composed of the polyimide.

Because there are many factors which can alter the processability of a polyimide, characterization of the polyimide is very important. The techniques used for proper characterization are discussed next.

Polyimides: Characterization of Polyamic acids/ Polyamic acid salts and polyimides

When considering a research project that involves synthesis and processing of polyimides from an aqueous solution, the methods of polymer characterization must be appropriate and well understood. Since the processing of aqueous polyamic acid salt solutions is a relatively new technique, the chemistry of the precursors must be studied and understood. The chemistry of the resulting polyimides must also be verified for structure and completion of imidization. Spectroscopic techniques are common for studying the chemistry of polyamic acids and their conversion to polyimides.

The thermal properties of polyamic acid salts and polyimides are also very important. The temperatures for conversion to polyimide need to be characterized, as well as the glass transition temperature and the temperature of degradation for the resulting polyimide. While

many techniques are available for estimating the glass transition temperature of polymers, the use of dynamic scanning calorimetry (DSC) will be the focus of this review. The use of thermal gravimetric analysis for probing imidization temperature ranges and degradation temperatures will also be discussed.

It is extremely important to know the molecular weight of the polyamic acids and resulting polyimides for producing polymers with controlled molecular weight. The use of intrinsic viscosity, inherent viscosity, and gel permeation chromatography (GPC) to characterize the molecular weights will be reviewed. Although melt viscosity measurements do not provide a *measure* of molecular weight, such measurements can be used to study the relative change in molecular weight for a given polyimide chemistry during dynamic temperature cycles. Therefore, the use of melt rheology will be discussed with these topics. If all polyimides were linear, amorphous, single phase polymers, then concerns of the polyimide microstructure would not exist. As it is, the microstructures of polyimides produced from aqueous polyamic acid salts are varied and require examination.

Typical mechanical properties of commercial polyimides have been tabulated above. It is very useful to measure the mechanical properties of polymides produced from aqueous polyamic acid salts for comparison and to gain understanding of the polymer microstructure. Since these polyimides will be used to create a composite interphase region, the mechanical properties can also be used to develop micro-mechanical models of composite failure.

Polyimides: Spectroscopic Investigation of Chemical Structure

Many features of polymer chemical structure can be obtained with a variety of spectroscopic techniques. Some useful spectroscopic techniques are low angle light scattering (LALS), x-ray scattering, nuclear magnetic resonance (NMR),electron spectroscopy for chemical analysis (ESCA) and Fourier transform infrared spectroscopy (FTIR).

The molecular weight and second virial coefficient can be found with LALS techniques. Information about periodic molecular structure can be determined from x-ray scattering. Chemical structure can be deduced and molecular weight can sometimes be estimated using NMR techniques. While these methods of analysis are powerful and important, they will not be included in this review for reasons of brevity.

FTIR can be used to identify the signature chemical bonds of a polyimide and has been used by many researchers in the recent literature to asses the completion of polymerization or the extent of imidization [25,71,80,88-91]. FTIR attenuated total reflectance (ATR) is an adaptation of the infrared technique which allows infrared spectra to be obtained for polymers in the solid state.

The IR bands typically used for determining the completion of polymerization of the polyamic acid monomers are characteristic of the anhydride groups which would remain from the dianhydride monomer. The IR bands resultant from the anhydride are located at 1830 cm^{-1} on the infrared spectrum. The IR bands characteristic of the carboxylic acid groups on the polyamic acid are located at 1550 cm^{-1} and at 3300 cm^{-1} . Identification of the polyimide is made by the imide bands at 1780 cm^{-1} due to symmetrical carbonyl stretching vibrations, at 1730 cm^{-1} due to asymmetrical carbonyl stretching vibrations, at 1380 cm^{-1} due to stretching vibrations of C-N,

and at 720 cm^{-1} due to bending vibrations of cyclic C=O. Caution should be made in using the bands near 1780 cm^{-1} and 1730 cm^{-1} to characterize differences in extent of imidization at high conversions, because these bands are insensitive to changes that might be detected by a thermal technique. Further complications causing interference at the 1780 cm^{-1} can occur if the sample is heated or the polyimide film has anisotropic orientation. Pride has shown that during a heating step, the band at 1780 cm^{-1} is affected by anhydride absorptions [79]. Pride also has shown with a dichroic effect that an isotropy of a polyimide film cast on a substrate increases with the extent of imidization, which can complicate the use of infrared spectroscopy to follow the imidization reaction [79]. Chen et al. used FTIR to show that while complete imidization occurred at temperatures as low as 200°C, the mechanical properties were not maximized until an imidization temperature was increased to 350° [90].

Polyimides: Thermal Properties

One of the most important features of polyimides is high temperature stability. Polyimides are typically used in applications that are not load bearing applications, such as protective films and coatings. In some typical load bearing applications they are not the *primary* load bearing structure, such as use as an adhesive or in fiber reinforced composites. Therefore, the thermal stability requirements do not always include maintaining a certain strength or modulus at the application temperature. Often, the main requirement for polyimide thermal stability is resistance to thermal degradation or retention of weight [76]. It is possible for crosslinking reactions of a reorganizational type to occur at elevated temperatures, where gaseous

products are not evolved. Due to this consideration, the weight retention criterion must often be combined with maintenance of physical microstructure.

The excellent thermal stability of polyimides is one of the important features which makes this class of polymers so important. Many polyimides have glass transition temperatures above 200°C and some are thermally stable up to temperatures as high as 400°C [1-2,20-21,25,77-78,80-81,87-89]. A typical consequence of increased thermal stability is a high melt viscosity which limits processability [20]. Recently, some polyimides have been developed that have more flexible polymer chain linkages, increasing the possibilities for processing, yet slightly sacrificing the thermal stability [20-21]. Thermal degradation can change the microstructure of the polyimide, leading to changes in the physical properties. Degradation of a linear polyimide can result in crosslinking or fragmentation of the polymer molecules. Either of these forms of degradation will result in changes to the physical properties.

To characterize the thermal stability and the thermal properties of a polyimide that is intended to be used as an interphase material in a composite, it is desirable to measure the glass transition temperature, the temperature of onset of degradation, and to probe for chemical changes that may occur at the processing temperatures which will alter the microstructure. The glass transition temperature is most easily measured with DSC [20-21]. The temperatures at which degradation occurs has been characterized by many researchers using TGA [80]. To probe for chemical changes that may occur at the processing temperatures, TGA, pyrolysis gas chromatography and TGA-mass spectrometry may be used. A gel fraction measurement of a polyimide sample that has been treated at processing conditions is very useful for qualifying any crosslinking type of changes that do not evolve gaseous products.

Polyimides: Effect of Chemical Structure and End Groups on Thermal Stability

The thermal stability of a polymer molecule will be governed by the strength of the weakest bond in the polymer chain. Since a polymer molecule is a series of repeat units connected together, the weakest bond will be present at least once in each repeat unit. A correlation has actually been noted between E_a values for the degradation of polyimides in an inert atmosphere and the bond dissociation energy of the weakest bond [76]. This explains the emphasis that is placed on highly aromatic backbone polyimides. There are also considerations of the secondary structure which can change the density by sterically effecting the chain packing, or alter the proximity of functional groups which may influence any possible crosslinking reactions. It has been found that the diamine structure has a greater influence on polyimide thermal stability than the dianhydride structure. This is attributed to a greater electron density in the diamine region making it a likely point of oxidation [76].

Endcapping polyimide chains has been shown to be very important for maintaining high temperature thermal stability. Historically polyimides were synthesized with an excess of dianhydride or diamine, thereby terminating the polymer chains with the respective excess monomer. Using this technique it was shown that anhydride end groups were slightly more stable than amine end groups. However, anhydride endgroups are susceptible to degradation by hydrolysis followed by decarboxylation/ decarbonylation [76]. Thus, it has been shown by many researchers that high temperature thermal stability can only be attained by capping polyimide chains with monofunctional chainstoppers [20,76,81].

Polyimides: Effect of Polyimide Physical State on Thermal Stability

The physical state of a polyimide will affect its thermal stability. Cella explains that a polyimide film will have increased thermal stability as the film thickness is increased, due to a higher weight to surface area ratio [76]. The higher surface area allows for greater diffusion of small molecules which may influence degradation. According to this reasoning, powder samples, which have a higher surface area than films, will suffer more from thermal degradation and thick molded parts will resist thermal degradation more. Figure 2-7 shows the effect of film thickness on polyimide stability for ODAN/MPD/PPD films in air at 371°C.

A polyimide sizing on a carbon fiber can be viewed as a very thin film on the fiber substrate. In this case, the weight to surface area ratio is low, and degradation is more likely than for thicker films. However, when a matrix polymer is introduced to the sized fibers, the system can be considered a polymer blend.

The mode of preparation of the polyimide can have an effect on the thermal stability. As described earlier, imidization of a polyamic acid can be achieved by solution imidization, chemical imidization, or bulk thermal imidization. In general, a polyimide made by solution imidization will have a higher molecular weight, which will lead to better resistance to thermal degradation. However, the tendency for solvent retention can lead to less resistance to thermal degradation. Polyimides made via chemical imidization will also have a tendency for solvent retention, and the formation of isoimide structures. These isoimide structures can rearrange at higher temperatures and do not necessarily accelerate thermal degradation.

Polyimides made by bulk thermal imidization of polyamic acids are regarded as the least thermally stable. This is attributed to a lower ultimate molecular weight caused by hydrolysis

due to the presence of water produced during the condensation reaction. This comparison is made with laboratory prepared samples where special attention is given to complete solvent removal for the polyimides made by chemical imidization and solvent imidization. For a commercial application, complete solvent removal may prove to be too time consuming. Other considerations for degradation during bulk thermal imidization of polyamic acid films cast from solution include solvent type, solution viscosity, solution age and imidization temperature cycle. Even during bulk thermal imidization, it is estimated that 1-8 wt% degradation can occur [76].

Polyimides: Environmental Effects on Thermal Stability

The effect of atmosphere on the thermal stability of polyimides is an important consideration. In an inert atmosphere or a vacuum, polyimides have been shown to sustain temperatures of 350-400°C for several hours [76]. However degradation of these same polyimides will occur rapidly at the same temperature in air, and even more rapidly in humid air. Bell et al. has shown that the T_g of various novel polyimides can vary by as much as 80°C when imidization is compared using nitrogen and air atmospheres. A trend was not consistent for either atmosphere yielding a consistently higher T_g [78].

If a polyimide is cast onto a substrate, the surface chemistry of the substrate becomes important to polyimide thermal stability. The level of impurities on the substrate is important as impurities can catalyze polyimide degradation. The degree of interfacial adhesion between the polyimide and the substrate will determine the porosity at the interface which is important when considering the diffusion of water and oxygen. As mentioned before, the presence of oxygen or

water dramatically accelerates degradation. Cotts has shown that the type of glass substrate alters the stability of ODAN/MPD/PPD polyimide at 371°C. When a Pyrex is used as a substrate, the polyimide retains about 87% weight after 100 hours, however when a soft glass slide is used as a substrate, the polyimide only retains about 52% weight after 100 hours [76].

A polyimide sizing on a carbon fiber is a particular case where the substrate influence is very important. It has been shown that dramatic differences in the elevated-temperature weight retention of PMR-15 type composites are dependant on the type of carbon fiber used [76]. Based on the results of Pride, [79] which show that a polyamic acid cast on a substrate and subsequently thermally imidized can develop increased an isotropy with increasing temperature, it is important to consider the implications of a polyamic acid cast on a carbon fiber and subsequently imidized on thermal stability. A polyimide layer on a carbon fiber substrate that develops anisotropic orientation will have a closer packing of molecules which will increase the density, thereby decreasing the diffusion of water or oxygen molecules. It is implied that each of these factors will contribute to an increased resistance to thermal degradation.

Polyimides: Mechanisms for Degradation

Although mechanistic information concerning polyimide degradation is available in the literature, there are no universally accepted mechanisms. Most proposed mechanisms are based on analysis of the degradation products, both volatile off-gases and solid residues, and at least partially, on speculation. The most prevalent products evolved during thermolysis of a polyimide are CO_2, CO and H_2O [76]. Cella concludes that all of the major volatile decomposition products

evolved during thermolysis of a polyimide implicate the imide ring as the site of initial degradation in air or an inert atmosphere [76].

As already mentioned, the presence of water can rapidly accelerate the degradation of polyimides. A model compound study by Sazanov shows the degradation of N-phenylphthalimide at 400-500°C in vacuo and in a moist environment has a decomposition rate that is 15 times faster under the hydrolytic conditions [76]. Moisture present in the atmosphere is not the only source of water for hydrolytic degradation. Water can arise from several sources such as cyclization of diacids and amic acids, condensation of unreacted amine with acid or anhydride groups, and condensation of unreacted amines with imide linkages to form imidines [76]. The results of hydrolytic degradation are chain scission, weight loss, and crosslinking.

Development of degradation mechanisms can also be accomplished by examination of the polymer residue after thermal treatment. These techniques are limited to solid state examinations as the residue is often insoluble. Analysis of residual polymer indicates that thermolysis of polyimides originates in the imide ring and oxidative crosslinking occurs predominantly at the amine fragments [76].

Polyimides: Molecular Weight Determination

There are many techniques available for molecular weight determination of polymers. Some of these techniques are osmotic pressure, light scattering, intrinsic viscosity, NMR, and GPC. Most of these techniques only give a single moment of the molecular weight distribution, providing only limited information about the complete polymer molecular weight. Universal

calibration GPC is the only technique mentioned which provides quantitative information about the entire distribution of molecular weights.

A common feature of all these techniques is that the polymer examined is in a dilute solution. This feature is necessary, because isolation of the polymer molecules from neighboring polymer molecules is necessary for a molecular weight determination. The choice of solvent system is very important when making molecular weight measurements. The universal calibration GPC technique will be explained and the application of this technique to polyimide characterization will be reviewed. While the other techniques for molecular weight determination are often useful, they do not fit into the scope of this study, and they will not be reviewed.

Universal calibration GPC makes use of size exclusion chromatography measurements coupled with intrinsic viscosity measurements. Calibration of the chromatographic column with polystyrene standards is necessary with the solvent system that will be used for sample measurement. In this manner the elution volume of the mobile phase is correlated with the hydrodynamic size of a polymer. The in-line intrinsic viscosity measurements of both the polystyrene standards and the samples being measured allows use of the relationship

$$\log[\eta]_1 M_1 = \log[\eta]_2 M_2$$

where $[\eta]_1$ is the intrinsic viscosity of the polystyrene calibration sample, M_1 is the molecular weight of the polystyrene calibration sample, $[\eta]_2$ is the intrinsic viscosity of the measured sample and M_2 is the molecular weight of the measured sample. The time dependance of the elution volume is thus correlated with a molecular weight for the measured sample, and the molecular weight distribution is measured.

Intrinsic viscosity measurements of polymers in dilute solution are very important for the universal calibration GPC technique. Intrinsic viscosity measurements have also been used without GPC to study the relative molecular weights of a given polyimide [80]. Cotts attempted viscosity measurements of concentrated solutions of polyamic acids for characterizing molecular weight but was not successful because of the sensitivity of this technique to solution changes other than molecular weight [6].

It is also important that the polymers are uncharged and the hydrodynamic dimensions are not influenced by intramolecular interactions. It is not possible to make an accurate measurement of the intrinsic viscosity of charged polyelectrolytes due to the interactions between charged species. Cotts showed that polyamic acids of pyromellitic dianhydride-4-4'-diaminodiphenylether displayed polyelectrolye effects in NMP that is used as received [6]. If the NMP is purified by distillation, the polyelectrolyte effects are eliminated. Also, LiBr can be added to the NMP to serve as a scavenger ion and suppress the electrostatic interactions. The polyelectrolyte effect is shown in Figure 2-8 from Cotts [6]. In Figure 2-8, the reduced viscosity for several polyamic acid solutions is shown as a function of concentration. The increased reduced viscosities at low concentrations are a result of the increased hydrodynamic volume of the polyamic acid resulting from the polyelectrolyte effect.

The effectiveness of adding LiBr to the NMP mobile phase for GPC to suppress a polyelectrolyte effect with oxydiphthalic anhydride/oxydianiline (ODPA/ODA) polyimide was also shown by McGrath et al. [80]. This study investigated the molecular weights of ODPA/ODA polyimides and the polyamic acid precursors. The addition of LiBr to the NMP mobile phase was not sufficient for measuring the molecular weights of the polyamic acids

because the polyamic acid absorbed to the chromatographic column media. McGrath et al discovered that by stirring NMP over P_2O_5 prior to use eliminated the polyelectrolyte effect for both the ODPA/ODA polyimide and the respective polyamic acid, allowing molecular weight distributions of both to be measured.

Polyimides: Melt Rheology

The rheological properties of a polymer melt can be characterized in the oscillation mode of a torsional rheometer using a parallel plate fixture. At small frequencies the frequency dependent viscosity, also called the complex viscosity, closely resembles the steady state, shear viscosity at low shear rates. This relationship is expressed by the Cox-Merz rule:

$$\lim |\eta^*(\omega)| = \eta(\gamma).$$

Measurement of the complex viscosity, at low frequencies, can be used to characterize the structure property relationships of a polymer. At very small frequencies, the complex viscosity of many polymers will remain approximately constant with respect to frequency. This viscoelastic regime is known as the zero shear plateau and the viscosity in this regime is known as the zero shear viscosity, η_0. The zero shear viscosity is represented qualitatively in Figure 2-9. Since a measured value of viscosity is generally dependent on the frequency of measurement, the zero shear viscosity is a suitable parameter for comparison of the melt rheology of different polymers. This eliminates the need for arbitrarily choosing a standard, fixed frequency for

comparison.

The zero shear viscosity is also very useful for relating the molecular structure to the rheological properties. There are several mathematical models, both empirical and phenominalogical, that make use of the zero shear viscosity to calculate parameters such as critical entanglement molecular weight, molecular weight between entanglements, characteristic ratio, and self diffusion coefficients [3].

There is a very strong molecular weight dependence on the melt rheological behavior of polymers. If the molecular weight of a polymer is below the critical entanglement molecular weight, the zero shear melt viscosity, η_0, is directly proportional to the weight average molecular weight, M_w. However, when the molecular weight of a polymer is above the critical entanglement molecular weight,η_0 varies with the 3.4 power of M_w. These relationships have been shown to be empirically valid for many linear polymers [3-4]. These relationships are shown in Figure 2-10,

where

$$\eta_0 \approx K_1 \cdot M_w , \qquad \text{for } M_w < M_c$$

and

$$\eta_0 \approx K_2 \cdot M_w^{3.4}, \qquad \text{for } M_w > M_c .$$

The temperature dependance on rheological properties is very important. Typically, the melt viscosity of a polymer decreases with increasing temperature. However, thermally activated reactions causing chain extension or crosslinking will cause the melt viscosity to increase. If

crosslinking does occur, the storage modulus will dominate over the loss modulus. This will lead to a diminishing zero shear plateau, and could eliminate the possibility of measuring the zero shear viscosity all together.

By measuring the rheological properties during simulated processing temperatures, a knowlege of the melt viscosity during the processing cycle can be developed. This information is very important for developing processing conditions and understanding the physical state of the polymer during and after processing. Typically a processing window is defined by measuring the melt viscosity of a polymer over a specific temperature range. The range of temperatures at which the melt viscosity is at a level that represents processable conditions defines the processing window.

The melt stability of polymers has been studied by several researchers using rheological techniques [20-21,82]. Srinivas et al. studied the degradation of semicrystalline polyimides during isothermal holds using melt rheology [20-21]. After isothermal holds of varying time and termperature, the subsequent crystallization kinetics of the polyimides were supressed. The melt rheology tests showed an increase in complex viscosity during an isothermal hold which verified chemical changes that explained the supression in crystallization kinetics.

Polyimides: Mechanical Properties

The mechanical properties of polyimides typically reported include tensile properties and shear properties. It is very important to measure the tensile properties of polyimides which are designed for structural applications. The shear properties are important for polyimides which are designed as adhesives. Since polyimides used for composite applications will undergo complex

local loading histories, both tensile and shear properties are important for composite design considerations. As discussed previously, some typical properties of commercial polyimides are shown in Table 2-I. The mechanical properties of polyimides will be dependent upon many factors such as the degree of crosslinking, the molecular weight and molecular weight distribution, the imidization conditions, and the degree of an isotropy.

From a structure-property perspective, polyimides are typically stiff, rigid macromolecules which are sometimes semicrystalline. The focus of this thesis is amorphous polyimides and the discussion will be limited to such. Because of their molecular structure, unbranched, linear polyimides will typically have a high modulus. Elongation of high molecular weight polyimides is possible resulting in plastic deformation and local molecular orientation. As mentioned previously with work by Kochi et al. [5], cold drawing polyimide films can result in drastic increases in polymer modulus.

The tensile properties of novel polyimides have been studied by few researchers [25,23,77-78,83]. The tensile yield strength, ultimate strength, modulus, yield strain and ultimate strain are typical properties reported. Bell has reported unusually high moduli ranging from 2.3 GPa to 9.2 GPa for novel polyimide films synthesized with fluorene-derived diamines [77]. Polyamic acid films were cast onto a glass substrate, dried of solvent, and imidized using a staged thermal imidization cycle. The films were stripped from the glass substrate and tested for tensile properties. As described previously, the imidization of a polyamic acid on a substrate can result in an anisotropic molecular orientation. While Bell attributes the unusually high modulus to chain rigidity resulting from the bulky fluorine diamine segments, anisotropic orientation would provide a better explaination. Bell did not examine the possiblity of orientation.

The lap shear strength of metal bonded with polyimide adhesives have been studied [23,25,84]. Progar and Pike compared the lap shear strengths of titanium adherends bonded with LaRC-TPI polyimde [84]. The LaRC-TPI polyimide adhesive was applied as a polyamic acid from diglyme and also as an aqueous polyamic acid salt. The adhesives were thermally imidized before bonding the adherends. The lap shear strengths were very similar for the different sample preparation methods which was important for the development of water soluble polyimide precursors.

Polyimides: Microstructure

As shown thus far, polyimides can be processed using several techniques, imidized under a variety of conditions, and physically altered by the thermal and mechanical history. The microstructure of a polyimide will be dependent upon these and many other factors. There is a scarcity of polyimide microstructure characterization in the literature. The microstructure is defined by the particular molecular structure of the polyimide, and the morphology of the polyimide- whether it is amorphous, anisotropically oriented, semicrystalline, linear, branched, crosslinked, or consisting of several phases. The microstructure is very important for interrelating all the polyimide characterization discussed previously.

The mechanical properties simply describe the performance characteristics. An understanding of the microstructure provides an explanation relating the mechanical properties and the thermal properties to the chemical structure, molecular weight and molecular weight distribution, the processing techniques, the imidization conditions, and the thermal and mechical

history.

Since so much information is required for an understanding of the microstructure, there have been very few studies which have addressed this issue [25,77-78]. One of the main objectives of this thesis is to develop an understanding of the failure mechanics of polyimide interphase composites. The microstructure of the polyimide interphase is extremely important for understanding mechanisms of load transfer and mode of failure.

The interphase composites considered in this thesis are manufactured with Ultem-type polyimide interphases, and a PEEK or PPS matrix. The miscibility of the interphase polyimide with the matrix polymer will further alter the microstructure of the interphase. The literature review for blends of polyimides with PEEK and PPS will be discussed later.

Polyether ether ketone

High performance thermoplastics have the benefits of solvent resistance, light weight, as well as high strength, modulus and toughness over a wide temperature range. Most high performance thermoplastics are semicrystalline which enhances the aforementioned characteristics. Polyether ether ketone (PEEK) is a widely available semicrystalline high performance thermoplastic that has utility for many applications, including composite manufacture.

The following sections will examine the importance of PEEK as a high performance thermoplastic, the commercial availability, typical characterization of PEEK as pertaining to the goals of this thesis, and a discussion of the use of PEEK as a composite matrix polymer.

PEEK: commercial availability

The first polyether ketone was developed at DuPont in the early 1960s. By the early 1980s, PEEK was commercially available from ICI. PEEK is available in a few different grades from limited manufacturers. Victrex PEEK is available as powder, granules, or film. Carbon fiber prepreg with PEEK matrix is also available and will be discussed in a later section. Some of the properties of two different grades of Victrex PEEK are listed in Table 2-III. These two grades of PEEK are commonly studied in the literature. Jonas and Legras report values of M_n for 150 grade PEEK and 450 grade PEEK as 12,000 g/mol and 50,000 g/mol, respectively [92].

Table 2-III. Some properties of two different grades of PEEK supplied by Victrex.

	150 grade Victrex PEEK	450 grade Victrex PEEK
density (g/cm^3)	1.32	1.32
flexural modulus (GPa)	3.53	3.66
tensile strength (MPa)	94	92
yield strain (%)	4.7	4.9
notched Izod impact strength (J/m)	61	83
CTE (m/m/°C)	$47x10^{-6}$	$47x10^{-6}$
HDT (°C)	156	160

PEEK: characterization

The high performance characteristics of PEEK make it a very useful polymer. However, one characteristic, the resistance to solvents, has made characterization of this polymer very difficult. PEEK is soluble in only a few solvents. Some of the solvents require high temperatures while other solvents such as sulfuric acid, sulfonate the PEEK molecules, which alters the polymer complicating characterization. Solution properties of PEEK have been studied by Berk and Berry [93], Bishop et al.[94], and Roovers et al. [95,96]. The characterization techniques and some typical results will be discussed in the following sections.

The emphasis of the topics discussed will be focused on PEEK characterization that applies to the goals of this thesis. The thermal properties of PEEK are important for processing considerations as well as applications. Thermal properties that are of primary concern are the typical glass transition temperature, T_g, the typical melting temperature for the crystalline phase, T_m, and the flow characteristics at various melt processing temperatures. The bulk mechanical properties are of importance for engineering design. These properties include tensile and flexure properties at room temperature and elevated temperatures, and impact strength. The microstructure of PEEK will be discussed which is strongly dependent upon the crystalline morphology and content.

The use of PEEK as a composite matrix polymer will be addressed. Some benefits, applications and limitations of PEEK matrix composites will be examined. The manufacturing methods for PEEK matrix composites will be reviewed, as well as the characterization of PEEK matrix composites in the literature.

PEEK: characterization: thermal properties

This section will review the important thermal properties of PEEK and the characterization techniques used for evaluating the thermal properties. The glass transition temperature is dependent upon parameters such as the thermal history and molecular weight of the polymer. The T_g of PEEK has been measured with DSC, DMA torsional braid analysis and . The values for T_g of PEEK are typically around 144°C [97-100].

Physical aging is a thermal relaxation mechanism which occurs between 50-140°C for PEEK [97]. The physical aging of PEEK has been studied by D'Amore et al.,[101] and Ogale and McCullough [98]. The effects of physical aging are an increase in density, decrease in permeability, and changes in strength, modulus, yield strain, failure strain and T_g. As the crystalline content increases, the effects of physical aging will not be as noticeable since the closely packed crystalline phase will dominate the performance characteristics. When evaluating the mechanical properties of PEEK and PEEK matrix composites, it is important to consider the effects of physical aging on the response of the test specimens.

The melting temperature of the crystalline phase of PEEK is dependent upon the crystalline morphology. The crystallization of PEEK is very complicated and is dependent upon parameters such as the thermal history, the molecular weight and the presence of nucleation sites. Of particular importance for PEEK crystallization behavior is the temperature history in the melt. The nucleation density has been shown to change with time in the temperature range of 380-400°C [97]. The T_m is most commonly measured using DSC. The typical melting temperature of PEEK reported is around 335°C [97].

Upon cooling, DSC thermograms show a complicated crystallization exotherm consisting

of a sharp peak and formation of a shoulder with continued cooling. The same shouldered peak is seen during a heating scan, demonstrating two regions of crystalline melting. This double melting behavior is not fully understood and there is disagreement in the literature explaining this phenomenon.

Nguyen et al. attribute this double melting phenomenon to a reorganization of the crystalline phase during the dynamic temperature scan [97]. As the temperature is increased, the crystalline phase is continually melting and recrystallizing which results in a perfection of the crystalline phase. Lee and Porter support this theory [102].

Bassett et al. attribute the phenomenon of double melting behavior of PEEK to the formation of two different crystalline morphologies which have different melting temperatures [103]. They claim that reorganization during heating is not the cause of the shouldered DSC peak.

Further discussion of this phenomenon is beyond the scope of this work and the reader is referred to work in the literature for further information [97,99,100,102,103].

An important consideration for the thermal behavior of a polymer is degradation at elevated temperatures. As explained in a previous section for polyimides, degradation can be manifested as decomposition of molecular weight or crosslinking, leading to a networked microstructure that will impede crystallization. Studies of thermal degradation of PEEK have been done by Jonas and Legras [92], and Day et al. [104]. It was shown by both researchers that the thermal stability of PEEK is greatly reduced by an oxidative atmosphere.

Jonas and Legras used 150 Grade PEEK from ICI in a study which examined isothermal hold temperatures from 385°C to 440°C in air and nitrogen for various time periods up to 30

minutes. The samples were dissolved in sulfuric acid and the molecular weights were estimated using size exclusion chromatography. It was shown that at isothermal hold temperatures greater than 400°C in air, the weight average molecular weight increased significantly during the 30 minute hold time. The thermal stability was shown to be much better in nitrogen, where three moments of the molecular weight distribution, M_n, M_w and M_z, were unchanged for hold times up to 30 minutes and temperatures up to 440°C. An important criticism of this work is that sulfuric acid sulfonates PEEK to varying degrees which has been shown to alter the solution behavior of PEEK [93,94,96]. Thus, accurate measurement of molecular weights are not possible using sulfuric acid as a solvent.

Day et al. showed that PEEK is stable at a temperature of 400°C in nitrogen, which is nonoxidative, for periods up to 6 hours [104]. However, in air at the same temperature, the gel fraction of PEEK increases with time. As shown in Figure 2-11, the gel fraction increases up to 40% after 6 hours in air at 400°C. Day et al. used solution techniques to characterize PEEK samples after controlled conditions of environment and temperature. Methane sulfonic acid was used as a solvent which does not sulfonate the PEEK, unlike sulfuric acid. Using these PEEK solutions, techniques of viscometry, UV-visible spectroscopy, NMR and FTIR were used to study the degradation behavior. It was concluded that in an oxidative, high temperature environment chain scission was followed by crosslinking [104].

The heat distortion temperature, HDT, is a common parameter reported for industrial applications of a polymer. The HDT for PEEK is reported as 156°C by the ICI Victrex data sheet [105].

PEEK: Bulk mechanical properties

The mechanical properties of semi-crystalline polymers are dependent upon many factors such as crystalline content, molecular weight, free volume content, rate of testing, environmental conditions, and temperature history. Although mechanical properties are dependent upon many considerations it is useful to note some typical properties and the mechanical behavior of PEEK.

The tensile properties are commonly reported for polymers. As seen in Table 2-III, the tensile strength and yield strain are reported from a PEEK product data sheet. Nguyen and Ishida report a similar value for tensile strength (100 MPa) [97]. They also report values for tensile modulus of 4 GPa and tensile strain-to-failure of 150% [97].

As commonly seen with ductile thermoplastics loaded in tension, PEEK shows a linear elastic region followed by yielding and then plastic deformation. The maximum elongation is dependant upon many factors but is usually within the range of 60-150% [97,105].

PEEK: Melt Rheology

The melt viscosity of a thermoplastic is an important parameter for processing PEEK. A major drawback to the melt processing of PEEK is the high temperature necessary for processing. Typical processing temperatures for PEEK are within 350°C to 400°C. Although the processing temperatures are high compared to other thermoplastic polymers, the melt viscosity in this range is comparable to the melt viscosities of polycarbonate and rigid PVC in their respective processing temperature ranges. This is seen in Figure 2-12 where the melt viscosities for several thermoplastics are compared within their appropriate processing temperature ranges [105].

PEEK: Crystallization/Microstructure

The crystalline content of PEEK is commonly quantified using DSC. The area under the melting endotherm is used to calculate a heat of melting which can be related to the crystalline fraction using the enthalpy for melting of a 100% crystalline PEEK formation. This enthalpy was determined by Blundell and Osborn to be 130 J/g [145].

For pure PEEK, the overall crystalline morphology will be dependent upon the thermal history and the crystallization conditions. The crystalline morphology of PEEK has been studied by Bassett et al. [103], and Lovinger et al. [99,100]. A spherulitic morphology has been observed when PEEK is crystallized from the melt [97]. As shown in the diagram in Figure 2-13, folded chain crystalline lamella form radially from a nucleation point to form a spherulitic structure. The amorphous interlamellar regions are thick compared to other semicrystalline polymers [97]. This is an important observation that will have implications on the discussion of PEEK/polyimide blends later in this chapter. Some spherulitic radii have been measured as large as 21.9 µm under carefully controlled crystallization conditions [97].

The crystallization kinetics are very rapid. Cooling rates greater than 700°C/minute are necessary to significantly retard the spherulitic growth [97,105].

Issues of transcrystallinity are important for composite applications. In composite applications, transcrystalline formations are crystalline domains that nucleate at the surface of a carbon fiber and radiate in a columnar growth formation [97]. Transcrystalline morphologies can drastically change the interfacial characteristics of a fiber-matrix interphase. There have been conflicting conclusions on the ability of PEEK to form transcrystalline domains with different carbon fibers, even by the same researcher. This will be discussed in further detail later in this

chapter.

PEEK: Benefits and Limitations as Composite Matrix

High performance thermoplastic matrix composites are finding increasing use as applications arise and necessary processing equipment is available. PEEK matrix composites can be made using several different techniques. The most common technique is consolidation of the widely used APC-2 prepreg from Fiberite. APC-2 is a melt impregnated tape which has excellent handling characteristics, a controlled fiber volume fraction, and uniformly aligned fibers. Cost is a limiting factor for this expensive prepreg.

PEEK matrix prepreg is also available as a commingled yarn from BASF where carbon fibers are intertwined with PEEK fibers to form a bundle tow prepreg [106,107]. This prepreg form also allows for controlled fiber volume fraction. However material handling is not as easy as with APC-2. Specially designed equipment is needed for controlled placement of the bundle tow prepreg.

There are methods that have been developed for PEEK matrix composite manufacture which avoid the need for ready-made prepreg. Powder based matrix impregnation techniques have been reported in the literature for making PEEK matrix composites. PEEK matrix powder is typically suspended in water or air and the carbon fiber tow is drawn through the suspended particles. For water based suspensions, the PEEK particles must be dispersed well and polymeric binders are needed in solution to adhere the particles to the carbon fiber tow [33,37,35,65]. For air based suspensions, narrow particle size distributions are needed for a uniform fluidized bed

and a mechanism is needed to adhere the particles to the fiber [108-110]. A common binding technique utilizes an electrostatic charge to temporarily adhere the powder particles to the carbon fiber tow which is immediately followed by a heating step to securely tack the particles to the carbon fiber [108]. Both of these powder based techniques require specialized equipment, careful development of processing conditions and a supply of PEEK powder with appropriate particle diameter [108-110]. The mean particle diameters have ranged from 3-40 µm for the aqueous suspension techniques [33,37,35,65] and from 30-70 µm for the air suspension techniques [108-110].

Another method for PEEK matrix composite manufacture is the simple stacking of PEEK film with carbon fiber tow for layup of the composite. This method can provide some control of fiber volume fraction, but special equipment is needed for carbon fiber tow placement. The high melt viscosity of PEEK would make void free consolidation very difficult using this method.

PEEK: Composite Applications

PEEK matrix composites find use in aerospace applications where light weight and strength are very important over a wide range of temperature [111]. The impact resistance of PEEK matrix composites is also attractive for aerospace applications [105].

PEEK: Characterization of PEEK Matrix Composites in Literature

Since the introduction of APC-2 prepreg, there have been many studies of PEEK matrix composites. The effect of thermal history on the properties and microstructure of the resulting

composite has been investigated by many researchers [107,112-119,101].

Davies et al. conducted a study on the cooling rate effects on many different mechanical properties of PEEK composites [118]. The cooling rate was shown to alter the composite properties by varying the level of crystallinity and development of residual stresses from thermal gradients. The mechanical properties used to evaluate the composites were 0° tension, 90° tension, ±45° tension, 0° compression, mode I fracture, mode II fracture, impact testing and R=0.1 fatigue. Davies et al. concluded that the performance of PEEK matrix composites suffers when the cooling rate is less than 10°C/minute. This is the recommended minimum cooling rate specified by Fiberite [105].

Denault and Vu-Khanh varied the consolidation time and temperature for APC-2 crossply laminates and commingled fabric PEEK laminates to study the effect on interlaminar adhesion. Electron microscopy and a short beam shear test were used to evaluate the interlaminar adhesion. At a consolidation temperature of 400°C, the short beam shear strength varied with residence time for both APC-2 and the commingled fabric composites. The short beam shear strength of the APC-2 composite was initially constant for residence times up to 110 minutes, and an approximate 15% decrease occurred for a residence time of 175 minutes. The short beam shear strength of the commingled fabric showed an initial increase for residence times up to 60 minutes, followed by a decrease for residence times of 110 and 175 minutes. Based on the short beam shear strengths, Denault and Vu-Khanh concluded that the fiber/matrix adhesion increased with consolidation residence time through an irreversible physiochemical adsorption of PEEK onto the carbon fiber. As mentioned earlier in this chapter, thermal degradation of PEEK at 400° is of concern in an oxidative environment. The diffusion of oxygen into the composite mold and

hence into the melted PEEK matrix should be considered especially at residence times of 175 minutes. Very special consolidation equipment is necessary to ensure the absence of oxygen during composite consolidation. This equipment was not addressed by Denault and Vu-Khanh. The loading conditions for short beam shear provide a complex stress state that cannot be correlated well to specific material properties [120]. This complex stress state is even more ambiguously defined for a crossply laminate or a fabric reinforced laminate. Caution should be exercised when making conclusions of composite material properties and mechanisms of fiber/matrix adhesion that are based on short beam shear strengths. The thermal degradation of the matrix material must also be carefully minimized.

The crystalline morphology of PEEK matrix composites has been studied by Lee and Porter [117], Jar [113], and Blundell et al. [115,116]. Transcrystalline formations can alter the fiber/matrix adhesion and thus are important for understanding the composite behavior. Lee and Porter showed the development of PEEK transcrystalline formations with Thornel 300 carbon fiber. As the residence time at 390°C was increased, the nucleation sites in the bulk matrix diminished, showing a more pronounced affect of transcrystalline nucleation [117].

Jar et al. studied the crystalline morphology of APC-2 prepreg and the resulting fracture surfaces in 0° and 90° tension. An important observation was that the bulk crystallinity and the spherulite size was dependent upon the simulated consolidation temperature. Using thermal treatments of 350°, 370° and 390°C for 30 minutes in a forced convection oven, followed by a 3 hour, 300°C isothermal crystallization period, different crystalline morphologies were attained. The bulk crystallinity varied from 37% for the 390°C thermal treatment to 45% for the 350°C thermal treatment. The crystalline features showed fine crystallites for the 350° and 370°C

thermal treatments but large spherulites showing some transcrystallinity for the 390°C thermal treatment [113]. While it was not quantified by Jar et al., the different crystalline morphologies could lead to different composite mechanical responses, such as strength, and failure strain.

Blundell et al. used X-ray diffraction to monitor the growth of transcrystalline features in APC-2 laminates. It was shown that if a cooling rate within the Fiberite recommended range of 10°/min to 700°/min was used, the carbon fibers do not interact with the crystallization process [116].

Blundell et al. also did a study showing the crystalline morphology of APC-2 composites using an etching technique to remove some of the amorphous polymer on the surface of a cross section [115]. The remarkable micrographs from this study show spherulitic crystalline structures in the bulk PEEK matrix, but true transcrystalline features were rarely found. This contradicts the results of previous work done by some of the co-authors from this study [121]. In previous work, carbon fibers were imbedded in PEEK matrix between glass slides and examined under cross-polarized light. While transcrystalline features were dominant for this previous work, the sample preparation did not suitably model actual composite conditions. Blundell et al. explained the transcrystalline features from previous work as originating at fiber-fiber contact sites and locations where the fiber is in close contact with the glass cover slide [115]. Based on the micrographs of the etched APC-2 composite samples, Blundell et al. concluded that crystalline features can nucleate in three types of nucleation sites in APC-2 composites: (I.) nucleation from fiber-fiber contact points or regions where fibers are very close, (ii.) nucleation at fiber-PEEK interface, and (iii.) typical polymer nucleation in the bulk matrix [115]. This study has the rare benefit of using actual composite laminates. Thus the micrographs of the crystalline

features are representative of actual composite microstructures.

Polyphenylene Sulfide

Polyphenylene sulfide (PPS) is similar to PEEK in many respects. It is a semicrystalline high performance thermoplastic that can be used for many applications, including composite manufacture. High performance thermoplastics have the benefits of solvent resistance, light weight, high strength, and high modulus over a wide temperature range.

The following sections will examine the importance of PPS as a high performance thermoplastic, the commercial availability, typical characterization of PPS as pertaining to the goals of this thesis, and a discussion of the benefits and limitations of PPS as a composite matrix polymer. Excellent reviews of the properties of PPS have been written by Lopez and Wilkes [123] and Geibel and Leland [122].

PPS: Commercial Availability

PPS is sold by Phillips Petroleum Polymers Division under the trade name Ryton, and by Hoechst Celanese under the trade name Fortron. Many different grades of PPS are available from each supplier depending on the intended use. Some typical applications for PPS will be discussed in the following section.

PPS: Applications

Applications for PPS make use of the polymers good strength, excellent chemical resistance, flame resistance, thermal stability, and dimensional stability [122,123]. PPS has been processed as film, coatings, injection molded parts, fiber, and as a matrix for advanced composites. Specific applications for PPS have included pump impellers, ball valves, wear rings, electrical sockets, battery and telephone components, chip carriers, optical-fiber cables, electronic component encapsulants, and as a thermoplastic matrix for advanced composites [123]. Automotive applications include alternator components, engine sensors, and lamp sockets [124].

PPS: Characterization

The characterization of PPS is limited by the solvent resistance of the polymer. There are no known solvents for PPS below 210°C [122,123]. PPS is soluble in α-chloronaphthalene at 210°C [122,123]. This makes solution characterization techniques for molecular weight, such as intrinsic viscosity, light scattering and GPC, very difficult.

Some typical characterization techniques and their results will be presented in the following sections. The thermal properties of PPS have been investigated by many researchers. The complex nature of the response to thermal history makes thermal characterization of PPS very important. While PPS is typically recognized as a semicrystalline thermoplastic polymer, under specific oxidative conditions a “curing” behavior is noted which has implications on the polymer properties and microstructure. Some typical mechanical properties of PPS will be

discussed as well as their variance with crystalline content and "extent of cure". Since solution processing of PPS is not a viable alternative, melt processing techniques are used. The melt flow behavior of PPS has been addressed in the literature with consideration of the effects of "extent of cure". A discussion of the crystallization and crystalline morphology will be included but limited to the topics pertinent to the goals of this thesis.

PPS: Thermal Properties

The thermal properties of PPS are representative of a high performance thermoplastic. PPS shows a moderate T_g around 85°C [122,123] and a crystalline melting temperature around 285°C [122,123]. It is possible to obtain an amorphous PPS/carbon fiber composite using a suitable heat soak at 330°C followed by cooling below the T_g at a rate of 120°C/min or faster [125].

When heated above 500°C, the thermal degradation behavior shows less than 5% weight loss in air and no appreciable weight loss in nitrogen. A 40% weight retention is observed when heating to 1000°C in nitrogen [123].

Of particular importance to the thermal characteristics of PPS is a "curing" mechanism that occurs at elevated temperatures. Details of the curing reaction mechanism are not well understood. This curing process results in increases in molecular weight and crosslinking to various extent which alters many of the polymers characteristics. Curing is done in an oxygen containing environment and can be performed in the solid state or the melt state. The melt curing process typically occurs at melt temperatures of 315-425°C [123]. During melt curing the color

will darken and the polymer will thicken. After several hours of melt curing, PPS will gel to an infusible solid. The kinetics of melt curing are slow enough that changes due to melt curing will be negligible during typical melt processing techniques [123].

Solid state curing of PPS occurs below the crystalline melting temperature in the range of 175°C to 280°C. Solid state curing results in increases in molecular weight. As seen in Figure 2-14, after different solid state curing temperatures are held for various times, the melt flow of PPS is changed. As expected, the solid state curing kinetics increase with curing temperature as seen by the melt flow decreasing more quickly with higher solid state curing temperatures.

The curing of PPS has an effect on the resulting thermal stability, mechanical properties and crystallization behavior. Curing results in increases to toughness, ductility and insolubility. It has been shown that branched PPS has a greater thermal stability than that of the linear species [123]. The changes effecting the mechanical properties and crystallization behavior will be discussed later in appropriate sections of this chapter. It was noted by Lopez and Wilkes that there have been very few systematic studies on the effect of extent of cure on the properties of PPS [123].

PPS: Bulk Mechanical Properties

Although the mechanical properties will be dependent upon the molecular weight, crystalline fraction, thermal history and extent of cure, it is useful to identify some typical mechanical properties reported for PPS. For PPS a tensile strength of 65 MPa, failure strain of 1.1%, and a flexural strength 96 MPa has been reported [123]. Compared to other thermoplastic

polymers, PPS is brittle as characterized by the low failure strain. As the extent of cure increases for PPS the toughness increases. This is attributed to the plastic deformation attainable for the crosslinked species resulting in an increase in the failure strain. Ma et al. has shown that as the molecular weight of PPS is increased with curing, the elongation increases to 21% [126].

An important advantage of PPS is the mechanical response at elevated temperatures. Results are shown in Figure 2-15 from a study by Jones and Hill showing the flexural modulus of several materials as a function of temperature [127]. PPS retains a higher flexural modulus with temperature than nylon 66, while Vespel SP-1 polyimide performs better especially at higher temperatures. The glass filled systems are useful only for a general comparison since the compositions are not all the same. The flexural modulus of the PPS/glass composite is greater than the polysulfone/glass composite and the polycarbonate/glass composite however the glass content is also greater. It is important to note that unlike the polycarbonate and the polysulfone, PPS is a semicrystalline polymer. Thus, the flexural modulus does not decrease rapidly above its T_g as seen for the polycarbonate and polysulfone composites, but decreases steadily with increasing temperature.

PPS: Melt Rheology

The melt rheology of all polymers is dependent upon the molecular weight and molecular weight distribution. Complications arise for PPS due to the possibility of melt curing taking place during rheological testing. As previously mentioned, the melt curing will increase the molecular weight and create crosslinks, which can increase the melt viscosity.

There have been studies done on the melt viscosity of PPS and the effect of melt processing conditions on the properties [128-130] Ma et al. examined the melt viscosity of neat PPS and a PPS/carbon fiber system to study the effect of thermal history on the properties of PPS in both air and nitrogen environments [129]. Ma et al. used melt rheology to show that, after melt curing under controlled thermal histories, PPS still displayed Newtonian behavior indicating that even though branching is possible, linear species dominate [128]. A method for determining the molecular weight distribution of PPS using melt rheological measurements such as zero shear viscosity was also developed [128].

The melt viscosity of PPS is very low compared to other high performance thermoplastics [124]. Ma et al. showed that the complex viscosity of PPS at typical processing temperatures was an order of magnitude lower than the complex viscosity of PEEK at typical processing temperatures [128]. It was noted previously in this chapter that the melt viscosity of PEEK compares very favorably to melt viscosities for other thermoplastics.

PPS: Crystallization/Microstructure

The crystallization behavior of PPS has been studied by many researchers [131-137]. Brady studied the effect of crystalline content on the tensile properties of neat PPS and PPS/glass fiber composites [131]. Lovinger et al. [132], Lopez and Wilkes [133,135], and Lopez et al. [134] have studied the crystallization kinetics of PPS extensively. Chung and Cebe have examined the melting behavior of PPS [136,137].

The crystalline content of PPS is commonly quantified using DSC. The area under the

melting endotherm is used to calculate a heat of melting which can be related to the crystalline fraction using the enthalpy for melting of a 100% crystalline PEEK formation, ΔH^0. There is disagreement in the literature for the quantity of ΔH^0. Depending upon the method used for determination of ΔH^0, values range from 80 J/g to 146 J/g [122].

Although crystallization kinetics are slow, PPS crystallizes readily at temperatures above T_g and below T_m. It is possible to obtain amorphous PPS samples and samples with varying levels of crystallinity depending upon the thermal history. The thermal history is always important for concerns of crystallization kinetics, and the curing behavior of PPS complicates this issue more. Studies in the literature have shown that levels of crystallinity decrease after melt curing [122]. If a PPS sample has been crystallized, solid state curing will not immediately affect the crystalline domains that have formed. However, subsequent melting and recrystallization results in a lower ultimate crystalline content [122].

The morphology of melt crystallized PPS crystalline domains displays spherulitic structures. Spherulites are described by Lopez and Wilkes as having "volume filling characteristics" because of the large spacing between individual crystalline lamella [123]. These spaces are filled with amorphous PPS. The spherulites were shown by Lopez and Wilkes to have good connectivity between impinging spherulites [123]. The crystalline morphology could help to explain the brittle behavior at room temperature, although work investigating this topic was not found in the literature. The tensile properties of neat PPS were studied as a function of crystalline content by Brady which showed a surprising decrease in tensile strength after annealing to obtain higher levels of crystallinity [131].

As mentioned earlier, issues of transcrystallinity are important for composite applications.

Transcrystalline morphologies can drastically change the interfacial characteristics of a fiber-matrix interphase. Transcrystallinity of PPS with carbon fibers will be discussed in further detail later in this chapter.

PPS: Benefits and Limitations as a Composite Matrix:

The benefits of PPS as a high performance thermoplastic can be extended to composite applications. Specifically, PPS matrix composites are suited to applications which demand high temperatures and solvent resistance. While short fiber composites do not have the strength and stiffness that continuous fiber composites possess, it is possible to process short fiber composites using injection molding equipment. This is facilitated by the low melt viscosity of PPS. Thus, many applications of PPS matrix composites utilize chopped glass fiber or chopped carbon fiber reinforcement.

One of the limitations of PPS matrix composites has been poor toughness which has been attributed to a weak fiber/matrix adhesion [188]. The cost of PPS has also been a barrier for its wide use. However, with increased global applications of fiber reinforced composites, the market for PPS matrix composites is growing.

PPS: Composite Matrix Applications

PPS matrix composites are versatile from a processing standpoint. Glass and carbon fiber reinforcing material can be used as chopped fibers or continuous fibers. PPS matrix composites

have been used in the automotive, electrical/electronic, appliance, and industrial markets. They have found use as connectors, chip carriers, lamp sockets, switches, automotive brake components, engine sensors, pump housings, valves, seals and down-hole oil well equipment [124].

PPS: Characterization of PPS Matrix Composites

The characterization of PPS matrix composites in the literature is limited to studies which are designed to generate commercial interest for these composites [138,126]. There is a noticeable lack of complete, systematic examinations of the properties of carbon fiber/PPS matrix composites for the purpose of understanding the composite microstructure.

It has been historically difficult to manufacture PPS matrix, carbon fiber reinforced composites with good strength. This has been attributed to a weak interfacial bond between the PPS matrix polymer and the carbon fiber [125]. The transverse tensile strength has been shown to be very low at 32 MPa and an interlaminar shear strength of 70 MPa has been reported [138]. The interlaminar fracture toughness has been investigated by Ma et al. using a double cantilever beam Mode I delamination test [126]. The interlaminar fracture toughness of PPS matrix composites was shown to compare very well with PEEK matrix composites with values of 7.8 $in \cdot lb/in^2$ and 8.0 $in \cdot lb/in^2$, respectively. The good interlaminar fracture toughness was attributed to good bonding of PPS to the carbon fibers [123]. Due to the complex microstructure from variations in crystallinity and crosslinking, composites with different matrix properties are possible, including the development of transcrystalline regions which could affect fiber/matrix

adhesion. More importantly, however is the lack of structure-property investigations of PPS matrix composites in the literature.

While O'Connor et al. has shown a good interlaminar shear strength for PPS matrix composites from short beam shear testing [138], his results showing a very low transverse tensile strength are more important for making conclusions on the relative strength of the fiber/matrix adhesion. As explained earlier in the PEEK matrix section, interlaminar shear strength results from short beam shear testing must be interpreted with caution since the loading conditions used provide a complex stress state that cannot be correlated well to specific material properties [120]. Caution should also be exercised when making conclusions of a strong fiber/matrix adhesion based on interlaminar fracture toughness.

The low failure strain of neat PPS polymer is an important factor to consider when discussing the apparent fiber/matrix adhesion. When examining the micro-mechanics of composite loading, very stiff fibers are contrasted with a relatively ductile polymer matrix. The fibers are designed to support most of the loading and the matrix is designed to keep the fibers together. The matrix must survive the local micro-mechanical strains that are developed under load. Typical thermoplastic matrices will yield and plastically deform under these local strains. The brittle nature of PPS does not allow for yielding or plastic deformation which could lead to failure under the local strains resulting in composite failure. It is worth restating that the literature is noticeably lacking in structure-property investigations of PPS matrix composites which would provide satisfactory examination of the fiber/matrix adhesion.

O'Connor et al. measured the tensile strength of a PPS matrix composite with a fiber volume fraction of 59% that was annealed at 200°C for 2 hours to be 1640 MPa [138]. These

same composites also had a tensile modulus of 135 GPa, a tensile failure strain of 1.2%, a longitudinal flexure strength of 1289 MPa, and a longitudinal flexure modulus of 122 GPa [138].

Lee et al. developed a technique for quantifying the crystalline content of the PPS matrix in carbon fiber composites using X-ray diffraction [139].

Miller et al. used a dry powder prepregging process to make PPS/glass fiber composites [182]. The glass fiber tow was drawn through a bed of dry PPS powder. By vibrating the glass tow, the amount of PPS powder that was worked into the spaces between the individual fibers was controlled. The PPS powder was then fused to the tow while being drawn through ovens using infra-red and hot-air heating at 310°C [182]. The composites were characterized and shown to have void contents as high as 3% by volume and controlled fiber volume fractions between 52% and 62%. Some mechanical properties were shown as a function of fiber volume fraction. Interlaminar shear strength was measured to be in the range of 32-40 MPa and the longitudinal flexure strength was measured to be in the range of 1100-1300 MPa [182]. It was concluded in this study that the high void content did not significantly affect the mechanical properties.

As mentioned earlier with PEEK matrix composites, the issues of transcrystalline domains in semicrystalline matrix composites are important for understanding the fiber/matrix adhesion. The development of transcrystalline morphology has been studied in the literature [140-144]. The processing conditions, PPS molecular weight, the fiber type and the fiber surface properties are all very important for the development of transcrystallinity [123,125]. Lopez and Wilkes found that transcrystalline features with T300U carbon fibers developed most readily at lower annealing temperatures around 200°C [123].

Neyman et al. studied transcrystalline formation of two different molecular weights of PPS using several different carbon fibers [144]. Carbon fibers were used from each of the three different manufacturing precursors- pitch, PAN and rayon. Transcrystalline features were always found for samples made with pitch based carbon fiber and rayon based carbon fiber. The appearance of transcrystalline features was inconsistent for the PAN based carbon fiber [144].

Desio and Rebenfeld examined transcrystalline growth by studying the crystallization kinetics of PPS when carbon fibers are present [141-143]. In one study, two different PAN based carbon fibers were used, one of which was available both sized and unsized [141]. The results of this study showed that Thornel T300 carbon fiber increased the crystallization rate of PPS the most and led to the most extensive transcrystallinity. Sized AS-4 fibers moderately enhanced the crystallization rate of PPS and led to a less developed transcrystalline region. The sizing on the AS-4 fiber was not identified, but could be speculated to be the Hercules commercially available epoxy sizing. Unsized AS-4 had the least effect on the enhancement of crystallization rate and did not include a transcrystalline region at all [141].

Mehl and Rebenfeld studied the transcrystalline growth of Ryton® PPS from Phillips and Fortron® PPS from Hoechst Celanese using glass, aramid and carbon fibers. The carbon fibers used in the study were Thornel® T300 graphitized carbon fibers from Amoco and sized AS-4 high strength carbon fibers from Hercules [140]. Compared to the crystallization rate of neat Ryton® PPS, the crystallization rate of Ryton® PPS was dramatically enhanced by the presence of the T300 carbon fibers and moderately enhanced by the presence of the sized AS-4 carbon fibers. The crystallization rate of Fortron® PPS was only enhanced slightly over the crystallization rate of neat Fortron® PPS for both the T300 and sized AS-4 fibers [140].

As seen from the work referenced, there are many parameters which can influence the development of a transcrystalline interphase in PPS matrix composites. The processing conditions, PPS molecular weight, fiber type and fiber surface properties are all important parameters. While all these studies examine transcrystalline formation while systematically varying the constituent materials in an effort to understand the mechanisms for fiber-surface-nucleation, none of these studies examine the effect of the transcrystalline formations on the fiber/matrix adhesion. The literature is remarkably lacking in investigations concerning the transcrystalline microstructure of PPS on the overall composite performance.

Blends of Polyimide and PEEK: Background

When developing polymeric materials for specific applications, new polymers can be synthesized to meet the explicit design criteria. This can be complicated, cost prohibitive, or impractical. As polymeric materials find greater use and applications, specific design criteria can be met by blending two or more readily available polymers. For example, Ultem polyimide has been shown to be thermodynamically miscible with polyarylene ethers such as polyether ketone (PEK) and polyether ether ketone (PEEK) [146-148]. Blends of these polymers can have different processing considerations and properties very different from the neat polyimide. PEEK is more resistant to solvents than Ultem polyimide while the T_g of the polyimide is much greater. A blend of Ultem polyimide and PEEK results in a polymeric material that has a greater T_g than pure PEEK and a greater solvent resistance than pure Ultem polyimide. In this manner, specific design requirements can be met using polymer blends to tailor the overall properties of the

polymeric material. The miscible nature of the Ultem polyimide/PEEK system also led to the possible use of Ultem polyimide for bonding together composite laminates of PEEK matrix composites as a welded adhesive joint [149].

Karcha and Porter investigated the behavior of blends composed of polyimide/PEEK and polyimide/sulfonated PEEK [150,151]. The polyimides used in the studies were Ultem 1000 from GE and Torlon 4000T from Amoco. The PEEK was supplied from ICI and sulfonated using sulfuric acid. As-received PEEK was shown to be immiscible with Torlon 4000T. However miscibility was demonstrated over the entire composition range by a single T_g measured by DSC for Torlon 4000T and sulfonated PEEK [150].

The synthesis of novel polyimide BisP-BTDA was described earlier in this chapter. This polyimide is thermodynamically miscible with PEEK and PEK [80]. The T_g for different blend compositions of BisP-BTDA polyimide/PEEK as measured by dynamic mechanical analysis was modeled well by the Fox equation as seen in Figure 2-16 [80]. The Fox equation, equation (2-1), provides a simple estimation for the T_g of a two component polymer blend based on the individual glass transition temperatures and the composition of the blend [152].

$$\frac{1}{T_g} = \frac{W_1}{T_{g1}} + \frac{W_2}{T_{g2}} \qquad (2\text{-}1)$$

Where T_g = estimated glass transition of the blend
W_1, W_2 = weight fractions of the blend components
T_{g1}, T_{g2} = glass transition temperatures of the blend components.

Polymeric blends are not the focus of this thesis. However, for interphase composites,

compatibility of a polymer interphase with a different polymer matrix can be examined using the theories developed for polymer blends. Polymer blends are rarely thermodynamically miscible but this does not preclude polymer compatibility. As will be described in this section, thermodynamic miscibility of two high molecular weight polymers is a unique phenomenon while compatibility of two polymers simply describes a blend which has some desirable physical property [153].

The requirement for thermodynamic miscibility is that the Gibb's free energy of mixing, ΔG_{mix}, must be negative. As seen in equation (2-2), ΔG_{mix} is dependent upon the enthalpy of mixing, $\Delta H_{mix,}$ temperature, and the entropy of mixing, ΔS_{mix}.

$$\Delta G_{mix} = \Delta H_{mix} - T \cdot \Delta S_{mix} \qquad (2\text{-}2)$$

For high molecular weight polymers ΔS_{mix} is typically positive and small due to the small number of moles of each polymer in the blend. For nonpolar polymers, ΔH_{mix} is typically positive, resulting in a positive value for ΔG_{mix} which results in immiscibility. Miscibility can be assured if there are specific interactions that make the heat of mixing exothermic, ie. making $\Delta H_{mix} < 0$. The specific interactions between polymer molecules can be hydrogen bonding, acid/base reactions, charge transfer complex formations, or dipole-dipole interactions [153]. Since these specific interactions are dependent upon the presence of interacting functionalities on the repeat unit of both polymer chains, the molecular weight and the composition of the blend are important for qualifying thermodynamic miscibility. Compatible blends of polymers can display metastable compositions where local phase separation results in domains rich in an individual polymer.

Blends of Polyimide and PEEK: Characterization

One common method for qualifying miscibility is the examination of the glass transition behavior of a polymer blend. If a single T_g is found for a blend of two polymers, then thermodynamic miscibility is very likely. Two separate T_g's will be observed for an immiscible polymer blend. This method requires that the T_g's for the individual polymer components are significantly different from one another so that an apparent broadening is not confused with miscibility [153]. Neutron scattering is a relatively new method for qualifying the miscibility of a blend.

Suitable visual assessment of the morphology on an appropriate length scale is useful for describing the miscible behavior. Scanning electron microscopy (SEM) and transmission electron microscopy (TEM) can be used to examine the possibilities of microscale phase separation. For polymer blends where one component is a semicrystalline material, SEM is particularly useful for examining the phase behavior near crystalline structures, especially when the noncrystalline blend component can be preferentially removed with an etchant.

Blends of Ultem Polyimide/PEEK

The miscible nature of Ultem/PEEK blends has important consequences on the microstructure of the polymer blend. PEEK is a semicrystalline polymer and it is not possible for Ultem polyimide to be incorporated in the ordered crystalline phase. This results in a complex blend microstructure.

Since one of the main topics of this thesis concerns a polyimide composite interphase

which begins as a separate phase from the bulk PEEK matrix, and is then processed at temperatures where molecular mixing is possible, the interdiffusion of Ultem polyimide and PEEK is very important. Pertinent scientific studies of characterization of the microstructure, physical properties and diffusion characteristics of Ultem polyimide/PEEK blends will be discussed in the following sections.

Ultem Polyimide/PEEK Blends: Microstructure

A miscible blend of a noncrystallizable polymer with a crystallizable polymer is expected to have a complex microstructure. Binary blends of amorphous Ultem polyimide and semicrystalline PEEK are shown to have a complex microstructure that is dependent upon blend composition, and thermal history. The morphology of Ultem polyimide/PEEK blends has been studied by Hsiao and Sauer [154,155], Hudson et al. [156], and Crevecoeur and Groeninckx [157].

In a blend of the two polymers, the presence of Ultem polyimide does not prevent the crystallization of PEEK. When crystallization occurs, the Ultem polyimide is rejected from the PEEK crystalline phase. This has an effect an the T_g, T_m, and crystalline growth rate as will be discussed in the next section. Depending upon conditions such as blend composition and crystallization temperature, the exclusion of the Ultem polyimide from the PEEK crystalline domains can result different complex morphologies. Hsaio and Sauer identify three factors which influenced the morphology: (I.) segmental interactions between the two components, (ii.) diffusion of the noncrystallizable polymer, and (iii.) growth of the crystal front [154].

The three morphological features which are possible for miscible blends of crystallizable and noncrystallizable polymers are described as interlamellar segregation, interfibrillar segregation, and interspherulitic segregation. Simplified drawings of these three morphologies are shown in Figure 2-17. A fast crystalline growth rate and/or slow diffusion of the noncrystallizable component can result in the interlamellar morphology shown in Figure 2-17(a), characterized by noncrystallizable polymer trapped between the lamella of the crystalline phase. These conditions can also result in the interfibrillar morphology shown in Figure 2-17(b), characterized by noncrystallizable polymer residing between the lamellar bundles in the spherulitic structure. As described earlier in this chapter, PEEK spherulites have an expanded volume containing a significant amount of amorphous material in the spherulitic domain. This expanded volume provides spacing for amorphous PEEK and noncrystallizable Ultem polyimide. However, a slow crystalline growth rate and/or fast diffusion of the noncrystallizable polymer can result in the interspherulitic morphology shown in Figure 2-17(c.) characterized by isolated spherulitic structures in a matrix of amorphous polymer.

Some micrographs published by Hudson et al. of the important morphological structures described above are shown in Figure 2-18. A phase contrast micrograph showing spherulites which have grown to impingement on neighboring spherulites is shown in Figure 2-18(a). The light shaded regions surrounding individual spherulites are Ultem polyimide rich domains where the polyimide was rejected during crystalline growth. While this morphology can be classified as interspherulitic, the impingement of spherulites prevents complete rejection of the Ultem polyimide and some interlamellar or interfibrillar segregation is expected. A phase contrast micrograph showing isolated PEEK spherulites shown in Figure 2-18(b) clearly depicts

interspherulitic segregation. The micrograph in Figure 2-18© provides closer inspection of the spherulite edges from TEM.[156]

The blend composition will also influence the phase morphology for Ultem polyimide/PEEK blends. Hsaio and Sauer have shown that the interfibrillar morphology dominates for Ultem polyimide concentrations less than 50%. However, for Ultem polyimide concentrations of 50% and greater, the interspherulitic morphology occurs [154]. Using a higher molecular weight PEEK for their blends, Crevecoeur and Groeninckx concluded that interlamellar segregation does not occur based on calculated long spacings from SAXS measurements of blends with varying concentration. Therefore they deduced that the morphology was characterized by interfibrillar segregation [157]. The microscopy results of Hudson et al. shows the formation of interfibrillar and interlamellar morphologies to be consistent with the trends shown by Hsiao and Sauer [156]. For blends that were isothermally crystallized at 300°C with an Ultem polyimide concentration of 50%, a phase morphology of interspherulitic segregation occurred. The same blend composition that was crystallized at 270°C showed interfibrillar segregation where the PEEK spherulites impinged upon each other, leaving no space for possible interspherulitic segregation [156]. These observations will be important for a discussion of the level of crystallinity later in this section.

Ultem Polyimide/PEEK Blends: Properties

The thermal properties of Ultem polyimide/PEEK blends have been studied by many researchers. The glass transition behavior has been studied by Hsiao and Sauer [154,155], Harris

and Robeson [147], Crevecoeur and Groeninckx [157], and Goodwin and Simon [158].

Hsiao and Sauer show the effect of composition on T_g for binary Ultem polyimide/PEEK blends as seen in Figure 2-18. Blends that are completely amorphous follow the predicted trend from the Fox equation (2-2). Blends which have been annealed to promote crystalline growth of the PEEK component show positive deviation from the Fox equation predictions which is attributed partially to the crystalline domains creating mobility restrictions on the amorphous chains resulting in a broadening of T_g as measured by DSC [154]. Another factor which explains the increase in T_g for a specific blend composition with a significant crystalline fraction is the total amorphous phase composition. As the PEEK component crystallizes, fewer PEEK polymer chains are present in the amorphous phase. Therefore, the bulk amorphous phase composition increases in Ultem polyimide concentration. This results in a shift toward the higher T_g of the pure Ultem polyimide component [157]. Similar behavior was observed by Harris and Robeson [147], Crevecoeur and Groeninckx [157], and Goodwin and Simon [158] for the T_g of amorphous and semicrystalline Ultem polyimide/PEEK blends.

The crystallization kinetics and melting behavior has been studied by Hsiao and Sauer [154,155], Crevecoeur and Groeninckx [157], and Harris and Robeson [147]. Hsiao and Sauer used a series of isothermal crystallization experiments with Ultem polyimide/PEEK blends of systematically varied composition [154]. The results showed that, as the Ultem polyimide concentration was increased, the spherulitic growth rate decreased. Crevecoeur and Groeninckx also reported a decrease in the rate of crystallization with increasing Ultem polyimide composition [157]. The temperature for maximum crystallization, T_{maxc}, also increased with Ultem polyimide concentration. Harris and Robeson also reported an increase in T_{maxc} with

increasing Ultem polyimide concentration [147]. The equilibrium melting temperature of the PEEK crystalline phase was not affected by the presence or concentration of the Ultem polyimide phase. The increase in T_g with increasing Ultem polyimide concentration that was described above must also be considered in an explanation of these observations. Thermal crystallization of the PEEK component can only occur in the temperature range above T_g and below T_m. Thus, for a given isothermal crystallization temperature, T_x, as the Ultem polyimide concentration increases, the T_g increases, and the relative difference between T_x and T_g decreases. This effectively reduces the relative mobility of the crystallizing PEEK polymer chains [154]. This can also shift the location of the nucleation dominated crystallization regime and the diffusion dominated crystallization regime so that a specific T_x for several different blend compositions will result in very different microscopic crystalline growth.

Harris and Robeson showed that the degree of crystallinity of the PEEK component, as measured by DSC, passes through a maximum at blend compositions around 30-40 wt% Ultem polyimide [147]. This was explained by a possible increase in mobility in the interlamellar regions due to the presence of Ultem polyimide [147]. An increase in mobility violates the mechanism proposed by Hsiao and Sauer to explain the decrease in crystallization rate. Using WAXD, Hsiao and Sauer show a maximum in the degree of crystallinity at blend compositions around 50% Ultem polyimide [154]. This phenomenon was not commented on by Hsiao and Sauer. However the lamellar thickness as measured by SAXS for all blend compositions was greater than the lamellar thickness for pure PEEK [154]. An isothermal crystallization temperature of 300°C was used by both Harris and Robeson and Hsiao and Sauer.

The crystalline morphology of different blend compositions provides the basis for a

possible explanation regarding the maximum in degree of crystallinity for the PEEK component. As described previously, the rejection of Ultem polyimide during the crystallization of PEEK can result in different phase morphologies. When the concentration of Ultem polyimide is low, the phase morphology is classified as interfibrillar and is characterized by impinging PEEK spherulites which contain amorphous PEEK and Ultem polyimide in the expanded volume.

The Ultem polyimide behaves as a noncrystallizable diluent for the PEEK component [154]. As the diluent concentration increases, the phase morphology changes from interfibrillar to interspherulitic. The interspherulitic phase morphology is characterized by isolated PEEK spherulites separated in a matrix of amorphous PEEK and Ultem polyimide. Hsiao and Sauer noted that this phase morphology begins to occur for blend compositions of 50% Ultem polyimide [154]. This is the same composition for which the maximum in crystallinity of the PEEK component was reported. Since the PEEK spherulites are no longer impinging upon each other, the onset of this phase morphology allows complete development of the spherulites. This could explain the maximum in the degree of crystallinity.

As the concentration of Ultem polyimide is increased further, the phase morphology remains interspherulitic. However the further dilution of the PEEK polymer chains reduces the probability of intimate contact with other PEEK chains, thus reducing the crystallization kinetics and lowering the final crystallinity.

Harris and Robeson have extensively investigated the properties of Ultem polyimide/PEEK blends with systematically varied compositions [154,155]. Among the properties measure were tensile strength, tensile modulus, tensile impact strength, and heat deflection temperature (HDT). The blends were injection molded into appropriate geometries for

test specimens, cooled rapidly and then annealed for 30 minutes at 250°C, to promote crystallization of the PEEK component. The tensile strength and tensile modulus of Ultem polyimide/PEEK blends are shown as a function of blend composition in Figure 2-19. The tensile strength for all blend compositions is greater than that for pure PEEK. The local maximum in tensile strength around 30-40 wt% Ultem polyimide/PEEK blends is in accordance with a similar local maximum in crystalline fraction as described earlier. As expected from the tensile moduli of the individual components, the tensile modulus follows almost a monotonic decrease as the concentration of Ultem polyimide is decreased.

As shown in Figure 2-20, the tensile impact strength for all blend compositions is greater than the tensile impact strength for either pure component. It is interesting to note the large improvement in tensile impact strength from the case of pure PEEK at low to moderate concentrations of Ultem polyimide. The HDT of the blends is shown as a function of blend composition in Figure 2-21. The increase in HDT for the blends with increasing Ultem polyimide concentration can be attributed to a similar increase in blend T_g, and an increase in the crystalline fraction of the PEEK component, as were both shown earlier.

Ultem Polyimide/PEEK Blends: Interdiffusion

For a binary miscible blend of a crystallizable polymer with a noncrystallizable polymer, the diffusion of the noncrystallizable component is important to the resulting microstructure. Hsiao and Sauer used estimations of the diffusion coefficient, D_{12}, for the PEEK and Ultem polyimide blend to study the competing effects of crystallization of the PEEK and diffusion of

the Ultem polyimide. Using a ratio of the diffusion coefficient to the crystalline growth rate as a function of temperature and blend composition, a qualitative assessment of whether the blend morphology should be characterized by interlamellar segregation, interfibrillar segregation or interspherulitic segregation was made. Their results showed qualitative agreement with experimental results.

The diffusion coefficient used by Hsiao and Sauer was calculated using the Arrhenius equation shown in equation 2-3.

$$D_{12} = D_0 \cdot e^{\frac{-E_a}{R \cdot T}} \qquad (2\text{-}3)$$

where D_0 = empirically determined constant; E_a = activation energy; R = thermodynamic constant; T = temperature.

The values used for the parameters D_0 and E_a were 0.07 cm^2/s and 14 kcal/mole, respectively. Although these parameters were determined experimentally using an ATR technique for blends of Ultem polyimide with PEKK, Hsiao and Sauer used them for the Ultem/PEEK blends [154]. Values ranging from 2 x 10^{-12} to 4 x 10^{-12} cm^2/s were reported as typical for D_{12} [154].

An approximate calculation of the interdiffusion of PEEK and Ultem polyimide can be shown using these parameters for the case of Fickian diffusion. Considering a hypothetical system where thin films of pure PEEK and pure Ultem polyimide are brought into intimate

contact at elevated temperatures, the diffusivity can be calculated using equation (2-4).

$$t_{diff} = \frac{(2 \cdot \delta)^2}{D_{12}} \tag{2-4}$$

If an arbitrary diffusion distance, δ, of 10 μm is considered, then the time, t_{diff}, for complete interdiffusion of PEEK and Ultem polyimide within this distance is shown in Figure 2-22. It is important to note that only the amorphous phase of PEEK is available for interdiffusion. Although interdiffusion is possible at a temperature above the T_g of both polymers, any PEEK crystalline features will develop a barrier for interdiffusion. Above temperatures around 335°C the PEEK crystalline phase melts and the crystalline barriers to diffusion are eliminated.

There are many criticisms regarding the estimated diffusion times shown in Figure 2-22. Recall that the parameters for calculating D_{12} were actually obtained from measurements on an Ultem polyimide/PEKK blend. Although qualitative agreement was demonstrated for a method using the calculated D_{12} between predicted morphological microstructure and experimental observations in the Ultem polyimide/PEEK system, this predictive method was not shown for the Ultem polyimide/PEKK system. The crystallization kinetics and the growth rate are much slower for PEKK than for PEEK. Thus, very different predictions would follow for the morphological microstructures of PEKK blends. Therefore, the accuracy of the parameters D_0 and E_a and/or the method for prediction of the morphological microstructure must be viewed with caution.

Although PEEK and PEKK are very similar in many regards and both are miscible with

Ultem polyimide, there are important differences between the two polymers. The backbone chemical structure of PEEK contains entirely para-oriented aromatic bonding with 67% flexible ether linkages. The backbone chemical structure of PEKK has a combination of para-oriented and meta-oriented ketone linkages. Furthermore, PEKK only has 33% flexible ether linkages in the backbone. This change in molecular architecture can also change the mobility of the polymer chains, and hence alter the diffusion characteristics. A comparison of the zero shear melt viscosities for PEEK and PEKK would have provided very useful information for Hsiao and Sauer in their discussion of diffusion characteristics with Ultem polyimide.

Blends of Polyimide/PPS: Background

The properties described earlier in this chapter indicate that the solvent resistance, dimensional stability and maintenance of strength at high temperatures are the most advantageous qualities for PPS. The limitations of the performance of semicrystalline PPS center around its brittle nature.

Brittle polymers such as polystyrene are sometimes toughened with the addition of an elastomer [159]. Rubber toughened polystyrene forms an immiscible blend resulting in the elastomeric phase isolated in local domains. The brittle polystyrene surrounds the elastomeric domains, preventing their migration. The rubber toughening results in increasing the impact strength over pure polystyrene and providing ductility at high rates of loading [159].

The brittle nature of PPS can be altered with addition of an appropriate ductile polymer. Blends of polysulfone, PSF, and PPS were shown by Akhtar and White to be immiscible but yet

had improved the Izod impact strength monotonically with increasing PSF content.160 The tensile failure strain is greater than the pure PPS tensile failure strain for all blend compositions. Interestingly, a maximum in tensile failure strain was observed for a blend containing 50% PSF. Microscopic investigation revealed that the 50% PSF blend was characterized by continuous rod shaped domains of PSF embedded in a matrix of PPS [160].

Blends of Ultem Polyimide and PPS

As described earlier in this chapter, Ultem polyimide is an amorphous, ductile polymer which maintains good strength at high temperatures. These characteristics are beneficial for compatibility of the two polymers. A patent was issued to Giles of GE in 1984 disclosing blends of polyetherimides and polysulfides [161]. The focus of the results of this patent was on blends of Ultem 1000 and Ryton PPS. The applications detailed in the patent included use as films, molding compounds, composite matrices, coatings, electrical insulators and electronic packaging.

Blends of Ultem Polyimide and PPS: Characterization

The useful characterization techniques for Ultem polyimide/PPS blends are very similar to the useful characterization techniques outlined earlier for Ultem polyimide/PEEK blends. As mentioned above, examination of the glass transition behavior of a polymer blend can be useful for assessing the miscibility of the components. Microscopy is also a very useful technique for

characterizing the morphology of the blend, especially when phase separation occurs. Mechanical testing of a polymer blend provides critical information for assessing the compatibility of the components. Recall that compatibility does not imply thermodynamic miscibility. A compatible polymer blend results in a beneficial improvement for some design criteria.

Blends of Ultem Polyimide and PPS: Microstructure

Akhtar and White prepared blends of Ultem polyimide/PPS with a range of compositions using an injection molding technique [160]. The blends were then cryogenically fractured using liquid nitrogen to examine a cross section of the sample. Amazingly, after cryogenic fracture, Akhtar and White commented on the smoothness of the cavities and concluded that there is a lack of adhesion between the two phases. It is probable that loose Ultem polyimide domains were dislodged only because of extreme contraction of both polymers at the cryogenic temperatures. Contraction of both phases will occur with an extreme decrease in temperature, and it is possible that the dimensional changes alone would create enough force to separate the local phase domains. Also, any adhesive bond that might exist between Ultem polyimide and PPS would be "deactivated" to some extent at the cryogenic temperatures. Regardless, the micrographs shown by Akhtar and White clearly exhibit a two phase system and are shown in Figure 2-24. As seen in Figure 2-24(a) for a 15 wt% Ultem polyimide blend and Figure 2-24(b) for a 20 wt% Ultem polyimide blend, spherical domains of the polyimide approximately 1 to 2 um in diameter exist. As seen in Figure 2-24(c) and (d) different morphologies are possible at a

concentration of 50 wt% Ultem polyimide. In Figure 2-24(c) the microstructure is characterized by long filaments of polyimide in a matrix of PPS. In Figure 2-24(d), spherical domains of Ultem polyimide occur [160].

Blends of Ultem Polyimide and PPS: Properties

Binary blends of Ultem polyimide and PPS were prepared by injection molding for mechanical testing with a range of compositions by Giles [161] and Akhtar and White [160]. Two distinct Tg's were seen using DSC and the melting peak did not shift for all blend compositions [160]. The HDT was seen to increase with concentration of Ultem polyimide as seen in Figure 2-25 [161].

As seen in Figure 2-26, the notched Izod impact strength and unnotched Izod impact strength of the blends both increased with Ultem polyimide concentration [161]. This is a direct result of toughening of the PPS as described earlier. The presence of two distinct data points at 50 wt% Ultem polyimide was attributed to a phase inversion at this composition which was not easily controlled. Figure 2-27 shows the notched Izod impact strength measured by Akhtar and White which also exhibits a consistant increase with Ultem polyimide concentration for all blends [160]. The notched Izod impact strength was unexpectedly lower for pure Ultem polyimide than for the blend compositions containing greater than 50 wt% Ultem polyimide.

Also shown in Figure 2-27, are tensile moduli for different blend compositions. It is seen that the modulus remains relatively unchanged as the composition is varied. Even for the case of 100% Ultem polyimide the reported values of the tensile modulus are around 1.5 to 1.8 GPa

which is low compared to product literature data of 3.0 GPa for Ultem 1010 [15].

The failure strain measured by Akhtar and White is shown as a function of blend composition in Figure 2-28 [160]. The failure strain increases slowly with Ultem polyimide concentration up to 70 wt%. At 80 wt% Ultem polyimide, a maximum failure strain is measured. The failure strain results from Giles are shown in Figure 2-29 which do not show a maximum at intermediate compositions [161]. The yield strain is also shown in Figure 2-29 but only for compositions of 90 wt% and 100% Ultem polyimide. There is a converging trend of the yield strain and failure strain at 90 wt% Ultem polyimide concentration, indicating that for lower concentrations of Ultem polyimide, it is likely that yielding does not occur.

The tensile yield strength and the tensile ultimate strength measure by Giles are also shown in Figure 2-29. Once again, the yield strength is only reported for 90 wt% and 100% Ultem polyimide. By considering the converging nature of the yield strain and the failure strain at 90 wt% Ultem polyimide, the omission of yeild strengths at blend compositions less than 90 wt% Ultem polyimide is most likey due to the fact that yielding does not occur. The data measured by Akhtar and White for tensile strength as a function of blend composition is shown in Figure 2-28. A steady increase in tensile strength was measured for blend compositions of 20 wt% Ultem polyimide and greater [160].

The flexure and flexure modulus measured by Giles is shown in Figure 2-30. The flexure modulus is shown to be essentially unaffected by blend composition. The flexure strength increases with Ultem polyimide concentration.

While Akhtar and White conducted DSC experiments for measurement of the Tg's, there was no discussion of the crystalline melting behavior as a function of blend compostion.

Interphase Composites

A fiber reinforced composite is typically composed of fibers embedded in a matrix. The presence of a third phase immediately surrounding the fibers, yet different in material properties or microstructure than the bulk matrix is described as an interphase region or the interphase.

It is very desirable to develop mechanical models which accurately predict composite performance based on constitutive properties. This will develop the understanding of the mechanics of composite failure which will direct future endeavors for designing composites, modifying manufacturing processes and selection of materials.

Interphase Composites: Importance of Interphase

There have been several experimental studies in the literature demonstrating the effect of interfacial adhesion between the carbon fiber and bulk matrix in a composite system on the overall composite performance [36,169-171,180]. Composite failure is a result of the micromechanical stress distributions which can be altered by the presence of an interphase region.

Composite performance and durability have been shown to be dependent upon the interfacial adhesion between fibers and matrix. Interphase modifications have resulted in improvements to transverse flexure strength, transverse tensile strength, longitudinal tensile strength, short beam shear strength, fatigue lifetime, residual strength after fatigue, and impact resistance.

Interphase Composites: Uses, Benefits and Limitations

The use of interphase modifications to improve composite performance and durability are very important for the composite industry. An interphase typically accounts for less than 2% of the total mass of material in a composite. However, carefully modified interphases have been shown to improve longitudinal tensile strength by as much as 29% [162], compressive strength by as much as 50% and notched fatigue lifetime cycles by as many as two orders of magnitude [163]. Therefore, the benefits of implementing a carefully constructed interphase are obviously attractive.

Virtually any fiber reinforced structure can be modified to include an interphase region. The techniques for construction of an interphase will be discussed in the following section.

The present limitations of interphase composites are a thorough understanding of the failure mechanics and methods of interphase construction to obtain very specific fiber-matrix stress interactions and adhesion. As will be discussed later in this chapter, micromechanical models have been developed to further the understanding of interphase composite failure mechanics. The models have been used to formulate hypotheses regarding further improvements of interphase composites based on interphase modifications. The interphase modifications are described as desired material properties and levels of adhesion to the fiber surface. The ability to construct a polymeric interphase with precisely the desired material properties and adhesion to the fiber surface is a formidable task.

Interphase Composites: Manufacturing Techniques for Construction of Interphase

For the purposes of attaining the benefits of an interphase region on the bulk composite performance, a well-defined, tailored interphase region is necessary. To differentiate the interphase region from the bulk matrix in polymeric systems, the interphase must possess unique material properties or a significantly distinct microstructure arising from diffusion, crystalline morphology, chemical interaction with the fiber surface or a combination of the above. The interphase region can be constructed deliberately with the formation of a thin polymer layer [32-39,164] or can develop spontaneously due to the interactions of the matrix material with the surface of the carbon fiber [97,113-117,123,125,140-144,165-168].

As described earlier in this chapter specifically with polyimides, a polymeric sizing can be applied from solution onto carbon fibers to form an interphase. This method is the most common for deliberate interphase construction. Sizings can be applied to carbon fiber tow immediately after the carbon fiber manufacturing step, and the sized tow can be wound on a spool. The sized carbon fiber can then be processed to form a composite with any appropriate matrix polymer using a variety of composite manufacturing techniques.

Spontaneous development of an interphase region can occur for a binary polymer blend that is used for a matrix material. Preferential adsorption of one component of the blend will result in interphase formation [166]. Palmese and McCullough have studied interphase formation for an amine cured epoxy matrix, carbon fiber composite. The results show that the amine curing agent preferentially adsorbs onto the carbon fiber surface and diffuses into epoxy-rich sizings. This results in a gradient of matrix properties due to local variations in the degree of cure for the epoxy. The gradient of matrix properties essentially forms an interphase. By

controlling the composite processing conditions such as temperature and cure time, the diffusion and adsorption mechanisms can be suitably controlled to yield an interphase of desired characteristics [166].

A composite matrix that consists of a single polymer does not preclude the formation of an interphase. As described in detail earlier in this chapter for PEEK and PPS matrices, transcrystalline morphologies can develop under certain conditions. The nucleation of crystalline structures on the surface of the carbon fibers constitutes an interphase modification. It is well known that the material properties of crystalline domains are very different than the amorphous phase of a given polymer. The typical increase in density of the crystalline phase and the close packing of the polymeric chains result in increases in stiffness and decreases in ductility over the amorphous phase.

Another mode of spontaneous interphase development for a composite matrix consisting of a single polymer is molecular weight segregation. Pangelinan et al. have developed an analytical model that considers neutral, repulsive and attractive polymer-surface interactions for a carbon fiber, thermoplastic matrix composite. The results of the model predict the spatial variation of molecular weight species in the vicinity of a carbon fiber [165]. The model is based upon a Monte Carlo simulation and is applicable to thermoplastic matrix composites manufactured by melt impregnation. For binary and tertiary blends of monodisperse molecular weights the results show that segregation of the low molecular weight component occurs at the fiber interface [165]. Pangelinan et al. explained that segregation for typical thermoplastics used in composite manufacture result in an interphasial sheath with a composition rich in the low molecular weight species that is approximately 100nm thick [165]. It was also noted that

segregation equilibrium for a melt may take as long as 45 hours [165]. Also, as the breadth of the molecular weight distribution increases, the driving force for segregation also increases.

Interphase Composites: Characterization of Structure

The physical structure of carbon fiber reinforced composites must be characterized for proper development of structure-property relationships. The incorporation of an interphase region complicates the structure characterization due to the dimension scale of this important phase. Carbon fibers are typically 5-8 μm in diameter and an interphase region as mentioned in the previous section can be on the order of 0.1 μm. Examination of structures on this length scale requires extensive sample preparation. Scanning electron microscopy is a useful technique for examining the fiber spacing, fiber volume fraction, and void content. However, definitive verification of interphase thickness is not usually possible with SEM. Composite cross sections must be machined and polished for examination. An etching process can sometimes be used to preferentially remove the interphase polymer [169]. The gap created between the matrix and fiber then verifies the presence of the interphase, however, dimensions must be interpreted carefully.

Atomic force microscopy (AFM) is a new technique which is presently being modified to examine composite cross sections for the purpose of quantifying interphase dimensions.

As discussed previously, an interphase comprised of transcrystalline formations is possible, but the geometry is difficult to assess. Model composite samples can be prepared for the purpose of studying the conditions for transcrystalline growth, however formations in an

actual composite are difficult to characterize. As mentioned previously, the etching technique developed by Bassett et al. for actual PEEK matrix composites was useful in ascertaining the general absence of transcrystalline features [103]. It is possible that this method could applied to other composite systems for actual characterization of the structure of transcrystalline features.

The examination of failure surfaces can provide speculative information regarding the structure of the composite prior to failure. This requires extensive information about the properties of the constitutive phases.

Interphase Composites: Characterization of Properties

Many techniques have been used to characterize the properties of interphase composites. While general composite properties are useful for basic understanding of the composite behavior, it is most useful to identify specific characterization techniques which differentiate the effects of the interphase on the global composite properties. Only the most important and useful characterization techniques for interphase composites will be discussed in this section.

Adams et al. measured the transverse flexure strength of epoxy matrix composites made with unsized, unsized but surface treated, and epoxy-sized carbon fibers [170]. Their results showed that the transverse flexure strength was dependent upon the fiber treatment. Significant improvements in the transverse flexure strength were observed for the unsized but surface treated fibers over the unsized fibers. The presence of the epoxy-sizing on the fibers resulted in slight improvements in transverse flexure strength and transverse tensile strength over the unsized but surface treated fibers. The potential of using the transverse flexure strength for characterization

of the tensile strength of the fiber-matrix interface was established [170].

A very thorough study of the effect of fiber-matrix adhesion using epoxy matrix composites with three different fiber surface treatments was presented by Drzal and Madhukar [162]. The fibers used were AU-4 unsized, unsurface treated fibers, AS-4 unsized but surface treated fibers, and AS-4C surface treated fibers which were sized with a 100-200 nm thick layer of epoxy [162].

Results from a single fiber fragmentation test (SFFT) were presented first by Drzal and Madhukar which quantified the level of fiber-matrix adhesion for each composite system. The interfacial shear strength (ISS) results from the SFFT are shown in Table 2-IV along with results from many other mechanical tests from the paper. The other mechanical properties of the composites were discussed using the fiber-matrix adhesion strength as a basis of comparison.

Table 2-IV. Measured composite properties from Drzal and Madhukar [162]

	AU-4/epoxy	AS-4/epoxy	AS-4C/epoxy
interfacial shear strength (MPa)	37.2	68.3	81.4
longitudinal tensile strength (MPa)	1403 ± 107	1890 ± 143	2044 ± 256
longitudinal tensile modulus (GPa)	130 ± 9	138 ± 5	150 ± 9
longitudinal tensile modulus (GPa) [from rule of mixtures]	150	163	169
longitudinal flexure strength (MPa)	1662 ± 92	1557 ± 102	1827 ± 52
longitudinal flexure modulus (GPa)	154 ± 6	136 ± 11	147 ± 5
transverse flexure strength (MPa)	21.4 ± 5.8	50.2 ± 3.4	75.6 ± 14.0
transverse flexure modulus (GPa)	10.2 ± 1.5	9.9 ± 0.5	10.7 ± 0.6
Iosipescu shear strength (MPa)	55.0 ± 3.0	95.6 ± 5.1	93.8 ± 3.3
Iosipescu shear modulus (GPa)	7.2 ± 0.5	6.4 ± 1.0	7.9 ± 0.4
short beam shear strength (MPa)	47.5 ± 5.4	84.0 ± 7.0	93.2 ± 3.8

As seen from Table 2-IV, the transverse flexure strength and the short beam shear strength were strongly dependent upon the ISS. An increase in ISS resulted in a similar increase for each of these measured quantities. The longitudinal tensile strength showed an initial increase with ISS from the AU-4 fiber composite to the AS-4 fiber composite. However with a further increase in ISS, there was not a corresponding increase in longitudinal tensile strength. The same general behavior is demonstrated for the Iosipescu shear strength.

Failure surfaces from longitudinal tension tests were examined using SEM which showed bare fibers for the AU-4 fiber composites indicating interfacial failure. The failure mode changes

to interfacial and matrix failure for the AS-4 fiber composites and matrix dominated failure for the AS-4C fiber composites, as matrix material is increasingly visible on the failure surfaces [162]. Similar observations were made for failure surfaces from the transverse flexure test specimens.

The trends shown with longitudinal tensile strength and Iosipescu shear strength were explained by the different failure modes observed [162]. For the case of the AU-4 fibers, it is possible that the adhesive bond between the fiber and matrix is the limiting factor that is being tested. While for the composites made with AS-4 and AS-4C fibers, it appears that the material properties of the interphase region are being tested.

The failure mode was compared for the longitudinal tensile composite samples. The AU-4 fiber composites did not show much surface damage, but suffered internal delamination [162]. The AS-4 fiber composites showed a brush like failure mode characterized by fiber-matrix splitting. The AS-4C fiber composites failed in a brittle manner, fracturing transversely.

The slight increases in the longitudinal tensile modulus are apparently not due to the fiber-matrix adhesion. A comparison of the experimentally measured values of longitudinal modulus to the estimations from the rule of mixtures show the same degree of agreement. The longitudinal flexure strength and modulus do not correlate with the ISS. As ISS increases, the longitudinal flexure strength and modulus initially decrease for the AS-4 fiber composite and then increases for the AS-4C composite. Transverse flexure modulus and Iosipescu shear modulus is shown to be independent of ISS for these composites [162].

A study similar to that of Drzal and Madhukar was done by Chang et al. using the same

type of fibers with J2, an amorphous thermoplastic polyamide copolymer from DuPont, as the matrix material. The AU-4 and AS-4 fibers described above were used along with an AS-4CGP epoxy sized fiber. The composite mechanical testing results from the study by Chang et al. are shown in Table 2-V. The normalized interphase strength was determined using a meso-indentation technique (MIT). Due to complications of attaining an elastic response during MIT, the ISS could only be calculated for the AU-4 fiber composite. However, the normalized MIT strengths of the composites made with the AS-4 fiber and the AS-4CGP fiber were statistically similar and approximately 23% greater than the MIT strength for the AU-4 fiber. This normalized MIT strength was used to rank the interfacial adhesion.

Table 2-V. Measured composite properties from Chang et al. [171]

	AU-4/J2	AS-4/J2	AS-4CGP/J2
normalized MIT strength	1.00	1.23	1.23
longitudinal tensile modulus (GPa)	122.9 ± 3.8	124.4 ± 2.7	126.0 ± 7.4
longitudinal tensile strength (MPa)	1610 ± 80	1830 ± 60	1640 ± 20
longitudinal tensile failure strain (%)	1.21	1.31	1.17
transverse flexure modulus (GPa)	7.66 ± 0.38	8.09 ± 0.11	7.55 ± 0.16
transverse flexure strength (MPa)	54.5 ± 7.1	70.3 ± 10.0	69.5 ± 6.8
transverse flexure failure strain (%)	0.74	0.91	0.95
Iosipescu shear modulus (GPa)	5.22 ± 0.11	5.10 ± 0.12	4.97 ± 0.10
Iosipescu shear strength (MPa)	37.3 ± 3.4	68.2 ± 3.0	60.4 ± 4.1

The data shown in Table 2-V indicate that the transverse flexure strength, transverse flexure failure strain and the Iosipescu shear strength depend strongly upon the interfacial

adhesion for the J2 matrix composites. Drzal and Madhukar were not able to conclude that the Iosipescu shear strength was dependant upon ISS for the epoxy matrix composites since the failure mode was not consistent for all composites.

It is shown for the J2 matrix composites that the longitudinal tensile modulus and the Iosipescu shear modulus do not change with differences in interfacial adhesion. While there are variances of the longitudinal tensile strength, longitudinal tensile failure strain, and transverse flexure modulus with differences in interfacial adhesion, a clear trend is not apparent.

A similar study to the two previously described was done by Subramanian et al. for sized Apollo carbon fibers and an epoxy matrix [169]. A very important difference for this study was the fact that all the fibers were sized and surface treated. Apollo carbon fibers were used with three different controlled interphases. The sample designated 810 A received 100% of the standard industrial surface treatment and then a bisphenol A epoxy sizing was applied. The sample designated 820 A received 200% of the standard industrial surface treatment and was then sized with the same bisphenol A epoxy. The sample designated 820 O received 100% of the standard industrial surface treatment and then a polyvinylpyrrolidone (PVP) sizing was applied.

The composite mechanical testing results from the study by Subramanian et al. are shown in Table 2-VI. The ISS for the three composites was determined independently using two methods. A single fiber fragmentation test (SFFT) was used as well as the MIT. The SFFT yielded similar ISS values for the 810 A and 820 A composites and a 20% less ISS for the 810 O composite. The MIT yielded similar ISS values for the 810 A and 810 O composites, and an ISS for the 820 A that was "significantly greater than the other two"[169]. A qualitative comparision of the two tests was made and Subramanian et al. suggested that since the interfacial

failure mode of the SFFT was similar to the interfacial failure mode observed during longitudinal tensile testing, the SFFT ISS values should be adopted for further analysis.

Table 2-VI. Measured composite properties from Subramanian et al.[169]

	810 O	810 A	820 A
normalized ISS	1.0	1.2	1.2
longitudinal tensile strength (MPa)	3061 ± 113	2806 ± 41	2758 ± 22
longitudinal tensile modulus (GPa)	161.5 ± 5.9	191.3 ± 2.5	196.5 ± 1.4
longitudinal tensile failure strain (%)	1.66 ± 0.05	1.31 ± 0.04	1.28 ± 0.02
transverse flexure strength (MPa)	126.2 ± 22.1	81.8 ± 11.7	135.6 ± 9.6
transverse flexure modulus (GPa)	8.17 ± 0.21	7.94 ± 0.28	7.90 ± 0.28
transverse flexure failure strain (%)	1.39 ± 0.24	0.91 ± 0.14	1.54 ± 0.09

It is very difficult to make any definitive conclusions on the effects of ISS on the composite performance based on the data from Subramanian et al. shown in Table 2-VI. An important observation is that the longitudinal tensile strength is greatest for the 810 O composites which was shown to have the lowest ISS by SFFT. Based on this result Subramanian et al. suggested that local stress concentration effects do not contribute to the 810 O composite strength [169]. While the longitudinal tensile strength is greatest for the 810 O composite, the longitudinal tensile modulus is the lowest. Also, the longitudinal tensile failure strain is the largest indicating that there is ineffective load transfer from the matrix to the fiber [169]. These results are very important because they challenge the widely held notion that composite tensile strength increases with fiber-matrix adhesion.

The trends demonstrated by Drzal and Madhukar, and Chang et al. for transverse flexure strength increasing with ISS are not supported conclusively by the data in Table 2-VI. However, if the ISS values determined by MIT are considered, then the 820 A composite, which has the highest ISS, corresponds with the greatest transverse flexure strength. That comparison is the only validation of previous results though, since the 810 A composite and the 810 O composite were shown to have the same ISS by MIT, yet very different transverse flexure strengths.

Development of processing polyimide interphase PEEK matrix composites was done by Gonzalez [35]. The aqueous suspension prepregging technique was used with the ammonium salts of polyamic acids as binders to manufacture composites with a LaRC-TPI polyimide interphase and a BisP-BTDA polyimide interphase [35]. The polyimide interphase PEEK matrix composites were characterized using several mechanical testing techniques and the results of some of these tests are shown in Table 2-VII. Gonzalez also characterized PEEK matrix composites manufactured from APC-2 prepreg as a control.

Table 2-VII. Mechanical testing results from Gonzalez [35].

	LaRC TPI /PEEK	APC-2	BisP-BTDA /PEEK
MMHP (MPa)	686.7 ± 63.3	777.1 ± 99.4	812.9 ± 111.5
transverse flexure strength (MPa)	149.6 ± 6.9	172.5 ± 11.3	172.7 ± 3.9
transverse flexure modulus (GPa)	8.4 ± 0.2	9.5 ± 0.2	9.6 ± 0.2
transverse flexure failure strain (%)	1.91 ± 0.15	1.92 ± 0.21	1.92 ± 0.06
Iosipescu 90° shear strength (MPa)	85.06 ± 2.27	79.24 ± 2.59	84.77 ± 7.91
Isoipescu shear modulus (GPa)	4.37 ± 0.11	5.29 ± 0.06	4.19 ± 0.09
$[0/90]_{2s}$ notched tensile strength (MPa)	325.1	446.8	328.0

The MMHP listed in Table 2-VII is the maximum mean hardness pressure from the MIT data analysis. This value is correlated to the fiber-matrix adhesion and can be related to the ISS. It is difficult to make any conclusions on the effects of ISS on the mechanical properties of the PEEK matrix composites based on the results in Table 2-VII since the standard deviations are so large for the MMHP. However, the MMHP results can be used to qualitatively rank the ISS of the composites. A similar correlation to ISS that was made with the data from Subramanian et al. can be made for the transverse flexure strength. Specifically, the LaRC TPI/PEEK composite had the lowest transverse flexure strength and also was shown to have the lowest ISS. The transverse flexure strength for the other two composites was very similar. The transverse flexure modulus displayed the same behavior with regard to ISS ranking.

No correlation could be made between the Iosipescu shear strength, Iosipescu shear modulus, or the $[0/90]_{2s}$ notched tensile strength with regard to ISS. The study by Gonzalez focused on processing considerations of PEEK matrix composites using polyamic acid salt binders for the aqueous suspension prepregging technique. The composite manufacturing techniques and processing considerations of this thesis are based heavily upon the results of Gonzalez.

Interphase Composites: Mechanical Models

The mechanics of composite loading and stress transfer leading to composite failure are complex. It is useful to develop simplified models for a composite system from which the stresses and stress transfer can be studied. Model development requires an assumed geometry for

which a coordinate system can readily be defined. Many simplifying assumptions are necessary for this geometry. Some typical assumptions are that fibers are perfectly cylindrical, unidirectional, continuous and uniformly spaced. Further assumptions typically include elimination of voids, homogeneous fiber volume fraction throughout the composite. As seen in Figure 2-31, a model geometry described by hexagonally packed fibers is very different in principle than the actual composite cross section of a polyimide interphase, PEEK matrix, AS-4 carbon fiber composite.

Some simplifying assumptions must also be made regarding the material properties of the constituent elements of the composite. Typical material assumptions are that the fibers are transversely isotropic, all phases behave in a linearly elastic manner, and that the global composite behavior can be modeled by a representative volume element. Assumptions for the interactions of fibers and other phases such as the interphase and/or the matrix typically include perfect bonding between phases, and that failure of the representative volume element is attributed to a specific mechanism such fiber breakage or shear failure of the matrix.

All mathematical models for prediction of composite strength require inputs of constitutive properties. Important constitutive properties of the fiber include tensile modulus, tensile strength, tensile failure strain, and Poisson's ratio. Important constitutive properties of the matrix include shear modulus, tensile modulus, yield strains, and Poisson's ratio. Depending upon the complexity of the model, a combination of some of these constitutive properties or all of them may be necessary.

Details for the development of the rule of mixtures model for estimating composite strength are presented. The rule of mixtures model is very simplistic and will be shown to be

useful only for comparative purposes.

Other more complicated mechanical models will be described very briefly, and some of the important conclusions from each model will be noted. These mechanical models are described only for the purpose of developing an appreciation for the importance of manufacturing and evaluating composites with a carefully constructed and systematically modified interphase.

Rule of Mixtures

One of the simplest models for estimating unidirectional tensile strength is based upon the rule of mixtures. Necessary assumptions are that the unidirectional composite has fibers that are continuous, aligned parallel and uniform in properties [172]. Other important assumptions are that perfect bonding exists between the fibers and matrix so that slippage does not occur at the fiber-matrix interface and each component has a linear elastic response [172]. Thus, during longitudinal tension, the elastic strains experienced by the fiber, matrix and composite are assumed to be equal.

$$\epsilon_f = \epsilon_m = \epsilon_c \tag{2-4}$$

The load applied to the composite (P_c) is the sum of the loads carried by the fibers (P_f) and the matrix (P_m).

$$P_c = P_f + P_m \tag{2-5}$$

Equation (2-5) can be written in terms of the individual stresses, σ_c, σ_f, and $\sigma_{m,}$ applied to the composite, fiber and matrix, respectively, and their corresponding cross-sectional areas A_c, A_f, and A_m.

$$P_c = \sigma_c \cdot A_c = \sigma_f \cdot A_f + \sigma_m \cdot A_m \tag{2-6}$$

Dividing equation (2-6) by the cross sectional area of the composite, A_c, yields equation 2-7.

$$\sigma_c = \sigma_f \cdot \left(\frac{A_f}{A_c}\right) + \sigma_m \cdot \left(\frac{A_m}{A_c}\right) \tag{2-7}$$

Based on the assumptions for this model, the constituent volume fractions are equal to the respective cross sectional area fractions.

$$V_f = \frac{A_v}{A_c} \tag{2-8}$$

and

$$V_m = \frac{A_m}{A_c}$$

Substituting for the area fractions in equation (2-7) yields,

$$\sigma_c = V_f \cdot \sigma_f + V_m \cdot \sigma_m \qquad (2\text{-}9)$$

$_c$ = composite tensile strength
V_f = fiber volume fraction
σ_f = fiber tensile strength
σ_m = matrix tensile strength

Equation (2-9) indicates that the contributions to the composite strength of the fibers and the matrix are proportional to their volume fractions. This type of a relationship is called a rule of mixtures and σ_c from equation (2-9) is referred to as σ^{ROM}.

The stresses σ_f and σ_m in equation (2-9) are not the ultimate strengths of the constitutive materials, but they are stresses at a specific strain within the elastic region of deformation. To use equation 2-10 properly, a specific composite strain must be considered. Since the strains of the composite, fibers and matrix are equal in this model, and a linear elastic response is assumed for each component, Hooke's law can be used to calculate the individual contributions to composite strength by the fibers and the matrix.

$$\sigma_f = E_f \cdot \epsilon \qquad (2\text{-}10)$$

and

$$\sigma_m = E_m \cdot \epsilon$$

Since an the strain, ϵ, is not known, an experimentally measured value is typically needed.

Experimentally measuring the failure strain of a composite precludes the necessity for predicting the strength, since that value could then also be measured. Thus, the rule of mixture cannot be used for strength predictions. Another limitation of the rule of mixtures for estimating longitudinal strength is that the composite is considered as a fraction of two bulk components, fibers and matrix. The statistical nature of a distribution of fiber strengths is not considered. Thus, failure of individual fibers and the presence of discontinuous fibers are neglected.

The benefit of the rule of mixtures is simplicity. The rule of mixtures is most useful for comparing the relative performance of two similar composites that may or may not have the same fiber volume fraction and that fail in the same manner. Some example results are shown in Figure 2-32 for the rule of mixtures for composite strength with assumed values for the necessary parameters as detailed in the figure. The most important feature of this graph is the strength dependence on fiber volume fraction. As the fiber volume fraction changes from 50% to 60% there is an increase in estimated strength of approximately 20%.

Single Fiber in Continuous Matrix

The rule of mixtures does not provide a prediction of composite strength. It is generally assumed for high strength fibers, high stiffness fibers and a low stiffness matrix, that the fibers are the load bearing elements in unidirectional tension. These assumptions are satisfactory for carbon fiber reinforced polymer matrix composites. The rule of mixtures shows this qualitatively as the fiber contributions dominate the overall strength estimation. However, since experimental data for failure strain is needed to use the rule of mixtures, no predictions can be made without

experiments a priori.

As mentioned previously, it is very desirable to develop mechanical models which accurately predict composite performance based on constitutive properties. It is well accepted that the unidirectional tensile strength of carbon fiber/polymer matrix composites is dominated by the contributions of the fibers. The fibers support the tensile load and the matrix transfers the load among the fibers. When a sufficient number of the fibers fail, the entire composite fails. For this reason, models for composite strength typically focus on fiber fracture.

The simplest model for fiber fracture in a composite material considers a single fiber embedded in a continuous matrix. The diagram in Figure 2-33 shows the geometry of a single fiber model. The fiber of radius r_f is surrounded by a continuous matrix that is assumed to extend a distance r_m from the fiber center. Distances greater than r_m are considered bulk composite material and are modeled as having uniform properties.

Rosen developed a model in 1964 based on the single fiber geometry using a classical shear lag analysis for prediction of an ineffective length [173]. The classical shear lag model considers a single broken fiber based upon the geometry shown in Figure 2-33 with specific assumptions regarding the distribution of stresses. The extensional load is assumed to be supported entirely by the fiber. It is also assumed that the shear strains in the fiber are negligible. Thus, the matrix transmits axial load along the fiber length by shear stresses. These assumptions are appropriate for a system with very stiff and very strong fibers compared to the matrix.

Rosen's model proposed that there is a statistical distribution for the strength of individual fibers and that the strength of each fiber is based upon a weakest link theory. Furthermore, a composite is modeled as a bundle of these "weakest link" fibers. Thus, an

individual fiber fails due to statistically distributed flaws and the composite fails due to an accumulation of these fiber failures.

A shear lag analysis was used to calculate the length of each link in the fibers. This link length, describing the axial distance from a fiber fracture where the matrix shear stresses have fully decayed, was directly correlated to the ineffective length [173]. Results from this analysis are shown in Figure 2-34, where the ratio of the ineffective length, δ, to the fiber diameter, d_f, is shown as a function of the ratio of the fiber tensile modulus, E_f, to the matrix shear modulus, G_m, for several fiber volume fractions.

For a given fiber volume fraction, as E_f/G_m increases the ineffective length also increases. Physically, the shear stiffness of the matrix effectively decreases thereby decreasing the shear stresses in the matrix, and extending the necessary fiber surface area, hence axial distance, required for transmission of the load relinquished by the fracture in the fiber.

After considering the fiber link strength distributions, Rosen's analysis leads to predictions of composite tensile strength as a function of the ratio δ/d_f. These results, shown in Figure 2-35, indicate that the composite tensile strength increases as the ineffective length ratio decreases. From the development of later models, this prediction will be shown to be insufficient. The model developed by Rosen is useful for an introduction to the ineffective length concept, however the stress concentrations on neighboring fibers are neglected.

For the purposes of understanding the distribution of stresses during a single fiber fragmentation test, Whitney and Drzal developed a model considering a single fiber embedded in an unbounded matrix. It was assumed that perfect bonding existed between the fiber and matrix while both components were deformed elastically. The stresses were assumed to have a

functional dependence on radial and axial coordinates. The equilibrium equations and boundary conditions of the classical theory of elasticity were exactly satisfied throughout the fiber and matrix and compatibility was approximately satisfied [174]. The stresses were assumed to be axisymmetric in this model.

This modified shear lag analysis included axial loading in the matrix and shear stresses in the broken fiber. The model of Whitney and Drzal provides an improvement over the classical shear lag model in that it provides an estimation of all stress components and provides a shear stress distribution that satisfies the free edge boundary conditions at the fiber end [174]. The classical shear lag analysis incorrectly concludes that the shear stress is maximized at the end of the broken fiber, while the model of Whitney and Drzal shows an appropriately vanishing shear stress.

Using constitutive properties, estimations of ineffective length calculated from the model were compared to experimentally determined values from a single fiber fragmentation test of AS-4 fiber and Kevlar 49 fiber embedded in Epon 828 epoxy. The results showed that the predicted ineffective lengths were lower than the experimentally measured ineffective lengths. However, the lack of close agreement does not discount the validity of this model. The low estimates of ineffective length can be rationalized by the difficulties of attaining complete fiber fracture in the single fiber fragmentation test as described earlier.

Multiple Fibers in Continuous Matrix

The single fiber model has been shown to be useful for estimating the ineffective length which provides useful information regarding the transfer of stresses to a broken fiber away from the broken end. As mentioned earlier, the unidirectional tensile strength of carbon fiber/polymer matrix composites is dominated by the contributions of the fibers. When a sufficient number of the fibers fail, the entire composite fails.

While the ineffective length calculated from single fiber models is useful for relating the stresses around a fiber due to the fracture of that fiber, the absence of fiber-fiber stress interactions is a severe deficiency for prediction of composite strength. Since fiber-fiber stress interactions are important, a model must be considered which accounts for more than one fiber. The theories developed with the single fiber model were carried through for development of many models which consider multiple fibers in a continuous matrix.

A complex model was developed by Hedgepeth and VanDyke in 1967 which estimated the stress concentrations on unbroken fibers when various numbers of fibers in an array have broken [175]. This analysis was based on a modified shear lag method. Although stress concentration factors on unbroken fibers near one or more broken fibers were calculated for hexagonally packed and square packed fiber arrays, the model did not implement dimensions of fiber spacing, ie. fiber volume fraction. The model also did not account for constitutive properties of appropriate composite materials. The most important contribution of this model was the consideration of stress concentrations on unbroken fibers near a broken fiber. This model formed the basis for development of many subsequent models by other researchers.

A model was developed by Gao et al. based on a model composite system containing

several fibers in a continuous matrix as seen in Figure 2-36. Gao et al. used a modified shear lag approach which considered the ineffective length concept and also the effects of stress concentrations on neighboring fibers [176]. A Weibull distribution was used for the statistical analysis of fiber failure. The model presented the development of multiple fiber fractures due to stress concentrations surrounding a previously fractured fiber. Furthermore, for conditions where local stress concentrations dominate composite failure and for conditions where the ineffective length dominates composite failure, the composite tensile strength was predicted.

The ineffective length was shown to have a direct relationship to the local stress concentrations. In general, at the location of a fiber fracture, as δ decreased, the stress concentration on neighboring fibers increased. Also, the local stress concentrations were shown to increase sharply when 3 or 4 adjacent fibers were broken. After extensive numerical calculations it was observed that for all systems analyzed composite failure was always predicted for less than 8 adjacent fiber fractures [176]. Gao et al. suggest that an optimum ineffective length might exist for which composite tensile strength is maximized.

Concentric Cylinders Model

The calculation of stress fields using the models described previously for multiple fibers in a continuous matrix assume a specific, regular geometric packing of fibers. As already mentioned, this will not be the case for an actual composite cross section. Also, the fiber-fiber stress interactions in an array of many fiber becomes such a complex mathematical problem that the analysis quickly becomes too complicated for further improvement. A smearing technique

for the geometry of a hexagonally packed fiber array simplifies the model and allows significant progress in the development of complex mechanics.

Carman et al. details the formulation of a mechanical model for predictions of composite unidirectional tensile strength considering single or multiple fiber fracture [177]. The model proposed, which is based on mechanics of materials and classical elasticity concepts, considers a cracked fiber in the center of a hexagonal array of fibers, as shown in Figure 2-37. Simplification of geometry of the problem is achieved by assuming that the fibers adjacent to the broken fiber can be represented by an annular ring of material, as shown in figure . This simplification creates an axisymetric geometry that is commonly referred to as a "concentric cylinder model". Due to the smearing effect of the neighboring fibers into an annular ring, the individual fiber-fiber stress interactions are neglected, however trends in stress variations are typically accurate [178].

The model presented by Carman et al. contains a near-field analysis which considers the local stress redistribution immediately surrounding a broken fiber and a far-field analysis which considers the stress distributions at radial distances which include stress transfer to neighboring fibers [177]. Applications of the model included evaluation of the effects of fiber volume fraction, uniformity of fiber spacing, material properties, crack size and fiber eccentricity.

While the published model of Carman et al. does not explicitly include an interphase region in the analysis, the procedure of including such a consideration in the model development is mentioned at each critical step.

This general model was developed further by Case et al. whereby including the effects of multiple, adjacent fiber fractures and the stress concentrations were predicted as a function of axial distance along the fiber [179].

All of the models described thus far are based upon the assumption that perfect bonding between the fiber and matrix exists. As described earlier in this chapter, it has been shown that composites with tailored interphases demonstrate variability in fiber-matrix adhesion. A model was proposed by Subramanian et al. that included an interfacial efficiency factor to directly consider the variable transfer of stresses between the fiber and the matrix. Since interphase modification can directly result in alteration of the transfer of stresses between the fiber and matrix, this interfacial efficiency parameter is a direct consequence of the interphase.

The model of Subramanian et al. is based upon a modified shear lag analysis using a concentric cylinders model including the ineffective length and the stress concentrations on unbroken fibers due to a neighboring broken fiber [181]. The interfacial efficiency parameter, which can be measured experimentally, is developed to relate the load transfer between the fiber and the matrix. It turns out that the interfacial efficiency parameter is the ratio of the fiber strain to the matrix strain. The case of perfect bonding between the fiber and the matrix results in an efficiency parameter of 1.0. As the level of bonding decreases, so does the efficiency parameter.

Subramanian et al. conclude that the fiber-matrix interface can be completely characterized using two parameters: the interfacial shear strength (ISS) and the interfacial efficiency parameter [181]. Results of normalized tensile strength vs. interfacial shear strength from a parametric study of the model using typical constitutive properties of a carbon fiber/epoxy matrix composite system are shown in Figure 2-38. The most important observation from the figure is that a maximum exists for tensile strength as a function of ISS. The location of this maximum along the ISS axis is dependent upon the interfacial efficiency parameter. As the interfacial efficiency parameter decreases, the optimal ISS increases and the maximum

achievable tensile strength increases. Comparison of results from the model to experimental tensile strength results for carbon fiber/epoxy matrix composites with systematically modified interphases show good agreement.

The micro-mechanics of the model indicate that if interfacial debonding occurs prior to significant fiber fracture which manifests global composite failure, then plastic stress concentrations are used to predict subsequent fiber fracture and the interfacial failure is termed "plastic". If, however, no interfacial debonding occurs prior to significant fiber fracture, then the global composite failure is attributed to elastic stress concentrations and the interfacial failure is termed "elastic".

The results from this study provide the most compelling impetus for the work of this thesis. If composites can be manufactured for which the interphase properties can alter the interfacial shear strength while maintaining a constant interfacial efficiency, then the maximum in tensile strength predicted by the model of Subramanian et al. can be verified.

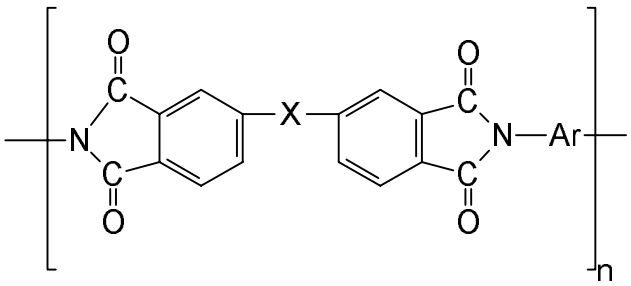

Figure 2-1. Generalized polyimide structure.

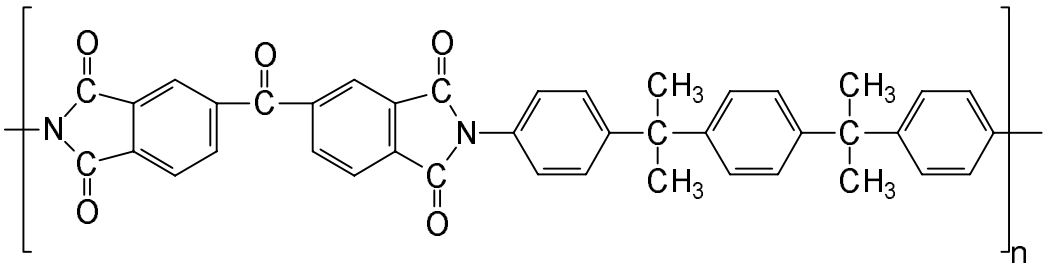

Figure 2-2. Chemical structure for BisP-BTDA polyimide.

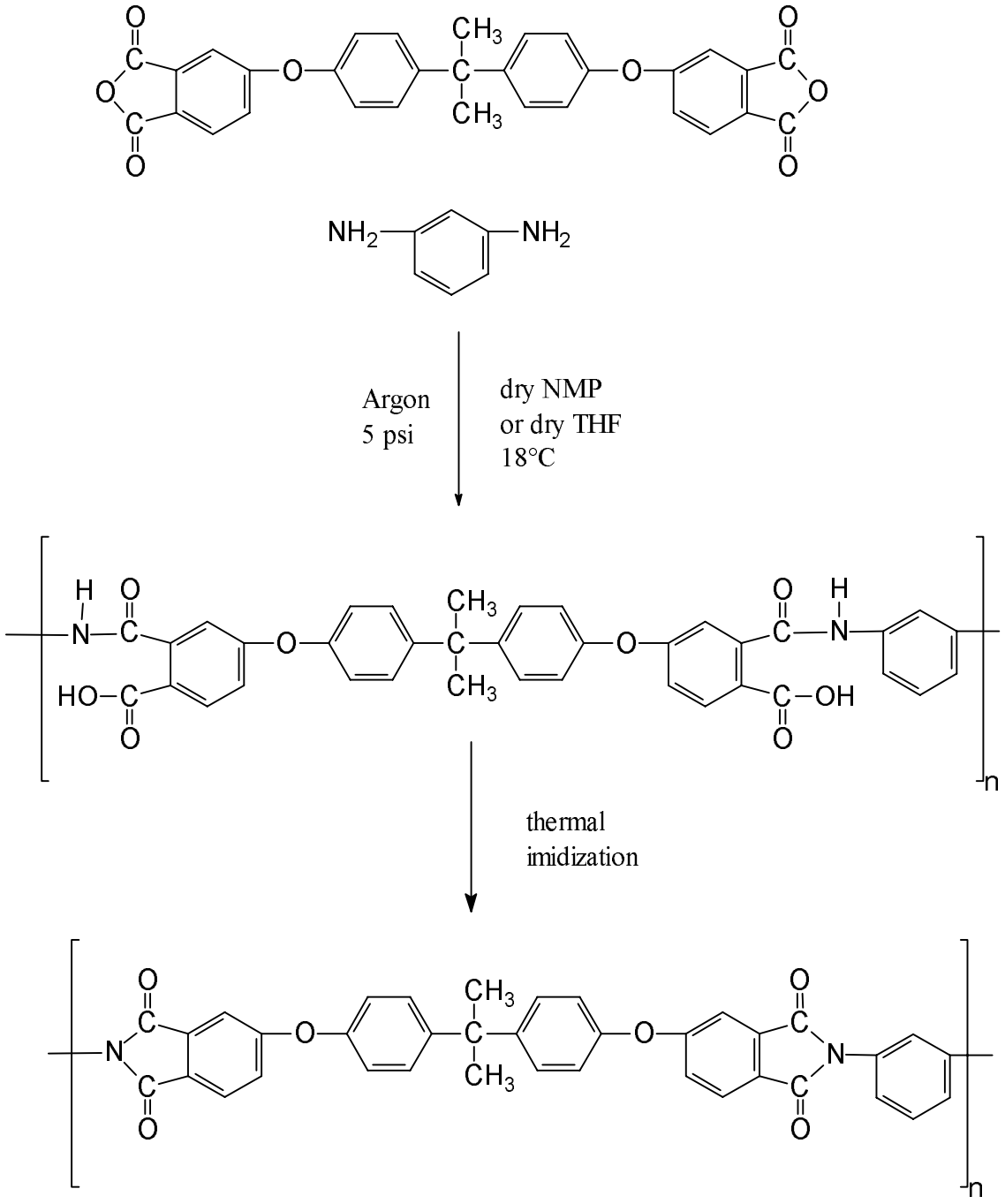

Figure 2-3. Synthesis of controlled molecular weight Ultem-type polyimide.

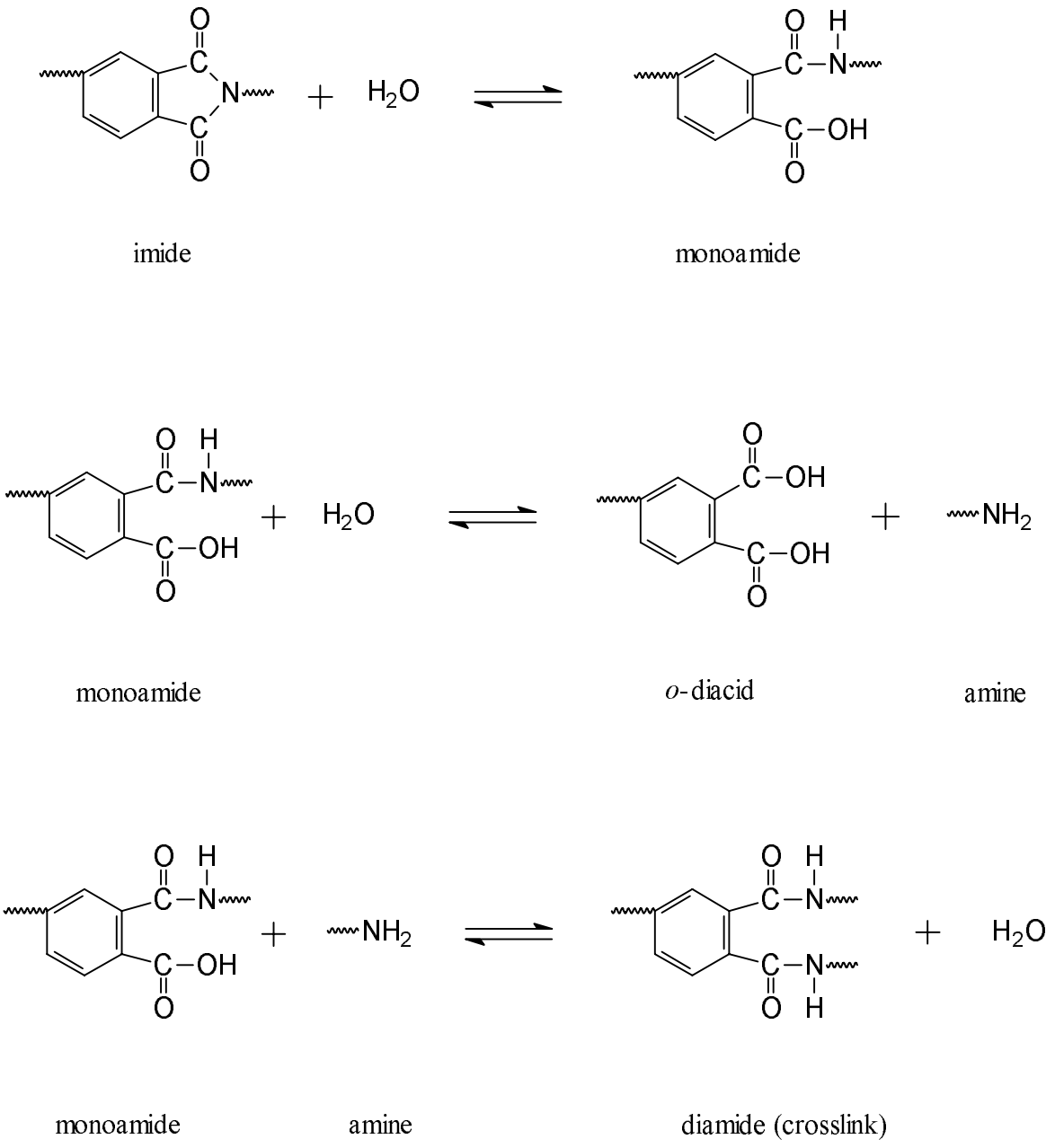

Figure 2-4. Possible side reactions proposed by Hermans and Streef during thermal imidization including a mechanism for forming crosslinks. [85]

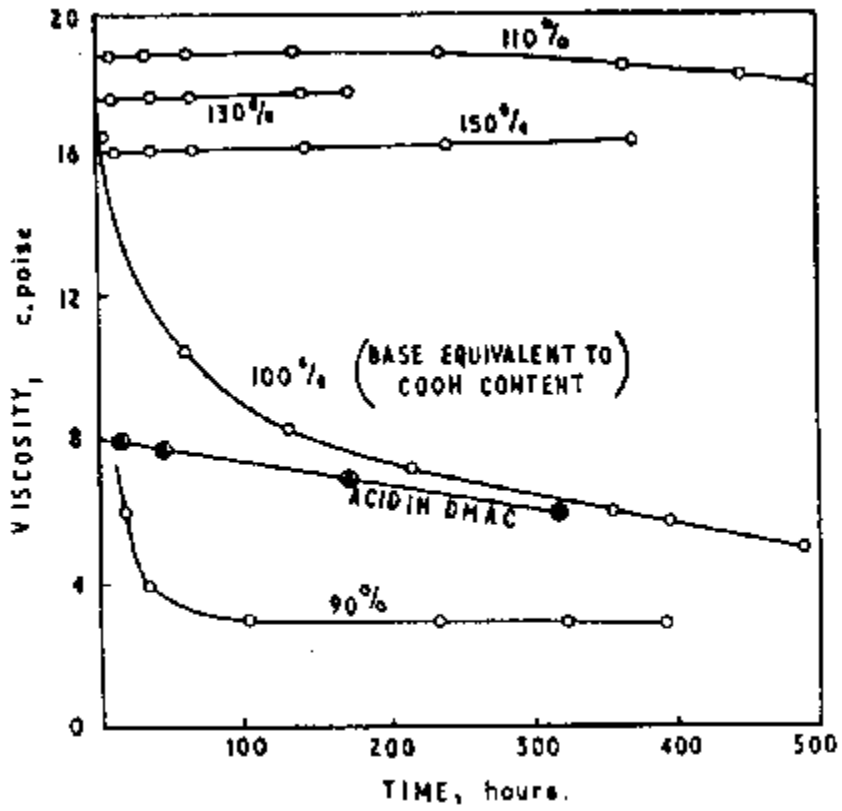

Figure 2-5. Viscosity change of 2 wt% solutions of TEA polyamic acid salts in dimthylacetimede. From Reynolds and Seddon [184].

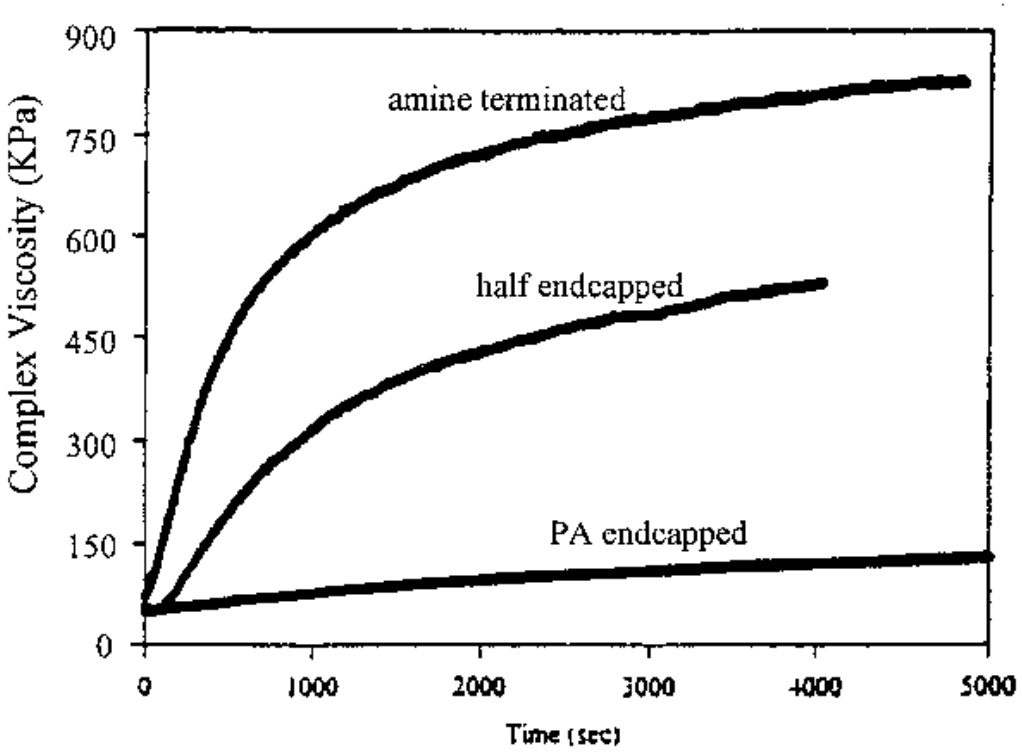

Figure 2-6. Isothermal viscosity sweeps for TPER polyimide with different end groups at 430°C. From Srinivas et al. [21].

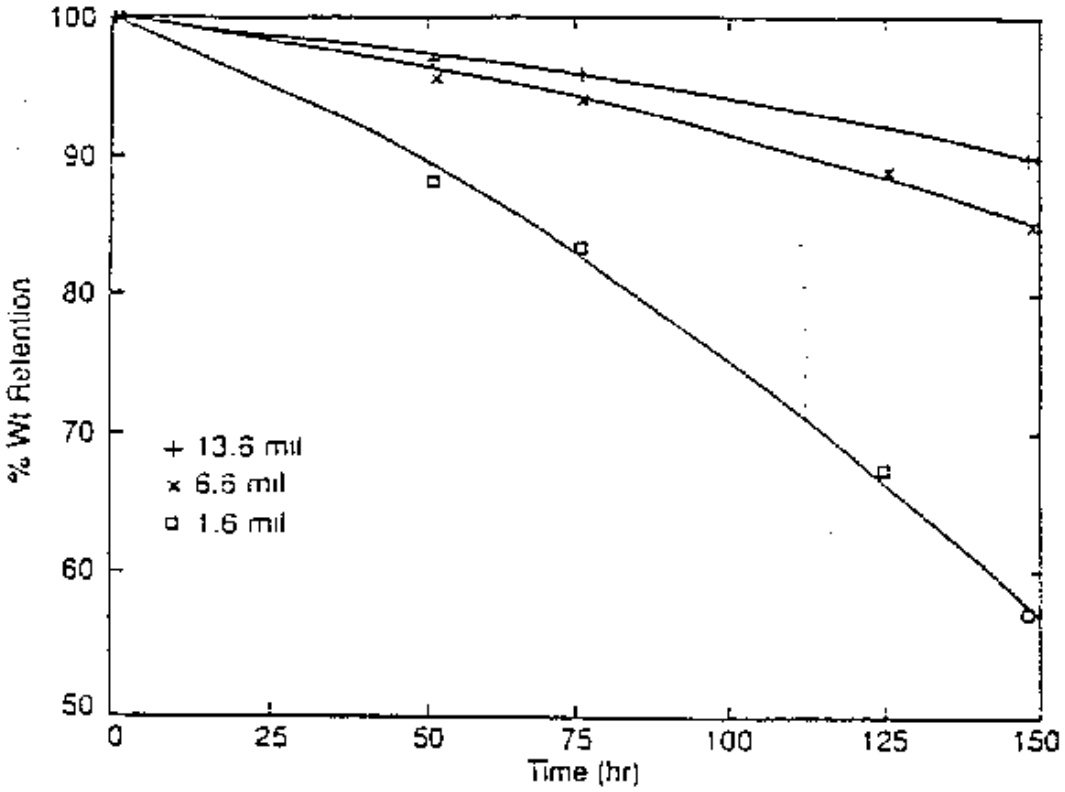

Figure 2-7. Effect of film thickness on polyimide thermal stability. Isothermal weight reduction at 371°C. From Cotts [76].

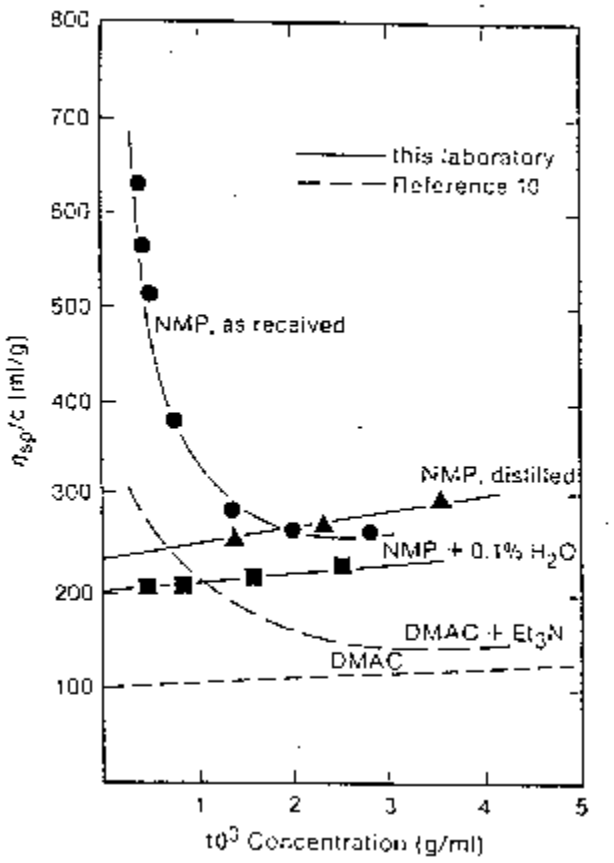

Figure 2-8. Reduced viscosity as a function of concentration for solutions of polyamic acids in NMP showing the polyelectrolyte effect. From Cotts [12].

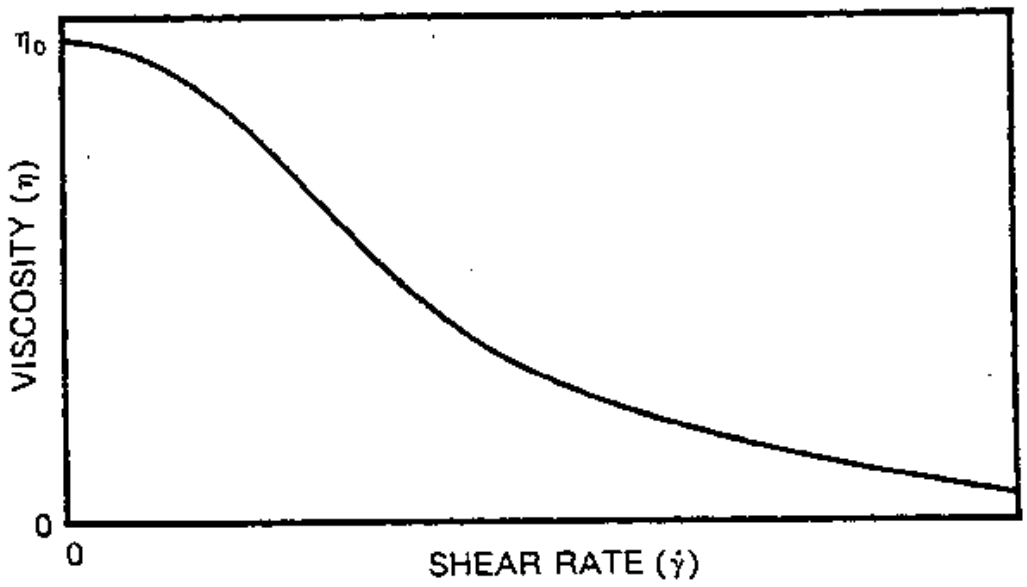

Figure 2-9. Melt viscosity vs. shear rate for a typical molten polymer identifying the zero shear viscosity, η_0. From Dealy and Wissbrun [4].

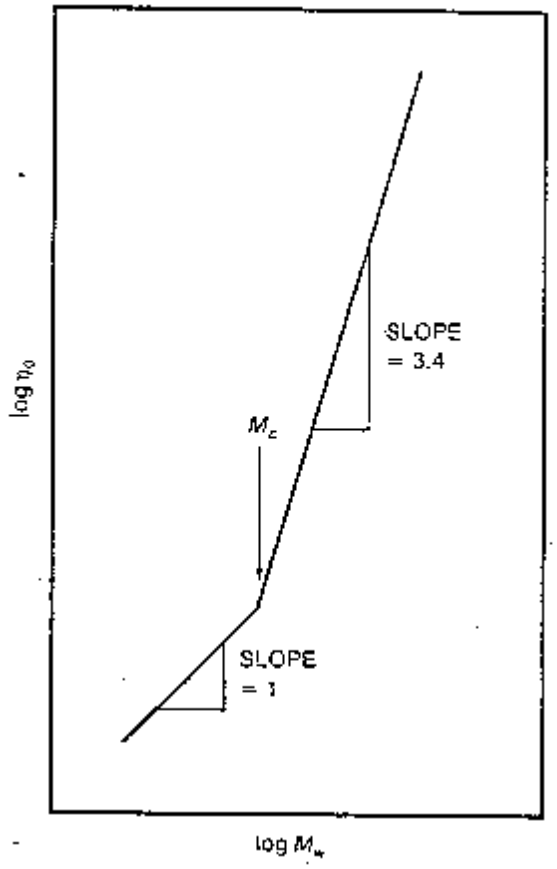

Figure 2-10. Molecular weight dependance of the zero shear viscosity. From Dealy and Wissbrun [4].

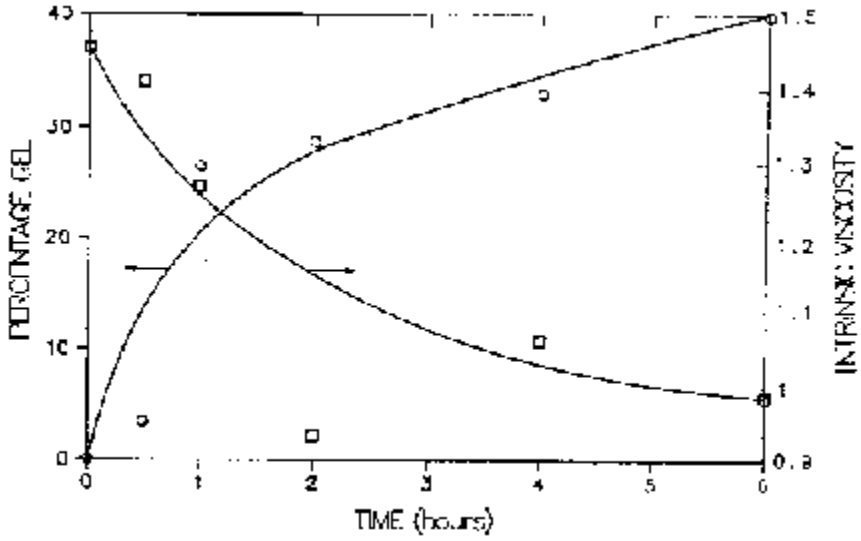

Figure 2-11. Percentage insoluble PEEK gel and intrinsic viscosities measured in methane sulphonic acid solution after heating in air for different lengths of time. From Day et al. [104].

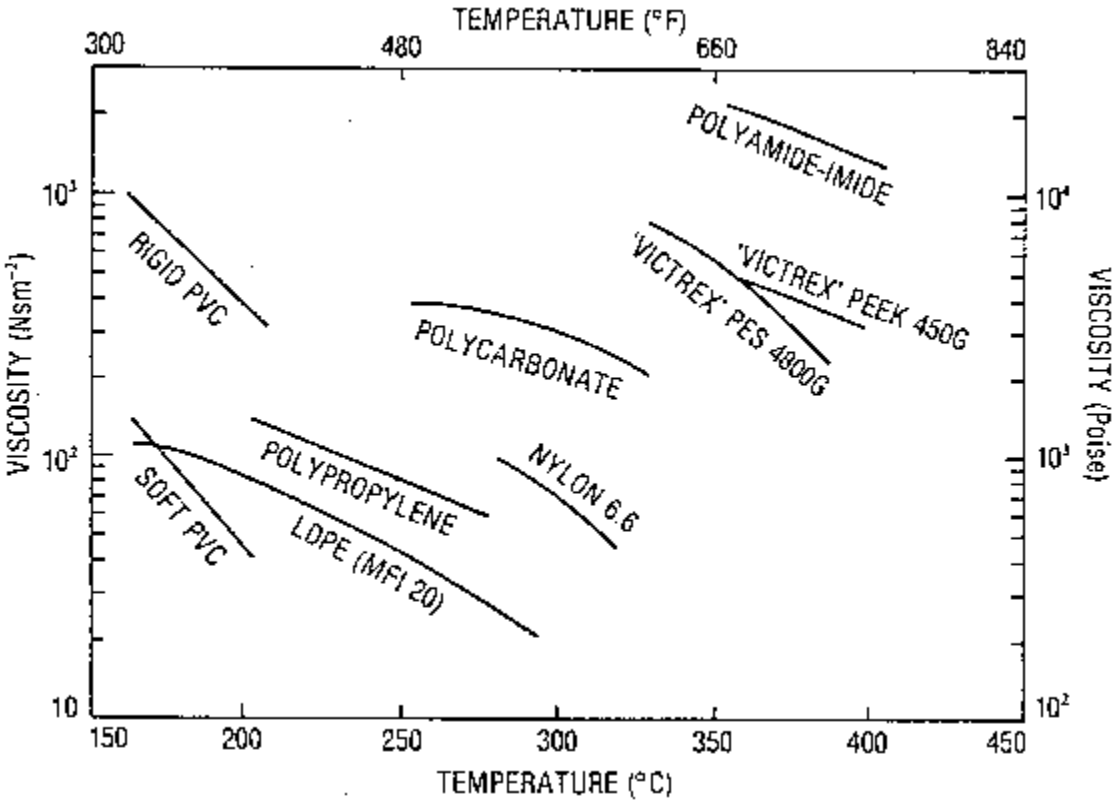

Figure 2-12. Steady shear melt viscosity vs. temperature for several thermoplastic polymers. From ICI Victrex PEEK product data sheet [185].

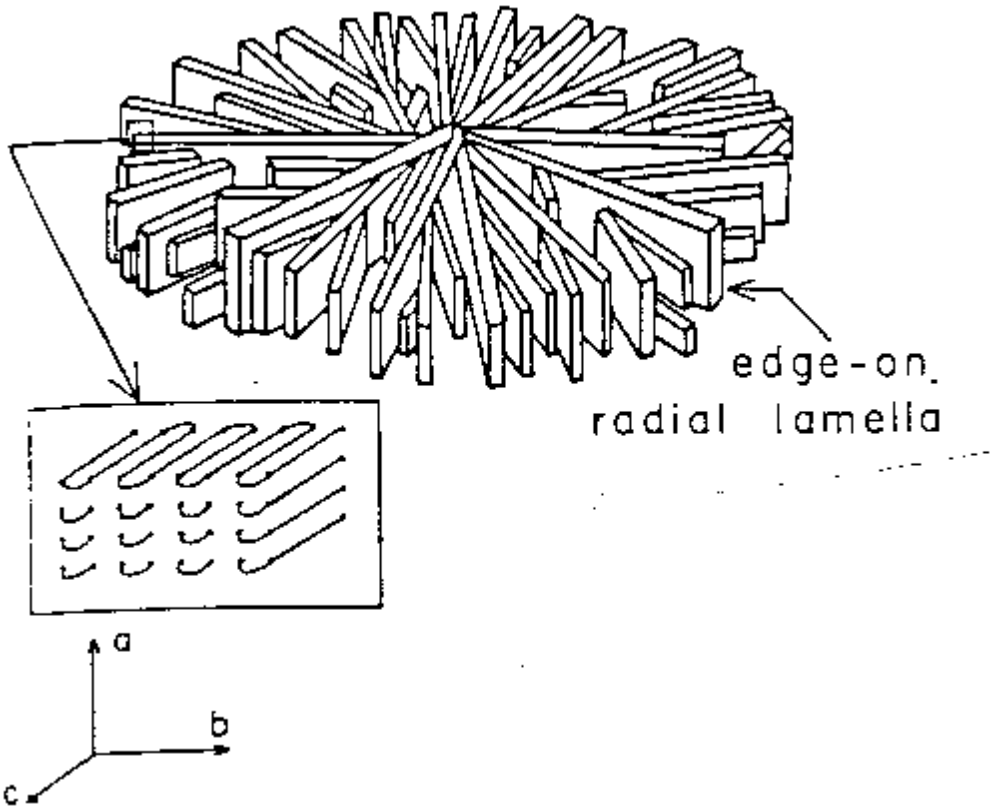

Figure 2-13. Schematic representation of a spherulite with cylindrical symmetry in a PEEK thin film. From Lovinger et al. [100].

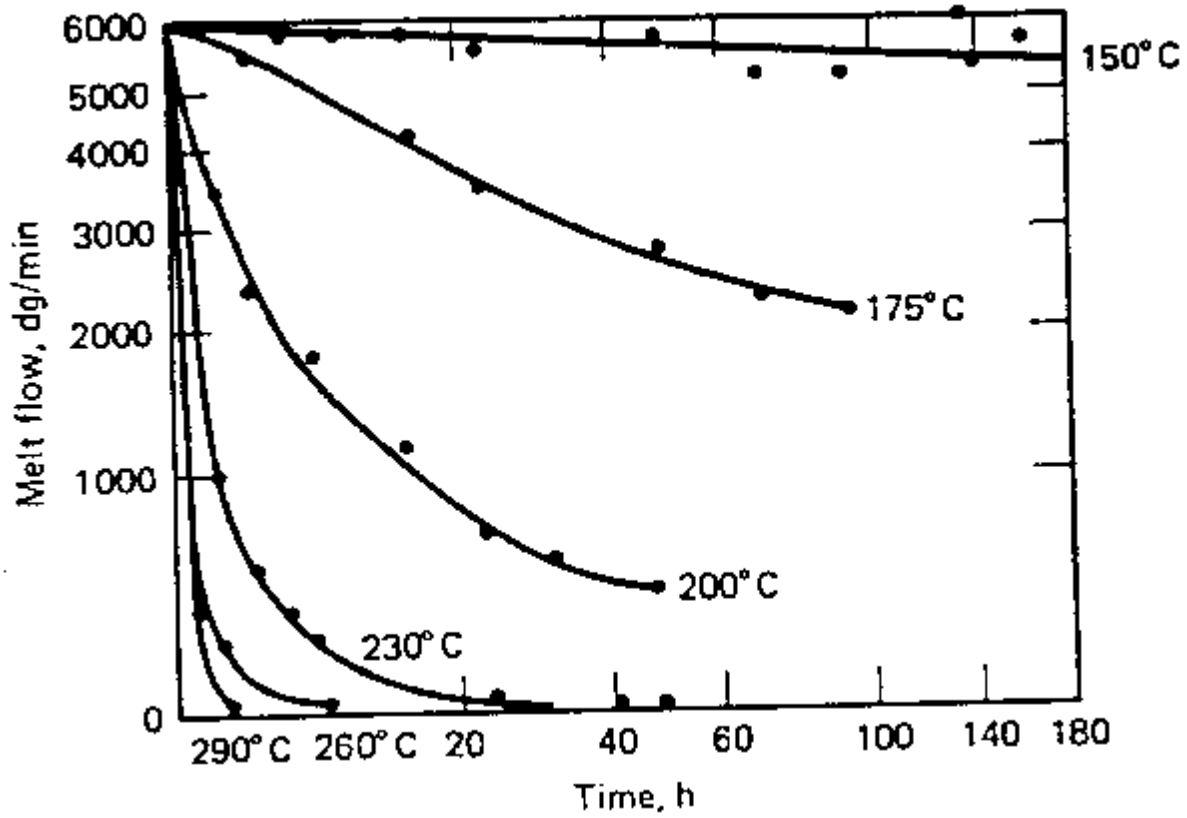

Figure 2-14. Subsequent melt flow as a function of solid state curing time at different curing temperatures. From Geibel and Leland [122].

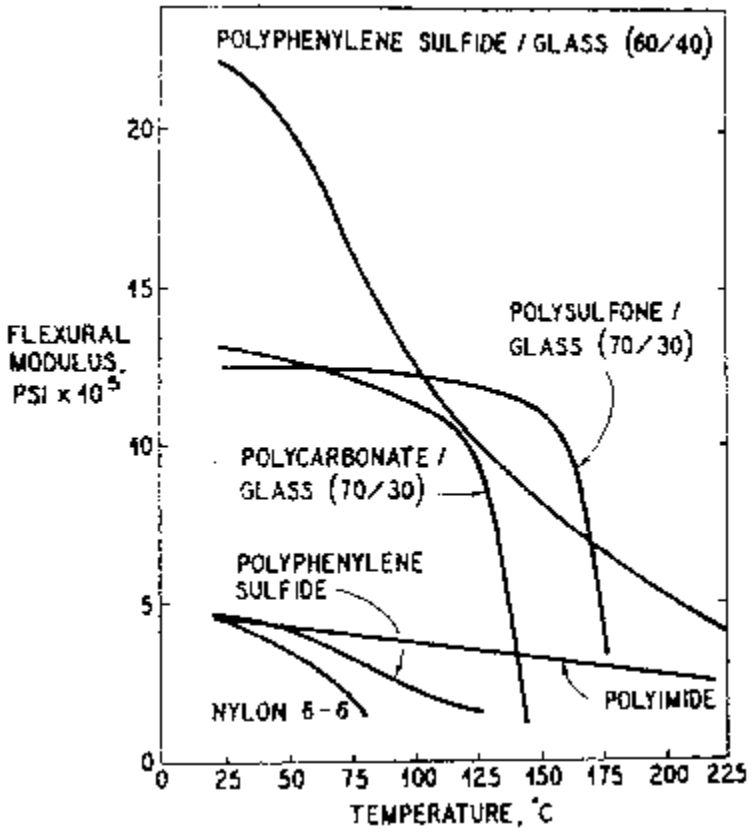

Figure 2-15. Flexural moduli af thermoplastic polymers and glass filled thermoplastic polymers as a function of temperature. From Geibel and Leland [122].

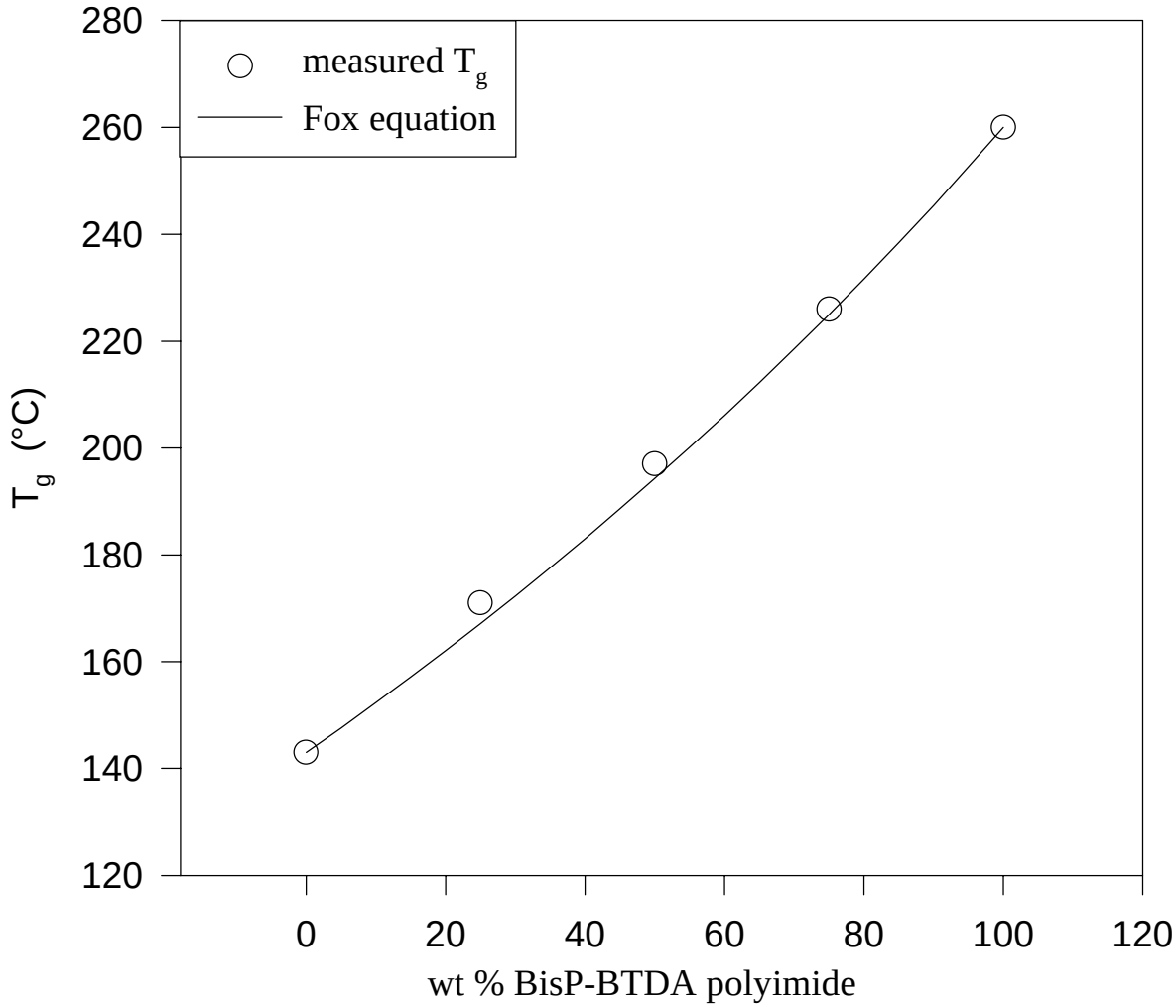

Figure 2-16. Glass transition temperature vs. weight percent BisP-BTDA polyimide for BisP-BTDA polyimide/PEEK blends and comparison to estimates from the Fox equation. From McGrath et al. [80].

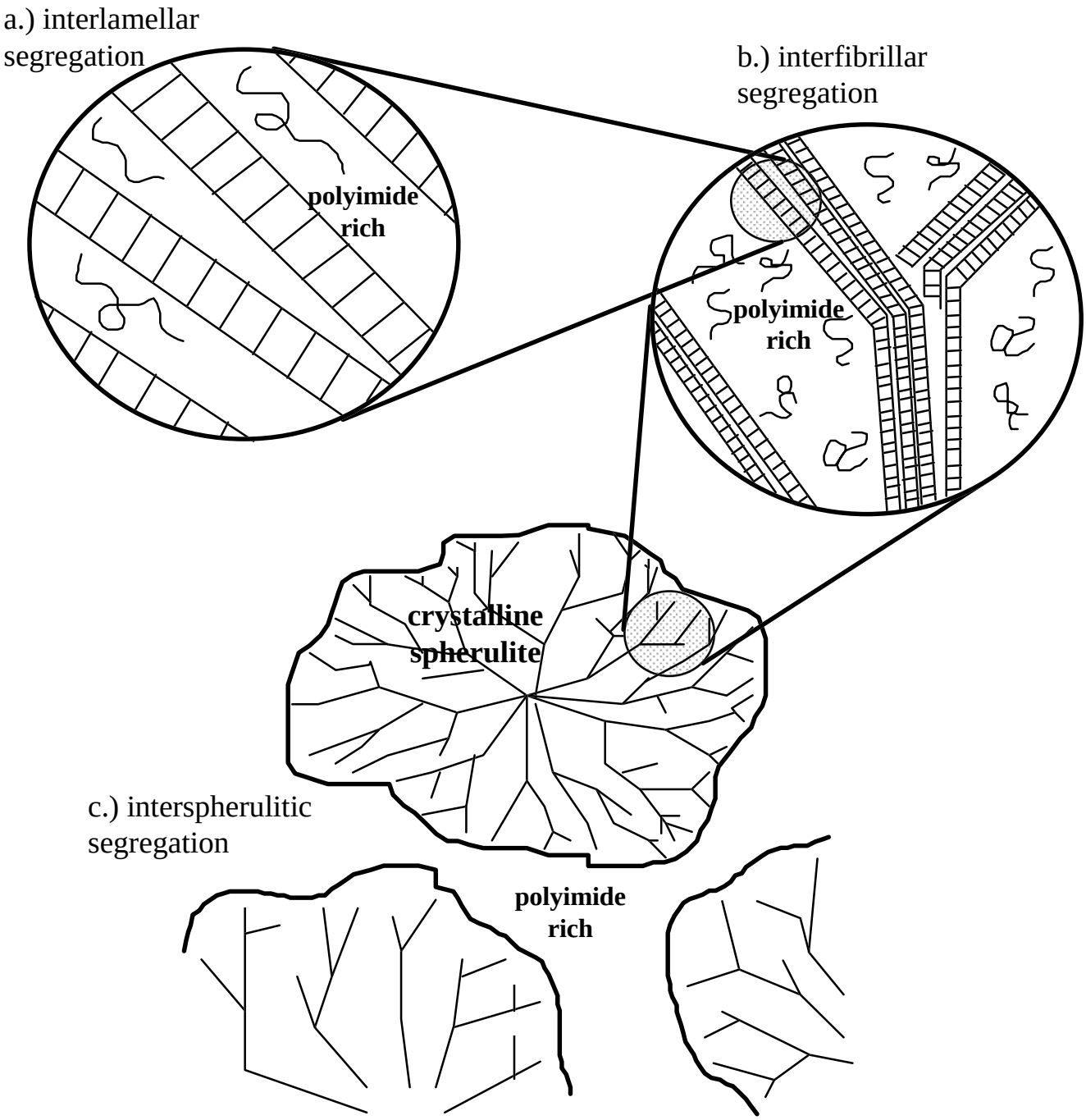

Figure 2-17. Possible phase morphologies for blends of crystallizable and noncrystallizable polymers: (a.) interlamellar segregation, (b.) interfibrillar segregation, and (c.) interspherulitic segregation.

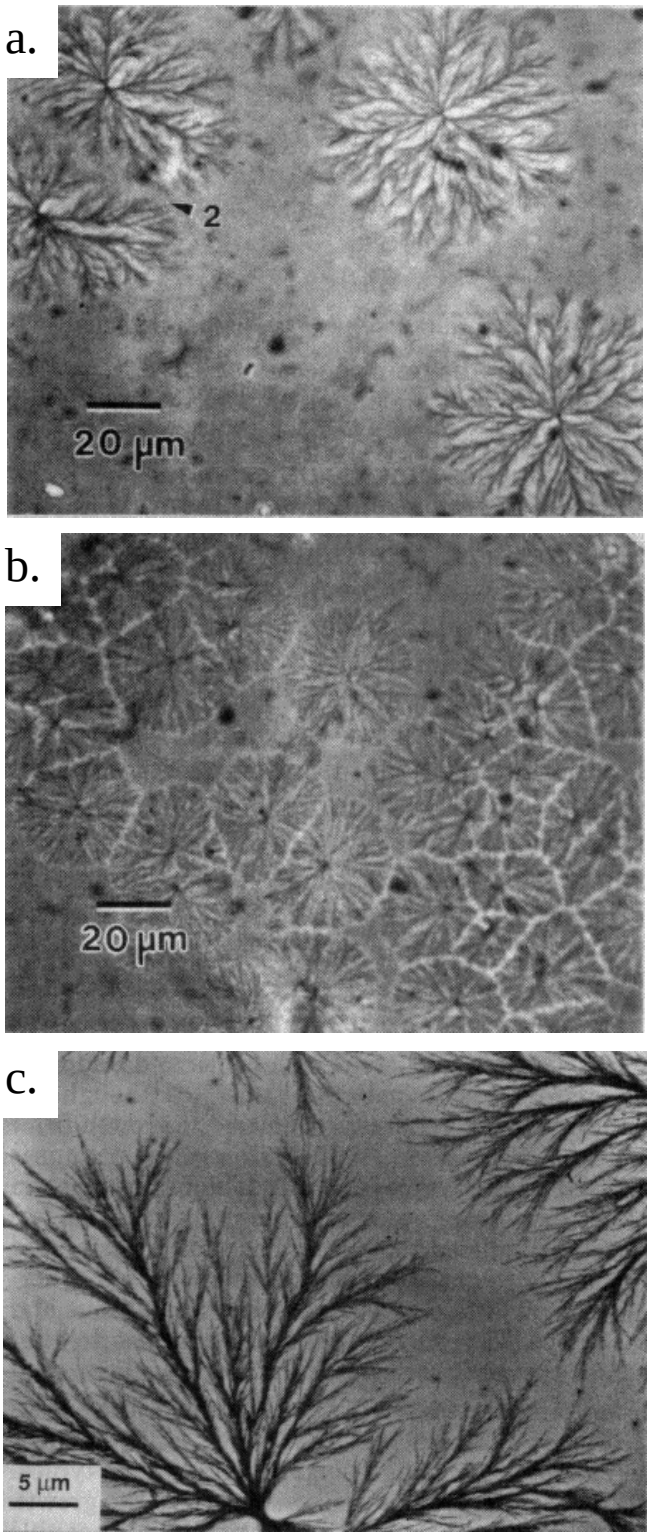

Figure 2-18. Microstructure morphology of Ultem polyimide/PEEK blends shown by Hudson et. al: (a.) phase contrast micrograph showing impinging spherulites, (b.) isolated spherulites representing interspherulitic segregation, and, (c.) transmission electron micrograph showing fine detail spherulite edge after interspherulitic segregation. From Hudson et. al [156].

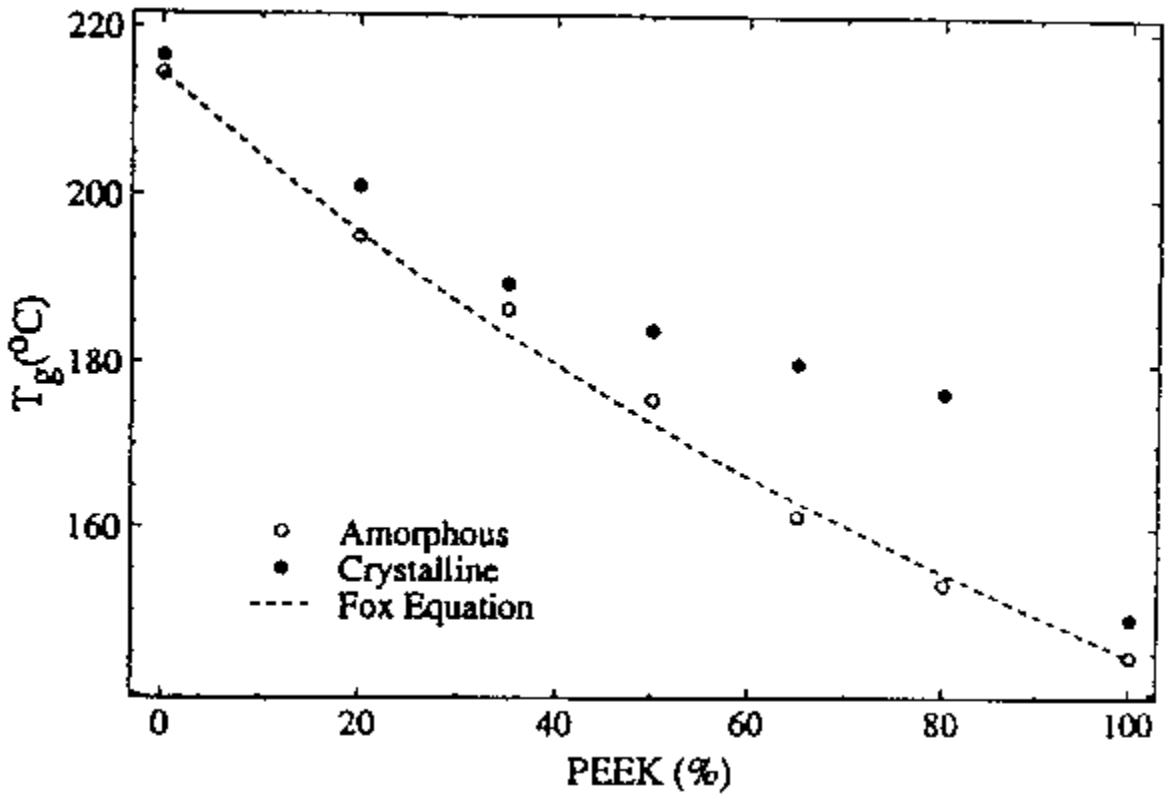

Figure 2-19. Glass transition temperatures vs. PEEK concentration for both crystallized and amorphous blends. The symbols represent the experimental data and the dashed line is predicted from the Fox Equation. From Hsiao and Sauer [154].

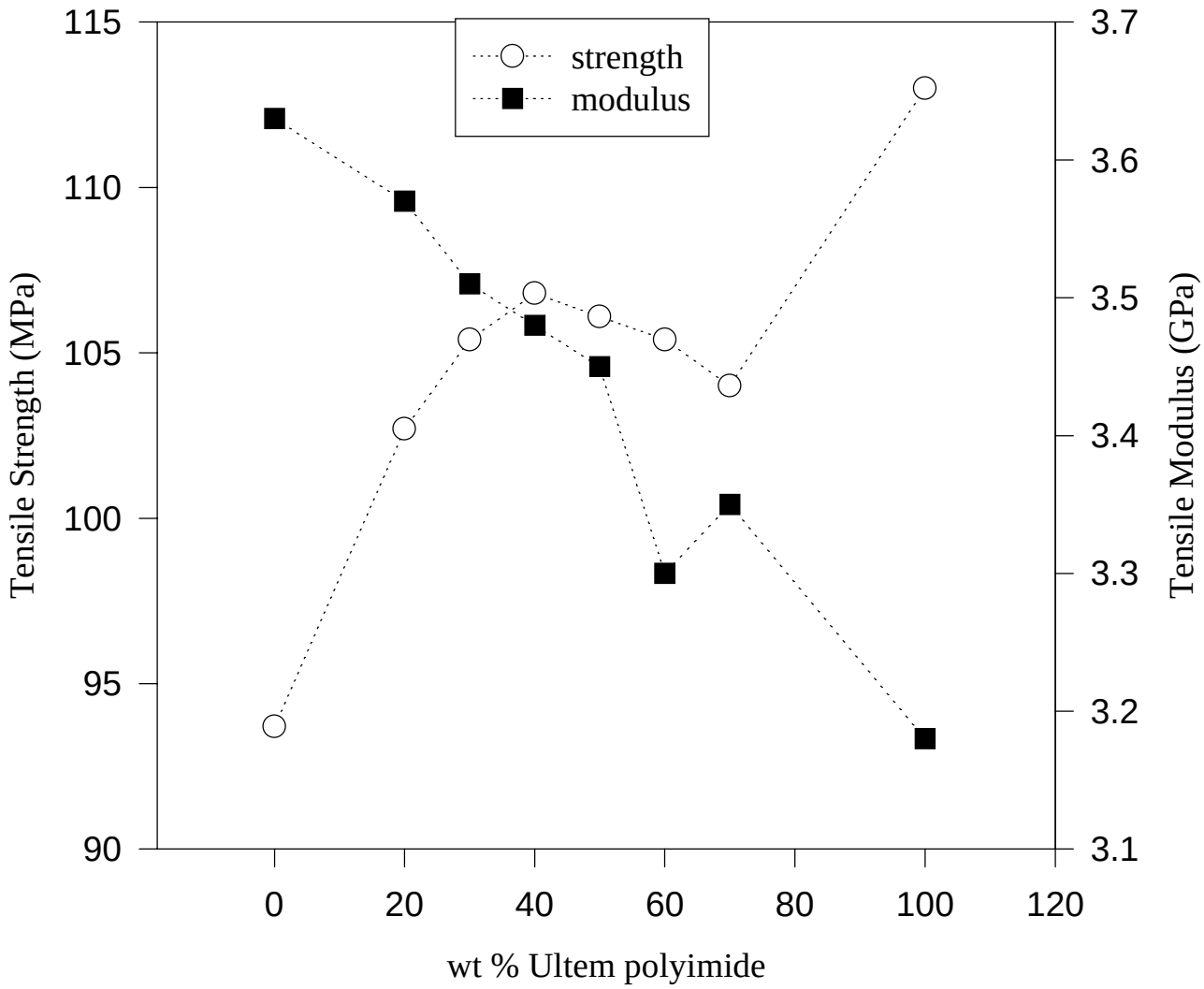

Figure 2-20. Tensile strength and tensile modulus vs. weight percent Ultem polyimide for Ultem/PEEK blends. From Harris and Robeson [147].

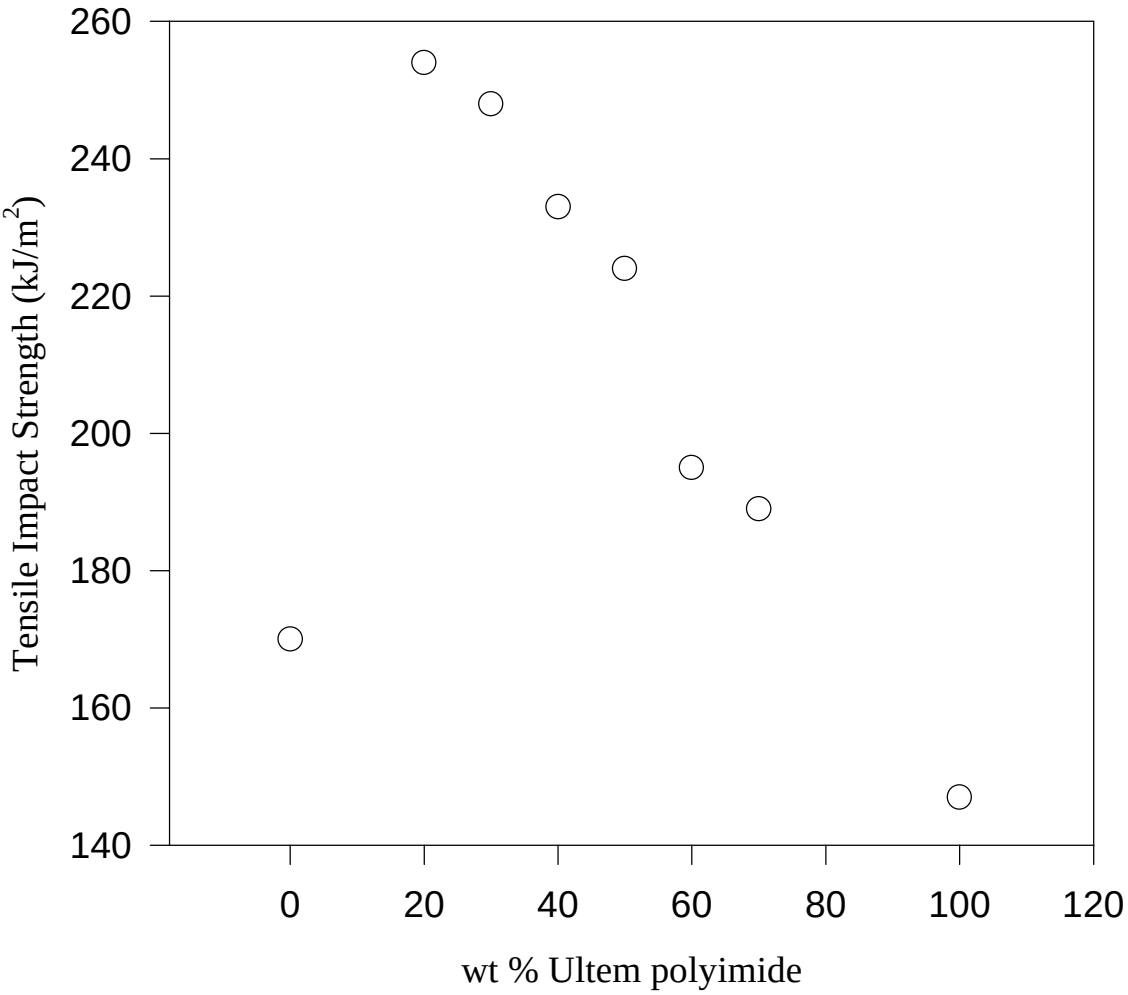

Figure 2-21. Tensile impact strength vs. weight percent Ultem polyimide for Ultem/PEEK blends. From Harris and Robeson [147].

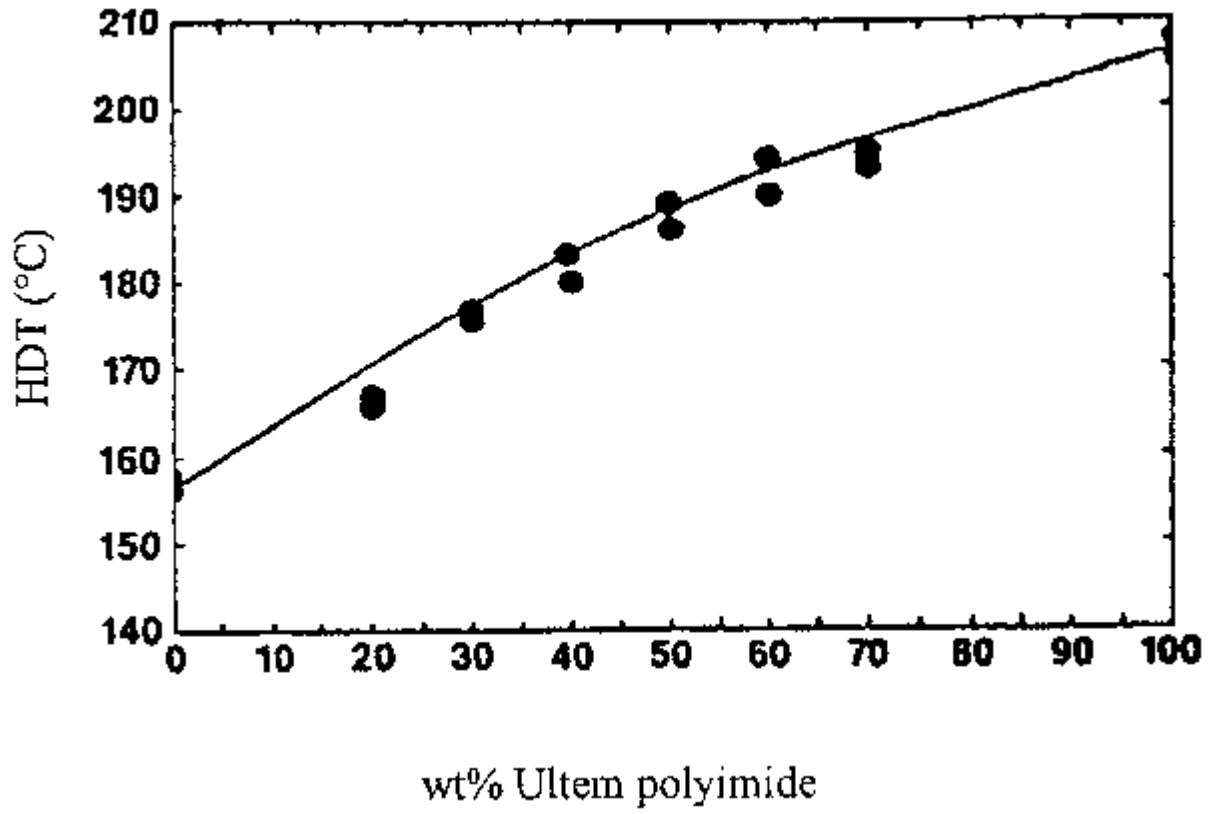

Figure 2-22. Heat deflection temperature (HDT) at 1.8 MPa for compositions of Ultem polyimide/PEEK blends. From Harris and Robeson [147]

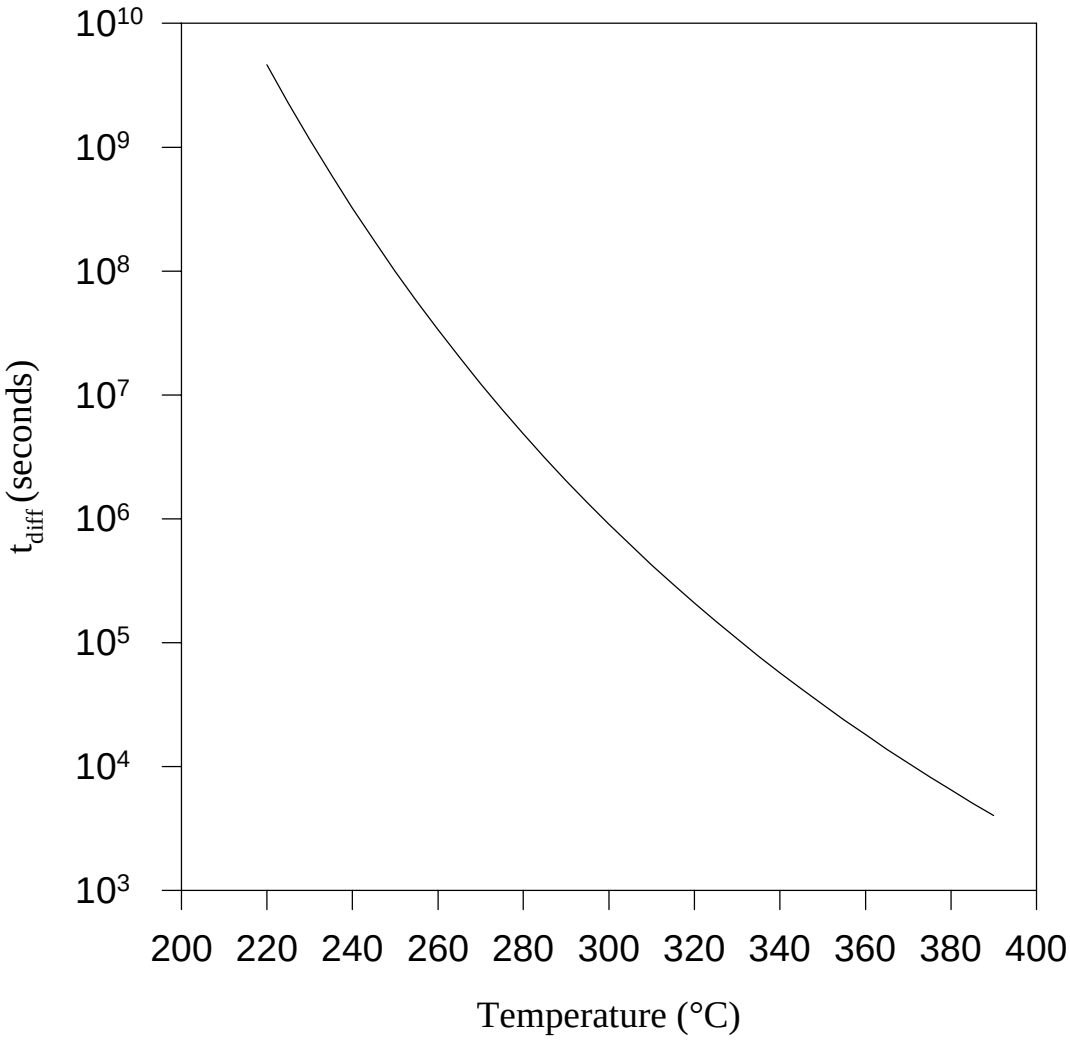

Figure 2-23. Estimated diffusion time for complete interdiffusion across a distance of 10 um for Ultem polyimide and PEEK .

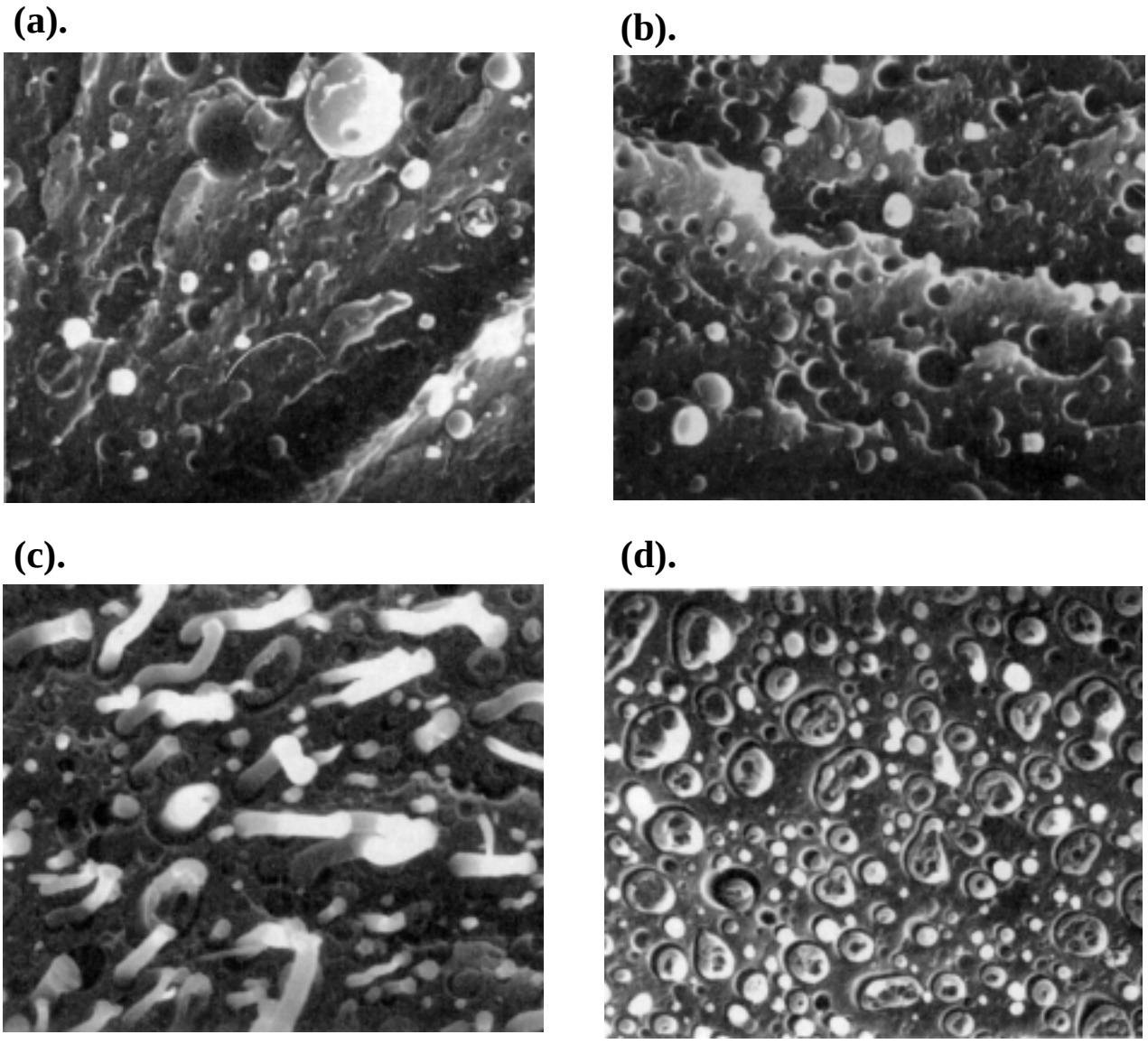

Figure 2-24. Morphology of Ultem polyimide/PPS blends from Akhtar and White [160]:
(a.) 15 wt% Ultem Polyimide, (b.) 20 wt% Ultem polyimide, (c.) and (d.) 50 wt% Ultem polyimide.

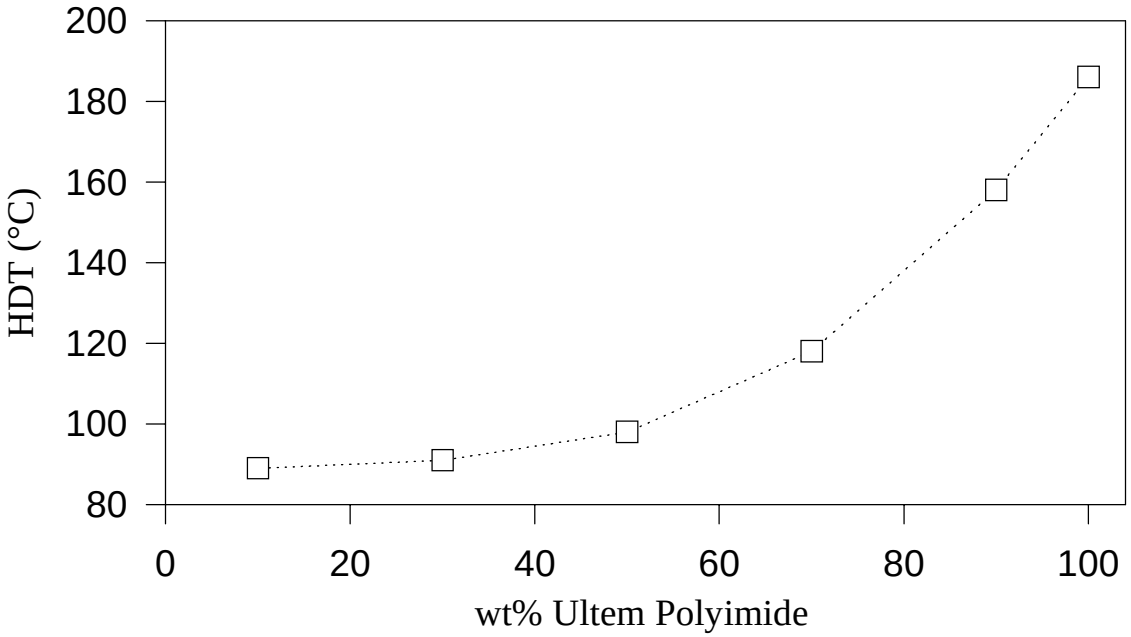

Figure 2-25. Heat deflection temperature (HDT) of Ultem polyimide/PPS blends of varying composition. From Giles [161].

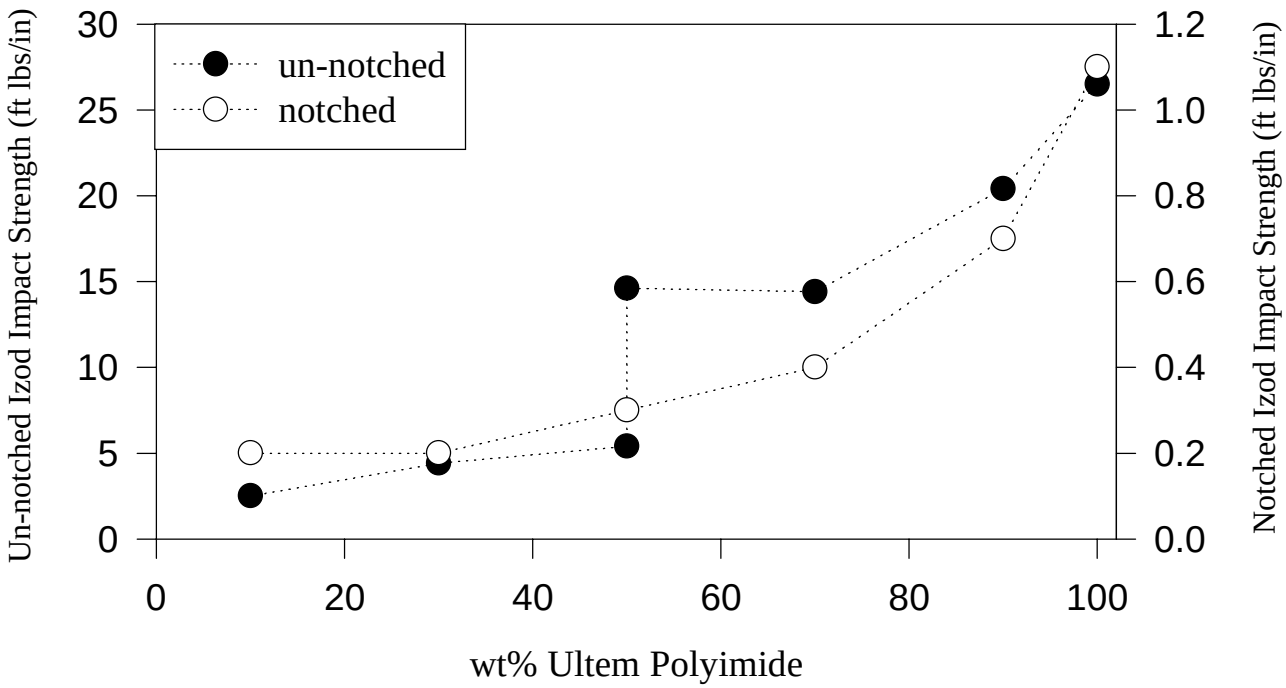

Figure 2-26. Notched and un-notched Izod impact strengths for blends of Ultem polyimide/PPS blends of varying composition from Giles [161].

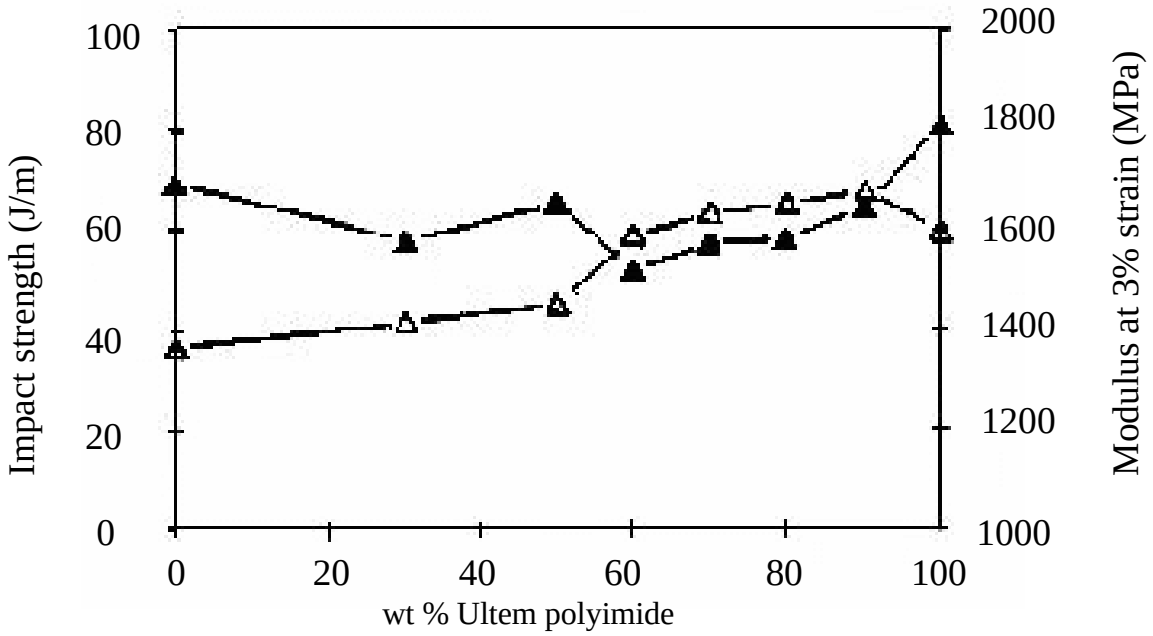

Figure 2-27. Notched Izod impact strength and tensile modulus at 3% strain of Ultem polyimide/PPS blends as measured by Ahktar and White [160].

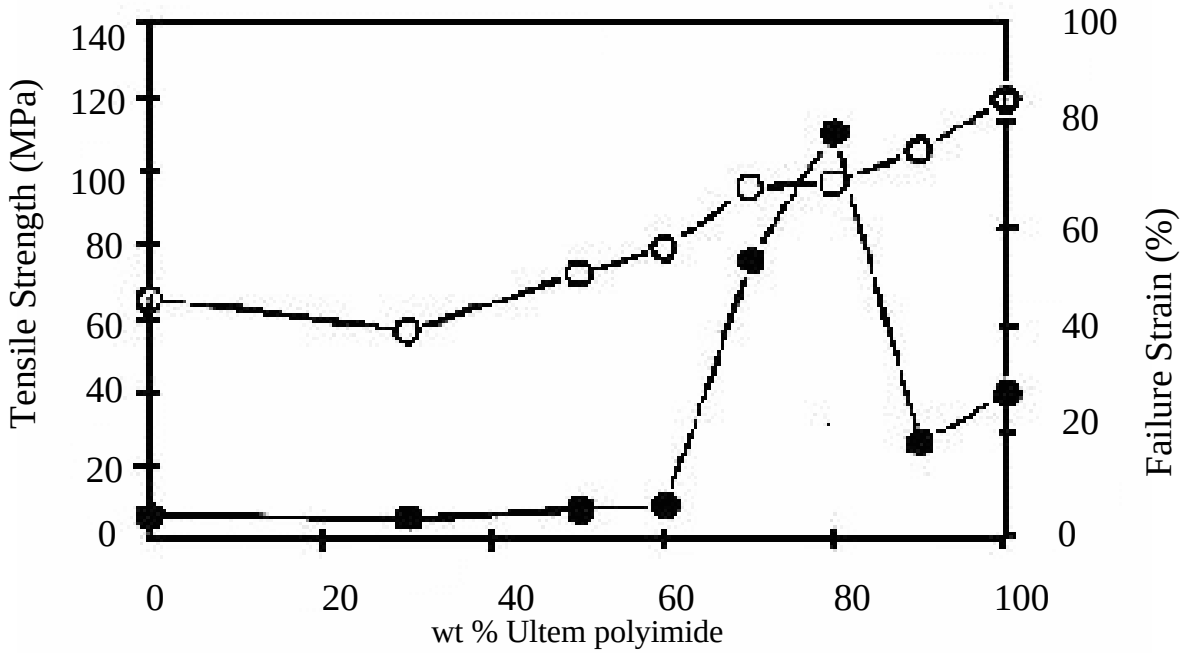

Figure 2-28. Tensile strength and failure strain of Ultem polyimide/PPS blends as measured by Ahktar and White [160].

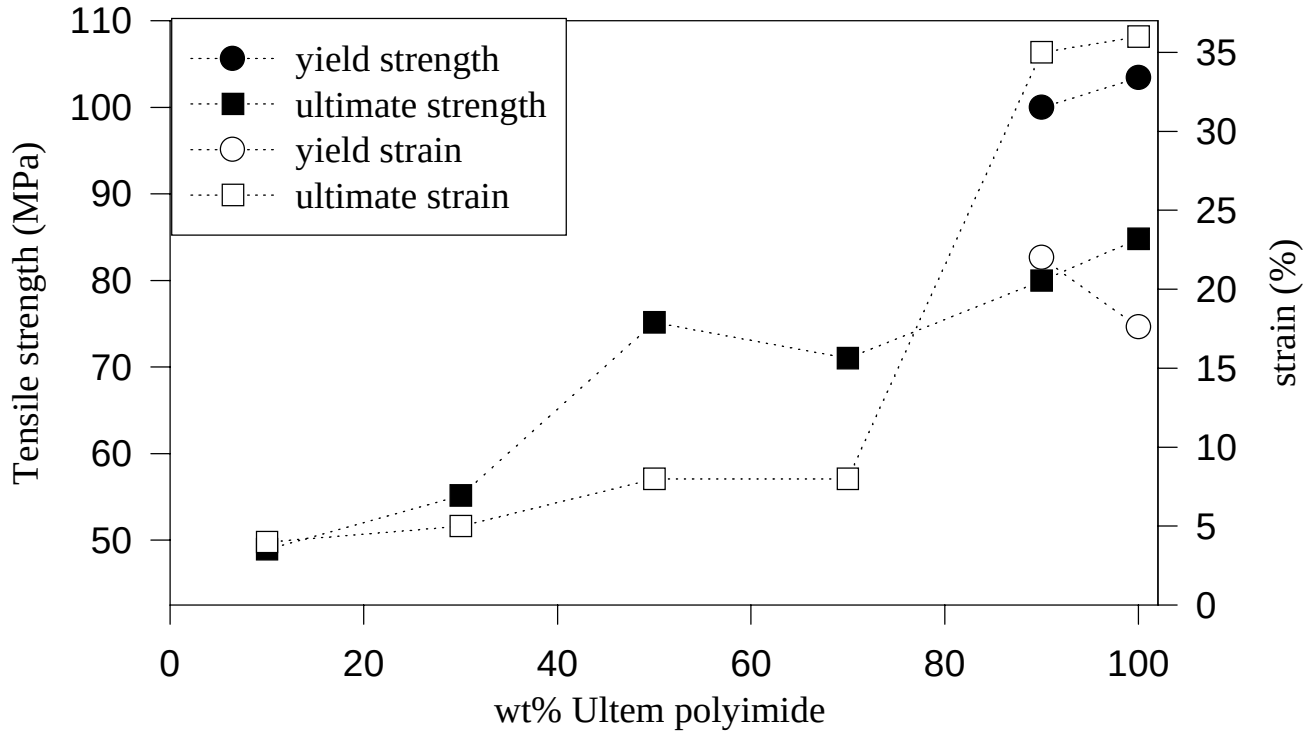

Figure 2-29. Tensile yeild strength, tensile ultimate strength, tensile yield strain and ultimate tensile strain for Ultem polyimide/PPS blends of varying composition. From Giles [161].

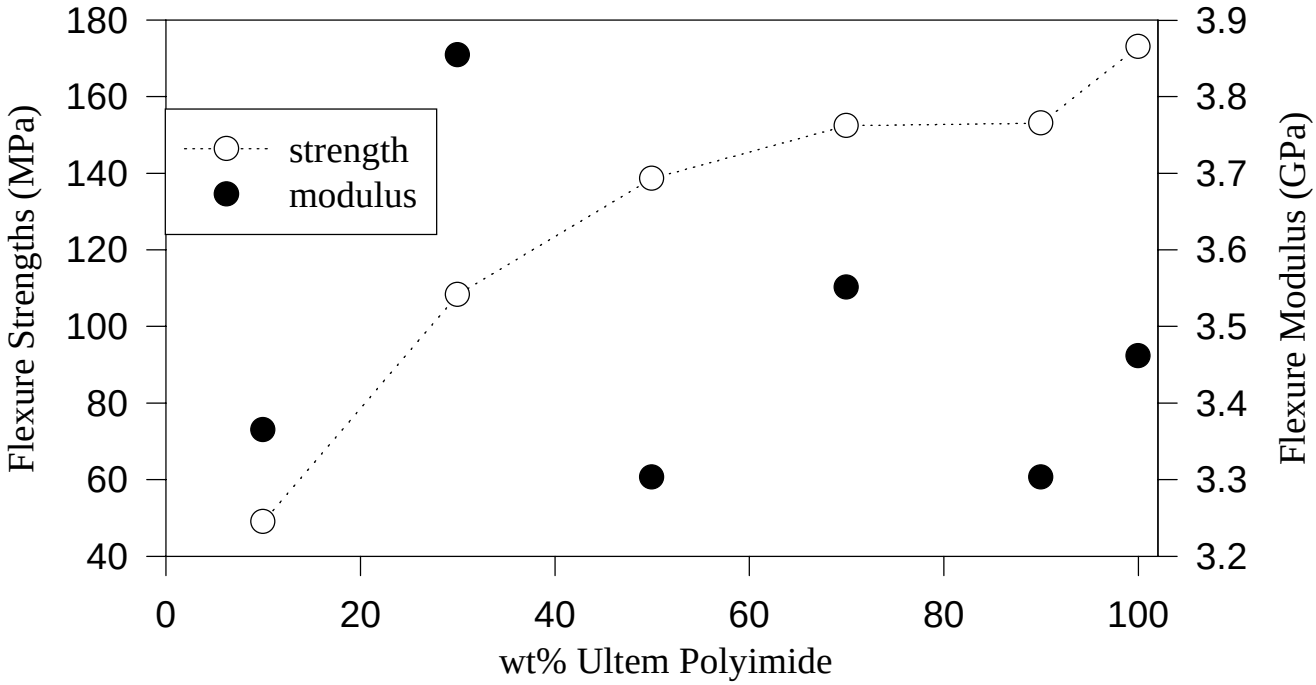

Figure 2-30. Flexure strength and flexure modulus of Ultem polyimide/PPS blends of varying composition. From Giles [161].

Ideal composite geometry

hexagonal packing
uniform fiber spacing
homogeneous
no voids

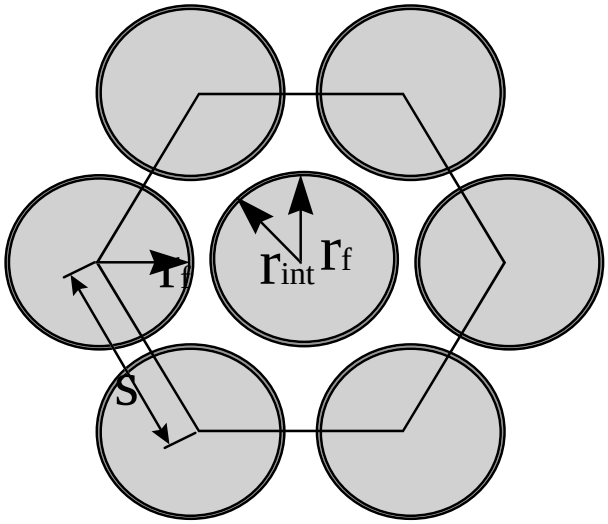

Actual composite cross section

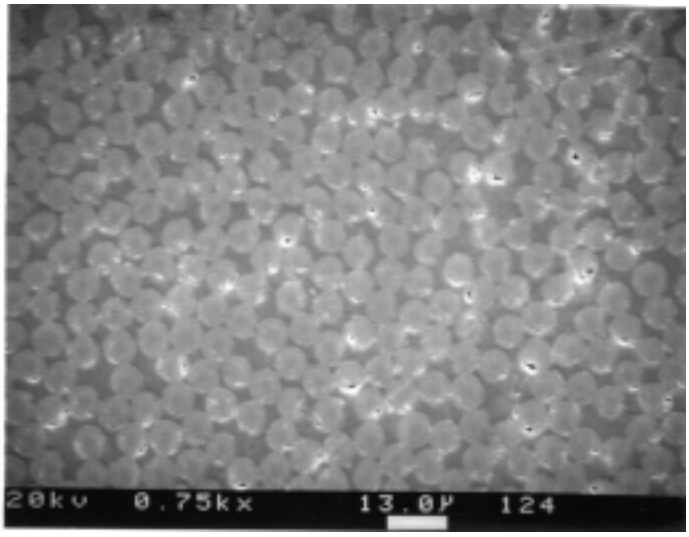

Figure 2-31. Geometry for model composite compared to geometry of actual composite cross section.

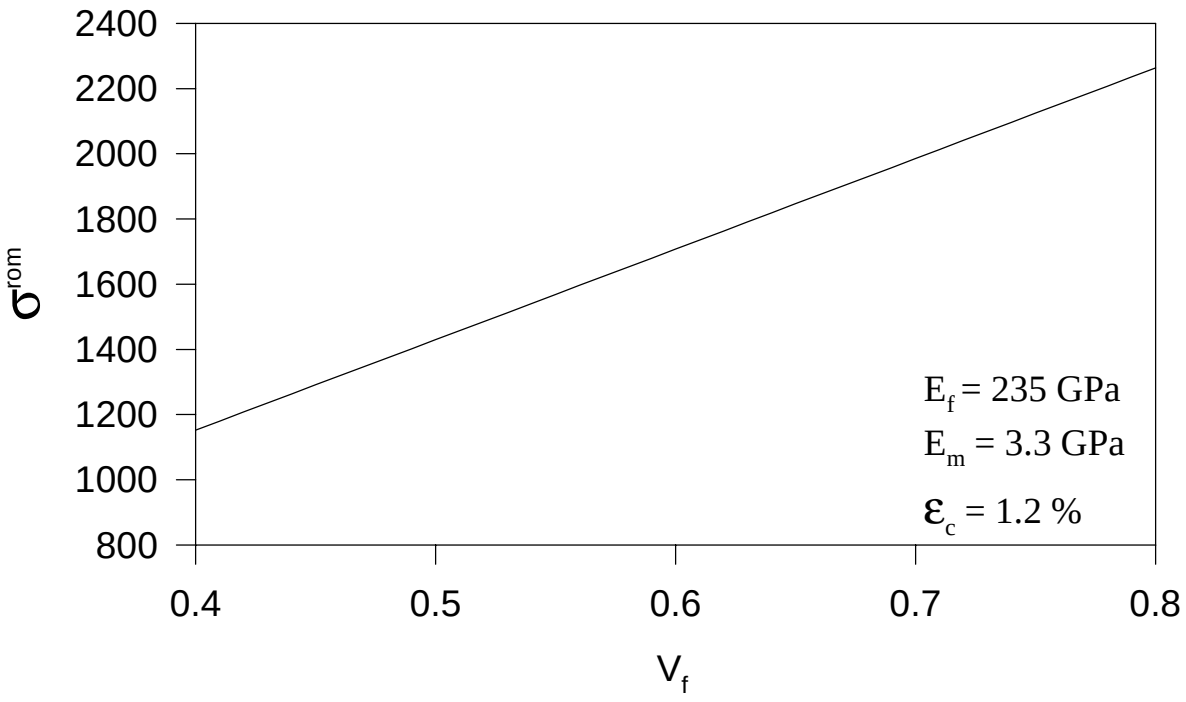

Figure 2-32. σ^{rom} (calculated from Eq. 2-10) vs. fiber volume fraction.

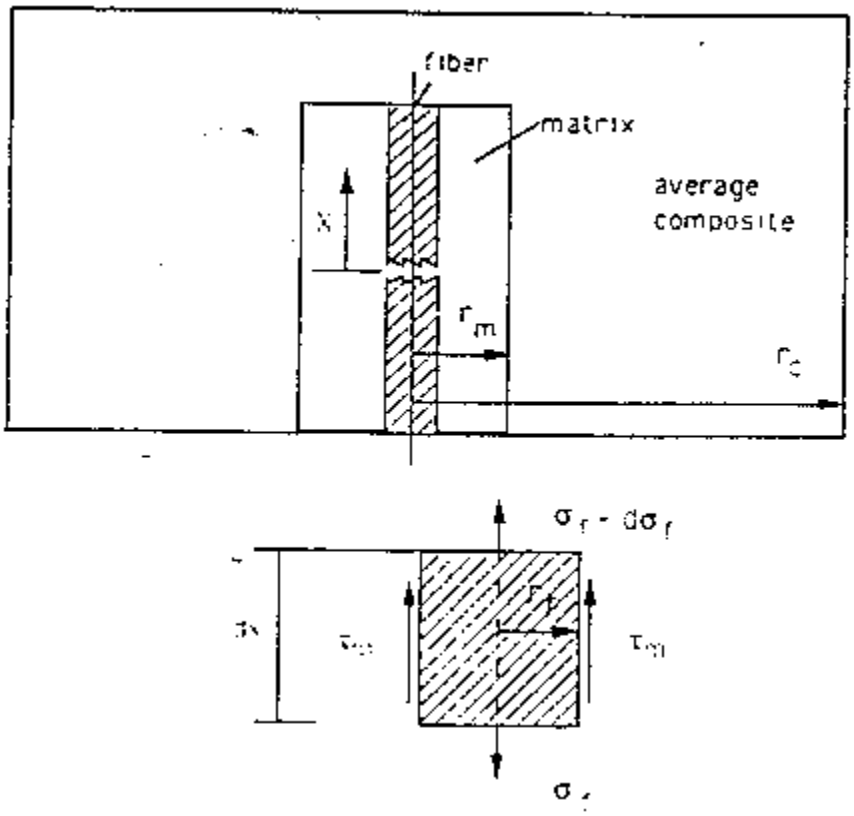

Figure 2-33. Single broken fiber in a continuous matrix surrounded by average composite material and the equilibrium element used in formation of shear lag model. From Gao et al. [176].

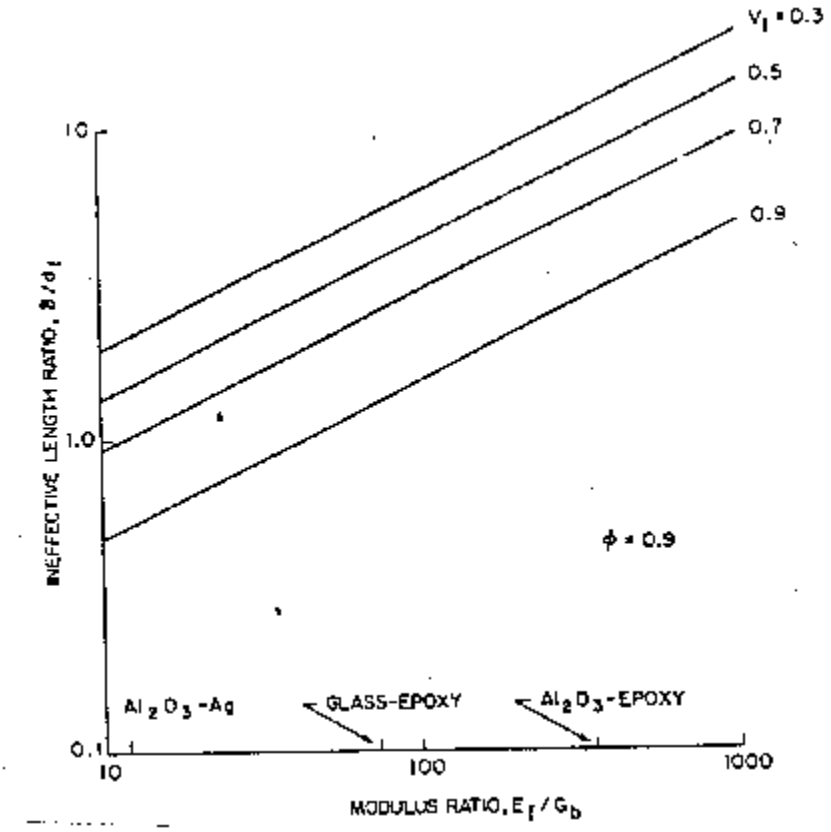

Figure 2-34. Calculated ineffective length ratio vs. ratio of fiber modulus to matrix shear modulus for several fiber volume fractions. From Rosen [173].

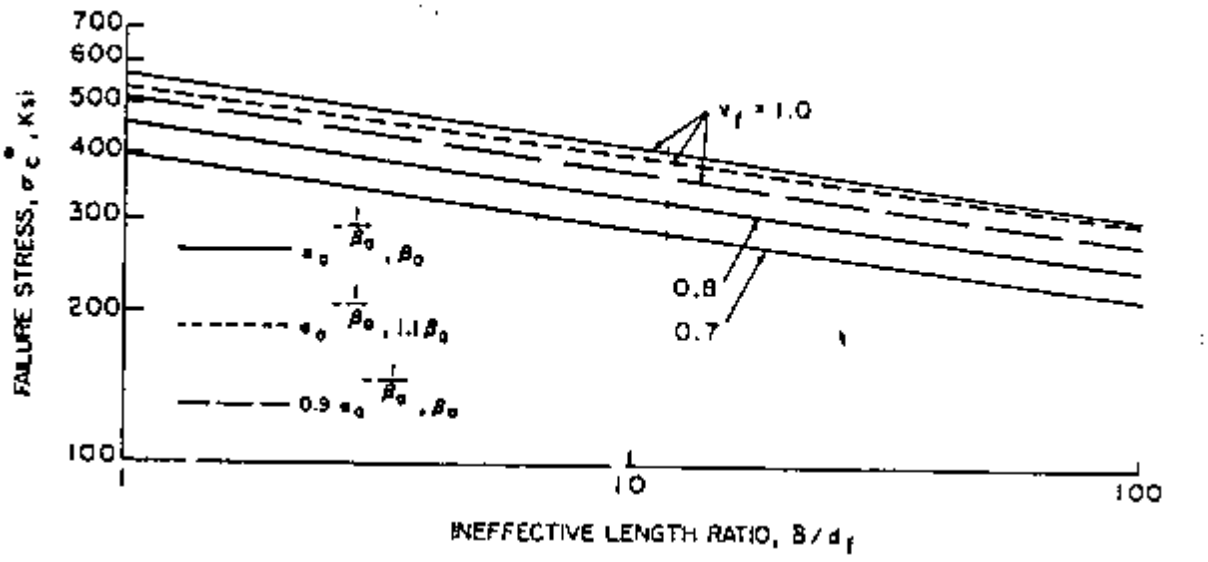

Figure 2-35. Failure stress vs. ineffective length ratio for several fiber volume fractions. From Rosen [173].

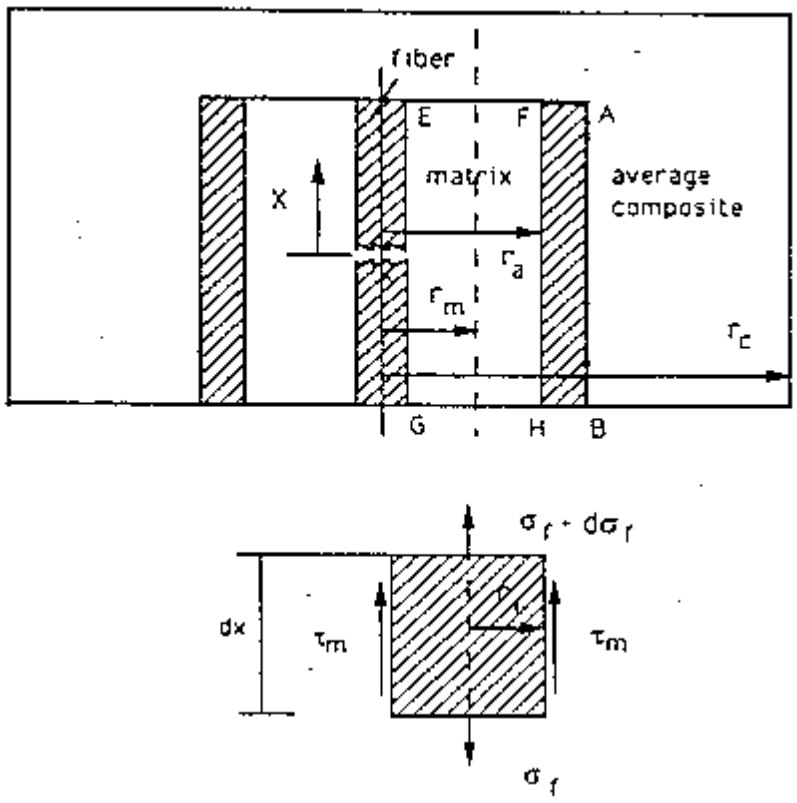

Figure 2-36. A single broken fiber with neighboring unbroken fibers in a continuous matrix surrounded by average composite material and the equilibrium element used in formation of shear lag model. From Gao et al. [176].

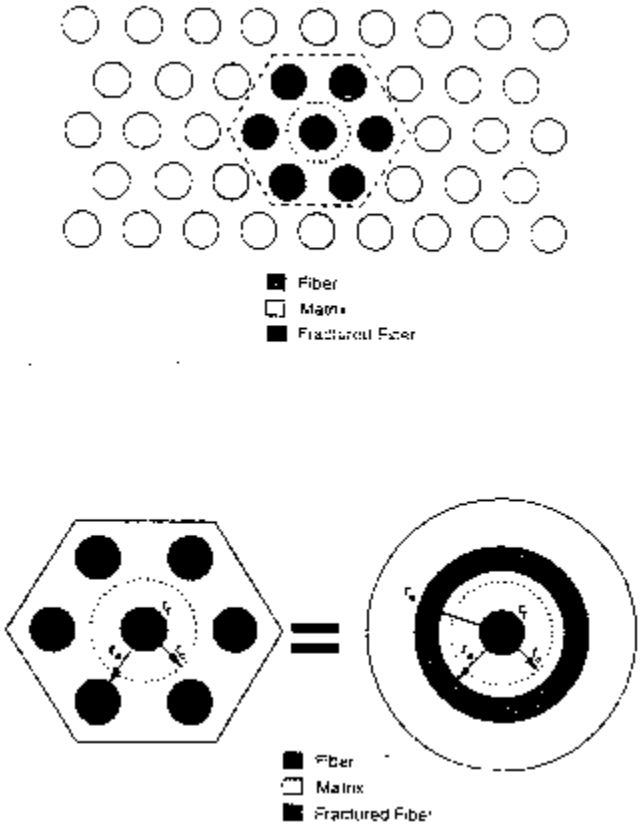

Figure 2-37. Hexagonally packed composite fibers that can be represented by an annular ring of neighboring fibers surrounding a broken, center fiber. From Case et al. [179].

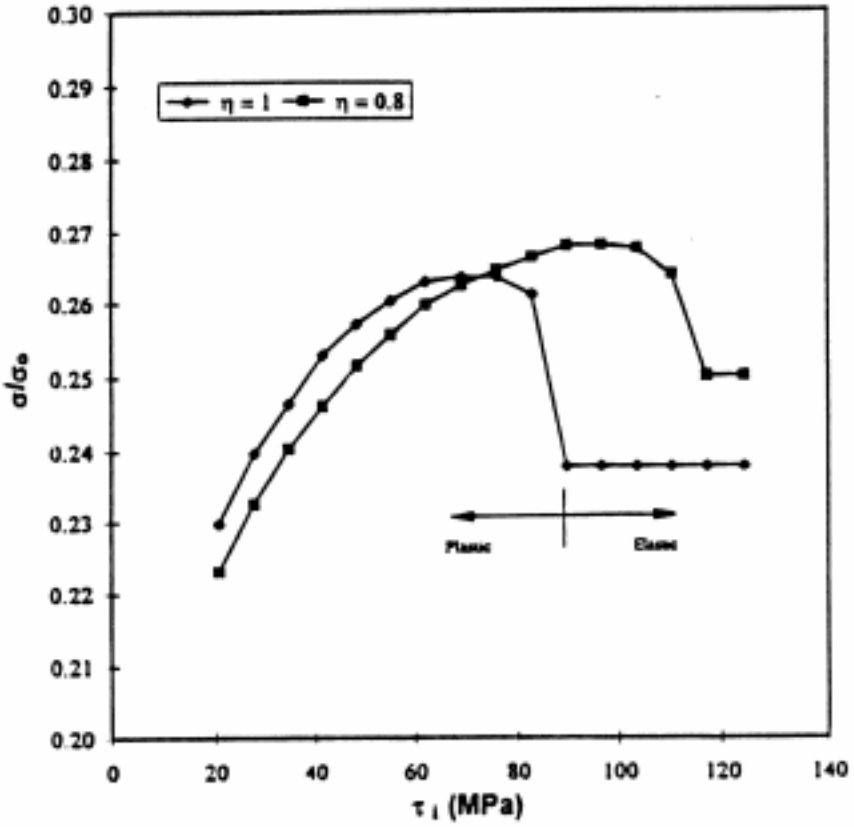

Figure 2-38. Predicted variation of normalized composite tensile strength vs. interfacial shear strength for two different assumed efficiency factors. From Subramanian et. al [169].

References

1 Mittal, K.L., Ed.,Polyimides; Plenum Press, New York, 1984.

2 Bessonov, M.I., Koton, M.M., Kudryavtsev, V.V., and Laius, L.S., Polyimides: Thermally Stable Polymers, Consultants Bureau, New York, 1987.

3 Ferry, J.D.,Viscoelastic Properties of Polymers, 3rd Edition, John Wiley and Sons, New York, 1980.

4 Dealy, J.M. and Wissbrun, K.F., Melt Rheology and Its Role in Plastics Processing, Van Nostrand Reinhold, New York, 1990.

5 Kochi, M. Yokota, R., Iizuka, T., and Mita, I., *Journal of Polymer Science: Part B: Polymer Physics*, **28**, 2463 (1990).

6 Cotts, P.M., Polyimides: Synthesis, Characterization and Applications, K.L. Mittal, Ed., Plenum, New York, 1984, p. 223.

7 Dine-Hart, R.A., and Wright, W.W., *J. Appl. Polym. Sci.*, **11**, 309 (1967).

8 Sroog, C.E., Endrey, A.L., Abramo, s.V., Berr, C.E., Edwards, W.M., and Olivier, K.L., *J. Polym. Sci.:Part A: Polym. Chem.*, **3**, 1373 (1965).

9 Shibaev, L.A., Stepanov, N.G., Kostereva, T.A., Novoselova, A.V., Spirina, T.N., and Sazanov, Y.N., *Journal of Thermal Analysis*, **38**, 1203 (1992).

10 Grenier-Loustalot, M.-F., Gillard, M., Joubert, F., and Grenier, P., *Journal of Polymer Science: Part A: Polymer Chemistry*, **31**, 2839 (1993).

11 Hsu, T.-C.J., and Liu, A.-L., *Journal of Applied Polymer Science*, **46**, 1821 (1992).

12 Cotts, P.M., *J. Polym. Sci.: Part B: Polym. Phys.*, **24**, 923 (1986).

13 Seymour, Raymond, B. Engineering Polymer Sourcebook, McGraw-Hill Publishing Company, New York, 1990.

14 Torlon product data sheet, DuPont Polymers.

15 Ultem data sheet, General Electic.

16 Vespel data sheet, DuPont Polymers.

17 Aurum data sheet, Mitsui Toatsu.

18 Arnold,C.A., PhD Dissertaion, Virginia polytechnic Institute and State University, Blacksburg, VA, (1989).

19 Brink, A.E., Lin, M.C., and Riffle, J.S., *Chem. Mater.*, **5**, 925 (1993).

20 S. Srinivas, M. Graham, M.H. Brink, S. Gardner, R.M. Davis, J.E. McGrath and G.L. Wilkes. *Polym. Eng. and Sci.*, **36,** 1928 (1996).

21 S. Srinivas, F.E. Caputo, M. Graham, S. Gardner, R.M. Davis, J.E. McGrath, and G.L. Wilkes. *Macromolecules*, **30**, 1012 (1997).

22 G.W. Meyer, J.L. Heidbrink, J.G. Franchina, R.M. Davis, S. Gardner, V. Vasudevan, T.E. Glass and J.E. McGrath, *Polymer*, **37**, 5077 (1996).

23 B. Tan, V. Vasudevan, Y.J. Lee, S. Gardner, R.M. Davis, T. Bullions, A.C. Loos, H. Parvatareddy, D.A. Dillard, J.E. McGrath and J. Cella, *J.of Polym. Sci. Part A:Polym. Chem.*, **35**, 2943 (1997).

24 Fowkes, F.M., Tischler, D.O., Wolfe, J.A., Lannigan, L.A., Ademu-John, C.M., and Halliwell, M.J., *J. of Polym. Sci.: Part A: Polym. Chem*., **22**, 547 (1984).

25 Arnold, C.A., Summers, J.D., Chen, Y.P., Bott, R.H., Chen, D., and McGrath, J.E.,

Polymer, **30**, 986 (1989).
26 Endrey, A.L., *US Patent 3,242,136* (1966).
27 J.V. Facinelli, A.E. Brink, S. Liu, H. Li, S. Gardner, R.M. Davis, J.S. Riffle, M. Marrocco, S. Harding. *J. Appl. Polym. Sci.*, **63,** 1571 (1997).
28 Facinelli, J.V., Gardner, S., Dong, L., Sensenich, C.L., Davis, R.M., and Riffle, J.S., *Macromolecules*, **29**, 7342 (1996).
29 Sensenich, C.L., Facinelli, J.V., Dong, L., Gardner, S., R.M. Davis, Riffle, J.S.,*Polymer Preprints, Division of Polymer Chemistry, American Chemical Society*,**37**, 400 (1997).
30 Tamada, T., Yokoyama, S., Kajikawa, K., Ishikawa, K., Takezoe, H., Fukuda, A., Kakimoto, M., and Imai, Y., *Thin Solid Films*, **244**, 754 (1994).
31 Hirano, K., Nishi, Y., Fukuda, H., Kakimoto, M., Imai, Y., Araki, T., and Iriyama, K., *Thin Solid Films*, **244**, 696 (1994).
32 The Effect of Polyimide Interphases on Properties of PEEK-Carbon Fiber Composites. S. Gardner, A. Gonzalez, R.M. Davis, J.V. Facinelli, J.S. Riffle, S. Case, J.J. Lesko, K.L. Reifsnider, *AIChE 1995 Annual Meeting.* November 12-17, 1995. Miami Beach, FL.
33 Yu, T.H. and Davis, R.M., *J. Thermoplast.Comp. Mater.*, **6**, 62 (1993).
34 Texier, A., Davis R.M., Lyon, K.R., Gungor, A., McGrath, J.E., Marand, H., and Riffle, J.S., Polymer, **34**, 896 (1993).
35 Gonzalez, A-I, M.S. Dissertation (Virginia Polytechnic Institute and State University, Blacksburg, VA, November 1992)
36 Gonzalez-Ibarra, A., Davis, R.M., Heisey, C.L., Wightman, J.P., and Lesko, J.J., *Journal of Thermoplastic Composite Materials*, **10**, 85 (1997).
37 Davis, R.M., and Texier, A., *ANTEC '91 Confer. Proceed.*, **37**, 2018 (1991).
38 Chuang, S.L., Chu, N.J., and Whang, W.T., *J. Appl. Polym. Sci*., **31**, 373 (1990).
39 Whang, W-T., and Liu, W-L., *SAMPE Quarterly*, October 1990, 3.
40 St. Clair, T.L., and Progar, D.J., *Journal of Adhesion*, **47**, 67 (1994).
41 Hou, T.H., Bai, J.M., and St. Clair, T.L., *Journal of Applied Polymer Science*, **36**, 321 (1988).
42 Hou, T.H., Bai, J.M., and St. Clair, T.L., *SAMPE Quarterly*, 20, July 1987.
43 Progar, D., St. Clair, T.L., Burks, H., Gautreaux, C., Yamaguchi, A., and Ohta, M., *SAMPE Journal*, 53, January/February 1990.
44 Burks, H.D., St. Clair, T.L., and Gautreaux, C.R., *SAMPE Journal*, **26**, 59 (1990).
45 Hou, T.H., Bai, J.M., *35th International SAMPE Symposium*, 1594, April 2-5, 1990.
46 Progar, D., St. Clair, T.L., Burks, H., Bautreaux, C., Yamaguchi, A., and Ohta, M., *21st International SAMPE Technical Conference*, 544, September 25-28, 1989.
47 Burks, H.D., St. Clair, T.L., and Hou, T.-H., *SAMPE Quarterly*, **18**, 1 (1986).
48 Progar, D.J. and St. Clair, T.L., *NASA technical Memorandum 102586,*, LARC-1A: A Flexible Backbone Polymer (1990).
49 Pratt, J.R. and St. Clair, T.L., *SAMPE Journal*, **26**, 29 (1990).
50 Hou, T.H., Wakelyn, N.T. and St. Clair, T.L., *Journal of Applied Polymer Science*, **36**, 1731 (1988).
51 Harris, F.W., Beltz, M.W., and Hergenrother, P.M., *NASA Technical Support Brief LAR-*

13675, "Readily Processable Polyimide".
52 Bowles, K.J., *SAMPE Quarterly*, 6, July, 1990.
53 Hartness, T., Porter, D., and Reardon, J.P., *34th International SAMPE Symposium*, 211, May 8-11, 1989.
54 Kantz, M., *Plastics Engineering*, 27, January, 1990.
55 Bowles, K.J., *SAMPE Quarterly*, 6, July, 1990.
56 Nagumo, T., Nakamura, H., Hakakura, T., and Sakai, H., 1304, *Proc. 1st Japan International SAMPE Symposium*, Nov 28-Dec 1., 1989.
57 Moyer, D.J.D., and Wightman, J.P., *Proceedings of the American Society for Composites Seventh Technical Conference : composite materials, mechanics, and processing*: October 13-15, 1992, Keller Conference Center, Lancaster, PA.
58 Gan, S., Sereris, J.C., and Gibbs, H.H., *Proceedings of the American Society for Composites Seventh Technical Conference : composite materials, mechanics, and processing* : October 13-15, 1992, Keller Conference Center, Lancaster, Pa.
59 Jeng, J.S., Ono, K., and Yang, J.M., *World Meeting on Acoustic Emission*, S268.
60 Chenock, T.A., and Aglan, H., 27, *SAMPE Quarterly*, July, 1990.
61 McConnel, V.P., *High Performance Composites:Sourcebook 1998*, **5**, 26 (1997).
62 Johnston, N.J., St. Clair, T.L., and Baucom, R.M., Polyimide Matrix Composites: Polyimidesulfone/:aRC-TPI (1:1) Blend, *24th International SAMPE Symposium and Exhibition*, Reno, NV, May 8-11, 1989.
63 Johnston, N.J. and St. Clair, T.L., *SAMPE Journal*, **23**, 12 (1987).
64 Johnston, N.J. and St. Clair, T.L., *SAMPE Preprints*, **18**, 53 (1986).
65 Texier, A., Davis R.M., Lyon, K.R., Gungor, A., McGrath, J.E., Marand, H., and Riffle, J.S., *Polymer*, **34**, 896 (1993).
66 Varughese, B., Muzzy, J., and Baucom, R.M., *21st Intern. SAMPE Tech. Confer.*, Sept. 25-28, 1989.
67 Bower, G.M., and Frost, L.W., *J. Polym. Sci.*, **A1**, 3135 (1963).
68 Frost, L.W., and Kesse, I., *J. Appl. Polym. Sci.*, **8**, 1039 (1964).
69 Ahne, H. Domke, W.-D., Rubner, R., and Schreyer, M., Chapter 39., Polymers for High Technology, 457 (1987).
70 Orwoll, R.A., St. Clair, T.L., and Dobbs, K.D., *J. Polym. Sci.:Part B: Polym. Phys.*, **19** (1981).
71 Palmese, G.R., and Gillham, J.K., *Journal of Applied Polymer Science*, **34**, 1925 (1987).
72 Clemenson, P.I., Pandiman, D., Pearson, J.T., and Lavery, A.J., *Polymer Engineering and Science*, **37**, 966 (1997).
73 Gregor, H.P., and Gregor, J.M., *J. Of Chem. Phys.*, **66**, 1934 (1977).
74 Gregor, H.P., and Greff, R.J., *J. Chem. Phys.*, **67**, 5742 (1977).
75 Kielland, J., *J. of American Chem. Soc.*, **59**, 1675 (1937).
76 Cella, J. A., *Polymer Degradation and Stability* **36**, 99 (1992).
77 Bell, V.L., *Journal of Polymer Science*, **14**, 225 (1976).
78 Bell, V.L., *Journal of Polymer Science*, **14**, 2275 (1976).
79 Pryde, C.A., *J.of Appl.Polym. Sci.: Part A: Polymer Chemistry*, **27**, 711 (1989).
80 McGrath, J.E., Rogers, M.E., Arnold, C.A., Kim, Y.J. and Hedrick, J.C., *Makromol.*

Chem., Macromol. Symp., **51**, 103 (1991).
81 Kim, Y.J., Glass, T.E., Lyle, G.D., and McGrath, J.E., *Macromolecules*, **26**, 1344 (1993).
82 Widmaier, J.M., Eouriaghli, T.E., Leger, L., and Marmonier, M.F., *Polymer*, **30**, 549 (1989).
83 Pike, R.A., Polyimides: Synthesis, Characterization and Applications, K.L. Mittal, Ed., Plenum, New York, 1984, p. 15.
84 Progar, D.J., and Pike, R.A., *Int. J. Adhesion and Adhesives*, **8**, 25 (1988).
85 Hermans, P.H., and Streef, J.W., *Die Makromol. Chemie.* **74**, 133 (1964).
86 Vincent, G.G., Anderson, T.E., *US Patent 3,652,511* (1972).
87 Stoakley, D.M., St. Clair, A.K., and Baucom, R.M., *SAMPE Quarterly*, October (1989).
88 Qiu, W., Li, C., Zeng, W., Liu, J., Lu, L., and Wang, X., *Journal of Applied Polymer Science*, **56**, 1295 (1995).
89 Rao, V.L., and Bijimol, J., *Makromol. Chem.*, **192**, 1025 (1991).
90 Chen, K.M., Wnat, T.H., King, J.S., and Hung, A., *J. Appl. Polym. Sci.*, **48**, 291 (1993).
91 Lee, H. And Lee, Y., *J. of Appl. Polym. Sci.*, Johnston, N.J., St. Clair, T.L., **40**, 2087 (1990).
92 Jonas, A., and Legras, R., *Advanced Thermoplastic Composites, Characterization, Processing; Chapter 2*, Hanser Pub., 57 (1993).
93 Wei-Berk, C. and Berry, G.C., *J.Polym. Sci.:Part B: Polym. Phys.*, **28**, 1873 (1990).
94 Bishop, M.T., Karasz, F.E., Russo, P.S., and Langley, K.H., *Macromolecules*, **18**, 86 (1985).
95 Wang, F., Roovers, J., and Toporowski, P.M., *Macromolecules*, **26**, 3826 (1993).
96 Roovers, J., Cooney, J.D., and Toporowski, P.M., *Macromolecules*, **23**, 1611 (1990).
97 Nguyen, H.X., and Ishida, H., *Polymer Composites*, **8**, 57 (1987).
98 Ogale, A.A., and McCullough, R.L., *Comp. Sci. & Tech.*, **30**, 137 (1987).
99 Lovinger, A.J., and Davis, D.D., *Journal of Applied Physics*, **58**, 2843 (1985).
100 Lovinger, A.J., Hudson, S.D., and Davis, D.D., *Macromolecules*, **25**, 1752 (1992).
101 D'Amore, A., Cocchini, F., Pompo, A., Apicella, A., and Nicolais, L., *J. Appl. Polym. Sci.*, **39**, 1163 (1990).
102 Lee, Y., and Porter, R.S., *Macromolecules*, **20**, 1336 (1987).
103 Bassett, D.C., Olley, R.H., and Al Raheil, I.A.M., *Polymer*, **29**, 1745 (1988).
104 Day, M., Sally, D., and Wiles, D.M., *J.of Appl. Polym. Sci.*, **40**, 1615 (1990).
105 ICI Fiberite APC-2 product data sheet.
106 Denault, J., and Vu-Khanh, T., *Polym. Compos.*, **13**, 361 (1992).
107 Denault, J., and Vu-Khanh, T., *Journal of Thermoplastic Composite Materials*, **6**, 190 (1993).
108 Bucher, R.A., PhD Dissertaion, Virginia polytechnic Institute and State University, Blacksburg, VA, (1994).
109 Muzzy, J., Varughese, B., Thammongkol, V., and Tincher, W., *SAMPE Journal*, **25**, 15 (1989).
110 Muzzy, J., *U.S. Patent #5,094,883*, March 10, 1992.
111 Advanced Thermoplastic Composites, Ed. H.H. Kausch, Hanser Publishers, New York,

1993.
112 Lee, Y., Lee, E.H., and Mansur, L.K., *Surface and Coatings Technology*, **51**, 267 (1992).
113 Yar, P.-J., Cantwell, W.J., and Kausch, H.H., *Composites Science and Technology*, **43**, 299 (1992).
114 Olley, R.H., Bassett, D.C., and Blundell, D.J., *Polymer*, **27**, 344 (1986).
115 Blundell, D.J., Crick, R.A., Fife, B., Peacock, J., Keller, A., and Waddon, A., *J. Mater. Sci*., **24**, 2057 (1988).
116 Blundell, D.J., Chalmers, J.M., MacKenzie, M.W., and Gaskin, W.F., *SAMPE Quarterly*, **16**, 22 (1985).
117 Lee, Y., and Porter, R.S., *Polym. Eng. & Sci.*, **26**, 633 (1986).
118 Davies, P., Cantwell, W.J., Jar, P.-Y., Richard, H., Neville, D.J., and Kausch, H.H., *Compos. Materials: Fatigue and Fracture (Third Volume)*, T.K. O'Brien, Ed., American Society for Testing and Materials, Philadelphia, 1991, pp 70-88.
119 D'Amore, A., Pompo, A., and Nicolais, L., *Compos. Sci. & Tech.*, **41**, 303 (1991).
120 personal consultation with Professor K.L. Reifsnider
121 Peacock, J.A., Fife, B., Nield, E., and Crick, R.A., *International Conf. on Compos. Interfaces*, Cleveland, OH, May 27-30 (1986).
122 Geibel, J., and Leland, J., Encyclopedia of Chemical Technology, 4th Edition, **vol. 19**, John Wiley & Sons, pp 904-933, 1996.
123 Lopez, L.C. and Wilkes, G.W., *JMS-Rev. Mocromol. Chem. Phys*., **C29**, 83 (1989).
124 Stevens, T., *Materials Engineering*, **107**, 26 (1990).
125 Davies, P. And Plummer, Ch.J.G., *Advanced Thermoplastic Composites, Characterization,Processing; Chapter 5*, Hanser Pub., 141 (1993).
126 Ma, C.C.M., O'Connor, J.E., and Lou, A.Y., *SAMPE Q.*, **15**(7), 12 (1984).
127 Jones, R.V., and Hill, H.W. Jr., *Adv. Chem. Ser.*, **140**, 174 (1975).
128 Ma, C.C.M., Hsiue, L.-T., Wu, W.-G., and Liu, W.-L., *J. Appl. Polym. Sci.*, **39**, 1399 (1990).
129 Ma, C.C.M., Hsia, H.-C., Liu, W.-L., and Hu, J.-T., *Polym. Compos.*, **8**, 256 (1987).
130 Kraus, G., and Whitte, W.M., *Proceedings from the 28th Macromolecular Symposium of the IUPAC*, Amherst, MA, July 12, 1982.
131 Brady, D.G., *J. Appl. Polym. Sci.*, **20**, 2541 (1976).
132 Lovinger, A.J., Davis, D.D., and Padden, F.J., *Polymer*, **26**, 1595 (1985).
133 Lopez, L.C. and Wilkes, G.W., *Polymer*, **30**, 882 (1989).
134 Lopez, L.C., Wilkes, G.W., and Geibel, J.J., *Polymer*, **30**, 147 (1989).
135 Lopez, L.C. and Wilkes, G.W., *Polymer*, **29**, 106 (1988).
136 Chung, J.S., and Cebe, P., *Polymer*, **33**, 2312 (1992).
137 Chung, J.S., and Cebe, P., *Polymer*, **33**, 2325 (1992).
138 O'Connor, J.E., Beever, W.H., and Geibel, J.F., *31st International SAMPE Symposium*, April 7-10, 1986, 1313.
139 Lee, T.H., Boey, F.Y.C., and Khor, K.A., *Polym. Compos.*, **16**, 481 (1995).
140 Mehl, N.A., and Rebenfeld, L., *J. Appl. Polym. Sci.*, **57**, 187 (1995).
141 Desio, G.P., and Rebenfeld, L., *J. Appl. Polym. Sci.*, **44**, 1989 (1992).
142 Desio, G.P., and Rebenfeld, L., *J. Appl. Polym. Sci.*, **45**, 2005 (1992).

143 Desio, G.P., and Rebenfeld, L., *J. Appl. Polym. Sci.*, **39**, 825 (1990).
144 Neyman, G., Lando, J.B., and Ishida, H., *Composite Interfaces*, **2**, 351 (1994).
145 Blundell, D.J. and Osborn, B.N., *Polymer*, **24**, 953 (1983).
146 Harris, J.M, and Robeson, L.M., *J. Polym. Sci.: Part B: Polym. Phys.*, **25**, 311 (1987).
147 Harris, J.M., and Robeson, L.M., *J. Appl. Polym. Sci.*, **35**, 1877 (1988).
148 Harris, J.M., *ACS Polymer Preprint*, **28**, 56 (1987).
149 Bastien, L.J., and Gillespie, J.W., *Polymer Engineering and Science*, **24**, 1720 (1991).
150 Karcha, R.J., and Porter, R.S., *Journal of Polymer Science: Part B: Polymer Physics*, **31**, 821 (1993).
151 Karcha, R.J., and Porter, R.S., *Journal of Polymer Science: Part B: Polymer Physics*, **27**, 2153 (1989).
152 Olabissi, O., Mobeson, L.M., and Shaw, M.T., *Polymer-Polymer Miscibility*, Academic Press, New York, 1979.
153 Krause, S., *Polymer Blends, Volume 1., Chapter 2,* Ed. D.R. Paul and S. Newman, Academic Press, New York, 15 (1978).
154 Hsaio, B.S., Sauer, B.B., *Journal of Polymer Science: Part B: Polymer Physics*, **31**, 901 (1993).
155 Hsaio, B.S., Sauer, B.B., *Journal of Polymer Science: Part B: Polymer Physics*, **31**, 917 (1993).
156 Hudson, S.D., Davis, D.D., Lovinger, A.J., *Macromolecules*, **25**, 1759 (1992).
157 Crevecoeur, G., and Groeninckx, G., *Macromolecules*, **24**, 1190 (1991).
158 Goodwin, A.A., and Simon, G.P., *Polymer*, **37**, 991 (1996).
159 Riew, C.K. (Ed.), *Rubber-Toughened Plastics*, American Chemical Society, Washington DC, 1989.
160 Akhtar, S., and White, J.L., *Polymer Engineering and Science*, **31**, 84 (1991).
161 Giles, H.F., *U.S. Patent 4,455,410.*, June 19, 1984.
162 Drzal, L.T. and Madhukar, M., *Journal of Material Science*, **28**, 569 (1993).
163 Reifsnider, K.L., *Composites*, **25**, 461 (1994).
164 Cagliostro, D.E., *Polym. Eng. & Sci.*, **28**, 562 (1988).
165 Pangelinan, A.B., McCullough, R.L., and Kelley, M.J., *J. Polym. Sci:Part B:Polym. Phys.*, **32**, 2383 (1994).
166 Palmese, G.R., and McCullough, R.L., *Journal of Adhesion*, **44**, 29 (1994).
167 Jabbari, E., and Peppas, N.A., *Polymer*, **36**, 575 (1995).
168 Jordan, E.A., Ball, R.C., Donald, A.M., Fetters, L.J., Jones, R.A.L., and Klein, J., *Macromolecules*, **21**, 235 (1988).
169 Subramanian, S., Lesko, J.J., Reifsnider, K.L., and Stinchcomb, W.W., *J. Compos. Mater.*, **30**, 309 (1996).
170 Adams, D.F., King, T.R., and Blackketter, D.M., *Composites Science and Technology*, **39**, 341 (1990).
171 Chang, Y.S, Lesko, J.J., Case, S.W., Dillard, D.D., and Reifsnider, K.L., *Journal of Thermoplastic Composite Materials*, **7**, 311 (1994).
172 Agarwal and Broutman, "Analysis and Performance of Fiber Composites",
173 Rosen, B.W. *AIAA Journal*, **2** (1964) 1985.

174 Whitney, J.M., and Drzal, L.T., *Toughened Composites, ASTM STP 937,* N. Johnston, Ed., American Society for Testing and Materials, Philadelphia, PA, p. 179, 1987.
175 Hedgepeth, J.M., and Van Dyke, P., *J. Compos. Mater.*, **1**, 294 (1967).
176 Gao, Z., Reifsnider, K.L., and Carman, G., *J. Compos. Mater.,* **26**, 1678 (1992).
177 Carman, G.P., Lesko, J.J., and Reifsnider, K.L., *Composite Materials: Fatigue and Fracture, Fourth Volume, ASTM STP 1156,* W.W. Stinchcomb and N.E. Ashbaugh, Eds., American Society for Testing and Materials, Philadelphia, PA, p. 430, 1993.
178 Case, S.W.*PhD Dissertation* (Virginia Polytechnic Institute and State University, Blacksburg, VA, May 1996).
179 Case, S.W., Carman, G.P., Lesko, J.J., Fajardo, A.B., and Reifsnider, K.L., *J. Compos. Mater.*, **29**, 208 (1995).
180 Jenkins, S.D., Emmerson, G.T., McGrail, P.T., and Robinson, R.M., *Journal of Adhesion*, **45**, 15 (1994).
181 Subramanian, S., Reifsnider, K.L., and Stinchcomb, W.W., *Journal of Composites Technology & Research*, **17**, 289 (1995).
182 Miller, A., Wei, C., and Gibson, A.G., *Composites, Part A*, **27A**, 49 (1995).
183 Baxandall, L.G., *Macromolecules*, **22**, 1982 (1989).
184 Reynolds, R.J.W., and Seddon, J.D., *J. Polym. Sci., Pt. C.*, **23**, 45 (1968).
185 ICI Victrex PEEK product data sheet.
186 personal communication with ICI Victrex technical service.
187 Liang, K., Grebowicz, J., Valles, E., Karasz, R.E., and MacKnight, W.J., *J. Appl. Polym. Sci., Part B, Polym. Phys.*, **30**, 465, (1994).
188 personal consultation with J. Geibel., Phillips Petroleum Chemical Division.

Chapter Three: Structure-Property Relationships of Model Interphase Ultem-type Polyimides Made from Water Soluble Precursors and Model Matrix PEEK/Polyimide Blends Made From Aqueous Suspension

Introduction

The effects of interphase modifications to improve composite performance and durability are important topics in the composite industry. In order to better understand the micro-mechanics of failure of interphase composites, mathematical models which incorporate an interphase region with significantly different material properties from the matrix polymer have been developed by Reifsnider et al. [1-7]. To make use of these models, information regarding the material properties of the interphase region and of the bulk matrix is required [2].

Carbon fiber, polyether ether ketone (PEEK) matrix composites with an Ultem-type polyimide interphase have been fabricated and tested in Chapter Four of this thesis. The composites were fabricated using the aqueous suspension prepregging technique which provides the application of the interphase polymer at the same time as the matrix polymer. Aqueous suspension prepregging has been done by many researchers using a polyimide precursor, a polyamic acid salt, which is dissolved in water, and neutralized with a base [8-13]. The matrix polymer powder is dispersed in the aqueous polyamic acid salt solution. The polyamic acid salt behaves as a stabilizer, adsorbing to the surface of the matrix powder particles, and electrostatically stabilizing the suspension. The fiber tow is then coated with the polyimide precursor and the matrix powder in a single prepregging step. The polyamic acid salt also serves as a binder, adhering the matrix powder to the carbon tow. After drying the water from the prepreg, a heating cycle is used to convert the polyamic acid to the polyimide by way of thermal

imidization. During this heating cycle volatilization of the counterion occurs. By selection of the base used for making the polyamic acid salt, the molecular weight of the final polyimide can be controlled.

Prior to the beginning of this work it was a widely held belief that molecular weight control of polyamic acids that were dissolved in water was not possible. Hydrolytic degradation of polyamic acids typically occurs when they are subjected to aqueous conditions [14-18]. Hydrolysis results in decreased molecular weight of the polyamic acid and ultimately the polyimide.

Molecular weight control of water soluble polyimide precursors has been demonstrated by Facinelli et al. with Ultem-type polyamic acid salt [18]. A systematic increase in ultimate polyimide molecular weight was developed using several different bases for synthesis of different polyamic acid salts. Molecular weight control was demonstrated with a particularly important polyimide having a glass transition temperature of 218°C and a number average molecular weight of 13,400 made from the Ultem-type polyamic acid triethylammonium salt [18].

Water soluble Ultem-type polyamic acid salts were used in the aqueous suspension prepregging of PEEK matrix composites. The polyamic acid salt is converted to a polyimide in a subsequent heating step. By controlling the molecular weight of the interphase polyimide, it is intended that the material properties of the interphase can be controlled. These properties must be known for using the mathematical models mentioned previously.

Since techniques have not yet been developed for measuring the properties of the actual interphase region of a composite, model interphase samples were prepared and characterized.

The model interphase samples were prepared according to the same methods used for aqueous suspension prepregging and subsequent composite consolidation. The model interphase polyimides were characterized for molecular weight, chemical identification, thermal properties, and rheological properties. For interphase composite manufacture with a PEEK matrix, the processing temperature is 380°C for thirty minutes. The thermal stability of the polyimide interphase material at this temperature is important when considering an interphase region that is primarily composed of the polyimide.

Since PEEK is miscible with Ultem polyimide [19], interdiffusion of the interphase polyimide and the bulk PEEK matrix is expected [20]. Thus, thermal, mechanical, and rheological properties of model matrix samples with varying compositions were measured.

Materials

A large batch of BPADA/MPD (Ultem-type) polyamic acid endcapped with phthalic anhydride was synthesized in a 5 liter reactor at the General Electric Research Center in Schenectady, New York, by Dr. Biao Tan from Professor McGrath's group of the Virginia Tech Chemistry Department. The reaction scheme is shown in Figure 3-1. The large batch of polyamic acid provided enough starting material so all experiments described in this chapter could be done using a single batch of polymer. This polyamic acid was used to make the model interphase samples for the structure property investigations of this chapter and the same batch of polyamic acid was used for subsequent composite manufacture as detailed in Chapter Four of this thesis.

The model matrix material was Victrex 380 Grade poly ether-ether-ketone (PEEK) supplied by ICI Americas. The PEEK was supplied as a powder with an 11µm median particle diameter as measured with a Shimadzu SPC-3 particle size analyzer. The PEEK is from the same batch used in subsequent composite manufacture as detailed in Chapter 4 and also the same batch used by Gonzalez [11] for polyimide interphase PEEK matrix composite manufacture.

The bases used for making the polyamic acid salts were ammonium hydroxide (NH_4OH), tetramethyl ammonium hydroxide (TMAH), and tripropylamine (TPA), all Fisher brand reagent grade.

Ultem 1000 polyetherimide obtained from General Electric was used for comparison of properties. The Ultem 1000 polyetherimide was supplied as pellets.

The solvent used for solubility tests was HPLC grade 2-methylpyrollidinone (NMP) from Fisher Scientific. For all aqueous solutions and suspension, deionized water with a resistivity of 16.7 ohms/cm^3 from a Nanopure II water filtering system was used.

Procedure
Calibration of Bases

All bases were purchased new, kept sealed and stored in a refrigerator. The concentration of the aqueous bases were determined by potentiometric titration using an MCI Automatic Titrator Model GT-05 (COSA Instruments Corporation). An aqueous HCl solution was prepared with an approximate concentration of 0.05 mol/l. This HCl solution was then standardized using a carefully prepared aqueous sodium carbonate solution. The sodium carbonate was stored as a

solid in a desiccator and dried in a vacuum oven at 105°C overnight prior to use. Three 0.1425 millimolar aqueous sodium carbonate solutions were prepared and used to standardize the HCl solution. The concentration of the standardized HCl solution was determined as the average of the three standardizations. The standardized HCl solution was then used to titrate the aqueous bases. The endpoint of the titration was calculated by the auto-titrator as the inflection point in the potential vs. volume of titrant plot. Each aqueous base was titrated three times and the results were averaged. The bases were kept in the original bottles with the caps sealed tightly with parafilm, and stored in a refrigerator.

Polyamic Acid Preparation

Polyamic acid made by Dr. Biao Tan from the monomers 2,2'-Bis[4-(3,4-dicarboxyphenoxy)- phenyl]propane dianhydride (BPADA) and meta-phenylene diamine (m-PDA) was supplied as a 25 wt% solution in NMP at a temperature of -5°C. The polyamic acid was endcapped with phthalic anhydride to provide a target molecular weight of 20,000 g/mole. The molecular weight distribution of this material was not measured by gel permeation chromatography (GPC) at this stage, since further processing steps were planned that would possibly alter the molecular weight.

The removal of NMP was accomplished by a precipitation procedure developed by Dr. Biao Tan. The polyamic acid/NMP solution was stored at a temperature of -5°C until the precipitation step. The polyamic acid was twice precipitated into water at room temperature to remove as much NMP as possible.

The first precipitation was done from the stock NMP solution where ~50 ml of the solution was slowly dripped into 500 ml water while mixing rapidly in an Osterizer laboratory blender. The precipitate was a stringy, yellow, granular solid. The mixture was blended for three minutes and then filtered using a Buchner funnel with 11 cm diameter Whatman #1 filter paper. The recovered polyamic acid was a stringy, yellow solid. This step was repeated four times to process a total of 200 ml of polyamic acid/NMP solution. The resulting batches of polyamic acid were then consolidated into a single batch and dried 24 hours in a vacuum oven at room temperature.

NMP has a boiling point of 203°C and complete removal of residual NMP from the polyamic acid is extremely difficult. A lower boiling solvent, tetrahydrofuran (THF), was used for the second precipitation. The recovered polyamic acid was dissolved in 500 ml of THF and was stirred with a magnetic stirrer for 15 hours in a sealed 1 liter round bottom flask.

The polyamic acid was precipitated from the THF in several small batches. For each batch precipitation, ~125 ml of the solution was slowly dripped into 500 ml water while stirring rapidly in an Osterizer laboratory blender. The precipitate was fine, light yellow flakes. The mixture was blended for three minutes and then filtered using a Buchner funnel with 11 cm diameter Whatman #1 filter paper. This step was repeated four times to process the 500 ml of polyamic acid/THF solution. The resulting batches of polyamic acid were then consolidated into a single batch and dried 48 hours in a hood and then 24 hours in a vacuum oven at room temperature. The recovered polyamic acid was light yellow, fine powder.

Finally, the solid polyamic acid was bottled and stored in a freezer at -5°C. At this stage, it was appropriate to measure the molecular weight distribution using GPC for a control case to

compare with further results.

Model Interphase Ultem-type Polyimide Characterization
Preparation of Test Samples

Since properties of the actual interphase region of a composite cannot be currently evaluated accurately, it was necessary to prepare polyimide model interphase material on a bulk scale so that properties could be measured. Ultem-type polyimides were prepared using exactly the same procedure for those used in the 10 series, 30 series and 50 series composites manufactured in Chapter Four of this thesis. The polyimides for all three of the composite systems are chemically identical as shown by FTIR. However, they have different molecular weights, as shown by GPC, due to the different salt preparation methods [18]. Bulk samples of Ultem-type polyimide were made from an NH_4^+ polyamic acid salt, a TMA^+ polyamic acid salt and also from a TPA polyamic acid salt. Figure 3-2 shows the chemical reactions for formation of the three polyamic acid salts. These bulk samples were designed to replicate the chemistry and physical state of the polyimide material in the 10 series, the 30 series, and the 50 series composites. Thus, the same batch of polyamic acid was used for the composite manufacturing process and the model interphase polyimide preparation procedure and the processing conditions were repeated exactly.

I) Ultem-type NH_4^+ polyamic acid salt (30 series composite model interphase): Deionized water at 70°C was mixed with 14.22 molar NH_4OH(aq). The polyamic acid was then added slowly while stirring rapidly. The NH_4OH was added in a 1.25:1 stoichiometric ratio to

acid functionalities of the polyamic acid (two per repeat unit) and a measured amount of polyamic acid was used to make a 5 wt% aqueous solution of polyamic acid . The 25% stoichiometric excess of base was used to ensure neutralization of amic acid functionalities and maintain stability of the aqueous polyamic acid salt as shown by Reynolds [21] and described in Chapter 2. This concentration of base also replicates conditions for composite manufacture of A. Gonzalez [11]. The solution was covered with Parafilm to prevent evaporation of base, and was stirred for one hour at 70°C to allow the polyamic acid salt to form and dissolve. The solution was then allowed to cool to room temperature and then it was filtered using a Buchner funnel and Fisher Brand No.41 filter paper. No insoluble polyamic acid residue was collected with the filter paper.

ii) Ultem-type TMA^+ polyamic acid salt (10 series composite model interphase): Deionized water at room temperature was mixed with 3.23 molar TMAH(aq). The polyamic acid was added slowly to the basic solution during rapid stirring. The TMAH was added in a 1.10:1 stoichiometric ratio to acid functionalities of the polyamic acid and a measured amount of polyamic acid was added to make a 5 wt% aqueous solution of polyamic acid. The 10% stoichiometric excess of base was used to ensure neutralization of amic acid functionalities and maintain stability of the aqueous polyamic acid salt as shown by Reynolds [21] and described in Chapter 2. It was found that 25% molar excess, as used with the NH_4OH dissolution procedure, was not needed for complete dissolution with TMAH, and that 10% molar excess was sufficient. The solution was covered with Parafilm to prevent evaporation of base, and was stirred at room temperature overnight, then it was filtered using a Buchner funnel and Fisher Brand No.41 filter paper. No insoluble polyamic acid residue was collected with the filter paper.

iii) Ultem-type TPA^+ polyamic acid salt (50 series composite model interphase): The polyamic acid salt precursor for this model interphase polyimide was prepared directly from the stock BPADA/m-PDA (Ultem-type) polyamic acid in NMP. The precipitation steps for polyamic acid preparation outlined in the previous section were not employed for this particular model interphase polyimide. Tripropylamine (TPA) was dissolved in methanol and then the BPADA/m-PDA (Ultem-type) polyamic acid in NMP was slowly added to the solution. The amount of TPA was carefully measured to yield a 1.25:1 stoichiometric ratio of TPA to acid functionalities of the polyamic acid. The amount of methanol used was equal to the volume of the polyamic acid/NMP added. The NMP/methanol/TPA/polyamic acid solution was mixed at room temperature overnight in a closed round bottom flask.

The precipitation of the TPA^+ polyamic acid salt was accomplished by slowly dripping the NMP/methanol/TPA/polyamic acid solution into 4-methyl-2-pentanone. An Osterizer laboratory blender was used to rapidly stir 750 ml 4-methyl-2-pentanone while ~50 ml of the NMP/methanol/TPA/polyamic acid solution was added. The precipitate was an off-white, fine powder. The precipitate was recovered using a Buchner funnel with 11 cm diameter Whatman No. 41 filter paper and was washed with 50 ml 4-methyl-2-pentanone. The solid TPA^+ polyamic acid salt was dried in a Model 532 Fisher convection oven at 65°C for two hours. To make an aqueous solution of the TPA^+ polyamic acid salt, the solid TPA^+ polyamic acid salt was added to an aqueous solution of TPA^+. The TPA^+ in the aqueous solution was carefully measured to provide a 0.25:1 stoichiometric ratio of base to acid functionalities of the polyamic acid. The TPA^+ polyamic acid salt prepared in the NMP/methanol solution was made with a 25% molar excess of TPA^+. However, after the TPA^+ polyamic acid salt was precipitated and the solid was

dried, the excess TPA^+ also was evaporated. Therefore additional TPA^+ added to the water provides the 25% molar excess of base used to ensure neutralization of amic acid functionalities and maintain stability of the aqueous polyamic acid salt as shown by Reynolds [21] and described in Chapter 2. The solution was covered with Parafilm to prevent evaporation of base, and was stirred at room temperature overnight, then it was filtered using a Buchner funnel and Fisher Brand No.41 filter paper. No insoluble polyamic acid residue was collected with the filter paper.

All three aqueous salt solutions were made in about 800 ml quantities. Approximately 400 ml of the each solution were saved for the model interphase study described below. Approximately 200 ml of each solution were sealed with Parafilm in a Nalgene bottle, and stored in a refrigerator for subsequent aqueous prepregging experiments.

The solutions were poured into specially made, shallow Teflon-film pans and dried in a hood at room temperature. The Ultem-type NH_4^+ solution dried completely in about 4 days. The Ultem-type TMA^+ solution and the Ultem-type TPA^+ solution dried completely in about 6 days.

Although most of the dry polyamic acid salts underwent a heat treatment cycle in a Model 532 Fisher Programmable air convection oven that was identical to that for the prepreg material, a small portion of these dry polyamic acid salt samples was reserved for thermal gravimetric analysis, (TGA). For the Ultem-type NH_4^+ Polyamic acid salt and the Ultem-type TMA^+ Polyamic acid salt a drying step of 65°C for one hour was followed by a further heat treatment step of 265°C for two hours to convert the Polyamic acid salt to polyimide. For the TPA^+ polyamic acid salt a drying step of 65°C for one hour was followed by a further heat treatment

step of 275°C for ten minutes to convert the polyamic acid salt to polyimide. The reason for the different thermal imidization cycles is that the process for making the Ultem-type TPA^+ polyamic acid salt was developed at an intermediate stage of this project. Dr. Venkat Venkatessan in Professor Riffle's group developed the procedure with the recommended thermal imidization cycle to obtain a substantially high molecular weight.

A portion of each polyimide was then melt pressed into a film for further study. The films were made in a specially manufactured mold made from 0.20" stainless steel shim stock. The mold was sandwiched between sheets of heavy duty aluminum foil that was treated with an aerosol Teflon based mold release agent. A Wabash Vacuum Hot Press was used to press the polyimide at a temperature of 380°C and a pressure of 100 psi for 30 minutes and then cooled at a rate of 10°C/min to simulate the actual consolidation temperature of the composite interphase.

Melt Rheology of Ultem-type Polyimides

Melt rheology samples were prepared by forming the polyimide into a circular slug. Approximately 0.6 g of polyimide were placed in a 25 mm diameter cylindrical steel mold. The sample in the mold was heated in a Model 532 Fisher programmable oven to a temperature 20°C above the glass transition temperature of the polyimide. This temperature was different for each polyimide ranging from 175°C to 240°C and was held for two hours. The oven was cooled as rapidly as possible by setting the setpoint to 25°C and waiting for the temperature to reach 40°C. This cooling step took about 20 minutes. At this point the mold was removed from the oven and let sit on a laboratory bench to cool further. When cool, the rheology sample was removed.

Rheological testing was done on a Bohlin VOR with a high temperature cell oven using nitrogen as the heating gas. The 25 mm parallel plate fixture was used with an approximate sample thickness of 1 mm. Prior to subsequent measurements, the amplitudes and frequencies which characterize the linear viscoelastic region were determined. The subsequent isothermal rheology tests were done within this linear viscoelastic range. The initial measurements of the dynamic temperature rheological tests were within the linear viscoelastic range, however this range was not maintained as the viscosities increased due to crosslinking. The purpose of the dynamic temperature rheological tests was to demonstrate crosslinking by an increase in melt viscosity.

Dynamic temperature tests from 250°C to 380°C were conducted in the oscillation mode with an amplitude of 35% (radians) and a frequency of 0.1 Hz or 0.4 Hz. A frequency of 0.1 Hz was used for the Ultem-type TMA^+ polyamic acid salt and the Ultem-type TPA polyamic acid salt. However, the lower melt viscosity of the Ultem-type NH_4^+ polyamic acid salt required a higher frequency (0.4 Hz) to obtain a recordable measurement. A heating rate of 5 °C/min was used. A torque bar with a calibrated torsional resistance of 11.45 g•cm was used for this test. Since the gap thickness will vary with temperature, and dynamic temperature tests were conducted, the plate gap spacing was calibrated at 315°C, which was a temperature in the middle of the range investigated.

Differential Scanning Calorimetry of Ultem-type Polyimides

A Seiko 220C differential scanning calorimeter, (DSC) in Professor Garth Wilkes' Laboratory was used to obtain dynamic heat capacity data for the polyimides. Chris Robertson graciously ran the DSC instrument which was calibrated with indium. Polymer samples were cut to fit into the DSC pans to obtain a sample mass of 10-15 mg. A dual scan procedure was used with a heating rate of 20°C/min from 60°C to 280°C under nitrogen purge. Since no melting type endotherm was observed, only heating scans were recorded for T_g measurement. Glass transition temperatures were found by using the midpoint of the heat capacity inflection.

Gel Permeation Chromatography

Gel permeation chromatography was done with a Waters GPS/ALC 150C chromatograph equipped with a differential refractometer detector and an on-line differential viscometric detector (Viscotek 150R) coupled in parallel in Professor Thomas Ward's Lab. Measurements were done by Dr. Qing Ji. The column used was a μStyragel HT3 + HT4 having pore sizes of 1,000 to 10,000Å. Online data collection with a personal computer and use of TriSEC GPC Software V2.70e (Viscotek) provided calculation of molecular weight distribution and the various moments of the distribution. The mobile phase was 2-methylpyrollidinone (NMP) stirred over 0.02 M phosphorous pentoxide, with a flow rate of 1.0 ml/min. Run parameters used were polymer concentrations of 4-5 mg/ml, injection volumes of 200 μl, and an inlet pressure of 56.9 KPa.

Solubility Test With Gel Fraction Measurement

Polyimide solubility was determined using NMP. Polyimides thermally imidized according to the schedules outlined previously were tested as well as samples which had also been subjected to the additional simulated consolidation heating cycle (380°/30 min). The mass of the polyimide samples was carefully measured (approximately 0.05 g) and placed in a screw top vial with about 5 ml of NMP. Each polyimide sample was run in triplicate. The vials were mixed overnight by tumbling end-over-end on a rotary wheel vial mixer.

The solutions were visually inspected and the presence of gel fractions were noted. The solutions with gel fractions were filtered using Whatman No. 1 filter paper and a Buchner funnel. The filter paper was wetted with chloroform, vacuum was applied to the Buchner flask, then the NMP/polyimide solution was poured onto the center of the filter paper. The recovered gel on the filter paper was washed three times with ~10 ml chloroform. The filter paper was then dried in a Fisher Model 532 programmable convection oven at 100°C for one hour, cooled in a desiccator cabinet, then weighted on a Sartorius Analytical balance accurate to 0.0001 g. The reported gel fraction is an average of three measurements.

Fourier Transform Infrared Spectroscopy with Attenuated Total Reflectance

Fourier Transform Infrared Spectroscopy with Attenuated Total Reflectance (FTIR-ATR) was done on solid polymer films using a BIO-RAD FTS-40A spectrometer by Ms. Christelle Laot in Dr. Eva Marand's laboratory. The spectrometer was equipped with a liquid nitrogen cooled mercury-cadmium-telluride detector. This model includes dynamic alignment to erase

scattered radiations from optical misalignment. No polarization was used with the radiation source. The samples were tested over the entire range of wavenumbers, 4,400 cm^{-1} to 400 cm^{-1}, for the instrument. A hemispherical, single internal reflection element composed of zinc selenide was used as a substrate for the polymer films during measurement. The ZnSe crystal was 25 mm in diameter, 12.5 mm in height with a plane and polish reflecting surface. The ZnSe crystal was mounted in a Harrick Scientific Corporation, Seagull attachment during measurement. Measurements were taken at room temperature.

The aqueous polyamic acid salts from the same batches of solutions described earlier were cast onto the crystal. The Ultem-type NH_4^+ polyamic acid salt was cast onto the crystal first. A drop of solution was put on the crystal and the water was evaporated in a hood. An FTIR-ATR spectrum was then measured for the polyamic acid salt sample. The Ultem-type NH_4^+ polyamic acid salt on the ZnSe crystal was then placed in a Model 532 Fisher Programmable air convection oven and heated according to the thermal imidization cycle described previously. Another FTIR-ATR spectrum was then measured for the polyimide sample. The crystal was cleaned and the other Ultem-type polyamic acid salts were examined using the same procedure to obtain spectra for the polyamic acid salt form and the subsequent polyimide form of the polymer.

Thermal Gravimetric Analysis

A Dupont Instruments model 951 Thermal Gravimetric Analyzer (TGA) was used to evaluate the imidization temperatures of the polyamic acid salts and the thermal stability of the

resulting polyimides. A nitrogen gas purge was used for all measurements. Measurements were taken on polymer samples weighing approximately 15-25 mg. Thermal cycles simulated the oven imidization cycle and the composite consolidation cycle used in composite manufacturing procedures. Following the simulated oven imidization cycle and the simulated consolidation cycle, the samples were pyrolyzed to assess thermal stability.

For the imidization cycle, the temperature was ramped at 10°C/min to 265°C, held for two hours, and then ramped at 10°C/min to 600°C. Since thermal imidization is a condensation reaction, water is evolved during the reaction. The weight loss that occurs at temperatures below the T_g of the resulting polyimide is attributed to loss of water, as well as loss of the basic counterion associated with the polyamic acid. The range of temperatures over which this weight loss occurs is defined as the imidization temperature range. The reported imidization temperatures are for purposes of comparing relative imidization reaction kinetics at a similar dynamic thermal cycle. The reported imidization temperatures should not be interpreted by the reader as the only temperatures which thermal imidization is possible for these materials.

For the simulated consolidation cycle the temperature was ramped at 10°C/min to 380°C, held for thirty minutes, and then ramped at 10°C/min to 900°C. Onset of degradation was characterized by the 5% weight loss temperature. For the imidization cycle, the samples lose weight as a consequence of imidization and so the temperature at which 5% weight loss occurred was measured only after imidization was complete.

Pyrolysis Gas Chromatography of Ultem-type Polyimides

The pyrolysis GC experiments were graciously ran with help of Dr. John Facinelli at the Allied Signal Research Center in Richmond, Virginia. The Ultem-type TMA^+ polyimide and the Ultem-type NH_4^+ polyimide which had each previously been thermally imidized at 265°C/2 hours were put in a closed cell and heated to 380°C for 15 minutes. After this heat treatment, the headspace gases were injected into a GC and a chromatogram was measured. The data was saved to a PC which also had a data base of elution times of many compounds, which simplified identification of the elution peaks.

Model Matrix Ultem-type polyimide/PEEK Blend Characterization
Preparation of Test Samples

Polymer films were manufactured to simulate the blend compositions of PEEK and polyimide that could occur in the matrix region of the composite. Since Ultem polyimide is miscible with PEEK [19], it was hypothesized that a concentration gradient of polyimide will be present immediately surrounding each carbon fiber. Thus, blends of Ultem-type polyimide and PEEK were made at 5 wt% Ultem-type polyimide and 50 wt% Ultem-type polyimide. The 5 wt% Ultem-type polyimide/PEEK blend is especially important because that is the same composition of the prepregging suspension for subsequent composite fabrication. The case of complete interdiffusion of the polyimide interphase and the bulk PEEK must be considered to address the antithesis that the effects of composite properties are due to the addition of a low molecular weight polyimide to the PEEK which merely plasticizes the matrix and alters the bulk

matrix properties.

Small samples of suspension were used to make representative matrix coupons for matrix characterization. The suspensions were made using a portion of the polyamic acid salt solutions that were made for the model interphase study. Small aqueous suspensions with a total solids content of 3.0 g were made with the polyamic acid salt solutions and 380 grade PEEK powder. The solids concentrations were varied with polyamic acid salt mass fraction of 5 wt%, and 50 wt%. As noted previously, the sample with the polyamic acid salt mass fraction of 0.05 was identical in composition to the matrix material used in the composite manufacturing. The suspensions were dried in a hood at room temperature, mixing occasionally to maintain a homogeneous distribution of PEEK powder and polyamic acid salt. When the suspensions were dry, they were pulverized using a mortar and pestle to homogenize each individual powder sample.

The homogenized powder samples were placed in specially made, shallow Teflon-film pans and subjected to a heat treatment cycle in a Model 532 Fisher Programmable air convection oven that was identical to that for composite prepreg material during a composite manufacturing procedure. The thermal imidization cycles described previously for each Ultem-type polyamic acid salt were used.

Model matrix films were pressed in a specially manufactured mold made from 0.20" stainless steel shim stock. The mold was sandwiched between sheets of heavy duty aluminum foil that were treated with an aerosol Teflon mold release agent. A Wabash Vacuum Hot Press was used to press the polyimide/PEEK blends at a temperature of 380°C and a pressure of 100 psi for 30 minutes and then cooled at a rate of 10°C/min to simulate the actual consolidation

temperature of the composite interphase.

Melt Rheology of Ultem-type polyimide/PEEK Blends

Rheological testing was done on a Bohlin VOR with a high temperature cell oven using nitrogen as the heating gas. The 25 mm parallel plate fixture was used with an approximate sample thickness of 1 mm. The plate gap spacing was calibrated at 380°C which was the temperature used for the rheology test.

Melt rheology samples were prepared by cutting the PEEK/PI film into pieces that could be stacked in between the parallel plates of the rheometer. The plates were preheated to 380°C so that the polymer film would flow quickly and the plate spacing was closed to about 1 mm for measurements. Any polymer that squeezed out beyond the edges of the plates was cut off with a razor blade.

Isothermal, dynamic frequency tests were conducted in the oscillation mode with an amplitude of 50% (radians). Prior to the isothermal, dynamic frequency tests, this amplitude was established as being within the linear viscoelastic region up to frequencies of 0.5 Hz. The frequency range for the dynamic frequency tests was 0.004 Hz to 0.4 Hz. The temperature throughout the test was 380 ± 1°C. A torque bar with a calibrated torsional resistance of 11.45 g•cm was used for this test.

Tensile Testing of Ultem-type Polyimide/PEEK Blends

A Polymer Labs Miniature Materials (MiniMat) Tester in Professor Ronald Kander's Lab, was used in the tensile mode to measure tensile properties of the PEEK/PI blends following ASTM Standard 1708-93. The films were cut into dogbone coupons using a dogbone blanking die. The dogbones were 1" long, 0.1" wide at the test area and had individually uniform thicknesses ranging from 0.04" to 0.05".

Tensile data were collected online with a personal computer using Polymer Labs MiniMat software. Tensile strength and strain data were collected. The first 2% strain was characterized by elastic deformation. Using the data from this region the Young's modulus was calculated as being the slope of the stress-strain curve. For each test sample composition, between 5 and 10 specimens were tested.

Differential Scanning Calorimetry of Ultem-type Polyimide/PEEK Blends

A Seiko 220C differential scanning calorimeter, calibrated with indium, was used to obtain dynamic heat capacity data for the PEEK/polyimide blends. Mr. Kurt Jordens graciously ran the DSC instrument in Professor Garth Wilkes' lab. Polymer samples were cut to fit into the DSC pans to obtain a sample mass of 10-15 mg. A triple scan procedure was used with a heating rate of 20°C/min to 400°C followed by a cooling rate of 10°C/min to 50°C under nitrogen. The polymer samples tested were 380 Grade PEEK, a 5 wt% Ultem-type PI/PEEK blend and a 50 wt% Ultem-type PI/PEEK blend. Since the blends exhibited melting endotherms, the triplicate scan procedure was useful for a statistical analysis of heats of melting. Glass transition

temperatures were found by using the midpoint of the heat capacity inflection. Temperatures of maximum crystallization were reported as the temperature at the peak of the crystallization exotherm. Melting and crystallization enthalpies were found by calculating the area under the respective peak which was executed by the Seiko DSC software. The crystalline fraction of the sample was determined by dividing the heat of fusion by 130 J/g, which is the heat of formation for 100% pure crystalline PEEK [22] and then dividing by the mass fraction of PEEK in the sample.

Results and Discussion

Model Interphase Characterization: FTIR ATR

FTIR spectra are shown in Figure 3-3 for three polyamic acid salts and the corresponding polyimides after a standard imidization cycle. Absorption bands around 1550 cm^{-1} are associated with secondary amide stretching vibrations [24,25]. Absorption bands at 1660 cm^{-1} are associated with secondary amide bending [26]. Absorption bands at 1780 and 1720 cm^{-1} are associated with the symmetric and assymetric carbonyl stretching, respectively, in the five membered imide ring [24-26]. Absorption bands at 1370-1380 cm^{-1} are associated with stretching vibrations of C-N for the polyimide [24-26].

Figure 3-3(a) shows the FTIR spectra for the Ultem-type TMA^{+} polyamic acid salt and the corresponding polyimide after the standard imidization cycle. Peaks at 1584, 1567 and 1554 cm^{-1} are representative of the amide stretching vibrations and the peak at 1660 cm^{-1} is representative of secondary amide bending. All of these peaks are not present for the resulting

polyimide, indicating that complete imidization has occurred according to the resolution of the FTIR detection capabilities. Essentially, completion of the imidization reaction can be quantitatively assured to at least 99% conversion of amic acid functionalities to imide functionalities. The formation of the characteristic imide absorption band peaks at 1779 and 1721 cm^{-1} also demonstate conversion of the polyamic acid to the polyimide. The presence of the peak at 1381 cm^{-1} for the C-N stretch is less obvious because it appears as a shoulder on a larger peak.

Figure 3-3(b) shows the FTIR spectra for the Ultem-type NH_4^+ polyamic acid salt and the corresponding polyimide after the standard imidization cycle. Once again, peaks at 1546 and 1537 cm^{-1} are representative of the amide stretching vibrations and the peak at 1657 cm^{-1} is representative of secondary amide bending. These peaks are not present for the resulting polyimide, indicating that essentially complete imidization has occurred. The characteristic imide absorption band peaks at 1719 and 1778 cm^{-1} indicate that with the loss of the carboxylic acid absorption peaks there is a corresponding gain of imide bond absorption peaks. The presence of a peak at 1380 cm^{-1} for the C-N stretch is less obvious because it appears as a shoulder on a larger peak.

Figure 3-3(c) shows the Ultem-type TPA^+ polyamic acid salt and the corresponding polyimide after the standard imidization cycle. Peaks at 1566, 1547 and 1537 cm^{-1} are representative of the amide stretching vibrations and the peak at 1660 cm^{-1} is representative of secondary amide bending. These peaks are not present for the resulting polyimide, indicating that essentially complete imidization has occurred. The characteristic imide absorption band peaks at 1720 and 1778 cm^{-1} indicate that with the loss of the carboxylic acid absorption peaks

there is a corresponding gain of imide bond absorption peaks. The presence of a peak at 1380 cm^{-1} for the C-N stretch is less obvious because it appears as a shoulder on a larger peak.

Figure 3-3(d) shows a comparison of the FTIR spectra for the three polyamic acid salts. This comparison shows that there is some difference between the three polyamic acid salts. The differences in the locations of the peaks at 1530-1580 cm^{-1} can be attributed to the presence of different ammonium counterions.

Figure 3-3(e) shows a comparison of the FTIR spectra for the three polyimides after a standard imidization cycle. An FTIR spectra was also measured for Ultem 1000 and it is shown in Figure 3-3(e). The comparison shows that there is no detectable difference between the four polyimides, indicating that they are all chemically identical.

In summary, the FTIR spectra in Figure 3-3(a-e) show that, although the polyamic acid salts differed slightly due to the different counterions present, the resulting polyimides were imidized to at least 99% conversion and were all identical in chemical structure to Ultem 1000.

Gel Permeation Chromatography

Gel permeation chromatography, (GPC), results for the Ultem-type TMA^+ polyimide and the Ultem-type NH_4^+ polyimide that were thermally imidized at 265°C for 2 hours are shown in Table I. The M_n of the Ultem-type TMA^+ polyimide is almost four times that of the M_n of the Ultem-type NH_4^+ polyimide. The polydispersities greater than 2 indicate that the change in molecular weight due to hydrolysis and then subsequent recombination during imidization leads to a broader distribution of molecular weights. The M_n of the Ultem-type NH_4^+ polyimide was

2,780 g/mol. Considering that the molecular weight of an Ultem-type polyimide repeat unit is 592 g/mol, the Ultem-type NH_4^+ polyimide is shown to have an average polydispersity less than 5. This material cannot strictly be considered a polymer, and rather is an oligomer. As will be discussed later, this material has been shown to crosslink at higher processing temperatures, ultimately resulting in a polymeric material.

The Ultem-type TPA^+ polyimide, imidized at 275°C for 10 minutes is also shown in Table 3-I and has an M_n almost as high as commercially available Ultem 1000 and is believed to be above the critical entanglement molecular weight. The polydispersity of 1.95 for the Ultem-type TPA^+ polyimide is indicative that the final molecular weight distribution was not altered appreciably from the initial molecular weight distribution of the polyamic acid. The synthesis of the polyamic acid follows a step growth polymerization scheme which typically yields a molecular weight distribution with a polydispersity of 2. The polyamic acid tabulated has a polydispersity of 1.67, however this is after twice precipitating the polyamic acid into water. The Ultem 1000 polyimide has a polydispersity of 1.87 which is expectedly close to 2.

Table 3-I. GPC, DSC and solubility test results for Ultem-type polyimides and Ultem-type polyamic acid.

	Ultem 1000	Ultem-type PAA* / PI	Ultem-type TMA^+ PI	Ultem-type NH_4^+ PI	Ultem-type TPA^+ PI
M_n	19,000	7,540* / 14,400	10,500	2,780	16,000
M_w	35,600	12,600* / 33,100	28,800	9,210	31,200
M_w/M_n	1.87	1.67* / 2.3	2.74	3.31	1.95
T_g	218°C	---* / 218°C	203°C	153°C	220°C
imidization temperatures		150-234°C	200-244°C	142-183°C	180-257°C
5% wt loss	539°C	--- * / 530°C	470°C	476°C	519°C
solubility (NMP)	yes	---* / yes	yes	yes	yes
after 380° Heat treatment					
gel fraction	---	---	13%	21%	0.6%
T_g	---	220°C	204°C	194°C	220°C

--- - not measured
* - data for Ultem-type polyamic acid

Thermal Gravimetric Analysis

Thermal gravimetric analysis yields a temperature range of imidization and temperatures for onset of degradation given as a 5 wt% weight loss temperature. The imidization temperatures are reported as the range of temperatures over which the decrease in mass is attributed to the condensation imidization reaction and release of volatile counterion components. These temperatures are shown in Table 3-I.

Figure 3-4 shows the TGA data for the PAA salts and the neat PAA focusing on the temperature range below 265°C for a discussion of the imidization kinetics. The differences in imidization temperatures for the three different Ultem-type polyamic acid salts can be partially attributed to the relative difference in volatilizing the specific counterion. Before a polyamic acid salt can undergo imidization it must first be converted back into the polyamic acid form [27]. This requires dissociation of the counterion and subsequent volatilization of the counterion. The results show an imidization temperature range for the Ultem-type TMA^+ polyamic acid salt that begins about 60°C higher than for the Ultem-type NH_4^+ polyamic acid salt and an imidization temperature range for the Ultem-type TPA^+ polyamic acid salt that begins about 40°C higher than for the Ultem-type NH_4^+ polyamic acid salt. It is interesting to note that the imidization temperature ranges for the Ultem-type TMA^+ polyamic acid and Ultem-type NH_4^+ polyamic acid salt begin at temperatures very near the glass transition temperatures for the respective resuting polyimides. The Ultem-type TPA^+ polyamic acid imidization temperature range begins about 40° below the T_g of its resulting polyimide.

The imidization temperature range for the neat Ultem-type polyamic acid is 150-234°C. This is a higher temperature range than the imidization temperature range for the Ultem-type NH_4^+ polyamic acid salt but begins at a lower temperature than for the Ultem-type TMA^+ polyamic acid salt and the Ultem-type TPA^+ polyamic acid salt.

The span of the imidization temperature range for the neat Ultem-type polyamic acid is 84°C, which is about comparable to the span of the imidization temperature range for the Ultem-type TPA^+ polyamic acid which is 77°C. However, the span of the imidization temperature range for the Ultem-type TMA^+ polyamic acid salt and the Ultem-type NH_4^+ polyamic acid salt are

about half as large at 44°C and 39°C, respectively.

The 5% weight loss temperatures are used to quantify the onset of degradation. Figure 3-5 shows a TGA cycle that simulates composite consolidation conditions for polyimides made from polyamic acid salts that were thermally imidized in a convection oven at the conditions described previously. Figure 3-6 is a summary of the critical temperatures identified from the TGA experiments comparing polyimides made from polyamic acid salts to pure polyamic acid and Ultem 1000. The 5% weight loss temperatures for both the Ultem-type TMA^+ polyimide and the Ultem-type NH_4^+ polyimide made from water soluble polyamic acid salts are 63-69°C lower than the 5% weight loss temperature for commercially available Ultem 1000. This can be attributed to a lower molecular weight for the Ultem-type NH_4^+ and the Ultem-type TMA^+ polyimides [28]. It is believed that both the Ultem-type TMA^+ polyimide and Ultem-type NH_4^+ polyimide made from water soluble polyamic acid salts have molecular weights that are below the critical entanglement molecular weight, therefore a lower degradation temperature is expected [28]. The assumption that the Ultem-type TMA^+ polyimide and Ultem-type NH_4^+ polyimide have a molecular weight that is below the critical entanglement molecular weight is based upon visual observation of the polyimides. After the Ultem-type TMA^+ polyamic acid salt and Ultem-type NH_4^+ polyamic acid salt were thermally imidized in a convection oven at 265°C for two hours, the resulting polyimide did not form a continuous film. The Ultem-type NH_4^+ polyimide was a powder and the Ultem-type TMA^+ polyimide initially appeared as flakes of polymer but the flakes had no mechanical integrity. Upon handling, the flakes readily broke into smaller pieces.

The 5% weight loss temperature for the Ultem-type TPA^+ polyimide was only 20°C lower

than the 5% weight loss termerature for Ultem 1000. The 5% weight loss temperature for the polyimide from the Ultem-type polyamic acid is only 9°C lower than for the Ultem 1000 polyimide. This is good evidence that the molecular weight of the Ultem-type TPA^+ polyimide and the Ultem-type polyimide made from the pure polyamic acid are similar to the Ultem 1000 polyimide and are all above the critical entanglement molecular weight.

Solubility Test with Gel Fraction Measurement

The solubility test results for the Ultem-type polyimides are shown in Table 3-I. The polyimides that were imidized under previously described thermal imidization conditions of 265°C for 2 hours for the Ultem-type TMA^+ polyimide and the Ultem-type NH_4^+ polyimide; and 275°C for 10 minutes for the Ultem-type TPA^+ polyimide were all soluble in NMP. After a heat treatment of 380°C for 30 minutes, the Ultem-type TMA^+ polyimide and the Ultem-type NH_4^+ polyimide were not completely soluble in NMP. The polyimide made from the Ultem-type NH_4^+ polyamic acid salt had a measured gel fraction of 21% and the polyimide made from the Ultem-type TMA^+ polyamic acid salt had a measured gel fraction of 13%. Although a gel fraction of 0.6% was measured for the Ultem-type TPA^+ polyimide after the heat treatment of 380°C for 30 minutes, the measured amount was so slight that it is considered insignificant.

The target molecular weight for synthesis of the Ultem-type polyamic acid was 20,000 g/mol, based on a calculation from the Carother's equation. An appropriate amount of phthalic anhydride was added to the polyamic acid as a nonreactive polymer endcap to maintain the molecular weight of 20,000 g/mol. After twice precipitating this polyamic acid into water, the

measured M_n was 7,540 g/mol. Since the M_n of the polyimide made from the Ultem-type NH_4^+ polyamic acid salt was 2,780 g/mol, it is reasonable to assume that there is a significant amount of reactive end groups present from hydrolyzed chains.

Upon heating the polyimide made from the Ultem-type NH_4^+ polyamic acid salt to 380°C, these reactive end groups could recombine to form a crosslinked structure. Thus, the crosslinked fraction becomes insoluble. Although the measured M_n for the polyimide made from the Ultem-type TMA^+ polyamic acid salt (10,500 g/mol) is higher than the measured M_n of the Ultem-type polyamic acid, it is reasonable to assume that there are still some reactive end groups present especially since the polydispersity of the polyimide made from the Ultem-type TMA^+ polyamic acid salt (2.7) is larger than 2, and also larger than the polydispersity for the Ultem-type polyamic acid (1.7). The reactive end groups present from the hydrolysis reaction could recombine during the 380°C heat treatment to form a crosslinked structure.

Differential Scanning Calorimetry of Ultem-type Polyimides

Differential scanning calorimetry was used to measure the T_g of the polyimides and the values are listed in Table 3-I. Figure 3-7 shows the DSC scans for the polyimides, with T_g's indicated, after oven imidization. It is shown in Figure 3-8 that the glass transition temperatures follow the Fox-Flory relationship:

$$T_g = T_g^{\infty} - \frac{c}{<M_n>} \qquad \text{Eq. 3-1}$$

using T_g^{∞}=230°C and c=215,779 where T_g^{∞} is the glass transition temperature for a linear polymer chain of infinite molecular weight, $<M_n>$ is the mean number average molecular weight and c is a constant. The relationship is based on the idea that the local mobility is greater for the segments at the end of a polymer chain than for segments in the middle of a polymer chain. Therefore the free volume of segments at the end of the chain will also be greater. A polymer sample with greater $<M_n>$ will have fewer chain ends per mole and thus a smaller total free volume than a polymer sample with a lower $<M_n>$. The smaller total free volume will yield a polymer with a higher T_g.

The Fox-Flory relation with T_g^{∞}=237°C and c=282,990 was shown by Facinelli et al. for similar Ultem-type polyimides processed from aqueous salts of polyamic acids [18]. In this study, polyimides were made from several different polyamic acid salt aqueous solutions, glass transition temperatures were measured by DSC and the molecular weights were characterized by GPC. The bases used for making these polyamic acid salts included tetramethylammonium hydroxide, tetraethylammonium hydroxide, tetrapropylammonium hydroxide, tetrabutylammonium hydroxide and triethylamine.

Melt Rheology of Ultem-type Polyimides

Since the end use of these polyimides will be as an additive in PEEK matrix composites, the processability of the polyimides during a typical thermal treatment for processing PEEK matrix composites was investigated. The thermal cycle of interest was a 5°C/min temperature ramp to 380°C, a 30 minute hold at 380°, and a 10°C/min cooling ramp to room temperature.

The cooling cycle is important for the PEEK matrix polymer since it is semicrystalline, but is not of primary concern for the polyimides. Thus, rheology measurements of neat polyimides were made during a 5°C/min heating ramp to 380°C, and 30 minute hold at 380°C. The complex viscosity and temperature are shown with time in Figure 3-9 which reflects the simulated composite consolidation cycle.

The initial complex viscosity of the Ultem-type TMA^+ polyimide was approximately 10,000 Pa·sec at 250°C. The complex viscosity decreased with increasing temperature until the hold temperature of 380°C was reached. At 380°C, the complex viscosity began to increase and continued to increase during the 30 minute isothermal hold. This was confirmation that crosslinking occurred during the 380°C isothermal hold.

The initial complex viscosity of the Ultem-type NH_4^+ polyimide was around 10 Pa·sec at 250°C. The complex viscosity remained around 10 Pa·sec during the initial heating ramp until around 334°C where the complex viscosity began to increase, slowly at first, then after the isothermal hold temperature of 380°C was reached, a rapid increase in complex viscosity occured. The complex viscosity of the Ultem-type TPA^+ polyimide was around 80,000 Pa·sec at 250°C. The complex viscosity decreased with increasing temperature until the hold temperature of 380°C was reached. At 380°C, the complex viscosity began to increase slowly and continued to increase during the 30 minute isothermal hold. This increase in complex viscosity is an indication that some crosslinking occurred during the isothermal hold.

A comparision of the complex viscosities at the begining of the 380°C isothermal hold for the polyimides made from the Ultem-type water soluble polyamic acid salts shows the expected trend from the measured molecular weights. The Ultem-type NH_4^+ polyimide initially

had a much lower M_n of 2,780 g/mole and hence had a melt viscosity that was 10 times lower than the Ultem-type TMA^+ polyimide which had an initial M_n of 10,500 g/mole. The Ultem-type TPA^+ polyimide had an initial M_n of 16,000 g/mole and a melt viscosity that was higher than the melt viscosity of the Ultem-type TMA^+ polyimide.

At the end of the simulated processing cycle, the complex viscosity of all the polyimides processed from water soluble polyamic acid salts is about 2,000 Pa·sec. Considering only the viscosity data during the isothermal hold at 380°C, the complex viscosity increased from about 200 Pa·sec to 2,000 Pa·sec at 0.1 Hz for the Ultem-type TPA^+ polyimide and from about 170 Pa·sec to 2,000 Pa·sec at 0.1 Hz for the Ultem-type TMA^+ polyimide, which is an increase by a factor of about 10 and 12, respectively. During this isothermal hold the complex viscosity increased from about 35 Pa·sec to 2,000 Pa·sec at 0.4 Hz for the Ultem-type NH_4^+ polyimide, which is an increase by a factor of about 57. If the increase in complex viscosity is attributed entirely to crosslinking, this would indicate that a much greater number of crosslinking sites are formed for the Ultem-type NH_4^+ polyimide.

The complex viscosity of the polyimides processed from water soluble polyamic acid salts is about three times higher than the complex viscosity of the Ultem 1000 polyimide at the end of the simulated processing cycle. Presumably the Ultem 1000 polyimide remains stable throughout the simulated consolidation and does not undergo significant crosslinking as supported by the relatively constant complex viscosity at the isothermal hold temperature of 380°C.

Pyrolysis Gas Chromotography

During the isothermal, 30 minute hold at 380°C of the TGA experiments, a 1 to 2 percent weight loss was observed. Specific weight loss amounts are tabulated in Table 3-II. Solubility experiments show that a crosslinked product results from this same isothermal hold. From these observations, it is proposed that the weight loss is a result of products of the crosslinking reaction. Pyrolysis-gas chromatography (pyrolysis-GC) was used to determine the products of the reaction. GC spectra are shown in Figure 3-10(a) and 10(b) for Ultem-type NH_4^+ polyamic acid and Ultem-type TMA^+ polyamic acid, respectively. The products of the pyrolysis of the Ultem-type NH_4^+ polyamic acid salt are acetaldehyde and NMP. The products of the pyrolysis of the Ultem-type TMA^+ polyamic acid salt are methanol and ethylene glycol. Figure 3-11 compares the chemical structures of the products with the chemical structure of the Ultem-type polyimide. No attempt at proposing a mechanism is made. As described in Chapter 2, thermal degredation mechanisms for polyimides are very complex and poorly understood [28]. FTIR ATR spectroscopy indicates that there are no chemical differences between the polyimides processed from the two different polyamic acid salts. Thus, the different products of pyrolysis could be an artifact of polymer molecular weight and thermal stability.

Blend Characterization
Tensile Testing of Ultem-type Polyimide/PEEK Blends

The discussion in this next section concerns characterization of binary Ultem-type polyimide/PEEK blends. The blends were prepared with compositions of 5 and 50 wt% Ultem-

type polyimide. For discussion purposes, the nomenclature of the samples is listed in Table 3-II.

Table 3-II. Nomenclature of binary Ultem-type polyimide/PEEK blends.

Label	composition and type of Ultem-type polyimide
10x05	5 wt% Ultem-type TMA^+ polyimide
10x50	50 wt% Ultem-type TMA^+ polyimide
30x05	5 wt% Ultem-type NH_4^+ polyimide
30x50	50 wt% Ultem-type NH_4^+ polyimide
50x05	5 wt% Ultem-type TPA^+ polyimide
50x50	50 wt% Ultem-type TPA^+ polyimide

The tensile properties of the model matrix, 5 wt% polyimide/PEEK blends, as well as neat PEEK and neat Ultem 1000 were measured using the DuPont Miniature Materials testing instrument. The tensile properties of these samples are shown in Table 3-III. As seen in Table 3-III, the tensile yield strengths of the three model matrix blends (10x05, 30x05 and 50x05) are not significantly different from each other or from the tensile yield strength of the pure 380 Grade PEEK sample. Comparing the tensile yield strengths with an estimated literature tensile strength of 93 MPa from the ICI Victrex data sheet shows good agreement.

Table 3-III. Tensile properties of 5 wt% Ultem-type polyimide/PEEK binary blends.

	tensile strength (MPa)	tensile modulus (GPa)	yield strain (%)	failure strain (%)
10x05[a]	80 ± 16	2.17 ± 0.13	6.3 ± 0.8	8.6 ± 1.3
30x05[b]	82 ± 12	2.05 ± 0.12	5.8 ± 1.1	8.9 ± 2.8
50x05[c]	94 ± 7	2.27 ± 0.05	7.1 ± 0.9	30.6 ± 13.1
380 Grade PEEK	85 ± 14	2.05 ± 0.14	5.7 ± 0.9	30.4 ± 24.0
PEEK	~ 93*	3.6 (ref [35])	~4.8*	90 (ref [36])
Ultem 1000	99 ± 5	2.07 ± 0.19	7.7 ± 0.4	26.6 ± 9.6
Ultem 1000	105**	2.92 (ref [34])	7.0**	60**

a - 5 wt%Ultem-type TMA^+ polyimide/PEEK blend
b - 5 wt% Ultem-type NH_4^+ polyimide/PEEK blend
c - 5 wt%Ultem-type TPA^+ polyimide/PEEK blend
* - estimated from ICI Victrex PEEK data sheet
** - from GE Ultem 1000 data sheet.

The reported tensile strength of 150 Grade PEEK from the ICI Victrex PEEK data sheet is 94 MPa and the reported tensile strength of 450 Grade PEEK from the ICI Victrex PEEK data sheet is 92 MPa [29]. The 380 Grade PEEK was available for a limited time to special customers of ICI Victrex. Although the data sheets do not include information on the 380 Grade, it was learned from ICI Victrex technical assistance that the only difference between the three grades was molecular weight and that the 150 Grade had the lowest molecular weight, the 450 Grade had the highest molecular weight and the 380 Grade was somewhere in between [30]. According to this information, an estimated tensile strength of 93 MPa for 380 Grade PEEK seems very reasonable. In similar fashion, an assumed value of 4.8% for the tensile yield strain is estimated from the tensile yield strain of 4.7% for the 150 Grade PEEK and 4.9% for the 450 Grade PEEK [29].

The measured tensile strength of the Ultem 1000 polyimide agrees very well with the reported tensile strength of 105 MPa from the General Electric Ultem Resin Design Guide [31]. The measured tensile strength for Ultem 1000 is greater than the tensile strength of the neat PEEK or the PEEK/PI blends. If a simple model such as the rule of mixtures is applied to an Ultem 1000/PEEK blend to determine the tensile strength, it would predict that any addition of Ultem 1000, which has a molecular weight above the critical entanglement value, to PEEK would increase the tensile strength of the blend above the tensile strength of the neat PEEK. Since the Ultem 1000 polyimide is a completely amorphous material and the PEEK is a semicrystalline material, the addition of significant amounts of Ultem polyimide to the PEEK would decrease the overall crystal fraction of the polymer blend which will be shown later in this chapter and has been noted for Ultem/PEEK blends in previous studies [32,33]. The tensile strength of a semicrystalline polymer is directly affected by the crystalline content. Thus an addition of Ultem 1000 polyimide to PEEK would decrease the overall blend crystalline content and hence could decrease the overall tensile strength. Therefore, in this case, the rule of mixtures would not be a suitable model for tensile strength of a PI/PEEK blend.

Since the standard deviations for some of the tensile test data are large, it is necessary to quantitatively compare the sets of data using a statistical comparison. The sets of data for the three model matrix samples and the neat PEEK sample were statistically compared using an unpaired *t*-test executed with SigmaStat Statistical Software v. 2.0. The unpaired *t*-test is used to test for a difference between two groups that is greater than what can be attributed to random sampling variation. The SigmaStat Statistical Software first tests for normally distributed populations using a Kolmogorov-Smirnov test, and then tests for equal variance by checking the

variability about the group means. If the sample populations each pass these tests, then the unpaired *t*-test is executed using a confidence interval of 95%. The unpaired *t*-test is a parametric test based on estimates of the mean and standard deviation parameters of the normally distributed populations from which the samples were drawn. If two sets of data pass an unpaired *t*-test, then there is 95% confidence that the difference in the mean values of the two groups is greater than would be expected by chance [38]. Therefore, there is a statistically significant difference between the groups.

The unpaired *t*-test results are shown in Table 3-IV. Each set of model matrix tensile data and neat PEEK tensile data was compared with one another. The results show that there are no statistically significant differences in tensile strength for any of the samples.

Table 3-IV. Unpaired *t*-test results comparing each set of model matrix and neat PEEK tensile data.

	tensile strength	tensile modulus	yield strain	failure strain
10x05[a] vs. 30x05[b]	fail	fail	fail	fail
10x05[a] vs. 50x05[c]	fail	fail	fail	pass
30x05[b] vs. 50x05[c]	fail	pass	pass	pass
10x05[a] vs. PEEK[d]	fail	fail	fail	pass
30x05[b] vs. PEEK[d]	fail	fail	fail	pass
50x05[c] vs. PEEK[d]	fail	pass	pass	fail

a - 5 wt%Ultem-type TMA^+ polyimide/PEEK blend
b - 5 wt% Ultem-type NH_4^+ polyimide/PEEK blend
c - 5 wt%Ultem-type TPA^+ polyimide/PEEK blend
d - neat 380 Grade PEEK
pass = statistically significant difference between data sets
fail = no statistical difference between data sets

The tensile moduli of the polyimide/PEEK blends, 380 Grade PEEK and the Ultem 1000 are shown in Table 3-III and the unpaired *t*-test results are shown in Table 3-IV. The unpaired *t*-test results show that there is not a statistically significant difference in the modulus for most of the samples. The 50x05 model matrix blend is statistically different from the 30x05 model matrix blend and the neat PEEK sample. However, the difference is only 10%. The linear elastic nature of the stress-strain response curve at strains less than 2% facilitated the calculations of modulus. The measured value of tensile moduli for the neat PEEK and the Ultem 1000 was lower than the respective literature values. This is a consequence of the testing of thin films with the Minimat instrument.

Although the ASTM D 1708-93 prodecure is a standardized testing method for tensile properties of plastics by use of micro-tensile specimens, it is much more desirable to measure tensile properties with larger test specimens. The literature values from commercial product data sheets for the tensile properties are reported using ASTM D 638 standardized testing procedure. This procedure uses larger test specimens which can be tested in a larger, more precise instrument. One of the biggest problems with the Minimat testing instruments is slippage of the specimen at the grips. The grips are simple, ridged metal clamps with a single screw which applies pressure to secure the specimen ends. As the specimen is deformed in tension there will be a corresponding deformation in the thickness of the sample, yet there is no compensation in grip pressure. This results in slippage of the specimen at the grips. This point should be kept in mind when considering the discussion of the measured tensile strain properties. Although the strain data and consequently the moduli data from the Minimat tensile tests suffer in comparison to strain and moduli measurements from more sophisticated instruments, the results are internally

consistent and provide a meaningful comparison within the data set.

The yield strain of the model matrix blends, 380 Grade PEEK and the Ultem 1000 are shown in Table 3-III and the unpaired *t*-test results are shown in Table 3-IV. The unpaired *t*-test results show that there is not a statistically significant difference in the yield strain for most of the samples. In similar fashion to the *t*-test results for comparing tensile modulus, the yield strain of the 50x05 model matrix blend is statistically different than the yield strain of the 30x05 model matrix blend and the neat PEEK sample. The yield strains for the neat 380 Grade PEEK and the neat Ultem 1000 were greater than the literature values. This is a good indication that grip slippage occured with the polymer specimens during tensile testing. If slippage occured, then the crosshead would move a greater distance than the actual displacement of elongation allowed by the test specimen. This would lead to measured strains that are artificially high. This would not affect the measured load or the calculated stress of the specimen. However the tensile moduli would not be accurate. If the measured strains are artificially higher than actual values, the calculated moduli would suffer a similar artificial decrease. Since the modulus is the slope of the stress-strain curve in the linear viscoelastic region, if the ordinate (strain) of the plot is artificially increased then the slope (modulus) will be artificially decreased. This also provides an explaination for the smaller measured modlulus of Ultem 1000 than the literature value.

The failure strain of the model matrix blends, 380 Grade PEEK and the Ultem 1000 are shown in Table 3-III and the unpaired *t*-test results are shown in Table 3-IV. Contrary to the trends of the strength, modulus and yield strain results, the unpaired *t*-test results show that there is a statistically significant difference in the failure strain for almost all of the sets of data. These results are explained by the difficulty in pressing a perfectly, void-free film, the microstructre of

the samples and the limitations of the MiniMat testing instrument.

The standard deviation for the failure strain for the neat 380 Grade PEEK samples is very large which can be attributed to the difficulty in melt-pressing a void-free film of PEEK. Some of the PEEK films had some very small, visible voids that appeared to be a result of entrapped air. Some samples were visibly free of voids. This resulted in measured failure strain as high as 73.0% and as low as 16.2% for the 380 Grade PEEK samples. The voids present in the samples would act as stress concentrations, which would result in coupon failure at lower strains. The large, visible voids were not observed in the Ultem-type polyimide/PEEK blends. It is not known why these macroscopic voids occured with the neat 380 Grade PEEK and not with the blends.

It is likely that the failure strains of the 10x05 (TMA^+) and 30x05 (NH_4^+) blends were much lower than the failure strain for the 50x05 (TPA^+) blend and the 380 Grade PEEK because of a decrease in the amount of molecular entanglements in the amorphous material due to the presence of the low molecular weight polyimide. The molecular weights of the polyimides in the 10x05 (TMA^+) and 30x05 (NH_4^+) blends are both believed to be less than the critical entanglement molecular weight for an Ultem-type polyimide and are present in bulk concentrations of about 5 wt%. Although this is a low concentration of the polyimide, the actual local concentrations of polyimide in the amorphous phase of the model matrix samples may be greater.

Since PEEK is a semicrystalline polymer and the Ultem-type polyimide is completely amorphous, there will be a complex microstructure for a blend of these two polymers. Hudson et al. have shown that blends of these two polymers that have been subjected to heat treatments

which allow the PEEK content to crystallize resulting in a crystalline PEEK phase and an amorphous Ultem polyimide/PEEK phase [32]. In low concentrations the polyimide will not alter the final fraction of crystalline PEEK. This will result in a microstructure containing crystalline PEEK domains surrounded by an amorphous Ultem-type polyimide/PEEK blend. In the case of the model matrix samples, the amorphous Ultem-type polyimide/PEEK domains will have a composition of polyimide greater than 5 wt%. This will accentuate the affects of the low molecular weight component upon plastic tensile deformation.

Although the model matrix tensile samples are shown to poorly represent the actual matrix material **at high strains** due to sample defects and grip slippage, these high tensile strain properties are less important than the lower strain properties. In the actual composite material, bulk loading occurs only at low strains because the reinforcing fibers bear most of the load. The tensile modulus for AS-4 carbon fiber is 234 GPa and the strain to failure is 1.61% [37]. Therefore in the actual composite system fiber tensile strains of greater than 1.61% will inevitably lead to catostrophic failure of the composite and are irrelevant when modelling the matrix behavior. The fibers have a high modulus and a low strain to failure compared to the model matrix properties, therefore only low strains of the model matrix samples are reasonable for comparison to the actual composite matrix system.

The 10x05 (TMA^+) and 30x05 (NH_4^+) blends loaded in tension failed in a consistent brittle mode of failure. The failure appeared macroscopically to be entirely elastic, as no necking was visible. The stress-strain curves showed little to no plastic deformation as failure typically occured immediately after a local maximum in the stress which characterized the yielding point. These observations can be explained by a low molecular weight polyimide dispersed in the

PEEK, decreasing the number of molecular entanglements, thereby decreasing the extent of plastic deformation before failure.

Melt Rheology of Ultem-type Polyimide/PEEK blends

The complex melt viscosity of binary model matrix blends was characterized. Figure 3-12 shows that the low frequency complex viscosity (at a frequency of 0.002 sec^{-1}) of the 10x05 (TMA^+) blend is higher than that of the 30x05 (NH_4^+) blend which is higher than that of the 50x05 (TPA^+) blend. All three model matrix blends have a much higher melt viscosity at low frequencies than 380 Grade PEEK. All three model matrix blends also have a much higher melt viscosity at low frequencies than the 5wt% Ultem 1000/PEEK blend.

An explanation for the higher melt viscosity for the model matrix polyimide/PEEK blends is an increase in molecular weight of the polyimide component by a crosslinking reaction. It is important to recall the complex viscosity of the model interphase polyimides during a simulated consolidation temperature cycle from Figure 3-9 at this point. It was shown in Figure 3-9 that the melt viscosities of all the model interphase polyimides increased during an isothermal hold at 380°C. This provides evidence that chemically active species are present in the interphase polyimides. Therefore it follows that the model matrix blends also have chemically active species present in the polyimide component allowing for possible chain extension and/or crosslinking. Due to the miscible nature of PEEK and Ultem polyimide, the 5 wt% blend could effectively dilute the polyimide component thereby limiting the opportunity for polyimide crosslinking. The preparation of the model matrix samples for melt

rheology used the same procedure as for composite prepregging and fabrication except that carbon fibers were not present. Therefore, the melt rheology of the model matrix blends provides information about the competing mechanisms of polyimide/PEEK interdiffusion, which would supress polyimide crosslinking, and crosslinking of the polyimide component, which would hinder interdiffusion.

The trend of increasing blend melt viscosity does not follow the expected trend of polyimide component molecular weight. The initial number average molecular weights of the polyimide components, as measured by GPC and discussed earlier in this chapter, are tabulated in Table 3-V along with the complex viscosity at a frequency of 0.004 s^{-1}. The melt viscosity of a miscible blend is expected to be somewhere between the melt viscosities of the two components of the blend [39-41]. This is found for the case of the 5wt% Ultem 1000/PEEK blend where the complex viscosity is between the complex viscosities for neat Ultem 1000 and neat 380 Grade PEEK at 0.004 s^{-1}. The complex viscosities for the model matrix blends at 0.004 s^{-1} are much greater than the neat 380 Grade PEEK indicating that the polyimide phase is contributing to a larger melt viscosity. The greatest blend melt viscosity is for the Ultem-type TMA^+ polyimide/PEEK blend which has an intermediate initial polyimide molecular weight. The Ultem-type NH_4^+ polyimide/PEEK blend has the lowest initial polyimide molecular weight yet has the second highest blend melt viscosity. The Ultem-type TPA^+ polyimide/PEEK blend has the highest initial polyimide molecular weight, yet has the lowest blend melt viscosity. These observations are explained by considering the initial polyimide molecular weight as well as the changes in polymer microstructure.

Table 3-V. Parameters of polyimides for discussion of molecular weight changes.

	initial PI M_n	η^* (ω=0.004s^{-1})	$\eta^*_{mmtx}/\eta^*_{Ultem1000/PEEK\ blend}$	chemical activity of polyimide component
10x05[a]	10,500	90,600 Pa·sec	21.6	high
30x05[b]	2,780	54,000 Pa·sec	13.0	high
50x05[c]	16,000	15,300 Pa·sec	3.6	low
PEEK[d]	N/A	4,900 Pa·sec		
Ultem 1000/ PEEK	19,000	4,200 Pa·sec		
Ultem 1000	19,000	1,600 Pa·sec		

a - 5 wt%Ultem-type TMA^+ polyimide/PEEK blend
b - 5 wt% Ultem-type NH_4^+ polyimide/PEEK blend
c - 5 wt%Ultem-type TPA^+ polyimide/PEEK blend
d - neat 380 Grade PEEK

If the chemical activity of the polyimide present in the model matrix blend is sufficiently high, then it is possible for chain extension and/or crosslinking reactions to occur which will increase the blend melt viscosity greatly. Since the melt viscosity of the Ultem 1000/PEEK blend lies between the melt viscosities of the constitutive components of the blend, the melt viscosities of the model matrix blends are normalized with respect to the Ultem1000/PEEK blend in Table V. The ratio of the melt viscosity of the model matrix blend to the melt viscosity of the Ultem1000/PEEK blend can be used to qualitatively rank the chemical acitvity of the polyimide components in the model matrix blends.

Although the Ultem-type NH_4^+ polyimide/PEEK blend has the lowest initial polyimide molecular weight, it has the second highest model matrix blend melt viscosity. The melt viscosity of the Ultem-type NH_4^+ polyimide/PEEK blend at 0.004 s^{-1} is 13.0 times greater than the melt viscosity of the Ultem 1000/PEEK blend. This could be attributed to a highly chemically active polyimide component in the blend.

The Ultem-type TMA^+ polyimide/PEEK blend has an intermediate initial polyimide molecular weight, yet it has the highest model matrix blend melt viscosity. The melt viscosity of the Ultem-type TMA^+ polyimide/PEEK blend at 0.004 s^{-1} is 21.6 times greater than the melt viscosity of the Ultem 1000/PEEK blend. This also can be attributed to a highly chemically active polyimide component in the blend. Since the initial polyimide molecular weight of the Ultem-type TMA^+ polyimide is 3.8 times greater than the molecular weight of the Ultem-type NH_4^+ polyimide, interdiffusion of the Ultem-type TMA^+ polyimide component will be slower. The slower interdiffusion would provide more opportunity for crosslinking among the polyimide component and it is reasonable that the melt viscosity of the Ultem-type TMA^+ model matrix blend is greater.

The Ultem-type TPA^+ blend has the lowest melt viscosity of the model matrix blends yet it has the greatest initial polyimide molecular weight. The melt viscosity of the Ultem-type TPA^+ polyimide/PEEK blend at 0.004 s^{-1} is 3.6 times greater than the melt viscosity of the Ultem 1000/PEEK blend. This can be attributed to a low chemical activity of the polyimide component. This behavior is similar to the Ultem 1000/PEEK blend where the initial polyimide molecular weight is high but the polyimide component in the blend is essentially non-reactive, thus the melt viscosity of the blend is low.

The data shown in Figure 3-12 for the Ultem-type TMA^+ polyimide/PEEK blend, the Ultem-type NH_4^+ polyimide/PEEK blend and the neat PEEK sample are from frequency sweeps starting from low frequency increasing in frequency up to 0.1 Hz and then decreasing in frequency back to the starting frequency. As seen in Figure 3-12, the curves do not overlap each other. There is a time difference of about 42 minutes from the first data point at 0.002 Hz and

the last data point at 0.002 Hz. For all these cases, during this 42 minute isothermal hold at 380°C, the complex viscosity of the blend increased. The increase in melt viscosity of PEEK during an isothermal hold has been attributed to chain scission follwed by crosslinking by Day et al. [42].

It is also possible that ketimine formation could occur between hydrolyzed polyimide chains and the ketone species in PEEK. The possible ketimine reaction is shown in Figure 3-13. Ketimine formation would result in branched or crosslinked polymer chains which would increase the blend melt viscosity, decrease further interdiffusion and hinder subsequent crystallization of the PEEK component. The ketimine reaction would also produce water, the presence of which could further hydrolyze the polyimide and promote further crosslinking reactions. Another possible explaination for the greater melt viscosity of the Ultem-type polyimide/PEEK blends is interaction of chemically active polyimide species with ionic endgoups on the PEEK chains.

Differential Scanning Calorimetry of Ultem-type Polyimide/PEEK blends

Differential scanning calorimetry was used to find the glass transition temperatures for the Ultem-type polyimide/PEEK blends and also to quantify the effect of the presence of the polyimide on the crystalline content of the PEEK fraction.

Hudson et al. has shown that the presence of Ultem 1000 polyimide in PEEK can decrease the crystallization kinetics, but a consistent crystalline fraction compared to neat PEEK is attainable utilizing longer crystallization times [32]. The examination of the microstructure of

PEEK/Ultem 1000 polyimide blends by Hudson et al. with PEEK mass fractions of 25%, 50% and 75% revealed that the polyimide segregates to the amorphous phase and the PEEK crystallizes much as in pure PEEK [32].

The DSC traces for the heating scan are shown in Figure 3-14 for model matrix polyimide/PEEK blends and the neat 380 Grade PEEK. As shown in Figure 3-14, a single glass transition temperature was found for the blends indicating no phase separation. Since the neat polyimides processed from water soluble polyamic acid salts can crosslink in the temperature range used to consolidate the composites, it is possible that during the pressing of the polymer blend films, the polyimide would not be well mixed with the PEEK before crosslinking could occur. While the concentration of Ultem-type polyimide is low, complicating the interpretation, the presence of a single T_g for the model matrix 5 wt% polyimide/PEEK blends suggests that the blend is well mixed. This will be addressed in more detail later.

The melting endotherms shown during the heating scan show that the fraction of crystalline PEEK in the samples does not vary significantly. The heats evolved during melting are very similar and differences in the melting temperatures are virtually undetectable. The glass transition temperatures and the heats of melting are tabulated in Table VI.

Table 3-VI. DSC results and calculated crystalline fractions for Ultem-type polyimide/PEEK blends and neat PEEK samples.

	Δh^f (J/g) (heating)	T_g (°C) (heating)	X_c (%) (heating)	Δh^f (J/g) (cooling)	T_g (°C) (cooling)	X_c (%) (cooling)
10x05[a] TMA^+ PI/PEEK	-41.9	161	34	43.0	153	35
30x05[b] NH_4^+ PI/PEEK	-45.6	162	37	44.1	153	36
50x05[c] TPA^+ PI/PEEK	-44.3	163	36	44.2	152	36
neat 380 Grade PEEK[d]	-48.4	155	37	43.9	149	34
5wt% Ultem 1000/PEEK	-43.8	164	35	42.9	151	35
10x50[e] 50%TMA^+ PI/PEEK	----	178	----	----	----	----
30x50[f] 50% NH_4^+ PI/PEEK	----	176	----	----	165	----
50x50[g] 50% TPA^+ PI/PEEK	----	184	----	----	177	----

a - 5 wt%Ultem-type TMA^+ polyimide/PEEK blend
b - 5 wt% Ultem-type NH_4^+ polyimide/PEEK blend
c - 5 wt%Ultem-type TPA^+ polyimide/PEEK blend
d - neat 380 Grade PEEK
e - 50 wt%Ultem-type TMA^+ polyimide/PEEK blend
f - 50 wt% Ultem-type NH_4^+ polyimide/PEEK blend
g - 50 wt%Ultem-type TPA^+ polyimide/PEEK blend

The DSC traces for the cooling scan are shown in Figure 3-15 for model matrix polyimide/PEEK blends and the neat 380 Grade PEEK. The crystallization exotherms during the subsequent cooling scan, shown in Figure 3-15, display features of very different crystallization kinetics. The most notable of these features is the temperature of maximum crystallinity, T_x^{max}, as defined by the temperature at the peak of the crystallization exotherm. The T_x^{max} values follow almost the exact same trend as the melt rheology results for the model matrix blends and neat PEEK. In this manner, the melt viscosities of the polyimide/PEEK blends can be used to

understand the crystallization kinetics of the PEEK component in the blend.

Table 3-VII. Ranking of model 5 wt% Ultem-type polyimide/PEEK blends and neat 380 Grade PEEK by complex melt viscosity and temperature of maximum crystallinity.

Ranking by highest η^* (ω=0.004s^{-1})	Ranking by lowest T_x^{max}(°C)
10x05[a]	10x05[a]
30x05[b]	30x05[b]
50x05[c]	Ultem 1000/PEEK[e]
PEEK[d]	50x05[c]
Ultem 1000/PEEK[e]	neat 380 Grade PEEK[d]

a - 5 wt%Ultem-type TMA^+ polyimide/PEEK blend
b - 5 wt% Ultem-type NH_4^+ polyimide/PEEK blend
c - 5 wt%Ultem-type TPA^+ polyimide/PEEK blend
d - neat 380 Grade PEEK
e - 5 wt% Ultem 1000/PEEK blend

The T_x^{max} for the 10x05 blend is the lowest at 266°C and this blend had the highest melt viscosity as seen in Figure 3-15. The T_x^{max} for the 30x05 blend is higher at 274°C and this blend had the second highest melt viscosity as seen in Figure 3-12. The retardation of the crystallization kinetics for the 30x05 blend and the 10x05 blend as identified by the lower T_x^{max} and the broad nature of the crystallization exotherm which can be attributed to the decrease in molecular mobility of the PEEK component due to the presence of a branched or crosslinked polyimide component.

The crystallization exotherms for the 5 wt% Ultem 1000/PEEK blend, 5 wt% Ultem-type TPA^+ polyimide/PEEK blend and the neat 380 Grade PEEK sample are more narrow than the 5 wt% Ultem-type TMA^+ polyimide/PEEK blend and 5 wt% Ultem-type NH_4^+ polyimide/PEEK blend. The polyimide components for the Ultem 1000/PEEK blend and the 5 wt% Ultem-type

TPA^+ polyimide/PEEK blend are considered to be non-reactive and of low chemical activity, respectively. Therefore, the retardation in crystallization kinetics is attributed to the presence of linear polyimide chains distributed throughout the PEEK component. Since the was no polyimide present in the neat 380 Grade PEEK sample, it had no impediments to the crystallization kinetics. Therefore, crystallization was a rapid and spontaneous process, as represented by the relatively sharp crystallization exotherm during the cooling scan.

Although a single T_g is found for the 5 wt% polyimide/PEEK blends, there is concern that 5 wt% polyimide is not a sufficient mass fraction to be detectable by DSC should phase separation occur. Therefore 50 wt% PEEK/PI blends were also examined by DSC and the traces are shown in Figure 3-16. Three scans were run for each sample. The DSC traces shown are typical traces for the 50% polyimide/PEEK blends during heating and cooling thermal histories.

The heating trace for the 10x50 blend shows a single T_g around 178°C followed by a smooth region until the melting endotherm around 320°C. If two distinct phases of Ultem-type TMA^+ polyimide and PEEK existed, a second T_g would be observed in this smooth region between 179° and 320°C since the T_g for the neat Ultem-type TMA^+ polyimide is 203°C. The cooling trace for the 10x50 blend does not show an obvious crystallization exotherm. However subsequent heating traces reveal melting endotherms identical in size and shape for the first heating trace, indicating that crystallization is indeed ocurring. The identification of a T_g on the cooling trace is not readily obvious, presumably due to masking of the change in heat capacity by the broad crystallization exotherm.

The heating trace for the 30x50 blend shows a single T_g around 176°C followed by a melting endotherm around 320°C. The T_g for the neat Ultem-type NH_4^+ polyimide is 153°C. If

two distinct phases of Ultem-type NH_4^+ polyimide and PEEK were present, a second T_g would be observed in the smooth region between 120° and 170°C. The cooling trace for the 30x50 blend does not show a clear crystallization exotherm. However, subsequent heating traces reveal melting endotherms identical in size and shape to the first heating trace, indicating that crystallization is indeed ocurring. A single T_g is visible on the cooling trace at 165°C.

The heating trace for the 50x50 blend shows a single T_g around 184°C followed by an exotherm that could be attributed to PEEK crystallization and a melting endotherm around 320°C. The T_g for the neat Ultem-type TPA^+ polyimide is 220°C. If two distinct phases of Ultem-type TPA^+ polyimide and PEEK were present, a second T_g would be observed in the smooth region between 190° and 250°C. The cooling trace for the 50x50 blend does not show a clear crystallization exotherm. However, subsequent heating traces reveal melting endotherms similar in size and shape to the first heating trace, indicating that crystallization is indeed ocurring. A single T_g is visible on the cooling trace at 177°C.

It is worth noting that a T_g is visible during the cooling traces for the 30x50 blend and the 50x50 blend but not visible for the 10x50 blend. The masking of the T_g during the cooling scan by a broad crystallization exotherm is evident when considering the DSC results for the 5 wt% Ultem-type polyimide blends from Figure 3-15. Since the crystallization exotherm occurs at the lowest temperature for the 10x05 blend, it follows that the 10x50 blend will also have a crystallization exotherm at the lowest temperature. These observations are all attributable to slower PEEK crystallization kinetics in the presence of the branched or crosslinked Ultem-type TMA^+ polyimide.

The glass transition temperatures of miscible blends can be predicted with the Fox

equation if the blend composition and the T_g's of the pure components are known [43]. The Fox equation is:

$$\frac{1}{T_g} = \frac{W_1}{T_{g1}} + \frac{W_2}{T_{g2}} \qquad \text{Eq. 3-2}$$

where T_g is the predicted glass transition temperature of the blend, T_{g1} and T_{g2} are the glass transition temperatures of component 1 and 2 respectively, and W_1 and W_2 are the mass fractions of component 1 and 2 respectively [43]. The measured T_g's of the Ultem-type polyimide/PEEK blends are compared to predicted values by the Fox equation in Figure 3-17. The measured T_g's used for the calculations were all obtained from DSC heating scans. The agreement for the Ultem-type TMA^+ polyimide/PEEK blend and the Ultem-type TPA^+ polyimide/PEEK blend is quite good. The positive deviations from predicted values by the Fox equation are attributed to the presence of the crystalline PEEK fraction which increases the concentration of polyimide in the amorphous region. Similar positive deviations from values predicted by the Fox equation were observed by Hsiao and Sauer for blends of Ultem 1000 and PEEK [20]. The extreme deviation at 50 wt% Ultem-type NH_4^+ polyimide is not understood and is attributed to the complex microstructure resulting from possibilities discusses earlier such as polyimide crosslinking, ketimine formation, and interaction of chemically active polyimide species with ionic endgoups on the PEEK chains.

Diffusion Calculations

Representative diffusion coefficients were calculated using Eq. 3-3 for a temperature dependent diffusion coefficient,

$$D = D_0 \cdot e^{-\frac{E_a}{R \cdot T}} \qquad \text{Eq. 3-3}$$

where D_o = diffusion coefficient constant (0.07 cm^2/s)
E_a = activation energy for diffusion (14 kcal/mole)
R = thermodynamic constant
T = temperature.

The constants D_o and E_a used in Eq.3-3 were determined by FTIR/ATR for Ultem 1000/PEKK blends by Hsiao and Sauer and used to model the diffusion of Ultem 1000 and PEEK [20]. The results from calculations of temperature dependent diffusion coefficients are shown in Figure 3-18. The temperature range examined in Figure 3-18 was 250°-380°C but the most important range of temperatures is 345°-380°C because this is above the melting temperature of PEEK. In this temperature range the diffusion coefficient varies between $2x10^{-10}$ and $1x10^{-9}$ cm^2/sec.

Although interdiffusion of Ultem polyimide and PEEK will occur at temperatures above the glass transition temperatures for both components, the extent of interdiffusion must be considered. For instance, temperatures around 230°C are above the T_g of PEEK and all of the Ultem-type polyimides. It is important to note that the ordinate for Figure 3-18 is a log scale. The diffusion coefficient is about three orders of magnitude smaller at 230°C than the diffusion coefficient at 340°C. Therefore it can be shown that any interdiffusion that occurs at

temperatures around 230°C is insignificant. Calculations show that the extent of interdiffusion at temperatures less than 345°C is insignificant compared to the interdiffusion which occurs above this temperature. Above 345°C crystalline PEEK melts and more of the PEEK is available for interdiffusion, with the possible exception of very small, ordered nucleation sites. Since the nucleation sites present will represent only a small fraction of the PEEK mass, they are considered insignificant with regard to the interdiffusion process.

Shown in Figure 3-19 are calculated diffusion times for Ultem polyimide to diffuse completely into PEEK with diffusion distances of 5.5 µm and 150 nm. The diffusion distance of 5.5 µm was chosen because the blends were made from a dispersion of 11 µm diameter PEEK powder particles and so the 5.5 µm diffusion distance represents the case of a completely mixed blend due to interdiffusion. The diffusion distance of 150 nm was chosen because this is the estimated polyimide layer thickness. Calculation of this layer thickness is shown in Appendix A of Chapter 4. The diffusion times were calculated using Eq.3-4

$$t_{diff} = \frac{(2 \cdot \delta)^2}{D(T)} \qquad \text{Eq. 3-4}$$

where t_{diff} is the diffusion time, δ is the diffusion distance and D(T) is the temperature dependant diffusion coefficient. The diffusion times show that interdiffusion over a distance of 150 nm of the PEEK and the Ultem polyimide occurs after about 30 minutes at 380°C. Since the isothermal hold during composite consolidation is 30 minutes at 380°C, this indicates that complete interdiffusion of the interphase polyimide into the PEEK matrix is expected. However the melt

viscosity results show that factors such as crosslinking occuring during the simulated consolidation isothermal hold at 380°C will limit the interdiffusion of the polymers.

The calculations for diffusion times provide simply an order of magnitude estimate of the diffusion behavior of linear Ultem 1000 polyimide and PEEK. It is not intended that these calculations would model the diffusion behavior of the Ultem-type polyimides made from water soluble polyamic acid salts. The initial molecular weights of all of these polyimides are less than the molecular weight of Ultem 1000, which would increase the diffusion coefficient for a given polyimide. However, branching or crosslinking which was shown to occur for these polyimides would drastically decrease the diffusion coefficient. Therefore, the diffusion calculations are for discussion purposes only and no conclusion can be made with regard to the interdiffusion of PEEK with the Ultem-type polyimides made from water soluble polyamic acid salts.

Conclusions

The purpose of this work was to prepare and characterize model interphase and model matrix samples to represent the polymeric material in Ultem-type polyimide interphase/PEEK matrix composites. For this work, controlled molecular weight Ultem-type polyimides from water soluble polyamic amic acid salts were made. The molecular weights of the Ultem-type polyimides from water soluble polyamic amic acid salts were measured using GPC. The Ultem-type NH_4^+ polyimide was oligomeric and had the lowest molecular weight (M_n = 2,780 g/mol), the Ultem-type TMA^+ polyimide had an intermediate molecular weight (M_n = 10,500 g/mol) and the Ultem-type TPA^+ polyimide had the highest molecular weight (M_n = 16,000 g/mol). Many of

the properties of the Ultem-type TPA^+ polyimide were similar to those of commercial Ultem 1000 polyimide.

The glass transition temperatures of the Ultem-type polyimides were measured using DSC. The Ultem-type NH_4^+ polyimide had the lowest T_g (153°C), the Ultem-type TMA^+ polyimide had an intermediate T_g (203°C) and the Ultem-type TPA^+ polyimide had the highest T_g (220°C) which is very close to the T_g measured for commercial Ultem 1000 (218°C).

It was verified using FTIR that the Ultem-type NH_4^+ polyimide, Ultem-type TMA^+ polyimide and Ultem-type TPA^+ polyimide were all chemically identical to commercial Ultem 1000 after thermal imidization. The glass transition temperatures of the Ultem-type polyimides displayed the expected trend of increasing T_g with increasing molecular weight. The Ultem-type TPA^+ polyimide had the best thermal stability of the Ultem-type polyimides from water soluble polyamic amic acid salts.

Although the Ultem-type NH_4^+ polyimide and the Ultem-type TMA^+ polyimide initially had molecular weights believed to be below the critical entanglement level, an increase in melt viscosity during a simulated processing thermal cycle and a measured gel fraction after a simulated processing thermal cycle both indicate that crosslinking occurs at temperatures above 350°C. After a simulated composite consolidation isothermal hold at 380°C for 30 minutes, the Ultem-type NH_4^+ polyimide had a gel fraction of 21% and the Ultem-type TMA^+ polyimide had a gel fraction of 13%. During the simulated composite consolidation isothermal hold at 380°C for 30 minutes, the melt viscosity of the Ultem-type NH_4^+ polyimide increased by a factor of 57, the melt viscosity of the Ultem-type TMA^+ polyimide increased by a factor of 12 and the melt viscosity of the Ultem-type TPA^+ polyimide increased by a factor of 10.

Model matrix Ultem-type polyimide/PEEK blends were prepared according to identical conditions as for aqueous suspension prepregging. A statistical analysis of the tensile test results for model matrix Ultem-type polyimide/PEEK blends showed that the tensile yield strengths were similar for all blends. This is an important conclusion because it provides verification that differences in composite performance would not be attributed to differences in matrix properties and therefore would be a result of interphase modification.

The melt viscosities of the model matrix Ultem-type polyimide/PEEK blends were characterized. The blends with Ultem-type TMA^+ polyimide and Ultem-type NH_4^+ polyimide had higher melt viscosities than the Ultem-type TPA^+ polyimide/PEEK blend. The results indicate that a complex microstructure exists due to the presence of chemically active polyimide species in the blend.

The miscibility of the Ultem-type polyimide and PEEK was verified by a single T_g for 5 wt% and also 50 wt% Ultem-type polyimide/PEEK blends. There was some correlation between the trends of temperature of maximum crystallization, T_x^{max}, and the blend melt viscosity.

Estimations of the diffusion time at 380°C for Ultem 1000 and PEEK indicate that a diffusion distance of 150 nm requires approximately thirty minutes. Although the interdiffusion of the Ultem-type NH_4^+ polyimide with PEEK and the Ultem-type TMA^+ polyimide with PEEK is expected to occur more rapidly than the predictied diffusion times due to lower initial molecular weights, any crosslinking or branching which occurs will severly limit interdiffusion.

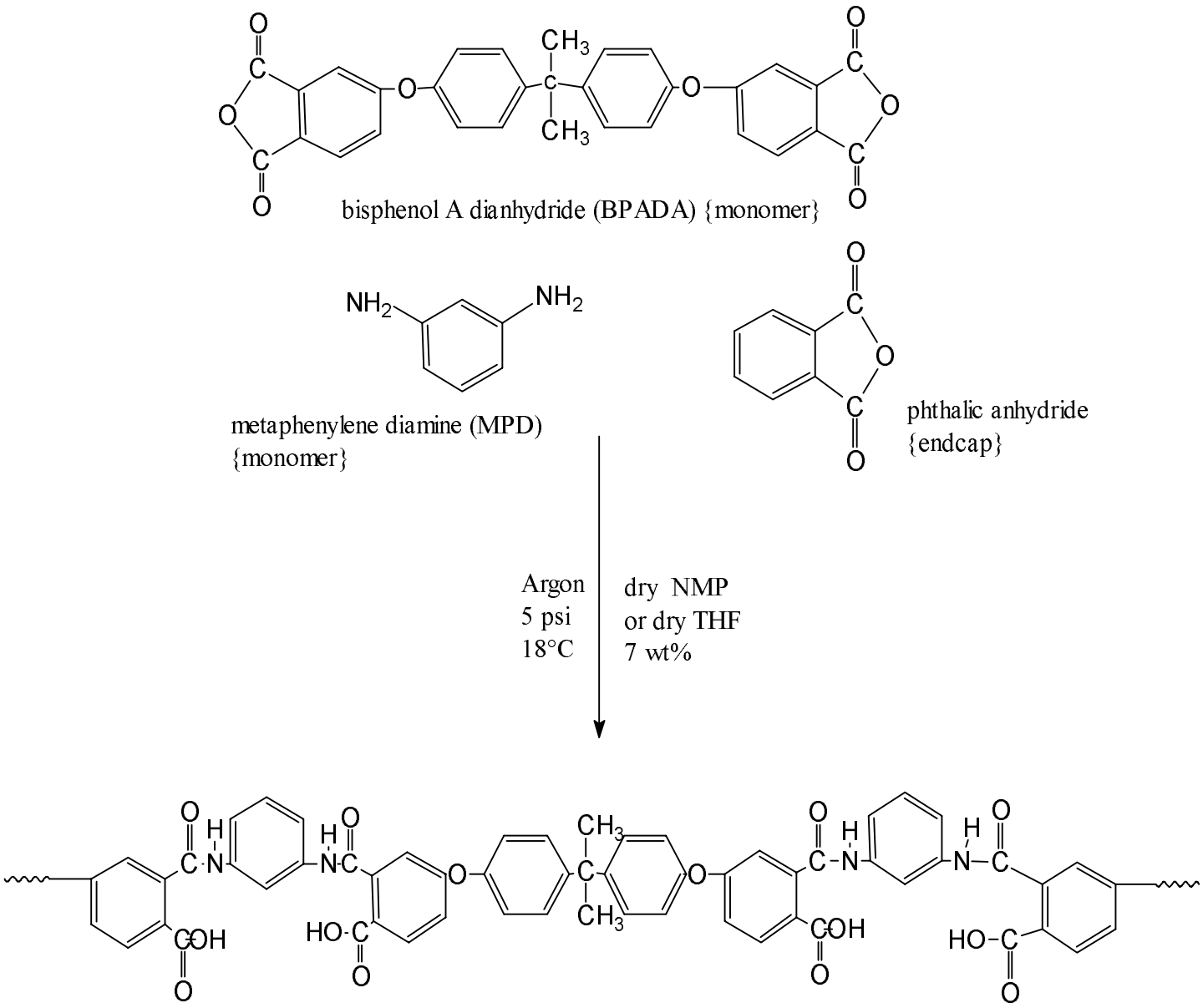

Figure 3-1. Chemical structures of monomers and the synthesis of Ultem-type polyamic acid.

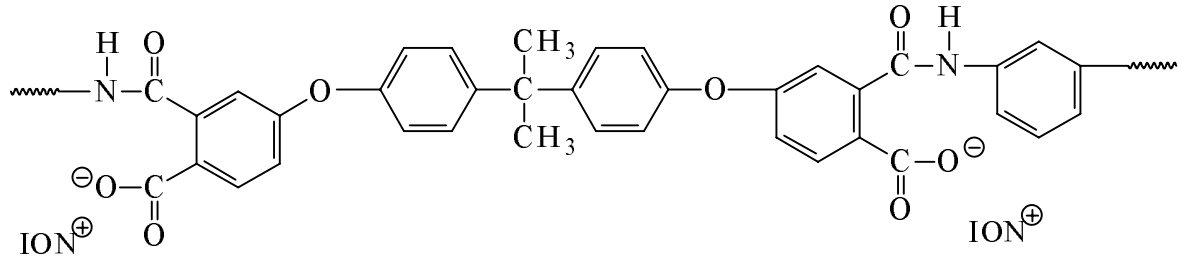

Ultem-type Polyamic Acid made water soluble by addition of basic counterion

Thermal Imidization

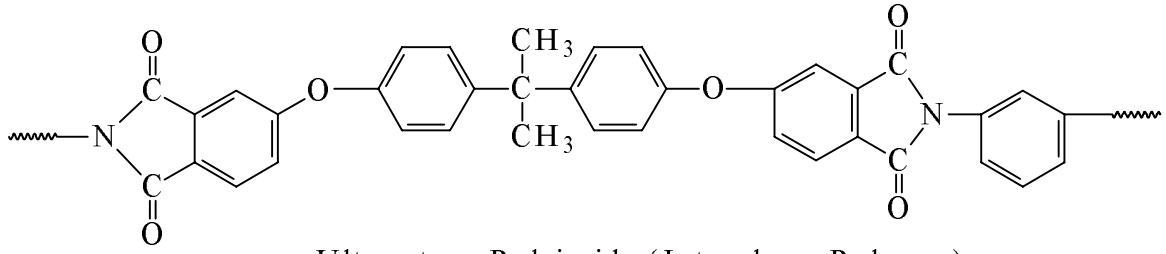

Ultem-type Polyimide (Interphase Polymer)

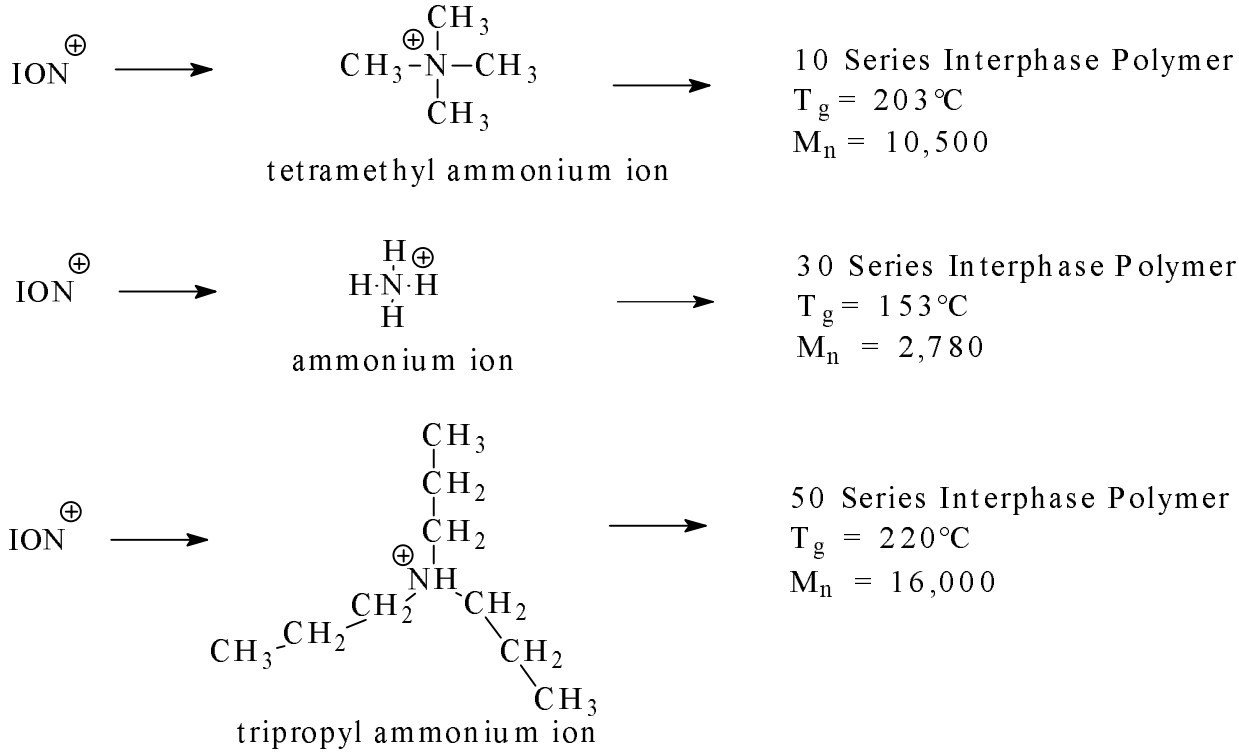

Figure 3-2. Formation of Ultem-type polyamic acid salts using different bases and the glass transition temperatures and number average molecular weight for the polyimide.

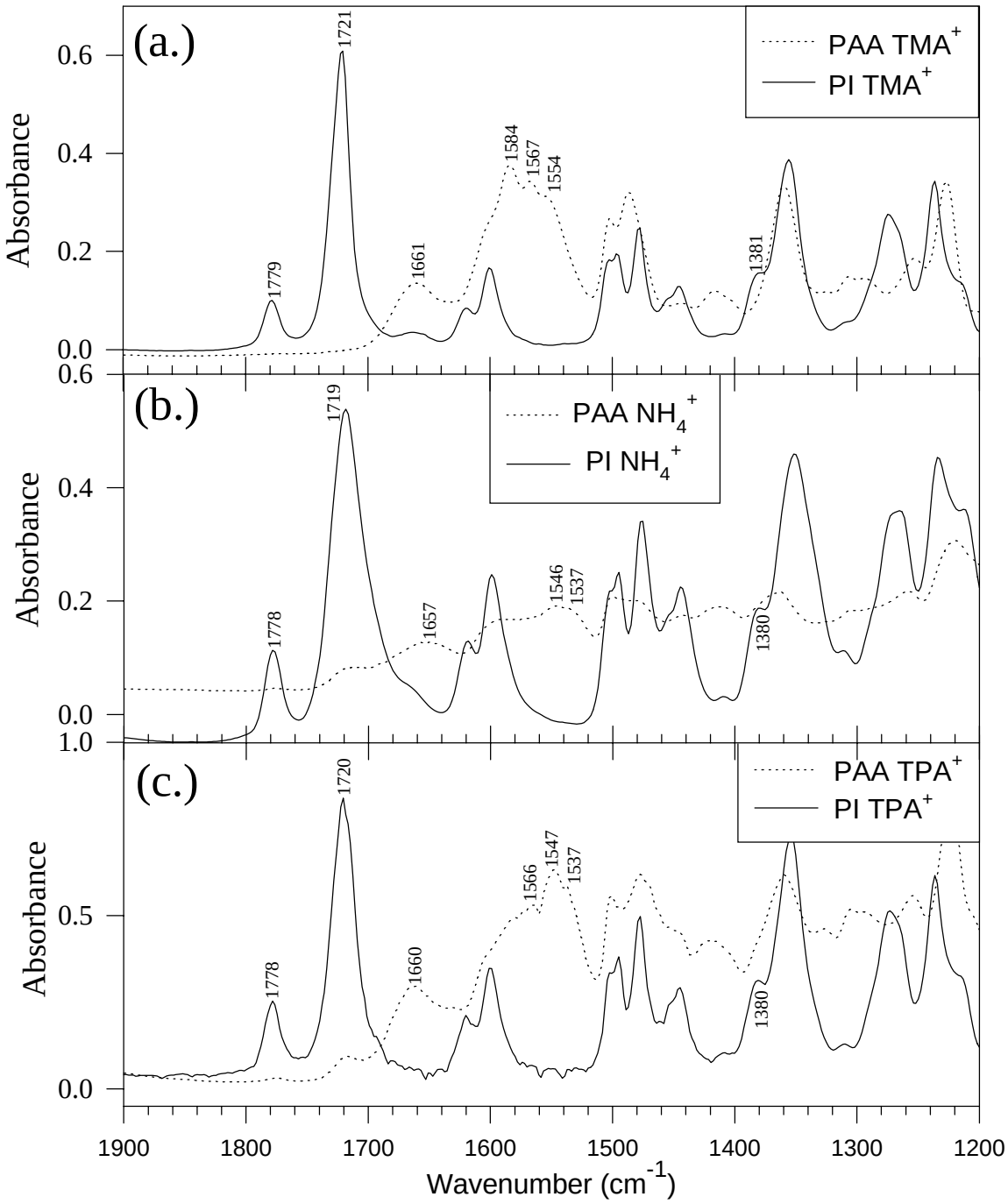

Figure 3-3. FTIR spectra for (a.) Ultem-type TMA^+ polyamic acid salt and Ultem-type TMA^+ polyimide, (b.) Ultem-type NH_4^+ polyamic acid salt and Ultem-type NH_4^+ polyimide, and (c.) Ultem-type TPA^+ polyamic acid salt and Ultem-type TPA^+ polyimide.

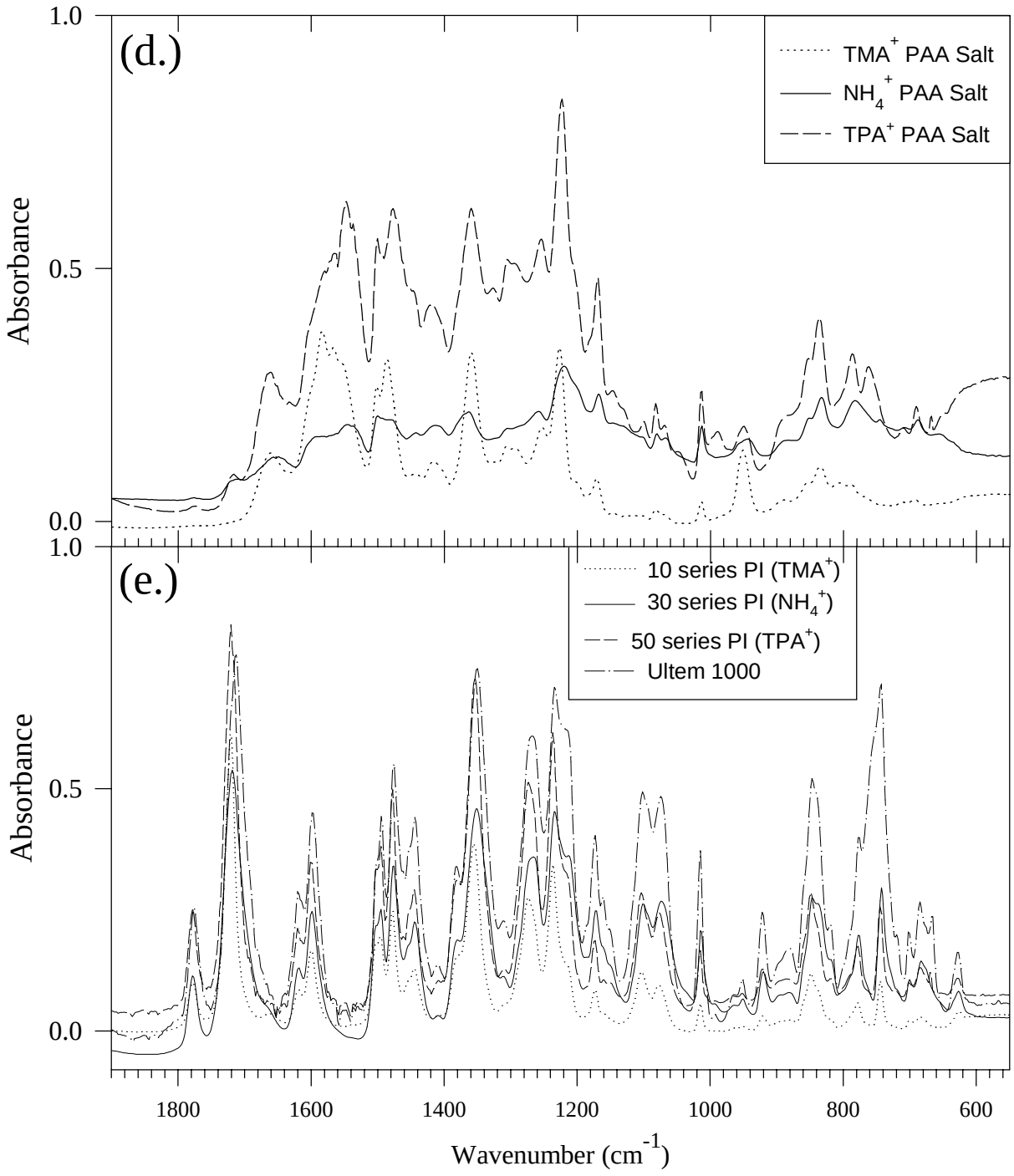

Figure 3-3. (continued) FTIR spectra showing that (d.) although the three Ultem-type polyamic acid salts have different spectra (e.) the chemical structures of all three resulting polyimides and commercial Ultem 1000 are identical.

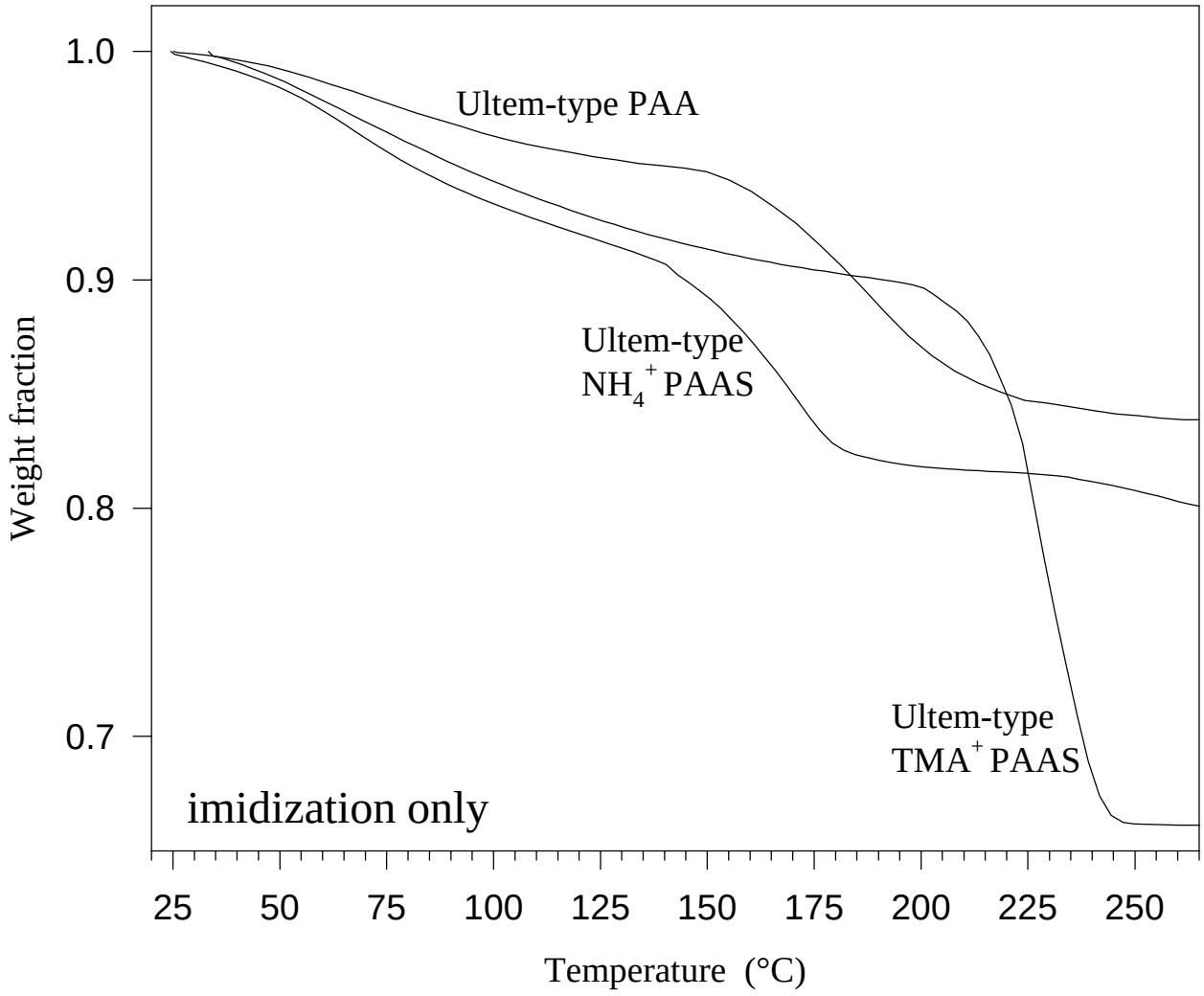

Figure 3-4. TGA scans for Ultem-type polyamic acid salts and neat Ultem-type polyamic acid showing weight loss due to imidization reaction.

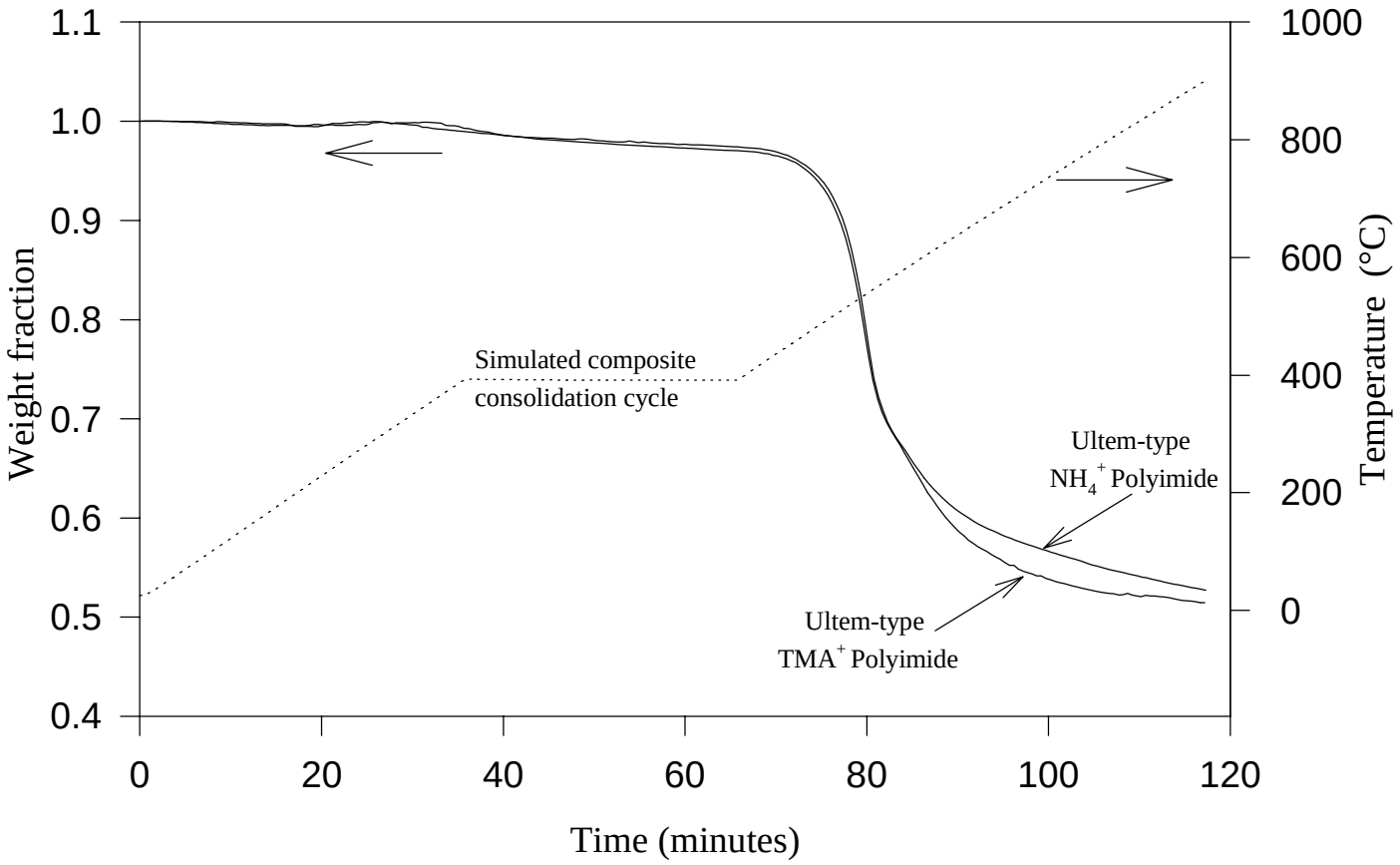

Figure 3-5. TGA scans of simulated consolidation conditions for Ultem-type TMA^+ polyimide and Ultem-type NH_4^+ polyimide.

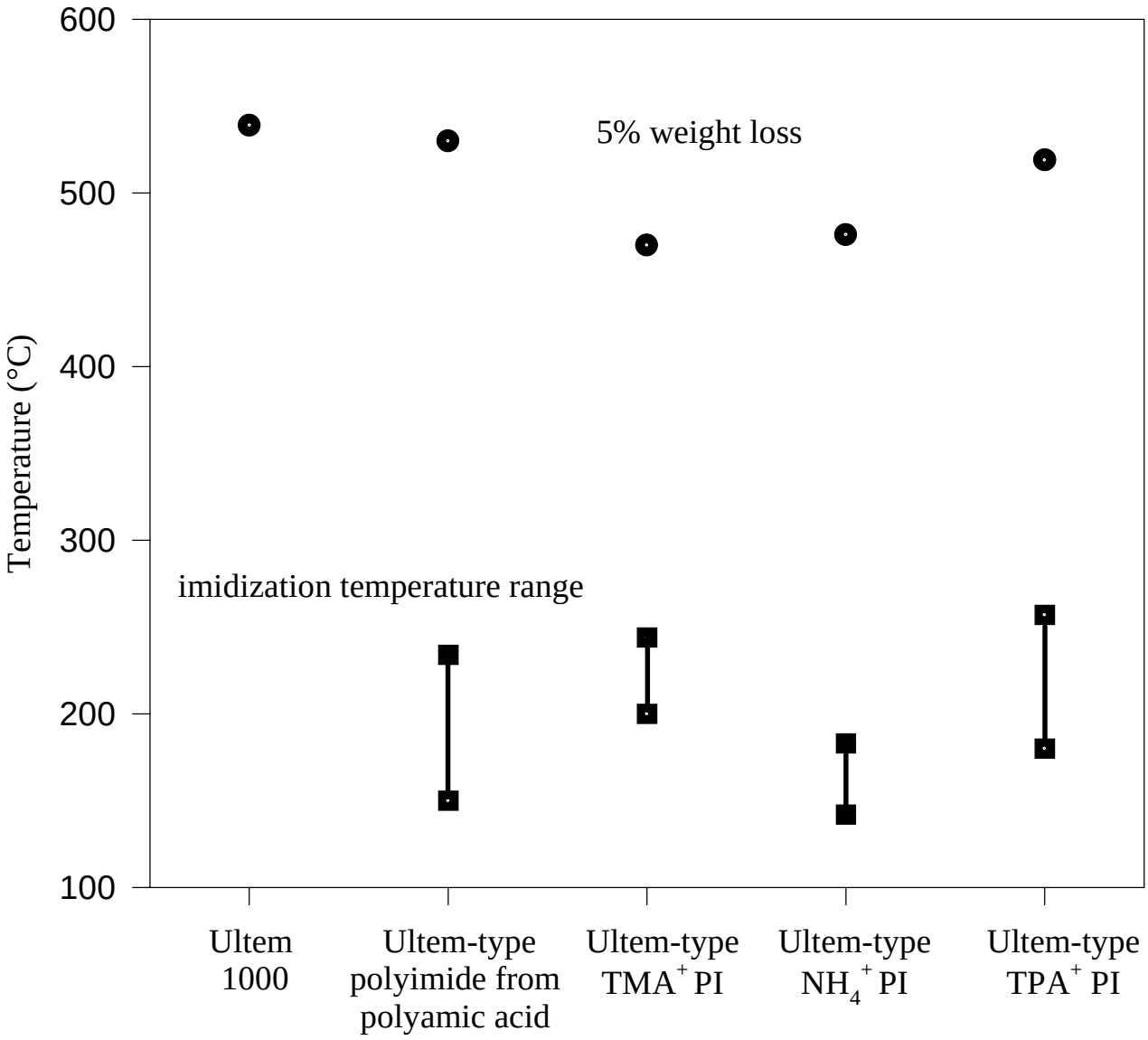

Figure 3-6. Imidization temperatures for model interphase polyamic acid salts and Ultem-type polyamic acid; and 5% weight loss temperatures Ultem-type polyimide.

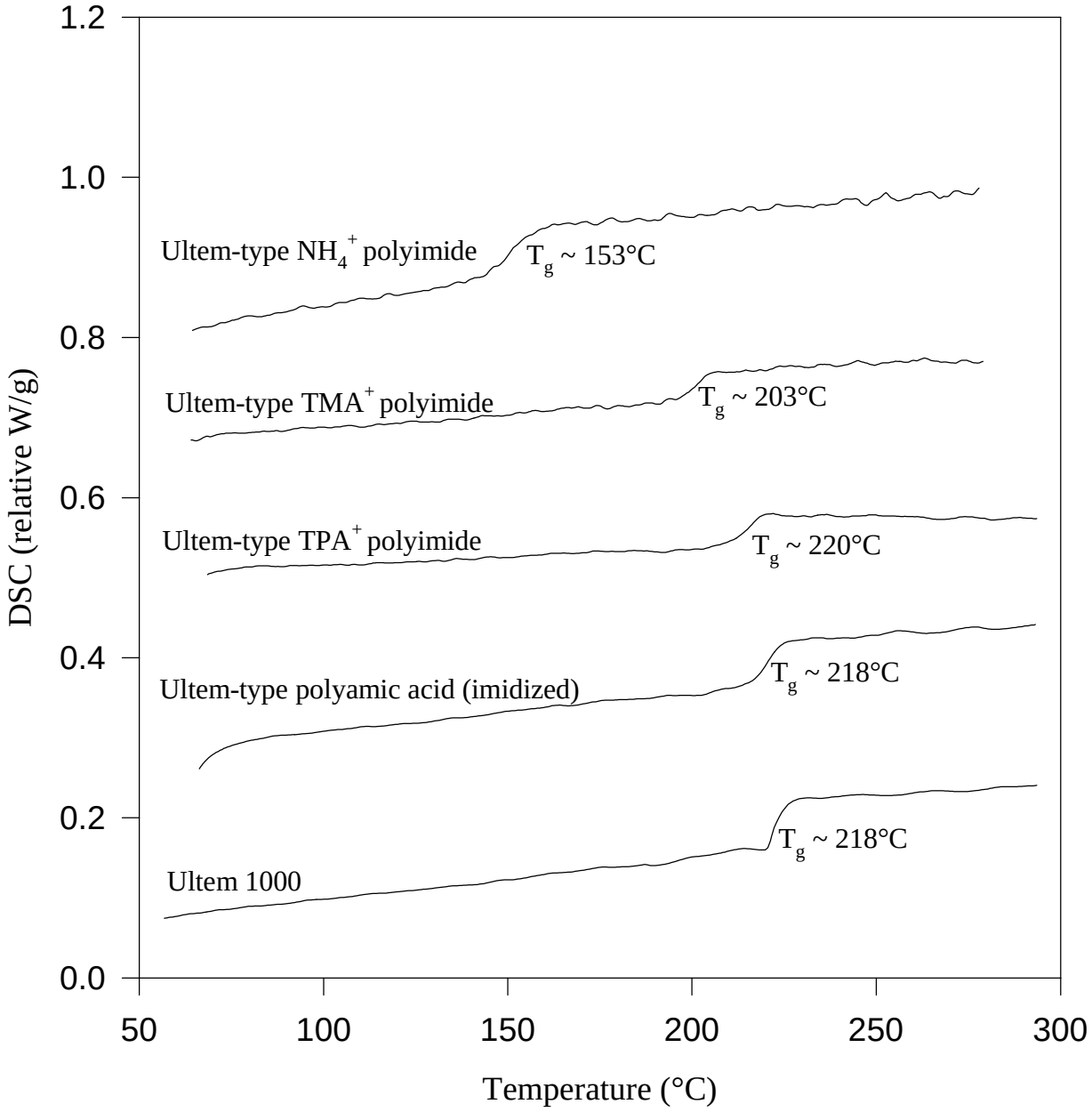

Figure 3-7. DSC scans for Ultem-type model interphase polyimides and commercial Ultem 1000.

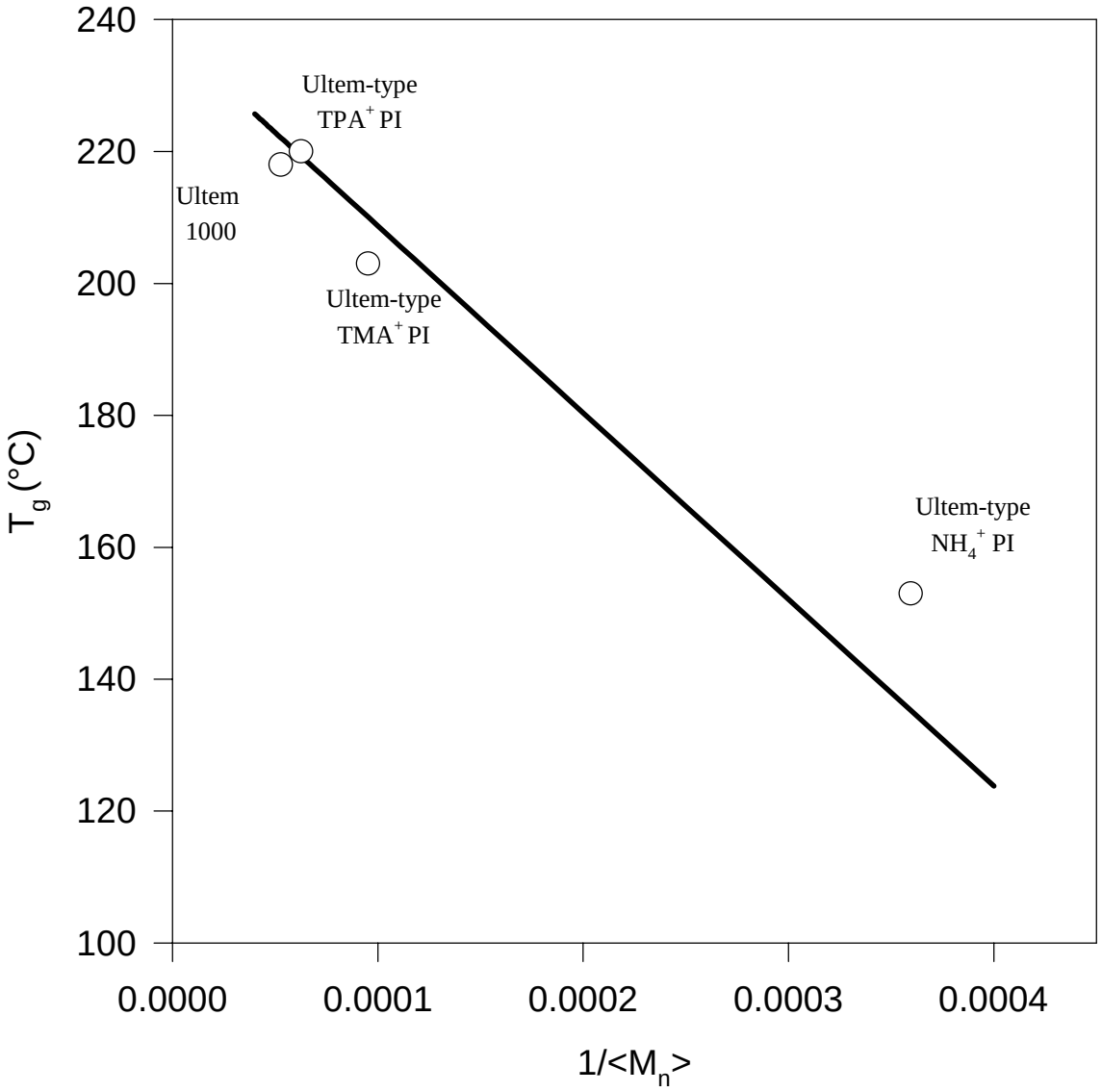

Figure 3-8. T_g of polyimides by DSC vs <M_n> compared to the Fox-Flory relationship using c=215,779 and T_g^{oo}= 230°C.

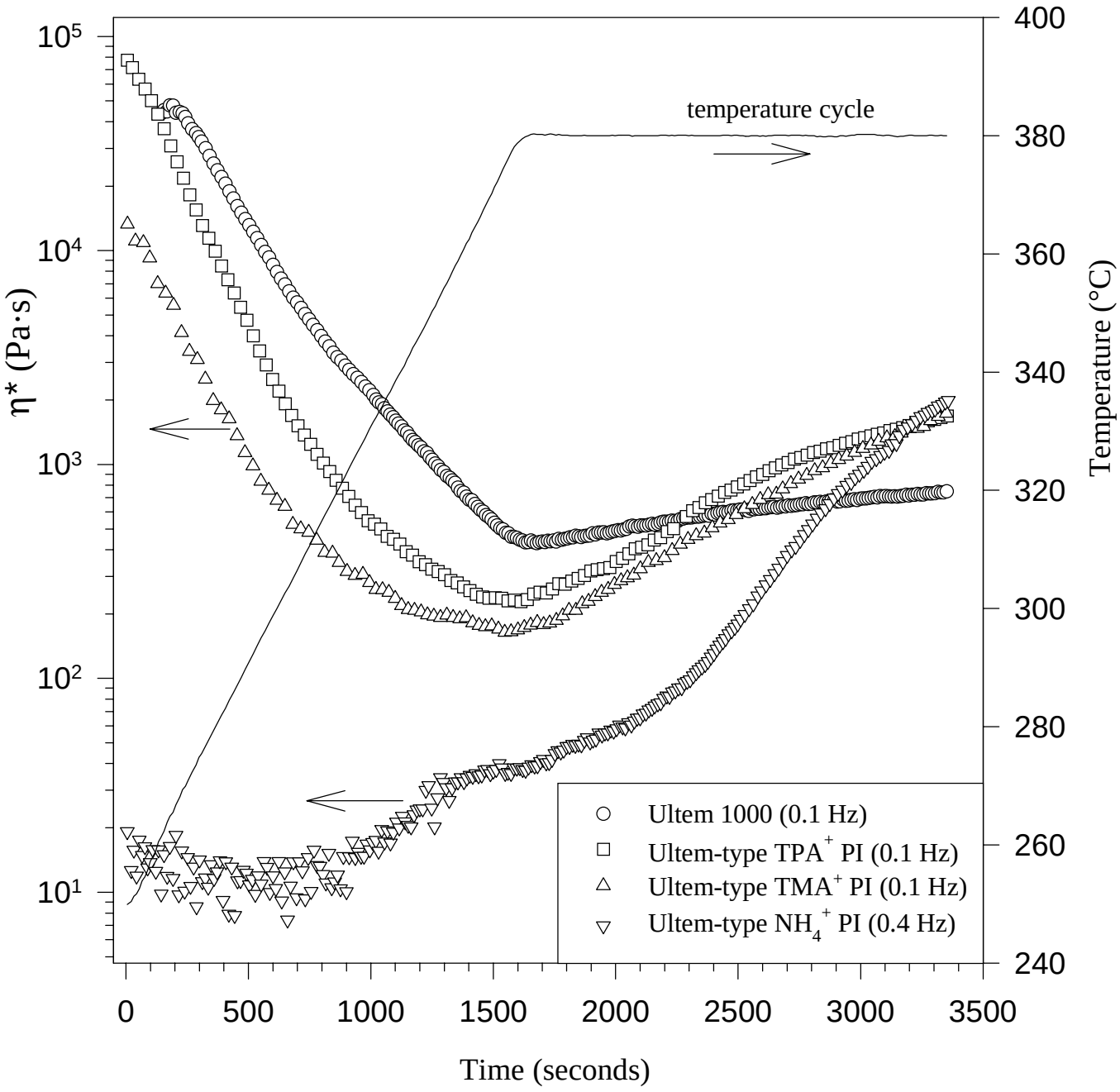

Figure 3-9. Complex viscosity of model interphase polyimides and Ultem 1000 during a simulated consolidation heating cycle.

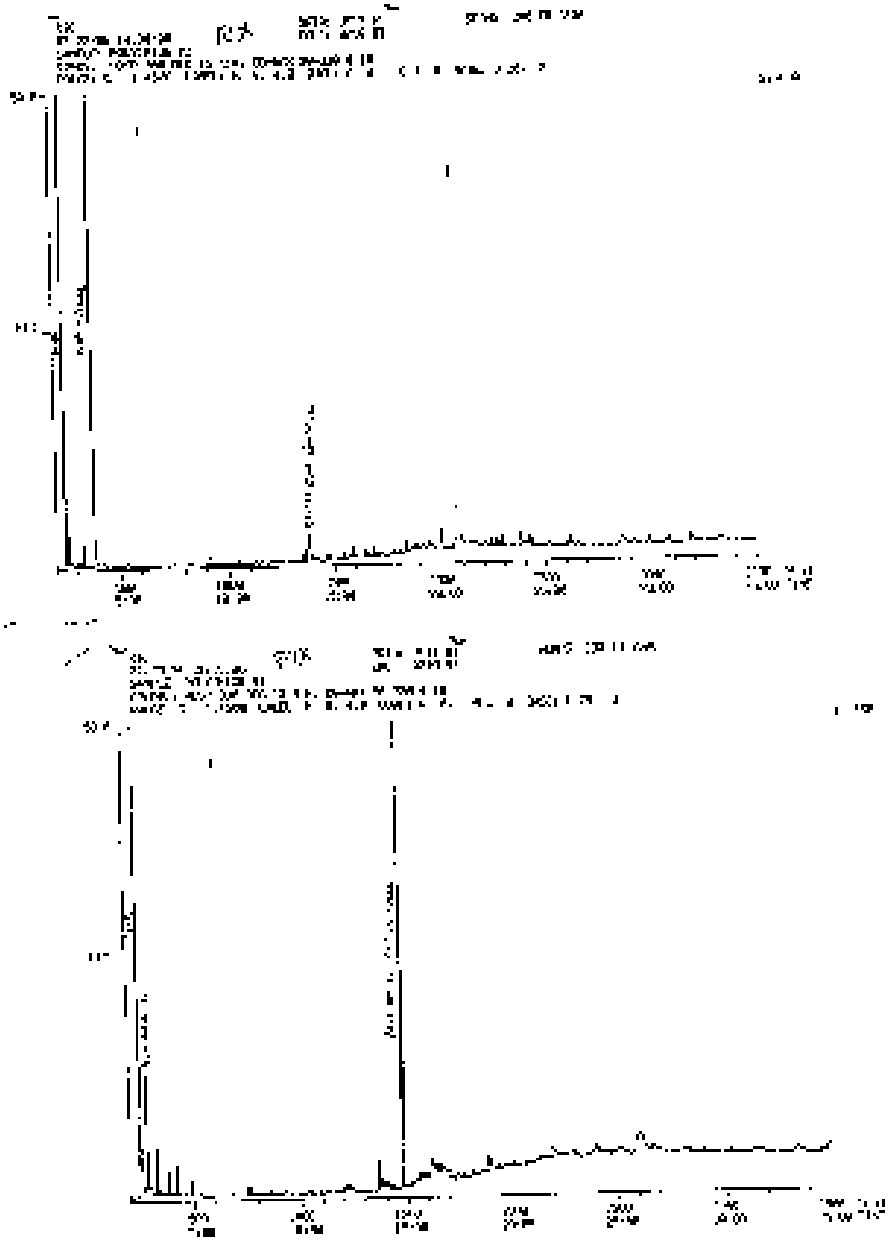

Figure 3-10. Gas chromatograph spectra after pyrolysis for (a.) Ultem-type NH_4^+ polyimide and (b.) Ultem-type TMA^+ polyimide.

(a.)

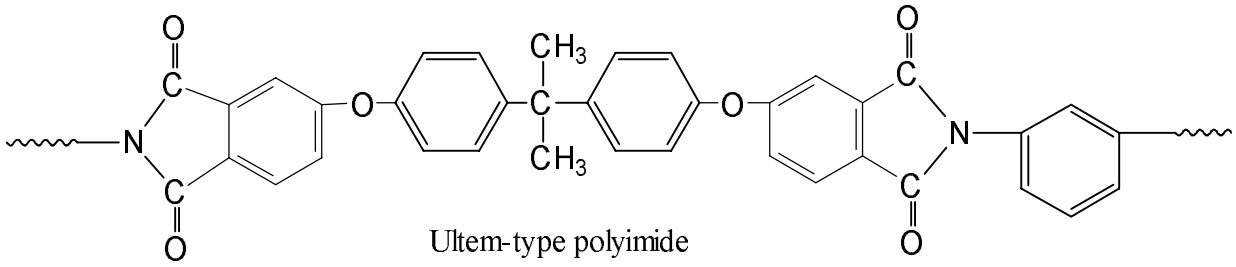

Ultem-type polyimide

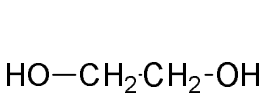

Ethylene glycol

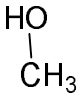

Methanol

Ultem-type TMA polyimide pyrolysis products

(b.)

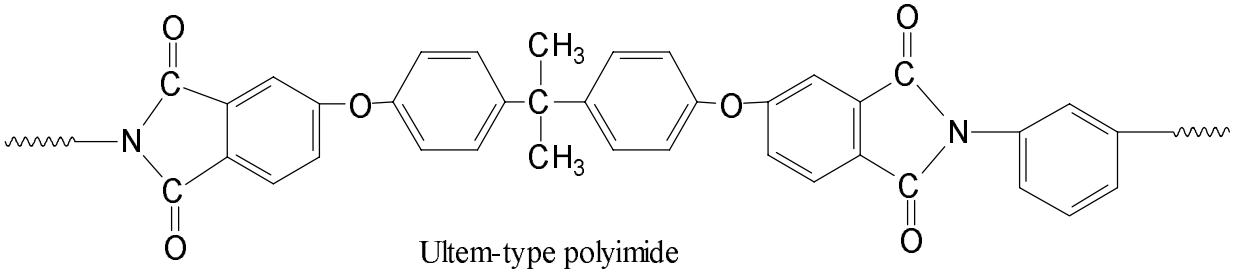

Ultem-type polyimide

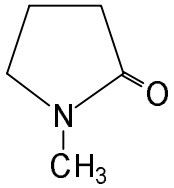

N-Methylpyrrolidone

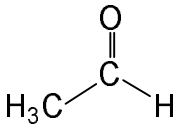

Acetaldehyde

Ultem-type NH_4 polyimide pyrolysis products

Figure 3-11. Chemical structures of Ultem-type polyimide and molecules detected by pyrolysis gas chromotography for (a.) Ultem-type NH_4^+ polyimide and (b.) Ultem-type TMA^+ polyimide.

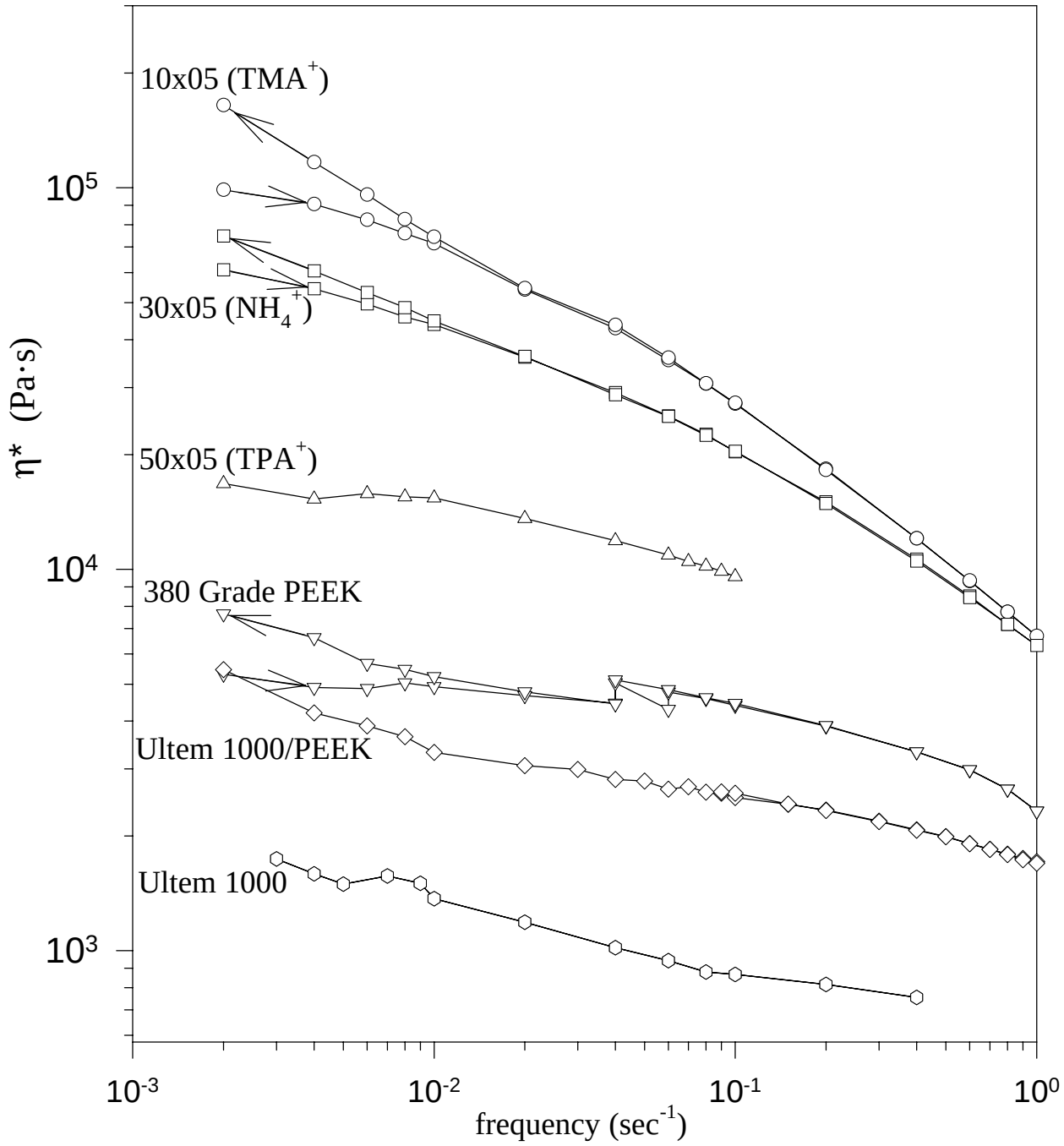

Figure 3-12. Complex viscosity vs. frequency for Ultem-type polyimide/PEEK model matrix blends, neat Ultem 1000 and 380 Grade PEEK at 380°C in nitrogen.

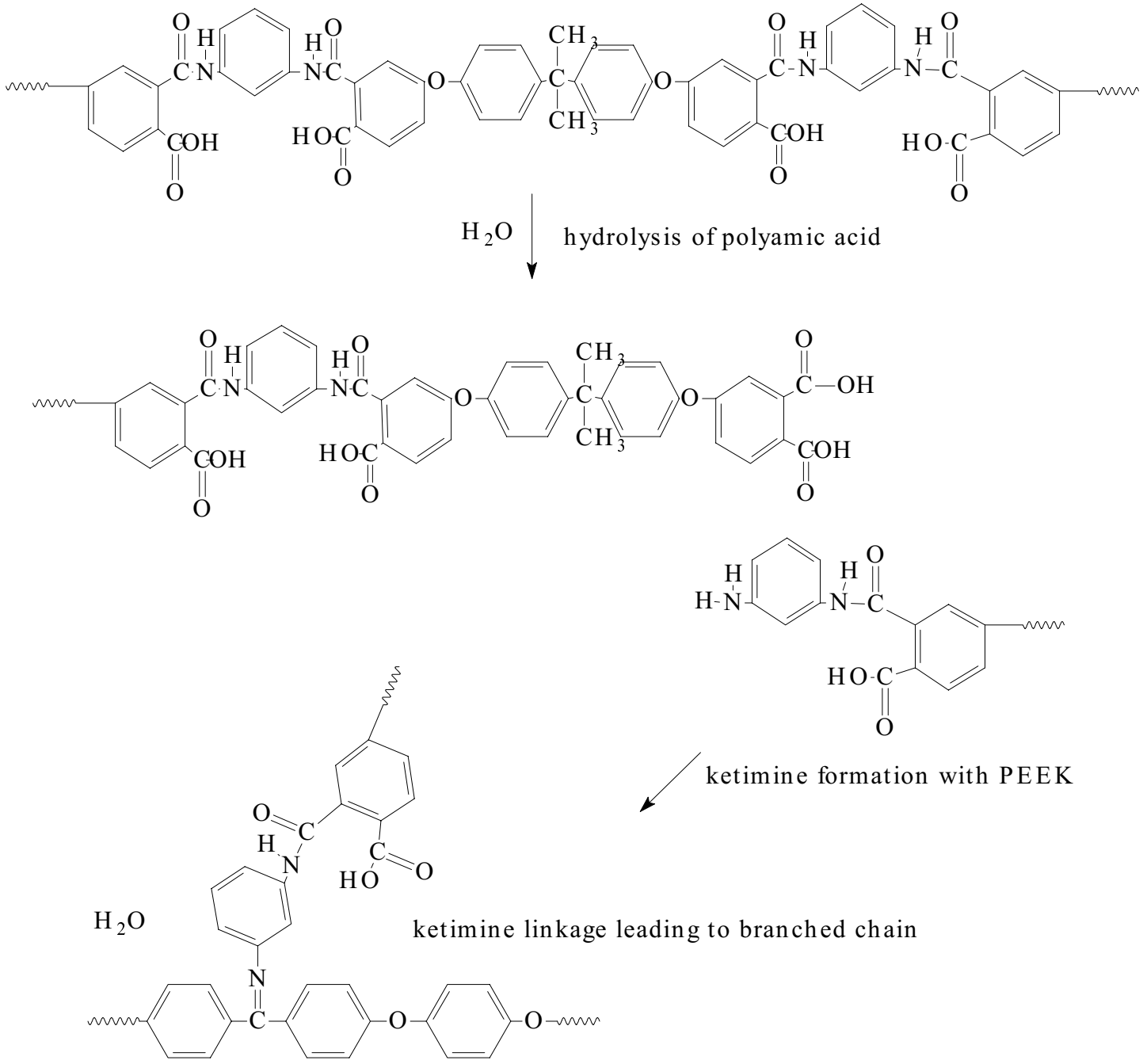

Figure 3-13. Hydrolysis and ketimine formation for Ultem-type polyimide and PEEK.

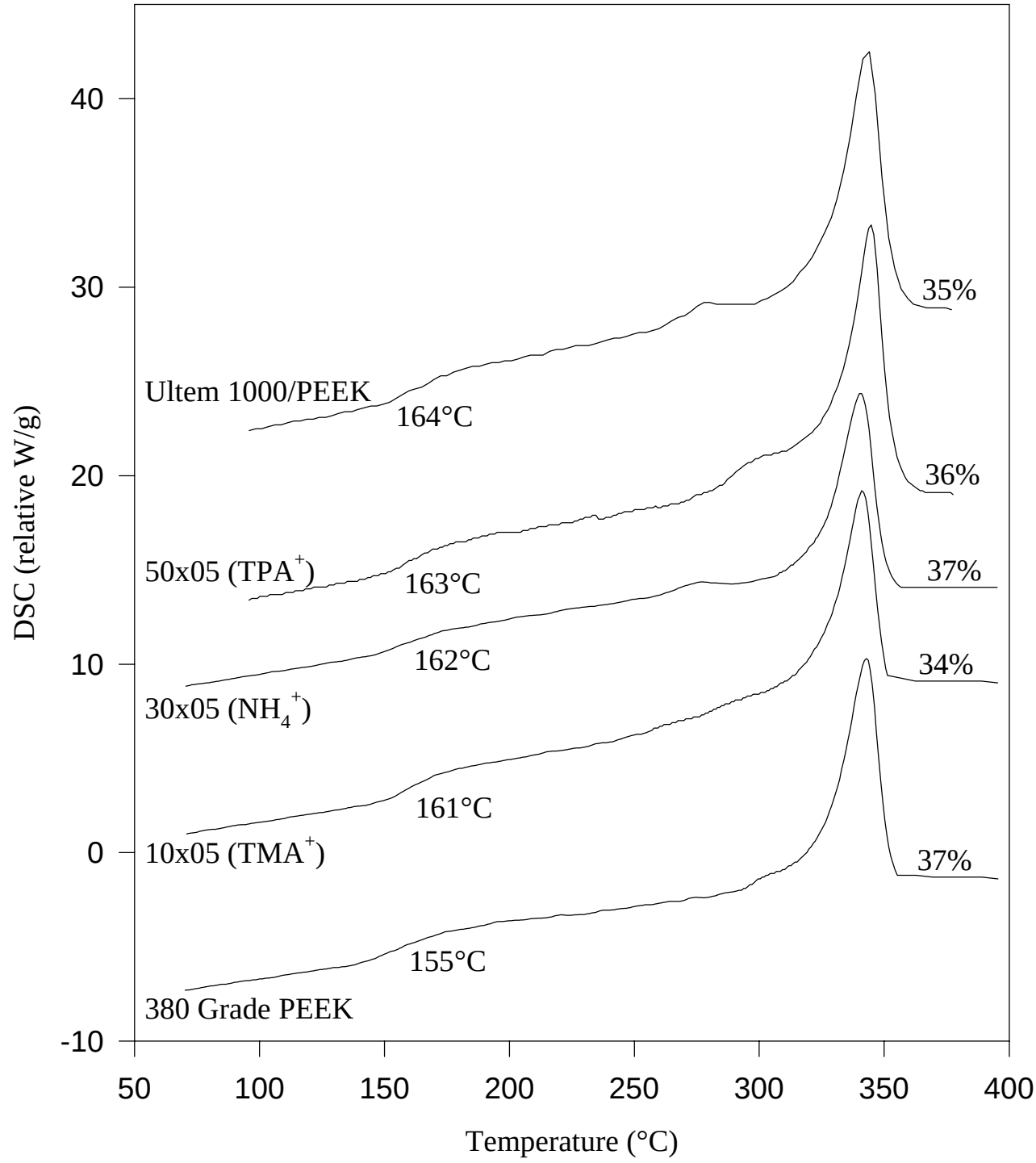

Figure 3-14. DSC heating scans at 20°C/min for model matrix blends and neat 380 Grade PEEK. Glass transition temperatures and calculated fraction crystallinity in the PEEK component are identified.

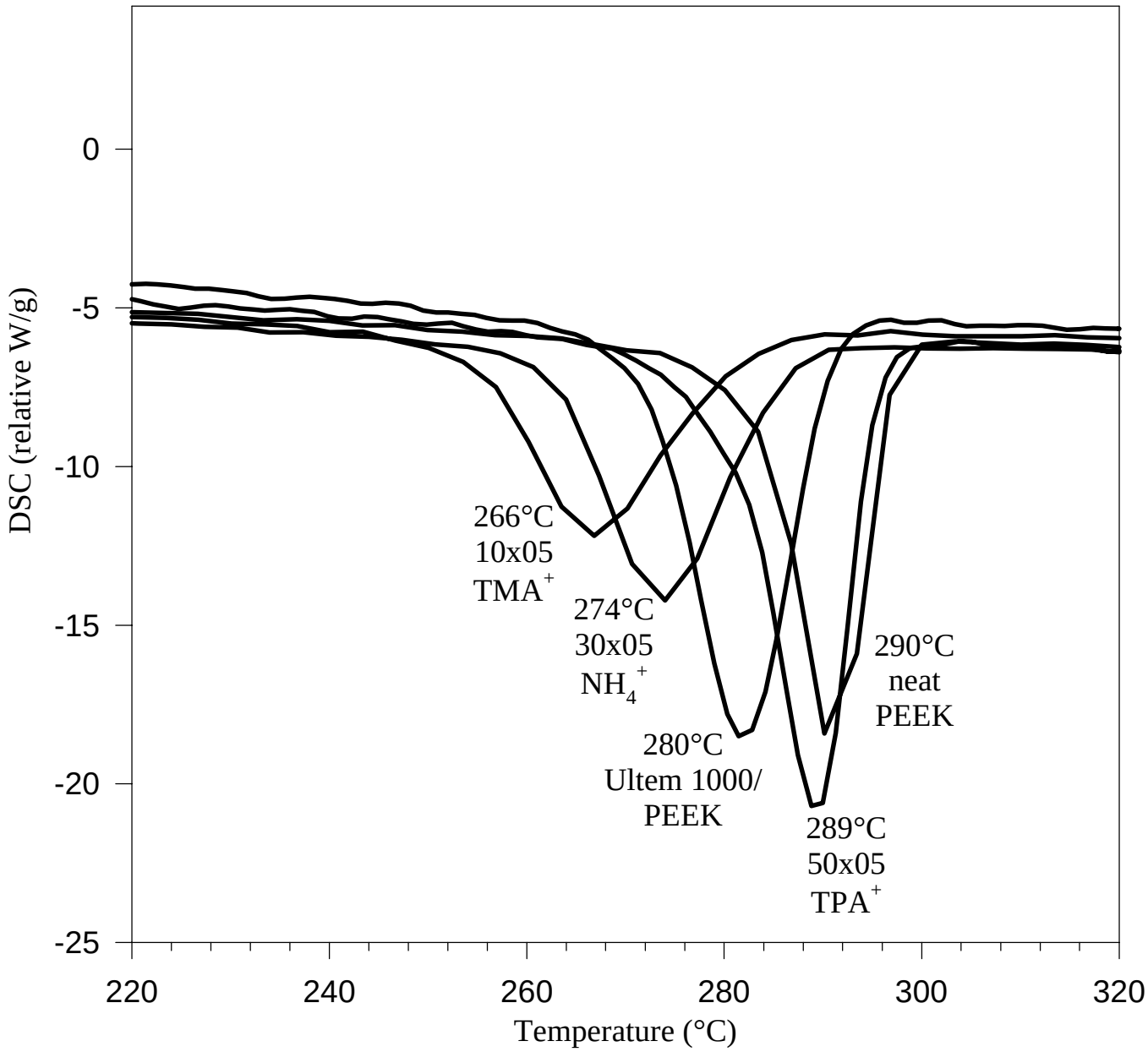

Figure 3-15. DSC cooling scan at 10°C/min of model matrix blends and neat 380 Grade PEEK with T_x^{max} labeled.

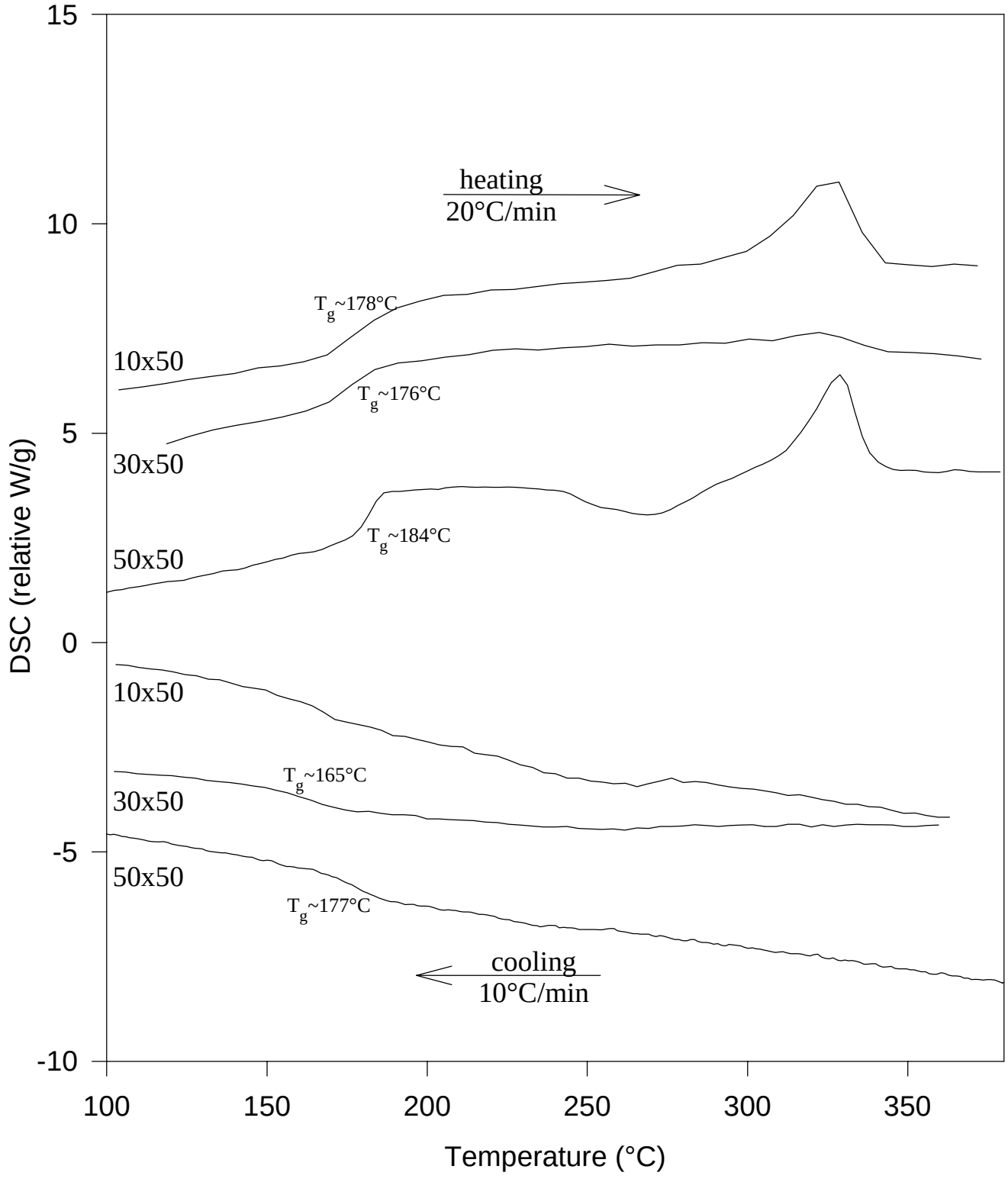

Figure 3-16. DSC traces for 10x50 50% TMA^+ PI/PEEK blend, 30x50 50% NH_4^+ PI/PEEK blend and 50x50 50% TPA^+ PI/PEEK blend.

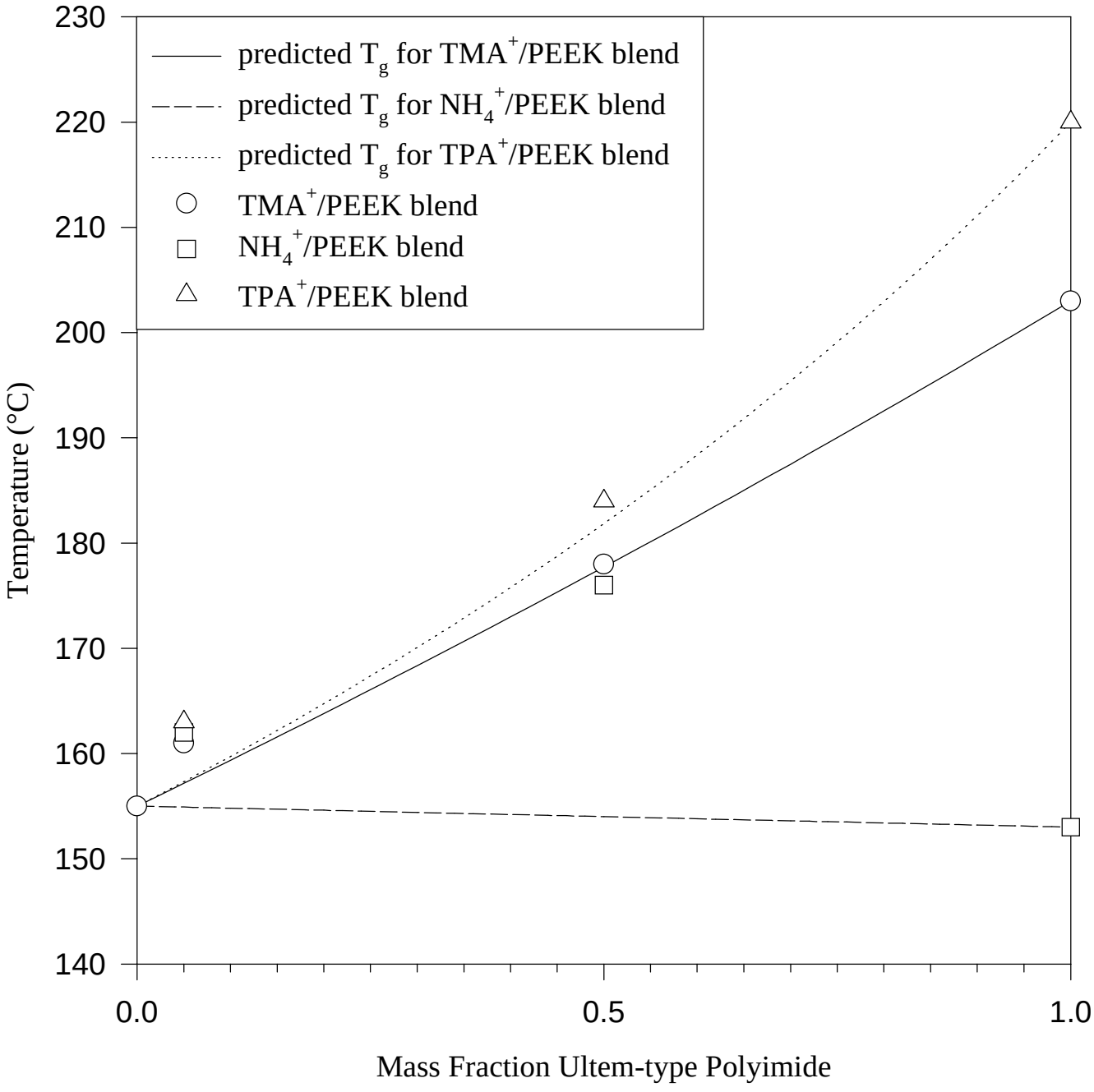

Figure 3-17. Glass transition temperatures for Ultem-type polyimide/PEEK blends of varying composition and predicted glass transition temperatures from the Fox equation.

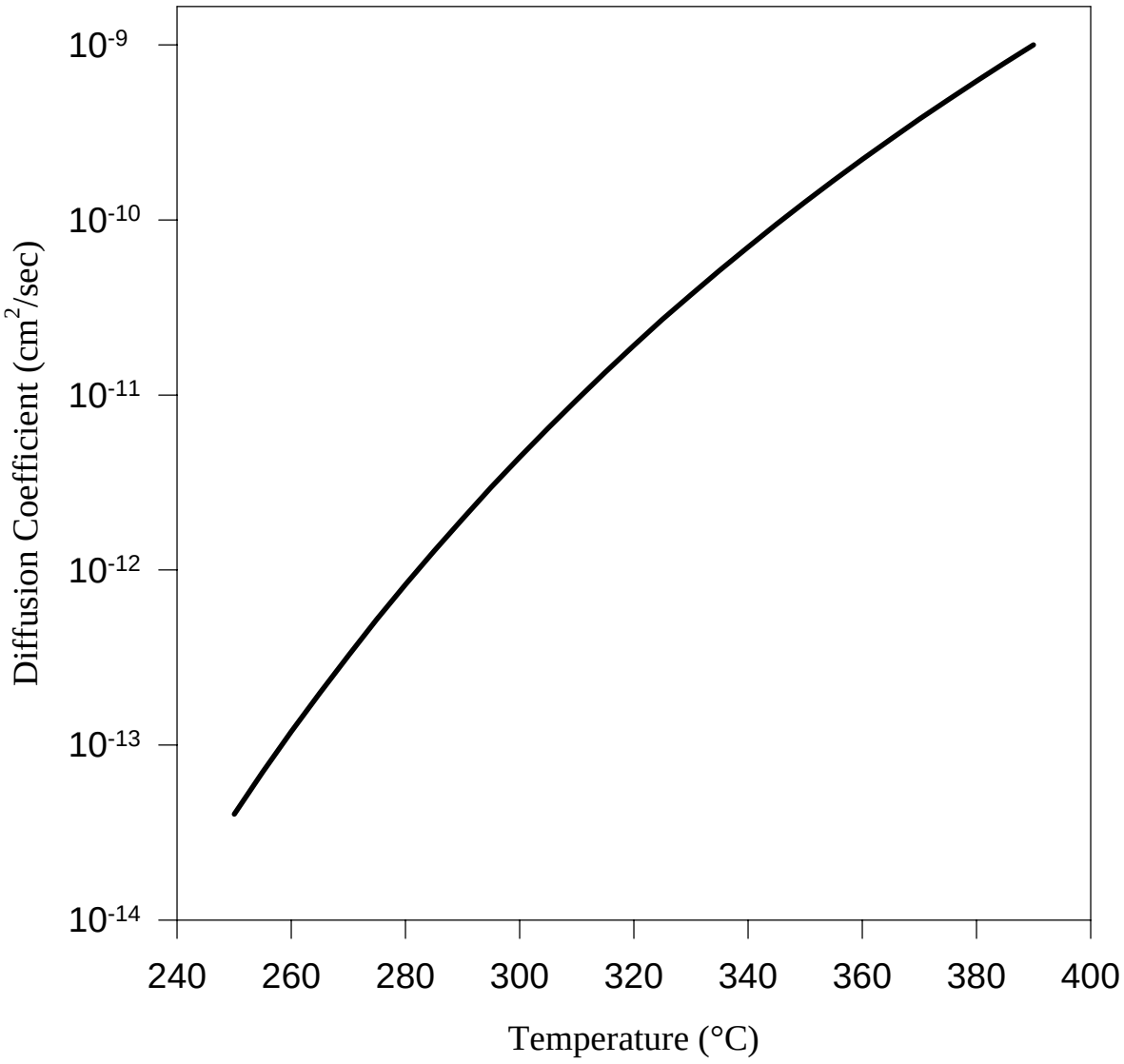

Figure 3-18. Calculated diffusion coefficient vs. temperature for Ultem-type polyimide/PEEK blends.

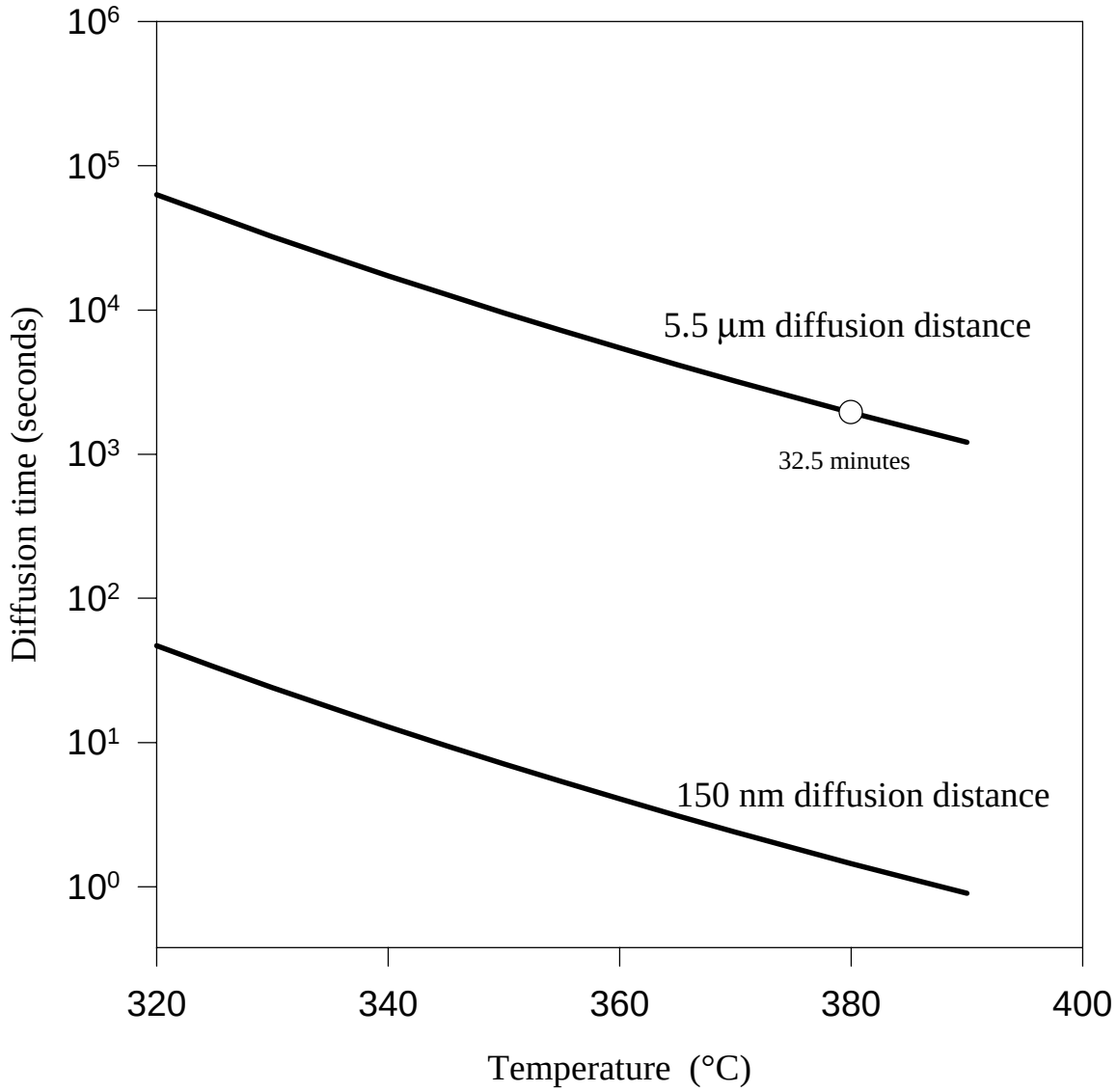

Figure 3-19. Calculated diffusion distances for PEEK/PI blends during a 30 minute isothermal hold as a function of temperature.

References

1 Reifsnider, K.L., *Composites*, **25**, 461 (1994).

2 Lesko, J.J., Swain, R.E., Cartwright, J.M., Chen, J.W., Reifsnider, K.L., Dillard, D.A., and Wightman, J.P., *Journal of Adhesion*, **45**, 43 (1994).

3 Subramanian, S., Lesko, J.J., Reifsnider, K.L., and Stinchcomb, W.W., *J. Compos. Mater.*, **30**, 309 (1996).

4 Chang, Y.S, Lesko, J.J., Case, S.W., Dillard, D.D., and Reifsnider, K.L., *Journal of Thermoplastic Composite Materials*, **7**, 311 (1994).

5 Gao, Z., Reifsnider, K.L., and Carman, G., *J. Compos. Mater.*, **26**, 1678 (1992).

6 Carman, G.P., Lesko, J.J., and Reifsnider, K.L., *Composite Materials: Fatigue and Fracture, Fourth Volume, ASTM STP 1156*, W.W. Stinchcomb and N.E. Ashbaugh, Eds., American Society for Testing and Materials, Philadelphia, PA, p. 430, 1993.

7 Case, S.W., Carman, G.P., Lesko, J.J., Fajardo, A.B., and Reifsnider, K.L., *J. Compos. Mater.*, **29**, 208 (1995).

8 The Effect of Polyimide Interphases on Properties of PEEK-Carbon Fiber Composites. S. Gardner, A. Gonzalez, R.M. Davis, J.V. Facinelli, J.S. Riffle, S. Case, J.J. Lesko, K.L. Reifsnider, *AIChE 1995 Annual Meeting.* November 12-17, 1995. Miami Beach, FL.

9 Yu, T.H. and Davis, R.M., *J. Thermoplast.Comp. Mater.*, **6**, 62 (1993).

10 Texier, A., Davis R.M., Lyon, K.R., Gungor, A., McGrath, J.E., Marand, H., and Riffle, J.S., Polymer, **34**, 896 (1993).

11 Gonzalez, A-I, M.S. Dissertation (Virginia Polytechnic Institute and State University, Blacksburg, VA, November 1992)

12 Gonzalez-Ibarra, A., Davis, R.M., Heisey, C.L., Wightman, J.P., and Lesko, J.J., *Journal of Thermoplastic Composite Materials*, **10**, 85 (1997).

13 Davis, R.M., and Texier, A., *ANTEC '91 Confer. Proceed.*, **37**, 2018 (1991).

14 Kochi, M. Yokota, R., Iizuka, T., and Mita, I., *Journal of Polymer Science: Part B: Polymer Physics*, **28**, 2463 (1990).

15 Cotts, P.M., Polyimides: Synthesis, Characterization and Applications, K.L. Mittal, Ed., Plenum, New York, 1984, p. 223.

16 Dine-Hart, R.A., and Wright, W.W., *J. Appl. Polym. Sci.*, **11**, 309 (1967).

17 Sroog, C.E., Endrey, A.L., Abramo, s.V., Berr, C.E., Edwards, W.M., and Olivier, K.L., *J. Polym. Sci.:Part A: Polym. Chem.*, **3**, 1373 (1965).

18 Facinelli, J.V., Gardner, S., Dong, L., Sensenich, C.L., Davis, R.M., and Riffle, J.S., *Macromolecules*, **29**, 7342 (1996).

19 Harris, J.M., and Robeson, L.M., *J. Appl. Polym. Sci.*, **35**, 1877 (1988).

20 Hsaio, B.S., Sauer, B.B., *Journal of Polymer Science: Part B: Polymer Physics*, **31**, 901 (1993).

21 Reynolds, R.J.W., and Seddon, J.D., *J. Polym. Sci., Pt. C.*, **23**, 45 (1968).

22 Baxandall, L.G., *Macromolecules*, **22**, 1982 (1989).

23 Jenkins, S.D., Emmerson, G.T., McGrail, P.T., and Robinson, R.M., *Journal of Adhesion*, **45**, 15 (1994).

24 Pryde, C.A., *J.of Appl.Polym. Sci.: Part A: Polymer Chemistry*, **27**, 711 (1989).
25 Rao, V.L., and Bijimol, J., *Makromol. Chem.*, **192**, 1025 (1991).
26 Seo, Y., Hong, S.M., Hwang, S.S., Park, T.S., Kim, K.U., Lee., S., and Lee, J., *Polymer*, **36**, 515 (1995).
27 Facinelli, J.V. *PhD Dissertation* (Virginia Polytechnic Institute and State University, Blacksburg, VA, (1996).
28 Cella, J. A., *Polymer Degradation and Stability* **36**, 99 (1992).
29 ICI Victrex PEEK product data sheet.
30 personal communication with ICI Victrex technical service.
31 Ultem data sheet, General Electic.
32 Hudson, S.D., Davis, D.D., Lovinger, A.J., *Macromolecules*, **25**, 1759 (1992).
33 Crevecoeur, G., and Groeninckx, G., *Macromolecules*, **24**, 1190 (1991).
34 Liang, K., Grebowicz, J., Valles, E., Karasz, R.E., and MacKnight, W.J., *J. Appl. Polym. Sci., Part B, Polym. Phys.*, **30**, 465, (1994).
35 Jar, P.-Y. and Plummer, Ch.J.G., Chapter 4, The Physical Structure and Mechanical Properties of Poly(Ether Ether Ketone), Advanced Thermoplastic Composites, Ed. H.H. Kausch and R. Legras, Hanser Publications, New York, NY (1993).
36 Harper, Handbook of Plastics, Elastomers and Composites, 2nd edition, McGraw-Hill,
37 Hercules AS-4 Carbon Fiber Product data sheet.
38 Sigma-Stat Statistical Software v. 2.0 User's Manual, Jandel Scientific, San Rafael, CA (1992-1995).
39 Burks, H.D., St. Clair, T.L., *SAMPE Quarterly*, 1, October 1987.
40 Roovers, J., and Toporowski, P.M., *Macromolecules*, **25**, 1096 (1992).
41 Yang, H.-H., Han C.D., and Kim, J.K., *Polymer*, **35**, 1503 (1994).
42 Day, M., Sally, D., and Wiles, D.M., *J.of Appl. Polym. Sci.*, **40**, 1615 (1990).
43 Fox, T.G. and Flory, P.J., *J. Appl. Phys.*, **21**, 571 (1950).

Chapter Four: Fabrication and Characterization of Carbon Fiber PEEK matrix composites with Ultem-type Polyimide Interphases of Tailored Properties for Studying the Effect of Interphase Modifications

Introduction

An important way to improve composite performance and durability is by modifying the interphase. The interphase region is defined as the transition zone between the reinforcing fiber and the bulk matrix in a composite. An interphase typically accounts for less than 2% of the total mass of material in a composite [1]. However, carefully modified interphases have been shown to improve composite longitudinal tensile strength by as much as 29% [3], compressive strength by as much as 50% and notched fatigue lifetime cycles by as many as two orders of magnitude [1,2]. Therefore, the benefits of implementing a carefully constructed interphase are obvious.

Many models based on the micro-mechanics of failure have been proposed for prediction of composite strength and lifetime. The most recent models proposed by Reifsnider et al. incorporate an interphase region with significantly different material properties from the matrix polymer [1,4-8]. These models have been used to formulate hypotheses regarding further improvements of composite performance and durability based on interphase modifications.

The most intriguing hypothesis is that a maximum composite tensile strength can be attained for an optimal interfacial shear strength between the fiber and the bulk matrix. The most direct method of altering the interfacial shear strength without changing any of the other constituent properties is by modifying the interphase properties. The work of this chapter concerns the fabrication of Ultem-type polyimide interphase/PEEK matrix composites to test the hypothesis of Reifsnider et al.

The aqueous suspension prepregging technique combines the matrix polymer with the fiber at the same time that the interphase polymer is deposited on the fiber [9-14]. Aqueous suspension prepregging has been done by many researchers using a polyimide precursor, a water soluble polyamic acid salt neutralized with a base [9-14]. The matrix polymer powder is dispersed in the aqueous polyamic acid salt solution. The polyamic acid salt behaves as a dispersant, adsorbing to the surface of the matrix powder particles, and electrostatically stabilizing the suspension. The fiber tow is then coated with the polyimide precursor and the matrix powder in a single prepregging step. The polyamic acid salt also serves as a binder, adhering the matrix powder to the carbon tow. After drying the water from the prepreg, a heating cycle is used to convert the polyamic acid to the polyimide by way of thermal imidization. The properties of the Ultem-type polyimide can be controlled by selection of the base and the method used for making the polyamic acid salt [15].

The main objectives of this chapter were (I) to fabricate polyether ether ketone (PEEK) matrix composites with three different Ultem-type polyimide interphases and (ii) to evaluate the performance of these composites to study the effects of the interphase on the bulk composite properties and to test the hypothesis of a maximum longitudinal tensile strength at an optimum interfacial shear strength.

The properties of the interphase were estimated by studying model interphase Ultem-type polyimide discussed in Chapter 3. After thermal imidization, the Ultem-type NH_4^+ polyimide was shown to have a T_g of 153°C and an M_n of 2,780. The Ultem-type TMA^+ polyimide was shown to have a T_g of 203°C and an M_n of 10,500 g/mol. The Ultem-type TPA polyimide was shown to have a T_g of 220°C and an M_n of 16,000 g/mol.

During a simulated composite consolidation temperature cycle, the melt viscosity of all three polyimides was shown to increase indicating crosslinking at temperatures above 350°C. The increase in melt viscosity was great for the Ultem-type NH_4^+ polyimide, moderate for the Ultem-type TMA^+ polyimide and slight for the Ultem-type TPA^+ polyimide. After the simulated composite consolidation temperature cycle the gel fraction of the Ultem-type NH_4^+ polyimide was shown to have a gel fraction of 21%, the Ultem-type TMA^+ polyimide was shown to have a gel fraction of 13% and the Ultem-type TPA^+ polyimide was shown to have a gel fraction of 0.6% .

Model matrix samples were prepared and analyzed in Chapter 3 to replicate the matrix/interphase compositions in the composites of this chapter. The tensile strengths and moduli of the model matrix blends were all very similar indicating that the mechanical properties of the bulk matrices should not be affected.

These factors indicate that while the interphase properties are varied for each composite, the matrix properties are not affected. Thus, any difference in composite performance can be attributed to the interphase modifications.

Since PEEK is miscible with Ultem-type polyimide, interdiffusion of the interphase polyimide and the bulk PEEK matrix is possible [24-26]. However, the crosslinking that occurs for the interphase polyimides indicate that interdiffusion of the PEEK and the Ultem-type polyimide may be limited. This would facilitate formation of an interphase with a very high concentration of Ultem-type polyimide.

Although significant interdiffusion would be limited by crosslinking of the Ultem-type polyimide, the miscible nature of *linear* Ultem-type polyimide indicates that good adhesion

should exist between the interphase and the bulk PEEK matrix.

There are many problems and obstacles regarding the research project described above. Fabrication of a series of composites containing an interphase with controlled properties, while maintaining similarity of all other properties is a difficult task. Some of the most difficult problems that will be addressed by this thesis are described next.

The aqueous suspension prepregging technique has been used successfully to fabricate PEEK matrix [33-36,38] and LaRC TPI matrix [10,12-14,16-21] composites.

Work has been done previously by Davis et al. [9-13] to assess the effects of systematically varied polyimide interphases that demonstrate a miscible interphase/matrix system and an immiscible interphase/matrix system. These are believed to be the first studies to specifically address such a concern for interphase composites. The work of this chapter extends the studies of Davis et al. to consider a series of systematically modified Ultem-type polyimide interphase PEEK matrix composites that demonstrate interphase/matrix compatibility.

The bulk of the investigations of interphase composites have been on thermosetting matrix systems. Due to the many advantages of engineering thermoplastic polymers, there is increasing interest in thermoplastic matrix, carbon fiber, interphase composites. The work of this chapter will address polyimide interphase composites that are fabricated with PEEK, a high performance thermoplastic.

Furthermore, the investigations of interphase composites reported in the literature usually contain the same matrix, but with interphase modifications ranging from an unsized, unsurface treated fiber to different fiber surface treatments and/or fiber with a polymeric sizing. This can result in differences of fiber/matrix adhesion or alteration of fiber properties rather than

modification of the interphase material properties. The systematically modified interphase composites studied in this thesis are unique because the same fiber and matrix are maintained throughout each composite series, and the same interphase polyimide is used. This minimizes speculation regarding the effects of system chemistry when interpreting the composite performance results.

Experimental

Materials

Composites were made with Hercules® AS-4 (lot#761-4m), unsized but surface treated 12k carbon fiber tow. This fiber is from the same batch used by Gonzalez [12-13] for polyimide interphase/PEEK matrix composite manufacture.

The matrix material was Victrex 380 Grade poly ether-ether-ketone (PEEK) supplied by ICI Americas (T_g = 143°C, T_m=335°C) [22]. The PEEK was supplied as a powder with ~11 µm median particle diameter as measured with a Shimadzu SPC-3 particle size analyzer. The chemical structure of PEEK is shown in Figure 4-1. This polymer is from the same batch used in the model matrix structure-property investigation as detailed in Chapter 3 and also the same batch used by Gonzalez [12-13] for polyimide interphase/PEEK matrix composite manufacture.

The binder polymer was an Ultem®-type polyamic acid which is a precursor to the Ultem®-type polyimide [15]. The chemical structure of Ultem-type polyamic acid is shown in Figure 4-2. Linear Ultem polyimide has been shown to be completely miscible with PEEK in all concentrations [24-26]. A large batch of BPADA/MPD (Ultem-type) polyamic acid endcapped with phthalic anhydride was synthesized in a 5 liter reactor at the General Electric Research

Center in Schenectady, New York, by Dr. Biao Tan from Professor McGrath's group of the Virginia Tech Chemistry Department. The large batch of polyamic acid provided enough starting material so all experiments could be done using a single batch of polymer. This polyamic acid was used for all composite manufacture and the same batch of polyamic acid was used for the model interphase material for the structure property investigation as detailed in Chapter 3.

The bases used for making the polyamic acid salts were ammonium hydroxide (NH_4OH), tetramethyl ammonium hydroxide (TMAH), and tripropylamine (TPA), all Fisher brand reagent grade.

For all aqueous solutions and suspensions, deionized water from a Nanopure II water filtering system with a resistivity of 16.7 Ω/cm^3 was used.

Procedure
Calibration of bases

The bases used for making the polyamic acid salts were ammonium hydroxide (NH_4OH), tetramethyl ammonium hydroxide (TMAH), and tripropylamine (TPA), all Fisher brand reagent grade. All bases were purchased new, kept in the original bottles with the caps sealed tightly with Parafilm, and stored in a refrigerator. The concentration of the aqueous bases were determined by potentiometric titration using an MCI Automatic Titrator Model GT-05 (COSA Instruments Corporation) using a 0.05 N HCl solution that was standardized against Na_2CO_3. The calibration of the bases is described in detail on page 171 of this thesis.

Polyamic acid preparation

Polyamic acid made by Dr. Biao Tan from the monomers 2,2'-Bis[4-(3,4-dicarboxyphenoxy)-phenyl]propane dianhydride (BPADA) and meta-phenylene diamine (m-PDA) was supplied as a 25 wt% solution in NMP at a temperature of -5°C. The polyamic acid chains were endcapped with phthalic anhydride to provide a target molecular weight of 20,000 g/mole. The polyamic acid was twice precipitated into water to remove the NMP. This procedure is described in detail on page 172 of this thesis.

Polyamic Acid Salt Preparation

Before making aqueous suspensions of PEEK matrix powder, solutions of polyamic acid salts were first prepared. The conversion of the polyamic acid salt to a polyimide along with a summary of the effect of counterion selection on some resulting polyimide properties is shown in Figure 4-3. The procedure for preparing aqueous solutions of Ultem-type NH_4^+ polyamic acid salt (30 series interphase), Ultem-type TMA^+ polyamic acid salt (10 series interphase), and Ultem-type TPA^+ polyamic acid salt (50 series interphase) is described on pages 174-177 of this thesis.

Suspension Preparation

After the aqueous polyamic acid salt solutions were made, they were used to make PEEK suspensions suitable for composite prepregging. The solution and the PEEK powder were mixed in a Waring blender at high speed for five minutes. The PEEK powder was added to make a 9.8 wt% PEEK solids content suspension. The mass of polyamic acid in solution was 5 wt% of the

mass of the PEEK powder. The suspensions were used immediately or were stored in a refrigerator.

A Shimadzu SAC-P3 Centrifugal Particle Size Analyzer was used to measure the size distributions of the suspensions. The instrument was used in the multi-function mode, which is a combination of gravimetric and centrifugal measurements. A few drops of the suspension was diluted in several milliliters of water until the turbidity of the suspension was reduced to a suitable level for measurements. The centrifuge was run at 240 rpm/min and a typical test took about 20 minutes. The median particle size for the suspensions were ~11 µm.

Prepregging

A detailed description of the prepregging process and techniques used in this work has been reported in previous studies by Yu and Davis [10], Texier et al [11], and by Gonzalez [12-13]. Using a modified Research Tool Corporation Model 30 Prepregger, the carbon fiber was continuously impregnated with the suspension. As seen in the schematic in Figure 4-4 the fiber was passed through a resin pot with an approximate volume of 0.25 l. The prepregged tow was then wound up on a drum at a line speed of ~10 cm/sec with a tow width of 0.33" and approximately 25% tow overlap. The prepreg was dried on the drum at room temperature for 30 minutes and then it was cut off the drum, and cut into square prepreg lamina, either 6" x 6" or 10"x10". The prepreg lamina were then placed in a freezer until composite panel lay-up and consolidation.

Composite Layup and Consolidation

Four different stacking schemes were used for composite manufacture. The composites made were four-ply, unidirectional panels ($[0]_4$); 16-ply unidirectional panels ($[0]_{16}$); 28-ply, cross-ply panels ($[0/90]_{7s}$); and 8-ply, cross-ply panels ($[0/90]_{2s}$) . The prepreg was taken immediately from the freezer and laid up in the appropriate stacking sequence. The stacked plies were heated in a Model 532 Fisher Programmable air convection oven according to a specially designed thermal treatment. The 10 series composite prepreg (Ultem-type TMA^+ interphase) and the 30 series composite prepreg (Ultem-type NH_4^+ interphase) were dried at 65°C for one hour followed by a two-hour hold at 265°C for imidization of the polyamic acid. The 50 series composite prepreg (Ultem-type TPA^+ interphase) was dried at 65°C for one hour followed by a 275°C, ten minute imidization hold. The cyclization of Polyamic acid to polyimide is a condensation reaction. Since water is a product, the cyclization must be done prior to consolidation in the matched mold to prevent the water from accumulating in the composite and forming voids.

The dried and heat treated prepreg was placed in a 6" x 6" or a 10" x 10" picture frame steel mold. A thermocouple was inserted into a corner of the mold to monitor the consolidation temperature and an IBM Model 30 personal computer was used to record the composite temperature and pressure history. The steel mold was treated with Frekote 34 mold release agent and the socket head cap screws that fasten the mold together were treated with a high temperature anti-seize compound.

A diagram illustrating the temperature and pressure program for the consolidation cycle is shown in Figure 4-5. A Wabash Vacuum Hot Press was used for composite consolidation. The

press was preheated to 390°C and the loaded mold was placed between the platens. Touch pressure was applied until the mold temperature was above 360°C. At this point, a vacuum of 28 in Hg was applied to the platen chamber and the consolidation platen pressure of 350 psi was applied. After the mold temperature reached 380°C, the temperature was maintained at this level for 30 minutes and then the mold was cooled at an approximate rate of 10°C/min. The consolidation pressure was applied until the mold temperature was at least 30°C below the glass transition temperature of the PEEK matrix (143°C).

Panel Evaluation
C-Scan

A Sperry Corporation S-80 C-Scan ultrasonic unit was used to qualitatively determine the level of consolidation of the panels. The 15 Khz transducer was used with a gain between 32 and 40 db. A scanning width of 0.1" was used with the fastest raster scanning speed.

Fiber Volume Fraction

The fiber volume fraction of most composites was determined by acid digestion according to the ASTM D3171-76 method. Densities of 1.3 $g \cdot cm^{-3}$ and 1.8 $g \cdot cm^{-3}$ were used for the PEEK matrix and the carbon fiber respectively. For the case of panels with regions of varying consolidation quality as determined by C-scan, samples were taken from two areas of the panel. The region of highest consolidation quality and the region of lowest consolidation quality were the two areas selected.

Image Analysis

An image analysis method was used to determine the void content of the composites. Samples of unidirectional laminates were mounted in epoxy, polished and examined under a scanning electron microscope (SEM) located in the chemistry departments surface analysis laboratory in the Hahn Hall. Buehler cold mount epoxide resin and hardener were used to mount the samples. Polishing was done on an automatic Buehler Polishing unit located in the Materials Response Group laboratory in Norris Hall using Buehler Carbimet Microcut Special Silicon Carbide Grinding Paper according to the polishing schedule outlined in Table 4-I. The polished sample was examined under SEM and representative micrographs were taken at magnifications of 500 x and 750 x.

Table 4-I. Polishing schedule of PEEK matrix composite surfaces for image analysis.

Duration	Grit Abrasive	Pressure	Polishing Direction
until surface ground level	120 grit	4lbs/pot	counter rotation
5 minutes	240 grit	4lbs/pot	counter rotation
5 minutes	320 grit	4lbs/pot	counter rotation
5 minutes	400 grit	4lbs/pot	matching rotation
10 minutes	600 grit	4lbs/pot	matching rotation
10 minutes	800 grit	4lbs/pot	matching rotation
10 minutes	1 µm grit	6lbs/pot	matching rotation
10 minutes	0.3 µm grit	6lbs/pot	matching rotation

The micrographs were scanned into electronic picture format using a Hewlet Packard scanner and a PC using PaperPort v.1.2 software package. Using grey scale imaging, the void content was determined.

Surface Chemistry by X-ray Photoelectron Spectroscopy

The surface chemistry of sized and unsized carbon fibers was determined by X-ray Photoelectron Spectroscopy (XPS). Carbon fiber samples were prepared to investigate the hypothesis that the Ultem-type polyimide prepared by the aqueous polyamic acid salt method, reacts with the carbon fiber at the elevated temperatures of composite consolidation. Carbon fibers were sized with aqueous solutions of Ultem-type polyamic acid salts using a single tow immersion procedure. AS-4 12k carbon fiber tow was cut into 10 cm lengths, bound at one end with masking tape and submersed in 50 ml of aqueous polyamic acid salt solution for six seconds. The aqueous polyamic acid salt solutions used were Ultem-type NH_4^+ polyamic acid salt, Ultem-type TMA^+ polyamic acid salt and Ultem-type TPA^+ polyamic acid salt prepared as described previously. After submersion in the polyamic acid salt solution, the sized tow was placed on a clean microscope slide and the end of the sample bound with masking tape was cut off. Two sized tow samples were prepared for each polyamic amic acid salt solution. The sized tow samples with the Ultem-type NH_4^+ polyamic acid salt and the Ultem-type TMA^+ polyamic acid salt were dried in a Fisher Model 532 programmable convection oven at 65°C for one hour followed by a two-hour hold at 265°C for imidization of the polyamic acid. This cycle replicates the exact procedure for heat treatment of the composite prepreg for the 10 series (TMA^+ polyamic acid salt) and 30 series (NH_4^+ polyamic acid salt) composites. The sized tow samples with the Ultem-type TPA^+ polyamic acid salt were dried in a Fisher Model 532 programmable convection oven at 65°C for one hour followed by a ten minute hold at 275°C for imidization of the polyamic acid. This cycle replicates the exact procedure for heat treatment of the composite prepreg for the 50 series (TPA^+ polyamic acid salt) composites. As received AS-4 carbon fiber

was into 10 cm lengths and placed on clean microscope slides to serve as an experimental control.

All samples were heated to 380°C for 30 minutes in a Blue M programmable furnace continuously purged with nitrogen. This cycle replicates the thermal treatment of the composites during consolidation. At this point, one sized tow sample from each group was set aside for XPS analysis. The other sized tow sample from each group was washed with chloroform, a good solvent for Ultem-type polyimide. The sized tow samples were each placed in a 35 ml screw cap vial which was then filled with chloroform. The vials were sealed and mixed on a rotating vial-mixing wheel for 24 hours. The vials were then drained of solvent, refilled with fresh chloroform, and mixed on the rotating vial-mixing wheel for 24 hours. The vials were then drained of solvent, the sized carbon tow samples were placed on a clean glass microscope slide and dried in a Fisher Model 532 programmable convection oven at 105°C for 12 hours. These samples were then submitted for XPS analysis.

The XPS experiments were done by Steve McCartney of the Virginia Tech National Science Foundation Science and Technology Center for High Performance Composites and Adhesives using a Perkin-Elmer PHI 5400 x-ray photoelectron spectrometer with a Mg Kα x-ray source (1253.6 eV). Spectra were collected at 15 kV and 400 W in a survey scan mode using a spot size of 1 mm x 3 mm and a take-off angle of 45°. The chamber pressure was maintained below 5×10^{-7} torr during measurement. Data acquisition and analysis were executed using PHI software v. 4.0 with binding energies referenced to 284.6 eV for graphite carbon.

Composite Characterization
Iosipescu Shear Testing

In-plane shear properties were measured using an Iosipescu shear test which was done by Dr. Wilson Tsang in The Material Response Group using a screw driven MTS. A modified Wyoming shear test fixture was used for testing the specimens. Figure 4-6 shows a schematic of the test coupons which were 3" x 0.75" and 16 plies thick with a V-notch in the middle of the coupon. Specimens were prepared according to procedures outlined by Ho et al. [28]. After the coupons were machined, an annealing process was employed to normalize the physical aging process. The coupons were annealed at 129°C, approximately 15°C below T_g, for 48 hours and then cooled to room temperature at a rate of 0.1°C/min. The coupons were equipped with back-to-back ±45° strain gage rosettes. Load data from a load cell and the strain data from the four strain gages were recorded by a Macintosh computer. If the strain data from the back-to-back gages was identical, then proper sample placement and loading were ensured.

Shear testing was done on specimens with a 90° orientation, meaning the unidirectional composite coupons were machined so that the fiber direction was in the direction of loading. This orientation was selected over the 0° orientation for two main reasons. With 0° specimen orientation, the strains measured by the two gages in the ±45° directions are usually unequal in magnitude, attributed to the presence of transverse normal strain in the test section [29]. With 90° specimen orientation, the strains measured by the two gages in the ±45° directions are typically equal in magnitude and opposite in sign. This leads to more accurate measurement of the in-plane shear modulus, not only because the shear strain can be measured more precisely, but also because the loading is more nearly pure shear loading. The other reason that the 90°

specimen orientation was selected is that measured shear strengths and shear moduli are typically greater for the 0° oriented specimens [29]. As established above, the loading for 0° oriented specimens is not a pure shear condition due to the transverse strains that develop in the test section. Therefore, the increases in shear strength and shear modulus due to the 0° orientation over the 90° orientation are artifacts of an unpure shear loading condition and do not accurately represent the in-plane shear properties of the composite.

Transverse Flexure Testing

Three point bending experiments according to ASTM D790-96 were done with 12.7 mm x 50.8 mm coupons [31]. Test specimens were machined using a diamond saw and the edges were polished with #400 grit silicon carbide abrasive paper. After the coupons were machined, an annealing process was employed to normalize the physical aging process. The coupons were annealed at 128°C, approximately 15°C below T_g, for 48 hours and then cooled to room temperature at a rate of 0.1°C/min. Testing was done using an Instron with a 1 KN load cell. A three point bending test fixture was used to support the sample and provide uniform loading conditions for all samples. The geometry of the transverse flexure test is shown in Figure 4-8. A 25/1 span to thickness ratio was used for testing. This is different that the 16/1 length to span ratio which was used by Gonzalez [12] because a larger span to thickness ratio is needed for fiber reinforced composites for a reliable determination of the modulus of elasticity [29]. The transverse flexure testing of APC-2 from the ICI Fiberite product data sheet was done with a span to thickness ratio of 25/1 [32].

Voltage Contrast X-ray Photoelectron Spectroscopy

Transverse flexure failure surfaces were examined with voltage contrast x-ray spectroscopy (VC-XPS) by Dr. Gerry Zajac at Amoco Research Center, Naperville, Il. This technique was developed by Miller et al. which is described in detail in [51]. The tensile side of the transverse flexure surface was examined with an x-ray spot size of 600 μm diameter using a Surface Science Laboratories SSX-100 spectrometer with a monochromatic Al Kα x-ray source. Five spots were examined for each sample providing an averaging over a relatively large area of the fracture surface. The SSX-100 low energy flood gun was used to bias the samples and thus separate the signals for the carbon fibers from the signals for the polymer material. Flood gun conditions were 2 mA emission current with an electron energy of 5-7 eV to produce separation of the C 1s peaks for the polymer and fiber. Since the carbon fiber is an electrically conductive material, and the polymer interphase and polymer matrix material is not, the electrical biasing produces shifts only in the measured binding energy of photoelectrons emitted from the carbon fiber surface. After the biasing is used to separate the XPS signals for the fiber and polymer at the surface, the intensities of signals from the fibers and the polymer material can be used to calculate the relative amount of each component at the surface.

Notched Fatigue Testing

Notched fatigue testing of the composites was done by Dr. Scott Case and Ms. Sneha Patel in the Materials Response Group at Virginia Tech. The testing procedure is detailed in the PhD thesis of Dr. Case [30]. An important parameter for fatigue testing is the R value which is the ratio of the compressive load to the tensile load. Dr. Case tested specimens from the 10

series Ultem-type TMA^+/PEEK composites and the 30 series Ultem-type NH_4^+/PEEK composites using an R value of 1.0. Dr. Case also tested specimens from APC-2 composites using an R value of 0.1 as detailed in his doctoral thesis [30]. Ms. Patel tested specimens from the 10 series Ultem-type TMA^+/PEEK composite, 30 series Ultem-type NH_4^+ /PEEK composite, and 50 series Ultem-type TPA^+ /PEEK composite using R = 0.1.

i.) R=1.0: Figure 4-7 shows a schematic of the test samples which were 28 ply crossply coupons ($[0/90]_{7s}$) with the 0° orientation along the length of the coupon. The coupons were machined and ground to have a length of 6" and a width of 1". Three samples from each group were left unnotched to measure the unnotched compression strength. Notched coupons were machined with a round 0.25" diameter notch in the center of the coupon. After the coupons were machined, an annealing process was employed to normalize the physical aging process. The coupons were annealed at 128°C, approximately 15°C below T_g, for 48 hours and then cooled to room temperature at a rate of 0.1°C/min. All fatigue coupons were equipped with extensometer mounting flanges so that an extensometer could be used to measure the displacement during the fatigue testing.

Fatigue testing was done with a 20 kip servo-hydraulic MTS test machine under load control mode. Quasi-static compression strengths were measured first and identified as the ultimate compressive strength (UCS). Subsequent fatigue testing experiments were done at several controlled fractions of the UCS. A frequency of 10 Hz was used. Fatigue testing was done at 65-85% UCS.

ii.) R=0.1: The schematic in Figure 4-7 also shows the test sample geometry which were 8 ply crossply coupons ($[0/90]_{2s}$) with the 0° orientation along the length of the coupon. The

coupons were machined and ground to have a length of 5" and a width of 1" cm. Notched coupons were machined with a round 0.25" diameter notch in the center of the coupon. After the coupons were machined, an annealing process was employed to normalize the physical aging process. The coupons were annealed at 128°C, approximately 15°C below T_g, for 48 hours and then cooled to room temperature at a rate of 0.1°C/min. All fatigue coupons were equipped with extensometer mounting flanges so that an extensometer could be used to measure the displacement during the fatigue testing.

Fatigue testing was done with a 20 kip servo-hydraulic MTS test machine under load control mode. Quasi-static, notched tensile strengths were measured first and identified as the ultimate tensile strength (UTS). Subsequent fatigue testing experiments were done at two controlled fractions of the UTS (80% and 87.5%). A frequency of 10 Hz was used.

Unidirectional Tension

Tension testing was done on 4-ply unidirectional panels from the 10 series Ultem-type TMA^+/PEEK, 30 series Ultem-type NH_4^+/PEEK, and 50 series Ultem-type TPA^+ /PEEK composites by the author and Mr. Brady Walther in the Material Response Group at Virginia Tech. Repeated loading tension testing was done on 4-ply unidirectional panels from the 10 series Ultem-type TMA^+/PEEK and 30 series Ultem-type NH_4^+/PEEK composites by Mr. Hans DeSmidt in the Material Response Group at Virginia Tech.

i.) Unidirectional tension testing: Tabs were bonded to the panels before the test samples were machined. Four rectangular, 12.7 cm x 2.54 cm x 0.25 cm, glass reinforced hardened epoxy

tabs were bonded on the panel ends perpendicular to the fiber direction. The test coupon geometry is shown in Figure 4-9. The tabbed panels were machined into 12.7 cm x 1.27 cm coupons with the length in the fiber direction using a diamond saw. Extensometer tabs were bonded to the panel in the center of the test region at a separation of 2.54 cm. Tension testing was done using a 20 kip servo-hydraulic MTS test machine under load control mode. The samples were loaded once, to failure, at a rate of 356 N/s.

ii.) Repeated loading unidirectional tension testing: Tabs were bonded to the panels before the test samples were machined. Four rectangular, 15.24 cm x 3.81 cm x 0.25 cm, hardened epoxy tabs were bonded on the panel ends perpendicular to the fiber direction. The test coupon geometry is shown in Figure 4-10. The tabbed panels were machined into 15.24 cm x 1.27 cm coupons with the length in the fiber direction using a diamond saw. Strain gages type CEA-06-125UW 350±.0.03 purchased from Micro Measurements, Inc. were bonded to each specimen. Tension testing was done using a 20 kip servo-hydraulic MTS test machine under load control mode. The specimens were loaded according to the scheme shown in Figure 4-10. Specimens were loaded quasi-statically three times to a level of 2224 N at a rate of 142 N/s. The longitudinal modulus was taken as the average value measured from these three loadings. The samples were then loaded to failure at a rate of 356 N/s. This testing was done by Mr. Hans DeSmidt, a student in the ESM Department at Virginia Tech.

Results and Discussion

Estimation of Interphase Thickness

The actual dimensions of the polyimide interphase in the composite cannot be experimentally measured at the present time. Experimental techniques for probing the dimensions accurately are currently under development at Virginia Tech and elsewhere. The interphase thickness can be estimated based on some assumptions of composite geometry, composition and microscopic morphology. A hexagonally packed fiber array can be used as an assumed geometry. This is shown in Figure 4-11 with seven fibers hexagonally arranged, each surrounded by an identical, uniform interphase region. The radius of each fiber, r_f, is assumed to be 4 μm and the distance between each adjacent fiber center around the hexagon is labeled S. Using a fiber volume fraction of 60%, and a bulk matrix composition of 95% matrix polymer and 5% interphase polymer, the interphase thickness is calculated to be 200 nm assuming that all of the interphase polymer remains at the fiber surface. This is clearly not the case in the composite fabrication step and so 200 nm is an upper bound for the interphase thickness. The necessary equations and sample calculations are shown at the end of this chapter in Appendix A.

Using the equations in Appendix A the interphase thickness can be calculated for several different fiber volume fractions using the same assumptions for geometry and bulk matrix composition. If a fiber volume fraction of 65% is used, the calculated interphase thickness is 160 nm and if a fiber volume fraction of 70% is used, the calculated interphase thickness is 130 nm.

There are many factors to consider when discussing the actual dimensions of the interphase. The interphase dimensions are calculated assuming that the interphase is a pure polyimide phase. As discussed in Chapter 3, the Ultem-type polyimide is miscible with PEEK at

all compositions, therefore interdiffusion of the two polymers is expected to occur [24-26]. This could result in an interphase with a composition gradient, high in polyimide concentration at the fiber surface, and diminishing in polyimide composition as the distance from the fiber surface increases. Polymer interdiffusion is strongly dependant on the molecular weight of the polymers. Since the molecular weights of the three different interphase polyimides are different, the interphase gradient microstructure is expected to vary with each system. While conventional polymer interdiffusion theory would lead to the conclusion that the lower molecular weight polyimide will diffuse more readily into the PEEK phase, the work by McCullough et al. describing molecular weight segregation leaving the lower molecular weight species at the carbon fiber surface is contradictory.

Also discussed in Chapter 3 was the tendency for the interphase polyimides to crosslink at the elevated temperatures experienced during composite consolidation. The crosslinking of the polyimide would hinder, if not prevent, interdiffusion of the interphase polyimide with the PEEK. If the interphase polyimide could diffuse into the PEEK before any crosslinking occurred, then the self-reactive functionalities of the interphase polyimide would become more dilute and the extent of crosslinking could be reduced. Since the crosslinking of the polyimides indicates that there are some chemically active functionalities such as amines, assumed to be at the ends of the polyimide chains, the possibilities for chemical interaction or physical adhesion to the carbon fiber surface must be considered.

Due to the complex nature of the interphase construction, the calculated interphase thickness should be considered as an order-of-magnitude approximation used to guide the further discussion of the composite properties. For the purposes of further discussions, a calculated

interphase thickness of 150 nm will be considered.

Panel Quality

The quality of the panels was assessed using ultrasonic C-scan. The C-scan images were used to choose the panels with a high quality of consolidation suitable for mechanical evaluation. Some of the panels had regions of lesser quality consolidation. These regions were not included in mechanical evaluation. Table 4-II lists the quality of consolidation as evaluated by ultrasonic C-scan as well as the fiber volume fraction for the composite panels. Figure 4-12 shows three C-scan images which are representative of good, fair and poor consolidation quality.

Fiber volume fractions were measured for each panel using 3-5 samples from each panel. For panels with varying degrees of consolidation quality throughout the panel as found by C-scan, an average fiber volume fraction was found using samples from the region of best consolidation quality and also the region of worst consolidation quality.

The microscopic inspection of the composite cross sections showed close packing of fibers, as expected with high fiber volume fractions. The measured void volumes of each unidirectional panel are included in Table 4-II as measured by image analysis of a composite cross section. The measured void volumes are very low, less than 1% for all unidirectional panels, and therefore the composite integrity is not sacrificed by the presence of a large void content.

Also shown in Table 4-II is a column labeled “test No.”. This column contains information about which mechanical test was used for the panel. The number corresponds to the mechanical tests listed in Table 4-IV.

Table 4-II. Quality of consolidation, fiber volume fraction, panel layup, void volume fraction, and mechanical test for which panel was used.

panel ID	size	layup	Consolidation Quality	V_f (%)	void volume	test No.
P101[a]	6"x6"	$[0/90]_{7s}$	good	67.6±2.5	N/A	3
P102[a]	6"x6"	$[0/90]_{7s}$	good	64.3±1.7	N/A	3
P103[a]	6"x6"	$[0/90]_{7s}$	fair	70.2±1.1	N/A	3
P104[a]	6"x6"	$[0/90]_{7s}$	good	68.6±0.9	N/A	3
P105[a]	6"x6"	$[0]_{16}$	fair	71.2±1.1	0.02%	1,2
P106[a]	6"x6"	$[0]_4$	good	68.8±0.9	0.23%	6
P107[a]	6"x6"	$[0]_4$	fair	72.1±0.3	0.35%	6
Q101[a]	10"x10"	$[0/90]_{2s}$	good	63.1±1.5	N/A	4
Q102[a]	10"x10"	$[0]_4$	good	64.8±1.0	0.27%	5
P301[b]	6"x6"	$[0/90]_{7s}$	good	61.6±1.2	N/A	3
P302[b]	6"x6"	$[0/90]_{7s}$	fair	62.3±0.2	N/A	3
P303[b]	6"x6"	$[0/90]_{7s}$	fair	66.4±0.4	N/A	3
P305[b]	6"x6"	$[0]_{16}$	fair	71.1±0.7	0.97%	1,2
P306[b]	6"x6"	$[0]_4$	fair	73.2±0.4	0.99%	6
P307[b]	6"x6"	$[0]_4$	poor	70.0±1.3	0.60%	6
Q301[b]	10"x10"	$[0/90]_{2s}$	good	64.3±1.7	N/A	4
Q302[b]	10"x10"	$[0]_4$	good	59.0±0.5	0.48%	5
Q501[c]	10"x10"	$[0/90]_{2s}$	good	67.5±1.3	N/A	4
Q502[c]	10"x10"	$[0]_4$	good	67.1±1.9	0.02%	5
Q503[c]	10"x10"	$[0]_{16}$	good	66.4±0.7	0.02%	2
A01[d]	6"x6"	$[0]_{16}$	good	61.2±0.3	0.51%	2
A02[d]	10"x10"	$[0]_4$	good	61.3±1.9	0.04%	5

a- Ultem-type TMA^+ polyimide interphase
b- Ultem-type NH_4^+ polyimide interphase
c- Ultem-type TPA^+ polyimide interphase
d- APC-2 prepreg from ICI

Sized Fiber Surface Chemistry by XPS

The surface chemical compositions of the AS-4 fiber, sized carbon fiber and chloroform washed sized carbon fiber are shown in Table 4-III.

Comparison of the surface chemistry of unsized AS-4 carbon fiber can be compared to data from several other researchers. It is important to note that since AS-4 carbon fiber is surface treated to remove weakly bound carbonaceous layers at the surface and increase the surface oxygen content [3], the surface chemistry of the AS-4 carbon fiber can vary slightly with each batch.

Table 4-III. Surface chemical compositions of carbon fiber tow.

fiber sample	C 1s (%)	O 1s (%)	N 1s (%)	Na 1s (%)	Zn 2p3 (%)
10x (sized)[a]	86.3	11.3	2.4	0.0	0.0
10x (washed)[a]	86.3	11.8	1.5	0.0	0.4
30x (sized)[b]	81.7	12.9	3.8	1.6	0.0
30x (washed)[b]	80.8	15.1	2.6	0.7	0.8
50x (sized)[c]	82.5	13.4	4.1	0.0	0.0
50x (washed)[c]	82.2	16.0	1.4	0.0	0.4
AS-4 (sized)[d]	84.2	13.6	1.3	0.9	0.0
AS-4 (washed)[d]	83.0	14.2	1.4	0.6	0.8
AS-4 [49]	85.0	12.0	3.6	0.34	0.0
AS-4 [34]	87.8	9.3	2.7	0.2	0.0
AS-4 [50]	83	12	4.0	0.7	0.0

a- Ultem-type TMA^+ polyimide interphase c- Ultem-type TPA^+ polyimide interphase
b- Ultem-type NH_4^+ polyimide interphase d- as received AS-4 fiber

The presence of zinc on the chloroform washed samples is a contamination occurring during the wash step of the procedure. The zinc could have been present in the chloroform or as a residue on the rubber seal of the vial screw cap. The level of zinc is very low and should not alter the interpretation of the surface chemistry results [33].

The concentration of nitrogen can be used as an indicator of the presence of polyimide. There is 1.3% nitrogen on the surface of the unsized AS-4 carbon fiber. The sized carbon fibers all have surface concentrations of nitrogen greater than 2%. This shows the presence of the polyimide on the fiber surface. The N/C ratio of the carbon fiber surfaces are plotted in Figure 4-13. The N/C ratios for the as received AS-4 fiber and the sized fibers are shown before and after the chloroform wash. The N/C ratios are 2.7, 4.7 and 4.9 for the 10 series, 30 series, and 50 series sized fibers, respectively. For both the 10 series and 50 series sized fibers, the N/C ratio for the washed samples is 1.7 which is equivalent to the N/C ratio for the AS-4 fiber. These results show that the Ultem-type polyimide was removed from the fiber surface during the chloroform wash for the 10 series and the 50 series sized fibers. For the 30 series sized fiber, the N/C ratio for the washed sample is 3.2 which is lower than the N/C ratio for the sized fiber, yet it is still more than twice the N/C ratio of the AS-4 fiber. This indicates there is still some Ultem-type polyimide remaining on the surface of the carbon fiber after the chloroform wash. The remaining Ultem-type polyimide on the 30 series sized fiber could be accounted for by a adhesion of the polyimide to the carbon fiber surface, or by crosslinking of a uniform Ultem-type polyimide coating forming an insoluble layer. It is possible that the Ultem-type NH_4^+ polyimide formed a uniform coating around the fibers which then crosslinked to form an insoluble sheath. The 30 series polyimide has a low molecular weight, hence a large concentration of free amine

endgroups, as discussed in Chapter 3, which are potentially reactive. The carbon fiber surface has a high concentration of oxygen atoms which are be present as hydroxyl groups, carboxylic acid functionalities and carbonyl groups [34]. These moieties are potentially reactive with the free amines present in the Ultem-type polyimide by covalent bonding or hydrogen bonding.

It is beyond the scope of this work to propose a mechanism for the adhesion of the polyimide to the carbon fiber surface or to qualify whether the adhesion is attributed to a chemical reaction or physical bonding of a crosslinked sheath. The important conclusion from this study is that the 30 series Ultem-type polyimide displays adhesion to the carbon fiber surface which is not disrupted by washing with a good solvent. Since the 30 series Ultem-type polyimide shows this adhesion and the 10 series and 50 series Ultem-type polyimides do not, these results correlate well with the hypothesis that the 30 series composites should have the strongest interfacial shear strength due to adhesion of the polyimide interphase.

Composite Properties

Although some of the composite fiber volume fractions were high compared to the "ideal" level of 60% fiber by volume, comparison of data from some mechanical tests (ie: transverse flexure and Iosipescu shear) to polyimide interphase/PEEK matrix composites made previously in Professor Davis' research group by Gonzalez [12] with closer to ideal fiber volume fractions, show close agreement. Mechanical properties of interphase composites have been reported in the literature by Drzal [3], Ho et al. [28] and Morton [35] where the fiber volume fractions are in the range of 70-72%.

Table 4-IV. Mechanical Testing Schedule

No.		10 series Ultem-type TMA^+	30 series Ultem-type NH_4^+	50 series Ultem-type TPA^+	APC-2 series
1	Iosipescu shear	✓	✓		
2	transverse flexure	✓	✓	✓	✓
3	notched fatigue (R=1.0)	✓	✓		
4	notched fatigue (R=0.1)	✓	✓	✓	✓
5	longitudinal tension	✓	✓	✓	✓
6	longitudinal tension (repeated loading scheme)	✓	✓		

The following sections will present experimental data of Ultem-type polyimide interphase/PEEK composites which will be compared to the mechanical testing data of similar composite specimens made from APC-2. Since the chemistry of the Ultem-type TPA^+ polyimide interphase was developed during the same period that other composite manufacturing and testing were done, the 50 series (Ultem-type TPA^+ polyimide interphase) composites were not available during all mechanical testing procedures. The details of the mechanical testing schedule are listed in Table 4-IV.

Shear Properties

Iosipescu (90°) shear testing gave similar results for the 10 series composite and the 30 series composite. Eight specimens from each panel were tested. The measured strains from the

back-to-back strain gage rosettes were virtually the same and the measured strains from the ±45° gages were virtually the same in magnitude and opposite in sign. The results from the Iosipescu shear testing are shown in Table 4-V. The shear strength of the 10 series composite and the shear strength of the 30 series composite were both very similar. The shear modulus for the 10 series composite and the shear modulus for the 30 series composite were also similar. It was determined from this test that the Iosipescu (90°) shear test is not sensitive to the interphase differences in the Ultem-type polyimide interphase/PEEK composites. Similar results have been shown by Gonzalez [12] with polyimide interphase/PEEK matrix composites. Gonzalez manufactured polyimide interphase/PEEK composites using BisP-BTDA polyimide and also LaRC TPI polyimide. Iosipescu (90°) shear testing was done on these composites and also APC-2 composites. The results from Gonzalez's Iosipescu shear testing are shown in Table 4-V for comparison.

Table 4-V. Iosipescu (90°) shear test results for PEEK composites.

Panel	V_f (%)	G_{12} (GPa)	$<G_{12}^{61\%}>$ (GPa)	shear strength (MPa)
10 series[a]	71.2	6.01 ± 0.10	4.01	85.55 ± 1.62
30 series[b]	71.0	5.80 ± 0.17	3.95	83.15 ± 3.12
BisP-BTDA/PEEK[c]	55.0	4.19 ± 0.09	5.61	84.77 ± 7.91
LaRC TPI/PEEK[c]	55.0	4.37 ± 0.11	5.76	85.06 ± 2.27
APC-2[c]	61.0	5.29 ± 0.06	5.29	79.24 ± 2.59

a- Ultem-type TMA^+ polyimide interphase
b- Ultem-type NH_4^+ polyimide interphase
c- composite data from Gonzalez [12]

Electron microscopy was used to examine the failure surfaces of the Iosipescu shear test specimens. Similar failure morphologies were seen for both 10 series and 30 series composite specimens as seen in the micrographs in Figure 4-14. Fibers were coated completely with polymer which was stretched and rippled. While a quantitative measure of the thickness of the polymer remaining on the carbon fiber in Figure 4-14 was not possible, the fact that no bare fibers were found indicates that for both composites, shear failure occurred *in the bulk matrix.*

Electron microscopy showed that the failure did not occur at the interface of the fiber and the interphase which would have resulted in clean fiber surfaces. Both mating failure surfaces of a single failed specimen were examined under SEM and the failure surfaces had a similar appearance which would occur with failure in the bulk matrix.

It was shown in Chapter 3 that the tensile properties of the model matrix samples from the 10 series system and the 30 series system did not differ significantly. The shear properties of the neat matrix polymer can be estimated using Eq. 4-1,

$$G = \frac{E}{2 \cdot (1 + \nu)} \qquad \text{Eq. 4-1}$$

where G = calculated shear modulus,
E = Young's tensile modulus,
and ν = Poisson's ratio

The tensile modulus for PEEK reported by Jar is 3.6 GPa [36] and the Poison's ratio reported by Folkes is 0.34 [37]. Using these data to calculate a shear modulus with Eq. 4-1 yields a value of 1.34 GPa. Comparing this calculated neat matrix shear moduli to the 10 series composite shear

modulus of 6.01 GPa and the 30 series composite modulus of 5.80 GPa, it is clear that although failure occurred primarily in the matrix, the fiber reinforcement did influence the composite shear modulus. This is consistent with results from other researchers.

The fiber volume fraction can have an effect on the shear modulus of the composite. By knowing the constitutive properties of the fiber and matrix the composite shear modulus can be estimated using Eq. 4-2, which is typically called a constant stress model and is derived using the assumption that the shear stress in the fibers is equal to the shear stress in the matrix [38].

$$G_{12} = \frac{G_m}{V_f \cdot \frac{G_m}{G_f} + (1 - V_f)} \qquad \text{Eq. 4-2}$$

where G_{12} =constant stress model composite shear modulus
G_m = matrix shear modulus
G_f = fiber shear modulus
V_f = fiber volume fraction.

Eq. 4-2 can also be used to correct experimentally measured shear moduli to a specific fiber volume fraction for comparison of measured shear moduli of composites with different fiber volume fractions [12]. To correct the shear modulus for fiber volume fraction, Eq. 4-2 is used as a ratio of two shear moduli and rearranged as Eq. 4-3.

$$G_{12}^{corr} = G_{12}^{exp} \cdot \frac{V_f^{act} \cdot \frac{G_m}{G_f} + (1 - V_f^{act})}{V_f^{corr} \cdot \frac{G_m}{G_f} + (1 - V_f^{corr})} \qquad \text{Eq. 4-3}$$

where G_m = matrix shear modulus
G_f = fiber shear modulus
V_f^{act} = actual fiber volume fraction of composite
V_f^{corr} = corrected fiber volume fraction reference
G_{12}^{corr} = corrected composite shear modulus at V_f^{corr}
G_{12}^{exp} = experimentally measured composite shear modulus at V_f^{act}.

The constant stress model is not mathematically rigorous and suffers from some limitations. Most importantly, the assumption of constant stresses in the fibers and the matrix leads to a mismatch of strains at the fiber-matrix interface.

A more rigorous model for predicting shear modulus of a unidirectional composite has been developed by Halpin and Tsai [38] based on a more exact micro mechanical analysis. From this analysis, equations have been developed to approximate the shear modulus of a composite for design purposes. The Halpin-Tsai equation for composite shear modulus is:

$$G_{12} = G_m \cdot \frac{1 + \xi \cdot \eta \cdot V_f}{1 - \eta \cdot V_f} \qquad \text{Eq. 4-4}$$

where

$$\eta = \frac{(G_f/G_m) - 1}{(G_f/G_m) + \xi} \qquad \text{Eq. 4-5}$$

and G_f = shear modulus of fiber
G_m = shear modulus of matrix
ξ = reinforcement geometry factor (1 for cylindrical fibers)
V_f = fiber volume fraction.

In a similar fashion to the constant stress model, the Halpin-Tsai model for predicting composite shear modulus can also be used in a ratio to correct measured composite shear moduli to a specific fiber volume fraction. The correction for fiber volume fraction using the Halpin-Tsai model is:

$$G_{12}^{corr} = G_{12}^{\exp} \cdot \frac{\dfrac{1+\xi\cdot\eta\cdot V_f^{act}}{1-\eta\cdot V_f^{act}}}{\dfrac{1+\xi\cdot\eta\cdot V_f^{\exp}}{1-\eta\cdot V_f^{\exp}}} \qquad \text{Eq. 4-6}$$

Where η is defined by Eq. 4-5
ξ = reinforcement geometry factor (1 for cylindrical fibers)
V_f^{act} = actual fiber volume fraction of composite
V_f^{corr} = corrected fiber volume fraction reference
G_{12}^{corr} = corrected composite shear modulus at V_f^{corr}
G_{12}^{exp} = experimentally measured composite shear modulus at V_f^{act}.

A comparison of the composite shear modulus predictions from Eq. 4-2 and Eq. 4-4 are shown by the curves in Figure 4-15 as a function of fiber volume fraction. The composite shear modulus predictions are made using a matrix shear modulus values of 1.34 GPa as calculated above and a fiber shear modulus of 28 GPa from ref [38]. Also shown in Figure 4-15 are experimentally measured composite shear moduli. The predictions from the Halpin-Tsai model

(Eq. 4-4) are closest to the measured data. Thus, it follows that the Halpin-Tsai model for composite shear moduli is the more appropriate approach for corrections of experimental data for fiber volume fraction using Eq. 4-6. The corrected mean shear moduli in Table 4-V, $<G_{12}^{61\%}>$ are from this correction scheme.

A comparison of the corrected composite shear moduli is shown in Figure 4-16. The solid symbols represent the experimentally measured composite shear moduli. The open symbols show corrected composite shear moduli to reference fiber volume fractions of 61%. The lines drawn through the open symbols are to guide the reader.

Transverse Flexure Properties

The data from the transverse flexure test shown in Table 4-VI provide compelling results that the differences in interphase properties directly affect the fiber-matrix adhesion in the composite. The flexure strength of the composites show differences of up to 17% for the 30 series composites and the 10 series composites. The flexure moduli of all the composites are very similar. The strain reported from the flexure tests is the tensile strain at the midspan of the specimen in the outer ply induced by the bending moment. The mechanics of the bending test create a compression load on the top surface of the specimen and a tensile load on the bottom surface of the specimen. The strain represents the compressive and tensile strains at failure on the top and bottom surface of the specimen, respectively. The flexure toughness was calculated as the area under the stress-strain response curve from the transverse flexure test.

The coupon failure mode for the transverse flexure testing was consistent for all samples

and was characterized by fracture at the beam center due to normal stresses which broke the beam into two nearly symmetric pieces. Some of the failed coupons were held together by the outer layer of polymer matrix that was on the top surface of the loaded beam. This would indicate that fracture initiated on the bottom surface of the beam where the bending moment creates tensile stresses normal to the load. There was no indication of fracture due to interlaminar shear stresses which would be characterized by splitting of the beam on the level of the mid-plane.

Table 4-VI. Transverse flexure results for PEEK composites.

	flexure strength (MPa)	flexure modulus (GPa)	failure strain (%)	toughness (MPa)
10 series[a]	126.8 ± 5.4	10.11 ± 0.15	1.31 ± 0.07	0.83 ± 0.08
30 series[b]	146.1 ± 10.3	10.86 ± 0.24	1.43 ± 0.13	1.01 ± 0.17
50 series[c]	141.1 ± 13.3	10.39 ± 0.10	1.48 ± 0.18	1.11 ± 0.25
APC-2[d]	147.9 ± 11.8	9.90 ± 0.08	1.49 ± 0.11	1.11 ± 0.17

a- Ultem-type TMA^+ polyimide interphase
b- Ultem-type NH_4^+ polyimide interphase
c- Ultem-type TPA^+ polyimide interphase
d- APC-2 prepreg from ICI

The sets of data for the four composites were statistically compared using an unpaired *t*-test executed with SigmaStat Statistical Software v. 2.0. The unpaired *t*-test is used to test for a difference between two groups that is greater than what can be attributed to random sampling variation. The SigmaStat Statistical Software first tests for normally distributed populations using a Kolmogorov-Smirnov test, and then tests for equal variance by checking the variability about the group means. If the sample populations each pass these tests, then the unpaired *t*-test is

executed using a confidence interval of 95%. The unpaired *t*-test is a parametric test based on estimates of the mean and standard deviation parameters of the normally distributed populations from which the samples were drawn. If two sets of data pass an unpaired *t*-test, then there is 95% confidence that the difference in the mean values of the two groups is greater than would be expected by chance. Therefore, there is a statistically significant difference between the groups.

The unpaired *t*-test results are shown in Table 4-VII. Each set of PEEK matrix composite transverse flexure data was compared with one another. The results show that there is a statistically significant difference in transverse flexure strength between the 10 series composite and every other composite. The results also show that the transverse flexure strength for the 30 series, the 50 series and the APC-2 composites are not statistically different.

The transverse flexure moduli for all the PEEK matrix composites are all statistically different from one another. These differences are expected and attributed to differences in fiber volume fraction. The transverse properties of composites are mildly affected by small changes in fiber volume fraction. The transverse flexure moduli are shown as a function of fiber volume fraction in Figure 4-17

Table 4-VII. Unpaired *t*-test results comparing each set of PEEK matrix composite transverse flexure data.

	transverse flexure strength	transverse flexure modulus	strain-to-failure	transverse flexure toughness
10 series[a] vs. 30 series[b]	pass	pass	pass	pass
10 series[a] vs. 50 series[c]	pass	pass	pass	pass
30 series[b] vs. 50 series[c]	fail	pass	fail	fail
10 series[a] vs. APC-2[d]	pass	pass	pass	pass
30 series[b] vs. APC-2[d]	fail	pass	fail	fail
50 series[c] vs. APC-2[d]	fail	pass	fail	fail

a- Ultem-type TMA^+ polyimide interphase
b- Ultem-type NH_4^+ polyimide interphase
c- Ultem-type TPA^+ polyimide interphase
d- APC-2 prepreg from ICI
pass = statistically significant difference between data sets
fail = no statistical difference between data sets

The *t*-test results show that the strain-to-failure results of the 10 series composite are statistically different from every other composite. The *t*-test results also show that the differences in the mean values of all the other pairs are not great enough to reject the possibility that the difference is due to random sampling variability. There is not a statistically significant difference among the strain-to-failure of the 30 series, 50 series and APC-2 composites. The strain-to-failure results show that the 10 series composite has the lowest strain to failure. This is an important consideration for composite design issues. In composite design, the transverse flexure strength is not as important as the transverse strain to failure. When designing a composite laminate, a specific lamina stacking sequence is used to tailor the properties of the composite laminate to suit the loading condition. For example, when considering a crossply composite laminate, the tensile loads applied to the composite in the 0° direction will bear

predominantly upon the 0° oriented lamina and the 90° oriented lamina must survive the corresponding transverse elongation. In this manner, the tensile loads applied to the composite in the 90° direction will bear predominantly upon the 90° oriented lamina, and the 0° oriented lamina must survive the corresponding transverse elongation. The transverse lamina are not intended to support a tensile load. Thus, the transverse strain to failure is more important than the transverse strength from a design perspective.

The transverse flexure strength is a very important property because it furthers the development of the composite structure-property relationships and provides a means of comparing the interfacial adhesion of the composites. There is a 17% increase in transverse flexure strength for the 30 series composite specimens and a 13% increase in transverse flexure strength for the 50 series composite specimens over the 10 series composite specimens. The transverse flexural strength has been shown by Adams, et al. [39] to be dependent upon different sizings or interphases of the composite. Drzal and Madhukar [3] have shown that the flexural strength correlates well with the interfacial shear strength (ISS) for composites made with AU-4, AS-4 and AS-4C fibers and Epon 828 epoxy matrix, cured with mPDA. Chang, et al. [5] showed a similar correlation of transverse flexure strength with ISS for composites made with AU-4, AS-4, and AS-4GCP fibers and J2 polyamide copolymer matrix. The normalized transverse flexure strength has been plotted as a function of normalized ISS from the data of Drzal and Madhukar [3] and Chang, et al. [5] in Figure 4-18. This data clearly shows a correlation of increasing transverse flexure strength with increasing ISS.

Although quantitative ISS values cannot be gained from the correlation of ISS to transverse flexure strength data, a relative ranking of ISS, or fiber-matrix interfacial adhesion can

be made. Following the trends of the transverse flexure strength, this relative ranking is:

$$ISS_{10\ series} < ISS_{50\ series} \simeq ISS_{30\ series} \simeq ISS_{APC\text{-}2}.$$

This relative ranking of composite interfacial shear strength is very important for a discussion of the effects of interfacial shear strength on overall composite performance and understanding the micro mechanics of composite failure.

A comparison of the flexure toughness of the composite samples provides the most striking difference of the composites. There is an 18% increase in toughness for the 30 series composite system over the 10 series composite system and a 25% increase in toughness for the 50 series composite system over the 10 series composite system.

Microscopic examination of the failure surfaces for the transverse flexure specimens revealed very different topographies for the composites. The bending nature of the three point bending test creates tensile loading on the lower side of the test specimen (beam) and compressive loading on the top side of the test specimen. The tension side of the failure surface was the focus of the examination as this is the side where failure initiates.

Micrographs from the transverse flexure failure specimens are shown in Figure 4-19. The 10 series composite failure surface shown in Figure 4-19(a.) shows some bare fiber matrix material that appeared to be pulled away from the fiber. The 30 series composite failure surface shown in Figure 4-19(b.) has no bare fibers visible. There are channels and ridges where fibers were pulled from the mating surface, but polymer matrix material covered the region. A similar failure surface is seen for the 50 series composite failure surface in Figure 4-19(c.) with no bare

fibers visible. The APC-2 composite failure surface shown in Figure 4-19(d.) shows no bare fibers but a different surface morphology. There were not as many ridges or channels which could be a result of the lower fiber volume fraction as compared to the polyimide interphase/PEEK matrix composites. Also, the rippled texture of the APC-2 failure surface is very different from the polyimide interphase/PEEK matrix composites suggesting that the failure mechanism for the polyimide interphase/PEEK matrix composites was influenced by the presence and properties of the polyimide interphase region.

Voltage Contrast X-ray Photoelectron Spectroscopy

The C_f/C_m ratio is a quantitative parameter used to determine how cohesive or adhesive the failure was. The C_f/C_m ratio is defined as the ratio of the area of exposed fiber to the area of exposed polymer based on the shift of the C 1s binding energy. Miller et al. ranks the nature of the failure surface based on the C_f/C_m ratio [51]. For a C_f/C_m ratio less than 0.2 the failure is described as being cohesive in the matrix with excellent interfacial bonding [51]. For a C_f/C_m ratio of 0.2-0.6 the failure is described as being mostly cohesive in the matrix with good interfacial bonding [51]. A C_f/C_m ratio greater than 1.2 required for the nature of the failure to be classified as adhesive failure [51].

The C_f/C_m ratio for the 10 series Ultem-type TMA^+ polyimide interphase composite was 0.05 ± 0.02; the C_f/C_m ratio for the 30 series Ultem-type NH_4^+ polyimide interphase composites was 0.12 ± 0.04; and the C_f/C_m ratio for the 50 series Ultem-type TPA^+ polyimide interphase composites was 0.28 ± 0.03. The C_f/C_m ratio is very low for all three of the Ultem-type

polyimide interphase/PEEK matrix composites indicating good to excellent interfacial bonding and mostly cohesive to fully cohesive failure in the matrix [52]. For the case of the Ultem-type polyimide interphase/PEEK matrix composites, it is important to note that the cohesive failure could occur in the polyimide interphase region or the bulk matrix. The C_f/C_m ratio indicates that the fibers are covered with polymer however accurate interpretation of the composition of this polymer is not probable. The very low standard deviation coupled with the low values for the C_f/C_m ratio indicate that the composites were very well made, that the failure did not occur at the fiber/polymer interface and that the composites were very uniform at the cross section [52].

Notched Fatigue Properties (R=1.0)

The notched fatigue testing with R=1.0 is a fully reversible fatigue loading scheme. The coupons are loaded cyclically in tension and compression with the same magnitude of load. It is well known that the compression strength of a composite is typically lower than the tensile strength, thus failure is expected in the compressive mode. Compressive failure of a crossply laminate is typically a result of fiber microbuckling, fiber-matrix debonding, matrix cracking or shear failure.

This experiment was conducted prior to the capabilities of fabricating the interphase for the 50 series composites. Therefore, the 50 series composites were not available for R=1.0 notched fatigue testing.

The notched fatigue sample geometry is shown in Figure 4-7. The circular notch in the center of the sample provides a carefully designed stress concentration in the composite laminate.

The effect of this stress concentration on the compressive properties of a crossply composite can be studied by using a fatigue-based testing scheme. The quasi-static ultimate compressive strengths (UCS) of the notched coupons was determined to be 304.0 ± 22.8 MPa. This was the statistical average from 5 test specimens from the 10 series composites and from 1 test specimen from the 30 series composite. This average was used due to the limited supply of test coupons. The results from the R=1.0 notched fatigue testing are shown in Table 4-VIII. A plot of residual strength vs. log of the number of cycles fatigued is shown in Figure 4-20. The lines in Figure 4-20 represent best fit linear regressions of each data set. A statistical analysis on the linear regressions resulted in the conclusion that they are not statistically different.

The results from the R=1.0 notched fatigue testing do not show a difference between the 10 series and 30 series composites. It is estimated from the transverse flexure strength that the differences in interfacial shear strength are greatest for these composites. This indicates that the R=1.0 notched fatigue testing is not sensitive to the differences in composite interphase in the Ultem-type polyimide interphase composites. The scatter in the data is large, which decreases the probability that the two sets of data will be statistically different. The large scatter is attributed to the complex failure modes of the compressive failure.

Table 4-VIII. Loading level and number of fatigue cycles before failure for R=1.0 notched fatigue testing.

loading level (% UCS)	30 series[b] cycles		loading level (% UCS)	10 series[a] cycles
0.85	607		0.85	831
0.85	342		0.85	30062
0.825	3		0.80	432
0.825	2883		0.775	4996
0.825	972558		0.75	2051
0.80	15202		0.75	12500
0.80	20977		0.75	20023
0.775	62200		0.75	30621
0.775	1000872		0.75	681141
0.75	1007681		0.70	66182
			0.65	519616

a- Ultem-type TMA^+ polyimide interphase b- Ultem-type NH_4^+ polyimide interphase

Notched Fatigue Properties (R=0.1)

The quasi-static ultimate tensile strengths (UTS) of the notched coupons are tabulated in Table 4-IX and Table 4-X identified by one cycle of loading. The 10 series composites have the highest UTS of those studied amounting to a 35% increase in UTS over the 30 series composites and a 25% increase in UTS over the 50 series composites. The notched fatigue testing of the $[0/90]_{2s}$ composites at R=0.1 was conducted at 80% of UTS and 87.5% UTS. The residual strength and average split length are shown in Table 4-IX with the number of cycles loaded for the 80% UTS fatigue experiments. The residual strength and average split length are shown in

Table 4-X with the number of cycles loaded for the 87.5% UTS fatigue experiments.

It is important to carefully consider the crossply panel construction and the damage growth with regard to the stress concentration to properly understand the meaning of the UTS comparisons. Since the panels have a crossply layup, the lamina alternate from 0° orientation to 90° orientation. In tensile loading, the lamina with the 0° orientation bear most of the load. After enough of the fibers in the 0° orientation have broken, the composite will fail. The circular notch provides a stress concentration at the horizontal edges of the notch which increases the propensity for fiber breakage. If the stress concentration can be relieved, then the amount of fiber breakage can be reduced. One way for the stress concentration to be relieved is by the growth of longitudinal splits at the horizontal edges of the circular notch as shown in Figure 4-21. If these splits were to grow the entire length of the coupon, then the single coupon would actually become two separate, load-bearing coupons without the circular notch stress concentration.

Because the relief of the stress concentrations is so important, the growth of the longitudinal splits during cyclic fatigue testing was studied. Figure 4-22 shows the split length measured after different numbers of cycles of loading. The curve on each graph represents a second order fit of the data. For each composite system, the fatigue experiments were conducted at 80% and 87.5% of the UTS.

The 10 series composite shows the most rapid growth of longitudinal splits with number of cycles of fatigue at 80% UTS. The 30 series composite shows the slowest growth of longitudinal splits with number of cycles of fatigue at 80% UTS. The split growth can be compared quantitatively by utilizing the polynomial function of the second order fit to the experimental data. These fits each show a reasonable representation of the experimental data as

Table 4-IX. R=0.1 Notched fatigue results for 80% UTS

Panel	number of cycles	residual strength (MPa)	% average UTS	average split length (mm)
10 series[a]	1	475.74	100	0
10 series[a]	100	456.44	96	11
10 series[a]	10000	509.18	107	19
10 series[a]	100000	406.77	106	20
30 series[b]	1	353.01	100	0
30 series[b]	100	330.61	94	5.25
30 series[b]	10000	404.04	114	10.5
30 series[b]	100000	458.5	130	18.25
50 series[c]	1	379.21	100	0
50 series[c]	100	370.94	98	6.5
50 series[c]	10000	436.10	115	13.5
50 series[c]	100000	467.12	123	20
APC-2[d]	1	385.07	100	0
APC-2[d]	100	376.46	98	---
APC-2[d]	100	381.97	99	---
APC-2[d]	10000	407.48	106	13.51
APC-2[d]	100000	416.45	108	19.86

a- Ultem-type TMA^+ polyimide interphase
b- Ultem-type NH_4^+ polyimide interphase
c- Ultem-type TPA^+ polyimide interphase
d- APC-2 prepreg from ICI, data from ref [30]

Table 4-X. R=0.1 Notched fatigue results for 87.5% UTS.

Panel	number of cycles	residual strength (MPa)	% average UTS	average split length (mm)
10 series[a]	1	475.74	100	0
10 series[a]	100	415.41	87	12.5
10 series[a]	666*	N/A	N/A	N/A
10 series[a]	4571*	N/A	N/A	N/A
30 series[b]	1	353.01	100	0
30 series[b]	100	371.63	105	2
30 series[b]	10000	404.38	115	12.75
30 series[b]	100000	458.50	124	19.5
50 series[c]	1	379.21	100	0
50 series[c]	100	370.94	105	8
50 series[c]	10000	436.10	124	15.25
50 series[c]	100000	467.12	118	20
APC-2[d]	1	385.07	100	0
APC-2[d]	100	375.77	98	6.84
APC-2[d]	100	395.76	103	6.74
APC-2[d]	10000	441.96	115	18.19
APC-2[d]	100000	477.12	124	---
APC-2[d]	100000	463.33	120	---

a- Ultem-type TMA^+ polyimide interphase
b- Ultem-type NH_4^+ polyimide interphase
c- Ultem-type TPA^+ polyimide interphase
d- APC-2 prepreg from ICI, data from ref [30]
*- failed during cyclic loading

seen in Figure 4-22. The second order polynomial function that was used to fit the data was:

$$y = b_1 \cdot [\log(N)]^2 + b_2 \cdot \log(N) \qquad \text{Eq. 4-7}$$

where y = split length; N = number of cycles; b_1 = constant determined by fit; b_2 = constant determined by fit

Sigma Plot, V 2.0 was used to automatically fit the polynomial function to the experimental data. The constants found to best fit the data are shown in Table 4-XI for each composite system at 80% UTS and 87.5% UTS.

Table 4-XI. Constants for equation 4-10 from second order fit.

	b_1 80%UTS	b_2 80% UTS	b_1 87.5% UTS	b_2 87.5% UTS
10 series[a]	-0.6118	7.0395	0	6.25
30 series[b]	0.1480	2.1316	0.3388	1.3289
50 series[c]	0.0033	3.3224	-0.1974	4.5329
APC-2[d]	0.5945	0.9995	0.5763	2.2425

a- Ultem-type TMA^+ polyimide interphase
b- Ultem-type NH_4^+ polyimide interphase
c- Ultem-type TPA^+ polyimide interphase
d- APC-2 prepreg from ICI

The curves from the second order polynomial functions for 80% UTS fatigue experiments are shown in Figure 4-22, with the experimental data. The differential of the polynomial function yields an equation which can be used to calculate the instantaneous slope of the function. This slope can be considered the longitudinal split growth rate as a function of number of cycles. The longitudinal split growth rates are shown in Figure 4-23 as a function of number

of cycles. These longitudinal split growth rates can be used for quantitative comparison of the different composite split growth rates. The initial longitudinal split growth rate for the 10 series composite is at least two times greater than any other composite system. Thus, the 10 series composite system can relieve the stress concentrations much faster than the other composites.

The ability of the 10 series composite system to relieve to stress concentrations could contribute to the effect that the 10 series composite system has the highest quasi-static UTS. The longitudinal split growth is measured as a function of cyclic fatigue at 80% UTS and at 87.5% UTS. Although the 10 series composites do not survive fatigue cycles up to 10,000 at 87.5% UTS, the initial split growth rate is greater than the split growth rate at 80% UTS. The rapid longitudinal split growth rate could be due to a weak interphase, or a "slip" interphase, providing cohesive interphase failure at moderate levels of strain. The cohesive interphase failure could contribute to relief of stress concentrations during the quasi-static tensile test, thus yielding a greater UTS than for the other composite systems. A weaker interphase for the 10 series composites is consistent with observations from transverse flexure experiments.

The 30 series composites have the slowest initial split growth rate of the polyimide interphase composites at 80% UTS fatigue cycling as seen in Figure 4-23(a). The 30 series composites thus have the least ability to initially grow longitudinal splits and relieve the stress concentrations. The slow longitudinal split growth rate could be due to a stronger interphase which could limit the growth of longitudinal splits. By restraining the growth of longitudinal splits, the stress concentrations are not relieved as effectively. This idea can extend to the mechanics of the quasi-static tension testing, maintaining the stress concentrations with a strong interphase which would contribute to the effect that the 30 series composite system has the

lowest quasi-static UTS. A stronger interphase for the 30 series composites is consistent with observations from transverse flexure experiments.

The 50 series composite has an intermediate initial split growth rate between the 10 series and the 30 series composites at 80% UTS fatigue cycling. Also, the UTS of the 50 series composites is intermediate between the 10 series and the 30 series composites. These results are consistent with the mechanics postulated. An intermediate interphase strength between the 10 series and 30 series composites is consistent with observations from transverse flexure experiments.

Although the longitudinal split length for all three polyimide interphase composites is about the same after 1,000,000 cycles of fatigue at 80% UTS, the amount and the type of damage in the coupon will not necessarily be the same. The rapid initial growth of longitudinal splits for the 10 series composite relieves the stress concentrations more quickly and limits the amount of fiber breakage and matrix cracking in the region of the stress concentrations. Thus, the split growth rate is more important for composite durability than the actual split length after a given number of fatigue cycles.

Similar trends occur with the 87.5% UTS fatigue cycling as for the 80% UTS fatigue cycling as seen in Figure 4-23(b). Again, the initial split growth rate of the 30 series composites is the lowest among the polyimide interphase composites, the initial split growth rate of the 10 series composites is greatest and the initial split growth rate of the 50 series composites is intermediate. The 10 series composite does not survive fatigue cycles up to 10,000. The 10 series composite coupons fatigued above 100 cycles at 87.5% UTS failed at 666 cycles and 4,571 cycles. This failure could be due to cohesive interphase failure throughout the composite

coupon, fiber breakage from the more aggressive cyclic loading stress (87.5% of 475 MPa for the 10 series composites is 416 MPa which is greater than 100% UTS of any other composite system examined) or a combination of these factors.

The residual strength after cyclic fatigue loading provides valuable information about composite durability. It is interesting to note the trends of composite residual strength as a function of cycles of fatigue at 80% UTS shown in Figure 4-24(a.). All the composites show an initial decrease in residual strength after 100 cycles of fatigue, followed by an increase in residual strength to values greater than the initial quasi-static strength. As explained previously, the increase in residual strength is attributed to the relief of stress concentrations at the edges of the circular notch. The 30 series composite shows an exceptional increase in residual strength of 30% from the quasi-static UTS and the 50 series composite shows an increase of 25% from the quasi-static UTS. The residual strength after 1000000 cycles of fatigue for the 10 series composite amounts to only a 6% increase from the quasi-static UTS, however the magnitude of strength is far greater than for any other composite system. The large value of tensile strength and the small margin of improvement with cyclic fatigue for the 10 series composite could indicate that this system is near the tensile performance limits for an AS-4/PEEK matrix composite. The APC-2 composite shows a similar initial decrease in residual strength followed by an increase in residual strength with cyclic fatigue. At much larger numbers of fatigue cycles, damage accumulation will result in an eventual decrease in residual strength however, the notched fatigue testing was stopped before this could be observed [40].

The trends of composite residual strength as a function of cycles of fatigue at 87.5% UTS are shown in Figure 4-24(b.). For the 87.5% UTS cyclic fatigue loading, only the 10 series

composite and the 50 series composite showed an initial decrease in residual strength. As previously noted, the 10 series composite did not survive a number of fatigue cycles above 4571. The initial decrease in residual strength for the 50 series composite at 87.5% UTS cyclic fatigue is only 2% at 100 cycles. Upon further cyclic fatigue loading a continual increase in residual strength is shown to a final value 23% greater than the quasi-static UTS. The 30 series composite shows a continual increase in residual strength with cyclic fatigue to a final value 24% greater than the quasi-static UTS. The APC-2 composite also shows a continual increase in residual strength with cyclic fatigue up to 10000 cycles.

The dependance of initial split growth rate as a function of the interfacial shear strength is approximated in Figure 4-25. As explained previously, the transverse flexure strength is used as a qualitative measure of the interfacial shear strength. The trends in Figure 4-25(a) and 4-25(b) clearly show that as the composite transverse flexure strength decreases, there is a corresponding increase in the initial split growth rate. This further illustrates the importance of the interfacial shear strength on composite durability, specifically on the relief of stress concentrations.

Longitudinal Tension

Longitudinal tension testing of 4-ply unidirectional PEEK matrix composites was done using a single, quasi-static loading ramp of 356 N/sec. The longitudinal tensile test results are shown in Table 4-XII. The tensile strength is tabulated along with the tensile strength normalized with respect to the 30 series composite strength value.

Table 4-XII. Longitudinal tension test results for PEEK matrix composites.

Panel	tensile strength (MPa)	normalized tensile strength	tensile modulus (GPa)	failure strain (%)
10 series[a]	1969 ± 110	1.13 ± 0.06	146.1 ± 2.7	1.27 ± 0.09
30 series[b]	1749 ± 168	1.00 ± 0.10	132.6 ± 6.6	1.30 ± 0.05
50 series[c]	1824 ± 144	1.08 ± 0.08	150.0 ± 16.8	1.22 ± 0.07
APC-2[d]	2057 ± 115	1.18 ± 0.06	140.9 ± 5.5	1.41 ± 0.07

a- Ultem-type TMA^+ polyimide interphase
b- Ultem-type NH_4^+ polyimide interphase
c- Ultem-type TPA^+ polyimide interphase
d- APC-2 prepreg from ICI

The primary reason for measuring the longitudinal tensile strength of the Ultem-type polyimide interphase/PEEK matrix composites is to test the hypothesis of Subramanian et al. which proposes that a maximum tensile strength exists at an optimum interfacial shear strength (ISS) for a given composite system [4]. This hypothesis was first discussed in Chapter Two of this thesis and is shown graphically from data of Subramanian et al. in Figure 2-38 [4].

It was shown earlier in this chapter that the transverse flexure strength can be used to rank the relative ISS for a given composite system. Therefore the plot of normalized transverse flexure strength vs. longitudinal tensile strength for the Ultem-type polyimide interphase/PEEK matrix composites shown in Figure 4-26 can be qualitatively compared to Figure 2-38. The curve in Figure 4-26 is a second order polynomial fit to the data by the curve fitting function of SigmaPlot 3.0 and is only intended to suggest a possible trend of the data. The trend suggested by the data shows qualitative agreement to the hypothesis of Subramanian et al.

The sets of longitudinal tension data for the four composites were statistically compared using an unpaired *t*-test executed with SigmaStat Statistical Software v. 2.0 as described earlier

in the transverse flexure test section. The unpaired *t*-test is used to test for a difference between two groups that is greater than what can be attributed to random sampling variation. A 95% confidence interval was used to determine if the difference in the mean values of the two groups is greater than would be expected by chance. The *t*-test results for the unidirectional tension test are shown in Table 4-XIII. The results show that the tensile strength for each data set is statistically unique with exception of the 30 series vs. the 50 series composites. There is not a statistically significant difference between the tensile strength of the 30 series and the 50 series composites.

Table 4-XIII. Unpaired *t*-test results comparing each set of PEEK matrix composite longitudinal tensile data.

	tensile strength	tensile strain-to-failure	tensile modulus
10 series[a] vs. 30 series[b]	pass	fail	pass
10 series[a] vs. 50 series[c]	pass	fail	fail
30 series[b] vs. 50 series[c]	fail	pass	pass
10 series[a] vs. APC-2[d]	pass	pass	pass
30 series[b] vs. APC-2[d]	pass	pass	pass
50 series[c] vs. APC-2[d]	pass	pass	fail

a- Ultem-type TMA^+ polyimide interphase
b- Ultem-type NH_4^+ polyimide interphase
c- Ultem-type TPA^+ polyimide interphase
d- APC-2 prepreg from ICI

The panel made from the APC-2 prepreg has the highest strength. This system has been optimized by Fiberite and the details of the optimization are proprietary information and not available. Since little is known about the construction of the APC-2 prepreg the structure-

property relationships of the composite cannot be related to the interphase. Among the Ultem-type polyimide interphase composites, the 10 series composite has the highest tensile strength. This interphase composite system was shown to have the weakest fiber-matrix adhesion of the three Ultem-type polyimide interphase composites by transverse flexure testing. Although the differences in tensile strength are slight, they are statistically significant and consistent with the trend shown by the UTS of notched coupons shown in the R=0.1 notched fatigue results.

The tensile moduli shown in Table 4-XII. indicate that there is a significant statistical difference among several of the pairs of composite systems which can be accounted for by differences in fiber volume fraction. A mathematical model of the composite system is next presented to compare the strength and modulus of the composites with respect to fiber volume fraction.

Development of the Rule of Mixtures for Composite Strength

A unidirectional composite may be modeled by assuming that the fibers are continuous, aligned parallel and uniform in properties [38]. Other important assumptions are that perfect bonding exists between the fibers and matrix so that slippage does not occur at the fiber-matrix interface and each component has a linear elastic response [38]. Thus, during longitudinal tension, the elastic strains experienced by the fiber, matrix and composite are equal.

$$\epsilon_f = \epsilon_m = \epsilon_c \qquad \text{Eq. 4-8}$$

The load applied to the composite (P_c) is the sum of the loads carried by the fibers (P_f) and the matrix (P_m).

$$P_c = P_f + P_m \qquad \text{Eq. 4-9}$$

Eq. 4-9 can be written in terms of the individual stresses, σ_c, σ_f, and σ_m, applied to the composite, fiber and matrix, respectively, and their corresponding cross-sectional areas A_c, A_f, and A_m.

$$P_c = \sigma_c \cdot A_c = \sigma_f \cdot A_f + \sigma_m \cdot A_m \qquad \text{Eq. 4-10}$$

Dividing Eq. 4-10 by the cross sectional area of the composite, A_c, yields Eq. 4-11.

$$\sigma_c = \sigma_f \cdot \left(\frac{A_f}{A_c}\right) + \sigma_m \cdot \left(\frac{A_m}{A_c}\right) \qquad \text{Eq. 4-11}$$

Based on the assumptions for this model, the constituent volume fractions are equal to the respective cross sectional area fractions.

$$V_f = \frac{A_v}{A_c}, V_m = \frac{A_m}{A_c} \qquad \text{Eq. 4-12}$$

Substituting for the area fractions in Eq. 4-11 yields,

$$\sigma_c = V_f \cdot \sigma_f + V_m \cdot \sigma_m \qquad \text{Eq. 4-13}$$

σ_c = composite tensile strength V_f = fiber volume fraction
σ_f = fiber tensile strength σ_m = matrix tensile strength

Eq. 4-13 indicates that the contributions to the composite strength of the fibers and the matrix are proportional to their volume fractions. This type of a relationship is called a rule of mixtures and σ_c from Eq. 4-13 is referred to as σ^{ROM} [38].

The stresses σ_f and σ_m in Eq. 4-13 are not the ultimate strengths of the constitutive materials, but they are stresses at a specific strain within the elastic region of deformation. To use Eq. 4-13 properly, a specific composite strain must be considered [38]. Since the strains of the composite, fibers and matrix are equal in this model, and a linear elastic response is assumed for each component, Hooke's law can be used to calculate the individual contributions to composite strength by the fibers and the matrix. The actual stress-strain response curves for unidirectional tensile testing of all composites was nearly linear. Hooke's law is:

$$\sigma_i = E_i \cdot \epsilon \qquad \text{Eq. 4-14}$$

where the variable "I" is meant to represent either "f" for the fiber or "m" for the matrix. The strain, ϵ, used to calculate the individual contributions to composite strength for the rule of mixtures strength, σ^{ROM}, is the measured composite strain from Table 4-XIV. The Hercules AS-4 carbon fiber data sheet reports E_f = 234.6 GPa [23] and Jar reports E_m = 3.6 GPa for neat

PEEK [36]. Using these values with Eq. 4-14 and Eq. 4-13 the rule of mixtures composite strength, σ^{ROM}, is calculated and tabulated in Table 4-XIV.

The ratio of measured strength to predicted strength by the rule of mixtures, also from Table 4-XIV, is close to 1.0 for all composites, which shows good agreement between predicted and measured strengths. This indicates that the composites are modeled well by the assumptions made for the rule of mixtures model. Specifically, the composite has fibers that are continuous, aligned parallel and uniform in properties. Good bonding exists between the fibers and matrix so that no slippage occurs at the fiber-matrix interface and each component can be considered to have a linear elastic response.

The data sheet for Hercules AS-4 carbon fiber reports a fiber tensile strain-to-failure of 1.61% [23]. As seen in Table 4-XII, the largest tensile strain for any of the composites is 1.41%. Thus, all the composites fail before the fibers can be loaded to their individual maximum strain. The strain limitation for the composite is attributed to fiber defects, composite voids and discontinuous fibers in the composite. The data sheet for ICI PEEK reports a tensile yield strain of 4.7% [41], therefore the matrix can be considered to deform elastically up to the limiting tensile strain the fibers (1.61%). An ultimate composite longitudinal tensile strength σ^{ULT}, can be calculated using Eq. 4-13 and Eq. 4-14 with a maximum composite strain of 1.61%. The calculated values of σ^{ULT} are tabulated in Table 4-XIV. The σ^{ULT} represents the longitudinal tensile strength of a perfect composite with no broken fibers, no fiber defects, no matrix voids and perfect bonding between fiber and matrix. This ultimate longitudinal tensile strength can be used to make some important comparisons of the Ultem-type interphase/PEEK matrix composites. To discuss these comparisons properly, the micromechanics of load transfer around

a broken fiber are presented next.

Table XIV. Rule of mixture predictions for strength, ratios of measured strength to predicted strength by the rule of mixtures, and strength reduction factor.

Panel	V_f (%)	σ^{ROM} (MPa)	$\sigma^{measured}/\sigma^{ROM}$	σ^{ULT} (MPa)	S_T*
10 series[a]	64.8	1938 ± 143	1.018 ± 0.043	2461	1.25 ± 0.07
30 series[b]	59.0	1811 ± 65	0.966 ± 0.089	2245	1.28 ± 0.14
50 series[c]	67.1	1926 ± 115	1.004 ± 0.116	2547	1.35 ± 0.12
APC-2[d]	61.3	2035 ± 102	1.011 ± 0.031	2331	1.13 ± 0.06

a- Ultem-type TMA^+ polyimide interphase
b- Ultem-type NH_4^+ polyimide interphase
c- Ultem-type TPA^+ polyimide interphase
d- APC-2 prepreg from ICI
* defined in Eq. 4-15

All of the polyimide interphase/PEEK matrix composites were manufactured using the same aqueous suspension prepregging technique. Inherently, all of these composites should statistically have the same number of discontinuous fibers and the same concentration of fiber defects. Since the characteristics of the fibers are the same for all of the polyimide interphase/PEEK matrix composites, differences in composite performance can be attributed to load transfer by the interphase and matrix components. The differences in composite strength are a factor of how the matrix and interphase transfer the load in the presence of a defect or a broken fiber. It has been shown by Subramanian et al. [4] and Jayaraman et al. [42-44] that the local stress concentrations developed by fiber breaks ultimately result in composite tensile failure. The stress concentrations considered are significant on a micro-mechanical level and propagate damage through the composite.

The transfer of load in a composite becomes very important when there is a break in a fiber. The load must be taken by other fibers immediately surrounding the break in the failed fiber. The load can be transferred back to the broken fiber a certain axial distance from the failure location. This distance is called the critical fiber length or ineffective length [45]. The fiber behaves as though it is not damaged at distances greater than the ineffective length from the break.

When considering a single broken fiber in a composite and the load transfer to neighboring fibers, the case of a short ineffective length is contrasted with the case of a long ineffective length in Figure 4-27. It has been shown by Reifsnider [1], Madhukar and Drzal [3], and Monette et al. [46-47], among others, that a stronger interfacial shear strength will result in a shorter ineffective length for a given composite fiber/matrix system and a weaker interfacial shear strength will result in a longer ineffective length for a given fiber/matrix system. A composite with a short ineffective length is shown in Figure 4-27(a). As seen by the stress profiles, the load will be transferred to neighboring fibers at a high stress level, but the stress profile returns to a uniform loading level across the matrix a short axial distance along the fiber from the break. This stress concentration on neighboring fibers increases the probability of breaking the neighboring fiber at the loading point. Thus, the interfacial shear strength can be too large for optimum loading of the carbon fibers. The mode of failure for unidirectional composite coupons with this type of interfacial stress transfer, shown in Figure 4-27(c), is characterized by transverse cracks propagating through the composite with little or no fiber-matrix splitting. It is hypothesized by Subramanian et al. that the interphase behaves as an elastic material during load transfer and they describe this type of interfacial failure as “elastic”

[4]. Subramanian et al. maintains that interphase properties can be tailored such that an optimum balance between stress concentration and ineffective length will maximize longitudinal tensile strength [4].

A composite with a long ineffective length is shown in Figure 4-27(b). As seen by the stress profiles, the load will be transferred to neighboring fibers at a moderately high stress level, and the stress profile returns to a uniform loading level across the matrix a long axial distance along the fiber from the break. Although the stress concentrations on neighboring fibers have been relieved, a larger area of the neighboring fibers are subjected to a moderately greater stress which increases the probability of loading the neighboring fiber at point defect. In this case, the interfacial shear strength can be too weak for optimum loading of the carbon fibers. The mode of failure for unidirectional composite coupons with this type of interfacial stress transfer, shown in Figure 4-27(d), is characterized by fiber-matrix splitting along the length of the composite. It is the hypothesis of Subramanian and Reifsnider et al. that the interphase deforms inelastically during transfer of load and they describe this type of interfacial failure as “plastic” [4].

The sketch in Figure 4-27(e) shows the relative effect of different ineffective lengths on the stress transferred to neighboring fibers. The curve for the broken fiber with a small ineffective length shows a greater local stress on the neighboring fibers at z=0 on the x-axis. At increasing distances along the fiber length the stress decreases rapidly up to z=Lc(1) which represents this system’s ineffective length. At distances greater than the ineffective length the neighboring fibers are subjected to the average stress level applied to all fibers in the composite. The curve for the broken fiber with the large ineffective length shows a smaller local stress on the neighboring fibers at z=0 on the x-axis. This stress decreases more gradually at distances

along the fiber length up to z=Lc(2) which represents this system's ineffective length. At distances greater than the ineffective length the neighboring fibers are subjected to the average stress level applied to all fibers in the composite.

All of the PEEK matrix composites displayed the same mixed-mode of failure during longitudinal tension testing. The coupons shattered into many, long, thin pieces at failure. The failure was "explosive", resulting in significant fiber-matrix splitting, however, each thin, broken piece had ends resembling transverse cracking type failure. Only a small portion of the composite coupon which was bonded to the tabbing material remained in the grips. Since all coupons failed with the same mixed-mode, it is assumed that the strengths can be compared with the use of a strength reduction factor, S_T, defined as the ratio of σ^{ULT} to the measured composite strength.

$$S_T = \frac{\sigma^{ULT}}{\sigma^{experimental}} \qquad \text{Eq. 4-15}$$

The strength reduction factors tabulated in Table 4-XIV are used to rank the level of the micro-mechanical stress concentrations in the polyimide interphase/PEEK matrix composites. It is important to note that since σ^{ULT} was calculated for each individual composite and respective fiber volume fraction, S_T will not be dependent upon fiber volume fraction. The values for S_T are close for all the polyimide interphase composites, so an appropriate statistical comparison of the data sets is important. The unpaired *t*-test executed with SigmaStat Statistical Software v. 2.0, as described earlier, was used with a 95% confidence interval. The *t*-test results for comparison of the S_T values from each data set are shown in Table 4-XV.

Among the polyimide interphase/PEEK matrix composites, the 10 series composite has the lowest S_T. The unpaired *t*-test results show that the S_T for the 10 series composites is not statistically different from the S_T for the 30 series composites. The 10 series composite has a lower ISS than the 30 series composite as concluded from transverse flexure strength results. The 10 series composite also reduces the stress concentrations at the circular notch more effectively than the 30 series composite for the R=0.1 notched fatigue testing of the crossply composites. It would follow that the 10 series composite reduces the local micro-mechanical stress concentrations caused by broken fibers most effectively in the longitudinal tension testing. The greater longitudinal tensile strength and greater longitudinal tensile strain-to-failure of the 10 series composite could be explained by the reduction of micro-mechanical stress concentrations from broken fibers. The fact that the S_T is not statistically different for the 10 series and 30 series composites indicates that the S_T is not a useful indicator of the micro-mechanical stress concentrations of the Ultem-type polyimide/PEEK composites. The merit of the S_T however, will be shown in the next section as well as in Chapter 7.

The 30 series and the 50 series composites have an S_T that is not statistically different from one another. This is expected since the approximated ISS of the two composites was shown to be statistically equivalent from the transverse flexure strength results.

Table 4-XV. Unpaired *t*-test results comparing each set of PEEK matrix composite strength reduction factor data.

	S_T
10 series[a] vs. 30 series[b]	fail
10 series[a] vs. 50 series[c]	pass
30 series[b] vs. 50 series[c]	fail
10 series[a] vs. APC-2[d]	pass
30 series[b] vs. APC-2[d]	pass
50 series[c] vs. APC-2[d]	pass

a- Ultem-type TMA^+ polyimide interphase
b- Ultem-type NH_4^+ polyimide interphase
c- Ultem-type TPA^+ polyimide interphase
d- APC-2 prepreg from ICI

The APC-2 composite prepreg was manufactured using a technique other than aqueous suspension prepregging, therefore caution must be exercised when comparing this composite to the polyimide interphase/PEEK composites. It is possible that the APC-2 composite had a lower number of initial discontinuous fibers in the composite, therefore the number of initial locations for micromechanical stress concentrations would also be fewer. Also, although the APC-2 prepreg was made with AS-4 fiber, it was not from the same lot number that was consistently used for all the polyimide interphase PEEK matrix composites. Therefore, the fiber properties themselves could have been different such as fiber tensile strength and modulus.

Development of the Rule of Mixtures for Composite Strength

The "rule of mixtures" model of Eq. 4-13 can be developed further. Since the strain in the model is assumed to be the same for the composite, the fibers and the matrix, Eq. 4-13 can

be differentiated with respect to a single strain, ϵ.

$$\frac{d\sigma_c}{d\epsilon} = \frac{d\sigma_f}{d\epsilon} \cdot V_f + \frac{d\sigma_m}{d\epsilon} \cdot V_m \qquad \text{Eq. 4-16}$$

The differentials in Eq. 4-16 each represent a slope of the stress-strain response curve at a specific strain. If the stress-strain response curves of the composite, fibers and matrix are linear within the strains of interest, the differentials are constants represented by the elastic moduli.

$$E_c = V_f \cdot E_f + V_m \cdot E_m \qquad \text{Eq. 4-17}$$

E_c = composite modulus
V_f = fiber volume fraction
E_f = fiber modulus
E_m = matrix modulus

Eq. 4-17 indicates that the contributions to the composite modulus of the fibers and the matrix are proportional to their volume fractions. Once again this relationship is called a rule of mixtures and E_c from Eq. 4-17 can be referred to as E^{ROM} [38].

Table 4-XVI. shows the composite fiber volume fractions, rule of mixture predictions for modulus, and the ratio of measured modulus to predicted modulus by the rule of mixtures. The rule of mixture predictions were calculated using the PEEK tensile modulus from Jar, 3.6 GPa [36], and the fiber tensile modulus from a Hercules AS-4 product data sheet, 234 GPa [23]. As seen in Table 4-XVI, the ratio of measured modulus to predicted modulus by the rule of mixtures is very similar for all the composites. This demonstrates that when differences in fiber volume fraction are normalized, all the composites have very similar moduli.

Table 4-XVI. Longitudinal tensile modulus, rule of mixture predictions for modulus and ratios of measured modulus to predicted modulus by the rule of mixtures.

Panel	V_f (%)	tensile modulus (GPa)	E^{ROM} (GPa)	$E^{measured}/E^{ROM}$
Q102[a]	64.8	146.1 ± 2.7	153.0	0.96 ± 0.02
Q302[b]	59.0	132.6 ± 6.6	139.6	0.95 ± 0.05
Q502[c]	67.1	154.1 ± 16.8	158.3	0.95 ± 0.11
A02[d]	61.3	140.0 ± 5.5	144.9	0.97 ± 0.04

a- Ultem-type TMA^+ polyimide interphase
b- Ultem-type NH_4^+ polyimide interphase
c- Ultem-type TPA^+ polyimide interphase
d- APC-2 prepreg from ICI

Figure 4-28 shows the composite tensile moduli compared to predictions from the rule of mixtures. The ratios of measured tensile moduli to the predicted moduli by the rule of mixtures are labeled in Figure 4-28.

The E^{ROM} values predicted by Eq. 4-17 show very good agreement with the experimental values of modulus, indicating that the composites are modeled well by the assumptions made for the rule of mixtures model. Specifically, the composite has fibers that are continuous, uniform in properties and aligned parallel. Good bonding exists between the fibers and matrix so that no slippage occurs at the fiber-matrix interface and each component can be considered to have a linear elastic response.

Longitudinal Tension (repeated loading scheme)

The results from the unidirectional tension testing done by H. DeSmidt are shown in Table 4-XVII. The P106 and P107 composite panels are the 10 series composites and the P306 and P307 composite panels are the 30 series composites. The data from each individual panel

are shown independently.

The tensile test results shown in Table 4-XVII show the trend that the 30 series composites have a higher strength and a higher strain to failure than the 10 series composites. This is contradictory to the tensile test results from work done by the author and B. Walther.

Due to the repeated loading testing scheme, as shown in Figure 4-10, the results shown in Table 4-XVII cannot be strictly considered tensile data. The composite specimens were loaded quasi-statically three times to a level of 2224 N at a rate of 142 N/s. Then the samples were loaded to failure at a rate of 356 N/s. The three loadings to 2224 N can be considered three cycles of fatigue to a stress level of about 20% of the ultimate tensile strength for the 10 series

Table 4-XVII. Tensile test results with a repeated loading scheme for Ultem-type polyimide interphase/PEEK composites.

Panel	V_f (%)	repeated loading tensile strength (MPa)	tensile modulus (GPa)	failure strain (%)
P106[a]	68.8	1330 ± 160	140.3 ± 9.7	1.00 ± 0.15
P107[a]	72.1	1240 ± 95	127.5 ± 4.8	0.99 ± 0.10
P306[b]	73.2	1710 ± 213	138.6 ± 9.6	1.18 ± 0.17
P307[b]	70.0	1920 ± 170	144.4 ± 4.1	1.26 ± 0.08

a- Ultem-type TMA^+ polyimide interphase b- Ultem-type NH_4^+ polyimide interphase

and 30 series composites. The ultimate tensile strengths used are the tensile strengths for the 10 series and 30 series composites from the single loading unidirectional tension test results.

Rosen et al. developed a model for a unidirectional composite under tensile loading

which showed that fiber breakage begins to occur at 40% of the ultimate tensile load [45]. It is noted from Rosen's study that the interfaces of broken fibers may become debonded because of stress concentrations created at the fiber ends and thus may contribute to the separation of the composite at a given cross section. If there are discontinuous fiber ends inherent in the composite due to the manufacturing process, then these fiber ends could be susceptible to the stress concentrations thereby causing fiber-matrix debonding at the locations of stress concentrations. From Rosen's findings, it is assumed that any damage that was created during the first three cycles of tensile loading is not characterized by fiber breakage.

Applying the stress concentrated dominated micro-mechanics discussed earlier provides an interpretation to the repeated loading tension test results. It has been demonstrated that the 10 series composites have the weakest ISS and greatest tendency for fiber-matrix debonding under a tensile load. For these reasons the 10 series composite interphase was described earlier as a "slip" interphase as compared to the 30 series composite interphase. During the first three cycles of tensile loading, it is possible that due to a lower ISS extensive fiber-matrix debonding occurred, damaging the composite significantly. After the three loading cycles to 2224 N, the composite was loaded to failure. The loads greater than 2224 N would result in further damage from fiber-matrix debonding and the overall strength of the composite would be reduced. This is consistent with the notched fatigue data.

The R=0.1 notched fatigue results showed that the 10 series composite had the greatest longitudinal split growth rate under tensile load. The growth of longitudinal splits resulted in an increase in residual strength for the notched, cross-ply panels. The circular notch provides a large stress concentration which must be relieved to increase the residual strength. The relief of

this stress concentration is accomplished by longitudinal splitting which is enhanced with a low ISS. The cross-ply stacking sequence provides a transverse stability which will limit the longitudinal split damage from tearing the composite completely along its length. This same trend is **not** expected for an unnotched, unidirectional composite. If sufficient fiber-matrix debonding occurs the unidirectional composite will fail as a result of splitting along its length as discussed previously and shown by the diagram in Figure 4-27(d).

Further comparison of the composites from the repeated loading unidirectional tension testing is done by calculating a rule of mixtures strength and an ultimate composite strength from Eq. 4-13, and a strength reduction factor, S_T, from Eq. 4-15. These calculated values are shown in Table 4-XVIII.

Table 4-XVIII. Rule of mixture predictions for strength, ratios of experimental strength to rule of mixture predictions, calculated composite ultimate strength and strength reduction factor.

Panel	V_f (%)	σ^{ROM}* (MPa)	$\sigma^{measured}/\sigma^{ROM}$	σ^{ult}**	S_T***
P106[a]	68.8	1626	0.82	2617	1.97
P107[a]	72.1	1678	0.74	2729	2.20
P306[b]	73.2	2027	0.84	2766	1.62
P307[b]	70.0	2077	0.92	2655	1.38

a- Ultem-type TMA^+ polyimide interphase b- Ultem-type NH_4^+ polyimide interphase
*- from Eq. 4-13 using experimental ϵ from Table 4-XVII.
**- from Eq. 4-13 using theoretical ϵ of 1.61%.
***-from Eq. 4-15.

The ratio of measured strength to predicted strength by the rule of mixtures is 0.82 and 0.74 for the P106 and P107 composites, respectively. The ratio of measured strength to predicted

strength by the rule of mixtures is 0.84 and 0.92 for the P306 and P307 composites, respectively. While this ratio for the P307 composite is high, it is not as great as the value for the 30 series composite from the single loading longitudinal tension test results, which was 0.97. This shows that there is not good agreement between predicted and measured strengths for both composites and indicates that the composites are not modeled well by the assumptions made for the rule of mixtures model. This is contradictory to the results from the single loading longitudinal tension test results and is an indication that the composites were damaged during the first three cycles of tensile loading.

The strain-to-failure for the P106 and P107 composites were much lower than the strain-to-failure of the 10 series composite single loading longitudinal tension testing. The strain-to-failure for the 10 series composite from the single loading longitudinal tension testing was 1.27 ± 0.09%. This is another indication that the 10 series composites were damaged during the first three cycles of tensile loading. The strain-to-failure for the P306 and P307 composites were closer to the strain-to-failure of the 30 series composite single loading longitudinal tension testing. The strain-to-failure for the 30 series composite from the single loading longitudinal tension testing was 1.30 ± 0.05%. This indicates that the 10 series composites were damaged more than the 30 series composites during the first three cycles of tensile loading.

Photographs of the failure modes are shown in Figure 4-29. Macroscopically, the P106 specimens failed in a longitudinal direction, splitting the coupon along the fibers, while the P307 specimens failed in a transverse direction, breaking the coupon in the middle. Both the P107 and P306 specimens failed more in a longitudinal direction, splitting the coupons along the fiber direction. An important difference, however, was that the specimens in the P107 group were

much more frayed and broom-like; more like the P106 than the P307 composite specimens. The P306 specimens were not as frayed, and although they failed in the longitudinal direction, there was less damage area, since there were fewer splits by comparison with the P107 group. These failure modes are very important in demonstrating the different mechanics of failure. Considering the trend that the ISS for the 10 series composites is lower than the ISS for the 30 series composite, the failure modes are consistent with stress concentration dominated micromechanics.

Conclusions

The interphase thickness was estimated to have an upper bound of 200 nm for a 5 wt% interphase/95% matrix component system based on a hexagonally packed array of cylindrical fibers with a diameter of 8 mm and a fiber volume fraction of 60%. This upper bound was based on assumptions that all of the interphase polymer is distributed evenly around each of the fibers and that no interdiffusion of the pure phases occurs.

A series of PEEK matrix Ultem-type polyimide interphase composites of high quality were fabricated using the aqueous suspension prepregging technique. The void volume content was measured to be no greater than 0.99% for any of the unidirectional composites.

Interactions between the Ultem-type polyimide and the fiber surface were probed with X-ray photoelectron spectroscopy (XPS) with sized and sized, then solvent washed fiber samples. The results showed possible interactions between the Ultem-type NH_4^+ polyimide and the fiber surface. It is possible that the interactions were due to hydrogen bonds or covalent bonds

between the free amine functionalities of the Ultem-type NH_4^+ polyimide and oxygen containing species on the fiber surface. However, it is also possible that the Ultem-type NH_4^+ polyimide formed a uniform coating around the fibers which then crosslinked to form an insoluble sheath. The Ultem-type TMA^+ polyimide and the Ultem-type TPA^+ polyimide did not show any interactions with the fiber surface by XPS of the sized and the sized, then washed fibers indicating that the level of adhesion for the Ultem-type NH_4^+ polyimide and the carbon fiber surface was greatest.

Iosipescu shear testing was not shown to be sensitive to the changes of composite interphase for the Ultem-type NH_4^+ polyimide interphase and the Ultem-type TMA^+ polyimide interphase. The experimentally measured shear moduli of the polyimide interphase/PEEK matrix composites from this chapter and from Gonzalez [12] were modeled well by the Halpin-Tsai model for estimating shear moduli.

A direct correlation was shown for transverse flexure strength and interfacial shear strength using data from Chang et al. [5] and Madhukar and Drzal [3]. As the interfacial shear strength increases, the transverse flexure strength increases. This relationship was used to rank the relative level of interfacial shear strengths for the Ultem-type polyimide/PEEK matrix composites. Using this correlation the trends showed that the interfacial shear strength of the 10 series Ultem-type TMA^+ polyimide interphase composite was lowest and the 30 series Ultem-type NH_4^+ polyimide interphase composite and the 50 series Ultem-type TPA^+ polyimide interphase composite were greater and comparable. Examination of the transverse flexure failure surfaces by VC-XPS provided a quantitative measurement showing that the failure for all Ultem-type polyimide interphase composites was mostly cohesive to fully cohesive in nature.

The notched fatigue experiments using R=1.0 were shown to be insensitive to the interphase differences for the Ultem-type NH_4^+ polyimide composites and the Ultem-type TMA+ polyimide composites.

The notched fatigue results from experiments using R=0.1 showed a strong sensitivity to interphase differences for the 10 series, 30 series and 50 series composites. The 10 series composites had the highest quasi-static ultimate tensile strengths (UTS) of the crossply panels amounting to a 35% increase in UTS over the 30 series composites and a 25% increase in UTS over the 50 series composites. The split lengths measured as a function of loading cycles were used to study the relief of the stress concentrations caused by the circular notch. The split growth rate was found by taking the derivative of a second order polynomial fit to the split length vs. loading cycle data. The 10 series composite showed the most rapid longitudinal split growth rate and the 30 series composite showed the slowest longitudinal split growth rate at both 80% UTS and 87.5% UTS. The 50 series composite had an intermediate split growth rate. The trends of split growth rate were shown to be consistent with the ranking of ISS from the transverse flexure strength results. As the relative ISS estimated from transverse flexure strength increased the initial split growth rate decreased.

The longitudinal tensile strength of the 10 series composite was 12% greater than the longitudinal tensile strength of the 30 series composite and 8% greater than the 50 series composite. A plot of normalized transverse flexure strength vs. longitudinal tensile strength showed qualitative agreement to the hypothesis proposed by Subramanian et al. [4]. The estimates of composite strength using the rule of mixtures showed very good agreement to the experimental data indicating that the assumptions for the rule of mixtures were applicable to the

Ultem-type polyimide interphase/PEEK matrix composites, specifically, the composite has fibers that are continuous, aligned parallel and uniform in properties, good bonding exists between the fibers and matrix and each component has a linear elastic response. The estimates of composite modulus from the rule of mixtures also showed good agreement to the experimental data.

The repeated loading scheme for longitudinal tensile testing was shown to yield different results than the single loading longitudinal tensile test. It was demonstrated that damage occurred in the Ultem-type polyimide interphase/PEEK matrix composites during the three initial loadings.

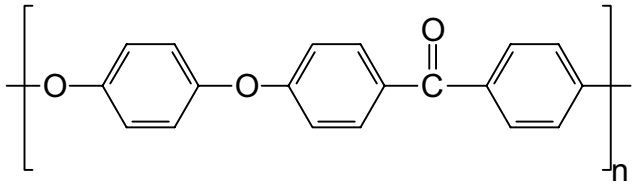

Figure 4-1. Chemical structure of polyether ether ketone.

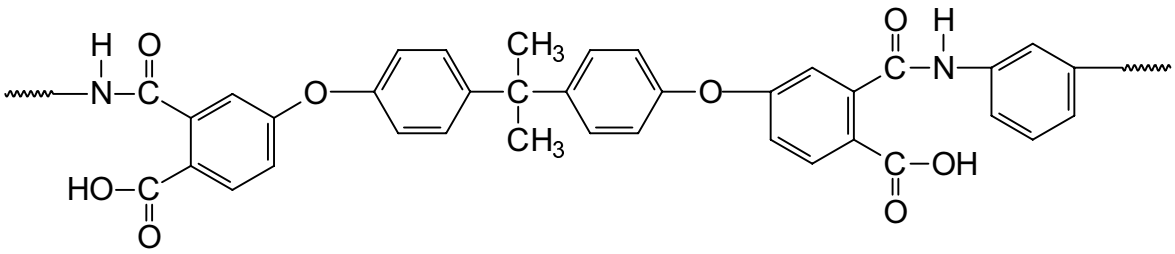

Figure 4-2. Chemical structure of Ultem-type polyamic acid.

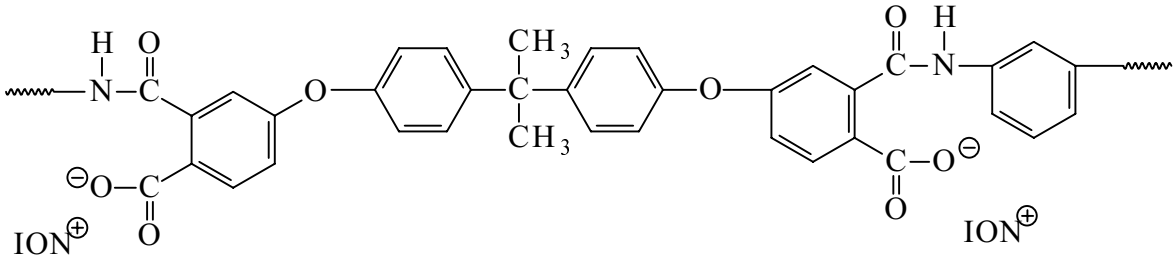

Ultem-type Polyamic Acid made water soluble by addition of basic counterion

Thermal Imidization

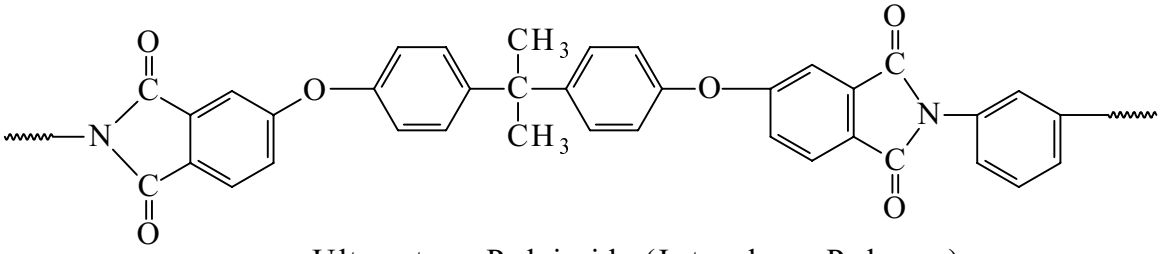

Ultem-type Polyimide (Interphase Polymer)

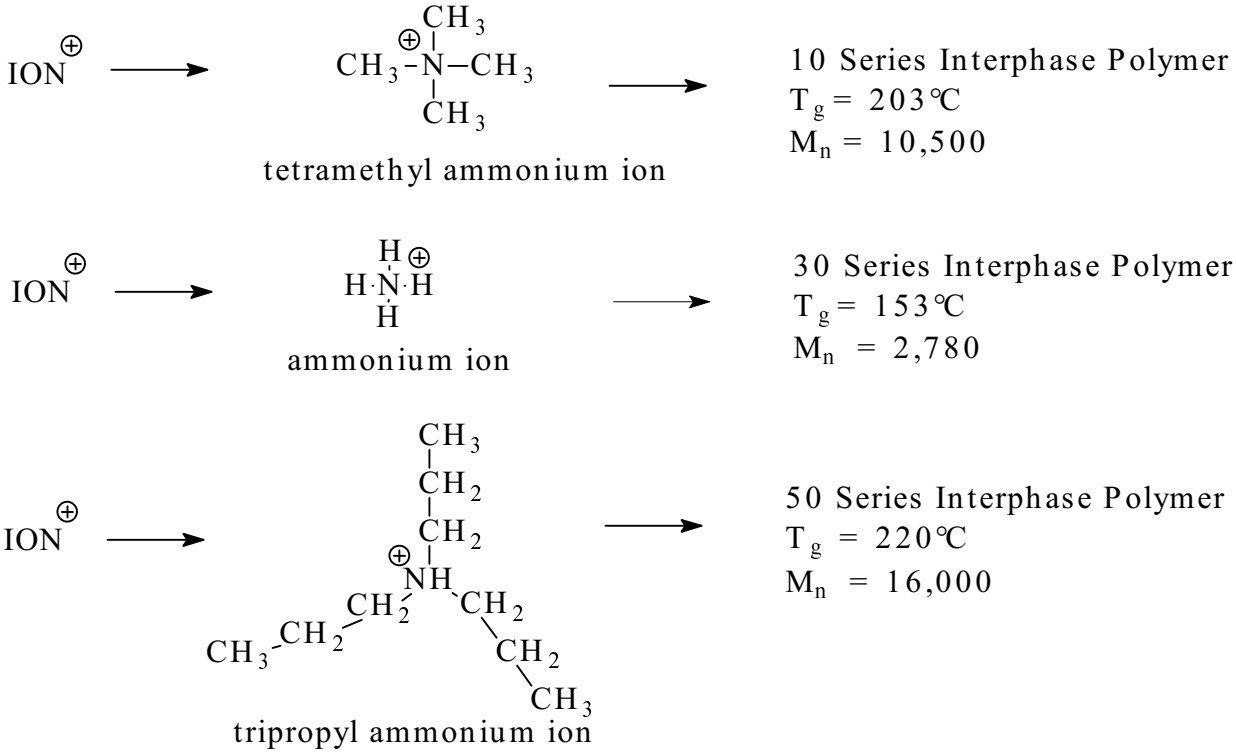

Figure 4-3. Formation of Ultem-type polyamic acid salts using different bases and the glass transition temperatures and number average molecular weight for the polyimide.

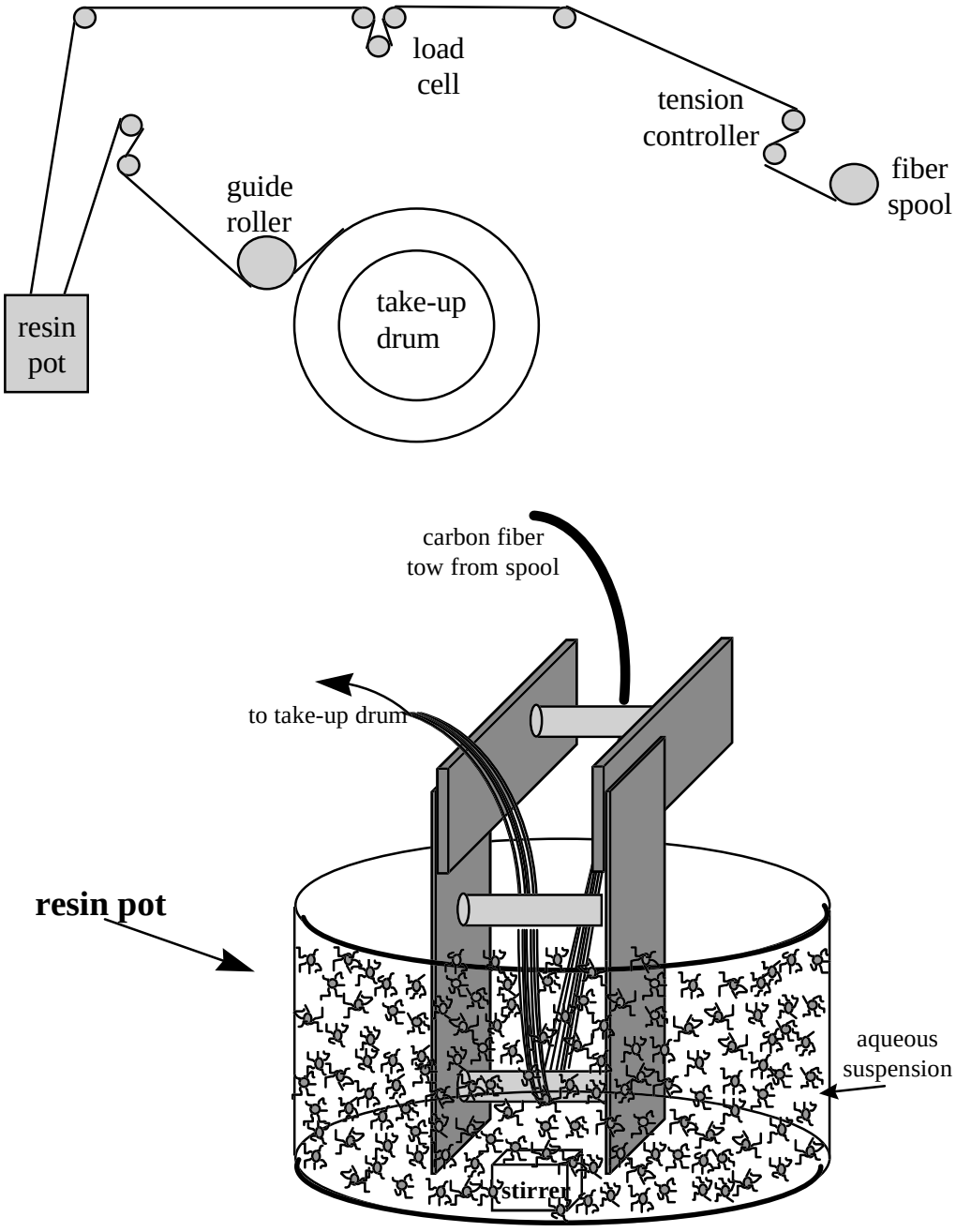

Figure 4-4. Schematic drawing of modified Research Tool Corporation Model 30 Drumwinder Prepregger with an enlarged view of the resin pot used for aqueous suspension prepregging.

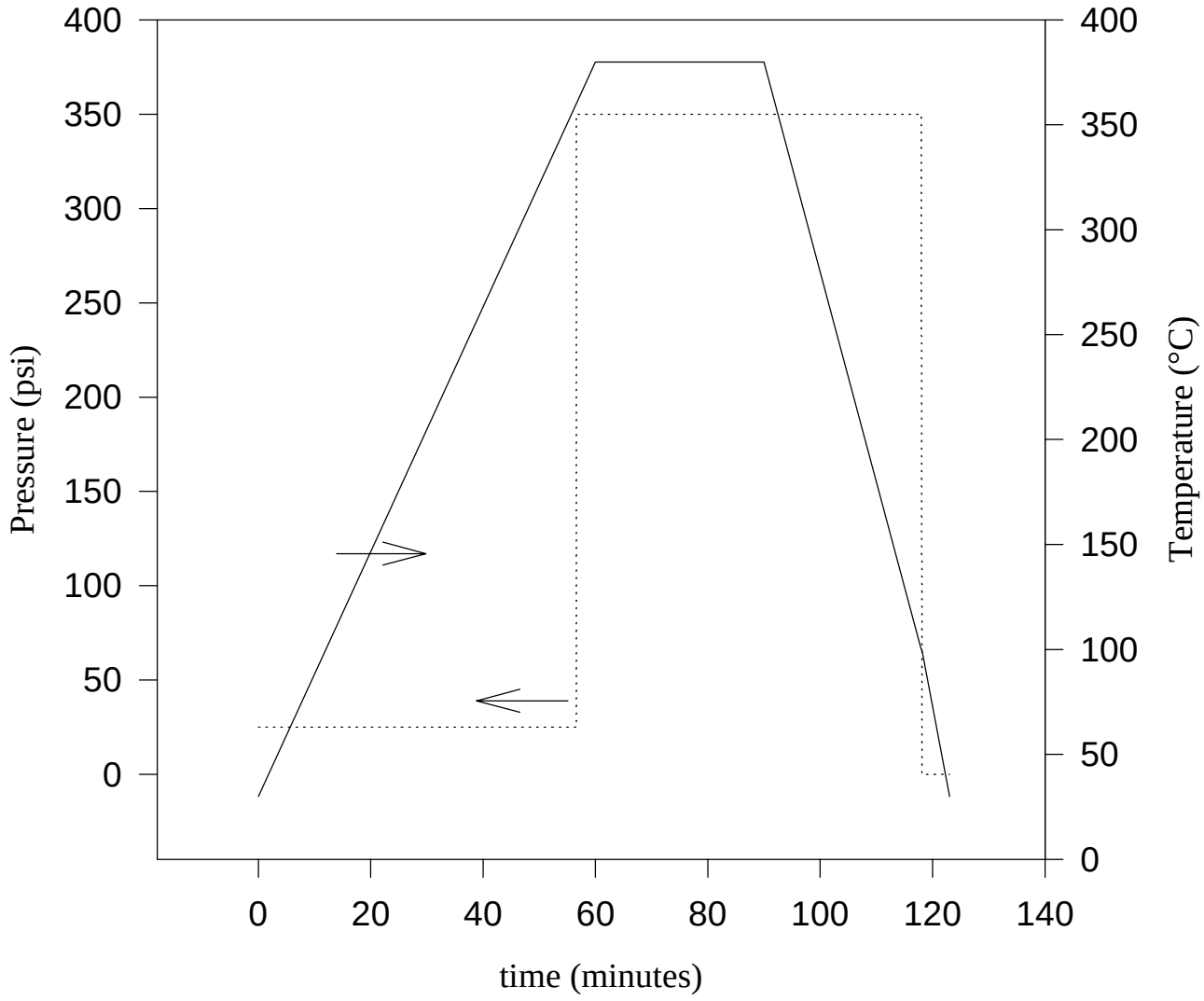

Figure 4-5. Temperature and pressure schedule for consolidation of PEEK matrix composites.

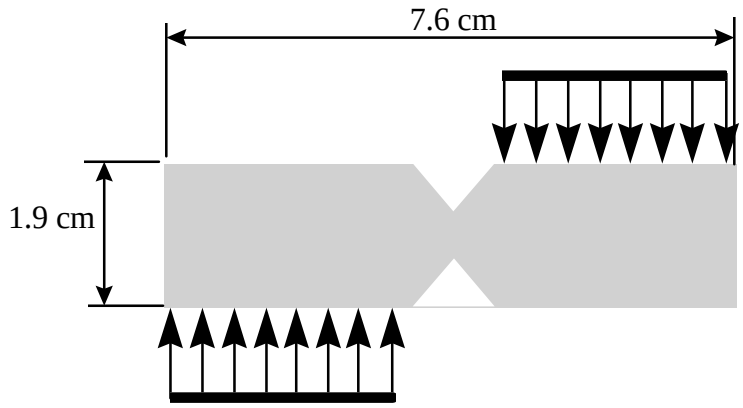

Figure 4-6. Iosipescu shear loading geometry.

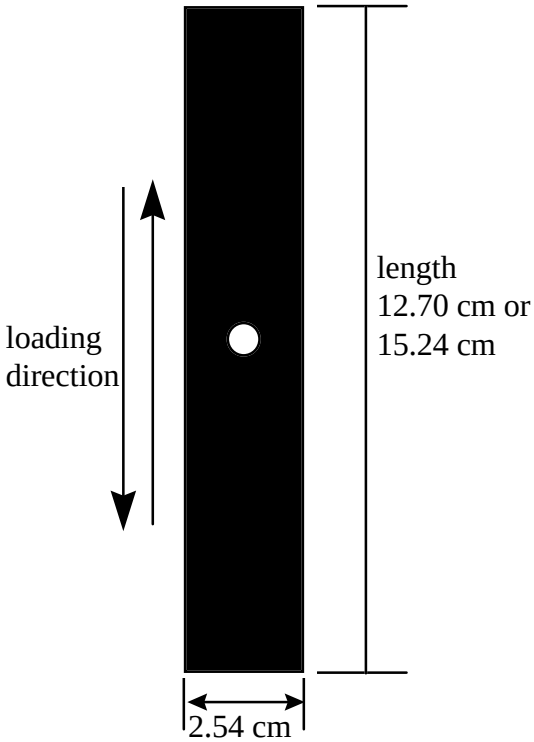

Figure 4-7. Notched fatigue specimen loading geometry for R=1.0 and R=0.1 notched fatigue experiments.

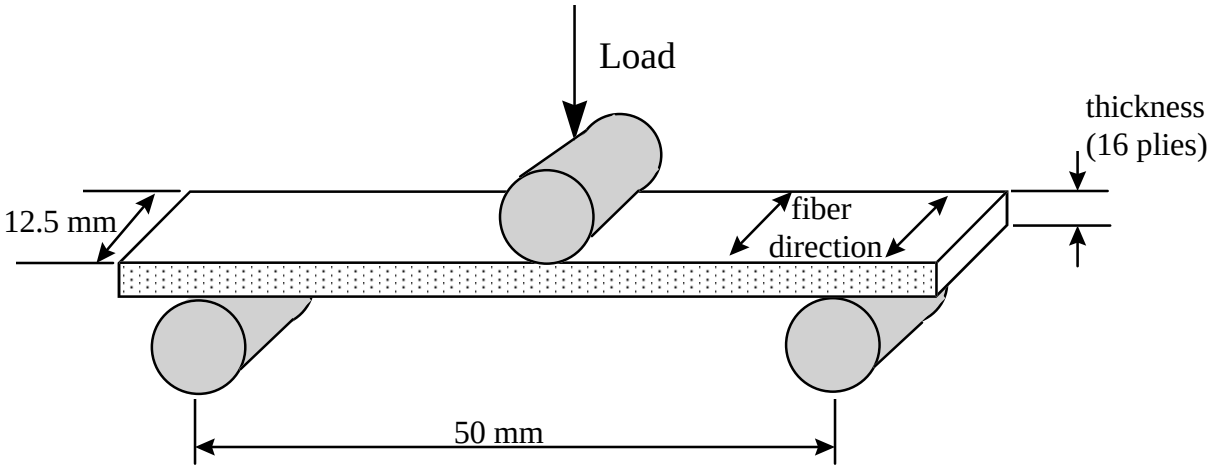

Figure 4-8. Transverse flexure specimen loading geometry.

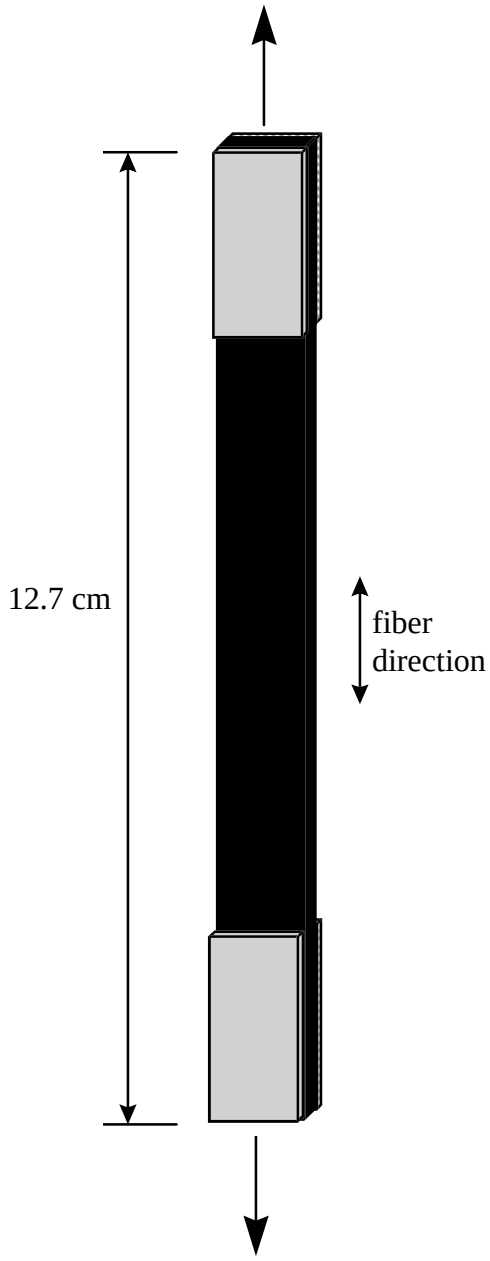

Figure 4-9. Unidirectional tension test geometry.

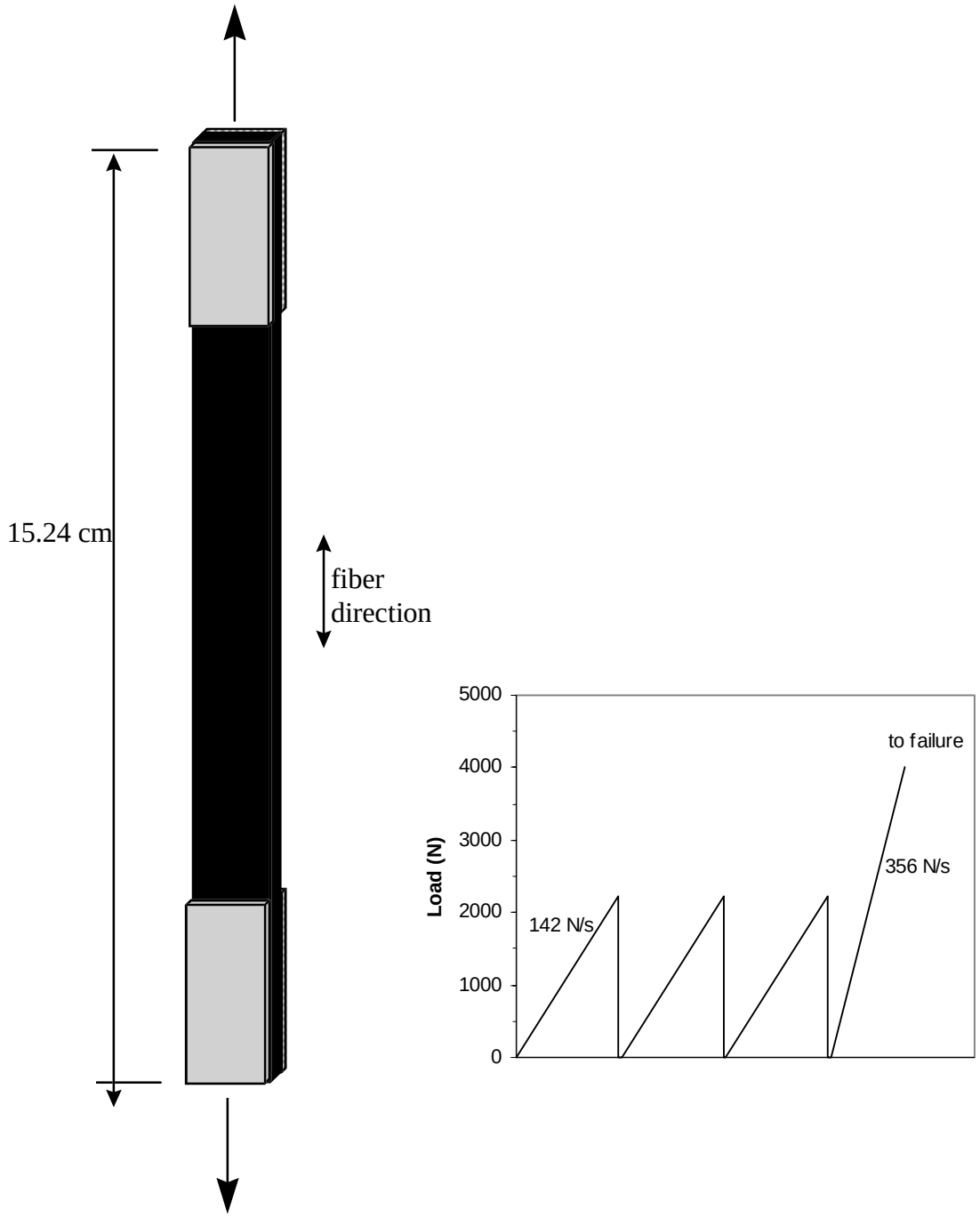

Figure 4-10. Repeated loading scheme unidirectional tension test geometry and loading scheme.

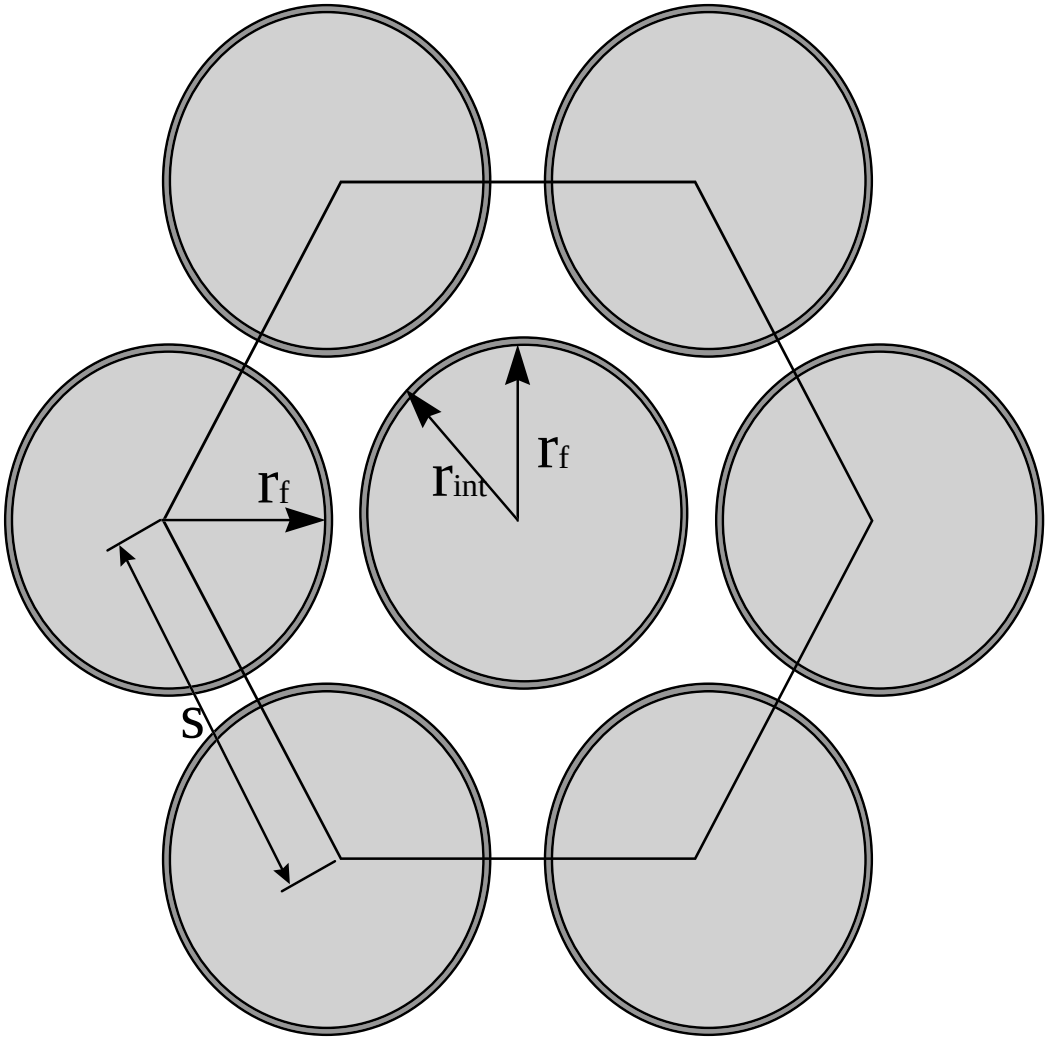

Figure 4-11. Diagram of fibers with interphase layer in a hexagonal packing for calculation of estimated interphase thickness.

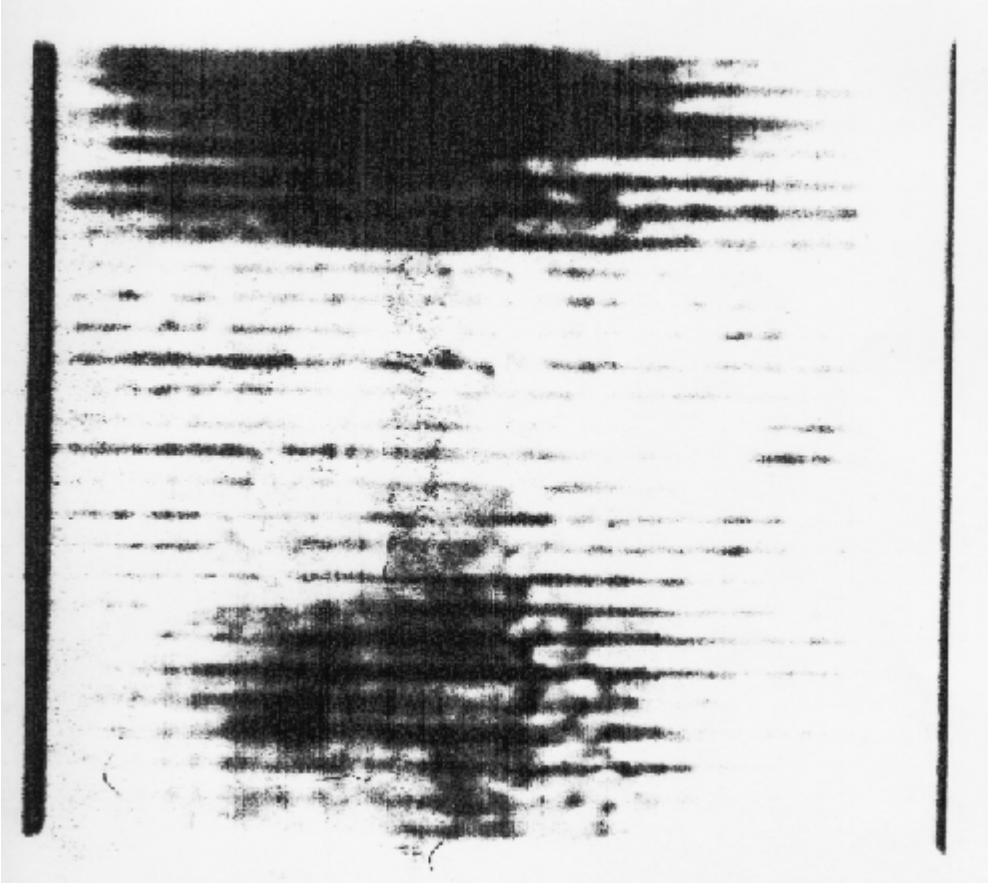

Figure 4-12(a). C-Scan image of panel P307 which is representative of “poor” consolidation.

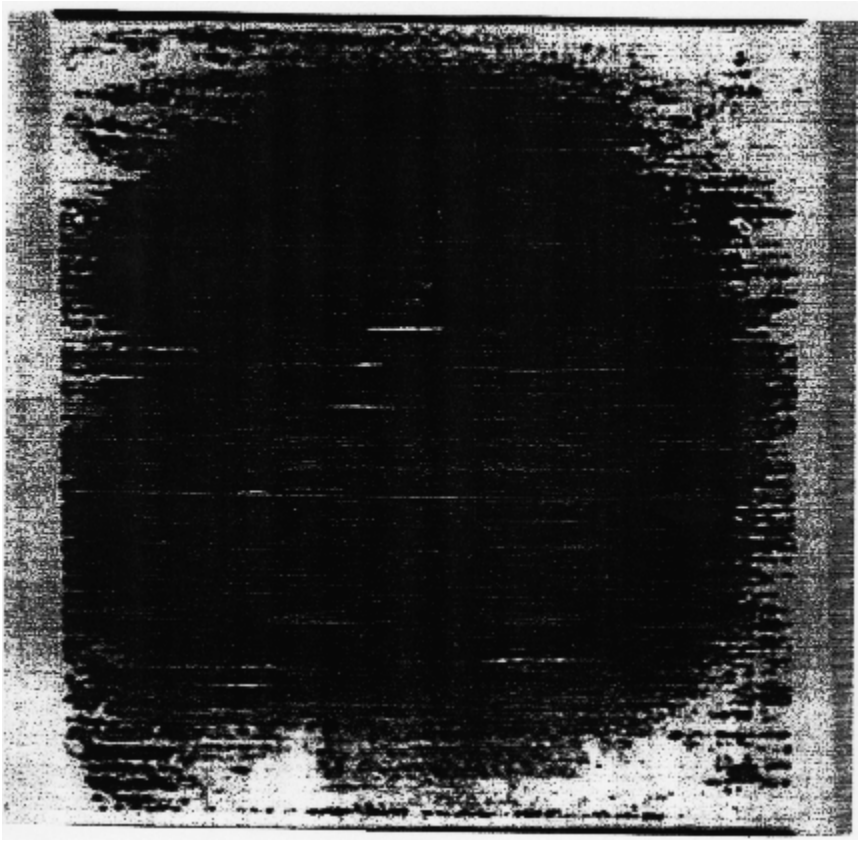

Figure 4-12(b). C-Scan image of panel P105 which is representative of “fair” consolidation.

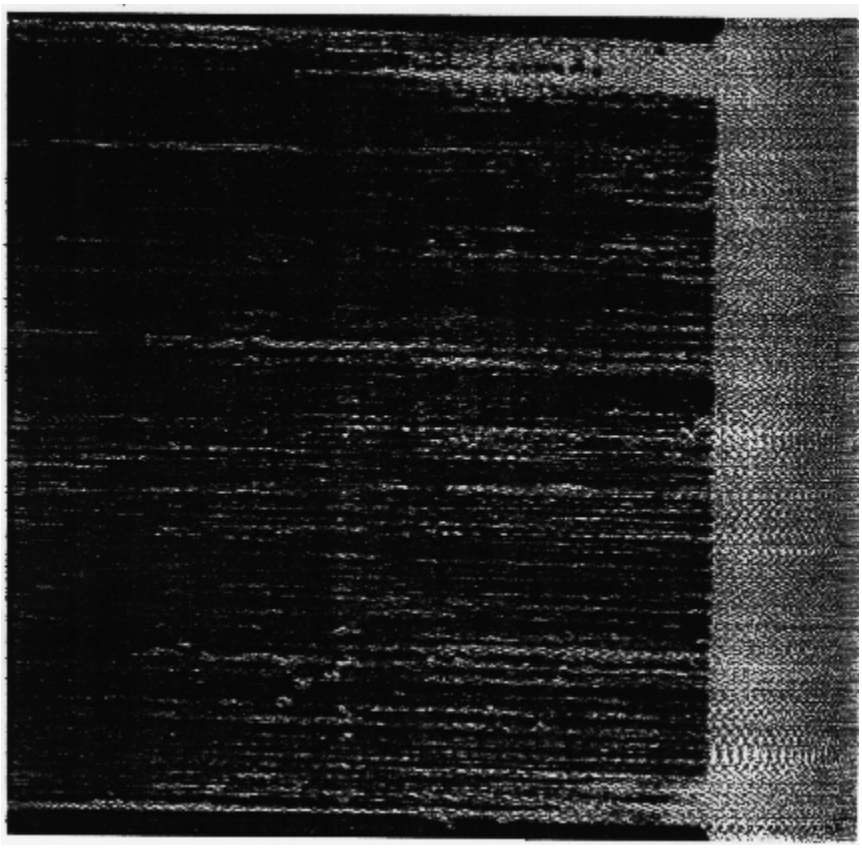

Figure 4-12(c). C-Scan image of panel Q502 which is representative of “good” consolidation.

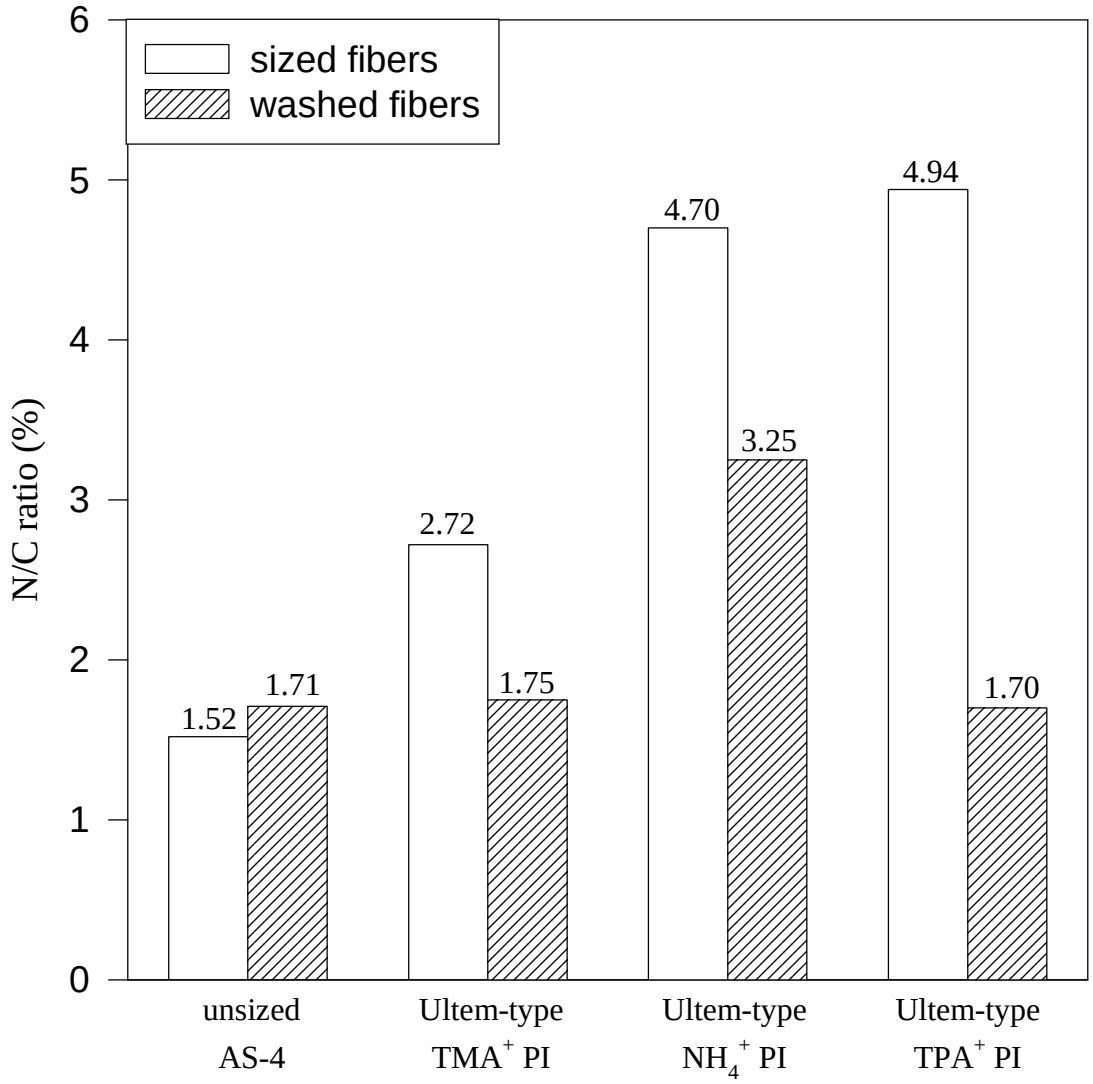

Figure 4-13. N/C ratios of atomic concentration on fiber surfaces.

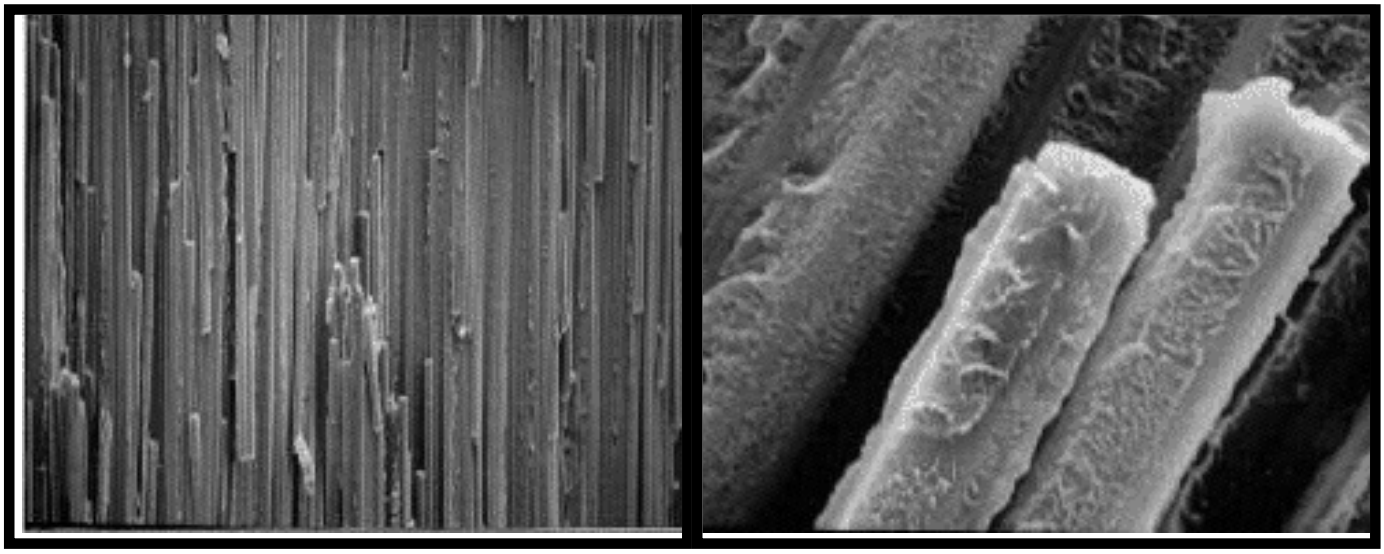

(a.) (b.)

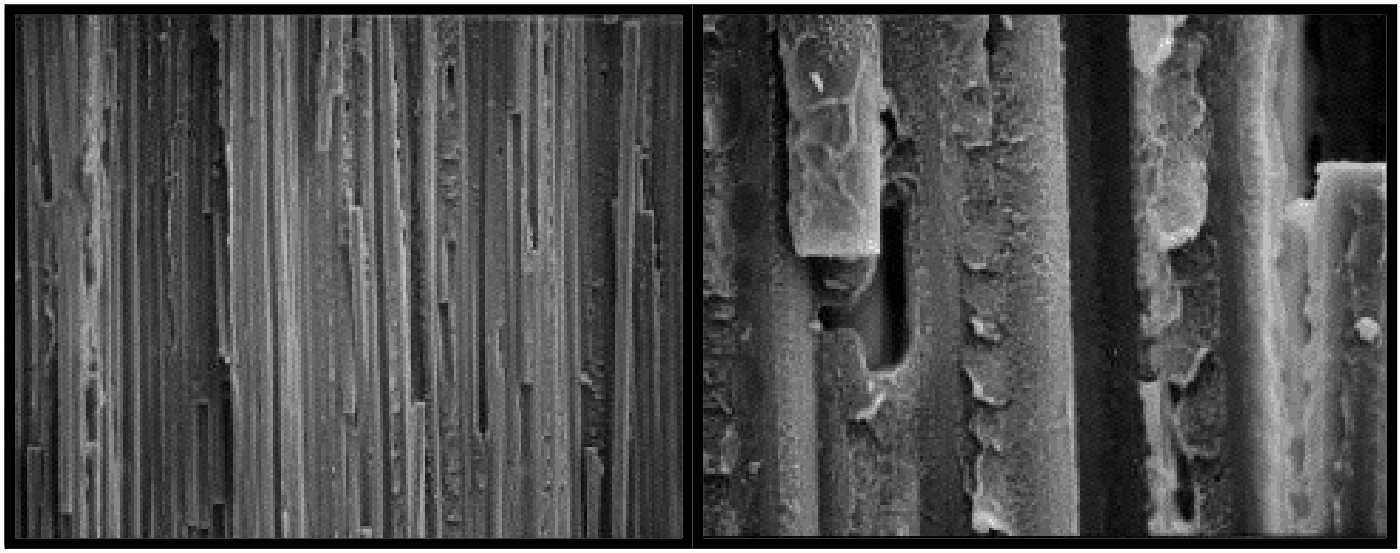

(c.) (d.)

Figure 4-14. Iosipescu 90° shear failure surfaces for (a.) 10 series composite at 500x, (b.) 10 series at 2500x, (c.) 30 series at 500x, and (d.) 30 series at 2500x.

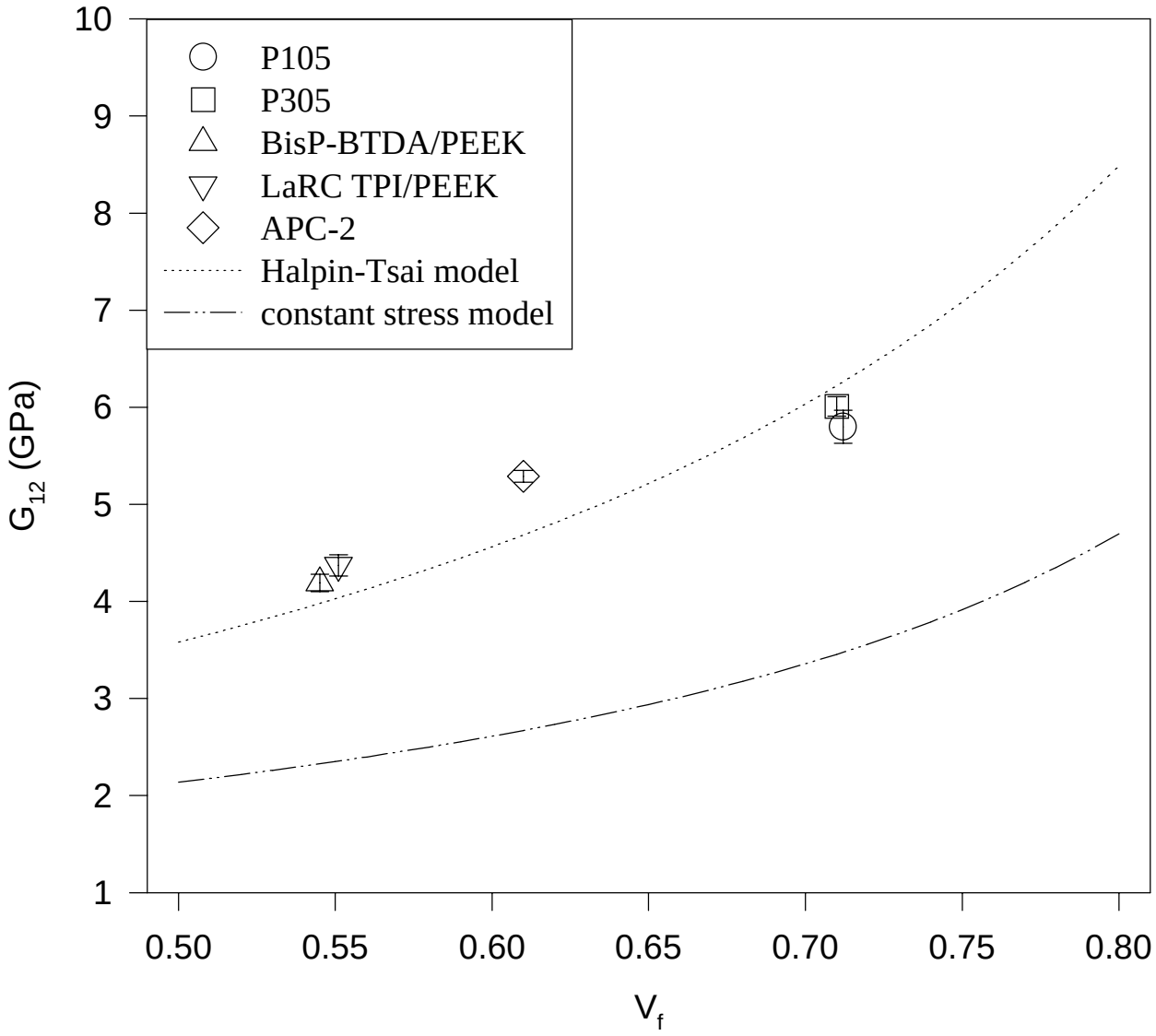

Figure 4-15. Iosipescu shear modulus from (90°) shear testing and calculated shear moduli from constant stress model (Eq. 4-2) and Halpin-Tsai model (Eq. 4-4).

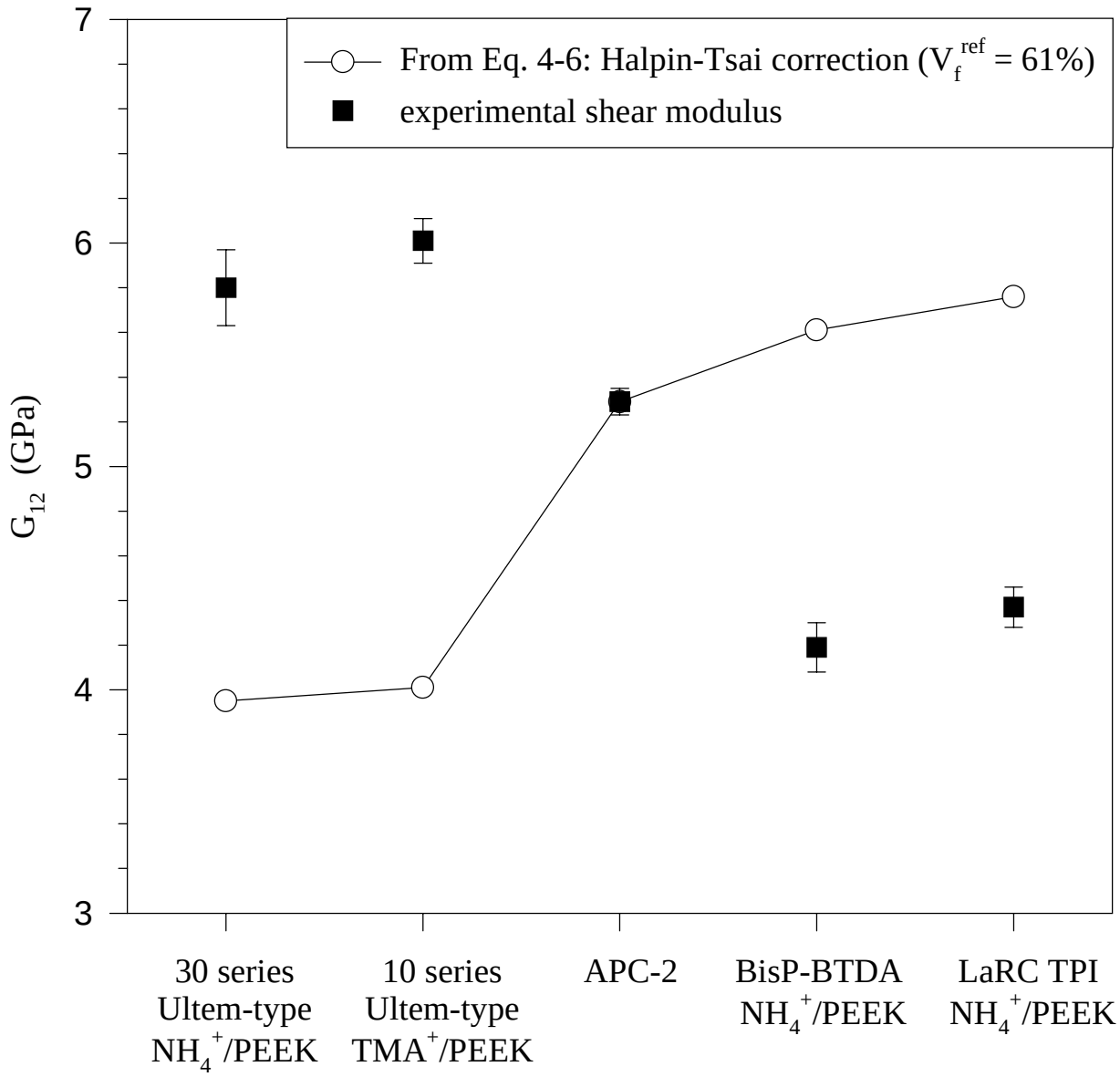

Figure 4-16. Shear modulus corrected to a fiber volume fraction of 61% using Eq. 4-6 and data from Iosipescu shear testing of PEEK matrix composites including BisP-BTDA NH_4^+/PEEK and LaRC TPI NH_4^+/PEEK composites from Gonzalez [12]

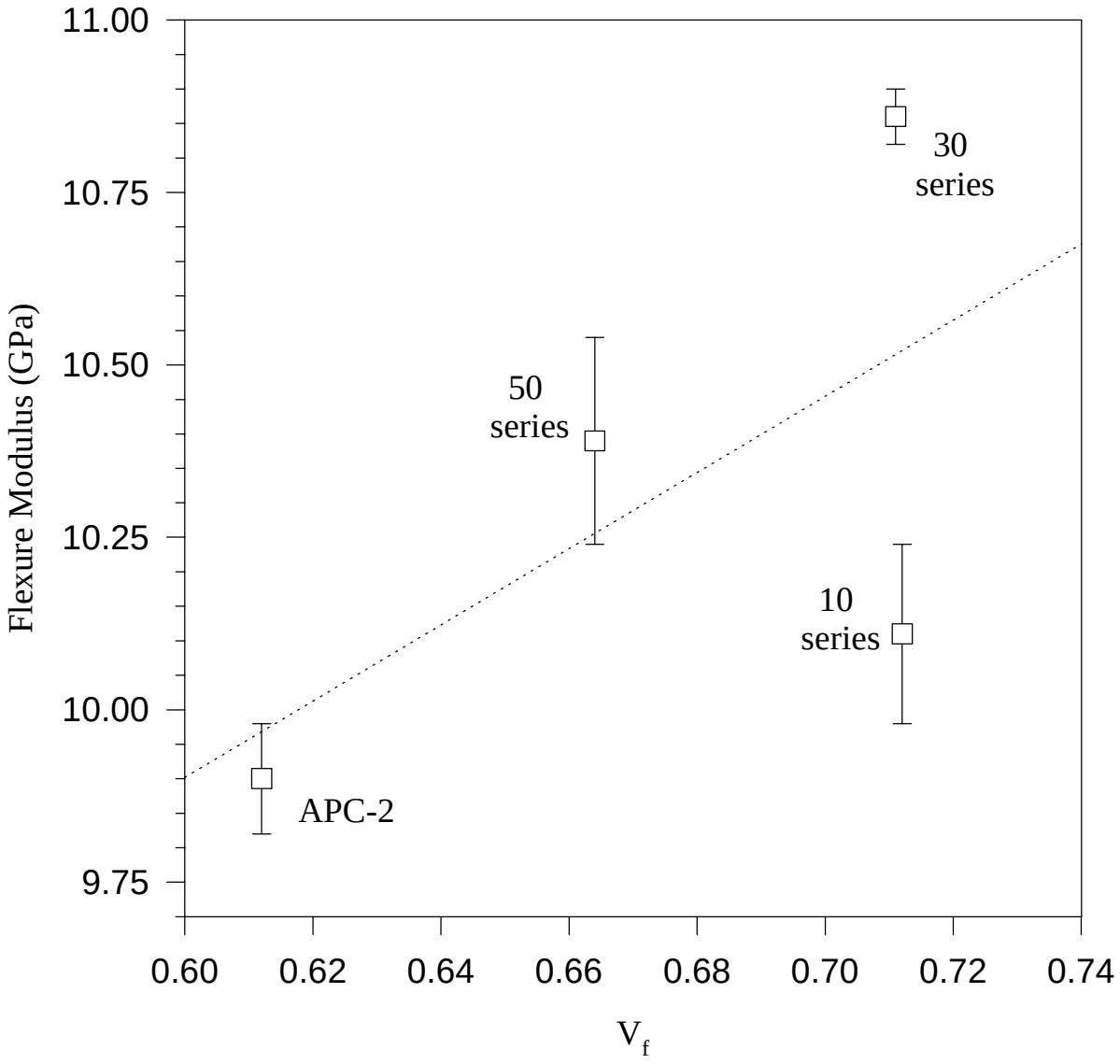

Figure 4-17. Transverse flexure modulus vs. composite fiber volume fraction.

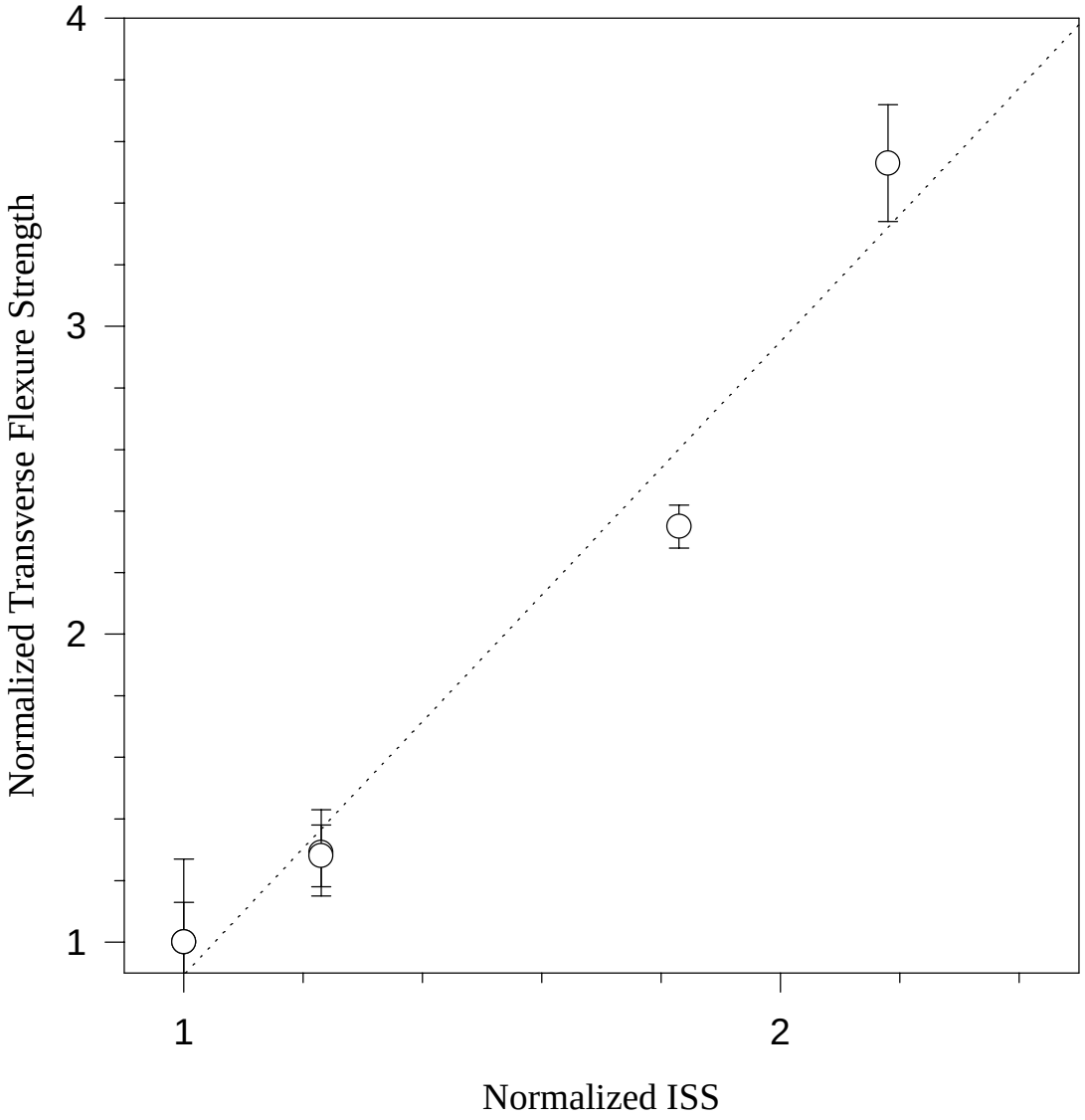

Figure 4-18. Normalized ISS vs. normalized transverse flexure strength data from Chang et al. [5] and Madhukar and Drzal [3].

(a.)

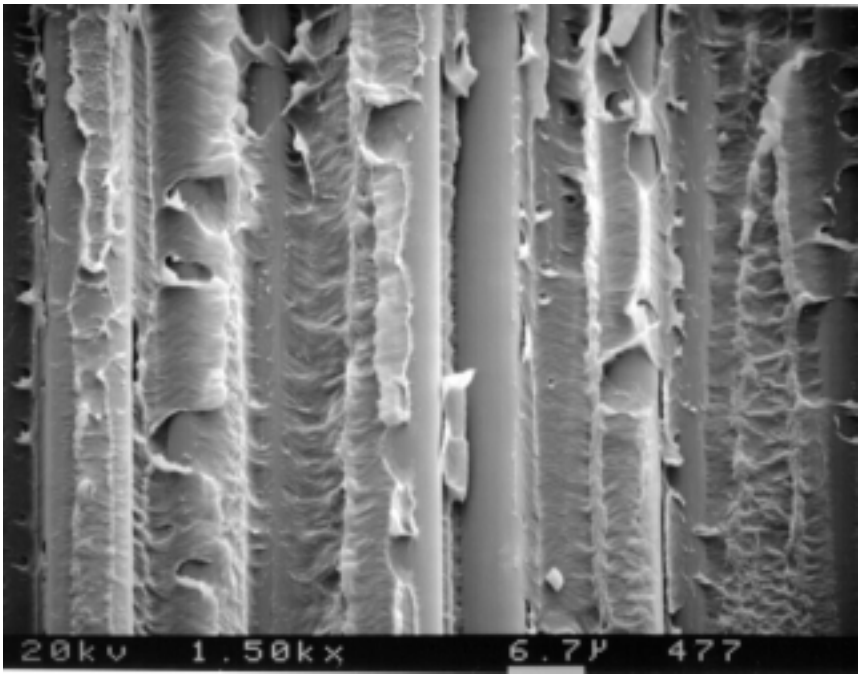

(b.)

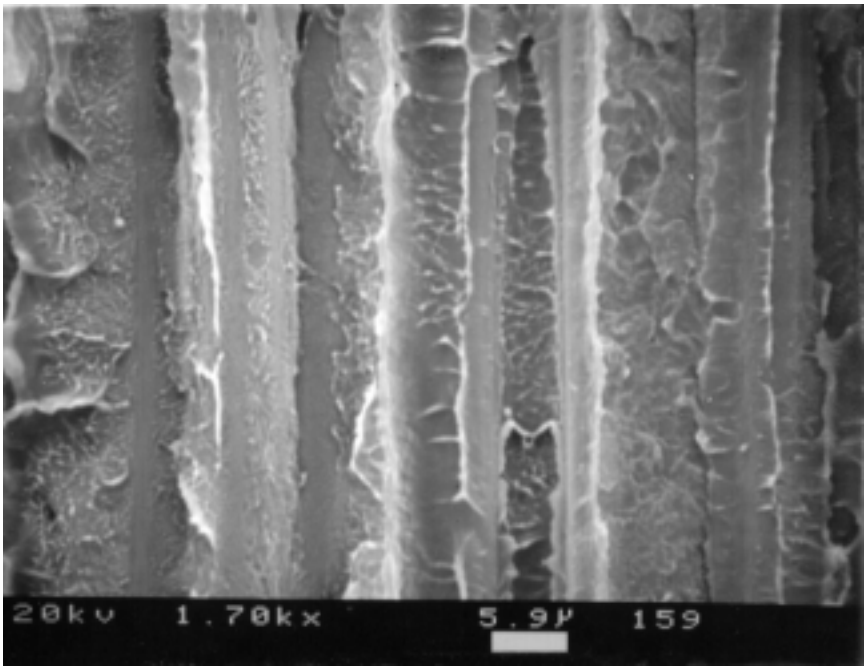

Figure 4-19. Transverse flexure failure surfaces for (a.) 10 series composite and (b.) 30 series composite.

(c.)

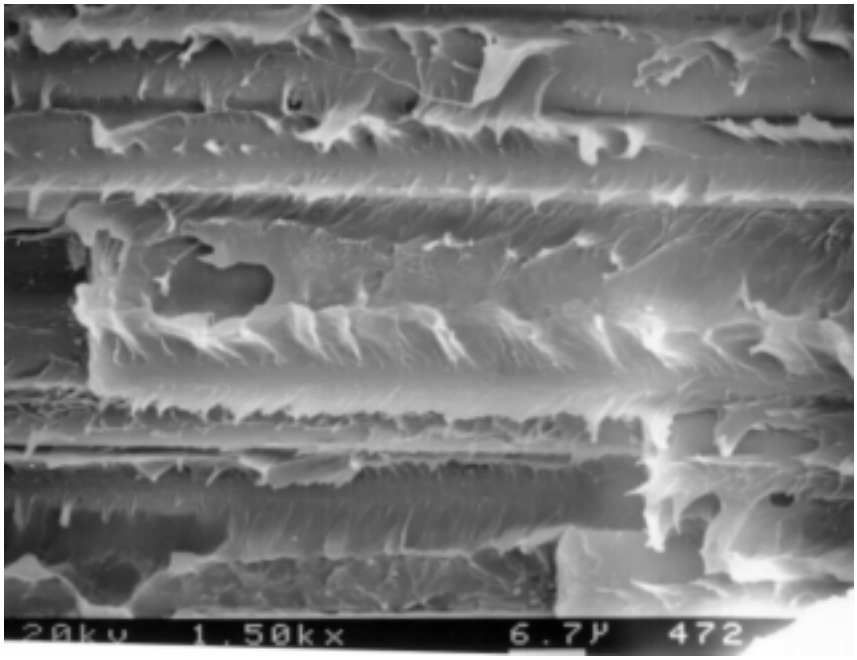

(d.)

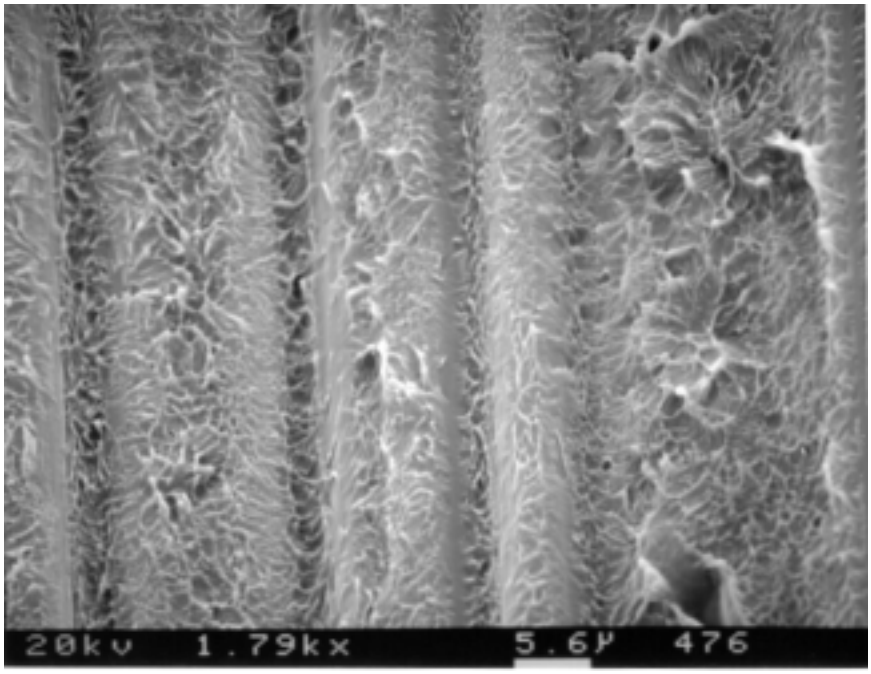

Figure 4-19. (continued) Transverse flexure failure surfaces for (c.) 50 series composite and (d.) APC-2 composite.

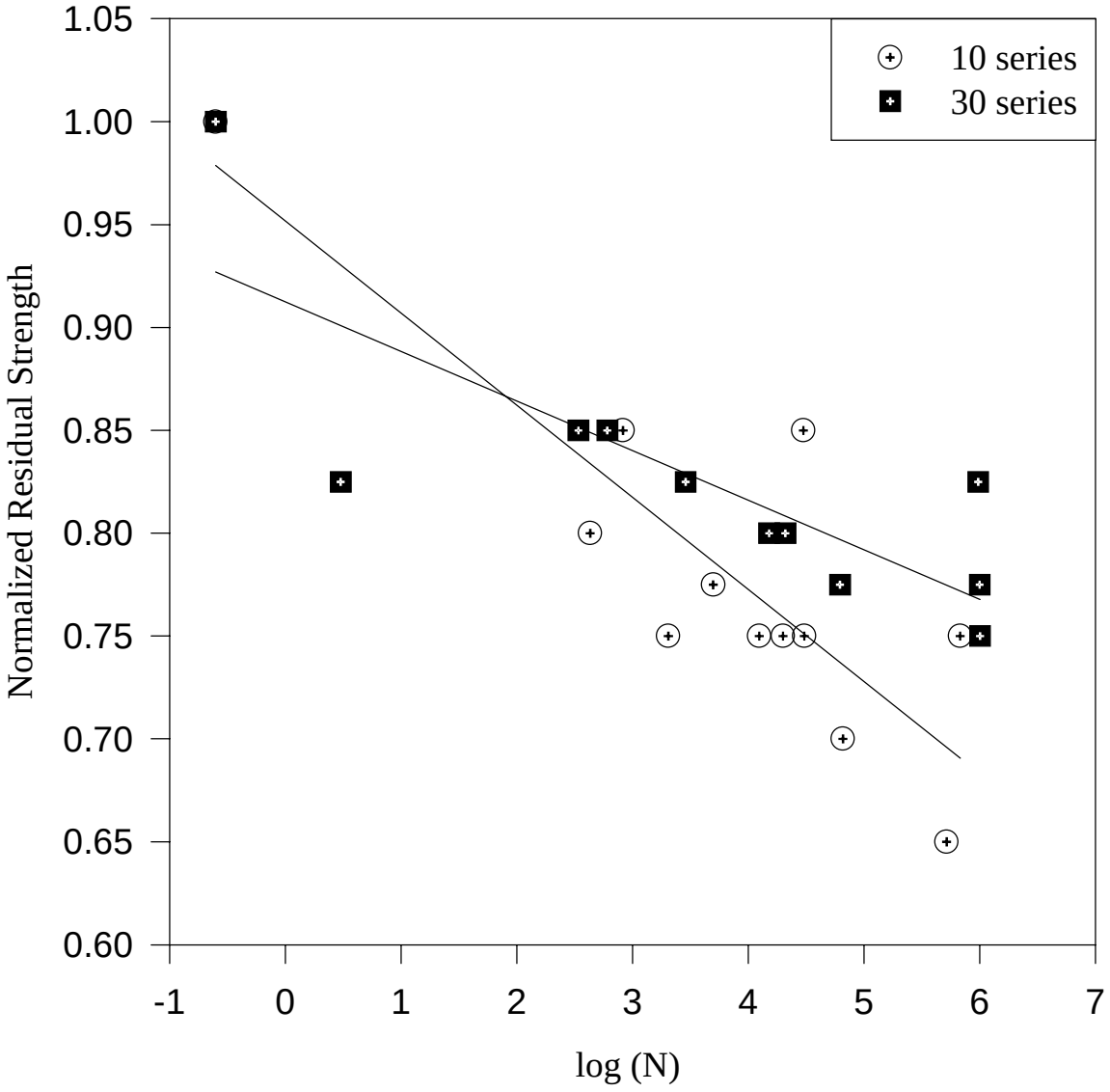

Figure 4-20. Normalized strength vs. log N for R=1.0 notched fatigue experiments. The lines shown are linear best-fit linear regressions to each data set.

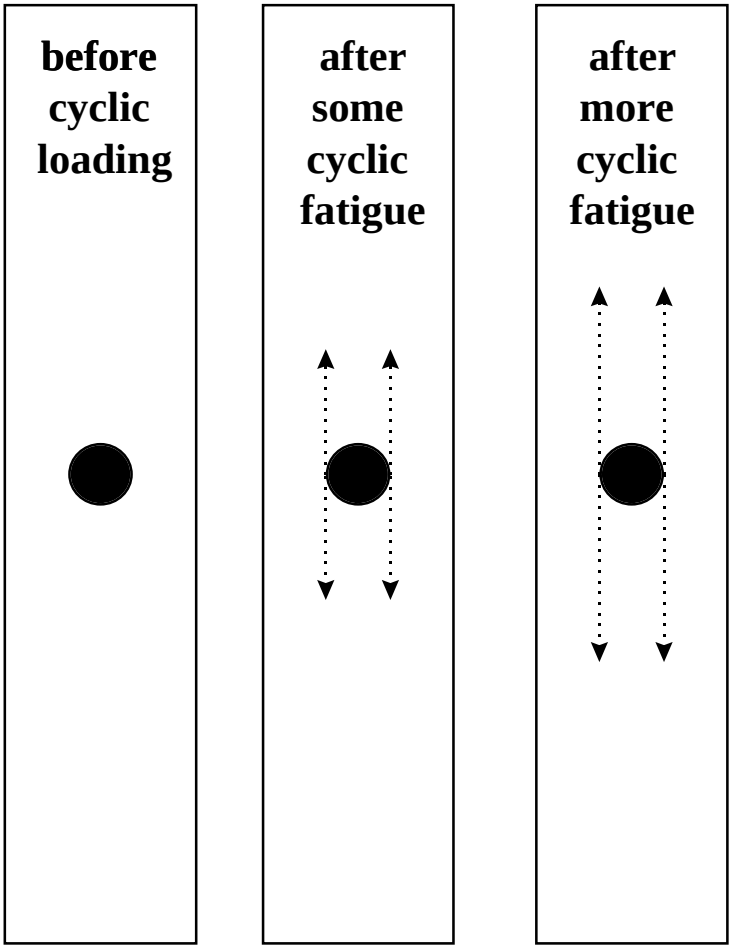

Figure 4-21. Longitudinal split growth for relief of stress concentrations in notched crossply composites during R=0.1 notched fatigue experiments.

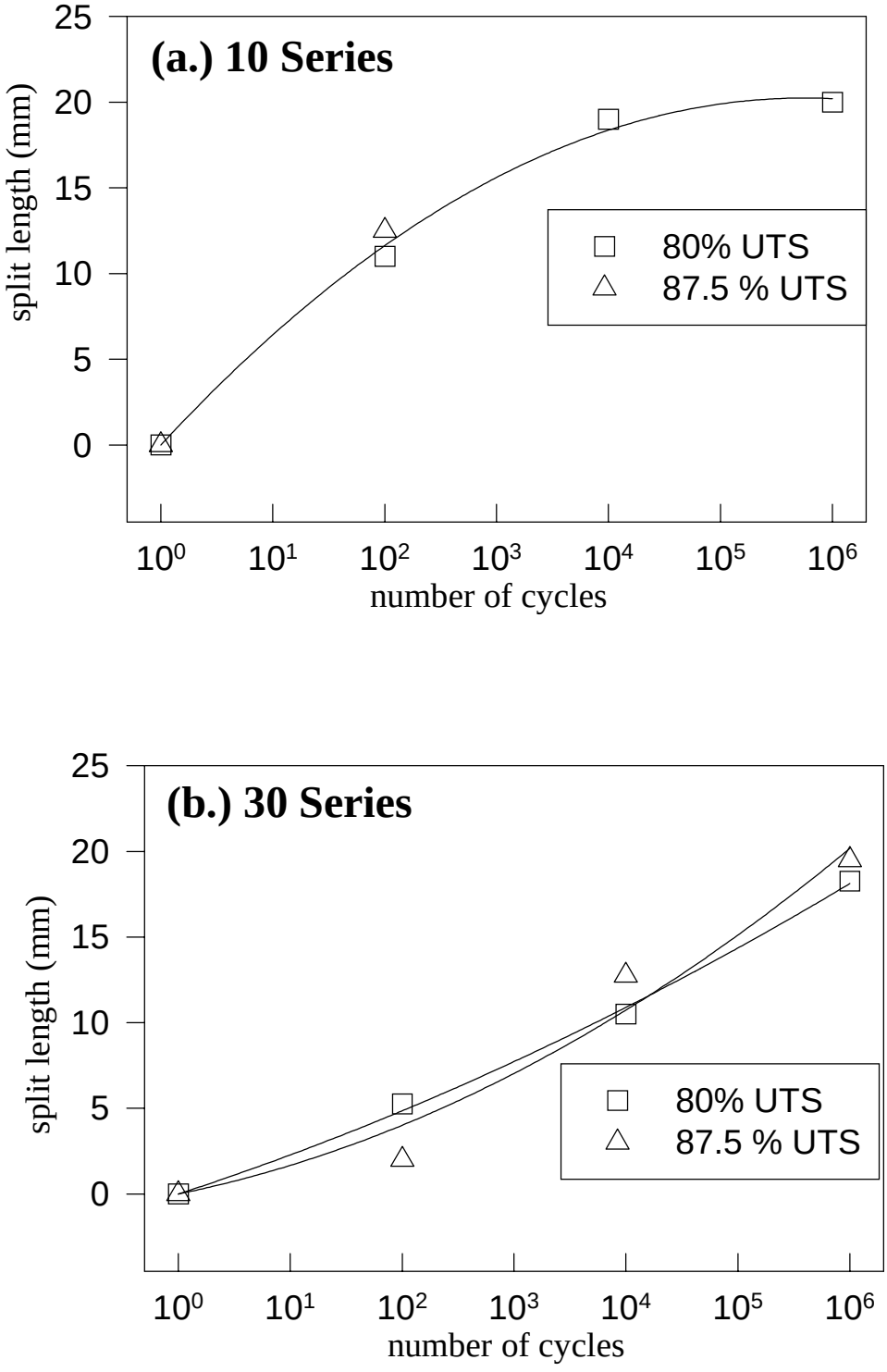

Figure 4-22. Split length vs. number of cycles for R=0.1 notched fatigue testing at 80% UTS and 87.5% UTS for (a.) 10 series composites and (b.) 30 series composites.

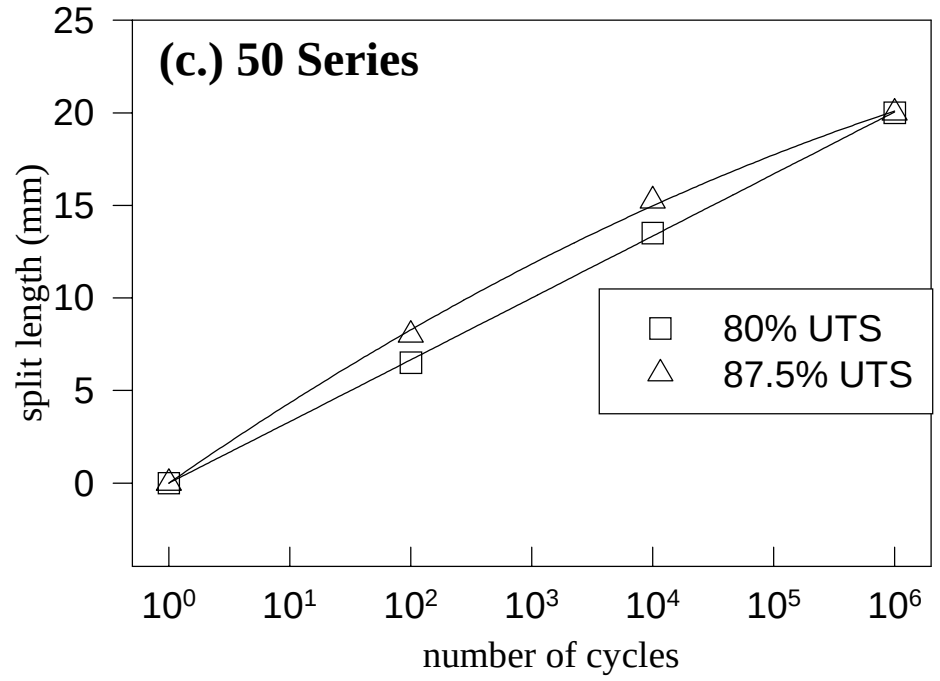

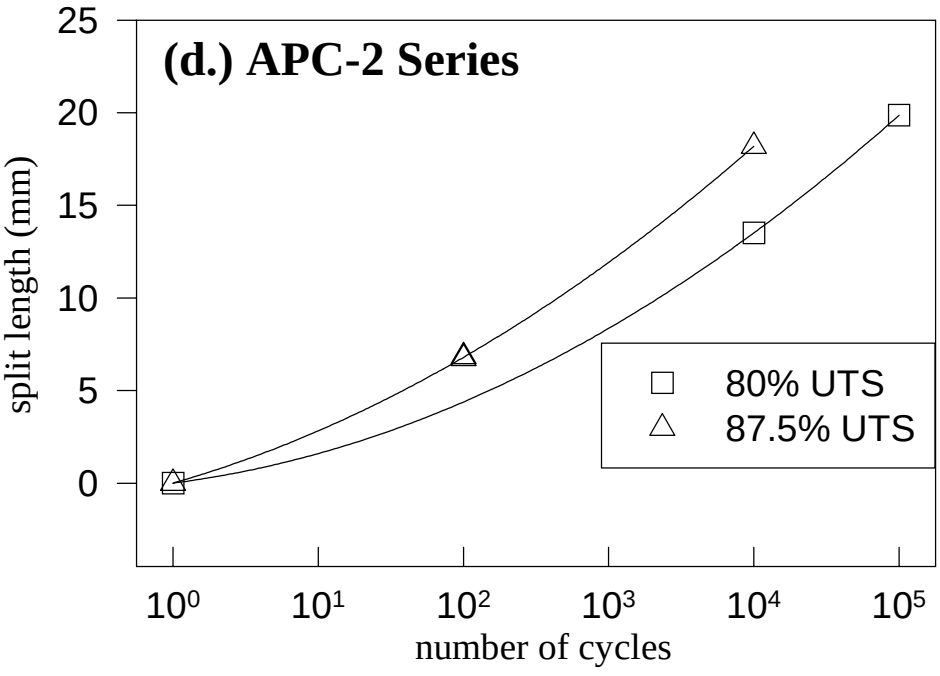

Figure 4-22. (continued) Split length vs. number of cycles for R=0.1 notched fatigue testing at 80% UTS and 87.5% UTS for (c.) 50 series composites and (d.) APC-2 composites.

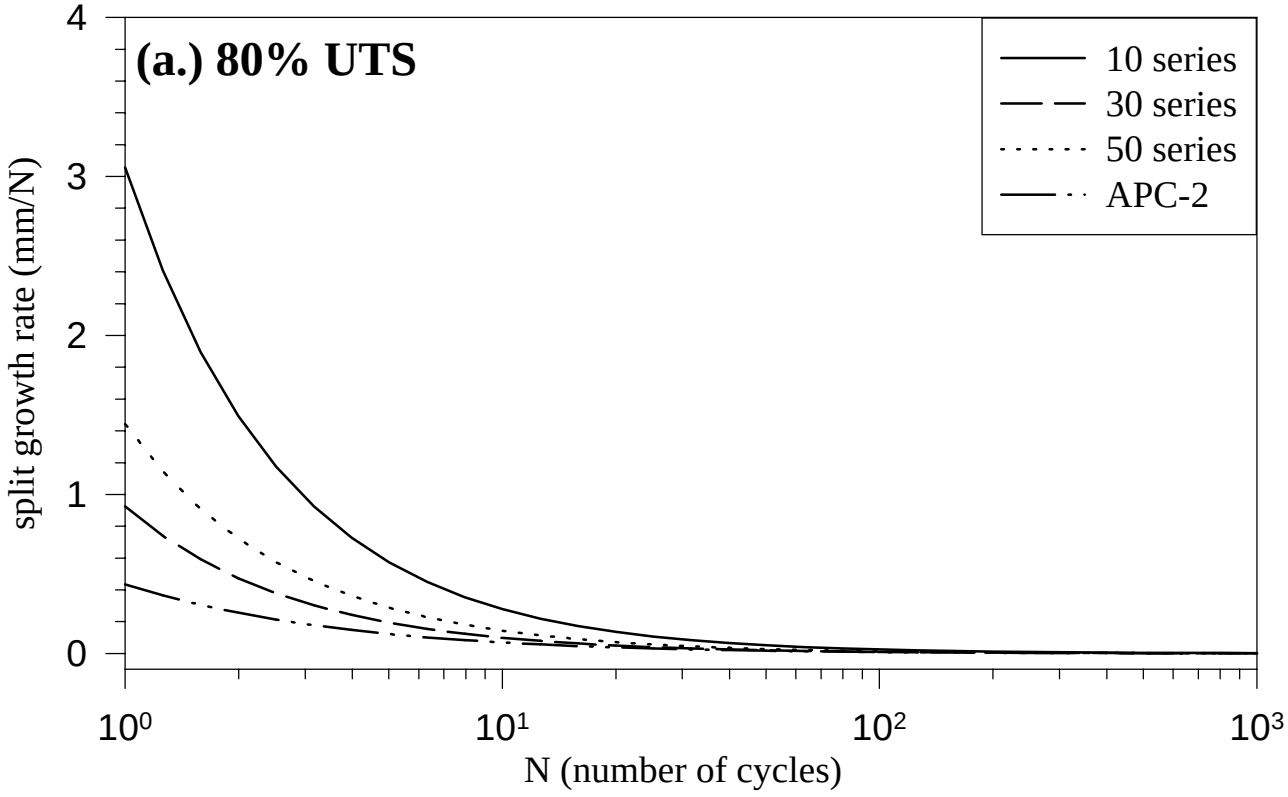

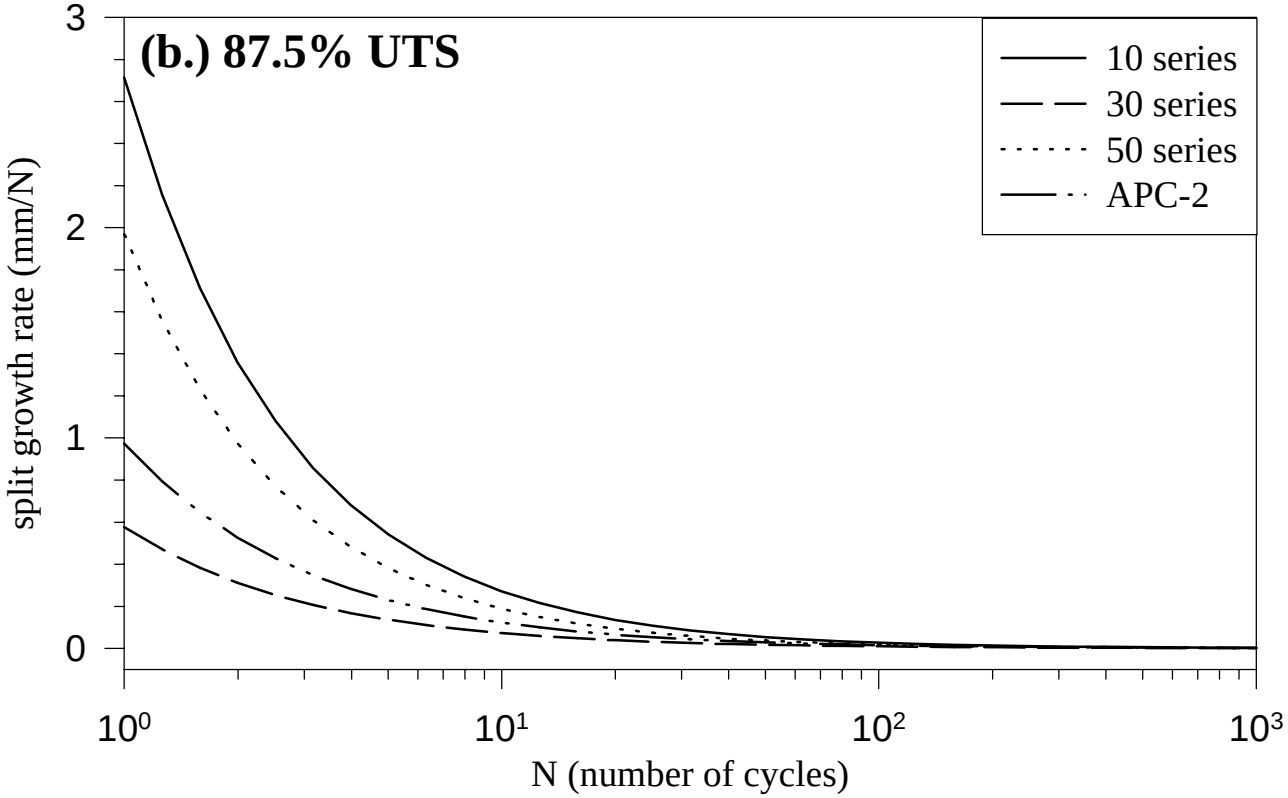

Figure 4-23. Split growth rates for notched fatigue (R=0.1) results of PEEK matrix composites at (a.) 80% UTS and (b.) 87.5% UTS.

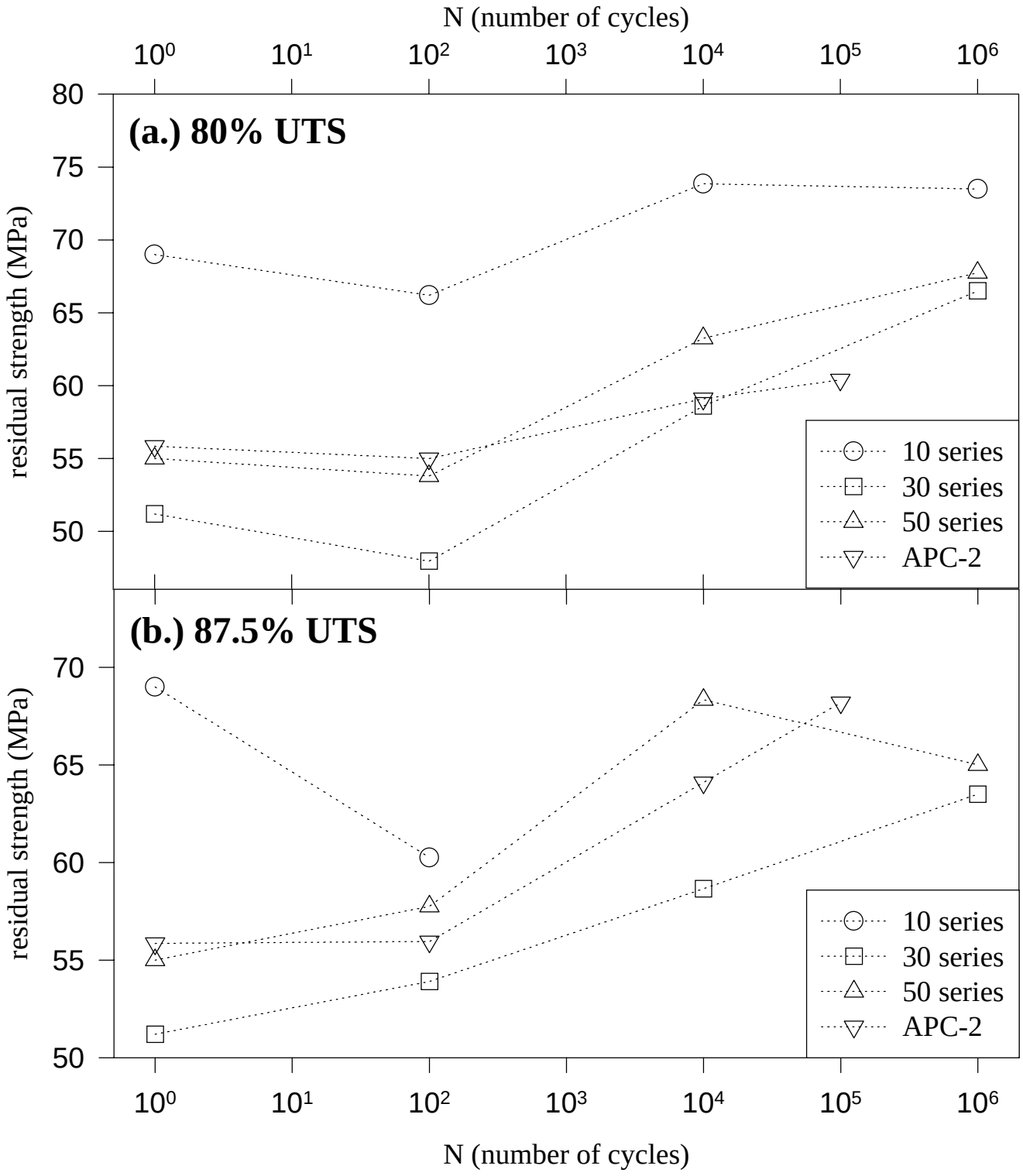

Figure 4-24. Residual tensile strength of notched PEEK composites after various numbers of loading cycles (a.) at 80% UTS and (b.) at 87.5% UTS.

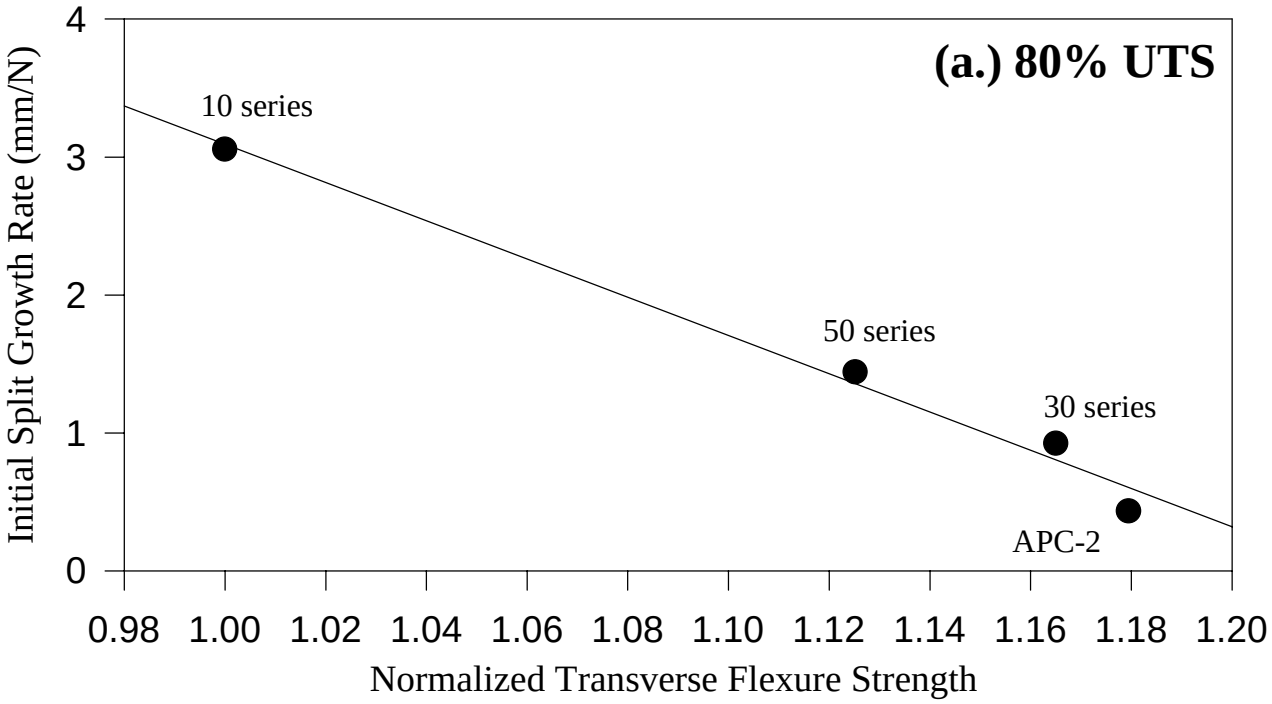

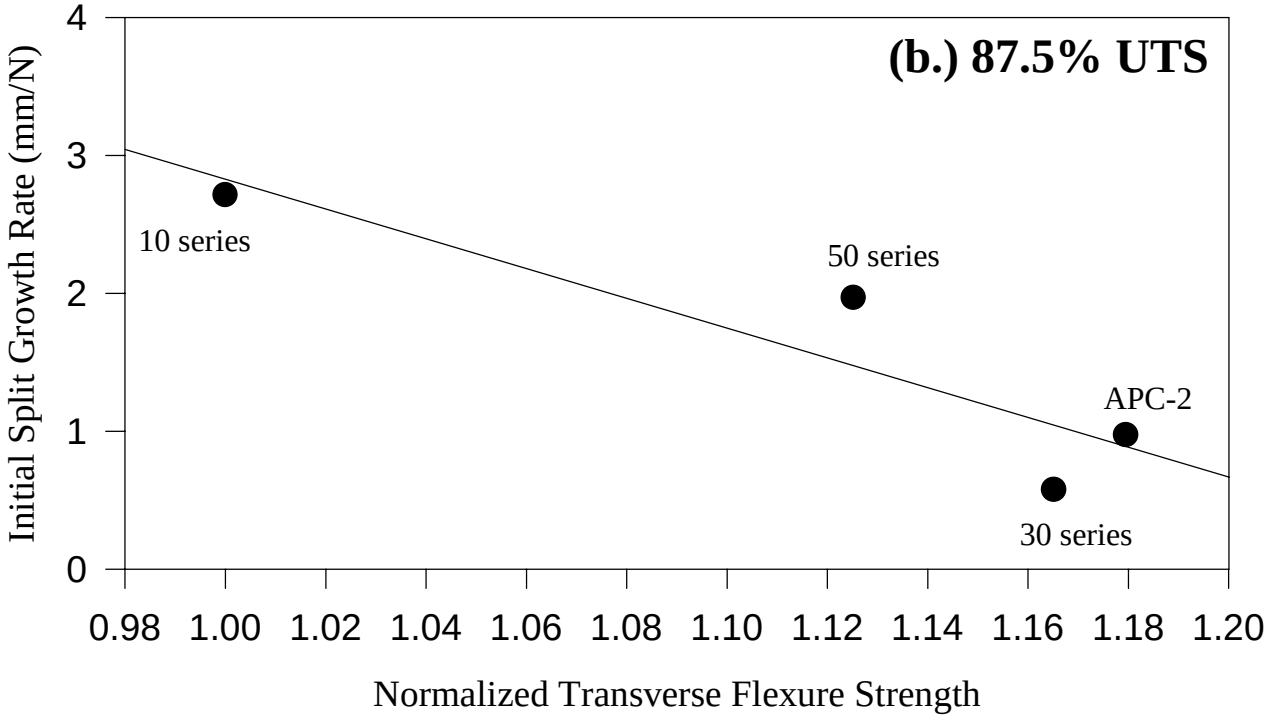

Figure 4-25. Initial split growth rate from R=0.1 notched fatigue experiments at (a.) 80% UTS and (b.) 87.5% UTS vs. normalized transverse flexure strength.

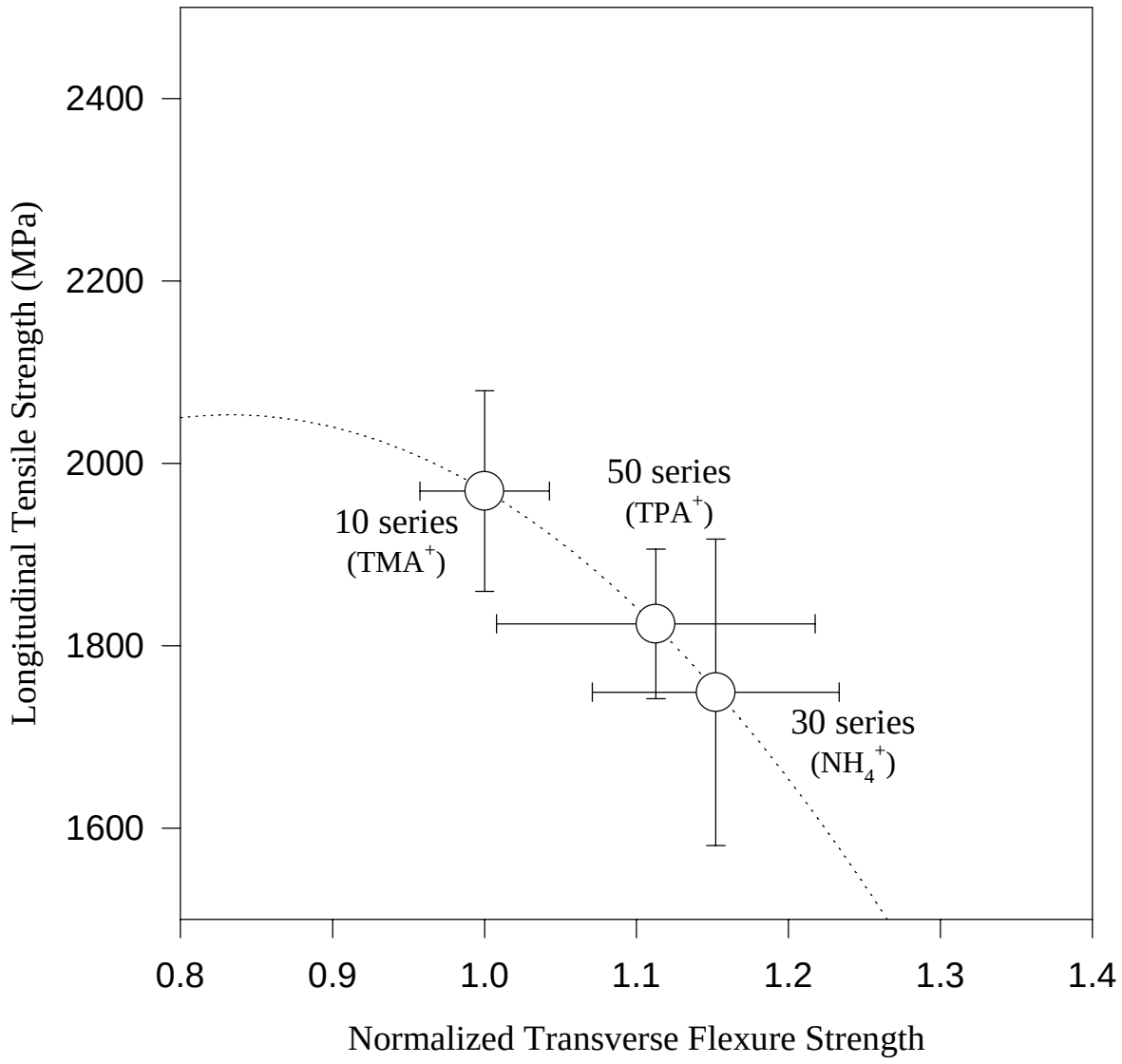

Figure 4-26. Longitudinal tensile strength vs. normalized transverse flexure strength for PEEK matrix composites with a second order polynomial fit.

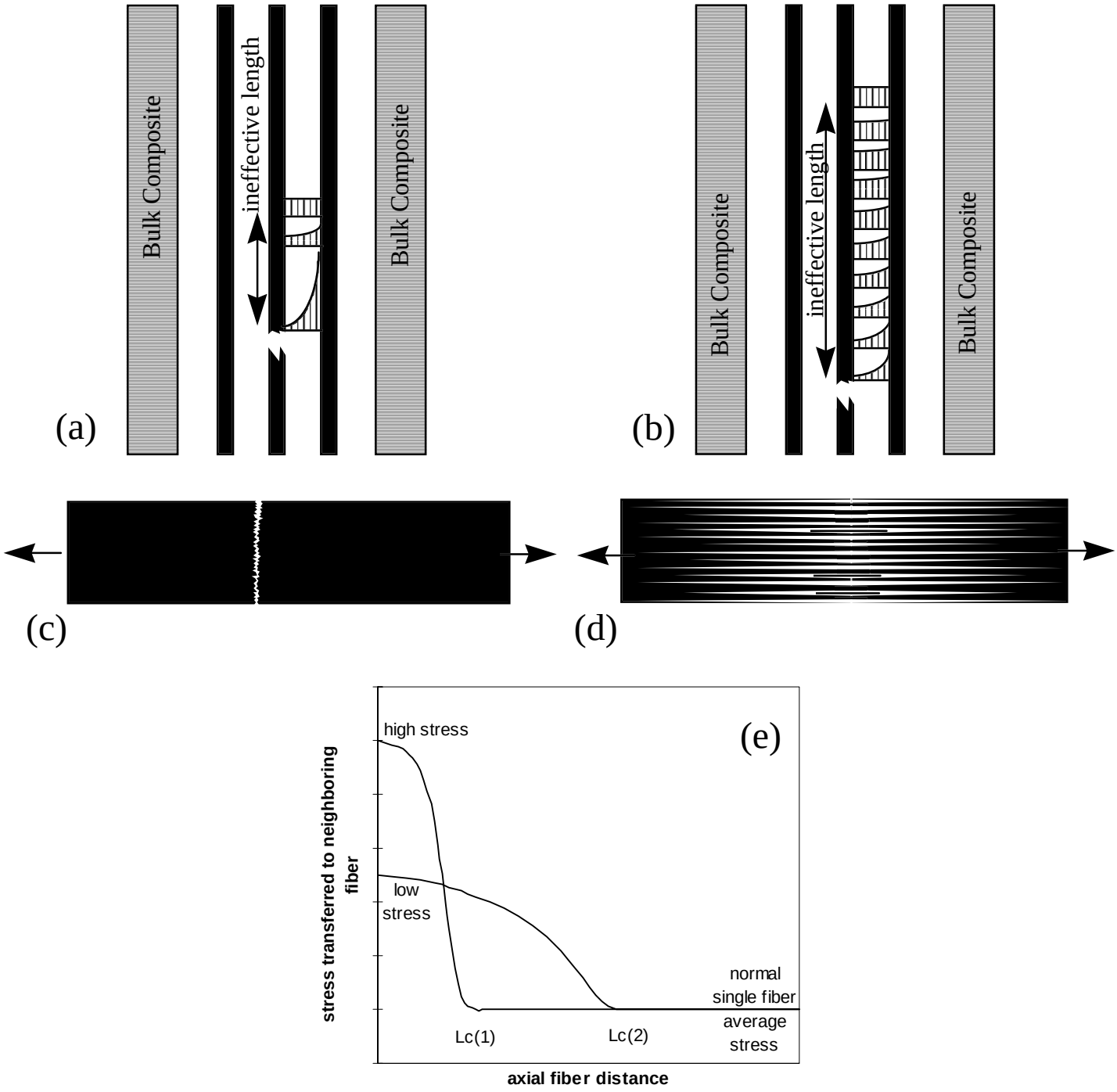

Figure 4-27. Comparison of relative ineffective lengths. The stress profiles for stresses transferred to neighboring fibers are shown in (a) for a short ineffective length and (b) for a long ineffective length. The macroscopic tensile failure modes are shown in (c) for the extreme case of a short ineffective length and (d) for the extreme case of a long ineffective length. The stresses transferred to neighboring fibers are also sketched as a function of arbitrary axial fiber distance for a short ineffective length, at point Lc(1), and a long ineffective length, at point Lc(2).

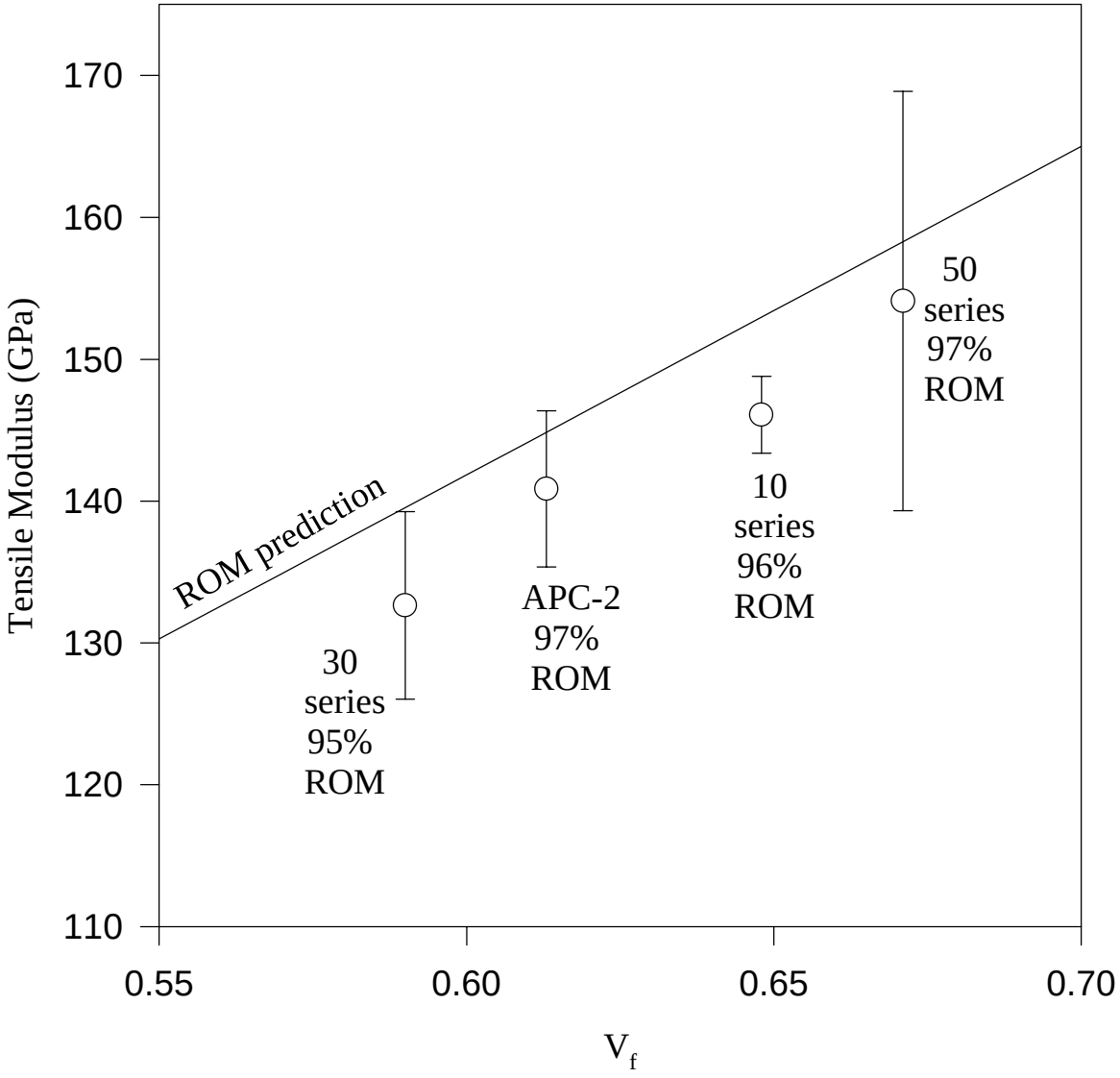

Figure 4-28. Tensile modulus for PEEK matrix composites compared to estimates from the rule of mixtures.

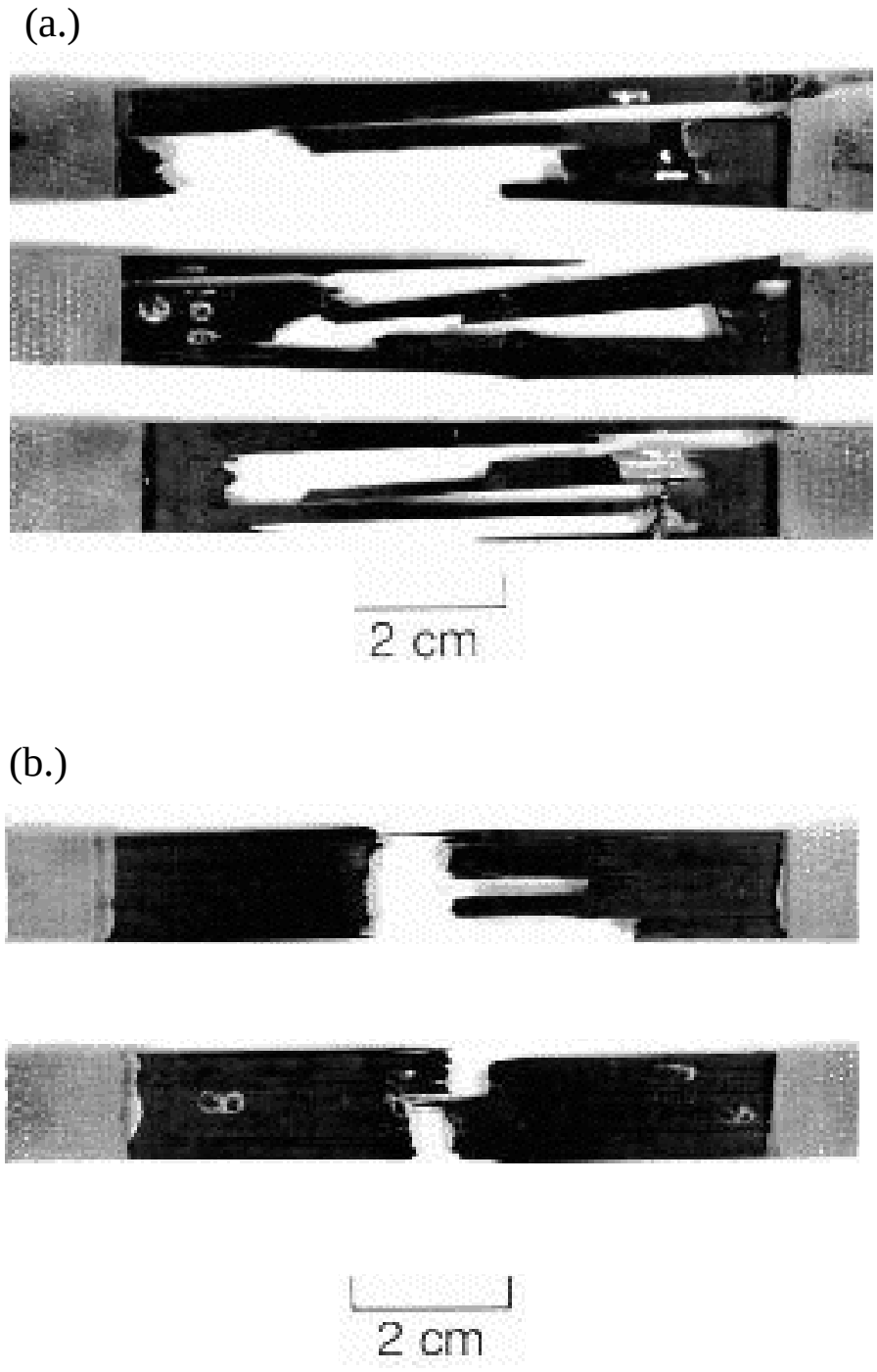

Figure 4-29. Photographs of failed repeated loading tensile specimens showing failure mode for (a.) 10 series composite and (b.) 30 series composite.

Appendix A. Calculation of estimated interphase thickness based on hexagonal packing of carbon fibers.

Considering a hexagonally packed system of equally spaced fibers as shown in Figure 4-11 where the radius of a single fiber is 4.0 microns, the fiber volume fraction is 60% and the volume ratio of matrix to interphase is 95:5.

The area of a hexagon with sides of length s is

$$A_{hex} = \frac{3 \cdot s^2}{2} \cdot \tan\left(\frac{\pi}{3}\right) \qquad \text{Eq. A-1}$$

The area of the hexagon is the sum of the area of the fibers and the area of the bulk matrix, so...

$$A_{hex} = A_f + A_m \qquad \text{Eq. A-2}$$

and

$$A_m = A_{hex} - A_f$$

The area of the fibers inside the hexagon is

$$A_f = \pi \cdot r_f^2 + 6 \cdot \left(\frac{1}{3} \cdot \pi \cdot r_f^2\right) = 3 \cdot \pi \cdot r_f^2 \qquad \text{Eq. A-3}$$

The area of the hexagon is 60% fiber area as defined by the fiber volume fraction, thus the area of the hexagon is 40% matrix area, and...

$$A_f = V_f \cdot A_{hex}$$

$$A_m = \left(1 - V_f\right) \cdot A_{hex} = \left(1 - V_f\right) \cdot \frac{A_f}{V_f} \qquad \text{Eq. A-4}$$

Substituting Eq A-1, Eq A-3 and Eq. A-4 into equation Eq. A-2 yields...

$$\frac{3 \cdot s^2}{2} \cdot \tan\left(\frac{\pi}{3}\right) = 3 \cdot \pi \cdot r_f^2 + \left(1 - V_f\right) \cdot \frac{3 \cdot \pi \cdot r_f^2}{V_f} = 3 \cdot \pi \cdot r_f^2 \cdot \left(1 + \frac{1 - V_f}{V_f}\right)$$

solving for the distance between fiber centers where the fiber radius is $r_f := 4.0$ microns and the fiber volume fraction is $V_f := 0.60$

$$s := \left[\frac{2 \cdot \pi \cdot r_f^2 \cdot \left(1 + \frac{1 - V_f}{V_f} \right)}{\tan\left(\frac{\pi}{3} \right)} \right]^{0.5}$$

yields $s = 9.835$ microns

The distance between the fiber edges is $d := s - 2 \cdot r_f$ and so $d = 1.835$ microns

The area of the polyimide interphase is

$$A_{int} = \pi \cdot r_{int}^2 - \pi \cdot r_f^2$$

The bulk matrix is 95% PEEK by volume, so the volume fraction of the bulk matrix that is polyimide interphase is $\phi_{int} := 0.05$

and so $\phi_{int} \cdot A_m = A_{int}$

substituting

$$\phi_{int} \cdot A_m = \pi \cdot r_{int}^2 - \pi \cdot r_f^2 \qquad \text{Eq. A-5}$$

substituting Eq. A-1 and Eq. A-3 into Eq. A-2 gives

$$A_m = A_{hex} - A_f = \frac{3 \cdot s^2}{2} \cdot \tan\left(\frac{\pi}{3} \right) - 3 \cdot \pi \cdot r_f^2$$

and substituting into Eq. A-5 yields

$$\phi_{int} \cdot \left(\frac{3 \cdot s^2}{2} \cdot \tan\left(\frac{\pi}{3} \right) - 3 \cdot \pi \cdot r_f^2 \right) = \pi \cdot r_{int}^2 - \pi \cdot r_f^2$$

rearranging gives

$$r_{int} := \left[\frac{\phi_{int}}{\pi} \cdot \left(\frac{3 \cdot s^2}{2} \cdot \tan\left(\frac{\pi}{3} \right) - 3 \cdot \pi \cdot r_f^2 \right) + r_f^2 \right]^{0.5}$$

and solving $r_{int} = 4.195$ microns

the thickness of the interphase is found by $thick_{int} := r_{int} - r_f$

and solved to be $thick_{int} = 0.195$ microns

References

1 Reifsnider, K.L., *Composites*, **25**, 461 (1994).

2. Lesko, J.J., Swain, R.E., Cartwright, J.M., Chen, J.W., Reifsnider, K.L., Dillard, D.A., and Wightman, J.P., *Journal of Adhesion*, **45**, 43 (1994).

3 Drzal, L.T. and Madhukar, M., *Journal of Material Science*, **28**, 569 (1993).

4 Subramanian, S., Lesko, J.J., Reifsnider, K.L., and Stinchcomb, W.W., *J. of Compos.Mat*., **30**, 309 (1996).

5 Chang, Y.S, Lesko, J.J., Case, S.W., Dillard, D.D., and Reifsnider, K.L., *Journal of Thermoplastic Composite Materials*, **7**, 311 (1994).

6 Gao, Z., Reifsnider, K.L., and Carman, G., *J. Compos. Mater.*, **26**, 1678 (1992).

7 Carman, G.P., Lesko, J.J., and Reifsnider, K.L., *Composite Materials: Fatigue and Fracture, Fourth Volume, ASTM STP 1156,* W.W. Stinchcomb and N.E. Ashbaugh, Eds., American Society for Testing and Materials, Philadelphia, PA, p. 430, 1993.

8 Case, S.W., Carman, G.P., Lesko, J.J., Fajardo, A.B., and Reifsnider, K.L., *J. Compos. Mater.*, **29**, 208 (1995).

9 The Effect of Polyimide Interphases on Properties of PEEK-Carbon Fiber Composites. S. Gardner, A. Gonzalez, R.M. Davis, J.V. Facinelli, J.S. Riffle, S. Case, J.J. Lesko, K.L. Reifsnider, *AIChE 1995 Annual Meeting.* November 12-17, 1995. Miami, FL.

10 Yu, T.H. and Davis, R.M., *J. Thermoplast.Comp. Mater.*, **6**, 62 (1993).

11 Texier, A., Davis R.M., Lyon, K.R., Gungor, A., McGrath, J.E., Marand, H., and Riffle, J.S., Polymer, **34**, 896 (1993).

12 Gonzalez, A-I, M.S. Dissertation (Virginia Polytechnic Institute and State University, Blacksburg, VA, November 1992).

13 Gonzalez-Ibarra, A., Davis, R.M., Heisey, C.L., Wightman, J.P., and Lesko, J.J., *Journal of Thermoplastic Composite Materials*, **10**, 85 (1997).

14 Davis, R.M., and Texier, A., *ANTEC '91 Confer. Proceed.*, **37**, 2018 (1991).

15 Facinelli, J.V., Gardner, S., Dong, L., Sensenich, C.L., Davis, R.M., and Riffle, J.S., *Macromolecules*, **29**, 7342 (1996).

16 Pratt, J.R. and St. Clair, T.L., *SAMPE Journal*, **26**, 29 (1990).

17 Johnston, N.J., St. Clair, T.L., and Baucom, R.M., Polyimide Matrix Composites: Polyimidesulfone/:aRC-TPI (1:1) Blend, *24th International SAMPE Symposium and Exhibition*, Reno, NV, May 8-11, 1989.

18 Johnston, N.J. and St. Clair, T.L., *SAMPE Journal*, **23**, 12 (1987).

19 Johnston, N.J. and St. Clair, T.L., *SAMPE Preprints*, **18**, 53 (1986).

20 Texier, A., Davis R.M., Lyon, K.R., Gungor, A., McGrath, J.E., Marand, H., and Riffle, J.S., *Polymer*, **34**, 896 (1993).

21 Varughese, B., Muzzy, J., and Baucom, R.M., *21st Intern. SAMPE Tech. Confer.*, Sept. 25-28, 1989.

22 Jonas, A. and Legras, R., *Chapter 3, Assessing the Crystallinity of PEEK*, Advanced Thermoplastic Composites, Ed. H.H. Kausch and R. Legras, Hanser Publications, New York, NY (1993).

23 Hercules AS-4 Product data sheet.

24 Harris, J.M, and Robeson, L.M., *J. Polym. Sci.: Part B: Polym. Phys.*, **25**, 311 (1987).
25 Harris, J.M., and Robeson, L.M., *J. Appl. Polym. Sci.*, **35**, 1877 (1988).
26 Harris, J.M., *ACS Polymer Preprint*, **28**, 56 (1987).
27 Reynolds, R.J.W., and Seddon, J.D., *J. Polym. Sci., Pt. C.*, **23**, 45 (1968).
28 Ho, H., Tsai, M.Y., Morton, J., and Farley, G.L., Journal of Composites Technology & Research, **15**, 52 (1993).
29 Tarnopol'skii, Kincis, Static Test Methods for Composites, 1985
30 Case, S.W.*PhD Dissertation* (Virginia Polytechnic Institute and State University, Blacksburg, VA, May 1996).
31 ASTM Standard D 790M-92 Standard Test Methods for Flexural Properties of Unreinforced and Reinforced Plastics and Electical Insulating Materials
32 ICI Fiberite APC-2 product data sheet.
33 personal consultation with Professor J.P. Wightman.
34 Heisey, C.L., Wood, P.A., McGrath, J.E., and Wightman, J.P., Journal of Adhesion, **53**, 117 (1995).
35 Morton, J., Ho, H., Tsai, M.Y., and Farley, G.L., Journal of Composite Materials, **26**, 708 (1992).
36 Jar, P.-Y. and Plummer, Ch.J.G., Chapter 4, The Physical Structure and Mechanical Properties of Poly(Ether Ether Ketone), Advanced Thermoplastic Composites, Ed. H.H. Kausch and R. Legras, Hanser Publications, New York, NY (1993).
37 Folkes, M.J. *J. of Compos. Sci. & Tech.*, **46**, (1993) 77.
38 Agarwal and Broutman, "Analysis and Performance of Fiber Composites", John Wiley and Sons, New York, NY, 1990.
39 Adams, D.F., King, T.R., and Blackketter, D.M., *Composites Science and Technology*, **39**, 341 (1990).
40 personal consultation with Professor K.L. Reifsnider.
41 ICI Victrex PEEK product data sheet.
42 Jayaraman, K., Reifsnider, K.L., and Swain, R.E., Journal of Composites Technology & Research, **15**, 3 (1993).
43 Jayaraman, K., Reifsnider, K.L., and Swain, R.E., Journal of Composites Technology & Research, **15**, 14 (1993).
44 Jayaraman, K., Gao, Z., and Reifsnider, K.L., Journal of Composites Technology & Research, **16**, 21 (1994).
45 Rosen, B.W. *AIAA Journal*, **2** (1964) 1985.
46 Monette, L., Anderson, M.P., and Grest, G.S., Polymer Composites, **14**, 101 (1993).
47 Monette, L., Anderson, M.P. and Grest, G.S., Journal of Material Science, **28**, 79 (1993).
48 ICI Fiberite APC-2 PEEK/AS-4 composite prepreg product data sheet.
49 Zhuang, H. And Wightman, J.P., *Journal of Adhesion*, **62**, 213 (1997)
50 Chung, Deborah D, Carbon Fiber Composites, Butterworth-Heinemann, Boston, p.91 (1994).
51 Miller, J.D., Harris, W.C., and Zajac, G.W., *Surface and Interface Analysis*, **20**, 977 (1993).
52 Personal communication with James Miller and Gerry Zajac, Amoco Chemicals.

Chapter 5: Structure-Property Relationships of Model Interphase BisP-BTDA Polyimides Made from Water Soluble Precursors and Model Matrix Polyimide/PEEK Blends Made From Aqueous Suspension

Introduction

The effects of interphase modifications to improve composite performance and durability are important topics in the composite industry because of the need to increase performance while minimizing cost. In order to better understand the micro-mechanics of failure of interphase composites, mathematical models which incorporate an interphase region with significantly different material properties from the matrix polymer have been developed by Reifsnider et al. [1-7]. To make use of these models, information regarding the material properties of the interphase region and of the bulk matrix is required [3].

Carbon fiber, polyether ether ketone (PEEK) matrix composites with a BisP-BTDA polyimide interphase have been fabricated and tested in work related to this study. The composites were fabricated using the aqueous suspension prepregging technique which provides the application of the interphase polymer at the same time as the matrix polymer. Aqueous suspension prepregging has been done by many researchers using a polyimide precursor, a polyamic acid salt, which is dissolved in water, and neutralized with a base [8-13]. The matrix polymer powder is dispersed in the aqueous polyamic acid salt solution. The polyamic acid salt behaves as a stabilizer, adsorbing to the surface of the matrix powder particles, and electrostatically stabilizing the suspension. The fiber tow is then coated with the polyimide precursor and the matrix powder in a single prepregging step. The polyamic acid salt also serves as a binder, adhering the matrix powder to the carbon tow. After drying the water from the

prepreg, a heating cycle is used to convert the polyamic acid to the polyimide by way of thermal imidization. By selection of the base used for making the polyamic acid salt, the final properties of the polyimide can be modified.

Poly ether-ether-ketone (PEEK) is a high performance thermoplastic polymer. The T_g of PEEK is typically around 145°C and the typical observed melting is around 340°C [14]. PEEK has very good strength and toughness properties which makes it a suitable composite matrix material. Water soluble BisP-BTDA polyamic acid salts were used in the aqueous suspension prepregging of PEEK matrix composites which are described in detail in Chapter 6 of this thesis. The polyamic acid salt is converted to a polyimide in a subsequent heating step. By modifying the physical properties of the interphase polyimide, it is intended that the material properties of the composite interphase can be altered. These properties must be known for using the mathematical models mentioned previously.

Since techniques have not yet been developed for measuring the properties of the actual interphase region of a composite, model interphase samples consisting of blends of PEEK and BisP-BTDA polyimide were prepared and characterized. The model interphase samples were prepared according to the same methods used for aqueous suspension prepregging and subsequent composite consolidation. The model interphase polyimides were characterized for thermal properties, rheological properties, and gel fraction. For interphase composite manufactured with a PEEK matrix, the processing temperature is 380°C for thirty minutes. The thermal stability of the polyimide interphase material at this temperature is important when considering an interphase region that is primarily composed of the polyimide.

Since PEEK is miscible with BisP-BTDA polyimide [15], interdiffusion of the interphase

polyimide and the bulk PEEK matrix is expected. Thus, thermal, mechanical, and rheological properties of model matrix samples with varying compositions were measured.

The BisP-BTDA polyimide interphase/PEEK matrix composites are discussed in Chapter 6. As a control case, PEEK matrix composites were fabricated with a "fugitive" binder, hydroxypropyl cellulose (HPC) supplied by Aqualon. The HPC was utilized for dispersion of the aqueous suspension and binding the powder to the carbon fiber, as described in Chapter 6. Prior to the composite lay-up, the prepreg was heated in a convection oven at 325°C for pyrolysis of the HPC. The Aqualon product data sheet reports HPC burnout temperatures of 250-500°C [16].

Model matrix samples were prepared with 5 wt% HPC and 95 wt% PEEK to investigate the bulk matrix properties of the "fugitive" binder control case composites. These HPC/PEEK model matrix samples are characterized in this chapter.

The goals of this work are (I.) processing of BisP-BTDA polyimides from aqueous polyamic acid salts, (ii.) characterization of polyimides including thermal analysis, measuring gel fractions, and melt rheology, and (iii.) polyimide/PEEK and HPC/PEEK model matrix characterization including thermal analysis, assessment of crystalline content, melt rheology, and tensile properties.

Materials

A 40 g batch of BisP-BTDA polyamic acid endcapped with phthalic anhydride to provide a target molecular weight of 40,000 g/mole was synthesized by Dr. Biao Tan from Professor McGrath's group of the Virginia Tech Chemistry Department. The polyamic acid was supplied as a solid powder and stored in a freezer at -5°C. This large batch of polyamic acid provided enough starting material so all experiments described in this chapter could be done using a single batch of polymer. This polyamic acid was used to make the model interphase samples for the structure property investigations of this chapter and the same batch of polyamic acid was used for subsequent composite manufacture as detailed in the Chapter 6 of this thesis.

The matrix material was Victrex 380 Grade poly ether-ether-ketone (PEEK) supplied by ICI Americas. The PEEK was supplied as a powder with an 11µm median particle diameter as measured with a Shimadzu SPC-3 particle size analyzer. The PEEK is from the same batch used in subsequent composite manufacture as detailed in Chapter 6 and also the same batch used by Gonzalez [11] for polyimide interphase PEEK matrix composite manufacture.

The bases used for making the polyamic acid salts ammonium hydroxide (NH_4OH) and tetramethyl ammonium hydroxide (TMAH) were both Fisher brand reagent grade. Klucel hydroxypropylcellulose, type 99-EFF, lot # FP10-10085 was supplied by Aqualon. For all aqueous solutions and suspension, deionized water with a resistivity of 16.7 ohms/cm^3 from a Nanopure II water filtering system was used.

Calibration of Bases

All bases were purchased new, kept sealed and stored in a refrigerator. The concentration of the aqueous bases were determined by potentiometric titration using an MCI Automatic Titrator Model GT-05 (COSA Instruments Corporation). The titration procedure has been described in detail in Chapter 3. The bases were kept in the original bottles, sealed tightly with parafilm and stored in a refrigerator.

Model Interphase BisP-BTDA Polyimide Characterization
Preparation of Test Samples

Since properties of the actual interphase region of a composite cannot be currently evaluated accurately, it was necessary to prepare polyimide model interphase material on a bulk scale so that properties could be measured. BisP-BTDA polyimides were prepared using exactly the same procedure for those used in the 70 series and 80 series composites manufactured subsequently in the work of Chapter 6 in this thesis. Bulk samples of BisP-BTDA polyimide were made from an NH_4^+ polyamic acid salt and a TMA^+ polyamic acid salt. Figure 5-1 shows the chemical reactions for formation of the two polyamic acid salts. The bulk sample polyimide made from the BisP-BTDA NH_4^+ polyamic acid salt was designed to replicate the chemistry and physical state of the polyimide material in the 80 series composites. The bulk sample polyimide made from the BisP-BTDA TMA^+ polyamic acid salt was designed to replicate the polyimide material in the 70 series composites. Thus, the same batch of PAA was used for the composite manufacturing process and the model interphase polyimide preparation procedure and the processing conditions were repeated exactly.

i.) BisP-BTDA NH_4^+ PAA salt (80 series composite model interphase): Deionized water at 70°C was mixed with 14.22 molar NH_4OH(aq). The polyamic acid was then added slowly while stirring rapidly. The NH_4OH was added in a 1.25:1 stoichiometric ratio to acid functionalities of the PAA (two per repeat unit) and a measured amount of PAA was used to make a 5 wt% aqueous solution of polyamic acid . The 25% stoichiometric excess of base was used to ensure neutralization of amic acid functionalities and maintain stability of the aqueous polyamic acid salt as shown by Reynolds [17] and described in Chapter 2. This concentration of base also replicates conditions for composite manufacture of Gonzalez [11]. The solution was covered with Parafilm to prevent evaporation of base, and was stirred for one hour at 70°C to allow the PAA salt to form and dissolve. The solution was then allowed to cool to room temperature and then it was filtered using a Buchner funnel and Fisher Brand No.41 filter paper. No insoluble polyamic acid residue was collected with the filter paper.

ii.) BisP-BTDA TMA^+ PAA salt (70 series composite model interphase): Deionized water at room temperature was mixed with 3.23 molar TMAH(aq). The PAA was added slowly to the basic solution during rapid stirring. The TMAH was added in a 1.10:1 stoichiometric ratio to acid functionalities of the PAA and a measured amount of PAA was added to make a 5 wt% aqueous solution of polyamic acid. The 10% stoichiometric excess of base was used to ensure neutralization of amic acid functionalities and maintain stability of the aqueous polyamic acid salt as shown by Reynolds [17] and described in Chapter 2. It was found that 25% molar excess, as used with the NH_4OH dissolution procedure, was not needed for complete dissolution with TMAH, and that 10% molar excess was sufficient. The solution was covered with Parafilm to prevent evaporation of base, and was stirred at room temperature overnight, then it was filtered

using a Buchner funnel and Fisher Brand No.41 filter paper. No insoluble polyamic acid residue was collected with the filter paper.

The aqueous salt solutions were made in about 800 ml quantities. Approximately 400 ml of the each solution was reserved for the model interphase study described below. Approximately 200 ml of each solution was stored in a Nalgene bottle sealed with parafilm, and stored in a refrigerator for subsequent aqueous composite prepregging experiments.

The solutions were poured into specially made, shallow Teflon-film pans and dried in a hood at room temperature. The BisP-BTDA NH_4^+ solution dried completely in about 3 days. The BisP-BTDA TMA^+ solution dried completely in about 7 days.

Although most of the dry polyamic acid salts underwent a heat treatment cycle in a Model 532 Fisher Programmable air convection oven that was identical to that for the prepreg material, a small portion of these dry polyamic acid salt samples was reserved for thermal gravimetric analysis, (TGA). For this test a drying step of 65°C for one hour was followed by a further heat treatment step of 265°C for two hours to convert the polyamic acid salt to polyimide.

Melt Rheology of BisP-BTDA Polyimides

Rheology testing was done on a Bohlin VOR with a high temperature cell oven using nitrogen as the heating gas. A 25 mm parallel plate fixture was used with an approximate sample thickness of 1 mm. Prior to subsequent measurements, the amplitudes and frequencies which characterize the linear viscoelastic region were determined. The subsequent isothermal rheology tests were done within this linear viscoelastic range. The initial measurements of the dynamic

temperature rheological tests were within the linear viscoelastic range, however this range was not maintained as the viscosities increased due to crosslinking. The purpose of the dynamic temperature rheological tests was to demonstrate crosslinking by an increase in melt viscosity.

Melt rheology samples were prepared by cutting the polyimide film, which had been thermally imidized, into circular shapes and stacking them between the plates of the Bohlin VOR. The plates of the VOR were preheated to 290°C. After inserting the polyimide sample and the oven temperature had returned to 290°C, the plates were closed to an approximate spacing of 1.0 mm, excess polyimide was trimmed around the edges of the plates using a razor blade and the measurements were made. Approximately 0.6 g of polyimide was used for each sample.

Dynamic temperature tests from 290°C to 380°C were conducted in the oscillation mode with an amplitude of 35% (radians) and a frequency of 0.1 Hz. A heating rate of 5 °C/min was used. A torque bar with a calibrated torsional resistance of 11.45 g•cm was used for this test. Since the gap thickness will vary with temperature, and dynamic temperature tests were conducted, the plate gap spacing was calibrated at 315°C, which was a temperature in the middle of the range investigated.

Differential Scanning Calorimetry of BisP-BTDA Polyimides

A Seiko 220C differential scanning calorimeter (DSC) in Professor Garth Wilkes Laboratory was used to obtain dynamic heat capacity data for the polyimides. Chris Robertson graciously ran the DSC instrument which was calibrated with indium. Prior to the DSC

experiment the polyimides had been dried and imidized in a convection oven using a temperature cycle of 65° for one hour followed by 265°C for two hours. Polymer samples were cut to fit into the DSC pans to obtain a sample mass of 10-15 mg. A dual scan procedure was used with a heating rate of 20°C/min from 60°C to 350°C under nitrogen purge. Since no melting type endotherm was observed, only heating scans were recorded for T_g measurement. Glass transition temperatures were found by using the midpoint of the heat capacity inflection.

Thermal Gravimetric Analysis

A Dupont Instruments Model 951 Thermal Gravimetric Analyzer (TGA) was used to evaluate the imidization temperatures of the polyamic acid salts and the thermal stability of the resulting polyimides. A nitrogen gas purge was used for all measurements of the polyimides. Measurements were taken on polymer samples weighing approximately 15-25 mg. Thermal cycles simulated the oven imidization cycle and the composite consolidation cycle used in composite manufacturing procedures. TGA was also used to evaluate the pyrolysis of the HPC "fugitive" binder using an air purge. Following the simulated oven imidization cycle or the simulated consolidation cycle, the samples were pyrolyzed to assess thermal stability.

For the imidization cycle, the temperature was ramped at 10°C/min to 265°C, held for two hours, and then ramped at 10°C/min to 600°C. Since thermal imidization is a condensation reaction, water is evolved during the reaction. The weight loss that occurs at temperatures below the T_g of the resulting polyimide is attributed to loss of water, as well as loss of the basic counterion associated with the polyamic acid. The range of temperatures over which this weight

loss occurs is defined as the imidization temperature range. The reported imidization temperatures are for purposes of comparing relative imidization reaction kinetics at a similar dynamic thermal cycle. The reported imidization temperatures should not be interpreted by the reader as the only temperatures for which thermal imidization is possible for these materials.

For the simulated consolidation cycle the temperature was ramped at 10°C/min to 380°C, held for thirty minutes, and then ramped at 10°C/min to 900°C. Onset of degradation was characterized by the 5% weight loss temperature. For the imidization cycle, the samples lose weight as a consequence of imidization and so the temperature at which 5% weight loss occurred was measured only after imidization was complete.

For the examination of the pyrolysis of the HPC "fugitive" binder the temperature was ramped to 325°C at 10°C/min and held for two hours, then ramped to 380°C at 10°C/min and held for 30 minutes and then ramped to 600°C at 10°C/min. This thermal cycle simulated the actual composite fugitive binder pyrolysis thermal cycle with a two hour isothermal hold at 320°C and the composite consolidation thermal cycle of a 30 minute isothermal hold at 380°C.

Model Matrix Blend Characterization
Preparation of Test Samples

Polymer films were manufactured to simulate the blend compositions of PEEK and polyimide that could occur in the matrix region of the composite. Since BisP-BTDA polyimide is miscible with PEEK [15], it is hypothesized that a concentration gradient of polyimide will be present immediately surrounding each carbon fiber, rich in polyimide at the fiber surface, and

rich in PEEK in the bulk matrix. Model matrix samples of 5wt% BisP-BTDA polyimide and 95 wt% PEEK having the same composition of the prepregging suspension for subsequent composite fabrication were prepared.

The case of complete mixing of the polyimide interphase and the bulk PEEK must be considered to address the possibility that the effects of composite properties are due to the addition of a polyimide component to the PEEK which merely alters the matrix properties.

Small samples of suspension were used to make representative matrix coupons for matrix characterization. The suspensions were made using a portion of the polyamic acid salt solutions that were made for the model interphase study. Small aqueous suspensions with a total solids content of 3.0 g were made with the polyamic acid salt solutions or HPC aqueous solution and 380 grade PEEK powder. The suspensions were dried in a hood at room temperature, mixing occasionally to maintain a homogeneous distribution of PEEK powder and binder. When the suspensions were dry, they were pulverized using a mortar and pestle to homogenize each individual powder sample.

The homogenized powder samples were placed in specially made, shallow Teflon-film pans and subjected to a heat treatment cycle in a Model 532 Fisher Programmable air convection oven that was identical to that for the respective composite prepreg material during a composite manufacturing procedure. The thermal imidization cycle for the BisP-BTDA polyamic acid salts was 65°C for one hour followed by 265° C for two hours. The temperature cycle for HPC burnout was one hour at 100°C followed by two hours at 325°C.

Model matrix films were pressed in a specially manufactured mold made from 0.20" stainless steel shim stock. The mold was sandwiched between sheets of heavy duty aluminum

foil that were treated with an aerosol Teflon mold release agent. A Wabash Vacuum Hot Press was used to press the polyimide/PEEK blends at a temperature of 380°C and a pressure of 100 psi for 30 minutes and then cooled at a rate of 10°C/min to simulate the actual consolidation temperature of the composite interphase.

Melt Rheology of Model Matrix Blends

Rheology testing was done on a Bohlin VOR with a high temperature cell oven using nitrogen as the heating gas. The 25 mm parallel plate fixture was used with an approximate sample thickness of 1 mm. The plate gap spacing was calibrated at 380°C which was the temperature used for the rheology test.

Melt rheology samples were prepared by cutting the model matrix film into pieces that could be stacked in between the parallel plates of the rheometer. The plates were preheated to 380°C so that the polymer film would flow quickly and the plate spacing was closed to about 1 mm for measurements. Any polymer that squeezed out beyond the edges of the plates was trimmed with a razor blade.

Isothermal, dynamic frequency tests were conducted in the oscillation mode with an amplitude of 50% (radians). Prior to the isothermal, dynamic frequency tests, this amplitude was established as being within the linear viscoelastic region up to frequencies of 0.5 Hz. The frequency range for the dynamic frequency tests was 0.002 Hz to 0.1 Hz. The temperature throughout the test was 380 ± 1°C. A torque bar with a calibrated torsional resistance of 11.45 g•cm was used for this test.

Tensile Testing of Model Matrix Blends

A Polymer Labs Miniature Materials (MiniMat) Tester in Professor Ronald Kander's Lab, was used in the tensile mode to measure tensile properties of the model matrix blends following ASTM Standard 1708-93. The films were cut into dogbone coupons using a dogbone blanking die. The dogbones were 1" long, 0.1" wide at the test area and had individually uniform thicknesses ranging from 0.04" to 0.05".

Tensile data were collected online with a personal computer using Polymer Labs MiniMat software. Tensile strength and strain data were collected. The first 2% strain was characterized by elastic deformation. Using the data from this region the Young's modulus was calculated from the slope of the stress-strain curve. For each test sample composition, between 5 and 10 specimens were tested.

Differential Scanning Calorimetry of Model Matrix Blends

A Seiko 220C differential scanning calorimeter, calibrated with indium, was used to obtain dynamic heat capacity data for the PEEK/polyimide blends. Kurt Jordens graciously ran the DSC instrument in Professor Garth Wilkes lab. Polymer samples were cut to fit into the DSC pans to obtain a sample mass of 10-15 mg. A triple scan procedure was used with a heating rate of 20°C/min to 400°C followed by a cooling rate of 10°C/min to 50°C under nitrogen. The polymer samples tested were 380 Grade PEEK, a 5 wt% BisP-BTDA TMA^+/PEEK blend, a 5 wt% BisP-BTDA NH_4^+/PEEK blend and an HPC/PEEK blend. Since the blends exhibited melting endotherms, the triplicate scan procedure was useful for a statistical analysis of heats of

melting. Glass transition temperatures were found by using the midpoint of the heat capacity inflection. Temperatures of maximum crystallization were reported as the temperature at the peak of the crystallization exotherm. Melting and crystallization enthalpies were found by calculating the area under the respective peak which was executed by the Seiko DSC software. The crystalline fraction of the sample was determined by dividing the heat of fusion by 130 J/g, which is the heat of formation for 100% pure crystalline PEEK [18] and then dividing by the mass fraction of PEEK in the sample.

Results and Discussion

Model Interphase Characterization

The model interphase BisP-BTDA polyimides were characterized by thermal analysis and gel fraction from a solubility test. The molecular weight distribution could not be measured by gel permeation chromatography because the polyimides were not fully soluble in NMP after thermal imidization. The results from thermal analysis and gel fraction measurements are shown in Table 5-I. The BisP-BTDA polyamic acid that was never dissolved in water was thermally imidized according to the same heat treatment as for the two polyamic acid salts for thermal analysis.

Table 5-I. DSC and solubility test results for BisP-BTDA polyimides and BisP-BTDA polyamic acid.

	BisP-BTDA PI	BisP-BTDA TMA^+ PI	BisP-BTDA NH_4^+ PI
T_g	270°C	240°C	201°C
Imidization Temperatures	97-235°C	161-253°C	117-260°C
5% wt Loss Temperature	489°C	443°C	489°C
Gel fraction after 265°C (NMP)	not measured	29% (swollen gel)	97% (swollen gel)
Gel fraction after 380°C (NMP)	not measured	91% (solid gel)	100% (solid lump)

Solubility Test with Gel Fraction Measurement

The solubility test results including gel fractions for the BisP-BTDA polyimides are shown in Table 5-I. The polyimides that were thermally imidized under the previously described conditions of 265°C for 2 hours were not fully soluble in NMP. The BisP-BTDA TMA^+ polyimide was partially soluble giving rise to a dark yellow solution with a wispy, swollen gel. The BisP-BTDA NH_4^+ polyimide was slightly soluble giving rise to a light yellow solution with a larger amount of wispy, swollen gel observed than for the BisP-BTDA TMA^+ polyimide.

After a heat treatment of 380°C for 30 minutes, the BisP-BTDA TMA^+ polyimide was only slightly soluble and the BisP-BTDA NH_4^+ polyimide was not soluble at all in NMP. The BisP-BTDA TMA^+ polyimide had a measured gel fraction of 91% which was visible as a monolithic, swollen gel and the NMP solution turned light yellow in color. The BisP-BTDA NH_4^+ polyimide had a measured gel fraction of 100% which was visible as a contracted lump of slightly swollen material and the NMP solvent remained water-white.

Differential Scanning Calorimetry of BisP-BTDA Polyimides

Differential scanning calorimetry was used to measure the T_g of the polyimides and the values are listed in Table 5-I. Figure 5-2 shows the DSC scans for the polyimides, with T_g's indicated, after oven imidization. The T_g of the BisP-BTDA TMA^+ polyimide is about 40° greater than the T_g of the BisP-BTDA NH_4^+ polyimide. The T_g of the BisP-BTDA polyimide that was imidized directly from the polyamic acid is about 30° greater than the T_g of the BisP-BTDA TMA^+ polyimide and about 70° greater than the T_g of the BisP-BTDA NH_4^+ polyimide. Those trends are consistent with the trends of the Ultem-type polyimides discussed in Chapter 3 where the T_g's for the Ultem-type TMA^+ polyimide, the Ultem-type NH_4^+ polyimide and the polyimide from the Ultem-type polyamic acid were 203°, 153° and 218°C, respectively.

The glass transition temperatures indicate that the molecular weight of the BisP-BTDA TMA^+ polyimide is greater than the molecular weight of the BisP-BTDA NH_4^+ polyimide after thermal imidization. This follows the observations from the Ultem-type polyimides discussed in Chapter 3 where the molecular weight of the Ultem-type TMA^+ polyimide was about four times greater than the molecular weight of the Ultem-type NH_4^+ polyimide. The trends in T_g also indicate that the molecular weight of the BisP-BTDA polyimide that was imidized directly from the polyamic acid has the greatest molecular weight. The polyimides made from the two polyamic acid salts are not fully soluble in NMP and the gel fractions indicate that the molecular weights are actually very large. However, a comparison of the glass transition temperatures and the solubility test results for the BisP-BTDA NH_4^+ polyimide and the BisP-BTDA TMA^+ polyimide indicate that the BisP-BTDA NH_4^+ sample formed a polyimide with a lower initial molecular weight that then crosslinked extensively while the BisP-BTDA TMA^+ sample formed

a polyimide with a higher initial molecular weight that then crosslinked to a lesser extent.

Thermal Gravimetric Analysis

Thermal gravimetric analysis yields a temperature range of imidization and temperatures for onset of degradation given as a 5% weight loss temperature. The imidization temperatures are reported as the range of temperatures over which the decrease in mass is attributed to the condensation imidization reaction and release of volatile counterion components. These temperature ranges are shown in Table 5-I.

Figure 5-3(a) shows the TGA scan data for the polyamic acid salts during a thermal imidization cycle of two hours at 265°C followed by pyrolysis to 600°C. The difference in imidization temperatures from the BisP-BTDA NH_4^+ polyamic acid salt and the BisP-BTDA TMA^+ polyamic acid salt can be attributed to the relative difference in volatilizing the respective counterion. Before a polyamic acid salt can undergo imidization it must first be converted back into the polyamic acid form [19]. This requires dissociation of the counterion and subsequent volatilization of the counterion. The results show an imidization temperature range for the BisP-BTDA TMA^+ polyamic acid salt that begins 44°C higher in temperature than for the BisP-BTDA NH_4^+ polyamic acid salt.

Figure 5-3(b) shows the TGA scan for the BisP-BTDA polyamic acid during a thermal imidization cycle of 256°C/ 2 hours. The imidization temperature range for the neat BisP-BTDA polyamic acid is 97-235°C. This temperature range is lower than the imidization temperature range for the both BisP-BTDA polyamic acid salts. This can be explained by the absence of a

counterion which would hinder the thermal imidization process.

The span of the imidization temperature range for the neat BisP-BTDA polyamic acid is 138°C, which is comparable to the temperature range of the BisP-BTDA NH_4^+ polyamic acid salt (143°C) but larger than the temperature range of the BisP-BTDA TMA^+ polyamic acid salt (92°).

The 5% weight loss temperatures are used to quantify the onset of degradation. Since a crosslinking mechanism occurs for the model interphase BisP-BTDA polyimides, the structure of these polyimides are altered [20]. This altered structure will have an effect on the thermal stability of the final polyimide. To properly examine the thermal stability of the model interphase polyimide, it is very important to replicate the temperature history that the actual composite interphase will receive. Figure 5-4 shows a TGA scan for a simulated composite consolidation temperature cycle of BisP-BTDA polyimides made from polyamic acid salts that were thermally imidized in an oven at the conditions described previously. The 5 wt% loss temperatures reported are from these scans.

Figure 5-5 is a summary of the critical temperatures identified from the TGA experiments comparing the polyimides made from polyamic acid salts to a polyimide from direct thermal imidization of the polyamic acid. The 5% weight loss temperature for both the BisP-BTDA polyimide and the BisP-BTDA NH_4^+ polyimide was 489°C. The 5% weight loss temperature for the BisP-BTDA TMA^+ polyimide was 46° lower. The greater 5% weight loss temperature for the BisP-BTDA NH_4^+ than for the BisP-BTDA TMA^+ polyimide can be attributed to the greater extent of crosslinking of the polyimide [20].

The pyrolysis of the HPC “fugitive” binder was investigated using TGA as shown in

Figure 5-6. The results show that after the isothermal hold at 325°C for two hours there is 10% HPC char remaining. Therefore most of the "fugitive" binder will be pyrolyzed. However, a small amount is expected to remain in the composite.

Melt Rheology of BisP-BTDA Polyimides

Since the end use of these polyimides will be as an additive in PEEK matrix composites, the processability of the polyimides during a typical thermal treatment for processing PEEK matrix composites was investigated using melt rheology. The thermal cycle of interest was a 5°C/min temperature ramp to 380°C, a 30 minute hold at 380°, and a 10°C/min cooling ramp to room temperature. The cooling cycle is important for the PEEK matrix polymer since it is semicrystalline, but is not of primary concern for the polyimides. Thus, rheology measurements of neat polyimides were made with a frequency of 0.1 Hz and an amplitude of 35% during a 5°C/min heating ramp to 380°C, and 30 minute hold at 380°C. The complex viscosity and temperature are shown with time in Figure 5-7 which reflects the simulated composite consolidation cycle.

The melt rheology during the simulated consolidation thermal cycle also aids in the development of the structure-property relationships of the model interphase BisP-BTDA polyimides. The complex viscosity of the BisP-BTDA TMA^+ polyimide was approximately 29,000 Pa·sec at 290°C. The complex viscosity decreased with increasing temperature until just before the hold temperature of 380°C was reached. At 370°C, the complex viscosity began to increase and continued to increase during the 30 minute isothermal hold. This was confirmation

that crosslinking continued during the 380°C isothermal hold. The complex viscosity at the beginning of the thermal cycle corresponds to a measured gel fraction of 29% and the complex viscosity at the end of the thermal cycle corresponds to a measured gel fraction of 91%.

The complex viscosity of the BisP-BTDA NH_4^+ polyimide was around 49,000 Pa·sec at 290°C. The complex viscosity remained around 38,000 Pa·sec during the initial heating ramp until around 370°C where the complex viscosity began to increase. The complex viscosity at the beginning of the thermal cycle corresponds to a measured gel fraction of 97% and the complex viscosity at the end of the thermal cycle corresponds to a measured gel fraction of 100%.

With regard to the type of counterion used to make the polyamic acid salt, the apparent trends of the melt viscosity are reversed for the BisP-BTDA polyimides from the trends shown with the Ultem-type polyimides in Chapter 3. As seen in Figure 3-9 from Chapter 3, the Ultem-type NH_4^+ polyimide had a much lower initial molecular weight than the Ultem-type TMA^+ polyimide. It was also shown in Chapter 3 that both Ultem-type polyimides were completely soluble in NMP prior to the simulated consolidation thermal cycle. During the simulated consolidation thermal cycle the melt viscosity of both polyimides increased due to crosslinking. After the simulated consolidation thermal cycle the Ultem-type NH_4^+ polyimide had a measured gel fraction of 21% and the Ultem-type TMA^+ polyimide had a measured gel fraction of 13%. The larger gel content for the Ultem-type NH_4^+ polyimide explains the greater relative increase in melt viscosity.

The trends of melt viscosity for the BisP-BTDA polyimides show that the BisP-BTDA NH_4^+ polyimide has a higher initial melt viscosity than the BisP-BTDA TMA^+ polyimide. It was shown that, unlike the Ultem-type polyimides, both of the BisP-BTDA polyimides had a

measured gel content prior to the simulated consolidation thermal cycle. The crosslinking reaction occurred during the 265°C / 2 hour isothermal hold which was designed to imidize the polyamic acid salts. Because of these differences, with regard to crosslinking reactions which are important for processability concerns, the Ultem-type polyimides made from water soluble polyamic acid salts are more thermally stable than the BisP-BTDA polyimides made from water soluble polyamic acid salts.

The BisP-BTDA NH_4^+ polyimide had a 97% gel fraction after thermal imidization at 265°C and the BisP-BTDA TMA^+ polyimide had a 29% gel fraction. The trend of the higher melt viscosity of the BisP-BTDA NH_4^+ polyimide is explained by the higher gel fraction. After the simulated consolidation thermal cycle the BisP-BTDA NH_4^+ polyimide had a 100% gel fraction and the BisP-BTDA TMA^+ polyimide had a 91% gel fraction.

Model Matrix Blend Characterization
Tensile Testing of BisP-BTDA Polyimide/PEEK Blends

The discussion in this next section concerns characterization of binary BisP-BTDA polyimide/PEEK model matrix blends. The blends were prepared using the same preparation techniques as for subsequent composites. The tensile properties of the model matrix blends were measured using a MiniMat tensile testing instrument and the results are shown in Table 5-II. The tensile properties of pure 380 Grade PEEK was also measured and the results are also shown in Table 5-II.

With the exception of tensile strength, tensile data reported in the ICI Victrex data sheet

are also shown in Table 5-II The reported tensile strength of 150 Grade PEEK from the ICI Victrex PEEK data sheet is 94 MPa and the reported tensile strength of 450 Grade PEEK from the ICI Victrex PEEK data sheet is 92 MPa [21]. The 380 Grade PEEK was available for a limited time to special customers of ICI Victrex. Although the data sheets do not include information on the 380 Grade, it was learned from ICI Victrex technical assistance that the only difference between the three grades was molecular weight and that the 150 Grade had the lowest molecular weight, the 450 Grade had the highest molecular weight and the 380 Grade was somewhere in between [22]. According to this information, an estimated tensile strength of 93 MPa for 380 Grade PEEK seems very reasonable which is the value reported in Table 5-II.

Table 5-II. Tensile properties of model matrix blends and neat PEEK.

Model Matrix Blend	Tensile Strength (MPa)	Tensile Modulus (GPa)	Yield Strain (%)	Failure Strain (%)
HPC/PEEK	112 ± 3	2.59 ± 0.07	7.94 ± 1.07	41.25 ± 28.34
BisP-BTDA TMA^+/PEEK	109 ± 6	2.59 ± 0.07	6.86 ± 0.44	11.87 ± 3.41
BisP-BTDA NH_4^+/PEEK	110 ± 2	2.51 ± 0.03	7.58 ± 0.051	14.41± 6.10
380 Grade PEEK	93 ± 15	2.04 ± 0.14	5.68 ± 0.92	30.45 ± 23.98
PEEK	~93*	3.6 ref [23]	4.8 *	90 ref [24]

* tensile data estimated from ICI Victrex data sheet.

A quantitative comparison of the tensile data is desirable to verify which data sets are statistically different. The sets of data for the model matrix blends were statistically compared using an unpaired *t*-test executed with SigmaStat Statistical Software v. 2.0. The unpaired *t*-test

is used to test for a difference between two groups that is greater than what can be attributed to random sampling variation. The SigmaStat Statistical Software first tests for normally distributed populations using a Kolmogorov-Smirnov test, and then tests for equal variance by checking the variability about the group means. If the sample populations each pass these tests, then the unpaired *t*-test is executed using a confidence interval of 95%. The unpaired *t*-test is a parametric test based on estimates of the mean and standard deviation parameters of the normally distributed populations from which the samples were drawn.[25]

If two sets of data pass an unpaired *t*-test, then there is a 95% confidence that the difference in the mean values of the two groups is greater than would be expected by chance. Therefore, there is a statistically significant difference between the groups [25]. However, if the two sets of data fail an unpaired *t*-test, then it is concluded that the data sets are not statistically different.

The tensile data for the three model matrix blends were analyzed using the unpaired *t*-test and the results are shown in Table 5-III. The results show that there is not a significant statistical difference in the tensile strengths of the three model matrix samples. The *t*-test results indicate that the BisP-BTDA NH_4^+ /PEEK model matrix blend and the HPC/PEEK model matrix blend have a statistically significantly different tensile modulus, however, comparison of the actual data shows this difference to be less than 3%.

Table 5-III. Unpaired *t*-test results for comparisons of tensile data for model matrix blends.

	tensile strength	tensile modulus	yield strain	failure strain
HPC/PEEK vs. BisP-BTDA TMA^+/PEEK	fail	fail	fail	pass
HPC/PEEK vs. BisP-BTDA NH_4^+/PEEK	fail	pass	fail	fail
BisP-BTDA TMA^+/PEEK vs. BisP-BTDA NH_4^+/PEEK	fail	fail	pass	fail

pass = statistically significant difference between data sets
fail = no statistical difference between data sets

The tensile yield strain is shown to be statistically different for the BisP-BTDA TMA^+/PEEK model matrix blend compared to the BisP-BTDA NH_4^+/PEEK model matrix blend. The difference in the mean values of these yield strains is less than 10%.

The tensile failure strain is shown to be statistically different for the HPC/PEEK model matrix blend and the BisP-BTDA TMA^+/PEEK model matrix blend. The mean value for the tensile yield strain for the HPC/PEEK model matrix blend was the largest of all the samples tested.

Although the ASTM D 1708-93 procedure is a standardized testing method for tensile properties of plastics by use of micro-tensile specimens, it is much more desirable to measure tensile properties with larger test specimens. The literature values from commercial product data sheets for the tensile properties are reported using ASTM D 638 standardized testing procedure. This procedure uses larger test specimens which can be tested in a larger, more precise instrument. One of the biggest problems with the Minimat testing instruments is slippage of the specimen at the grips. The grips are simple, ridged metal clamps with a pair of screws which

apply pressure to secure the specimen ends. As the specimen is deformed in tension there will be a corresponding deformation in the thickness of the sample, yet there is no compensation in grip pressure. This results in slippage of the specimen at the grips. This point should be kept in mind when considering the discussion of the measured tensile strain properties. Although the strain data and consequently the moduli data from the Minimat tensile tests suffer in comparison to strain and moduli measurements from more sophisticated instruments, the results are internally consistent and provide a meaningful comparison within the data set.

The standard deviations for the strain-to-failure for the HPC/PEEK model matrix blend and the neat 380 Grade PEEK samples are very large. This is a consequence of the difficulty in melt-pressing a void free film of PEEK. Some of the PEEK films had some very small, visible voids that appeared to be a result of entrapped air. Some samples were visibly free of voids. This resulted in measured failure strain as high as 73.0% and as low as 16.2% for the 380 Grade PEEK samples. The voids present in the samples act as stress concentrations, decreasing the local cross sectional area and thereby increasing the stress at that location. The large, visible voids were not observed in the BisP-BTDA polyimide/PEEK blends. It is not known why these macroscopic voids occurred with the neat 380 Grade PEEK and not with the polyimide/PEEK blends. The HPC/PEEK blend had a higher mean failure strain than the pure PEEK sample. Visual observations for the HPC/PEEK blend were that the film was void free and brown in color. The pure PEEK film was grey in color. The brown color of the HPC/PEEK blend is an indication that residual HPC char from incomplete pyrolysis was present in the blend. The overall concentration of HPC char in the blend is very low as shown by the TGA experiments.

Although the model matrix tensile samples are shown to poorly represent the actual

matrix material **at high strains** due to sample defects and grip slippage, these high tensile strain properties are less important than the lower strain properties. In the actual composite material, bulk loading occurs only at low strains because the reinforcing fibers bear most of the load. The tensile modulus for AS-4 carbon fiber is 234 GPa and the strain to failure is 1.61% [26]. Therefore in the actual composite system fiber tensile strains of greater than 1.61% will inevitably lead to catastrophic failure of the composite and are irrelevant when modeling the matrix behavior. The fibers have a high modulus and a low strain to failure compared to the model matrix properties. Therefore only low strains of the model matrix samples are reasonable for comparison to the actual composite matrix system.

Melt Rheology of BisP-BTDA Polyimide/PEEK blends

The complex melt viscosity of binary model matrix blends was characterized. Figure 5-8 shows that the low frequency (0.002 sec^{-1}) complex viscosity of the BisP-BTDA NH_4^+/PEEK blend is higher than that of the BisP-BTDA TMA^+/PEEK blend. Also, the HPC/PEEK blend has the highest melt viscosity of the three model matrix blends which is unexpected. From the TGA results earlier in this chapter for HPC , it was shown that 10% of the HPC remains after a 325°C, 2 hour isothermal hold. It is possible that in the presence of PEEK, even more than 10% of the HPC would survive pyrolysis. The brown color observed for the HPC/PEEK blends indicates visually that the HPC was not completely pyrolyzed from the mixture. The Klucel product data sheet reports a weight average molecular weight of 80,000 for the grade of HPC used [16]. After the 325°C isothermal hold, the high molecular weight HPC would probably exist as a charred

material. The high melt viscosity of the HPC/PEEK blend could be attributed to the presence of high molecular weight HPC char.

Two of the model matrix blends have a much higher melt viscosity at low frequencies than 380 Grade PEEK. However, the melt viscosity of the BisP-BTDA TMA^+/PEEK blend is very similar to that of neat PEEK. This is a good indication that polyimide crosslinking, which has been shown to occur in the BisP-BTDA TMA^+ polyimide, may be somewhat suppressed in the model matrix blend. This could be attributed to the miscible nature of the two polymers.[15] The measured gel fraction of the BisP-BTDA TMA^+ polyimide was 29% and increases at temperatures above 370°C as shown by melt rheology. The melting temperature of PEEK is around 345°C. Thus, at temperatures above 345°C, the crystalline domains of PEEK would be melting and all the PEEK would be available for interdiffusion. This is contrary to the behavior of the Ultem-type polyimides discussed in Chapter 3. The Ultem-type TMA^+ polyimide began to crosslink at a temperature around 350°C as shown by melt rheology, only about 5° above the melting temperature of PEEK such that significant interdiffusion could not occur before the crosslinking began.

The data shown in Figure 5-8 for the BisP-BTDA TMA^+ polyimide/PEEK blend are from frequency sweeps starting from low frequency increasing in frequency up to 0.1 Hz and then decreasing in frequency back to the starting frequency. As seen in Figure 5-8, the curves do not overlap each other. There is a time difference of 42 minutes from the first data point at 0.002 Hz and the last data point at 0.002 Hz. During this 42 minute isothermal hold at 380°C, the complex viscosity of the blend increased from 5,117 Pa·s to 17,665 Pa·s. Therefore, although the crosslinking mechanism may be suppressed, it is not eliminated. During this isothermal hold the

melt viscosity of neat PEEK also increased from an initial value of 5,310 Pa·s to a final value of 7,650 Pa·s. The increase in melt viscosity of PEEK during an isothermal hold has been attributed to chain scission followed by crosslinking by Day et al. [27].

An explanation for the higher melt viscosity for the BisP-BTDA NH_4^+/PEEK model matrix blend is the large gel fraction of the polyimide component after thermal imidization. It is important to recall the complex viscosity of the model interphase polyimides during a simulated consolidation temperature cycle from Figure 5-7 at this point. It was shown in Figure 5-7 that the melt viscosity of the BisP-BTDA NH_4^+ polyimide was very high at the beginning of the thermal cycle and increased during the isothermal hold at 380°C. The complex viscosity of the BisP-BTDA TMA^+ polyimide increased significantly during the 380°C isothermal hold but was significantly lower than for the BisP-BTDA NH_4^+ polyimide early in the thermal cycle. The model matrix blend trends for melt viscosity are at least consistent with the model interphase polyimide trends. This provides evidence that chemically active species are present in the interphase polyimides. The BisP-BTDA polyimide/PEEK blends also have chemically active species present in the polyimide component allowing for possible chain extension and/or crosslinking.

Differential Scanning Calorimetry of BisP-BTDA Polyimide/PEEK blends

Differential scanning calorimetry was used to find the glass transition temperatures for the BisP-BTDA polyimide/PEEK blends and also to quantify the effect of the presence of the polyimide on the crystalline content of the PEEK fraction.

The DSC traces from a heating scan are shown in Figure 5-9 for the model matrix blends and the neat 380 Grade PEEK. A single glass transition temperature was found for the blends indicating no phase separation. Since the neat polyimides processed from water soluble polyamic acid salts have been shown to crosslink by melt viscosity measurements in the temperature range used to consolidate the composites, it is possible that during the pressing of the polymer blend films, the polyimide would not be well mixed with the PEEK before crosslinking could occur. While the concentration of BisP-BTDA polyimide is low, making interpretation inconclusive, the presence of a single T_g for the 5 wt% polyimide/PEEK blends is consistent with the interpretation that the blend is well mixed.

As seen in Figure 5-9, the glass transition temperatures are all similar and the calculated PEEK crystalline fractions for the three blends are also very close. These are indications that the microstructures of the blends are similar.

The DSC traces from a cooling scan are shown in Figure 5-10. Once again, a single T_g was observed, the values of T_g were all very similar and the calculated crystalline fractions were all very similar. The glass transition temperatures, the heats of melting, heats of crystallization and calculated crystalline fractions are tabulated in Table 5-IV.

The temperatures of maximum crystallinity, T_x^{max}, as defined by the temperature at the peak of the crystallization exotherm, are labeled in Figure 5-10. Among all the model matrix blends the T_x^{max} for the HPC/PEEK blend is the highest at 284°C.

Table 5-IV. Heats of melting, heats of crystallization, glass transition temperatures and calculated crystalline fractions of PEEK component for model matrix blends and neat PEEK.

	Δh^f (J/g) (heating)	T_g (°C) (heating)	X_c (%) (heating)	Δh^f (J/g) (cooling)	T_g (°C) (cooling)	X_c (%) (cooling)
HPC/PEEK	49.2	155	40	47.5	149	38
BisP-BTDA TMA^+ PI/PEEK	48.6	158	39	47.5	152	38
BisP-BTDA NH_4^+ PI/PEEK	48.0	157	39	47.3	152	38
neat 380 Grade PEEK	48.4	155	37	43.9	149	34

The crystallization of the neat 380 Grade PEEK sample was rapid and spontaneous, as represented by the relatively sharp crystallization exotherm during the cooling scan.

Conclusions

The purpose of this work was to prepare and characterize model interphase and model matrix samples to represent the polymeric material in BisP-BTDA polyimide interphase/PEEK matrix composites. For this work, BisP-BTDA polyimides were made from water soluble polyamic amic acid salts.

The BisP-BTDA NH_4^+ polyimide had a glass transition temperature of 201° and a gel fraction of 97%. The BisP-BTDA TMA^+ polyimide had a glass transition temperature of 240°C and a gel fraction of 29%. The melt viscosity of the BisP-BTDA NH_4^+ polyimide was higher at all temperatures during the simulated consolidation thermal cycle than the BisP-BTDA TMA^+ polyimide. After a simulated consolidation thermal treatment of 380°C/30 minutes, the BisP-

BTDA NH_4^+ polyimide had a gel fraction of 100% and the BisP-BTDA TMA^+ polyimide had a gel fraction of 91%. The increase in melt viscosity during a simulated thermal processing cycle and an increase in measured gel fraction after a simulated thermal processing cycle both indicate that crosslinking occurs at temperatures above 370°C.

The BisP-BTDA NH_4^+ polyimide had a 5% weight loss temperature of 489°C and the BisP-BTDA TMA^+ polyimide had a 5% weight loss temperature of 443°C. After a simulated pyrolysis temperature cycle of 325°C for two hours, 10 wt% of HPC remained.

Model matrix BisP-BTDA polyimide/PEEK blends were prepared according to identical conditions as for aqueous suspension prepregging. Tensile testing of model matrix blends showed that the tensile yield strengths were statistically similar for all blends. This is an important conclusion because it provides verification that even if all the BisP-BTDA polyimide diffused completely into the bulk matrix, the mechanical properties are similar. Therefore, any differences in composite performance can be attributed to differences in interphase properties.

The melt viscosities of the model matrix blends were characterized. The HPC/PEEK blend film was brown in color indicating the presence of charred HPC. The HPC/PEEK blend had the highest melt viscosity at low shear rates and the BisP-BTDA NH_4^+ polyimide/PEEK blend had the second highest melt viscosity at low shear rates. The melt viscosity of the BisP-BTDA TMA^+ polyimide/PEEK blend was very similar to the melt viscosity of neat PEEK during the first half of the rheological test. After a 42 minute residence time in the viscometer oven at 380°C the melt viscosity of the BisP-BTDA TMA^+ polyimide/PEEK blend was much higher than the corresponding melt viscosity of neat PEEK. These results are indications that chemically active species attributed to the polyimide are present in the blend. The high melt

viscosity of the HPC/PEEK blend compared to neat PEEK can be attributed to the presence of domains of charred HPC.

Miscibility of the BisP-BTDA polyimide and PEEK was suggested by a single T_g for 5 wt% BisP-BTDA polyimide/PEEK blends. The glass transition temperatures and calculated crystalline fraction of the PEEK component for the model matrix blends were all similar.

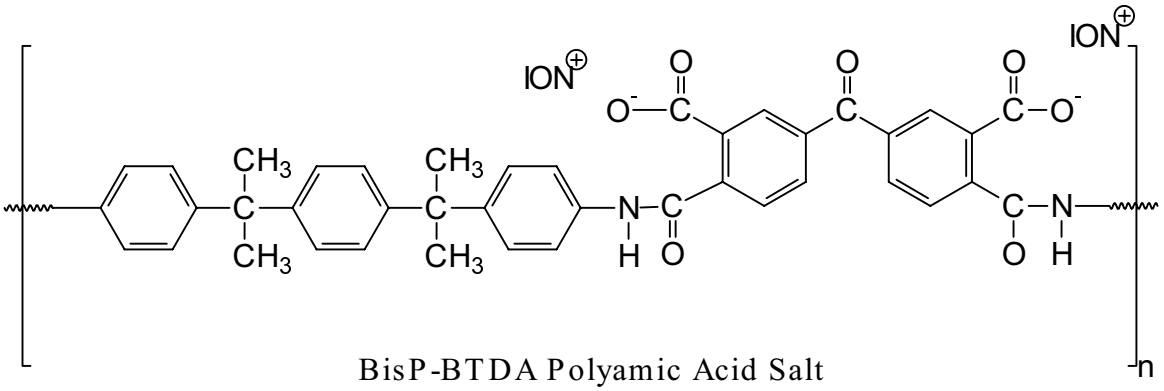

BisP-BTDA Polyamic Acid Salt

Thermal Imidization
265℃/ 2 hours

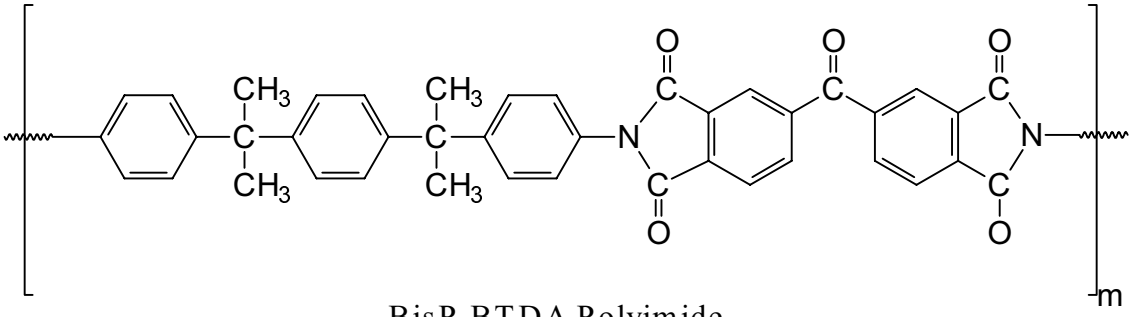

BisP-BTDA Polyimide

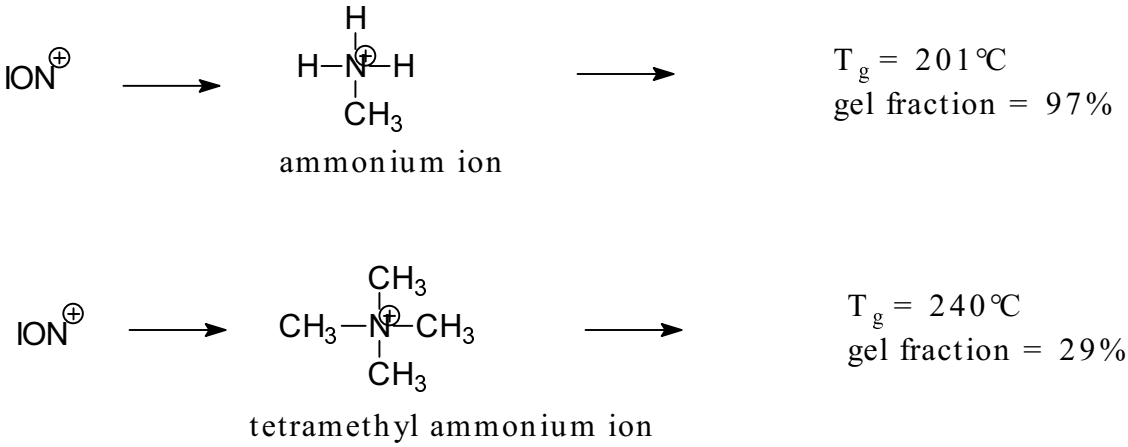

Figure 5-1. Formation of BisP-BTDA polyamic acid salt using two different bases for counterions and the resulting glass transition tempteratures and gel fractions of the resulting polyimide after thermal imidization.

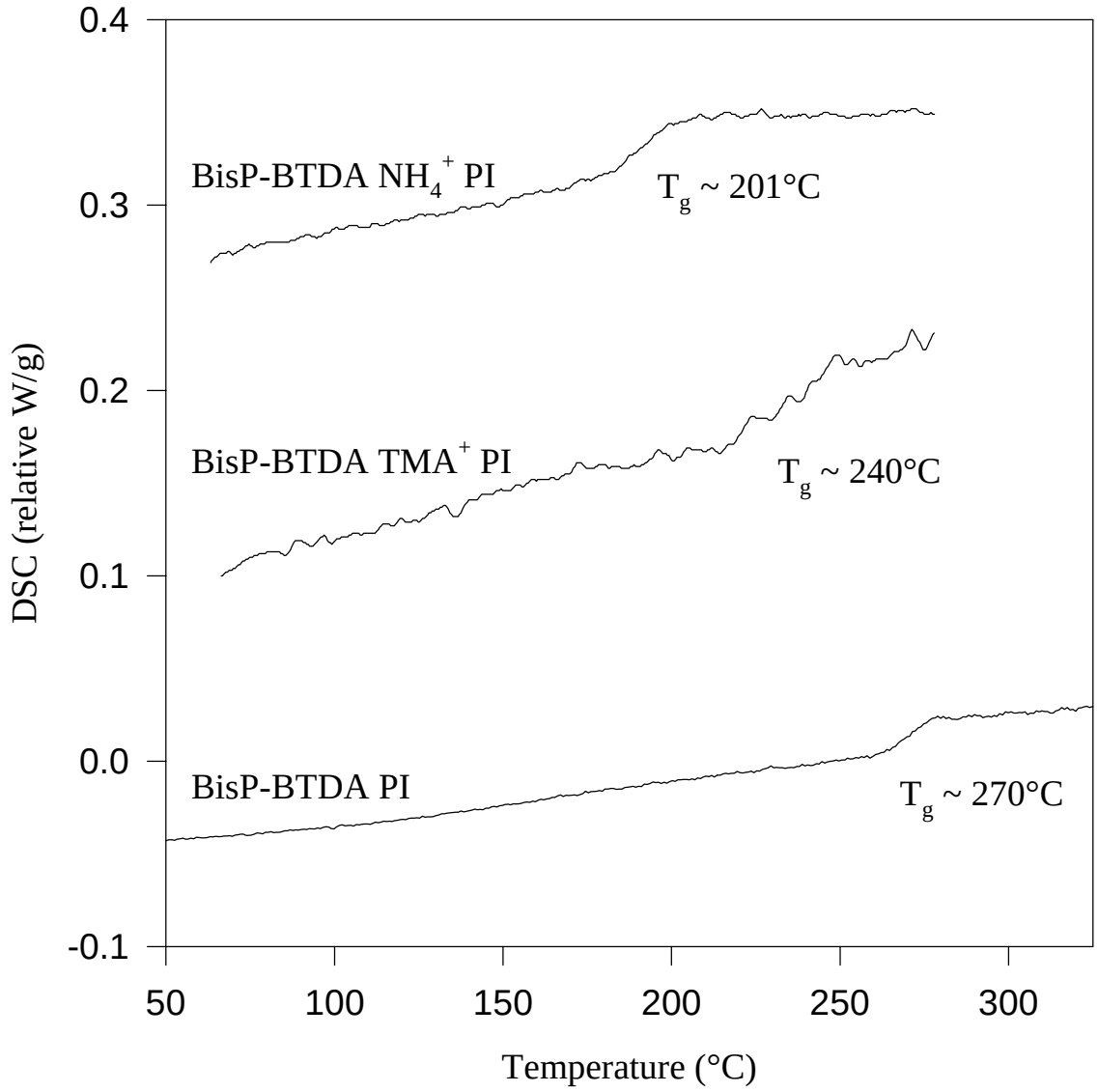

Figure 5-2. DSC traces for BisP-BTDA polyimides.

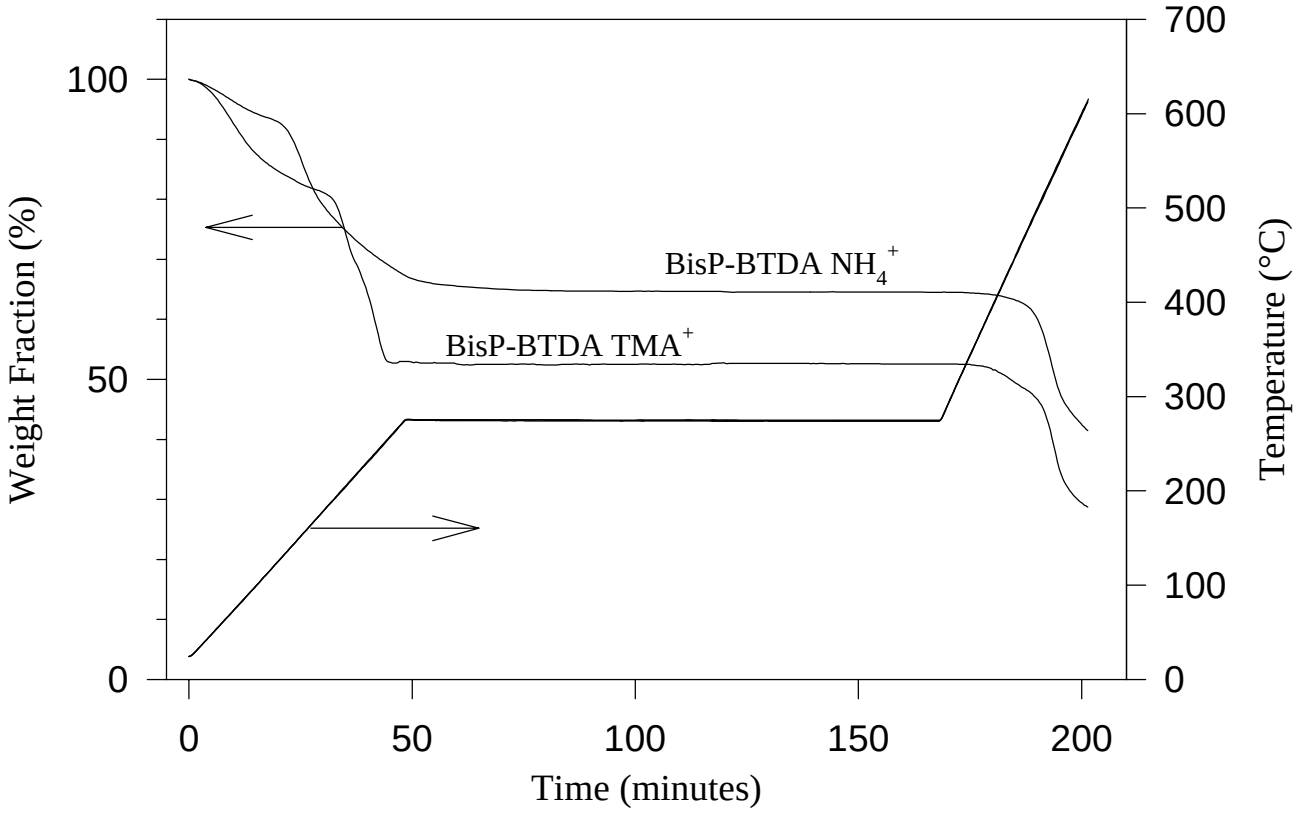

Figure 5-3(a). Weight loss of BisP-BTDA polyamic acid salts shown by TGA scan during standard thermal imidization cycle.

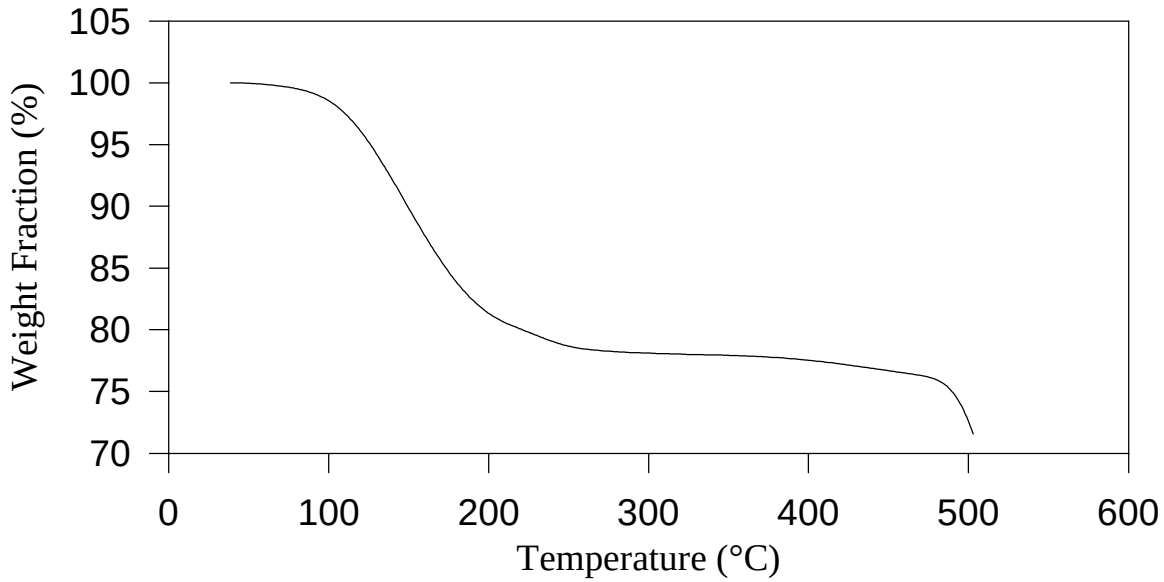

Figure 5-3(b). Weight loss of BisP-BTDA polyamic acid shown by a TGA scan during 10°C/min temperature ramp.

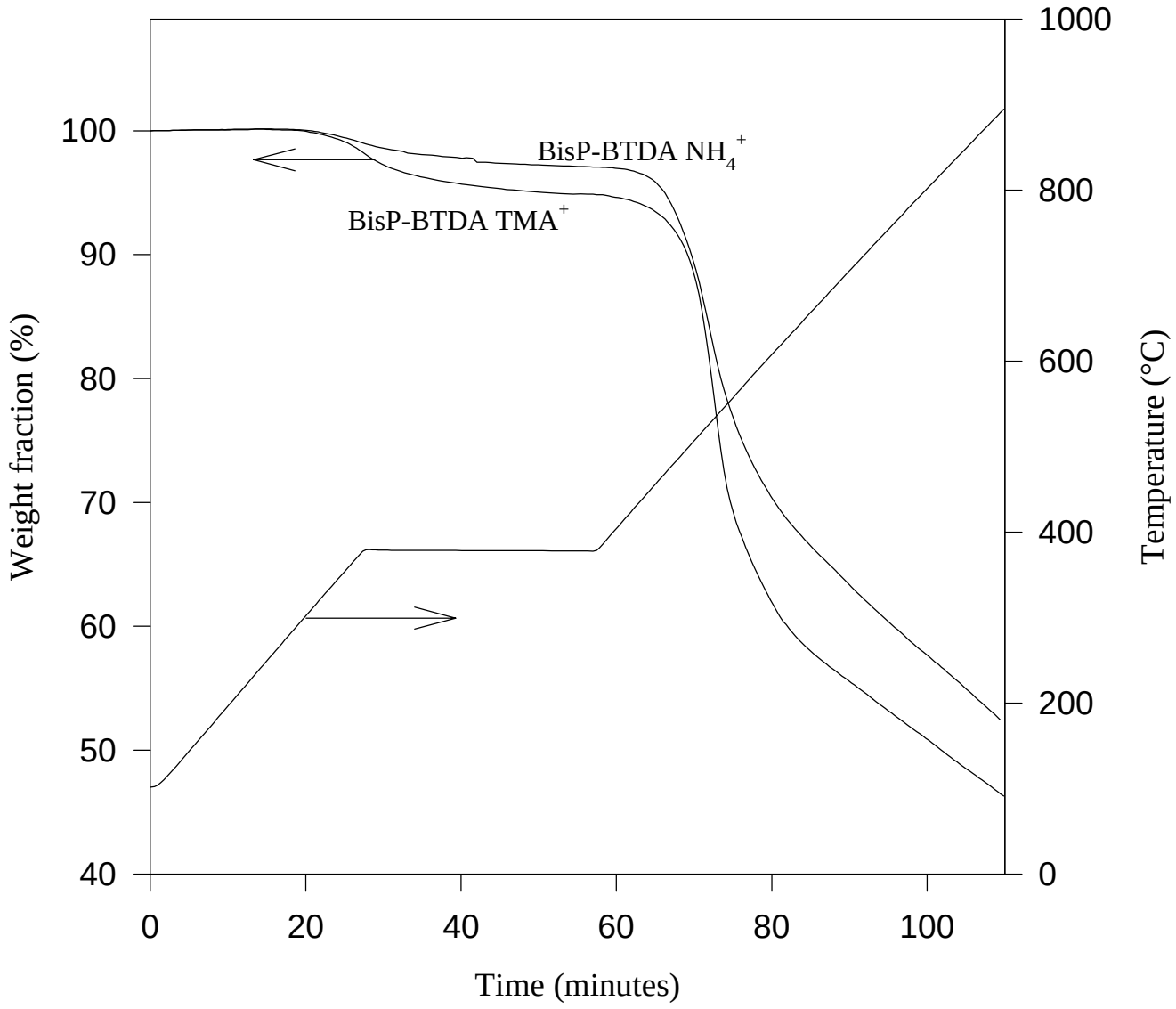

Figure 5-4. Weight loss of BisP-BTDA polyimides during simulated consolidation temperature cycle.

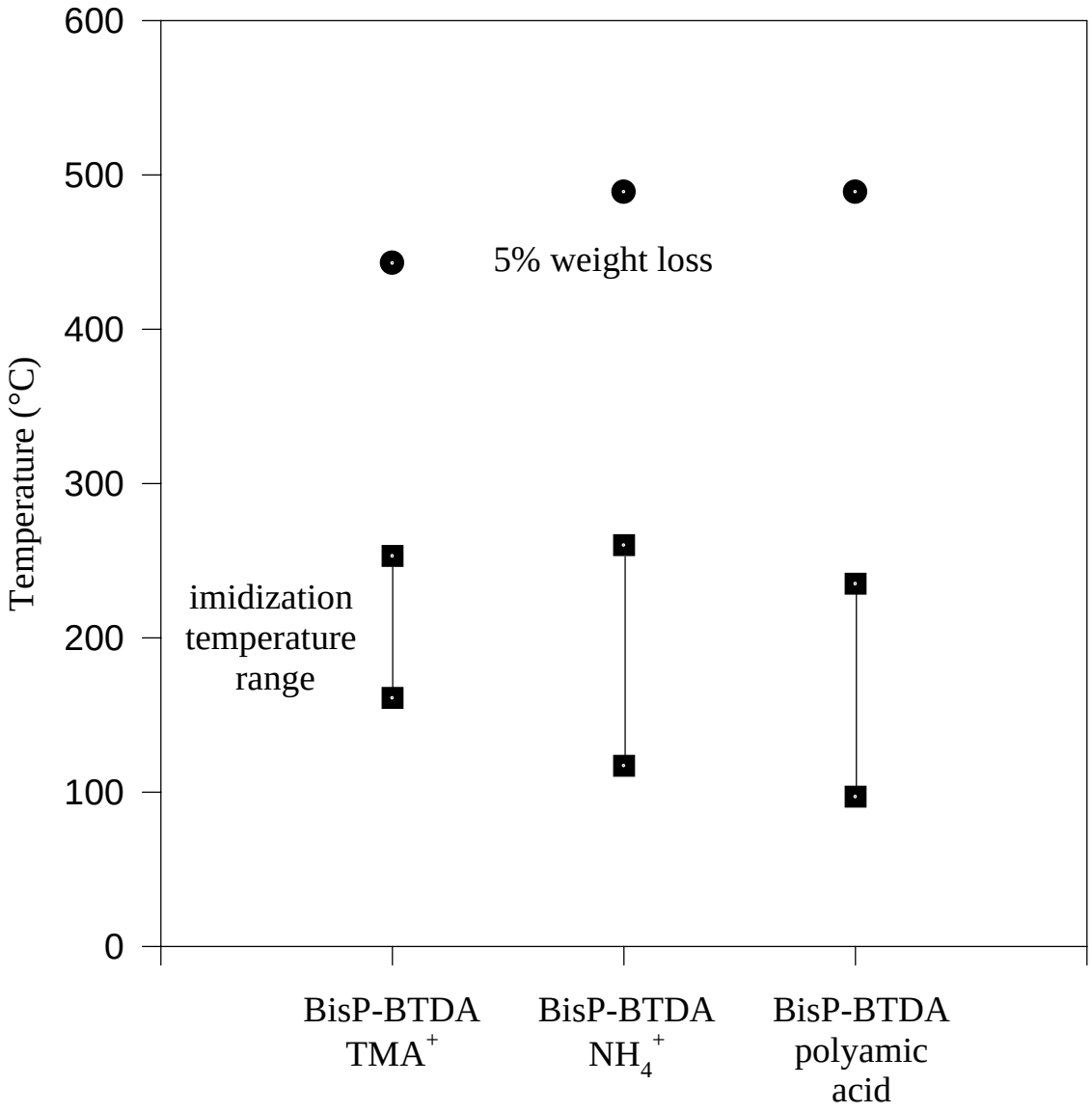

Figure 5-5. Imidization temperature ranges for BisP-BTDA polyamic acid salts and 5% weight loss temperatures for BisP-BTDA polyimides.

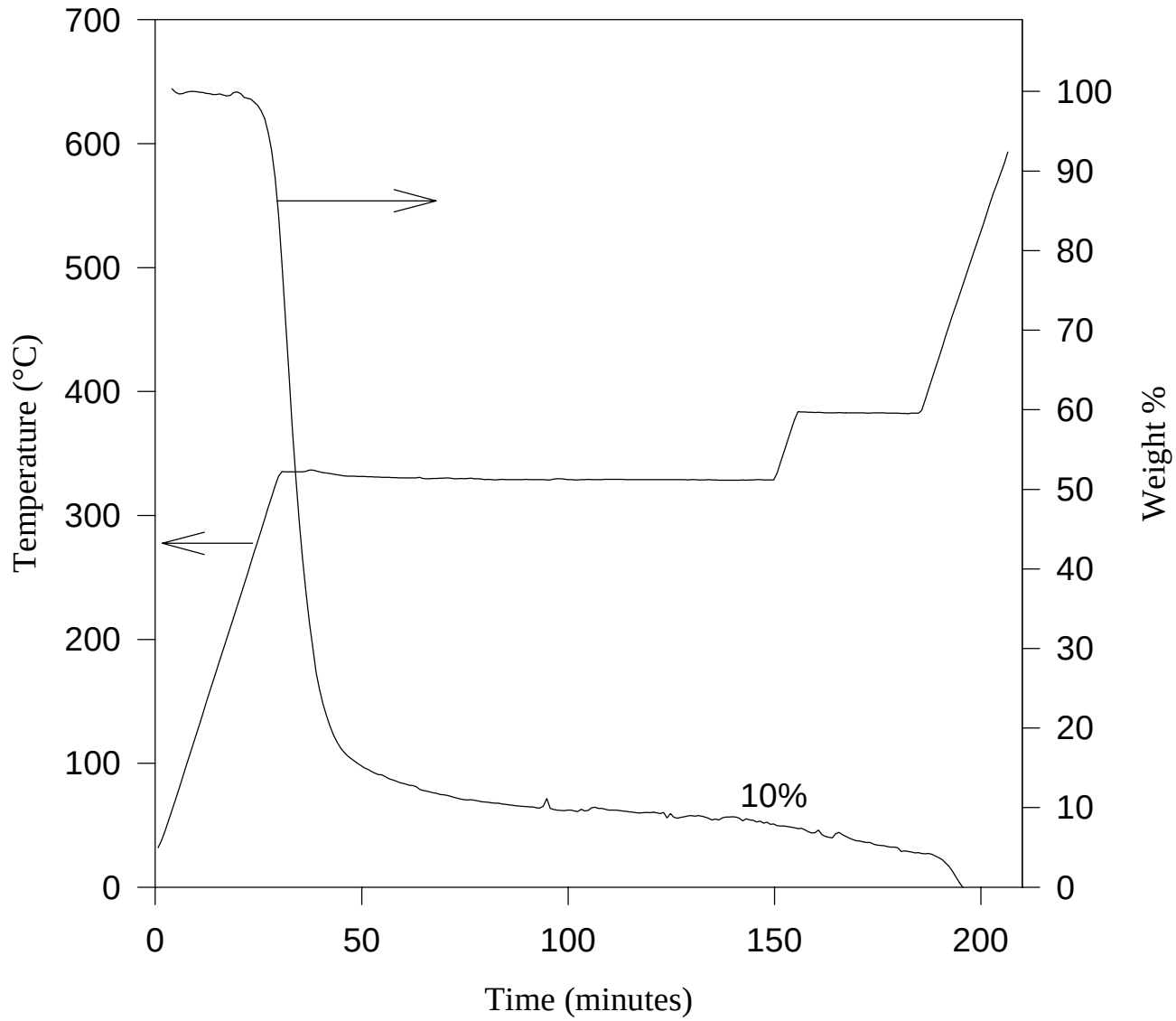

Figure 5-6. TGA scan for HPC fugitive binder during pyrolysis thermal cycle followed by simulated composite consolidation isothermal hold and a ramp to 600°C.

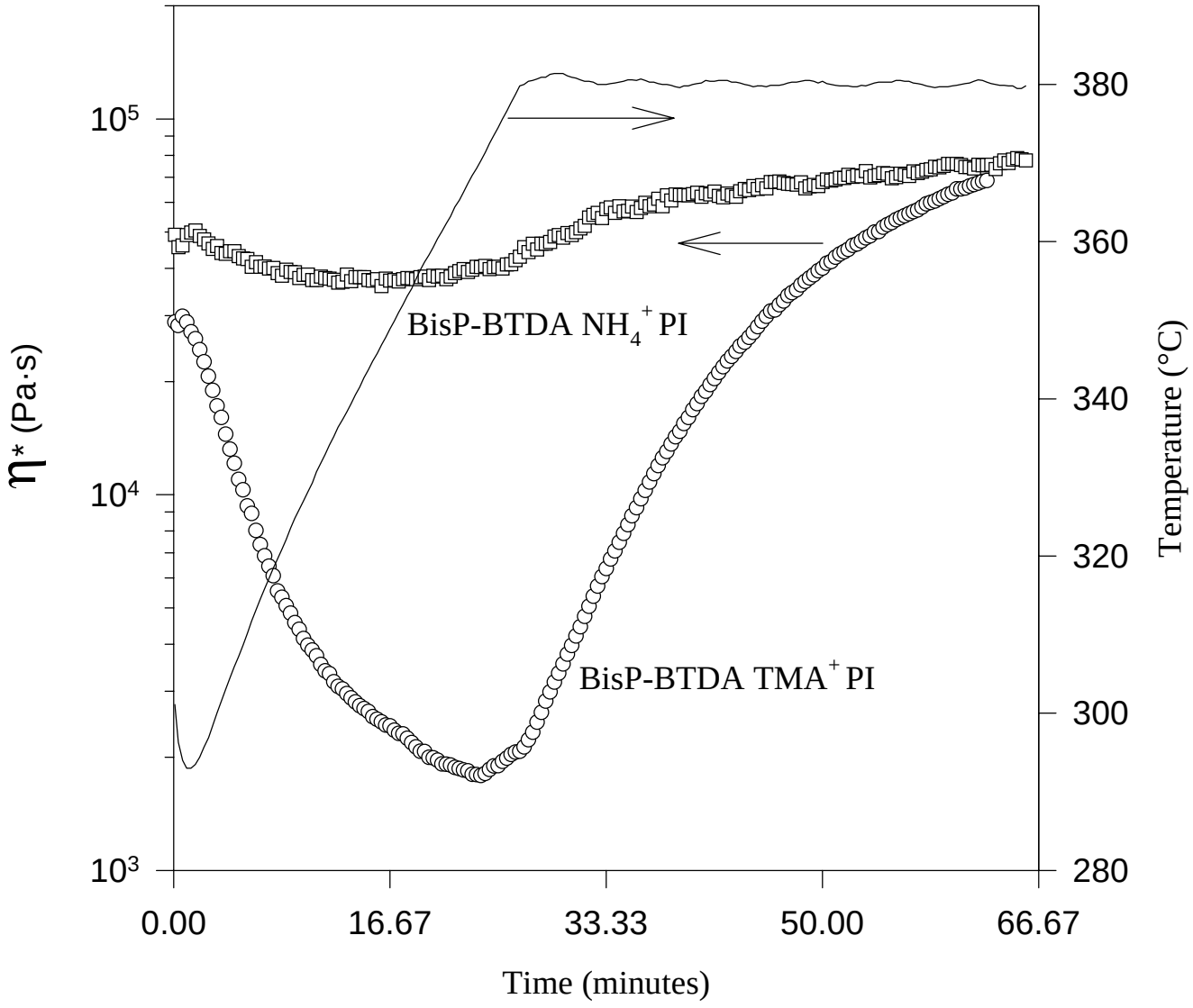

Figure 5-7. Complex viscosity vs time for BisP-BTDA polyimides during simulated consolidation thermal cycle.

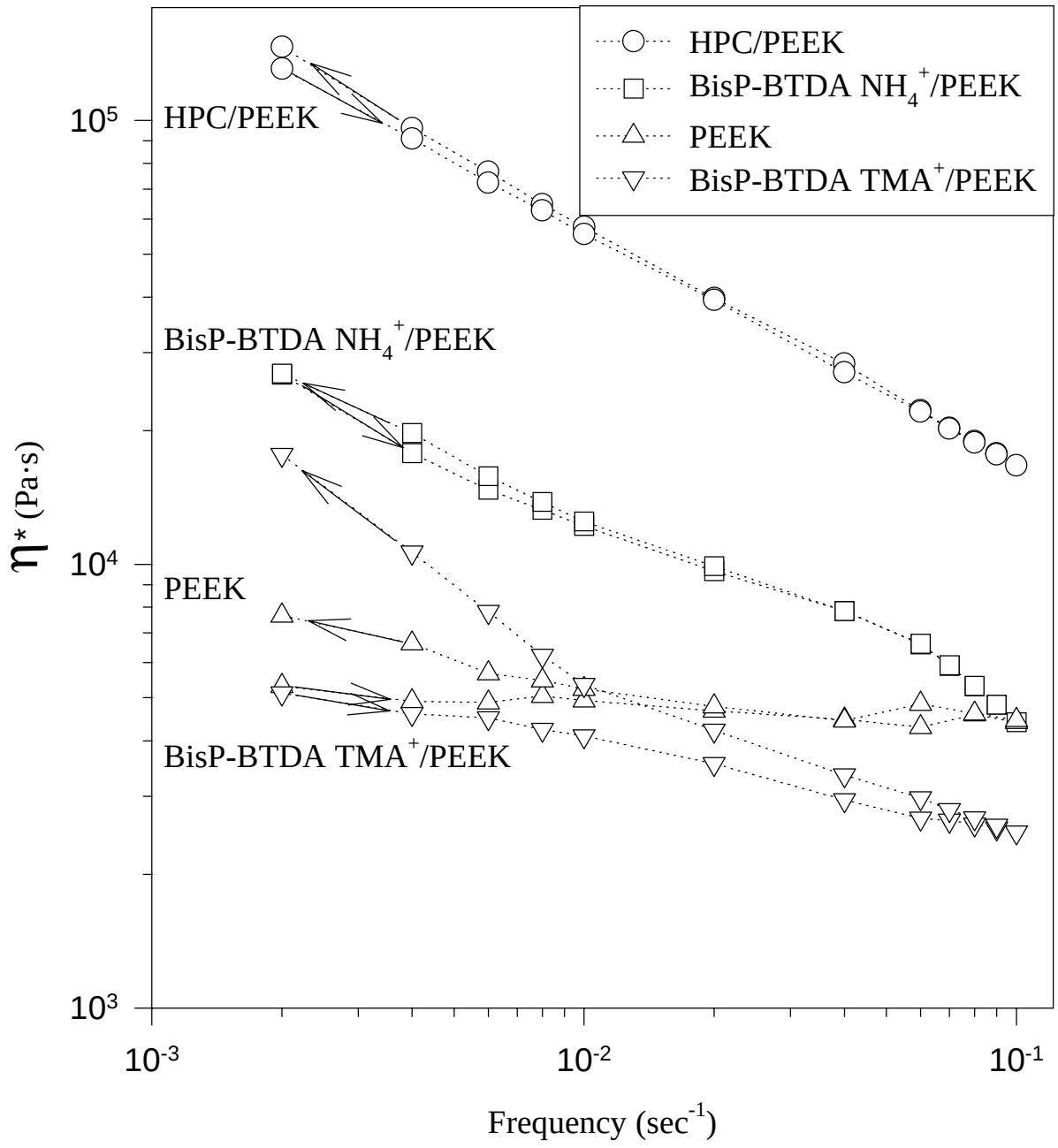

Figure 5-8. Complex viscosity vs frequency at an amplitude of 35% for model matrix PEEK blends and neat PEEK.

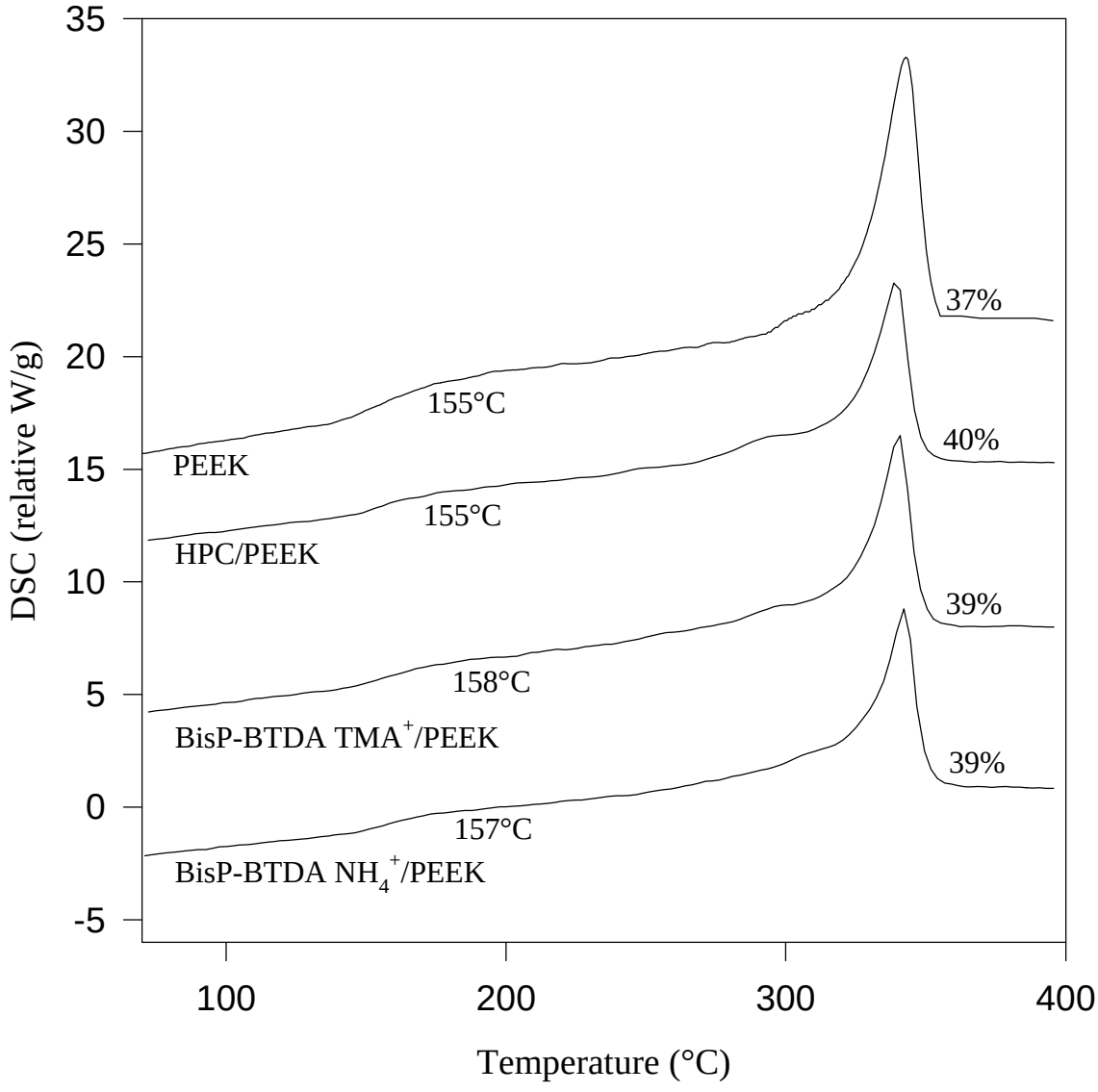

Figure 5-9. DSC traces for model matrix blends and neat PEEK.

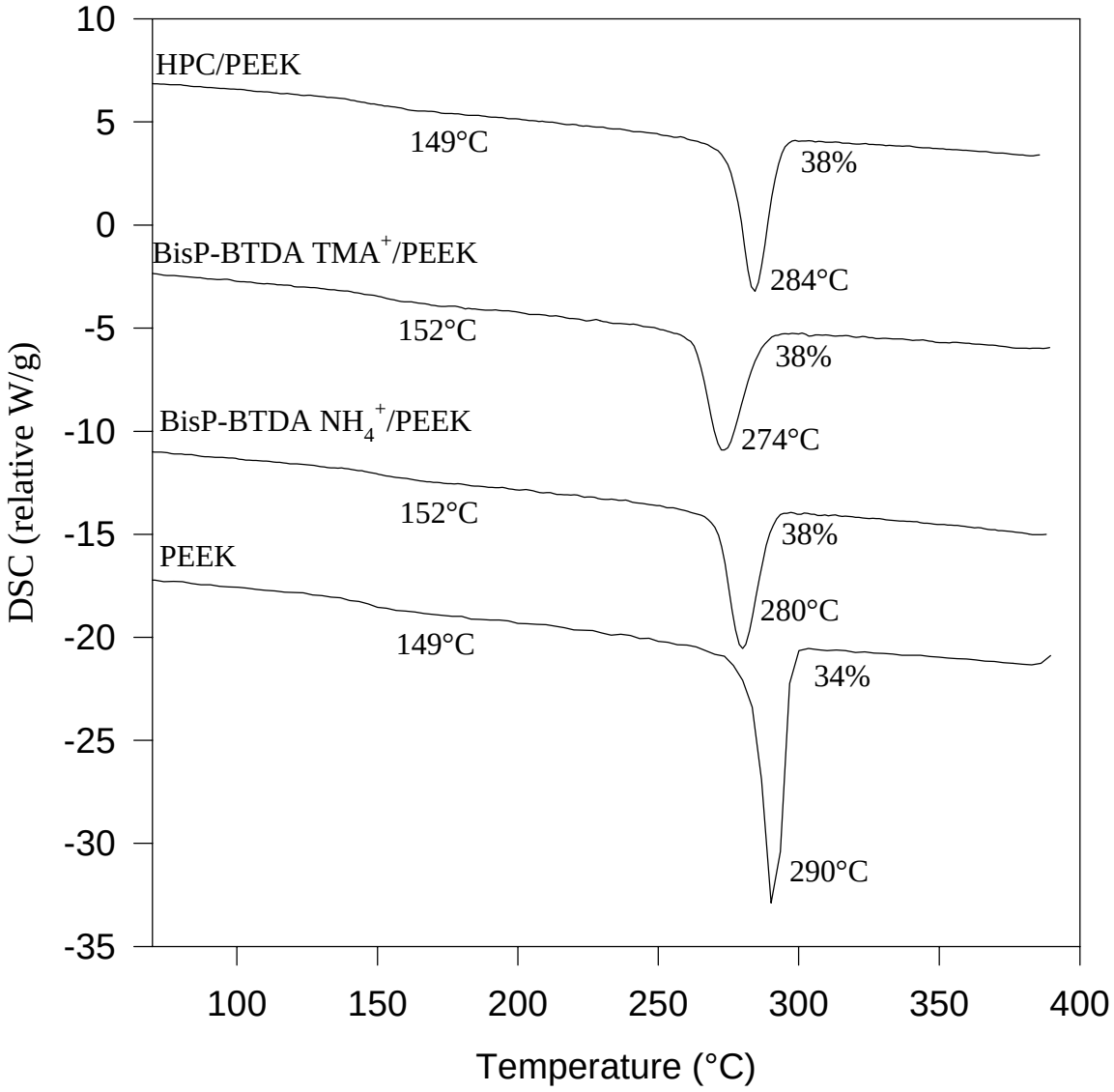

Figure 5-10. DSC cooling traces for model matrix PEEK blends and neat PEEK.

References

1 Reifsnider, K.L., *Composites*, **25**, 461 (1994).

2 Lesko, J.J., Swain, R.E., Cartwright, J.M., Chen, J.W., Reifsnider, K.L., Dillard, D.A., and Wightman, J.P., *Journal of Adhesion*, **45**, 43 (1994).

3 Subramanian, S., Lesko, J.J., Reifsnider, K.L., and Stinchcomb, W.W., *J. Compos. Mater.*, **30**, 309 (1996).

4 Chang, Y.S, Lesko, J.J., Case, S.W., Dillard, D.D., and Reifsnider, K.L., *Journal of Thermoplastic Composite Materials*, **7**, 311 (1994).

5 Gao, Z., Reifsnider, K.L., and Carman, G., *J. Compos. Mater.*, **26**, 1678 (1992).

6 Carman, G.P., Lesko, J.J., and Reifsnider, K.L., *Composite Materials: Fatigue and Fracture, Fourth Volume, ASTM STP 1156*, W.W. Stinchcomb and N.E. Ashbaugh, Eds., American Society for Testing and Materials, Philadelphia, PA, p. 430, 1993.

7 Case, S.W., Carman, G.P., Lesko, J.J., Fajardo, A.B., and Reifsnider, K.L., *J. Compos. Mater.*, **29**, 208 (1995).

8 The Effect of Polyimide Interphases on Properties of PEEK-Carbon Fiber Composites. S.Gardner, A. Gonzalez, R.M. Davis, J.V. Facinelli, J.S. Riffle, S. Case, J.J. Lesko, K.L. Reifsnider, *AIChE 1995 Annual Meeting.* November 12-17, 1995. Miami, FL.

9 Yu, T.H. and Davis, R.M., *J. Thermoplast.Comp. Mater.*, **6**, 62 (1993).

10 Texier, A., Davis R.M., Lyon, K.R., Gungor, A., McGrath, J.E., Marand, H., and Riffle, J.S., Polymer, **34**, 896 (1993).

11 Gonzalez, A-I, M.S. Dissertation (Virginia Polytechnic Institute and State University, Blacksburg, VA, November 1992)

12 Gonzalez-Ibarra, A., Davis, R.M., Heisey, C.L., Wightman, J.P., and Lesko, J.J., *Journal of Thermoplastic Composite Materials*, **10**, 85 (1997).

13 Davis, R.M., and Texier, A., *ANTEC '91 Confer. Proceed.*, **37**, 2018 (1991).

14 Jonas, A. and Legras, R., *Chapter 3, Assessing the Crystallinity of PEEK*, Advanced Thermoplastic Composites, Ed. H.H. Kausch and R. Legras, Hanser Publications, New York, NY (1993).

15 McGrath, J.E., Rogers, M.E., Arnold, C.A., Kim, Y.J. and Hedrick, J.C., *Makromol. Chem., Macromol. Symp.*, **51**, 103 (1991).

16 Aqualon, Klucel Hydroxypropylcellulose Physical and Chemical Properties, product data sheet.

17 Reynolds, R.J.W., and Seddon, J.D., *J. Polym. Sci., Pt. C.*, **23**, 45 (1968).

18 Baxandall, L.G., *Macromolecules*, **22**, 1982 (1989).

19 Facinelli, J.V. *PhD Dissertation* (Virginia Polytechnic Institute and State University, Blacksburg, VA, (1996).

20 Cella, J. A., *Polymer Degradation and Stability* **36**, 99 (1992).

21 ICI Victrex PEEK product data sheet.

22 telephone consultation with ICI Victrex technical service.

23 Jar, P.-Y. and Plummer, Ch.J.G., Chapter 4, The Physical Structure and Mechanical Properties of Poly(Ether Ether Ketone), Advanced Thermoplastic Composites, Ed. H.H. Kausch and R. Legras, Hanser Publications, New York, NY (1993).

24 Harper, Handbook of Plastics, Elastomers and Composites, 2nd edition, McGraw-Hill,New York, NY (1990).
25 Sigma-Stat Statistical Software v. 2.0 User's Manual, Jandel Scientific, San Rafael, CA (1992-1995).
26 Hercules AS-4 Product data sheet.
27 Day, M., Sally, D., and Wiles, D.M., *J.of Appl. Polym. Sci.*, **40**, 1615 (1990).

Chapter Six: Fabrication and Characterization of Carbon Fiber PEEK matrix composites with BisP-BTDA Polyimide Interphases of Tailored Properties for Studying the Effect of Interphase Modifications

Introduction

An important way to improve composite performance and durability is by modifying the interphase. The interphase region is defined as the transition zone between the reinforcing fiber and the bulk matrix in a composite. An interphase typically accounts for less than 2% of the total mass of material in a composite [1]. However, carefully modified interphases have been shown to improve composite longitudinal tensile strength by as much as 29% [2], compressive strength by as much as 50% and notched fatigue lifetime cycles by as many as two orders of magnitude [3]. Therefore, the benefits of implementing a carefully constructed interphase are obvious.

Many models based on the micro-mechanics of failure have been proposed for prediction of composite strength and lifetime. The most recent models proposed by Reifsnider et al. incorporate an interphase region with significantly different material properties from the matrix polymer [1,3-8]. These models have been used to formulate hypotheses regarding further improvements of composite performance and durability based on interphase modifications.

The most intriguing hypothesis is that a maximum composite tensile strength can be attained for an optimal interfacial shear strength between the fiber and the bulk matrix. The most direct method of altering the interfacial shear strength without changing any of the other constituent properties is by modifying the interphase properties. The work of this chapter concerns the fabrication of BisP-BTDA polyimide interphase/PEEK matrix composites to test

the hypothesis of Reifsnider et al.

The aqueous suspension prepregging technique combines the matrix polymer with the fiber at the same time that the interphase polymer is deposited on the fiber [9-14]. Aqueous suspension prepregging has been done by many researchers using a polyimide precursor, a water soluble polyamic acid salt neutralized with a base [9-14]. The matrix polymer powder is dispersed in the aqueous polyamic acid salt solution. The polyamic acid salt behaves as a stabilizer, adsorbing to the surface of the matrix powder particles, and electrostatically stabilizing the suspension. The fiber tow is then coated with the polyimide precursor and the matrix powder in a single prepregging step. The polyamic acid salt also serves as a binder, adhering the matrix powder to the carbon tow. After drying the water from the prepreg, a heating cycle is used to convert the polyamic acid to the polyimide by way of thermal imidization. The properties of the polyimide can be controlled by selection of the base and the method used for making the polyamic acid salt [15].

The main objectives of this chapter are (I) to fabricate polyether ether ketone (PEEK) matrix composites with two different BisP-BTDA polyimide interphases and control case PEEK matrix composites using hydroxypropylcellulose as a “fugitive” binder and (ii) to evaluate the performance of these composites to test the hypothesis of a maximum longitudinal tensile strength at an optimum interfacial shear strength.

The properties of the interphase have been estimated by studying model interphase BisP-BTDA polyimide discussed in Chapter 5. After thermal imidization, the BisP-BTDA NH_4^+ polyimide was shown to have a T_g of 201°C, a gel fraction of 97% and a high melt viscosity of 49,000 Pa·sec at 290°C. The BisP-BTDA TMA^+ polyimide was shown to have a T_g of 240°C, a

gel fraction of 29% and a lower melt viscosity of 29,000 Pa·sec at 290°C.

During a simulated composite consolidation temperature cycle, the melt viscosity of both polyimides was shown to increase. After the simulated composite consolidation temperature cycle the gel fraction of the BisP-BTDA NH_4^+ polyimide was shown to have a gel fraction of 100% and the BisP-BTDA TMA^+ polyimide was shown to have a gel fraction of 91%.

Model matrix samples were prepared and analyzed in Chapter 5 to replicate the matrix/interphase compositions in the composites of this chapter. The tensile strengths and moduli of the model matrix blends were all very similar indicating that the mechanical properties of the bulk matrices should not be affected.

These factors indicate that while the interphase properties are varied for each composite, the matrix properties are not affected. Thus, any difference in composite performance can be attributed to the interphase modifications.

Since PEEK is miscible with BisP-BTDA polyimide, interdiffusion of the interphase polyimide and the bulk PEEK matrix is possible [16]. However, the high gel fractions of the model interphase polyimides tested in Chapter 5 indicate that appreciable interdiffusion of the PEEK and the BisP-BTDA is not possible. The mobility of the BisP-BTDA polyimides will be severely limited by any crosslinking. This would facilitate formation of an interphase with a very high concentration of BisP-BTDA polyimide.

Although significant interdiffusion would be limited by crosslinking of the BisP-BTDA polyimide, the miscible nature of *linear* BisP-BTDA polyimide indicates that good adhesion should exist between the interphase and the bulk PEEK matrix.

Experimental
Materials

Composites were made with Hercules® AS-4 (lot#761-4m), unsized but surface treated 12k carbon fiber tow. This fiber is from the same batch used for the polyimide interphase/PEEK matrix composites described in the previous chapters.

The matrix material was Victrex 380 Grade poly ether-ether-ketone (PEEK) supplied by ICI Americas. The chemical structure for PEEK is shown in Figure 6-1. The PEEK was supplied as a powder with an 11µm median particle diameter as measured with a Shimadzu SPC-3 particle size analyzer. The PEEK is from the same batch used in previous Ultem-type polyimide interphase composite manufacture as detailed in Chapter 4 and also the same batch used by Gonzalez [12] for polyimide interphase PEEK matrix composite manufacture.

A 40 g batch of BisP-BTDA polyamic acid endcapped with phthalic anhydride was synthesized by Dr. Biao Tan from Professor McGrath's group of the Virginia Tech Chemistry Department. The large batch of polyamic acid provided enough starting material so all experiments described in this chapter could be done using a single batch of polymer. The BisP-BTDA polyamic acid was supplied as a solid powder and stored in a freezer at -5°C. The chemical structure for BisP-BTDA polyimide is shown in Figure 6-2.

The bases used for making the polyamic acid salts, ammonium hydroxide (NH_4OH) and tetramethyl ammonium hydroxide (TMAH), were both Fisher brand reagent grade.

Klucel hydroxypropylcellulose, type 99-EFF, lot # FP10-10085 was supplied by Aqualon.

For all aqueous solutions and suspension, deionized water with a resistivity of 16.7

ohms/cm^3 from a Nanopure II water filtering system was used.

Procedure

Calibration of Bases

All bases were purchased new, kept sealed and stored in a refrigerator. The concentrations of the aqueous bases were determined by potentiometric titration using an MCI Automatic Titrator Model GT-05 (COSA Instruments Corporation). The titration procedure has been described in detail in Chapter 3. The bases were kept in the original bottles, sealed tightly with Parafilm and stored in a refrigerator.

Polyamic Acid Salt Preparation

For aqueous suspensions of PEEK powder matrix, solutions of polyamic acid salts were first prepared. The formation of the BisP-BTDA polyamic acid salts and subsequent imidization are shown in Figure 6-3. As discussed in Chapter 5, the final properties of the BisP-BTDA polyimide are dependant upon the base selected making the polyamic acid salt. The glass transition temperature and the gel fraction of the polyimides are also shown in Figure 6-3. The procedure for preparation of BisP-BTDA polyamic acid salts is described in detail in Chapter 5. The procedure for preparing aqueous suspensions of BisP-BTDA polyamic acid salts and PEEK powder for prepregging is identical to the procedure used for Ultem-type polyamic acid salts with PEEK powder matrix from Chapter 4.

Hydroxypropyl Cellulose Fugitive Binder Preparation

Powdered hydroxypropyl cellulose (HPC) was sprinkled rapidly into stirred deionized water. The solution was covered with Parafilm to prevent evaporation of water, and was stirred at room temperature overnight, then it was filtered using a Buchner funnel and Fisher brand No. 41 filter paper. No insoluble HPC residue was collected with the filter paper.

Suspension Preparation

After the aqueous polyamic acid salt solutions were made, they were used to make PEEK suspensions suitable for composite prepregging. The solution and the PEEK powder were mixed in a Waring blender at high speed for five minutes. The PEEK powder was added to make a 9.8 wt% PEEK solids content suspension. The mass of polyamic acid in solution was 5 wt% of the mass of the PEEK powder. The suspensions were used immediately or were stored in a refrigerator.

A Shimadzu SAC-P3 Centrifugal Particle Size Analyzer was used to measure the size distributions of the suspensions. The instrument was used in the multi-function mode, which is a combination of gravimetric and centrifugal measurements. A few drops of the suspension was diluted in several milliliters of water until the turbidity of the suspension was reduced to a suitable level for measurements. The centrifuge was run at 240 rpm/min and a typical test took about 10 minutes. The median particle size for both BisP-BTDA polyamic acid salt stabilized suspensions and the HPC stabilized suspension was ~11 µm.

Prepregging

A detailed description of the prepregging process and techniques used in this work has been reported in previous studies by Yu and Davis [10], by Texier et. al [11], and by Gonzalez et. al [13]. Using a modified Research Tool Corporation Model 30 Prepregger, the carbon fiber was continuously impregnated with the suspension. As seen in the schematic in Figure 6-4 the fiber was passed through a resin pot with an approximate volume of 0.25 l. The prepregged tow was then wound up on a drum at a line speed of ~10 cm/sec with a tow width of 0.33" and approximately 25% tow overlap. The prepreg was dried on the drum at room temperature for 30 minutes and then it was cut off the drum, and cut into square prepreg lamina 6" x 6". The prepreg lamina were then placed in a freezer until composite panel lay-up and consolidation.

Composite Layup and Consolidation

Two different stacking schemes were used for composite manufacture. The composites made were four-ply, unidirectional panels ($[0]_4$) and 16-ply unidirectional panels ($[0]_{16}$). The prepreg was taken immediately from the freezer and laid up in the appropriate stacking sequence. The stacked plies were heated in a Model 532 Fisher Programmable air convection oven according to a specially designed thermal treatment. The thermal cycle was 65°C for one hour followed by a two-hour hold at 265°C for imidization of the polyamic acid. The cyclization of PAA to polyimide is a condensation reaction. Since water is a product, the cyclization must be done prior to consolidation in the matched mold to prevent the water from accumulating in the composite and forming voids.

The dried and heat treated prepreg was placed in a 6" x 6" picture frame steel mold. A thermocouple was inserted into a corner of the mold to monitor the consolidation temperature and an IBM Model 30 personal computer was used to record the composite temperature and pressure history. The steel mold was treated with Frekote 34 mold release agent and the socket head cap screws that fasten the mold together were treated with a high temperature anti-seize compound.

The composite consolidation cycle is shown in Figure 6-5. A Wabash Vacuum Hot Press was used for composite consolidation. The press was preheated to 390°C and the loaded mold was placed between the platens. Touch pressure was applied until the mold temperature was above 360°C. At this point, a vacuum of 28 in Hg was applied to the platen chamber and the consolidation platen pressure of 350 psi was applied. After the mold temperature reached 380°C, the temperature was maintained at this level for 30 minutes and then the mold was cooled at an approximate rate of 10°C/min. The consolidation pressure was applied until the mold temperature was at least 30°C below the glass transition temperature of the PEEK matrix (143°C) [24].

Panel Evaluation: C-Scan

A Sperry Corporation S-80 C-Scan ultrasonic unit was used to qualitatively determine the level of consolidation of the panels. The 15 Khz transducer was used with a gain between 32 and 40 db. A scanning width of 0.1" was used with the fastest raster scanning speed.

Fiber Volume Fraction

The fiber volume fraction of most composites was determined by acid digestion according to the ASTM D3171-76 method. Densities of 1.3 $g \bullet cm^{-3}$ and 1.8 $g \bullet cm^{-3}$ were used for the PEEK matrix and the carbon fiber respectively. For the case of panels with regions of varying consolidation quality as determined by C-scan, samples were taken from two areas of the panel. The region of highest consolidation quality and the region of lowest consolidation quality were the two areas selected.

Image Analysis

An image analysis method was used to determine the void content of the composites. Samples of unidirectional laminates were mounted in epoxy, polished and examined under a scanning electron microscope (SEM) located in the chemistry departments surface analysis laboratory in the Hahn Hall. Buehler cold mount epoxide resin and hardener were used to mount the samples. Polishing was done on an automatic Buehler Polishing unit located in the Materials Response Group laboratory in Norris Hall using Buehler Carbimet Microcut Special Silicon Carbide Grinding Paper according to the polishing schedule outlined in Table 7-I. The polished sample was examined under SEM and representative micrographs were taken at magnifications of 750 x.

Table 6-I. Polishing schedule of PEEK matrix composite surfaces for image analysis.

Duration	Grit Abrasive	Pressure	Polishing Direction
until surface ground level	120 grit	4lbs/pot	counter rotation
5 minutes	240 grit	4lbs/pot	counter rotation
5 minutes	320 grit	4lbs/pot	counter rotation
5 minutes	400 grit	4lbs/pot	matching rotation
10 minutes	600 grit	4lbs/pot	matching rotation
10 minutes	800 grit	4lbs/pot	matching rotation
10 minutes	1 µm grit	6lbs/pot	matching rotation
10 minutes	0.3 µm grit	6lbs/pot	matching rotation

These micrographs were scanned into .PCX format using a Microtek Scanmaker IIHR scanner and an IBM compatible PC using Adobe Photoshop 3.0 and Scanmaker Plug-in for Adobe Photoshop v.2.13. Using the grey scale imaging feature of SigmaScan v. 4.0, the void content was determined.

Composite Characterization:
Transverse Flexure Testing and Longitudinal Flexure Testing

Three point bending experiments according to ASTM D790-96 were done with 12.7 mm x 50.8 mm coupons. Test specimens were machined using a diamond saw and the edges were polished with #400 grit silicon carbide abrasive paper. After the coupons were machined, an annealing process was employed to normalize the free volume relaxation of the amorphous

content of the matrix polymer with regard to physical aging. The coupons were annealed at 128°C, approximately 15°C below T_g, for 48 hours and then cooled to room temperature at a rate of 0.1°C/min. Transverse flexure testing was done using an Instron with a 1 KN load cell and the longitudinal flexure testing was done using a 5 KN load cell. A three point bending test fixture was used to support the sample and provide uniform loading conditions for all samples. A 25/1 span to thickness ratio was used for testing. The longitudinal flexure testing was done with the fiber direction along the length of the coupon, as shown in Figure 6-6(a) and the transverse flexure testing was done with the fiber direction perpendicular to the length of the coupon, as shown in Figure 6-6(b).

Unidirectional Tension

Tension testing was done on 4-ply unidirectional panels from the 60 series HPC fugitive binder/PEEK and 80 series BisP-BTDA NH_4^+/PEEK composites by the author and Mr. Brady Walther in the Material Response Group at Virginia Tech.

Tabs were bonded to the panels before the test samples were machined. Four rectangular, 12.7 cm x 2.54 cm x 0.25 cm, glass reinforced hardened epoxy tabs were bonded on the panel ends perpendicular to the fiber direction. The test coupon geometry is shown in Figure 6-7. The tabbed panels were machined into 12.7 cm x 1.27 cm coupons with the length in the fiber direction using a diamond saw. Extensometer tabs were bonded to the panel in the center of the test region at a separation of 2.54 cm. Tension testing was done using a 20 kip servo-hydraulic MTS machine under load control mode. The samples were loaded to failure at a rate of 356 N/s.

Results and Discussion
Panel Quality

The quality of the panels was assessed using ultrasonic C-scan. The C-scan images were used to choose the panels with a high quality of consolidation suitable for mechanical evaluation. Some of the panels had regions of lesser quality consolidation. These regions were not included in mechanical evaluation. Table 6-II lists the quality of consolidation as evaluated by ultrasonic C-scan as well as the fiber volume fraction for the composite panels. Figure 6-8 shows a C-scan image which is representative of good consolidation quality.

Fiber volume fractions were measured for each panel using 3-5 samples from each panel. For panels with varying degrees of consolidation quality throughout the panel as found by C-scan, an average fiber volume fraction was found using samples from the region of best consolidation quality and also the region of worst consolidation quality.

The microscopic inspection of the composite cross sections showed close packing of fibers, as expected with high fiber volume fractions. The measured void volumes of each unidirectional panel are included in Table 6-II as measured by image analysis of a composite cross section. The measured void volumes are very low, less than 1% for all unidirectional panels, and therefore the composite integrity is not sacrificed by the presence of a large void content.

Also shown in Table 6-II is a column labeled “test No.”. This column contains information about which mechanical test was used for the panel. The number corresponds to the mechanical tests listed in Table 6-III.

Table 6-II. Quality of consolidation, fiber volume fraction, panel layup, void volume fraction, and mechanical test for which panel was used.

panel ID	size	layup	Consolidation Quality	V_f (%)	void volume	test No.
P605[a]	6"x6"	$[0]_{16}$	good	64.5±1.7	0.52%	1,2
P705[b]	6"x6"	$[0]_{16}$	good	65.8±0.4	0.24%	1,2
P805[c]	6"x6"	$[0]_{16}$	good	68.4±0.3	0.15%	1,2
A01[d]	6"x6"	$[0]_{16}$	good	61.2±0.3	0.51%	2
P606[a]	6"x6"	$[0]_4$	good	60.1±1.7	N/A	3
P607[a]	6"x6"	$[0]_4$	good	60.7±1.6	N/A	3
P806[c]	6"x6"	$[0]_4$	good	58.90±1.1	N/A	3
A02[d]	10"x10"	$[0]_4$	good	61.3±1.9	0.04%	3

a- HPC fugitive binder
b- BisP-BTDA TMA^+ polyimide interphase
c- BisP-BTDA NH_4^+ polyimide interphase
d- APC-2 from ICI

Composite Properties

The following sections will present experimental data of BisP-BTDA polyimide interphase/PEEK composites which will be compared to the mechanical testing data of similar composite specimens made from APC-2 prepreg tape. The details of the mechanical testing schedule are listed in Table 6-III.

Table 6-III. Mechanical Testing Schedule

No.		60 series HPC fugitive binder	70 series BisP-BTDA TMA^+	80 series BisP-BTDA NH_4^+	APC-2 series
1	longitudinal flexure	✓	✓	✓	
2	transverse flexure	✓	✓	✓	✓
3	longitudinal tension	✓		✓	✓

The experiments planned for the 60 series, 70 series and 80 series composites included longitudinal flexure, transverse flexure and longitudinal tension testing of all three composite systems. However, the supply of 11 µm diameter PEEK powder needed for the aqueous suspension prepregging technique was depleted before a 70 series BisP-BTDA TMA^+/PEEK composite panel could be made for longitudinal tension testing.

The experimental results reported in this chapter for the APC-2 composites are from the experiments detailed in Chapter 4. Longitudinal flexure testing of APC-2 composites was not planned.

Longitudinal Flexure

Two different failure modes are possible for longitudinal flexure testing of unidirectional composites. Interlaminar shear failure is possible which is characterized by planar failure near the center ply of the composite. Tensile failure is also possible which is characterized by breaking of the coupon into two pieces at the point of loading.

The failure mode was the same for the 60 series, 70 series and 80 series composites. All composite coupons failed in a tensile mode. Since the three point loading test fixture provides a bending moment at the beam center, a tensile load is applied to the bottom plies of the coupon and a compressive load is applied to the top plies of the coupon. All of the failed coupons showed a very clear distinction of a smooth, compressive type of failure on the top half of the coupon and a jagged, tensile-type of failure where fiber breakage and fiber pull-out occurred on the bottom half of the coupon.

The longitudinal flexure strength was calculated using Eq. 6-1, the longitudinal flexure modulus was calculated using Eq. 6-2 and the strain-to-failure was calculated using Eq. 6-3.

$$\sigma = \frac{3 \cdot P \cdot L}{2 \cdot b \cdot d^2} \qquad \text{Eq. 6-1}$$

$$E_B = \frac{L^3 \cdot m}{4 \cdot b \cdot d^3} \qquad \text{Eq. 6-2}$$

$$\epsilon = \frac{6 \cdot D \cdot d}{L^2} \qquad \text{Eq. 6-3}$$

where: σ = stress in the outer fibers at midspan
P = maximum load at a point just before failure
L = support span
b = width of beam tested
d = thickness of beam tested
E_B = modulus of elasticity in bending
m = slope of tangent to linear region of load-deflection curve
ϵ = maximum strain in the outer fibers
D = maximum deflection of the center of the beam

The longitudinal flexure properties are shown in Table 6-IV including the longitudinal flexure strength, the longitudinal flexure modulus, the failure tensile strain at the midspan of the specimen in the outerply induced by the bending moment, and the longitudinal flexure toughness calculated as the area under the longitudinal flexure stress-strain response curve.

Table 6-IV. Longitudinal flexure properties of Ultem-type interphase/PEEK matrix composites.

	V_f (%)	longitudinal flexure strength (MPa)	longitudinal flexure modulus (GPa)	longitudinal flexure strain-to-failure (%)	longitudinal flexure toughness (MPa)
60 series[a]	64.5	1648 ± 81	122.5 ± 6.2	1.46 ± 0.08	12.05 ± 0.74
70 series[b]	65.8	1571 ± 87	107.6 ± 2.7	1.55 ± 0.04	12.42 ± 0.57
80 series[c]	68.4	1592 ± 147	112.7 ± 5.6	1.37 ± 0.14	10.96 ± 2.81

a- HPC fugitive binder
b- BisP-BTDA TMA^+ polyimide interphase
c- BisP-BTDA NH_4^+ polyimide interphase

There are not large differences in the longitudinal flexure data for the three composites tested. A quantitative comparison of the data is desirable to verify which data sets are statistically different. The sets of data for the three composites were statistically compared using an unpaired *t*-test executed with SigmaStat Statistical Software v. 2.0. The unpaired *t*-test is used

to test for a difference between two groups that is greater than what can be attributed to random sampling variation [26]. The SigmaStat Statistical Software first tests for normally distributed populations using a Kolmogorov-Smirnov test, and then tests for equal variance by checking the variability about the group means. If the sample populations each pass these tests, then the unpaired *t*-test is executed using a confidence interval of 95%. The unpaired *t*-test is a parametric test based on estimates of the mean and standard deviation parameters of the normally distributed populations from which the samples were drawn. If two sets of data pass an unpaired *t*-test, then there is a 95% confidence that the difference in the mean values of the two groups is greater than would be expected by chance. Therefore, there is a statistically significant difference between the groups.

The unpaired *t*-test results for the HPC/PEEK composite and the BisP-BTDA/PEEK composites from the longitudinal flexure data are shown in Table 6-V. Each set of longitudinal flexure data was compared with one another. If the comparison of two sets of data passes the t-test, then it is concluded that there is a statistically significant difference between the groups. The results show that there is not a statistically significant difference in the longitudinal flexure strength or the longitudinal flexure toughness for any of the pairs of composites. These results provide a quantitative comparison showing that the transverse flexure moduli are similar

Table 6-V. Unpaired *t*-test results comparing each set of PEEK matrix composite longitudinal flexure data.

	Longitudinal flexure strength	Longitudinal flexure strain	Longitudinal flexure modulus	Longitudinal flexure toughness
60 series[a] vs 70 series[b]	fail	pass	pass	fail
60 series[a] vs 80 series[c]	fail	pass	fail	fail
70 series[b] vs 80 series[c]	fail	pass	fail	fail

a- HPC fugitive binder
b- BisP-BTDA TMA^+ polyimide interphase
c- BisP-BTDA NH_4^+ polyimide interphase

pass = statistically significant difference between data sets
fail = data sets are not significantly different

The longitudinal flexure modulus is shown to be statistically different for all of the pairs of composites. The 70 series BisP-BTDA TMA^+ polyimide interphase composite had the lowest longitudinal flexure modulus, the 80 series BisP-BTDA NH_4^+ polyimide interphase composite had the next highest longitudinal flexure modulus and the 60 series HPC fugitive binder composite had the highest longitudinal flexure modulus. Although the longitudinal flexure modulus shows these differences, since almost all of the other comparisons fail the *t*-test indicating no statistical difference, it is not possible to make any strong conclusions regarding the longitudinal flexure results.

Transverse Flexure Properties

The data from the transverse flexure test shown in Table 6-VI provide compelling results that the differences in interphase properties directly affect the fiber-matrix adhesion in the composite. The flexure strength of the composites show differences of up to 14% between the 60 series composites and the 80 series composites. The flexure modulus is calculated as the slope of the stress-strain response curve in the linear range from 0.2%-0.4% strain. The strain

reported from the flexure tests is the tensile strain at the midspan of the specimen in the outer ply induced by the bending moment. The mechanics of the bending test create a compression load on the top surface of the specimen and a tensile load on the bottom surface of the specimen. The strain represents the tensile strain at failure on the bottom surface of the specimen. The flexure toughness was calculated as the area under the stress-strain response curve from the transverse flexure test.

The coupon failure mode for the transverse flexure testing was consistent for all samples and was characterized by fracture at the beam center due to normal stresses which broke the beam into two nearly symmetric pieces. Some of the failed coupons were held together by the outer layer of polymer matrix that was on the top surface of the loaded beam. This would indicate that fracture initiated on the bottom surface of the beam where the bending moment creates tensile stresses normal to the load. There was no indication of fracture due to interlaminar shear stresses which would be characterized by splitting of the beam on the level of the mid-plane.

Table 6-VI. Transverse flexure results for PEEK composites.

	V_f (%)	flexure strength (MPa)	flexure modulus (GPa)	strain at failure (%)	toughness (MPa)
60 series[a]	64.5	133.1 ± 9.7	10.00 ± 0.13	1.38 ± 0.10	0.92 ± 0.13
70 series[b]	65.8	138.2 ± 9.6	9.23 ± 0.30	1.60 ± 0.06	1.11 ± 0.11
80 series[c]	68.4	120.8 ± 5.2	9.90 ± 0.17	1.27 ± 0.06	0.77 ± 0.07
APC-2[d]	61.2	147.9 ± 11.8	9.90 ± 0.08	1.49 ± 0.11	1.11 ± 0.17

a- HPC fugitive binder
b- BisP-BTDA TMA^+ polyimide interphase
c- BisP-BTDA NH_4^+ polyimide interphase
d- APC-2 prepreg from ICI

The sets of data for the four composites were statistically compared using an unpaired *t*-test executed with SigmaStat Statistical Software v. 2.0. As described in the previous section, the unpaired *t*-test is used to test for a difference between two groups that is greater than what can be attributed to random sampling variation. If two sets of data pass an unpaired *t*-test, then there is 95% confidence that the difference in the mean values of the two groups is greater than would be expected by chance. Therefore, there is a statistically significant difference between the groups.

The unpaired *t*-test results are shown in Table 6-VII. Each set of PEEK matrix composite transverse flexure data was compared with one another. The results show that there is a statistically significant difference in transverse flexure strength between the 80 series composite and each of the other two composites. The results also show that the transverse flexure strength for the 60 series and the 70 series are not statistically different.

Table 6-VII. Unpaired *t*-test results comparing each set of PEEK matrix composite transverse flexure data.

	transverse flexure strength	transverse flexure modulus	strain-to-failure	transverse flexure toughness
60 series[a] vs. 70 series[b]	fail	pass	pass	pass
60 series[a] vs. 80 series[c]	pass	fail	pass	pass
70 series[b] vs. 80 series[c]	pass	pass	pass	pass

a- HPC fugitive binder
b- BisP-BTDA TMA^+ polyimide interphase
c- BisP-BTDA NH_4^+ polyimide interphase
d- APC-2 prepreg from ICI

The *t*-test results show that the transverse flexure moduli for the 70 series composite is statistically different from the other two. It was shown in Chapter 4 that the transverse flexure modulus increased with composite fiber volume fraction. That trend is not as clear for the composites in this Chapter. The 60 series HPC fugitive binder composite had the lowest fiber volume fraction of the three experimental composites and the flexure modulus was among the greatest. This can be explained by the abnormally large standard deviation for the fiber volume fraction measurements of the 60 series composites. It is expected that the flexure modulus should increase monotonically with fiber volume fraction. The strain-to-failure results are statistically different for all of the composites. The 80 series composite has the lowest strain-to-failure and the 70 series composite has the highest strain-to-failure. This is an important consideration for composite design issues. In composite design, the transverse flexure strength is not as important as the transverse strain to failure. When designing a composite laminate, a specific lamina stacking sequence is used to tailor the properties of the composite laminate to suit the loading condition. For example, when considering a crossply composite laminate, the tensile loads applied to the composite in the 0° direction will bear predominantly upon the 0° oriented lamina and the 90° oriented lamina must survive the corresponding transverse elongation. In this manner, the tensile loads applied to the composite in the 90° direction will bear predominantly upon the 90° oriented lamina, and the 0° oriented lamina must survive the corresponding transverse elongation. The transverse lamina are not intended to support a tensile load. Thus, the transverse strain to failure is more important than the transverse strength from a design perspective.

The transverse flexure strength is a very important property because it furthers the

development of the composite structure-property relationships and provides a means of comparing the interfacial adhesion of the composites. There is a 14% increase in transverse flexure strength for the 70 series composite specimens and a 12% increase in transverse flexure strength for the 60 series composite specimens over the 80 series composite specimens.

The transverse flexure strength has been shown by Adams, et al. [30] to be dependent upon different sizings or interphases of the composite. Drzal and Madhukar [2] have shown that the flexural strength correlates well with the interfacial shear strength (ISS) for composites made with AU-4, AS-4 and AS-4C fibers and Epon 828 epoxy matrix, cured with mPDA. Chang, et al. [5] showed a similar correlation of transverse flexure strength with ISS for composites made with AU-4, AS-4, and AS-4GCP fibers and J2 polyamide copolymer matrix. The normalized transverse flexure strength has been plotted in Chapter 4 as a function of normalized ISS from the data of Drzal and Madhukar [2] and Chang, et al. [5] in Figure 4-18. This data clearly shows a correlation of increasing transverse flexure strength with increasing ISS.

Although quantitative ISS values cannot be gained from the correlation of ISS to transverse flexure strength data, a relative ranking of ISS, or fiber-matrix interfacial adhesion can be made. Following the trends of the transverse flexure strength, this relative ranking is:

$$ISS_{80\ series} < ISS_{60\ series} \simeq ISS_{70\ series}$$

This relative ranking of composite interfacial shear strength is very important for a discussion of the effects of interfacial shear strength on overall composite performance and understanding the micro mechanics of composite failure.

A comparison of the flexure toughness of the composite samples provides the most striking difference of the composites. There is an 45% increase in toughness for the 70 series composite system over the 80 series composite system and a 20% increase in toughness for the 60 series composite system over the 80 series composite system.

Microscopic examination of the failure surfaces for the transverse flexure specimens revealed similar topographies for the composites. The bending nature of the three point bending test creates tensile loading on the lower side of the test specimen and compressive loading on the top side of the test specimen. The tension side of the failure surface was the focus of the examination as this is the side where failure initiates.

Micrographs from the transverse flexure failure specimens are shown in Figure 6-10. The failure surfaces all had sufficient polymer material covering the carbon fibers. For all composite systems, some small, isolated, locations of bare fibers were found where adhesive failure occurred. It is not possible to quantify these observations with SEM. The failure surfaces all showed regions of ridged polymer material and troughs where fibers had been removed during failure. No clear differences were noted for the microscopic examination of the failure surfaces of the three composites.

Longitudinal Tension

Longitudinal tension testing of 4-ply PEEK matrix composites was done using a single, quasi-static loading ramp of 356 N/sec. The longitudinal tensile test results are shown in Table 6-VIII. The tensile strength is tabulated along with the tensile modulus and the tensile failure

strain.

Table 6-VIII. Longitudinal tension test results for PEEK matrix composites.

Panel	tensile strength (MPa)	tensile modulus (GPa)	failure strain (%)
60 series[a]	1899 ± 154	143.7 ± 10.7	1.25 ± 0.04
80 series[b]	1938 ± 159	141.3 ± 8.4	1.36 ± 0.07
APC-2[c]	2057 ± 115	140.9 ± 5.5	1.41 ± 0.07

a- HPC fugitive binder b- BisP-BTDA NH_4^+ polyimide interphase
c- APC-2 prepreg from ICI

The sets of data for the four composites were statistically compared using an unpaired *t*-test executed with SigmaStat Statistical Software v. 2.0 as described earlier in the longitudinal flexure test section. The unpaired *t*-test is used to test for a difference between two groups that is greater than what can be attributed to random sampling variation. A 95% confidence interval was used to determine if the difference in the mean values of the two groups is greater than would be expected by chance. The *t*-test results for the unidirectional tension test are shown in Table 6-IX. The results show that the tensile strength and the tensile modulus for the 60 series and 80 series composites are not statistically different.

Table 6-IX. Unpaired *t*-test results comparing each set of PEEK matrix composite longitudinal tensile data.

	tensile strength	tensile strain-to-failure	tensile modulus
60 series[a] vs. 80 series[b]	fail	pass	fail

a- HPC fugitive binder b- BisP-BTDA NH_4^+ polyimide interphase

The panel made from the APC-2 prepreg has the highest strength. This system has been optimized by Fiberite and the details of the optimization are proprietary information and not available. Since little is known about the construction of the APC-2 prepreg the structure-property relationships of the composite cannot be related to the interphase.

A unidirectional composite may be modeled by assuming that the fibers are continuous, aligned parallel and uniform in properties [27]. Other important assumptions are that perfect bonding exists between the fibers and matrix so that slippage does not occur at the fiber-matrix interface and each component has a linear elastic response [27]. Based upon these assumptions, a rule of mixtures can be developed for composite tensile strength as shown in Eq. 6-4. A complete derivation of the rule of mixtures for composite tensile strength is shown in Chapter 4 of this thesis.

$$\sigma_c = V_f \cdot \sigma_f + V_m \cdot \sigma_m \qquad \text{Eq. 6-4}$$

σ_c = composite tensile strength V_f = fiber volume fraction
σ_f = fiber tensile strength σ_m = matrix tensile strength

Eq. 6-4 indicates that the contributions to the composite strength of the fibers and the matrix are proportional to their volume fractions. This type of a relationship is called a rule of mixtures and σ_c from Eq. 6-4 is referred to as σ^{ROM}.

The stresses σ_f and σ_m in Eq. 6-4 are not the ultimate strengths of the constitutive materials, but they are stresses at a specific strain within the elastic region of deformation. To

use Eq. 6-4 properly, a specific composite strain must be considered. Since the strains of the composite, fibers and matrix are equal in this model, and a linear elastic response is assumed for each component, Hooke's law can be used to calculate the individual contributions to composite strength by the fibers and the matrix. Hooke's law for a general linear elastic material is

$$\sigma_i = E_i \cdot \epsilon \qquad \text{Eq. 6-5}$$

The notation is general with a subscript of "i", however Eq. 6-5 is applicable to the fiber or the matrix.

The strain, ϵ, used to calculate the individual contributions to composite strength for the rule of mixtures strength, σ^{ROM}, is the measured composite strain from Table 6-IX. The Hercules AS-4 carbon fiber data sheet reports E_f = 234.6 GPa [28] and the ICI PEEK data sheet reports E_m = 3.6 GPa [29]. Using these values with Eq. 6-4 and Eq. 6-5 the rule of mixtures composite strength, σ^{ROM}, is calculated and tabulated in Table 6-X.

The strength estimated by the rule of mixtures from Table 6-X shows good agreement to the measured tensile strength. This indicates that the composites are modeled well by the assumptions made for the rule of mixtures model. Specifically, the composite has fibers that are continuous, aligned parallel and uniform in properties. Good bonding exists between the fibers and matrix so that no slippage occurs at the fiber-matrix interface and each component can be considered to have a linear elastic response.

The data sheet for Hercules AS-4 carbon fiber reports a fiber tensile strain-to-failure of

1.61% [29]. As seen in Table 6-IX, the largest tensile strain for any of the composites is 1.41%. Thus, all the composites fail before the fibers can be loaded to their individual maximum strain. The strain limitation for the composite is attributed to fiber defects, composite voids and discontinuous fibers in the composite. The data sheet for ICI PEEK reports a tensile yield strain of 4.7% [31], therefore the matrix can be considered to deform elastically up to the limiting tensile strain the fibers (1.61%). An ultimate composite longitudinal tensile strength σ^{ULT}, can be calculated using Eq. 6-4 and Eq. 6-5 with a maximum composite strain of 1.61% whereby $\sigma_c = \sigma^{ULT}$. The calculated values of σ^{ULT} are tabulated in Table 6-X. The σ^{ULT} represents the longitudinal tensile strength of a perfect composite with no broken fibers, no fiber defects, no matrix voids and perfect bonding between fiber and matrix. This ultimate longitudinal tensile strength can be used to make some important comparisons of the BisP-BTDA/PEEK composites. To discuss these comparisons properly, the micromechanics of load transfer around a broken fiber should be considered. The reader is referred to the discussion of the micromechanics of load transfer for the PEEK matix composites contained in Chapter 4 of this thesis.

Table 6-X. Rule of mixture predictions for strength, ratios of measured strength to predicted strength by the rule of mixtures, and strength reduction factor.

Panel	V_f (%)	tensile strength (MPa)	σ^{ROM} * (MPa)	σ^{ULT} ** (MPa)	S_T ***
60 series[a]	60.4	1899 ± 154	1784 ± 65	2100	1.11 ± 0.09
80 series[b]	58.9	1938 ± 159	1880 ± 96	2063	1.07 ± 0.10
APC-2[d]	61.3	2057 ± 115	2035 ± 102	2331	1.13 ± 0.06

* - calculated from Eq. 6-4 using ε from Table 6-VIII
** - calculated from Eq. 6-4 using ε = 1.61%
*** - calculated from Eq. 6-6

a- HPC fugitive binder
b- BisP-BTDA NH_4^+ polyimide interphase
c- APC-2 prepreg from ICI

All of the PEEK matrix composites displayed the same mixed-mode of failure during longitudinal tension testing. The coupons shattered into many, long, thin pieces at failure. The failure was "explosive", resulting in significant fiber-matrix splitting, however, each thin, broken piece had ends resembling transverse cracking type failure. Only a small portion of the composite coupon which was bonded to the tabbing material remained in the grips. Since all coupons failed with the same mixed-mode, it is assumed that the strengths can be compared with the use of a strength reduction factor, S_T, defined as the ratio of σ^{ULT} to the measured composite strength.

$$S_T = \frac{\sigma^{ULT}}{\sigma^{experimental}} \qquad \text{Eq. 6-6}$$

The strength reduction factors, S_T, tabulated in Table 6-X are used to rank the level of the micro-mechanical stress concentrations in the polyimide interphase/PEEK matrix composites. It is important to note that since σ^{ULT} was calculated for each individual composite and respective fiber volume fraction, S_T will not be dependent upon fiber volume fraction. The values for S_T are close for the interphase composites, so an appropriate statistical comparison of the data sets is important. The unpaired *t*-test executed with SigmaStat Statistical Software v. 2.0, as described earlier, was used with a 95% confidence interval. A comparison of the S_T values for the 60 series and 80 series composites failed the *t*-test indicating that the values are not statistically different.

The "rule of mixtures" model of Eq. 6-4 can be developed further to estimate the

composite tensile modulus as shown in Eq. 6-7 and discussed in Chapter 4.

$$E_c = V_f \cdot E_f + V_m \cdot E_m \qquad \text{Eq. 6-7}$$

E_c = composite modulus V_f = fiber volume fraction
E_f = fiber modulus E_m = matrix modulus

Eq. 6-7 indicates that the contributions to the composite modulus of the fibers and the matrix are proportional to their volume fractions. Once again this relationship is called a rule of mixtures and E_c from Eq. 6-7 can be referred to as E^{ROM} [27].

Table 6-XI. shows the composite fiber volume fractions and the rule of mixture estimations of modulus. The rule of mixture estimations were calculated using the PEEK tensile modulus from Jar et. al, 3.6 GPa [29], and the fiber tensile modulus from a Hercules AS-4 product data sheet, 234 GPa [28].

Table 6-XI. Longitudinal tensile modulus, rule of mixture predictions for modulus and ratios of measured modulus to predicted modulus by the rule of mixtures.

Panel	V_f (%)	tensile modulus (GPa)	E^{ROM} (GPa)
60 series[a]	60.4	143.7 ± 10.7	143
80 series[b]	58.9	141.3 ± 8.4	139
A02[c]	61.3	140.0 ± 5.5	145

a- HPC fugitive binder b- BisP-BTDA NH_4^+ polyimide interphase
c- APC-2 prepreg from ICI

The E^{ROM} values calculated from Eq. 6-7 are very close to the experimental values of modulus, indicating that the composites are modeled well by the assumptions made for the rule of mixtures model. Specifically, the composite has fibers that are continuous, uniform in properties and aligned parallel [27]. Good bonding exists between the fibers and matrix so that no slippage occurs at the fiber-matrix interface and each component can be considered to have a linear elastic response [27].

Tensile Strength and Interfacial Shear Strength

As described in Chapter 2 of this thesis, a model was proposed by Subramanian et. al which is based on a modified shear lag analysis using a concentric cylinders model including the ineffective length and the stress concentrations on unbroken fibers due to a neighboring broken fiber [4]. This model predicts that a maximum composite tensile strength exists for a given optimum interfacial shear strength. This is represented in Figure 2-38 in Chapter 2. A major goal of the work of this thesis was to test the hypothesis proposed by the model of Subramanian et. al.

Using the correlation shown in Figure 4-18 of transverse flexure strength and interfacial shear strength, it is concluded that the transverse flexure strength can be used to qualitatively rank the interfacial shear strengths of the PEEK matrix composites. This is done by normalizing the transverse flexure strength by the lowest value which is 120.8 MPa for the 80 series BisP-BTDA NH_4^+/PEEK composite. Using this method for ranking the interfacial shear strength of the composites, the experimental longitudinal tensile strength is plotted against normalized

transverse flexure strength in Figure 6-10. This figure contains data for the PEEK matrix composites discussed in this chapter and data for the Ultem-type polyimide interphase/PEEK matrix composites discussed in Chapter 4. These data are all experimental values and are not corrected to a common fiber volume fraction.

Since the data points are close together and the error bars suggest overlapping of the data ranges, caution must be exercised when making conclusions on these data. The curve in Figure 6-10 is meant only to suggest a possible trend of the data. The trend suggests that a maximum tensile strength exists for the 10 series Ultem-type TMA^+ polyimide interphase/PEEK matrix composite. The trend also suggests qualitative reinforcement of the model proposed by Subramanian et. al [4].

It is important to note that since the APC-2 composite was fabricated from a commercial prepreg and the actual composition of the interphase is not known, the data for the APC-2 composite should not be included in the testing of the hypothesis of Subramanian et. al. Also, although the APC-2 prepreg was made with AS-4 fiber, it was not from the same lot number that was consistently used for all the polyimide interphase PEEK matrix composites. Therefore, the fiber properties themselves could have been different such as fiber tensile strength and modulus.

Conclusions

PEEK matrix composites with two different BisP-BTDA polyimide interphases have been fabricated, analyzed and compared to PEEK matrix composites with an HPC fugitive binder. A statistical analysis of the longitudinal flexure test results show that there is not a

difference among the longitudinal flexure strengths for the 60 series HPC/PEEK composites, the 70 series BisP-BTDA TMA^+/PEEK composite and the 80 series BisP-BTDA NH_4^+/PEEK composite. Only the longitudinal flexure failure strain showed a statistical difference among all three composites. The longitudinal flexure test was not shown to provide information for ranking the performance of the interphase composites.

A statistical analysis of the transverse flexure properties showed that the 60 series HPC/PEEK composites and the 70 series BisP-BTDA TMA^+/PEEK composite had comparable transverse flexure strengths which were greater than the transverse flexure strength of the 80 series BisP-BTDA NH_4^+/PEEK composite. The relationship shown from the data of Chang et. al [5] and Madhukar and Drzal [2] indicate direct correlation of interfacial shear strength with transverse flexure strength. Therefore, this correlation can be used to show qualitatively that the 60 series HPC/PEEK composites and the 70 series BisP-BTDA TMA^+/PEEK composite had comparable interfacial shear strengths which were greater than the interfacial shear strength of the 80 series BisP-BTDA NH_4^+/PEEK composite.

The longitudinal tensile strengths of the 60 series HPC/PEEK composite and the 80 series BisP-BTDA NH_4^+/PEEK composite were shown to be statistically similar, however this does not detract from the usefulness of the test.

The hypothesis proposed by Subramanian et. al [4] indicates that a maximum in tensile strength exists at an optimum interfacial shear strength. It is therefore possible that the tensile strengths of the 60 series HPC/PEEK composite and the 80 series BisP-BTDA NH_4^+/PEEK composite lie on either side of this maximum as shown in Figure 6-10.

The data from this chapter combined with the data from Chapter 4 for Ultem-type

polyimide interphase PEEK matrix composites for longitudinal tensile strength vs. normalized transverse flexure strength show qualitative reinforcement of the trends predicted by the model of Subramanian et. al [4].

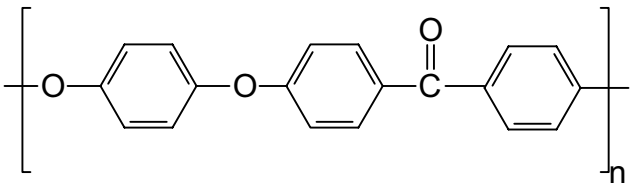

Figure 6-1. Chemical structure of polyether ether ketone.

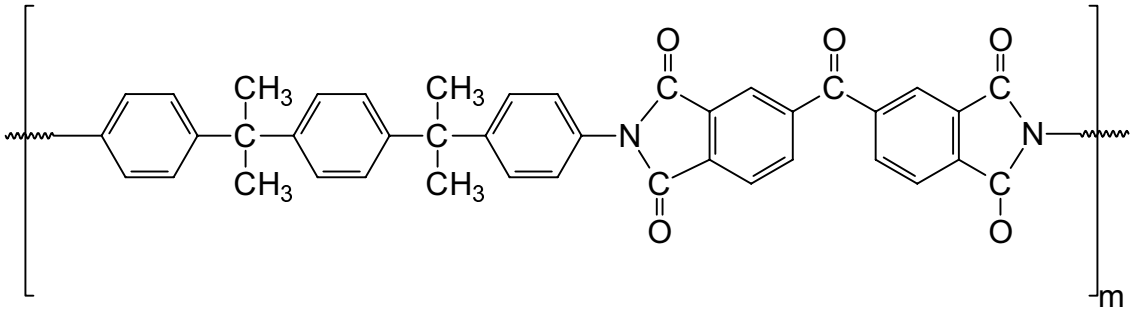

Figure 6-2. Chemical structure of BisP-BTDA polyimide.

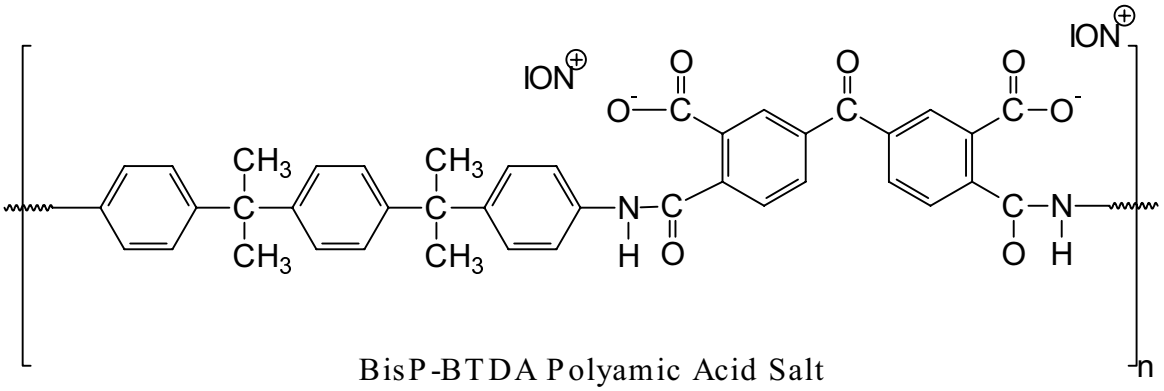

BisP-BTDA Polyamic Acid Salt

Thermal Imidization
265℃/ 2 hours

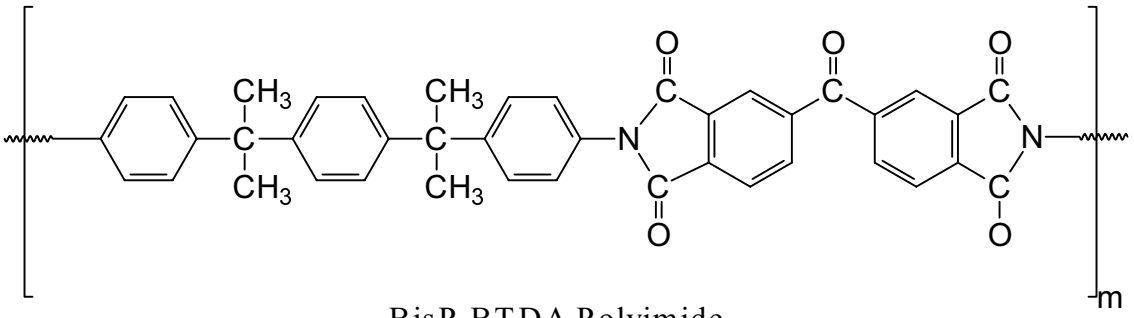

BisP-BTDA Polyimide

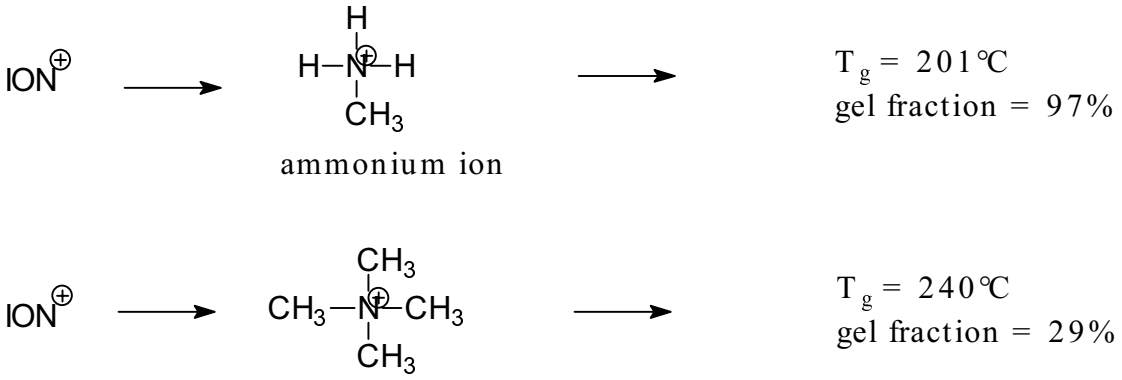

Figure 6-3. Formation of BisP-BTDA polyamic acid salt using two different bases for counterions and the resulting glass transition tempteratures and gel fractions of the resulting polyimide after thermal imidization.

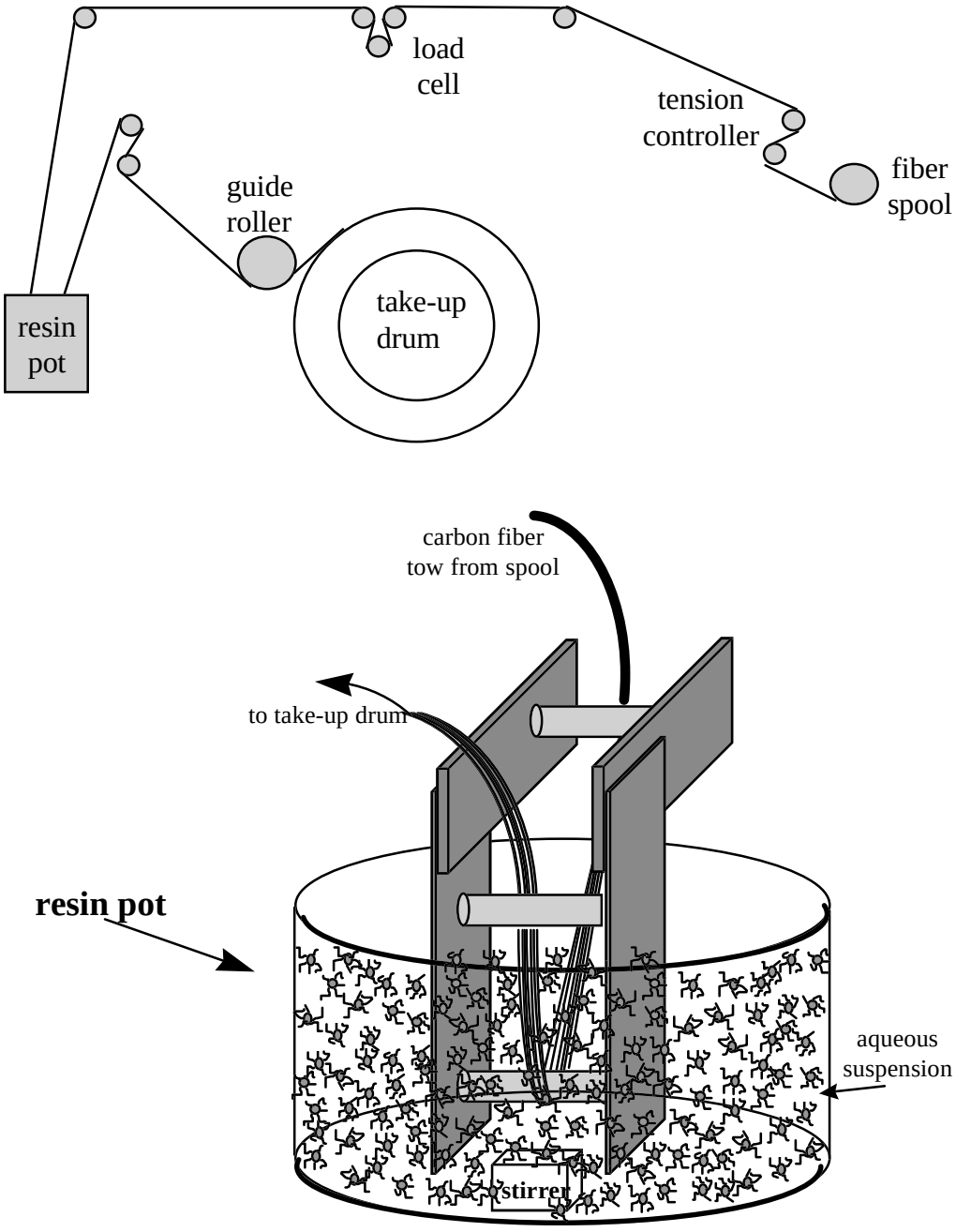

Figure 6-4. Schematic drawing of modified Research Tool Corporation Model 30 Drumwinder Prepregger with an enlarged view of the resin pot used for aqueous suspension prepregging.

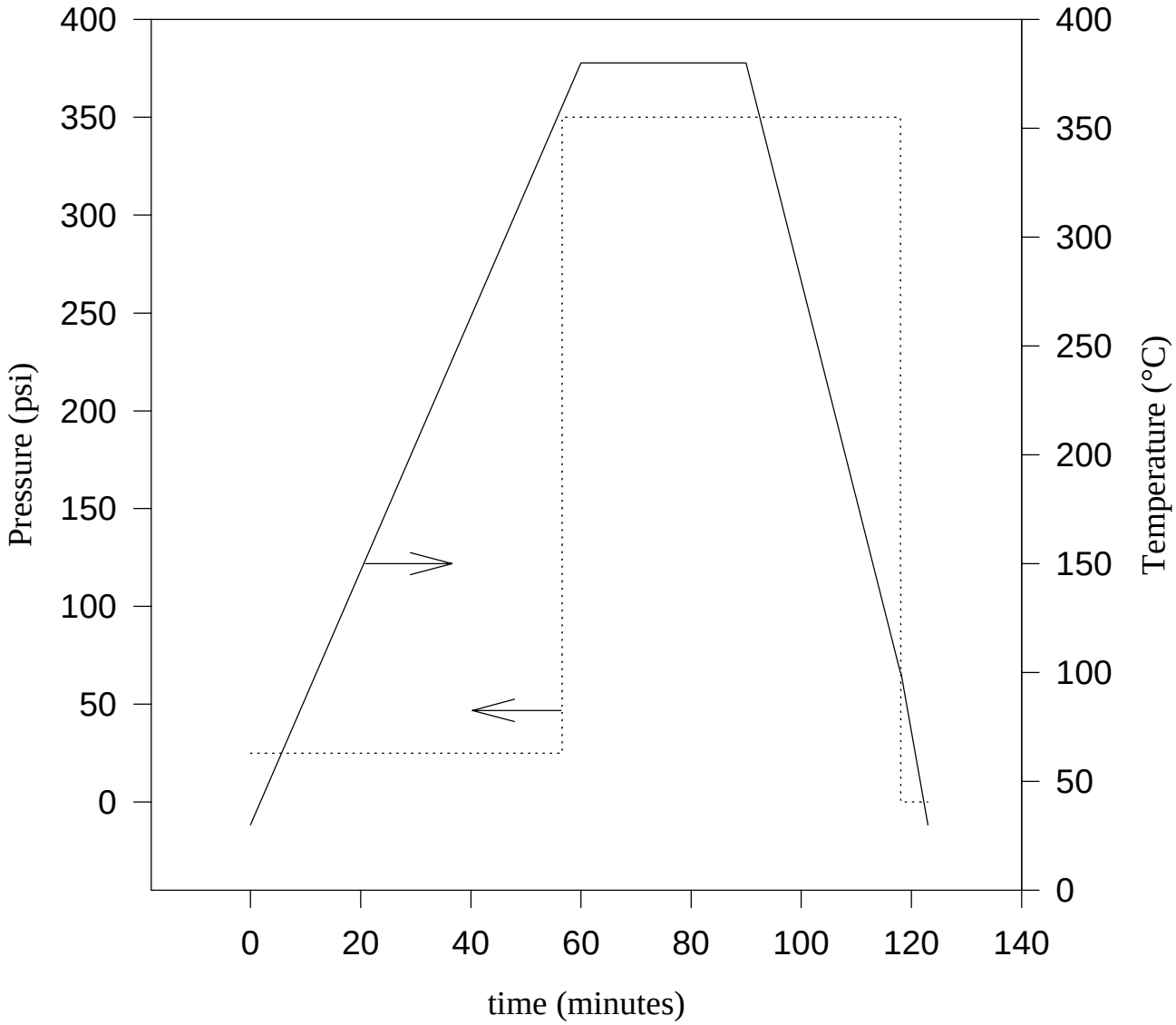

Figure 6-5. Temperature and pressure schedule for consolidation of PEEK matrix composites.

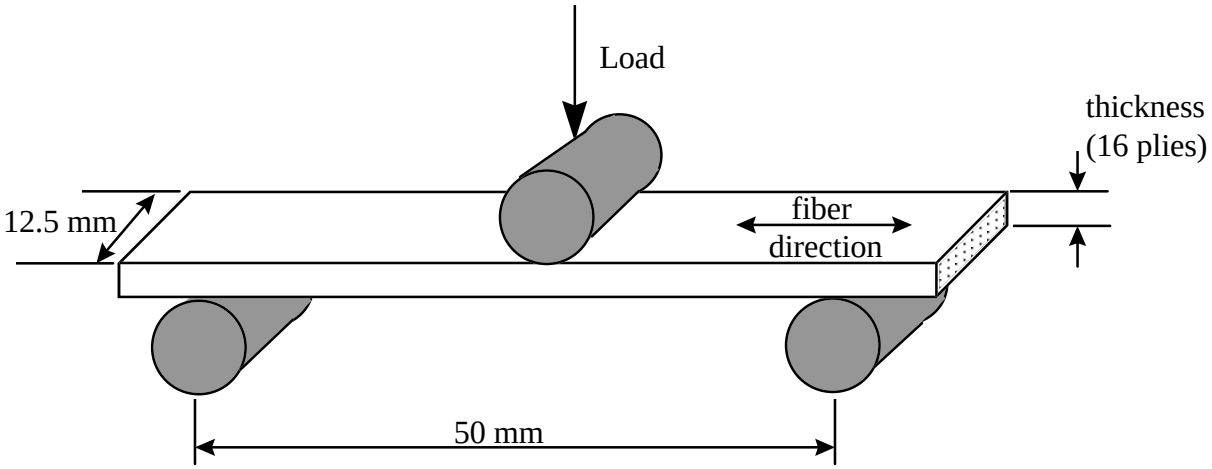

Figure 6-6(a) Composite longitudinal flexure testing geometry.

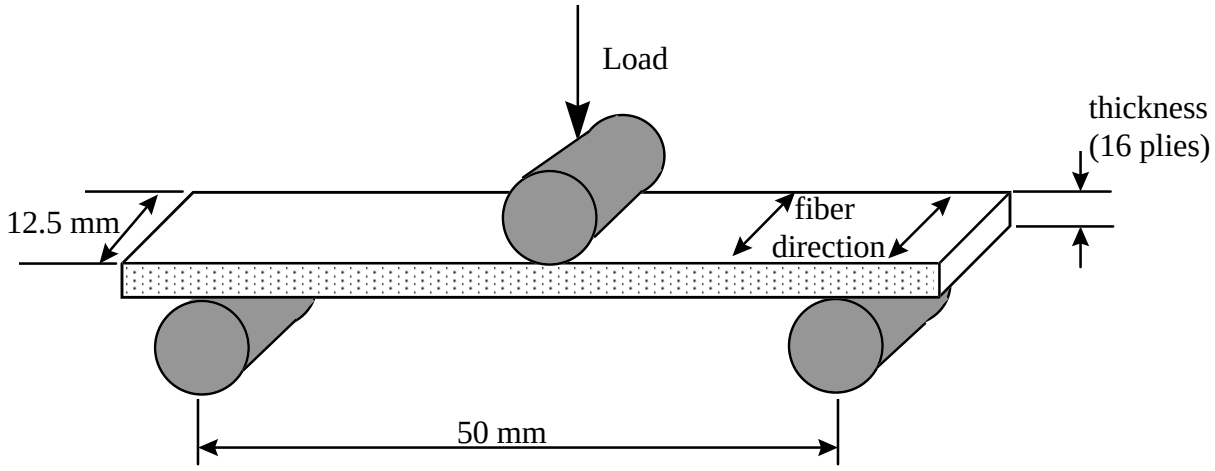

Figure 6-6(b) Composite transverse flexure testing geometry.

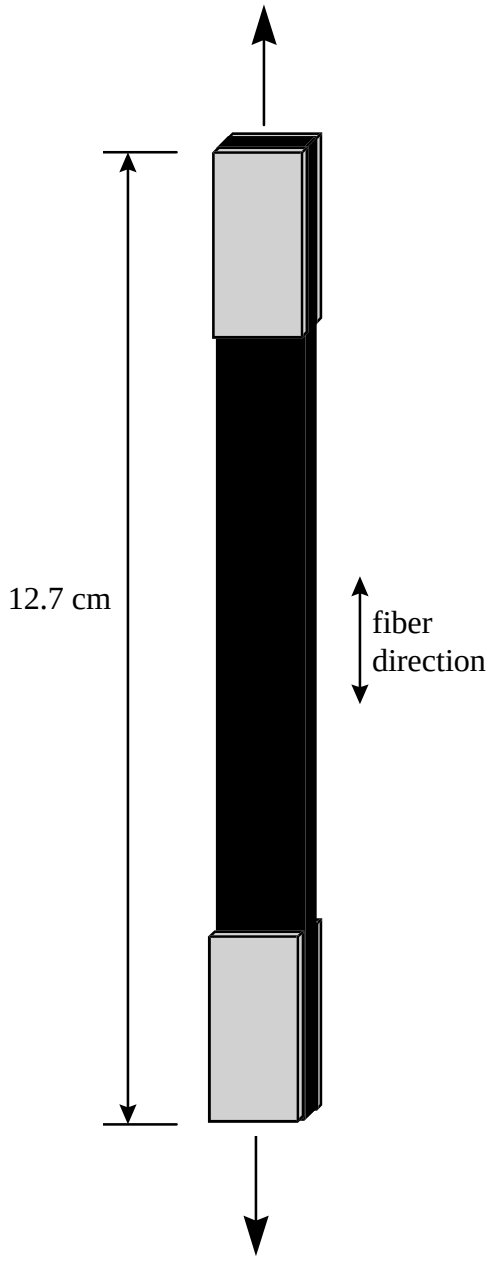

Figure 6-7. Unidirectional tension test geometry.

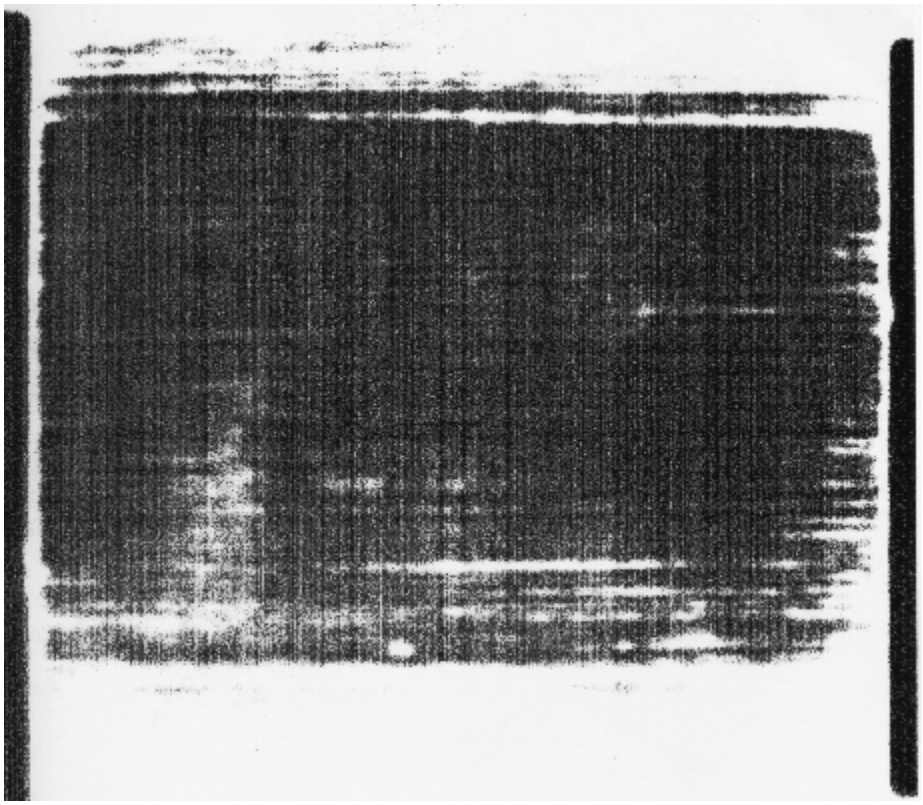

Figure 6-8. C-Scan image of panel P705 which is representative of “good” consolidation.

(a.)

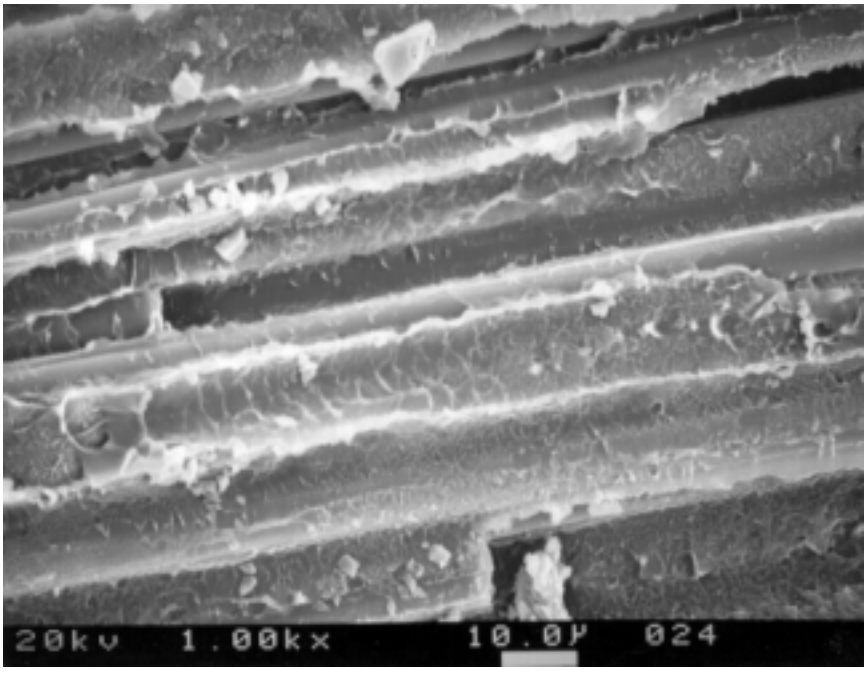

(b.)

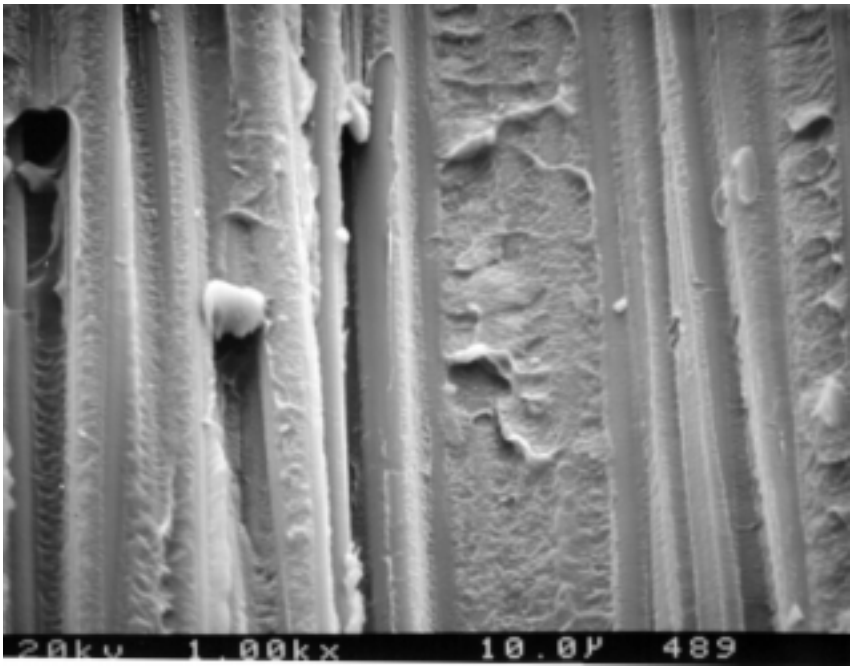

Figure 6-9. Micrographs of transverse flexure failure surfaces for (a.) 60 series HPC/PEEK composite and (b.) 70 series BisP-BTDA TMA+/PEEK composite.

(c.)

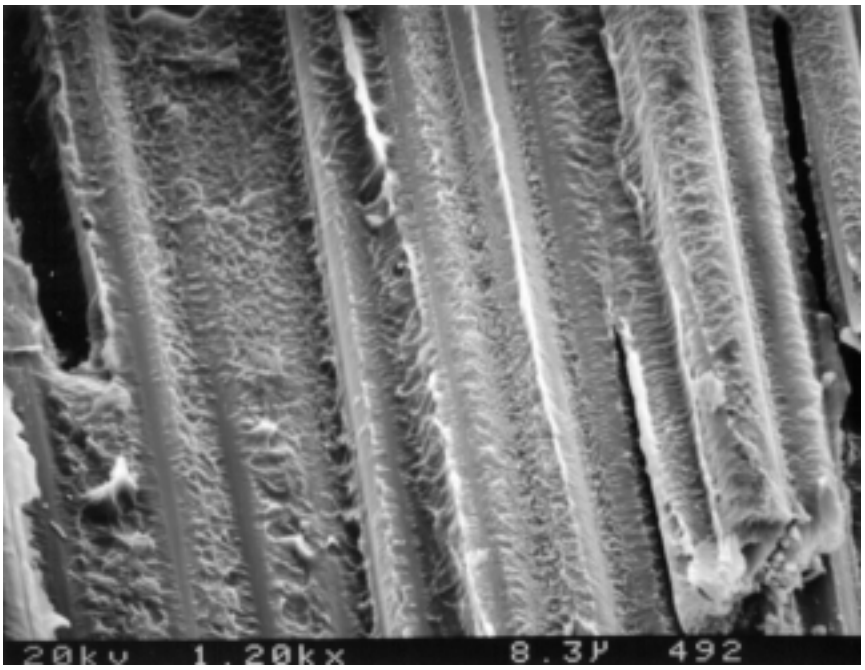

Figure 6-9. (continued) Micrograph of transverse flexure failure surfaces for (c.) 80 series BisP-BTDA NH4+/PEEK composite.

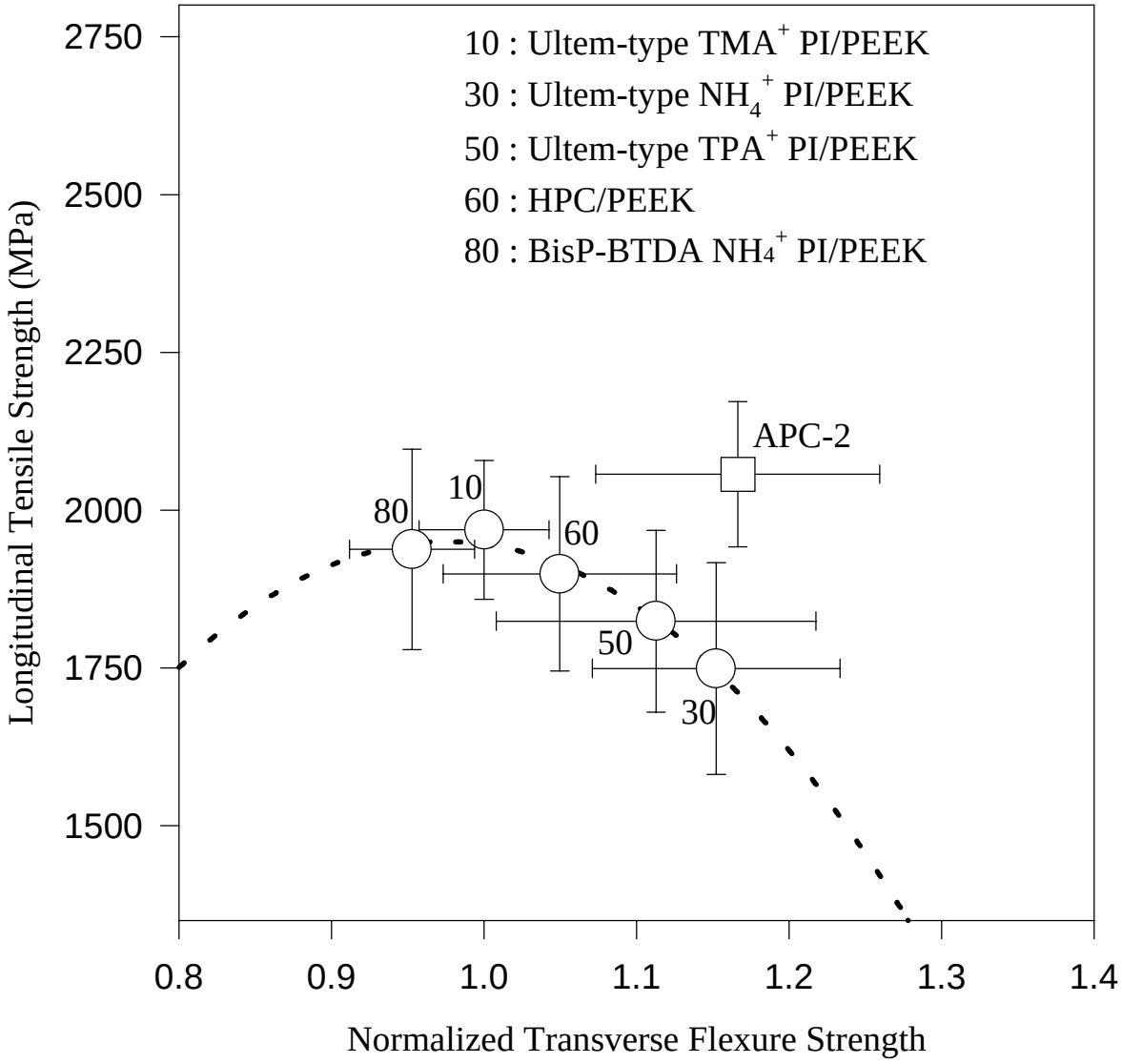

Figure 6-10. Experimentally measured longitudinal tensile strength vs. normalized transverse flexure strength (normalized to value for 10 series composite) of PEEK matrix composites.

References

1 Reifsnider, K.L., *Composites*, **25**, 461 (1994).

2. Drzal, L.T. and Madhukar, M., *Journal of Material Science*, **28**, 569 (1993).

3 Lesko, J.J., Swain, R.E., Cartwright, J.M., Chen, J.W., Reifsnider, K.L., Dillard, D.A., and Wightman, J.P., *Journal of Adhesion*, **45**, 43 (1994).

4 Subramanian, S., Lesko, J.J., Reifsnider, K.L., and Stinchcomb, W.W., *J. of Compos.Mat*., **30**, 309 (1996).

5 Chang, Y.S, Lesko, J.J., Case, S.W., Dillard, D.D., and Reifsnider, K.L., *Journal of Thermoplastic Composite Materials*, **7**, 311 (1994).

6 Gao, Z., Reifsnider, K.L., and Carman, G., *J. Compos. Mater.*, **26**, 1678 (1992).

7 Carman, G.P., Lesko, J.J., and Reifsnider, K.L., *Composite Materials: Fatigue and Fracture, Fourth Volume, ASTM STP 1156,* W.W. Stinchcomb and N.E. Ashbaugh, Eds., American Society for Testing and Materials, Philadelphia, PA, p. 430, 1993.

8 Case, S.W., Carman, G.P., Lesko, J.J., Fajardo, A.B., and Reifsnider, K.L., *J. Compos. Mater.*, **29**, 208 (1995).

9 The Effect of Polyimide Interphases on Properties of PEEK-Carbon Fiber Composites. S. Gardner, A. Gonzalez, R.M. Davis, J.V. Facinelli, J.S. Riffle, S. Case, J.J. Lesko, K.L. Reifsnider, *AIChE 1995 Annual Meeting.* November 12-17, 1995. Miami, FL.

10 Yu, T.H. and Davis, R.M., *J. Thermoplast.Comp. Mater.*, **6**, 62 (1993).

11 Texier, A., Davis R.M., Lyon, K.R., Gungor, A., McGrath, J.E., Marand, H., and Riffle, J.S., Polymer, **34**, 896 (1993).

12 Gonzalez, A-I, M.S. Dissertation (Virginia Polytechnic Institute and State University, Blacksburg, VA, November 1992).

13 Gonzalez-Ibarra, A., Davis, R.M., Heisey, C.L., Wightman, J.P., and Lesko, J.J., *Journal of Thermoplastic Composite Materials*, **10**, 85 (1997).

14 Davis, R.M., and Texier, A., *ANTEC '91 Confer. Proceed.*, **37**, 2018 (1991).

15 Facinelli, J.V., Gardner, S., Dong, L., Sensenich, C.L., Davis, R.M., and Riffle, J.S., *Macromolecules*, **29**, 7342 (1996).

16 McGrath, J.E., Rogers, M.E., Arnold, C.A., Kim, Y.J. and Hedrick, J.C., *Makromol. Chem., Macromol. Symp*., **51**, 103 (1991).

17 Pratt, J.R. and St. Clair, T.L., *SAMPE Journal*, **26**, 29 (1990).

18 Johnston, N.J., St. Clair, T.L., and Baucom, R.M., Polyimide Matrix Composites: Polyimidesulfone/:aRC-TPI (1:1) Blend, *24th International SAMPE Symposium and Exhibition*, Reno, NV, May 8-11, 1989.

19 Johnston, N.J. and St. Clair, T.L., *SAMPE Journal*, **23**, 12 (1987).

20 Johnston, N.J. and St. Clair, T.L., *SAMPE Preprints,* **18**, 53 (1986).

21 Texier, A., Davis R.M., Lyon, K.R., Gungor, A., McGrath, J.E., Marand, H., and Riffle, J.S., *Polymer*, **34**, 896 (1993).

22 Varughese, B., Muzzy, J., and Baucom, R.M., *21st Intern. SAMPE Tech. Confer.*, Sept. 25-28, 1989.

23 Baxandall, L.G., *Macromolecules*, **22**, 1982 (1989).

24 Jonas, A. and Legras, R., *Chapter 3, Assessing the Crystallinity of PEEK*, Advanced

Thermoplastic Composites, Ed. H.H. Kausch and R. Legras, Hanser Publications, New York, NY (1993).
25 Case, S.W.*PhD Dissertation* (Virginia Polytechnic Institute and State University, Blacksburg, VA, May 1996).
26 Sigma-Stat Statistical Software v. 2.0 User's Manual, Jandel Scientific, San Rafael, CA (1992-1995).
27 Agarwal and Broutman, "Analysis and Performance of Fiber Composites", John Wiley and Sons, New York, NY, 1990.
28 Hercules AS-4 Carbon Fiber Product data sheet.
29 Jar, P.-Y. and Plummer, Ch.J.G., Chapter 4, The Physical Structure and Mechanical Properties of Poly(Ether Ether Ketone), Advanced Thermoplastic Composites, Ed. H.H. Kausch and R. Legras, Hanser Publications, New York, NY (1993).
30 Adams, D.F., King, T.R., and Blackketter, D.M., *Composites Science and Technology*, **39**, 341 (1990).
31 ICI Victrex PEEK product data sheet.

Chapter Seven: Fabrication and Characterization of Carbon Fiber PPS matrix composites with Ultem-type Polyimide Interphases of Tailored Properties for Studying the Effect of Interphase Modifications

Introduction

An important way to improve composite performance and durability is by modifying the interphase. The interphase region is defined as the transition zone between the reinforcing fiber and the bulk matrix in a composite. An interphase typically accounts for less than 2% of the total mass of material in a composite [1]. However, carefully modified interphases have been shown to improve composite longitudinal tensile strength by as much as 29% [2], compressive strength by as much as 50% and notched fatigue lifetime cycles by as many as two orders of magnitude [1]. Therefore, the benefits of implementing a carefully constructed interphase are obvious.

Many models based on the micro-mechanics of failure have been proposed for prediction of composite strength and lifetime. The most recent models proposed by Reifsnider et al. incorporate an interphase region with significantly different material properties from the matrix polymer [1,3-7]. These models have been used to formulate hypotheses regarding further improvements of composite performance and durability based on interphase modifications.

The most intriguing hypothesis is that a maximum composite tensile strength can be attained for an optimal interfacial shear strength between the fiber and the bulk matrix. The most direct method of altering the interfacial shear strength without changing any of the other constituent properties is by modifying the interphase properties. The work of this chapter concerns the fabrication of Ultem-type polyimide interphase/PPS matrix composites to test the hypothesis of Reifsnider et al [8].

The aqueous suspension prepregging technique combines the matrix polymer with the fiber at the same time that the interphase polymer is deposited on the fiber [9-14]. Aqueous suspension prepregging has been done by many researchers using a polyimide precursor, a water soluble polyamic acid salt neutralized with a base [9-14]. The matrix polymer powder is dispersed in the aqueous polyamic acid salt solution. The polyamic acid salt behaves as a surfactant, adsorbing to the surface of the matrix powder particles, and electrostatically stabilizing the suspension. The fiber tow is then coated with the polyimide precursor and the matrix powder in a single prepregging step. The polyamic acid salt also serves as a binder, adhering the matrix powder to the carbon tow. After drying the water from the prepreg, a heating cycle is used to convert the polyamic acid to the polyimide by way of thermal imidization. The properties of the polyimide can be controlled by selection of the base and the method used for making the polyamic acid salt [15].

The main objectives of this chapter are (I) to fabricate polyphenylene sulfide (PPS) matrix composites with three different Ultem-type polyimide interphases and (ii) to evaluate the performance of these composites to test the hypothesis of a maximum longitudinal tensile strength at an optimum interfacial shear strength.

Some of the properties of the interphase have been estimated by studying model interphase Ultem-type polyimide discussed in Chapter 3. After thermal imidization, the Ultem-type NH_4^+ polyimide was shown to have a T_g of 153°C, and an M_n of 2,780 g/mol. The Ultem-type TMA^+ polyimide was shown to have a T_g of 201°C, and an M_n of 10,500 g/mol. The Ultem-type TPA polyimide was shown to have a T_g of 218°C, and an M_n of 16,000 g/mol. During a simulated composite consolidation temperature cycle, the melt viscosity of all three

polyimides was shown to increase at temperatures above 350°C.

Since PPS is immiscible with Ultem-type polyimide [16], interdiffusion of the interphase polyimide and the bulk PPS matrix is not possible. This is in contrast the Ultem-type polyimide/PEEK matrix system examined in Chapter 4. It is expected that the immiscible nature of the Ultem-type polyimide/PPS blend will result in two separate polymer phases which accentuate the effects of the polyimide interphase properties on the composite performance.

There are many problems and obstacles regarding the research project described above. Fabrication of a series of composites containing an interphase with controlled properties, while maintaining similarity of all other properties is a difficult task.

The aqueous suspension prepregging technique has been used successfully to fabricate PEEK matrix [9-12,14] and LaRC TPI matrix [10,12-14,17-22] composites.

Work has been done previously by Davis et al. [9,13] to assess the effects of systematically varied polyimide interphases that demonstrate a miscible interphase/matrix system and an immiscible interphase/matrix system. These are believed to be the first studies to specifically address such a concern for interphase composites. The work of this thesis extends the studies of Davis et al. to consider three systematically modified Ultem-type polyimide interphase PPS matrix composites.

The bulk of the investigations of interphase composites have been on thermosetting matrix systems. Due to the many advantages of engineering thermoplastic polymers, there is increasing interest in thermoplastic matrix, carbon fiber, interphase composites.

Furthermore, the investigations of interphase composites reported in the literature usually contain the same matrix, but with interphase modifications ranging from an unsized, unsurface

treated fiber to different fiber surface treatments and/or fiber with a polymeric sizing. This can result in differences of fiber/matrix adhesion or alteration of fiber properties rather than modification of the interphase material properties. The systematically modified interphase composites proposed for the work of this thesis are unique because the same fiber and matrix are maintained throughout each composite series, and the same interphase polyimide is used, but changes in interphase properties and characteristics will be a result of variances in interphase molecular weight. This minimizes speculation regarding the effects of system chemistry when interpreting the composite performance results.

Experimental
Materials

Composites were made with Hercules® AS-4 (lot#761-4m), unsized but surface treated 12k carbon fiber tow. This fiber is from the same batch used for the polyimide interphase/PEEK matrix composites described in the previous chapters.

The binder polymer was an Ultem®-type polyamic acid which is a precursor to the Ultem®-type polyimide.[15] The chemical structure for Ultem-type polyimide is shown in Figure 7-1. A large batch of BPADA/MPD (Ultem-type) polyamic acid endcapped with phthalic anhydride was synthesized in a 5 liter reactor at the General Electric Research Center in Schenectady, New York, by Dr. Biao Tan from Professor McGrath's group of the Virginia Tech Chemistry Department. The large batch of polyamic acid provided enough starting material so all experiments could be done using a single batch of polymer.

The bases used for making the polyamic acid salts were ammonium hydroxide (NH_4OH),

tetramethyl ammonium hydroxide (TMAH), and tripropylamine (TPA), all Fisher brand reagent grade.

The matrix material was GR-01 fiber spinning grade polyphenylene sulfide (PPS) supplied by Phillips Petroleum Chemicals Division (T_g = 85°C, T_m=285°C) [23]. The chemical structure of PPS is shown in Figure 7-2. The PPS was supplied as a powder with a very broad particle size distribution ranging from ~5 µm to greater than 1 mm in diameter. The powder was separated using a specially designed fluidized bed which was operated as an air classifier. A schematic of the fluidized bed is shown in Figure 7-3. The air flow rate and pressure was systematically varied in order to recover a narrow distribution of particle sizes. Details of the operation of the fluidized bed can be found in the report prepared by Mike Weber for the National Science Foundation, 1996 Summer Undergraduate Research Program requirement [24]. About ten pounds of PPS powder was separated with a median particle diameter of ~50 µm.

For all aqueous solutions and suspensions, deionized water from a Nanopure II water filtering system with a resistivity of 16.7 Ω/cm^3 was used.

Procedure

Calibration of bases

All bases were purchased new, kept sealed and stored in a refrigerator. The concentration of the aqueous bases were determined by potentiometric titration using an MCI Automatic Titrator Model GT-05 (COSA Instruments Corporation). The procedure for the calibration of the bases is identical to that used for the PEEK matrix composites and is described in detail in Chapter 4.

Polyamic acid preparation

Polyamic acid made by Dr. Biao Tan from the monomers 2,2'-Bis[4-(3,4-dicarboxyphenoxy)- phenyl]propane dianhydride (BPADA) and meta-phenylene diamine (m-PDA) was supplied as a 25 wt% solution in NMP at a temperature of -5°C. The polyamic acid chains were endcapped with phthalic anhydride to provide a target molecular weight of 20,000 g/mole. The preparation of the polyamic acid for use as in aqueous suspension prepregging with PPS powder matrix follows the exact procedure described for PEEK matrix composites. Details of the preparation of the polyamic acid can be found in Chapter 4.

Polyamic Acid Salt Preparation

For aqueous suspensions of PPS powder matrix, solutions of polyamic acid salts were first prepared. The formation of polyamic acid salt and subsequent imidization is shown in Figure 7-4. The procedure for preparation of Ultem-type polyamic acid salts for aqueous suspension prepregging with PPS powder matrix is identical to the procedure used for Ultem-type polyamic acid salts with PEEK powder matrix. The details of the procedures for Ultem-type NH_4^+ PAA salt preparation (30 series composite interphase), Ultem-type TMA^+ PAA salt preparation (10 series composite interphase) and Ultem-type TPA PAA salt preparation (50 series composite interphase) can be found in Chapter 4.

Suspension Preparation

After the aqueous polyamic acid salt solutions were made, they were used to make PPS suspensions suitable for composite prepregging. The solution and the PPS powder were mixed in a Waring blender at high speed for five minutes. The PPS powder was added to make a 9.8 wt% PPS solids content suspension. The mass of polyamic acid in solution was 5 wt% of the mass of the PPS powder. The suspensions were used immediately or were stored in a refrigerator.

A Shimadzu SAC-P3 Centrifugal Particle Size Analyzer was used to measure the size distributions of the suspensions. The instrument was used in the multi-function mode, which is a combination of gravimetric and centrifugal measurements. A few drops of the suspension was diluted in several milliliters of water until the turbidity of the suspension was reduced to a suitable level for measurements. The centrifuge was run at 240 rpm/min and a typical test took about 10 minutes. The median particle size for the suspensions were ~50 µm.

Prepregging

A detailed description of the prepregging process and techniques used in this work has been reported in previous studies by Texier et al [11] , by Yu and Davis [10] , and by Gonzalez et. al [13]. Using a modified Research Tool Corporation Model 30 Prepregger, the carbon fiber was continuously impregnated with the suspension. As seen in the schematic in Figure 7-5 the fiber was passed through a resin pot with an approximate volume of 0.25 l. The prepregged tow was then wound up on a drum at a line speed of ~10 cm/sec with a tow width of 0.33" and

approximately 25% tow overlap. The prepreg was dried on the drum at room temperature for 30 minutes and then it was cut off the drum, and cut into square prepreg lamina 10"x10". The prepreg lamina were then placed in a freezer until composite panel lay-up and consolidation.

Composite Layup and Consolidation

Two different stacking schemes were used for composite manufacture. The composites made were four-ply, unidirectional panels ($[0]_4$) and 16-ply unidirectional panels ($[0]_{16}$). The prepreg was taken immediately from the freezer and laid up in the appropriate stacking sequence. The stacked plies were heated in a Model 532 Fisher Programmable air convection oven according to a specially designed thermal treatment. The 10 series composite prepreg (Ultem-type TMA^+ interphase) and the 30 series composite prepreg (Ultem-type NH_4^+ interphase) were dried at 65°C for one hour followed by a two-hour hold at 265°C for imidization of the polyamic acid. The 50 series composite prepreg (Ultem-type TPA interphase) was dried at 65°C for one hour followed by a 275°C, ten minute imidization hold. The cyclization of PAA to polyimide is a condensation reaction. Since water is a product, the cyclization must be done prior to consolidation in the matched mold to prevent the water from accumulating in the composite and forming voids.

The dried and heat treated prepreg was placed in a 10" x 10" picture frame steel mold. A thermocouple was inserted into a corner of the mold to monitor the consolidation temperature and an IBM Model 30 personal computer was used to record the composite temperature and pressure history. The steel mold was treated with Frekote 34 mold release agent and the socket

head cap screws that fasten the mold together were treated with a high temperature anti-seize compound.

The composite consolidation cycle is shown in Figure 7-6. A Wabash Vacuum Hot Press was used for composite consolidation. The press was preheated to 320°C and the loaded mold was placed between the platens. Touch pressure was applied until the mold temperature was above 270°C. At this point, a vacuum of 28 in Hg was applied to the platen chamber and the consolidation platen pressure of 350 psi was applied. After the mold temperature reached 300°C, the temperature was maintained at this level for 30 minutes and then the mold was cooled at an approximate rate of 10°C/min. The consolidation pressure was applied until the mold temperature was at least 30°C below the glass transition temperature of the PPS matrix (85°C) [23].

Panel Evaluation

C-Scan

A Sperry Corporation S-80 C-Scan ultrasonic unit was used to qualitatively determine the level of consolidation of the panels. The 15 Khz transducer was used with a gain between 32 and 40 db. A scanning width of 0.1" was used with the fastest raster scanning speed.

Fiber Volume Fraction

Fiber volume fraction was determined by the Archemede's principle using a Sartorius balance with the specific gravity kit. Composite samples were weighed in air and in ethanol and

the composite density was determined using Eq. 7-1. The density of the ethanol was determined using a Mettler model DA-310 density/specific gravity meter. For the case of panels with regions of varying consolidation quality as determined by C-scan, samples were taken from two areas of the panel. The region of highest consolidation quality and the region of lowest consolidation quality were the two areas selected.

$$\rho_c = \frac{m^{air}}{m^{air} - m^{etOH}} \cdot \rho_{etOH} \qquad \text{Eq. 7-1}$$

Where: m^{air} = mass of composite sample in air
m^{etOH} = mass of composite sample in ethanol
ρ_{etOH} = density of ethanol.

The fiber volume fraction was calculated using the rule of mixtures rearranged in the form of Eq. 7-2.

$$V_f = \frac{\rho_c - \rho_m}{\rho_f - \rho_m} \qquad \text{Eq. 7-2}$$

Where:
ρ_c = density of composite as found from Eq. 7-1
ρ_f = density of carbon fiber
ρ_m = density of polymer matrix.

Image Analysis

An image analysis method was used to determine the void content of the composites. Samples of unidirectional laminates were mounted in epoxy, polished and examined under a scanning electron microscope (SEM) located in the chemistry departments surface analysis laboratory in the Hahn Hall. Buehler cold mount epoxide resin and hardener were used to mount the samples. Polishing was done on an automatic Buehler Polishing unit located in the Materials Response Group laboratory in Norris Hall using Buehler Carbimet Microcut Special Silicon Carbide Grinding Paper according to the polishing schedule outlined in Table 7-I. The polished sample was examined under SEM and representative micrographs were taken at magnifications of 750 x.

Table 7-I. Polishing schedule of PPS matrix composite surfaces for image analysis.

Duration	Grit Abrasive	Pressure	Polishing Direction
until surface ground level	120 grit	4lbs/pot	counter rotation
5 minutes	240 grit	4lbs/pot	counter rotation
5 minutes	320 grit	4lbs/pot	counter rotation
5 minutes	400 grit	4lbs/pot	matching rotation
10 minutes	600 grit	4lbs/pot	matching rotation
10 minutes	800 grit	4lbs/pot	matching rotation
10 minutes	1 µm grit	6lbs/pot	matching rotation
10 minutes	0.3 µm grit	6lbs/pot	matching rotation

These micrographs were scanned into .PCX file format using a Microtek Scanmaker IIHR scanner and an IBM compatible PC using Adobe Photoshop 3.0 and Scanmaker Plug-in for Adobe Photoshop v.2.13. Using the grey scale imaging feature of SigmaScan v. 4.0, the void content was determined.

Composite Characterization
Transverse Flexure Testing and Longitudinal Flexure Testing

Three point bending experiments according to ASTM D790-96 were done with 12.7 mm x 50.8 mm coupons [25]. Test specimens were machined using a diamond saw and the edges were polished with #400 grit silicon carbide abrasive paper. After the coupons were machined, an annealing process was employed to normalize the free volume relaxation of the amorphous content of the matrix polymer with regard to physical aging. The coupons were annealed at 70°C, approximately 15°C below T_g, for 48 hours and then cooled to room temperature at a rate of 0.1°C/min. Transverse flexure testing was done using an Instron with a 1 KN load cell and the longitudinal flexure testing was done using a 5 KN load cell. A three point bending test fixture was used to support the sample and provide uniform loading conditions for all samples. A 25/1 span to thickness ratio was used for testing. The transverse flexure testing was done with the fiber direction perpendicular to the length of the coupon, as shown in Figure 7-7(a) and the longitudinal flexure testing was done with the fiber direction along the length of the coupon, as shown in Figure 7-7(b).

Short Beam Shear

Short beam shear experiments according to ASTM D2344-84 were done with two sizes of coupons [26]. The smaller coupons were 6.34 mm x 16.5 mm x 2.5 mm thick and the larger coupons were 12.7 mm x 25.4 mm x 2.5 mm thick. Test specimens were machined using a diamond saw and the edges were polished with #400 grit silicon carbide abrasive paper. After the coupons were machined, an annealing process was employed to normalize the physical aging process. The coupons were annealed at 70°C, approximately 15°C below T_g, for 48 hours and then cooled to room temperature at a rate of 0.1°C/min. Testing was done using an Instron with a 5 KN load cell. A three point bending test fixture was used to support the sample and provide uniform loading conditions for all samples. A span to thickness ratio of 5 was used for the short beam shear testing. The loading geometry for the short beam shear testing is shown in Figure 7-8.

Unidirectional Tension

Tabs were bonded to the panels before the test samples were machined. Four rectangular, 12.7 cm x 2.54 cm x 0.25 cm, glass reinforced hardened epoxy tabs were bonded on the panel ends perpendicular to the fiber direction. The tabbed panels were machined into 12.7 cm x 1.27 cm coupons with the length in the fiber direction using a diamond saw. Extensometer tabs were bonded to the panel in the center of the test region at a separation of 2.54 cm. The specimen geometry for the longitudinal tension coupons is shown in Figure 7-9. Tension testing was done using a 20 kip servo-hydraulic MTS test machine under load control mode. The samples were

loaded to failure at a rate of 356 N/s.

Results and Discussion

Interphase Microstructure

Structure-property relationships of Ultem-type model interphase polyimides made from water soluble polyamic acid salts were developed in Chapter 3. To properly utilize these structure-property relationships in development of mechanical models for predicting composite failure, the geometry of each phase must be know. In an interphase composite, an important geometric parameter is the interphase thickness. The microstructure of the interphase must also be characterized. In the development of mechanical models for predicting composite failure, the structure-property relationships of the constitutive elements of the composite are applied. However, for present model development the properties of the interphase are assumed to be very similar to the properties of the bulk model interphase polyimides developed in Chapter 3. It is possible that the presence of the carbon fiber in the composite will affect the structure, hence the properties of the interphase polyimide. Interdiffusion of the polymer matrix and the interphase polyimide must also be considered.

The actual dimensions of the polyimide interphase in the composite cannot be experimentally measured at the present time. Experimental techniques for probing these dimensions are currently under development at Virginia Tech and elsewhere. The interphase thickness can be estimated based on some assumptions of composite geometry, composition and microscopic morphology.

It was shown in Chapter 4 that a hexagonally packed fiber array can be used as an assumed geometry, each surrounded by an identical, uniform interphase region. Using this geometry and an assumed fiber volume fraction of 60%, and a bulk matrix composition of 95% matrix polymer and 5% interphase polymer, the interphase thickness is calculated to be 200 nm. This calculation is based on the assumption that all of the interphase polymer remains in a single phase around the fiber surface which is a reasonable assumption for an immiscible blend. The necessary equations and sample calculations are shown in Appendix A of Chapter 4.

Using the equations in Appendix A the interphase thickness can be calculated for several different fiber volume fractions using the same assumptions for composite geometry, composition and microscopic morphology. If a fiber volume fraction of 40% is used, the calculated interphase thickness is 430 nm and If a fiber volume fraction of 65% is used, the calculated interphase thickness is 160 nm.

There are many factors to consider when discussing the actual dimensions of the interphase. The interphase dimensions are calculated assuming that the interphase is a pure polyimide phase. It has been shown by Akhtar and White [16] that while PPS is not miscible with Ultem 1000 polyimide, there is some degree of compatibility. Blends of PPS and Ultem 1000 showed a steady improvement in tensile strength with increasing polyimide composition [16]. If phase separation should occur for the immiscible PPS matrix and Ultem-type polyimide interphase, the microstructure of the interphase region would not have the gradient composition that was assumed for the PEEK matrix composites.

Polymer interdiffusion is strongly dependent on the molecular weight of the polymers. The number average molecular weight of Ultem 1000 was shown to be 19,000 in Chapter 3.

Since the immiscibility of PPS and Ultem-type polyimide was determined for high molecular weight Ultem 1000 [16], it is uncertain what the phase behavior might be for the Ultem-type polyimides processed from aqueous polyamic acid salts. Since the 10 series Ultem-type polyimide has an M_n of 10,500, the 30 series Ultem-type polyimide has an M_n of 2,780, and the 50 series Ultem-type polyimide has an M_n of 16,000, different phase behavior is possible. Since the molecular weights of the three interphase polyimides are different, the interphase microstructure is expected to vary with each system.

The polyimides processed from aqueous polyamic acid salts were shown to crosslink at elevated temperatures in Chapter 3, indicating that there are some chemically active functionalities, assumed to be at the ends of the polyimide chain. Thus, the possibilities for chemical interaction or physical adhesion to the carbon fiber surface must be considered. Structure-property relationships developed in Chapter 3 for the model interphase polyimide include characterization of model interphase polyimides after a simulated composite consolidation thermal treatment. This thermal treatment was a 30 minute isothermal hold at 380°C, designed to simulate the time-temperature cycle for manufacture of PEEK matrix composites. The processing cycle for the PPS matrix composites considered in this chapter includes a 30 minute isothermal hold at 300°C. This has important implications on the microstructure of the interphase in the PPS matrix composites. The crosslinking behavior of the model interphase polyimide was examined using melt rheology. When a simulated consolidation time-temperature cycle was utilized the melt viscosity was shown to decrease with temperature, up to about 350°C, where the melt viscosity began to increase. The melt viscosity during the simulated consolidation cycle suggests that any chemically active functionalities causing

crosslinking of the polyimide are activated above 350°C. Since the processing temperature for the PPS matrix composites is only 300°C, the crosslinking behavior is not expected to be as severe. However, this does not preclude any interactions of the interphase polyimide with the carbon fiber surface in the composite. Interactions of any chemically active functionalities with the carbon fiber surface could occur under the time-temperature cycle used for the PPS matrix composites.

Due to the complex nature of the interphase construction, the calculated interphase thickness should be considered as an order-of-magnitude approximation used to guide the further discussion of the composite properties.

Panel Quality

The quality of the panels was assessed using ultrasonic C-scan. The C-scan images were used to choose the panels with a high quality of consolidation suitable for mechanical evaluation. Some of the panels had regions of lesser quality consolidation. These regions were not included in mechanical evaluation. Table 7-II lists the quality of consolidation as evaluated by ultrasonic C-scan as well as the fiber volume fraction for the composite panels. Figure 7-10 shows a C-scan images which is representative of good consolidation quality.

Fiber volume fractions were measured for each panel using 3-5 samples from each panel. For panels with varying degrees of consolidation quality throughout the panel as found by C-scan, an average fiber volume fraction was found using samples from the region of best consolidation quality and also the region of worst consolidation quality.

Table 7-II. Quality of consolidation, fiber volume fraction and panel layup

panel ID	size	layup	Consolidation Quality	V_f (%)
PPS102[a]	10"x10"	$[0]_4$	good	61.0±3.1
PPS103[a]	10"x10"	$[0]_{16}$	good	59.0±3.8
PPS302[b]	10"x10"	$[0]_4$	good	39.5±0.7
PPS303[b]	10"x10"	$[0]_{16}$	good	63.4±0.3
PPS502[c]	10"x10"	$[0]_4$	good	61.1±1.4
PPS503[c]	10"x10"	$[0]_{16}$	good	56.8±2.0

a- Ultem-type TMA^+ polyimide interphase
b- Ultem-type NH_4^+ polyimide interphase
c- Ultem-type TPA polyimide interphase

The fiber volume fractions of the PPS matrix composites are all very close to one another except for the PPS302 panel. The fiber volume fraction of this panel is much lower than the rest. This panel is a unidirectional, 4-ply composite manufactured specifically for unidirectional tensile testing. As will be shown in the following discussion, there are mathematical corrections that can be applied for comparison of the unidirectional tensile data to account for variance in fiber volume fraction.

Composite Properties

The following sections will present experimental data of Ultem-type polyimide interphase/PPS composites. The details of the mechanical testing schedule are listed in Table 7-III.

Table 7-III. Mechanical testing schedule for PPS matrix composites

	10 series TMA^+/PPS	30 series NH_4^+/PPS	50 series TPA/PPS	layup
short beam shear	✓	✓	✓	$[0]_{16}$
transverse flexure	✓	✓	✓	$[0]_{16}$
longitudinal flexure	✓	✓	✓	$[0]_{16}$
longitudinal tension	✓	✓	✓	$[0]_4$

Short Beam Shear

The short beam shear testing results can be used to compare the relative interlaminar shear strengths of the composites tested. The ASTM D2344-84 standard test is not specified for measuring the interfacial shear strength but serves as a useful comparative testing [26].

All composite coupons tested failed in a horizontal shear mode. The short beam shear strengths were calculated using Eq. 7-3.

$$S_H = 0.75 \cdot \frac{P_B}{b \cdot d} \qquad \text{Eq. 7-3}$$

where S_H = shear strength, P_B = breaking load, b = width of coupon, d = thickness of coupon.

The short beam shear strengths (SBSS) are tabulated in Table 7-IV along with values normalized with respect to the SBSS for the TPA^+/PPS composite or the NH_4^+/PPS composite. Since two different sizes of short beam shear coupons were tested, the data is reported separately as $SBSS_{large}$ for the large coupons and $SBSS_{small}$ for the small coupons.

Table 7-IV. Short beam shear strengths for Ultem-type interphase/PPS matrix composites.

	V_f (%)	$SBSS_{large}$ (MPa)	normalized $SBSS_{large}$	$SSBS_{small}$ (MPa)	normalized $SSBS_{small}$
10 series[a]	59.0	57.4 ± 2.9	1.00	57.8 ± 3.8	1.05
30 series[b]	63.4	61.8 ± 3.4	1.08	55.3 ± 6.4	1.00
50 series [c]	56.8	75.7 ± 3.7	1.32	72.0 ± 4.8	1.30

a- Ultem-type TMA^+ polyimide interphase (panel PPS103)
b- Ultem-type NH_4^+ polyimide interphase (panel PPS303)
c- Ultem-type TPA polyimide interphase (panel PPS503)

For both sizes of short beam shear coupons, the 50 series composite had the greatest SBSS. The SBSS of the 50 series composite was 22-32% greater than the 10 series and 30 series composites. The results of these tests indicate that the interlaminar shear strength of the 10 series and 30 series composites are about the same and that the interlaminar shear strength of the 50 series composite is much greater. Guigon and Klinklin show increases of 15-33% in interlaminar shear strength for Narmco 5208 epoxy matrix/Courtaulds XAU carbon fiber over untreated fibers when the interphase was modified with two different amines [27].

One of the criticisms of the short beam shear test is that it does not provide quantitative data that can be related to micromechanical parameters [28]. It is a qualitative test used to rank

similar composites usually for the purposes of quality control. Another limitation of the test is that only the strength is a reportable parameter. Other mechanical tests yield a stiffness, a strain to failure and a toughness. The ranking of composites based on short beam shear testing is determined solely by the strength of the coupons. This does not provide as much insight to the performance of the composite as do other tests.

The 30 series and 50 series composite coupons reached a maximum load at failure and then the load dropped as the damaged coupon was folded in the three-point bending fixture. For the 30 series and 50 series composite coupons a loud, audible "pop" was heard when the coupon catastrophically failed at the peak of the load-deflection response curve, and then the load dropped off very rapidly. When this "pop" occurred, the fan-type edge was formed suddenly by several planes of shear delamination. The 10 series composite coupons did not fail in the same manner as the 30 series and 50 series composite coupons. There was not a loud "pop", but a quiet cracking sound and the load did not drop off as rapidly for the damaged coupon. Also, the formation of a fan-type edge did not occur, as the coupon continued to bend until the limits of the geometry of the three-point loading fixture were reached. Unfortunately, this significant observation can only be described and the standards of the test do not provide a qualitative means for comparing the toughness of the composites.

The small short beam shear test coupons from the three different composites failed in a more consistent manner than for the large short beam shear test. The load reached a maximum and then decreased as shear failure occurred delaminating the composite at several planes and creating a fan-type edge.

The failure mode of the short beam shear coupons display significant differences.

Pictures of failed small short beam shear test coupons are shown in Figure 7-11. As seen in Figure 7-11, the 10 series composite has a different appearance than the 30 series and 50 series composites. The 10 series composite shows more plastic deformation from the curved region at the midspan of the coupon. The 30 series and 50 series composites do not show curved areas of plastic deformation, and the fan-type edge formed by several planes of interlaminar shear failure is more pronounced.

Longitudinal Flexure

The longitudinal flexure properties provide more insight into the composite behavior in interlaminar shear failure. All longitudinal flexure coupons failed in a shear-type mode shown in Figure 7-12, as opposed to the tensile mode of failure observed with some of the PEEK matrix composites in Chapter 6. The longitudinal flexure strength was calculated using Eq. 7-4, the longitudinal flexure modulus was calculated using Eq. 7-5 and the strain-to-failure was calculated using Eq. 7-6.

$$\sigma = \frac{3 \cdot P \cdot L}{2 \cdot b \cdot d^2} \qquad \text{Eq. 7-4}$$

$$E_B = \frac{L^3 \cdot m}{4 \cdot b \cdot d^3} \qquad \text{Eq. 7-5}$$

$$\epsilon = \frac{6 \cdot D \cdot d}{L^2} \qquad \text{Eq. 7-6}$$

where: σ = stress in the outer fibers at midspan
P = maximum load at a point just before failure
L = support span
b = width of beam tested
d = thickness of beam tested
E_B = modulus of elasticity in bending
m = slope of tangent to linear region of load-deflection curve
ϵ = maximum strain in the outer fibers
D = maximum deflection of the center of the beam

The longitudinal flexure properties are shown in Table 7-V including the longitudinal flexure strength, the longitudinal flexure modulus, the failure tensile strain at the midspan of the specimen in the outerply induced by the bending moment, and the longitudinal flexure toughness calculated as the area under the longitudinal flexure stress-strain response curve.

Table 7-V. Longitudinal flexure properties of Ultem-type interphase/PPS matrix composites.

	V_f (%)	longitudinal flexure strength (MPa)	longitudinal flexure modulus (GPa)	longitudinal flexure strain-to-failure (%)	longitudinal flexure toughness (MPa)
10 series[a]	59.0	1105 ± 37	98.1 ± 3.8	1.34 ± 0.10	7.59 ± 0.48
30 series[b]	63.4	1282 ± 74	104.2 ± 8.4	1.37 ± 0.17	10.85 ± 1.35
50 series[c]	56.8	1370 ± 123	103.0 ± 5.3	1.70 ± 0.20	13.41 ± 0.68

a- Ultem-type TMA^+ polyimide interphase (panel PPS103)
b- Ultem-type NH_4^+ polyimide interphase (panel PPS303)
c- Ultem-type TPA polyimide interphase (panel PPS503)

The longitudinal flexure moduli for the three Ultem-type interphase/PPS matrix composites are not very different. A quantitative comparison of the data is desirable to verify which data sets are statistically different. The sets of data for the three composites were statistically compared using an unpaired *t*-test executed with SigmaStat Statistical Software v. 2.0. The unpaired *t*-test is used to test for a difference between two groups that is greater than what can be attributed to random sampling variation [29]. The SigmaStat Statistical Software first tests for normally distributed populations using a Kolmogorov-Smirnov test, and then tests for equal variance by checking the variability about the group means. If the sample populations each pass these tests, then the unpaired *t*-test is executed using a confidence interval of 95%. The unpaired *t*-test is a parametric test based on estimates of the mean and standard deviation parameters of the normally distributed populations from which the samples were drawn. If two sets of data pass an unpaired *t*-test, then there is a 95% confidence that the difference in the mean values of the two groups is greater than would be expected by chance. Therefore, there is a statistically significant difference between the groups.

The unpaired *t*-test results for the Ultem-type interphase/PPS matrix composite longitudinal flexure data are shown in Table 7-VI. Each set of PPS matrix composite longitudinal flexure data was compared with one another. The results show that there is not a statistically significant difference in the longitudinal flexure modulus for any of the pairs of composites. The longitudinal flexure moduli should be dependant upon fiber volume fraction, however the differences in fiber volume fraction are not great enough to create a significant difference. The *t*-test results provide a quantitative comparison showing that the transverse flexure moduli are similar.

The important differences in these composites are in longitudinal flexure strength, strain-to-failure and toughness. The results also show that there is a statistically significant difference in longitudinal flexure strength between the 10 series composite and both of the other composites. However the longitudinal flexure strength for the 30 series and the 50 series composites are not statistically different. The longitudinal flexure strain-to-failure for the 50 series composite has a statistically significant difference from both of the other composites. However, the longitudinal flexure strain-to-failure for the 10 series and 30 series composites are not statistically different. The longitudinal flexure toughness of the PPS composites are statistically different for all the composite pairs.

Table 7-VI. Unpaired *t*-test results comparing each set of PPS matrix composite longitudinal flexure data.

	Longitudinal flexure strength	Longitudinal flexure strain	Longitudinal flexure modulus	Longitudinal flexure toughness
10 series[a] vs 30 series[b]	pass	fail	fail	pass
10 series[a] vs 50 series[c]	pass	pass	fail	pass
30 series[b] vs 50 series[c]	fail	pass	fail	pass

a- Ultem-type TMA^+ polyimide interphase
b- Ultem-type NH_4^+ polyimide interphase
c- Ultem-type TPA polyimide interphase
pass = statistically significant difference between data sets
fail = data sets are not significantly different enough to reject the possibility that the difference is due to random sampling variability

The 50 series composite has the greatest longitudinal flexure strength, longitudinal flexure strain-to-failure and longitudinal flexure toughness of the Ultem-type interphase/PPS matrix composites. The longitudinal flexure strength of the 50 series composite is 20% greater

than the 10 series composite and 6% greater than the 30 series composite. However, the longitudinal flexure strain-to-failure for the 50 series composite is 19-21% greater than both the 10 series and 30 series composites. These factors combine to yield a longitudinal flexure toughness for the 50 series composite which is 43% greater than the 10 series composite and 19% greater than the 30 series composite.

The superior longitudinal flexure performance of the 50 series composite can be attributed largely to the greatest longitudinal flexure strain-to-failure . Since the composites all have very similar moduli, it is the ability of the 50 series composite to handle larger strains that allows it to be loaded to greater stresses.

Other researchers have attempted to correlate the longitudinal flexure strength to the longitudinal tensile strength for composites [2]. This will be discussed for the Ultem-type polyimide interphase/PPS matrix composites later in this chapter.

Drzal and Madhukar showed that the longitudinal flexure strength did not follow the same trends as the longitudinal tensile strength for epoxy matrix composites with different fiber surface treatments [2]. This is shown graphically in Figure 7-13 from Drzal and Madhukar's results. As the normalized ISS increases, the normalized longitudinal tensile strength increases, however the normalized longitudinal flexure strength initially decreases and then increases. There does not appear to be a trend of ISS with longitudinal flexure strength. This is understandable when considering the micromechanics of stress-concentration dominated fracture mechanics. Since the longitudinal flexure test does not provide a pure tensile loading, the failure mode will be mixed. The flexure test geometry applies a tensile load on the bottom surface of the test coupon while simultaneously applying a compressive load on the top surface of the test

coupon. This also results in a shear plane in the middle of the laminate. Since the flexure test geometry is a three point bending setup, the tensile and compressive loads will be maximized at midspan. The tensile and compressive loads will not be uniform along the length of the coupon, therefore, the presence of micromechanical stress concentrations distributed around the coupon due to discontinuous fibers will not factor in the manifestation of failure.

Transverse Flexure

The transverse flexure strength was calculated using Eq. 7-4, the transverse flexure modulus was calculated using Eq. 7-5 and the transverse flexure strain-to-failure was calculated using Eq. 7-6. The transverse flexure toughness was calculated as the area under the stress-strain response curve. The coupon failure mode for the transverse flexure testing was consistent for all samples and was characterized by tensile fracture near the beam center due to normal stresses. There was no indication of fracture due to interlaminar shear stresses which would be characterized by splitting of the beam on the level of the mid-plane.

The data from the transverse flexure test shown in Table 7-VII provide compelling results that the differences in interphase properties directly affect the fiber-matrix adhesion in the composite.

The stress-strain response behavior for the transverse flexure testing of the Ultem-type interphase/PPS matrix composites was similar for the 30 series and 50 series composites which failed at a maximum stress and then the stress dropped deliberately. The 10 series composite failed at a lower stress but failure was not catastrophic enough to fracture the coupon into

separate pieces. Further bending created more damage in the coupon which accumulated over a large coupon deflection, until the coupon was damaged enough that the stress fell off. The transverse flexure properties are shown in Table 7-VII.

Table 7-VII. Transverse flexure results for Ultem-type interphase/PPS matrix composites.

	V_f (%)	transverse flexure strength (MPa)	normalized transverse flexure strength*	transverse flexure modulus (GPa)	transverse flexure strain-to-failure (%)	transverse flexure toughness (MPa)
10 series[a]	59.0	16.2 ± 2.7	1.00 ± 0.17	2.23 ± 0.78	0.74 ± 0.29	0.152 ± 0.063
30 series[b]	63.4	43.8 ± 5.5	2.70 ± 0.13	8.02 ± 0.51	0.55 ± 0.09	0.166 ± 0.038
50 series[c]	56.8	35.0 ± 5.8	2.16 ± 0.17	7.56 ± 0.53	0.49 ± 0.07	0.105 ± 0.026

* - values normalized to transverse flexure strength of 10 series PPS composite
a- Ultem-type TMA^+ polyimide interphase (panel PPS103)
b- Ultem-type NH_4^+ polyimide interphase (panel PPS303)
c- Ultem-type TPA polyimide interphase (panel PPS503)

The sets of data for the three composites were statistically compared using an unpaired *t*-test executed with SigmaStat Statistical Software v. 2.0 as described earlier in the longitudinal flexure test section. The unpaired *t*-test is used to test for a difference between two groups that is greater than what can be attributed to random sampling variation. A 95% confidence interval was used to determine if the difference in the mean values of the two groups is greater than would be expected by chance. The *t*-test results for the transverse flexure test are shown in Table 7-VIII.

The transverse flexure strength of all the PPS matrix composites are statistically unique. The transverse flexure strain-to-failure is not statistically different for the 30 series composite

compared to either of the other composites. The transverse flexure modulus is not statistically different for the 30 series compared to the 50 series composite. The transverse flexure toughness is not statistically different for the 10 series compared to the 30 series composite.

Table 7-VIII. Unpaired *t*-test results comparing each set of PPS matrix composite transverse flexure data.

	Transverse Flexure Strength	Transverse Flexure Strain-to-Failure	Transverse Flexure Modulus	Transverse Flexure Toughness
10 series[a] vs 30 series[b]	pass	fail	pass	fail
10 series[a] vs 50 series[c]	pass	pass	pass	pass
30 series[b] vs 50 series[c]	pass	fail	fail	pass

a- Ultem-type TMA^+ polyimide interphase
b- Ultem-type NH_4^+ polyimide interphase
c- Ultem-type TPA polyimide interphase

The 30 series composite has the greatest transverse flexure strength, transverse flexure modulus and transverse flexure toughness of the Ultem-type interphase/PPS matrix composites. The 30 series composite transverse flexure strength is 15% greater that the transverse flexure strength for the 50 series composite and 58% greater than transverse flexure strength for the 10 series composite. The 30 series composite transverse flexure modulus is 73% greater than transverse flexure modulus for the 10 series composite. The 30 series composite transverse flexure toughness was 39% greater than the transverse flexure toughness for the 50 series composite. Since the strain to failure was greatest for the 10 series composite, even though the strength was much lower, the toughness was relatively high due to the compliant nature of the composite which accumulated damage over a wider range of strains.

The transverse flexure strength is a very important property because it furthers the development of the composite structure-property relationships and provides a means of comparing the interfacial adhesion of the composites. The transverse flexural strength has been shown by Adams, et al. [30] to be dependent upon different sizings or interphases of the composite. Drzal and Madhukar [2] have shown that the flexural strength correlates well with the interfacial shear strength (ISS) for composites made with AU-4, AS-4 and AS-4C fibers and Epon 828 epoxy matrix, cured with mPDA. Chang, et al. [4] showed a similar correlation of transverse flexure strength with ISS for composites made with AU-4, AS-4, and AS-4GCP fibers and J2 polyamide copolymer matrix. The normalized transverse flexure strength has been plotted as a function of normalized ISS from the data of Drzal and Madhukar [2] and Chang, et al. [4] in Figure 7-14. This data clearly shows a correlation of increasing transverse flexure strength with increasing ISS.

Although quantitative ISS values cannot be gained from the correlation of ISS to transverse flexure strength data, a relative ranking of ISS, or fiber-matrix interfacial adhesion can be made. Following the trends of the transverse flexure strength, this relative ranking is:

$$ISS_{\text{10 series}} < ISS_{\text{50 series}} < ISS_{\text{30 series}}$$

This relative ranking of composite interfacial shear strength is very important for a discussion of the effects of interfacial shear strength on overall composite performance and understanding the micromechanics of composite failure. This relative ranking is identical to the ranking for Ultem-type interphase/PEEK matrix composites discussed in Chapter 4.

Longitudinal Tension

The longitudinal tensile strength was calculated from the load at failure divided by the cross sectional area of the composite coupon. The tensile strain-to-failure was the strain of the composite coupon measured by an extensometer at the point of maximum load. The tensile modulus was calculated as secant modulus from 0.2 to 0.4% strain. This range of strains was within the linear region of the stress-strain response curve. The tensile toughness was calculated as the area under the stress-strain response curve up to the point of failure.

The longitudinal tensile test results are shown in Table 7-IX. The tensile strength is tabulated along with the tensile strength normalized with respect to the 30 series composite strength value.

Table 7-IX. Longitudinal tension test results for PPS matrix composites.

Panel	V_f (%)	tensile strength (MPa)	normalized tensile strength*	tensile modulus (GPa)	tensile strain-to-failure (%)	tensile toughness (MPa)
10 series[a]	61.0	1882 ± 55	1.94 ± 0.06	136.2 ± 7.2	1.34 ± 0.05	12.28 ± 0.76
30 series[b]	39.5	968 ± 20	1.0 ± 0.02	96.7 ± 3.1	0.99 ± 0.05	4.74 ± 0.54
50 series[c]	61.1	1779 ± 79	1.84 ± 0.08	127.9 ± 10.8	1.36 ± 0.11	12.25 ± 1.10

* - values normalized to longitudinal tensile strength of 30 series PPS composite
a- Ultem-type TMA^+ polyimide interphase (panel PPS102)
b- Ultem-type NH_4^+ polyimide interphase (panel PPS302)
c- Ultem-type TPA polyimide interphase (panel PPS502)

Among the Ultem-type polyimide interphase/PPS matrix composites, the 10 series composite had the highest tensile strength and tensile toughness. This interphase composite system was shown to have the weakest fiber-matrix adhesion of the three by transverse flexure testing and the weakest interlaminar shear strength by longitudinal flexure testing.

The tensile toughness is a useful indicator of composite tensile performance, and the differences in tensile toughness for the Ultem-type interphase composites support the trends of the tensile strengths. However, the much lower fiber volume fraction for the 30 series composite is an important factor in the differences in tensile properties, including toughness. Corrections can be applied to unidirectional tensile data to compensate for differences in fiber volume fraction, but these corrections are applicable to tensile strength and tensile modulus, not tensile toughness. Therefore, caution must be exercised when making conclusions based on the tensile toughness data.

The sets of data for the three composites were statistically compared using an unpaired *t*-test executed with SigmaStat Statistical Software v. 2.0 as described earlier in the longitudinal flexure test section. The unpaired *t*-test is used to test for a difference between two groups that is greater than what can be attributed to random sampling variation. A 95% confidence interval was used to determine if the difference in the mean values of the two groups is greater than would be expected by chance. The *t*-test results for the longitudinal tension test are shown in Table 7-X.

Table 7-X. Unpaired *t*-test results comparing each set of PPS matrix composite longitudinal tension data.

	Longitudinal Tensile Strength	Longitudinal Tensile Strain-to-Failure	Longitudinal Tensile Modulus
10 series[a] vs 30 series[b]	pass	pass	pass
10 series[a] vs 50 series[c]	pass	fail	fail
30 series[b] vs 50 series[c]	pass	pass	pass

a- Ultem-type TMA^+ polyimide interphase
b- Ultem-type NH_4^+ polyimide interphase
c- Ultem-type TPA polyimide interphase

The longitudinal tensile strengths of all the PPS matrix composites are statistically unique. The longitudinal tensile strain-to-failure for the 10 series compared to the 50 series composites are not statistically different. The longitudinal tensile moduli for the 10 series compared to the 50 series composites are not significantly different.

The differences in tensile strength are very dramatic. The tensile strength of the 10 series composite is 6% greater than the tensile strength of the 50 series composite but an impressive 49% greater than the tensile strength of the 30 series composite. This latter comparison, however, is affected by the large difference in fiber volume fraction between the specimens. The rule of mixtures can be applied to unidirectional tensile test data to compensate for differences in fiber volume fraction.

The Ultem-type interphase/PPS matrix composite coupons did not all fail in the same manner. In general, when failure occurred, the coupon shattered into many small pieces. However, as seen in Figure 7-15 the failure modes for the 10 series and 50 series composites were similar, resulting in a frayed, broom-like shape. The failure mode for the 30 series composite contrasts the failure mode of the other composites with fracture occurring in the

transverse direction, breaking the coupon in the middle. A discussion of stress concentration dominated mechanics and the implications on the longitudinal tensile strength and failure mode are included later in this chapter. The stress concentration dominated mechanics demonstrates that the failure mode of the 10 series and 50 series composites is indicative of a lower ISS and that the failure mode of the 30 series composites is indicative of a higher ISS. It is not clear whether the differences in fiber volume fraction influence the different composite tensile failure modes.

Table 7-XI shows the composite fiber volume fractions, rule of mixture predictions for strength (σ^{ROM}) and the experimentally measured tensile strength. The model for calculating the rule of mixtures strength was developed in Chapter 4. The assumptions for this model are that the fibers are continuous, aligned parallel and uniform in properties. Other important assumptions are that perfect bonding exists between the fibers and matrix so that slippage does not occur at the fiber-matrix interface and each component has a linear elastic response. Thus, during longitudinal tension, the elastic strains experienced by the fiber, matrix and composite are equal. The rule of mixtures strength can be calculated using Eq. 7-7.

$$\sigma^{ROM} = V_f \bullet \sigma_f + (1 - V_f)\sigma_m \qquad \text{Eq. 7-7}$$

σ^{ROM} = rule of mixtures tensile strength
V_f = fiber volume fraction
σ_f = fiber tensile strength
σ_m = matrix tensile strength

The stresses σ_f and σ_m in Eq. 7-7 are not the ultimate strengths of the constitutive materials, but they are stresses at a specific strain within the elastic region of deformation. To

use Eq. 7-7 properly, a specific composite strain must be considered. Since the strains of the composite, fibers and matrix are equal in this model, and a linear elastic response is assumed for each component, Hooke's law can be used to calculate the individual contributions to composite strength by the fibers and the matrix as seen in Eq. 7-8 and Eq. 7-9.

$$\sigma_f = E_f \cdot \epsilon \qquad \text{Eq. 7-8.}$$

$$\sigma_m = E_m \cdot \epsilon \qquad \text{Eq. 7-9.}$$

In this manner, the stresses of the constitutive components are calculated based on literature values for the fiber modulus, $E_{f,}$ and the matrix modulus, E_m. The strain used, ϵ, is the measured composite strain from Table 7-IX. The Hercules AS-4 carbon fiber data sheet reports E_f = 234.6 GPa [31] and the modulus of PPS is reported as E_m = 3.3 GPa [23]. Using these values with Eq. 7-7, Eq. 7-8 and Eq. 7-9, the rule of mixtures composite strength is calculated and tabulated in Table 7-XI.

Table 7-XI. Rule of mixture predictions for tensile strength compared to experimental data.

Panel	V_f (%)	σ^{ROM} * (MPa)	tensile strength (MPa)
10 series[a]	61.0	1938 ± 72	1882 ± 55
30 series[b]	39.5	947 ± 53	968 ± 20
50 series[c]	61.1	1970 ± 154	1779 ± 79

* calculated from Eq. 7-7.
a- Ultem-type TMA^+ polyimide interphase
b- Ultem-type NH_4^+ polyimide interphase
c- Ultem-type TPA polyimide interphase

The strength predicted by the rule of mixtures shows good agreement to the measured tensile strength. This indicates that the composites are modeled well by the assumptions made for the rule of mixtures model. Specifically, the composite has fibers that are continuous, aligned parallel and uniform in properties. Good bonding exists between the fibers and matrix so that no slippage occurs at the fiber-matrix interface and each component can be considered to have a linear elastic response.

The tensile moduli shown in Table 7-X. indicate that there is a large difference among the composite systems. Since all the composites were manufactured with the same type of carbon fiber, it is expected that the composite moduli would be similar. The differences in composite moduli can be explained by the differences in fiber volume fraction. Table 7-XI shows the composite fiber volume fractions, rule of mixture predictions for moduli, E^{ROM}, and the experimentally measured moduli. E^{ROM} was calculated using Eq. 7-10.

$$E^{ROM} = V_f \bullet E_f + (1 - V_f) E_m \qquad \text{Eq. 7-10}$$

E^{ROM} = rule of mixtures composite modulus V_f = fiber volume fraction
E_f = fiber modulus E_m = matrix modulus

The moduli predicted by the rule of mixtures is close to the measured modulus for the Ultem-type polyimide interphase PPS matrix composites. This is another indication that the PPS matrix composites are modeled well by the assumptions from which the model were developed. Specifically, the composite has fibers that are continuous, uniform in properties and aligned parallel. Good bonding exists between the fibers and matrix so that no slippage occurs at the

fiber-matrix interface and each component can be considered to have a linear elastic response. Of importance is that the modulus predicted for the 30 series composite is very close to the measured modulus, which indicates that, although the fiber volume fraction of the 30 series composite was lower than the other composites, the tensile modulus was very close to the expected value.

Table 7-XII. Rule of mixture predictions for tensile modulus compared to experimental data.

Panel	V_f (%)	E^{ROM} * (GPa)	tensile modulus (GPa)
10 series[a]	61.0	144.2	136.2 ± 7.2
30 series[b]	39.5	95.7	96.7 ± 3.1
50 series[c]	61.1	144.4	127.9 ± 10.8

*calculated from Eq. 7-10.
a- Ultem-type TMA^+ polyimide interphase
b- Ultem-type NH_4^+ polyimide interphase
c- Ultem-type TPA polyimide interphase

Figure 7-16 shows the composite tensile moduli vs. fiber volume fraction compared to predictions from the rule of mixtures. The rule of mixture predictions were calculated using the PPS tensile modulus from the literature, and the fiber tensile modulus from a Hercules AS-4 product data sheet [31]. The composite modulus has a very strong dependence upon fiber volume fraction, as seen by the curve in Figure 7-16. The ratios of measured tensile moduli to the predicted moduli by the rule of mixtures are labeled in Figure 7-16.

As mentioned earlier, the longitudinal tensile strength and longitudinal tensile modulus can be corrected for fiber volume fraction. This is accomplished with the use of the rule of mixtures. Since the rule of mixtures was shown to predict the longitudinal tensile strength and

longitudinal tensile modulus well for all PPS matrix composites regardless of the fiber volume fraction, corrections for fiber volume fraction using the rule of mixtures is considered appropriate.

Eq. 7-7 can be used to create a ratio of strengths predicted by the rule of mixtures as shown in Eq. 7-11 [34]. An important assumption for Eq 7-11 is that $\sigma^{experimental}$ is equal to σ^{ROM} as calculated by Eq. 7-7. It has been shown that this assumption is valid for the data.

$$\frac{\sigma^{61\%}}{\sigma^{experimental}} = \frac{0.61 \cdot \sigma_f + (1 - 0.61) \cdot \sigma_m}{V_f \cdot \sigma_f + (1 - V_f) \cdot \sigma_m} \qquad \text{Eq. 7-11}$$

where

$\sigma^{61\%}$ = composite tensile strength corrected to 61% fiber volume fraction
$\sigma^{experimental}$ = experimentally measured composite tensile strength
V_f = experimentally measured fiber volume fraction
σ_f = fiber tensile strength
σ_m = matrix tensile strength

From Eq. 7-11 the longitudinal tensile strength corrected to 61% fiber volume fraction can be calculated. A similar ratio can be made of Eq. 7-10 for moduli predicted by the rule of mixtures [34]. Once again, an important assumption for Eq 7-12 is that $E^{experimental}$ is equal to E^{ROM} as calculated by Eq 7-10. This has been shown to be a valid assumption for the data.

$$\frac{E^{61\%}}{E^{experimental}} = \frac{0.61 \cdot E_f + (1 - 0.61) \cdot E_m}{V_f \cdot E_f + (1 - V_f) \cdot E_m} \qquad \text{Eq. 7-12}$$

here

$E^{61\%}$ = composite modulus strength corrected to 61% fiber volume fraction
$E^{experimental}$ = experimentally measured composite modulus strength
V_f = experimentally measured fiber volume fraction
E_f = fiber tensile modulus
E_m = matrix tensile modulus

Eq. 7-12 can be used to calculate the tensile modulus of a composite corrected to 61% fiber volume fraction. The tensile strengths and tensile moduli corrected to 61% fiber volume fraction are tabulated in Table 7-XIII.

Table 7-XIII. Tensile moduli and tensile strength of Ultem-type polyimide interphase/PPS matrix composites corrected to 61% fiber volume fraction using Eq. 7-11 and Eq. 7-12.

	longitudinal tensile strength corrected to 61% fiber volume fraction*	longitudinal tensile modulus corrected to 61% fiber volume fraction**
10 series[a]	1882 ± 55	136.2 ± 7.2
30 series[b]	1459 ± 30	145.7 ± 4.7
50 series[c]	1776 ± 78	127.7 ± 10.8

a- Ultem-type TMA^+ polyimide interphase
b- Ultem-type NH_4^+ polyimide interphase
c- Ultem-type TPA polyimide interphase

* calculated from Eq. 7-11.
** calculated from Eq. 7-12.

The data sheet for Hercules AS-4 carbon fiber reports a fiber tensile strain-to-failure of 1.61% [31]. As seen in Table 7-IX, the largest tensile strain for any of the composites is 1.36%. Thus, all the composites fail before the fibers can be loaded to their individual maximum strain. The strain limitation for the composite is attributed to fiber defects, composite voids and discontinuous fibers in the composite. An ultimate composite longitudinal tensile strength σ^{ULT}, can be calculated using Eq. 7-13 [34].

$$\sigma^{UT} = V_f \bullet E_f \cdot \epsilon_f^{UT} + (1 - V_f) E_m \cdot \epsilon_f^{UT} \qquad \text{Eq. 7-13}$$

Where V_f = experimentally measured fiber volume fraction
E_f = fiber tensile modulus
E_m = matrix tensile modulus
ϵ_f^{ULT} = strain-to-failure of 1.61% representing ultimate possible fiber strain

The calculated values of σ^{ULT} are tabulated in Table 7-XIV. The σ^{ULT} represents the longitudinal tensile strength of a perfect composite with no broken fibers, no fiber defects, no matrix voids and perfect bonding between fiber and matrix. This perfect composite would permitted to support loads up to the ultimate strain of the fibers without suffering fiber matrix debonding. This ultimate longitudinal tensile strength can be used to make some important comparisons of the Ultem-type interphase/PPS matrix composites. To discuss these comparisons properly, the micromechanics of load transfer around a broken fiber are presented next.

Table 7-XIV. Ultimate composite tensile strength and strength reduction factor for Ultem-type polyimide interphase/PPS matrix composites.

	V_f (%)	σ^{ULT} * (MPa)	S_T**
10 series[a]	61.0	2321	1.23 ± 0.04
30 series[b]	39.5	1540	1.59 ± 0.3
50 series[c]	61.1	2325	1.31 ± 0.06

a- Ultem-type TMA^+ polyimide interphase
b- Ultem-type NH_4^+ polyimide interphase
c- Ultem-type TPA polyimide interphase

* calculated from Eq. 7-13
** calculated from Eq. 7-14

All of the polyimide interphase/PPS matrix composites were manufactured using the same aqueous suspension prepregging technique. Inherently, all of these composites should statistically have the same number of discontinuous fibers and the same concentration of fiber defects. Since the characteristics of the fibers are the same for all of the polyimide interphase/PPS matrix composites, differences in composite performance are attributed to load transfer by the interphase and matrix components. The differences in composite strength are a factor of how the matrix and interphase transfer the load in the presence of a defect or a broken fiber. It has been shown by Hedgepeth and VanDyke [32] and Subramanian et al. [3] that the local stress concentrations developed by fiber breaks ultimately result in composite tensile failure. The stress concentrations considered are significant on a micro-mechanical level and propagate damage through the composite.

The transfer of load in a composite becomes very important when there is a break in a fiber. The load must be taken by other fibers immediately surrounding the break in the failed fiber. The load can be transferred back to the broken fiber a certain axial distance from the failure location. This distance is called the critical fiber length or ineffective length. The fiber behaves as though it is not damaged at distances greater than the ineffective length from the break.

When considering a single broken fiber in a composite and the load transfer to neighboring fibers, the case of a short ineffective length is contrasted with the case of a long ineffective length in Figure 7-17. It has been shown by Reifsnider [1], Madukar and Drzal [2], and Monette et al. [33], among others, that a stronger interfacial shear strength will result in a shorter ineffective length for a given composite fiber/matrix system and a weaker interfacial

shear strength will result in a longer ineffective length for a given fiber/matrix system. A composite with a short ineffective length is shown in Figure 7-17(a). As seen by the stress profiles, the load will be transferred to neighboring fibers at a high stress level, but the stress profile reaches even loading a short axial distance along the fiber from the break. This stress concentration on neighboring fibers increases the probability of breaking the neighboring fiber at the loading point. Thus, the interfacial shear strength can be too large for optimum loading of the carbon fibers. The mode of failure for unidirectional composite coupons with this type of interfacial stress transfer, shown in Figure 7-17(c), is characterized by transverse cracks propagating through the composite with little or no fiber-matrix splitting. Subramanian et al. describe this type of interfacial failure as "elastic" [8]. It is the hypothesis of Subramanian et al. that interphase properties can be tailored such that an optimum balance between stress concentration and ineffective length will maximize longitudinal tensile strength [8].

A composite with a long ineffective length is shown in Figure 7-17(b). As seen by the stress profiles, the load will be transferred to neighboring fibers at a moderately high stress level. The stress profile becomes uniform at a long axial distance along the fiber from the break. Although the stress concentrations on neighboring fibers have been relieved, a larger area of the neighboring fibers are subjected to a moderately greater stress which increases the probability of loading the neighboring fiber at point defect. In this case, the interfacial shear strength can be too weak for optimum loading of the carbon fibers. The mode of failure for unidirectional composite coupons with this type of interfacial stress transfer, shown in Figure 7-17(d), is characterized by fiber-matrix splitting along the length of the composite. Subramanian et al. describe this type of interfacial failure as "plastic" [8].

The sketch in Figure 7-17(e) shows the relative effect of different ineffective lengths on the stress transferred to neighboring fibers. The curve for the broken fiber with a small ineffective length shows a greater local stress on the neighboring fibers at z=0 on the x-axis. At increasing distances along the fiber length the stress decreases rapidly up to z=Lc(1) which represents this system's ineffective length. At distances greater than the ineffective length the neighboring fibers are subjected to the average stress level applied to all fibers in the composite. The curve for the broken fiber with the large ineffective length shows a smaller local stress on the neighboring fibers at z=0 on the x-axis. This stress decreases more gradually at distances along the fiber length up to z=Lc(2) which represents this system's ineffective length. At distances greater than the ineffective length the neighboring fibers are subjected to the average stress level applied to all fibers in the composite.

All of the PPS matrix composites displayed a mixed-mode of failure during longitudinal tension testing. As seen in Figure 7-15, the 10 series and 50 series coupons shattered into many, long, thin pieces at failure. The failure was "explosive", resulting in significant fiber-matrix splitting, however, each thin, broken piece had ends resembling transverse cracking type failure. The 30 series coupons fractured with more of a transverse fracture, however, longitudinal splitting was still observed. It is assumed that the composites can be compared with the use of a strength reduction factor, S_T, defined as the ratio of σ^{ULT}, as calculated from Eq. 7-13, to the measured composite strength.

$$S_T = \frac{\sigma^{ULT}}{\sigma^{experimental}} \qquad \text{Eq. 7-14}$$

The strength reduction factors tabulated in Table 4-XIV are used to rank the level of the micro-mechanical stress concentrations in the polyimide interphase/PPS matrix composites. It is important to note that since σ^{ULT} was calculated for each individual composite and respective fiber volume fraction, S_T will not be dependent upon fiber volume fraction.

The unpaired t-test was used to determine the statistical uniqueness of the calculated strength reduction factors. As seen in Table 7-XV, all of the pairs of composites passed the t-test indicating that each S_T is statistically unique. Among the polyimide interphase/PPS matrix composites, the 10 series composite has the lowest S_T. The 10 series composite also has the weakest fiber-matrix adhesion as concluded from transverse flexure strength results. It follows that the 10 series composite reduces the local micro-mechanical stress concentrations caused by broken fibers most effectively in the longitudinal tension testing. The greater longitudinal tensile strength and greater longitudinal tensile strain-to-failure can be explained by the reduction of micro-mechanical stress concentrations from broken fibers.

The 30 series composite has the greatest S_T and the strongest fiber-matrix adhesion as concluded from the transverse flexure strength results. It follows that the micro-mechanical stress concentrations due to broken fibers are greater for the 30 series composite. The lower longitudinal tensile strength and lower longitudinal tensile strain-to-failure can be explained by the greater micro-mechanical stress concentrations from broken fibers.

The 50 series composite has an intermediate S_T and an intermediate fiber-matrix adhesion as concluded from the transverse flexure. It follows that the reduction of the micromechanical stress concentrations due to broken fibers is also intermediate.

Table 7-XV. Unpaired *t*-test results comparing each set of PPS matrix composite strength reduction factors and tensile data corrected to 61% fiber volume fraction.

	S_T	Longitudinal Tensile Strength Corrected to V_f = 61%	Longitudinal Tensile Modulus Corrected to V_f = 61%
10 series[a] vs 30 series[b]	pass	pass	pass
10 series[a] vs 50 series[c]	pass	pass	fail
30 series[b] vs 50 series[c]	pass	pass	pass

a- Ultem-type TMA^+ polyimide interphase
b- Ultem-type NH_4^+ polyimide interphase
c- Ultem-type TPA polyimide interphase

The strength reduction factor, S_T, is plotted against the normalized transverse flexure strength in Figure 7-18. As the normalized transverse flexure strength increases, the S_T also increases. Since the S_T is considered to be a measure of the level of the micro-mechanical stress concentrations in the polyimide interphase/PPS matrix composites, Figure 7-18 shows that as the normalized transverse flexure strength increases, the micromechanical stress concentrations increase which leads to failure at lower composite stress levels.

As mentioned previously, attempts have been made by other researchers to correlate longitudinal flexure strength with longitudinal tensile strength. As seen in Figure 7-19, the longitudinal flexure strength and the longitudinal tensile strength are plotted against the normalized transverse flexure strength. Since the normalized transverse flexure strength has been shown to be a good indicator of ISS, Figure 7-19 can be compared to the data from Drzal et al. in Figure 7-13. In similar fashion to the results of Drzal et al., a correlation cannot be made for the longitudinal flexure strength. As the normalized transverse flexure strength increases in

Figure 7-19, the longitudinal flexure strength initially increases and then decreases. The trend of the longitudinal tensile strength is that it first decreases slowly and then more rapidly with increasing normalized transverse flexure strength.

A model has been developed by Subramanian et al. based on stress concentration dominated fracture mechanics which accounts for constituent properties including an interphase [3]. The sketch in Figure 7-20 of composite tensile strength vs. ISS shows the results of the model. As the ISS increases, the longitudinal tensile strength initially increases to a maximum level. Upon further increase of ISS the longitudinal tensile strength decreases. The trend shown in Figure 7-21 for the normalized transverse flexure strength vs. tensile strength corrected to 61% fiber volume fraction for the Ultem-type interphase/PPS matrix composites is similar to the sketch in Figure 7-20 just to the right of the maximum in longitudinal tensile strength. This important observation is not conclusive evidence of verification of the model due to the presence of only three data points in Figure 7-21. However, the similarity of the trend of the experimental data to the model provides motivation for further study.

Conclusions

A series of PPS matrix Ultem-type polyimide interphase composites of high quality were fabricated using the aqueous suspension prepregging technique. Three different Ultem-type polyamic acid salts were used to tailor the interphase properties of the PPS matrix composites using the aqueous suspension prepregging technique.

The interlaminar shear strength (ILSS) was measured using a short beam shear test. The

ILSS of the 50 series Ultem-type TPA^+/PPS composite was greater than both the 10 series and 30 series composites.

The PPS matrix composites were tested using a longitudinal flexure test. All longitudinal flexure test samples failed in an interlaminar shear mode of failure. The 10 series Ultem-type TMA^+/PPS composite had the lowest longitudinal flexure strength. The longitudinal flexure strength of the 30 series and 50 series composites were shown to be statistically similar.

A direct correlation was shown for transverse flexure strength and interfacial shear strength using data from Chang et al.[5] and Madhukar and Drzal [2]. As the interfacial shear strength increases, the transverse flexure strength also increases. This relationship was used to rank the relative level of interfacial shear strengths for the Ultem-type polyimide/PPS matrix composites. Using this correlation the trends showed that the interfacial shear strength of the 10 series Ultem-type TMA^+ polyimide interphase composite was lowest and the interfacial shear strength of the 30 series Ultem-type NH_4^+ polyimide interphase composite was the greatest. The interfacial shear strength of the 50 series Ultem-type TPA^+ polyimide interphase composite was intermediate between the 10 series and 30 series composites.

The longitudinal tensile properties of the Ultem-type polyimide/PPS matrix composites were measured. Since the fiber volume fraction of the unidirectional tensile coupons varied significantly the longitudinal tensile strengths were corrected to 61% fiber volume fraction. The 30 series Ultem-type NH_4^+ polyimide interphase composite had the lowest corrected tensile strength, the 10 series Ultem-type TMA^+ polyimide interphase composite had the greatest corrected tensile strength and the 50 series Ultem-type TPA^+ polyimide interphase composite had an intermediate corrected tensile strength.

The hypothesis proposed by Subramanian et. al indicates that a maximum in tensile strength exists at an optimum interfacial shear strength [3]. The data for the Ultem-type polyimide interphase/PPS composites show qualitative reinforcement of the trends predicted by the model of Subramanian et. al.

The estimates of composite strength using the rule of mixtures showed very good agreement to the experimental data indicating that the assumptions for the rule of mixtures were applicable to the Ultem-type polyimide interphase/PPS matrix composites, specifically, the composite has fibers that are continuous, aligned parallel and uniform in properties, good bonding exists between the fibers and matrix and each component has a linear elastic response. The estimates of composite modulus from the rule of mixtures also showed good agreement to the experimental data.

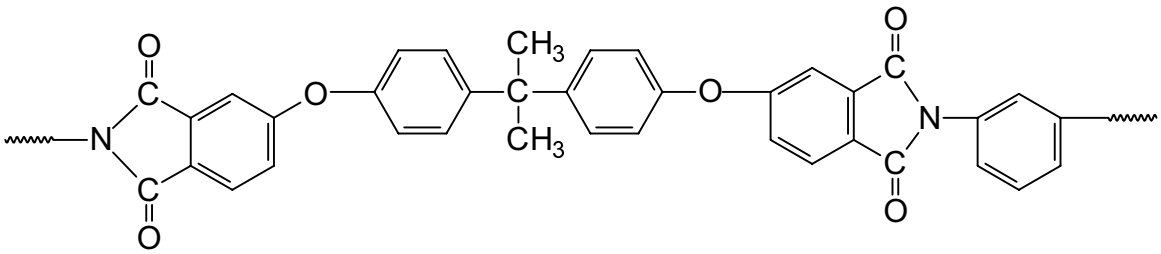

Figure 7-1. Chemical structure of Ultem-type polyimide.

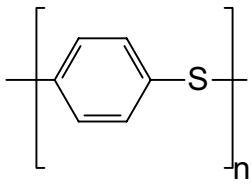

Figure 7-2. Chemical structure of PPS composite matrix polymer.

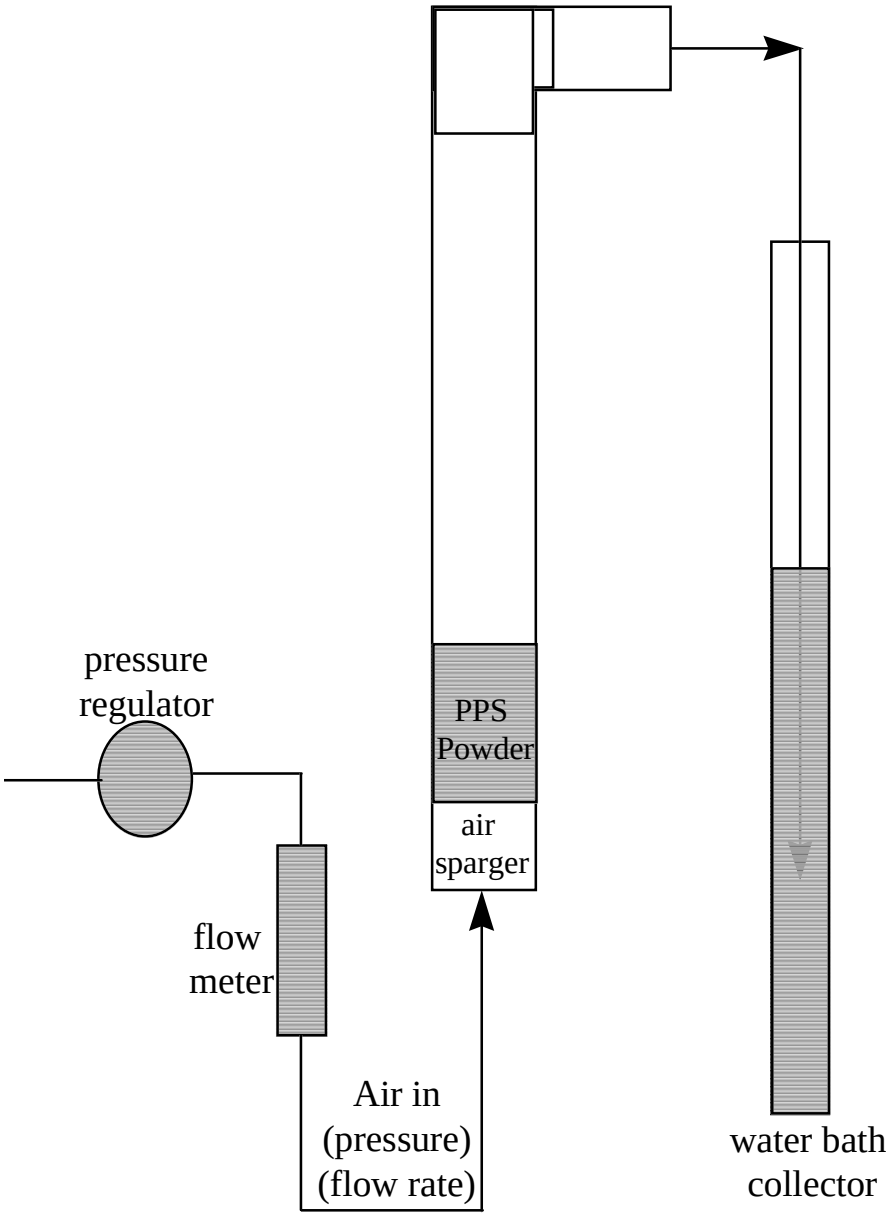

Figure 7-3. Schematic for air classifier used to separate PPS powder into size distributions suitable for aqueous suspension prepregging [24].

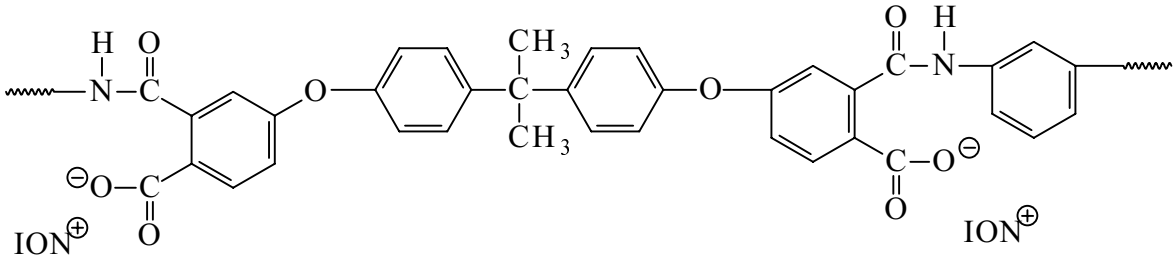

Ultem-type Polyamic Acid made water soluble by addition of basic counterion

Thermal Imidization

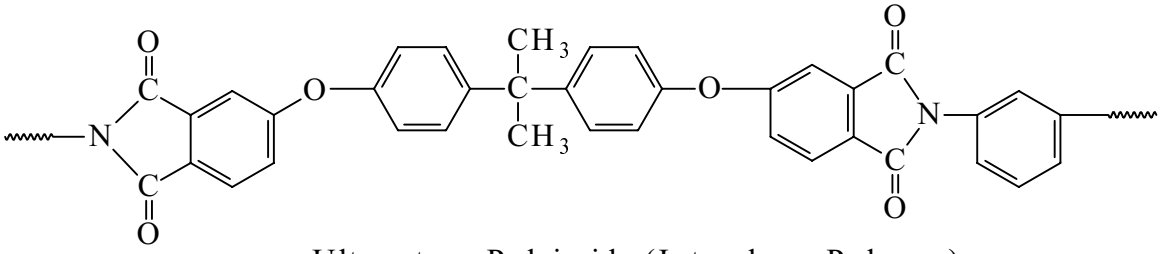

Ultem-type Polyimide (Interphase Polymer)

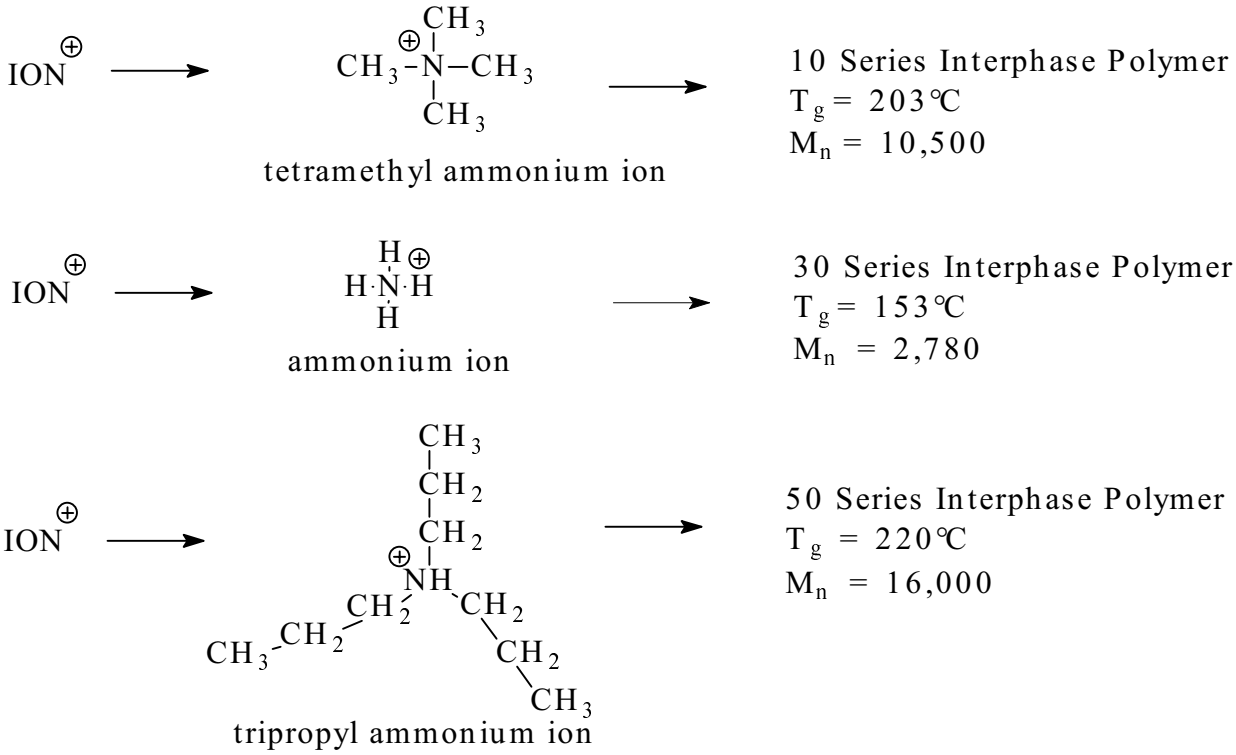

Figure 7-4. Formation of Ultem-type polyamic acid salts using different bases and the glass transition temperatures and number average molecular weight for the polyimide.

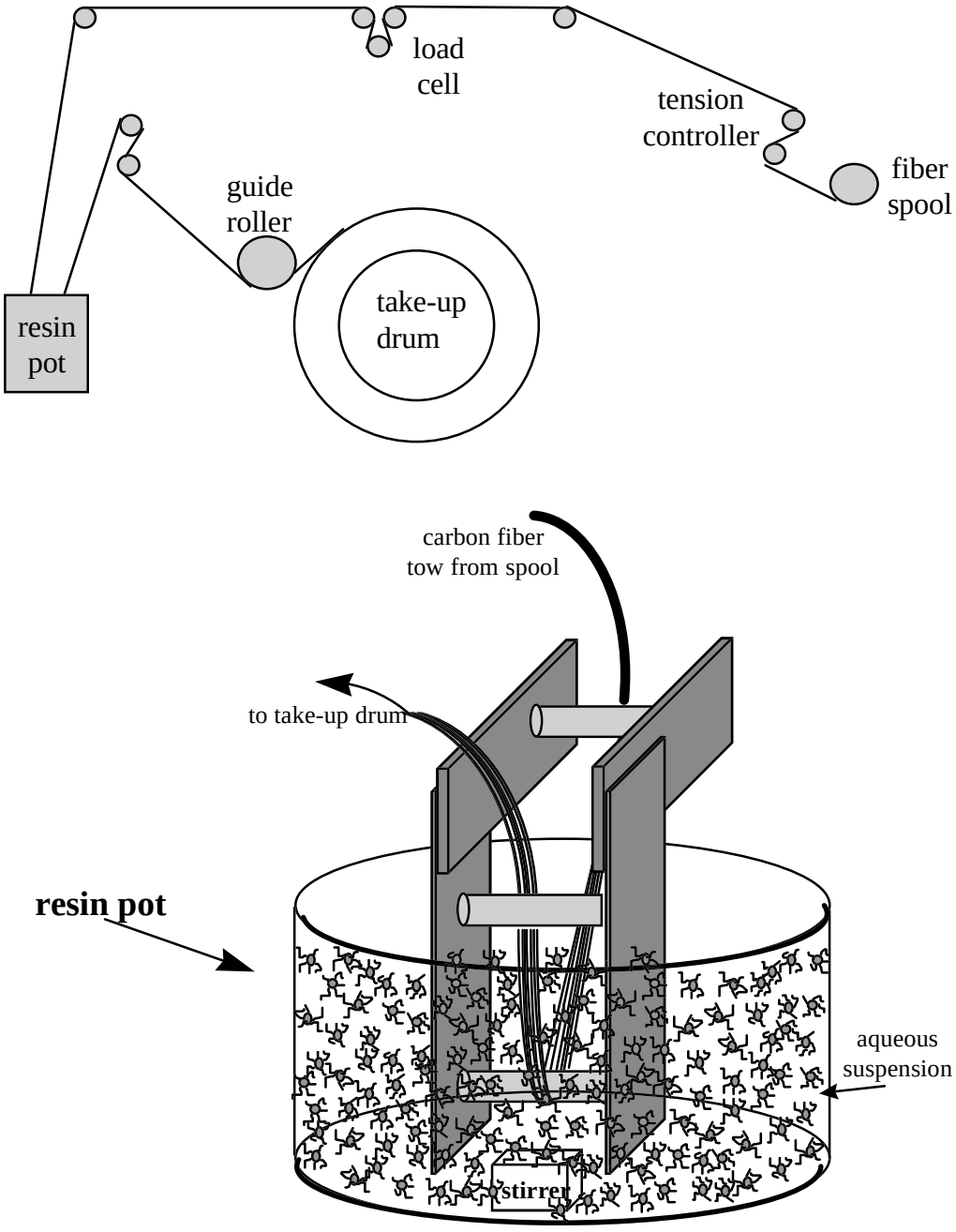

Figure 7-5. Schematic drawing of modified Research Tool Corporation Model 30 Drumwinder Prepregger with an enlarged view of the resin pot used for aqueous suspension prepregging.

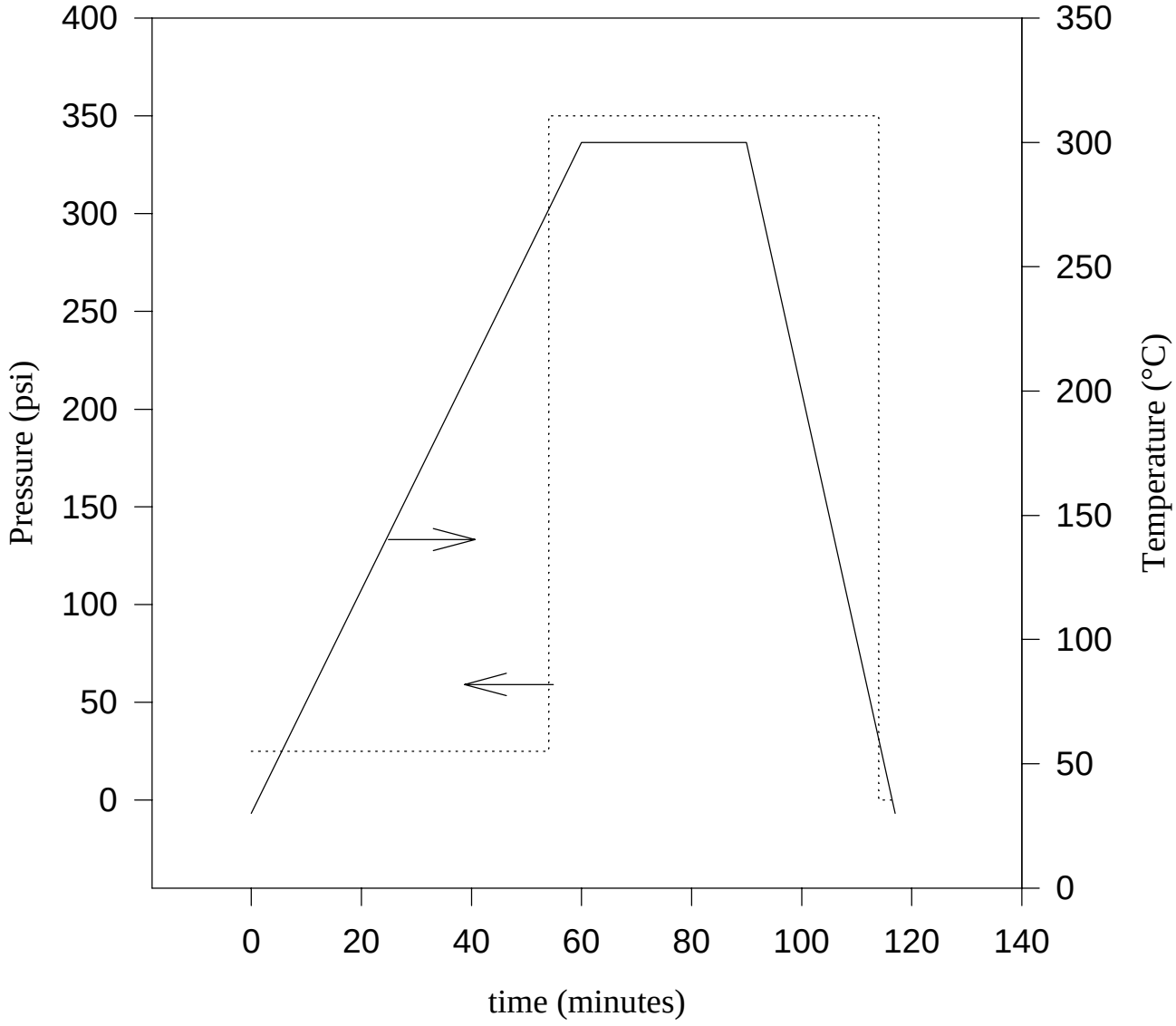

Figure 7-6. Temperature and pressure schedule for consolidation of PPS matrix composites.

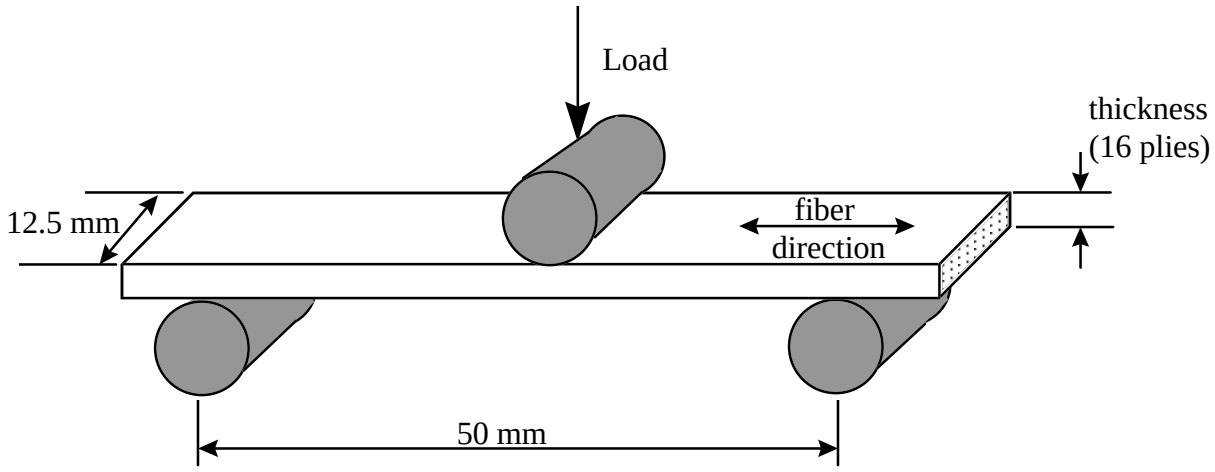

Figure 7-7(a) Composite longitudinal flexure testing geometry.

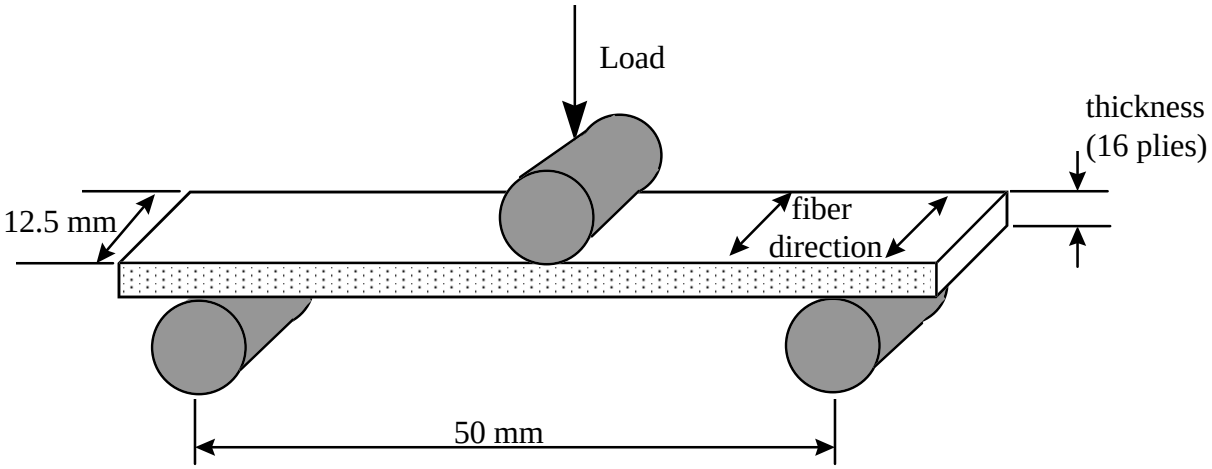

Figure 7-7(b) Composite transverse flexure testing geometry.

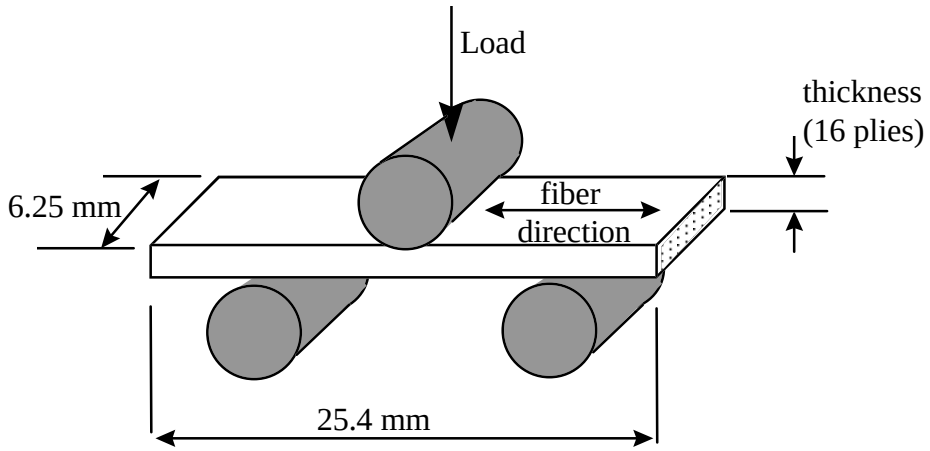

Figure 7-8. Composite short beam shear testing geometry.

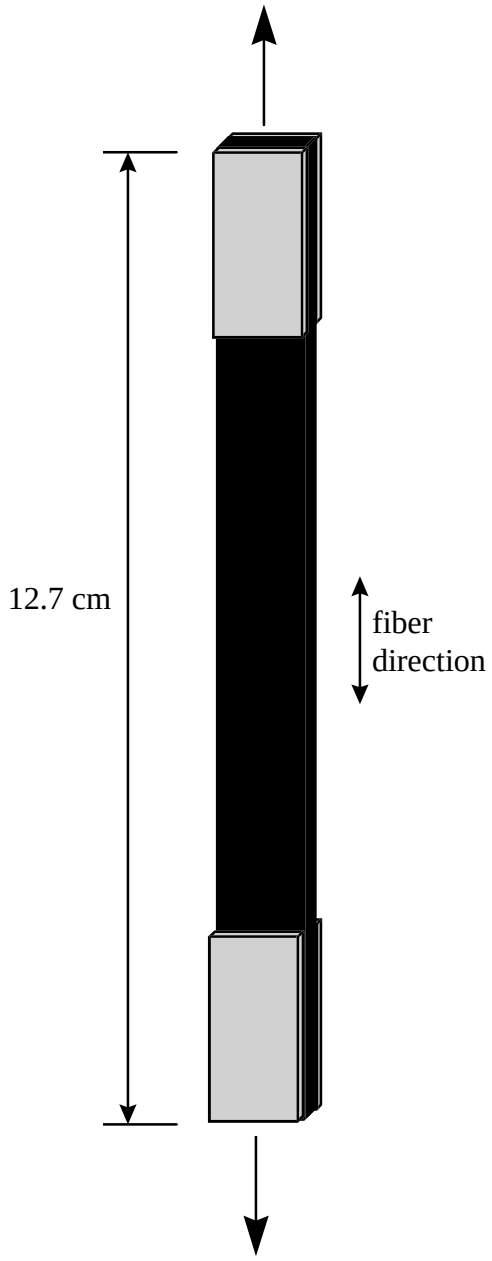

Figure 7-9. Unidirectional tension test geometry.

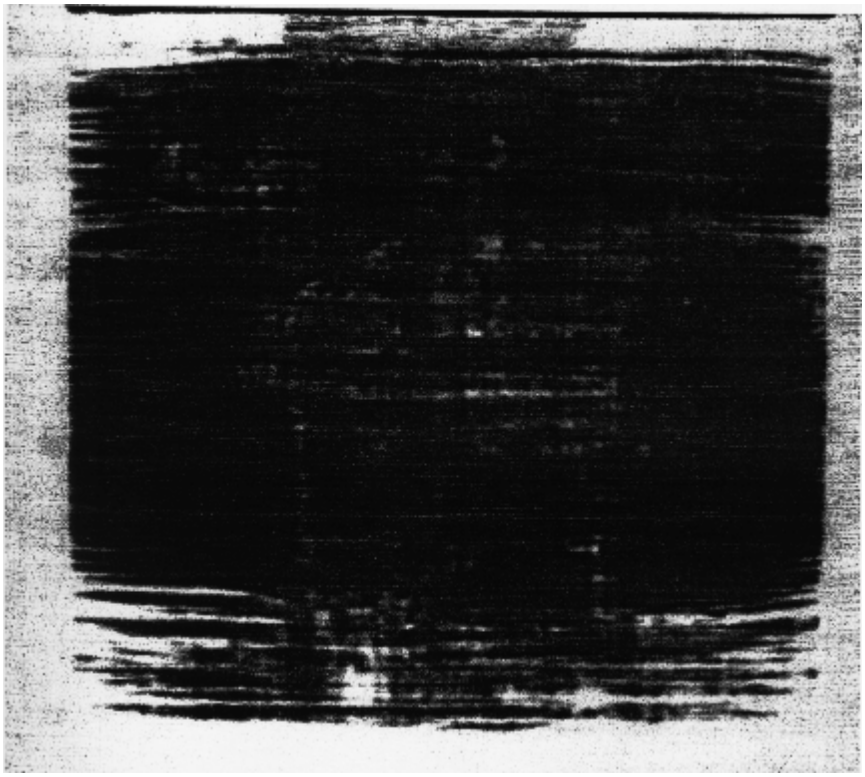

Figure 7-10. C-scan image of panel PPS302 which is representative of “good” consolidation.

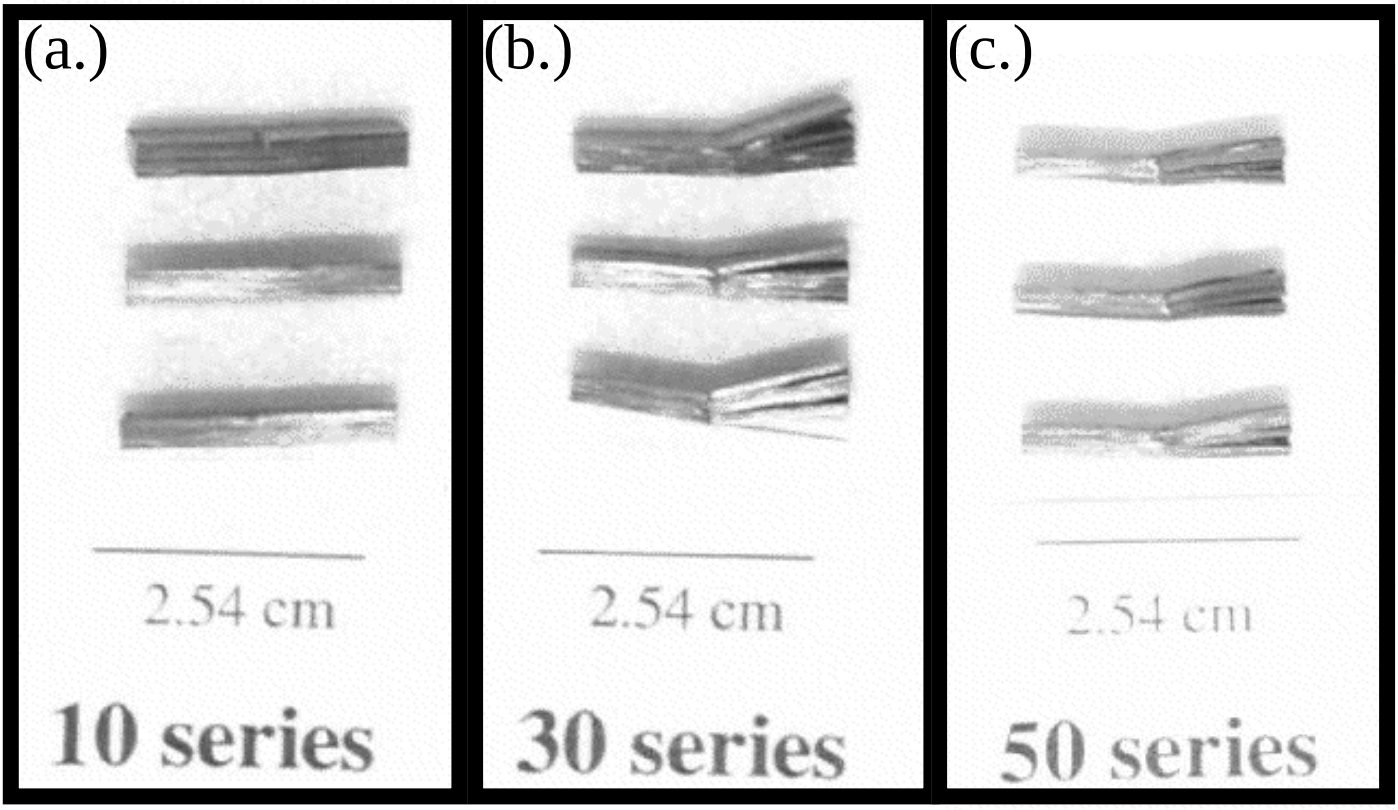

Figure 7-11. Photographs of failed short beam shear test coupons.

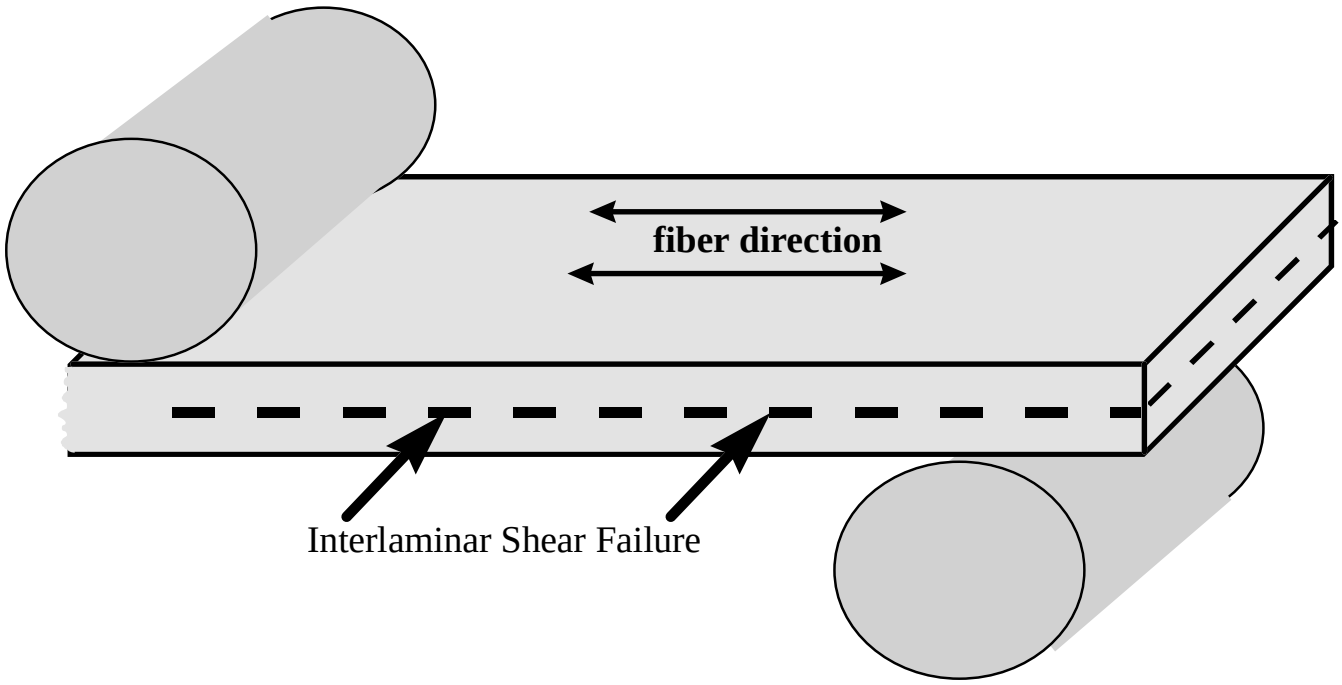

Figure 7-12. Longitudinal flexure shear failure mode.

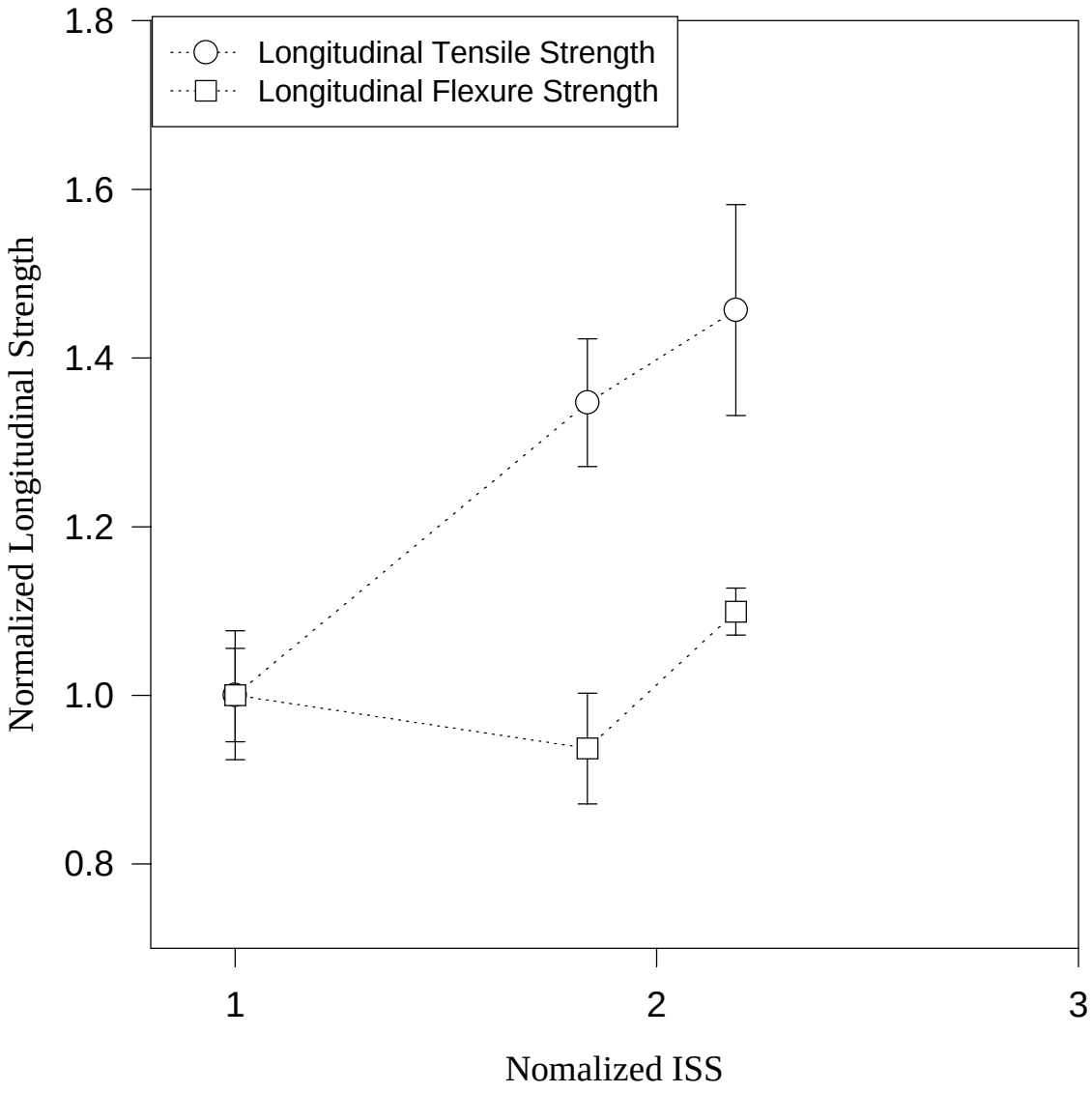

Figure 7-13. Normalized longitudinal composite strengths vs. normalized ISS from Drzal et. al for epoxy matrix/carbon fiber composites [2].

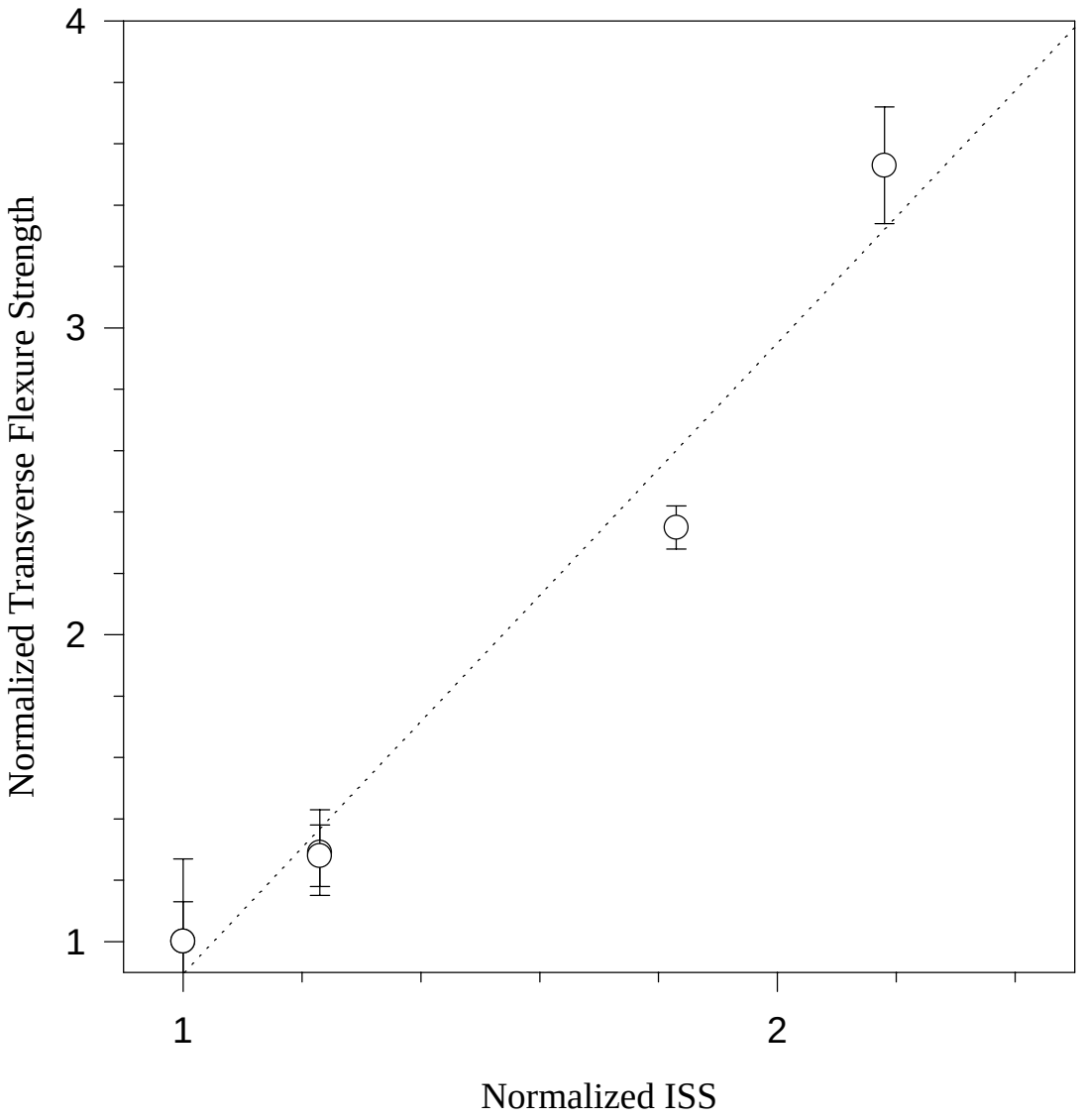

Figure 7-14. Normalized ISS vs. normalized transverse flexure strength data from Chang et al. [4] and Madhukar and Drzal [2].

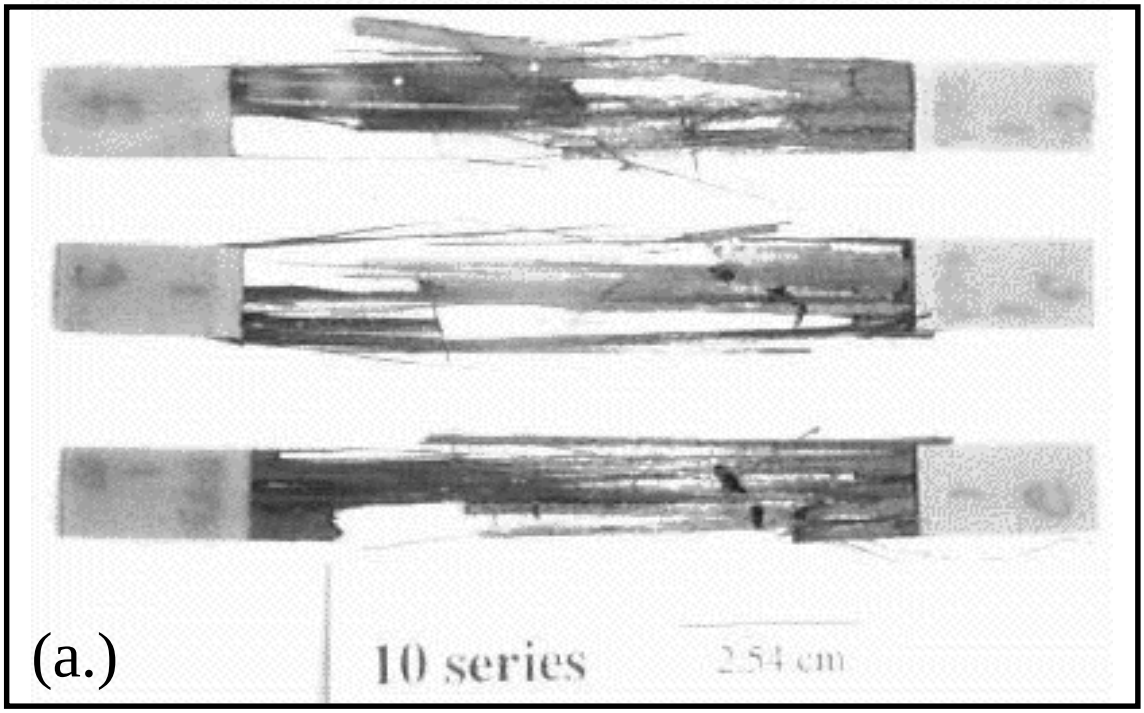

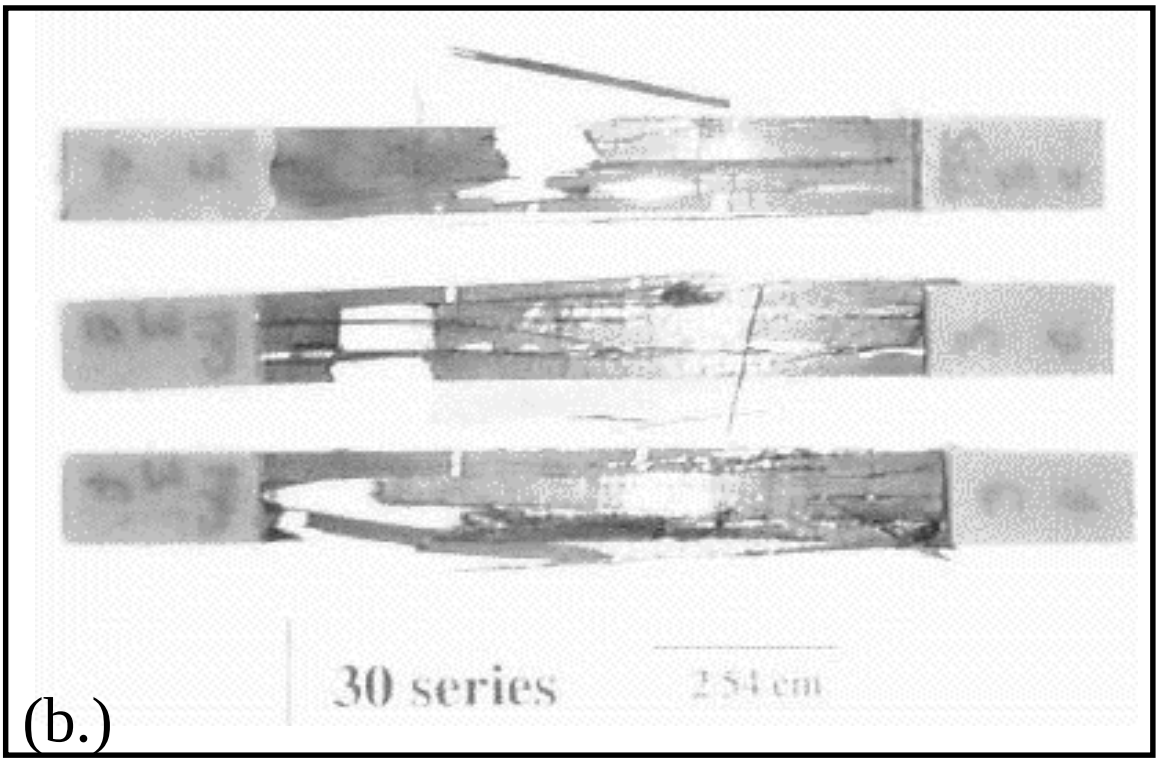

Figure 7-15. Photographs of failed longitudinal tension test coupons for (a.) 10 series PPS matrix composites, (b.) 30 series PPS matrix composites.

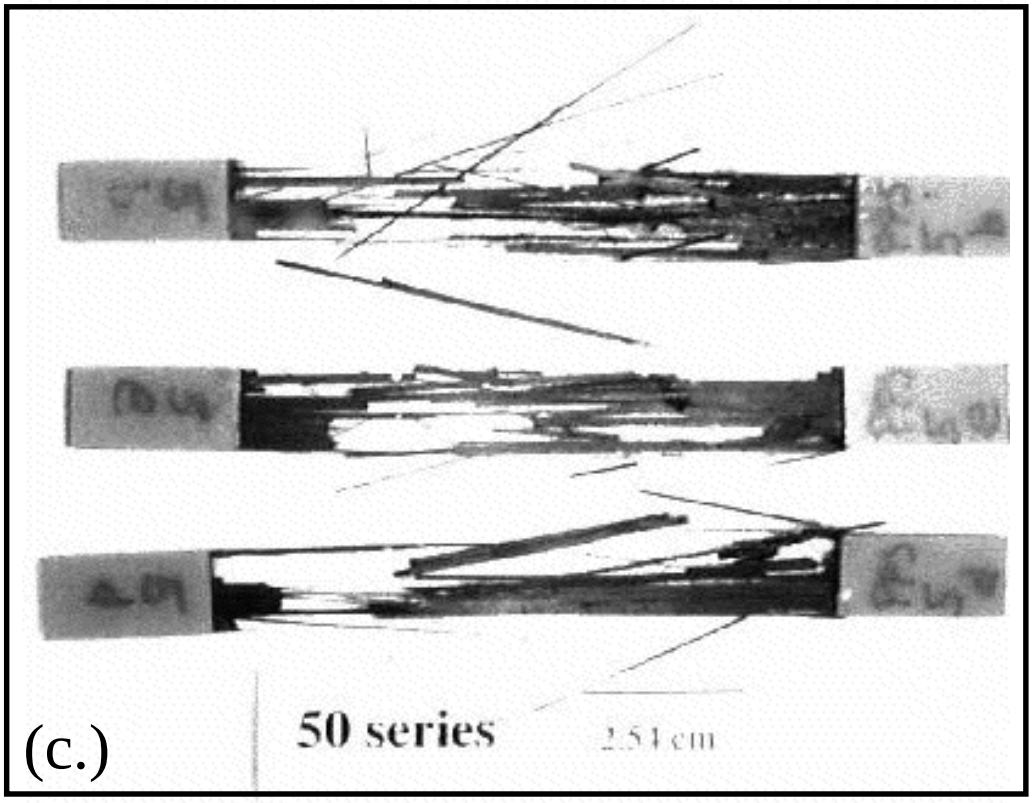

Figure 7-15 (continued). Photographs of failed longitudinal tension test coupons for (c.) 50 series PPS matrix composites.

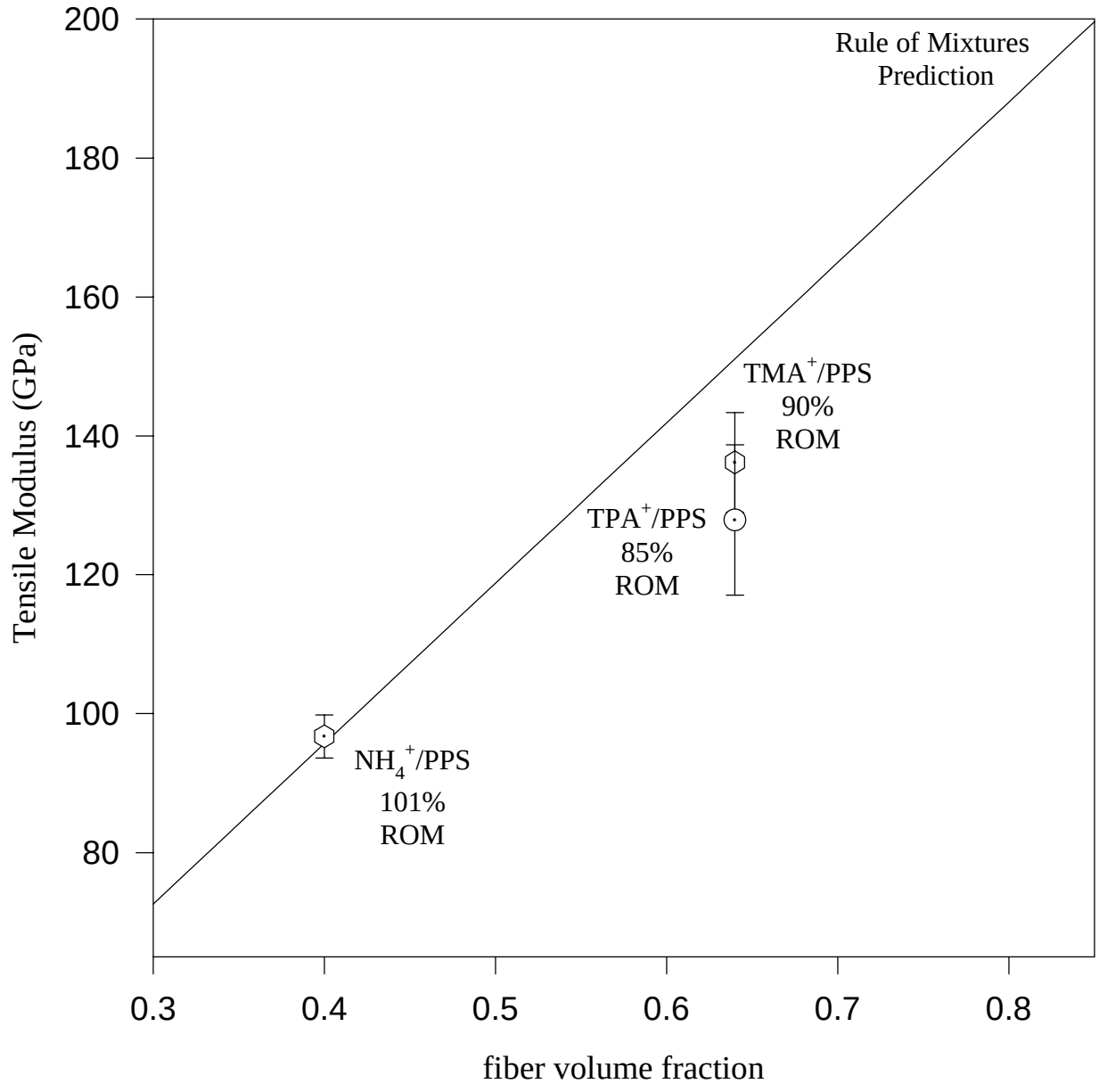

Figure 7-16. Fiber volume fraction vs. longitudinal tensile modulus for Ultem-type polyimide/PPS matrix composite coupons with comparison to predictions by the rule of mixtures.

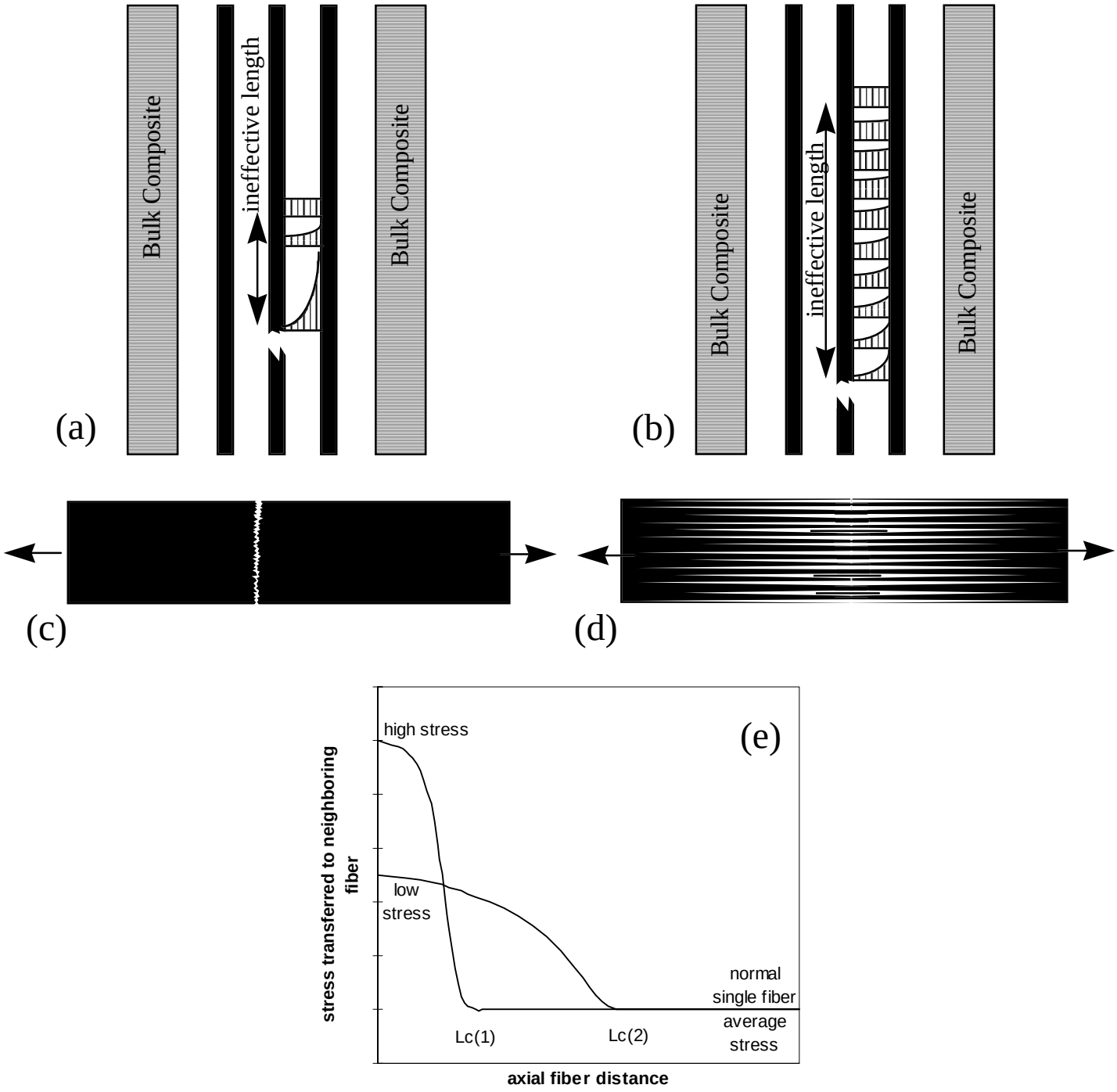

Figure 7-17. Comparison of relative ineffective lengths. The stress profiles for stresses transferred to neighboring fibers are shown in (a) for a short ineffective length and (b) for a long ineffective length. The macroscopic tensile failure modes are shown in (c) for the extreme case of a short ineffective length and (d) for the extreme case of a long ineffective length. The stresses transferred to neighboring fibers are also sketched as a function of arbitrary axial fiber distance for a short ineffective length, at point Lc(1), and a long ineffective length, at point Lc(2).

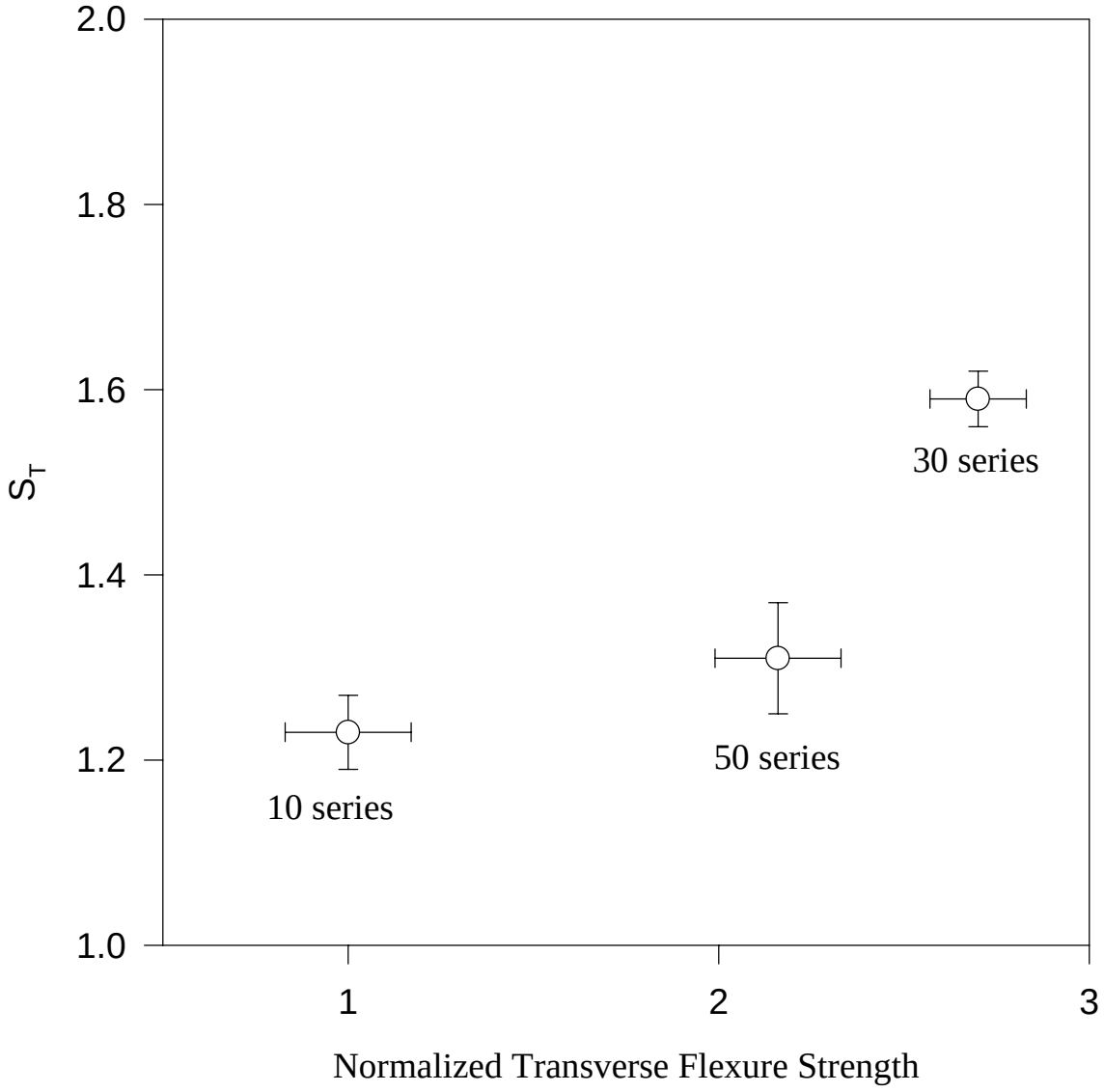

Figure 7-18. Strength reduction factor S_T vs. normalized transverse flexure strength.

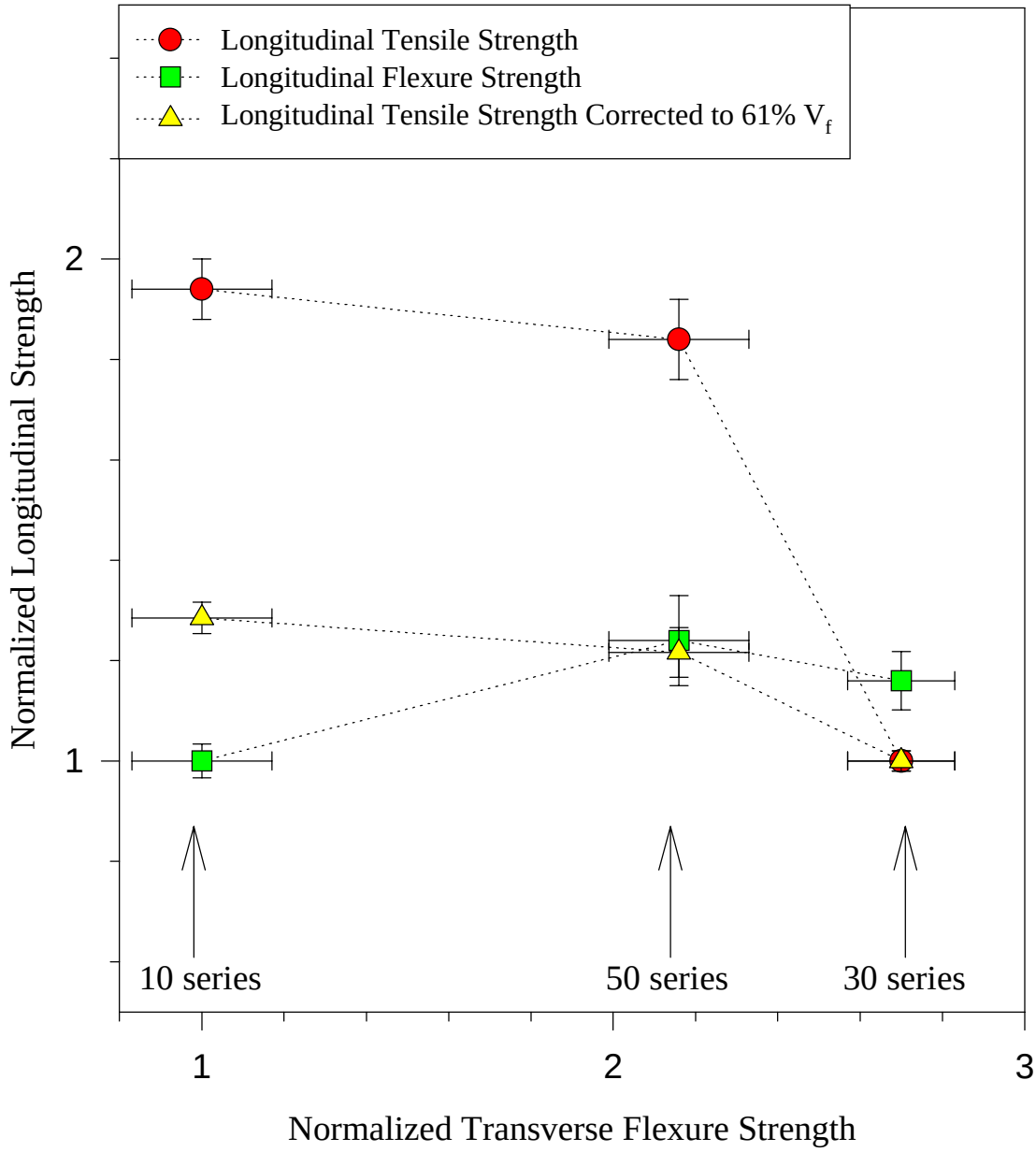

Figure 7-19. Normalized transverse flexure strength vs. normalized longitudinal tensile strength, normalized longitudinal flexure strength, and normalized longitudinal tensile strength corrected to 61% fiber volume fraction.

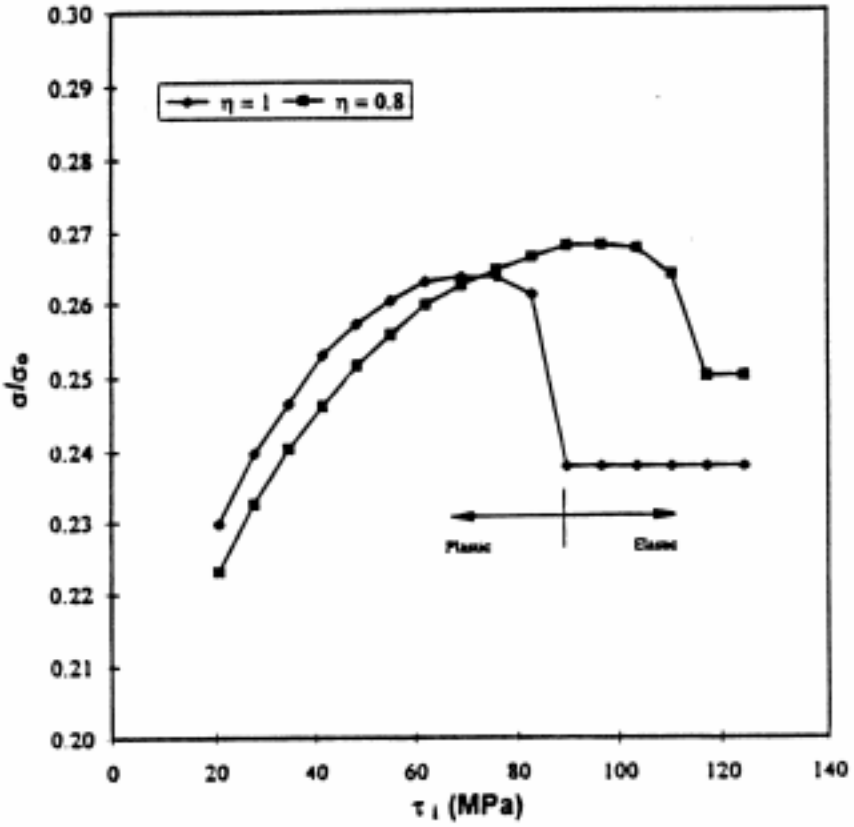

Figure 7-20. Predicted variation of normalized composite tensile strength vs. interfacial shear strength for two different composite systems. From Subramanian et. al [3].

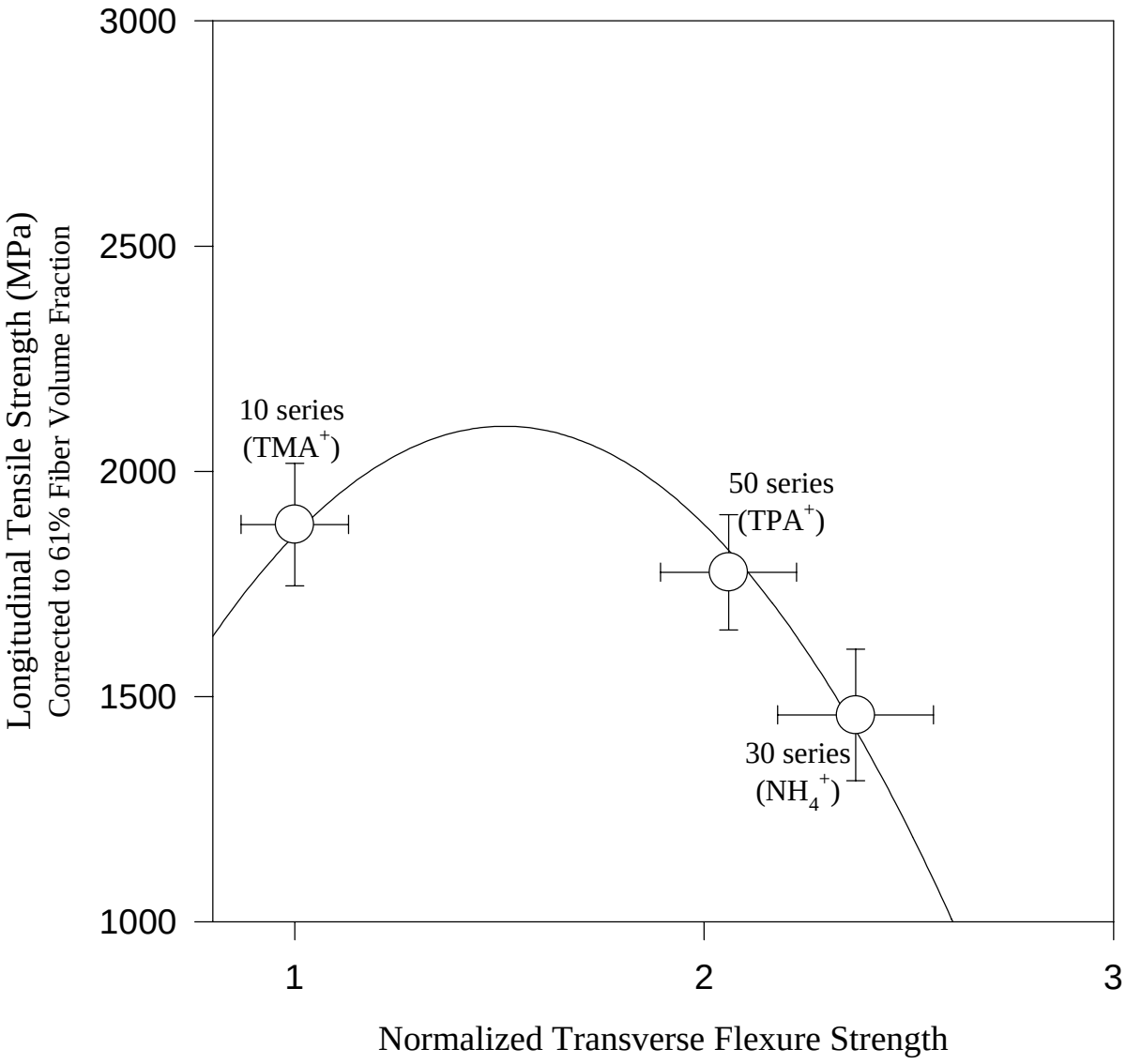

Figure 7-21. Longitudinal tensile strength corrected to 61% fiber volume fraction vs. normalized transverse flexure strength for Ultem-type polyimide interphase/PPS matrix composites.

References

1 Reifsnider, K.L., *Composites*, **25**, 461 (1994).

2 Drzal, L.T. and Madhukar, M., *Journal of Material Science*, **28**, 569 (1993).

3 Subramanian, S., Lesko, J.J., Reifsnider, K.L., and Stinchcomb, W.W., *J. Compos. Mater.*, **30**, 309 (1996).

4 Chang, Y.S, Lesko, J.J., Case, S.W., Dillard, D.D., and Reifsnider, K.L., *Journal of Thermoplastic Composite Materials*, **7**, 311 (1994).

5 Gao, Z., Reifsnider, K.L., and Carman, G., *J. Compos. Mater.*, **26**, 1678 (1992).

6 Carman, G.P., Lesko, J.J., and Reifsnider, K.L., *Composite Materials: Fatigue and Fracture, Fourth Volume, ASTM STP 1156,* W.W. Stinchcomb and N.E. Ashbaugh, Eds., American Society for Testing and Materials, Philadelphia, PA, p. 430, 1993.

7 Case, S.W., Carman, G.P., Lesko, J.J., Fajardo, A.B., and Reifsnider, K.L., *J. Compos. Mater.*, **29**, 208 (1995).

8 Subramanian, S., Reifsnider, K.L., and Stinchcomb, W.W., *Journal of Composites Technology & Research*, **17**, 289 (1995).

9 The Effect of Polyimide Interphases on Properties of PEEK-Carbon Fiber Composites. S. Gardner, A. Gonzalez, R.M. Davis, J.V. Facinelli, J.S. Riffle, S. Case, J.J. Lesko, K.L. Reifsnider, *AIChE 1995 Annual Meeting.* November 12-17, 1995. Miami, FL.

10 Yu, T.H. and Davis, R.M., *J. Thermoplast.Comp. Mater.*, **6**, 62 (1993).

11 Texier, A., Davis R.M., Lyon, K.R., Gungor, A., McGrath, J.E., Marand, H., and Riffle, J.S., Polymer, **34**, 896 (1993).

12 Gonzalez, A-I, M.S. Dissertation (Virginia Polytechnic Institute and State University, Blacksburg, VA, November 1992)

13 Gonzalez-Ibarra, A., Davis, R.M., Heisey, C.L., Wightman, J.P., and Lesko, J.J., *Journal of Thermoplastic Composite Materials*, **10**, 85 (1997).

14 Davis, R.M., and Texier, A., *ANTEC '91 Confer. Proceed.*, **37**, 2018 (1991).

15 Facinelli, J.V., Gardner, S., Dong, L., Sensenich, C.L., Davis, R.M., and Riffle, J.S., *Macromolecules*, **29**, 7342 (1996).

16 Akhtar, S., and White, J.L., *Polymer Engineering and Science*, **31**, 84 (1991).

17 Pratt, J.R. and St. Clair, T.L., *SAMPE Journal*, **26**, 29 (1990).

18 Johnston, N.J., St. Clair, T.L., and Baucom, R.M., Polyimide Matrix Composites: Polyimidesulfone/LaRC-TPI (1:1) Blend, *24th International SAMPE Symposium and Exhibition*, Reno, NV, May 8-11, 1989.

19 Johnston, N.J. and St. Clair, T.L., *SAMPE Journal*, **23**, 12 (1987).

20 Johnston, N.J. and St. Clair, T.L., *SAMPE Preprints,* **18**, 53 (1986).

21 Texier, A., Davis R.M., Lyon, K.R., Gungor, A., McGrath, J.E., Marand, H., and Riffle, J.S., *Polymer*, **34**, 896 (1993).

22 Varughese, B., Muzzy, J., and Baucom, R.M., *21st Intern. SAMPE Tech. Confer.*, Sept. 25-28, 1989.

23 Geibel, J., and Leland, J., Encyclopedia of Chemical Technology, 4th Edition, **vol. 19**, John Wiley & Sons, pp 904-933, 1996.

24 Weber, M. and Davis, R.M., National Science Foundation Science and Technology Center Summer Undergraduate Research Program Final Report, August, 1997.
25 ASTM Standard D 790M-96 Standard Test Methods for Flexural Properties of Unreinforced and Reinforced Plastics and Electical Insulating Materials
26 ASTM Standard D 2344-84 Standard Test Methods for Short Beam Shear Testing of Unidirectional Composite Materials
27 Guigon, M., and Klinklin, E., Composites, **25**, 534, (1994).
28 personal consultation with Professor K.L. Reifsnider
29 Sigma-Stat Statistical Software v. 2.0 User's Manual, Jandel Scientific, San Rafael, CA (1992-1995).
30 Adams, D.F., King, T.R., and Blackketter, D.M., *Composites Science and Technology*, **39**, 341 (1990).
31 Hercules AS-4 Carbon Fiber Product Data Sheet.
32 Hedgepeth, J.M., and Van Dyke, P., *J. Compos. Mater.*, **1**, 294 (1967).
33 Monette, L., Anderson, M.P., and Grest, G.S., Polymer Composites, **14**, 101 (1993).
34 Agarwal and Broutman, "Analysis and Performance of Fiber Composites", John Wiley and Sons, New York, NY, 1990.
35 Jayaraman, K., Reifsnider, K.L., and Swain, R.E., Journal of Composites Technology & Research, **15**, 3 (1993).
36 Jayaraman, K., Reifsnider, K.L., and Swain, R.E., Journal of Composites Technology & Research, **15**, 14 (1993).
37 Carman, G.P., Averill, R.C., Reifsnider, K.L., Reddy, J.N., Journal of Composite Materials, **27**, 589 (1993).
38 Jayaraman, K., Gao, Z., and Reifsnider, K.L., Journal of Composites Technology & Research, **16**, 21 (1994).
39 Rao, V., and Drzal, L.T., Polymer Composites, **12**, 48 (1991).
40 Bechel, V.T., and Kaw, A.K., International Journal of Solids Structures, **31**, 2053 (1994).
41 Gibson, R.F., "Principles of Composite Material Mechanics", McGraw-Hill, Inc., New York, 1994.
42 Swain, R.E., Reifsnider, K.L., Jayaraman, K., and El-Zein, M., Journal of Thermoplastic Composite Materials, **3**, 13 (1990).
43 Whang, W-T., and Liu, W-L., Sampe Quarterly, October 1990, 3.
44 Denault, J., and Vu-Khanh, T., Journal of Thermoplastic Composite Materials, **6**, 190 (1993).
45 Mittal, K.L., Ed.,Polyimides; Plenum Press, New York, 1984.
46 Bessonov, M.I., Koton, M.M., Kudryavtsev, V.V., and Laius, L.S., Polyimides: Thermally Stable Polymers, Consultants Bureau, New York, 1987.
47 Ferry, J.D.,Viscoelastic Properties of Polymers, 3rd Edition, John Wiley and Sons, New York, 1980.
48 Dealy, J.M. and Wissbrun, K.F., Melt Rheology and Its Role in Plastics Processing, Van Nostrand Reinhold, New York, 1990.
49 Cotts, P.M., *J. Polym. Sci.: Part B: Polym. Phys.*, **24**, 923 (1986).
50 Giles, H.F., *U.S. Patent 4,455,410.*, June 19, 1984.

51 Cagliostro, D.E., *Polym. Eng. & Sci.*, **28**, 562 (1988).
52 Pangelinan, A.B., McCullough, R.L., and Kelley, M.J., *J. Polym. Sci:Part B:Polym. Phys.*, **32**, 2383 (1994).
53 Palmese, G.R., and McCullough, R.L., *Journal of Adhesion*, **44**, 29 (1994).
54 Jabbari, E., and Peppas, N.A., *Polymer*, **36**, 575 (1995).
55 Rosen, B.W. *AIAA Journal*, **2** (1964) 1985.
56 Whitney, J.M., and Drzal, L.T., *Toughened Composites, ASTM STP 937*, N. Johnston, Ed., American Society for Testing and Materials, Philadelphia, PA, p. 179, 1987.
57 Case, S.W.*PhD Dissertation* (Virginia Polytechnic Institute and State University, Blacksburg, VA, May 1996).
58 Jenkins, S.D., Emmerson, G.T., McGrail, P.T., and Robinson, R.M., *Journal of Adhesion*, **45**, 15 (1994).
59 Miller, A., Wei, C., and Gibson, A.G., *Composites*, *Part A*, **27A**, 49 (1995).
60 Baxandall, L.G., *Macromolecules*, **22**, 1982 (1989).

Chapter Eight: Summary of Conclusions and Recommended Future Work

Structure-Property Relationships of Model Interphase Ultem-type Polyimides Made from Water Soluble Precursors

The purpose of this work was to prepare and characterize model interphase and model matrix samples to represent the polymeric material in Ultem-type polyimide interphase/PEEK matrix composites. For this work, controlled molecular weight Ultem-type polyimides from water soluble polyamic amic acid salts were made. The molecular weights of the Ultem-type polyimides from water soluble polyamic amic acid salts were measured using GPC. The Ultem-type NH_4^+ polyimide had the lowest molecular weight (M_n = 2,780 g/mol), the Ultem-type TMA^+ polyimide had an intermediate molecular weight (M_n = 10,500 g/mol) and the Ultem-type TPA^+ polyimide had the highest molecular weight (M_n = 16,000 g/mol). Many of the properties of the Ultem-type TPA^+ polyimide were similar to those of commercial Ultem 1000 polyimide.

The glass transition temperatures of the Ultem-type polyimides were measured using DSC. The Ultem-type NH_4^+ polyimide had the lowest T_g (153°C), the Ultem-type TMA^+ polyimide had an intermediate T_g (203°C) and the Ultem-type TPA^+ polyimide had the highest T_g (220°C) which is very close to the T_g measured for commercial Ultem 1000 (218°C).

It was verified using FTIR that the Ultem-type NH_4^+ polyimide, Ultem-type TMA^+ polyimide and Ultem-type TPA^+ polyimide were all chemically identical to commercial Ultem 1000 after thermal imidization. The glass transition temperatures of the Ultem-type polyimides displayed the expected trend of increasing T_g with increasing molecular weight. The Ultem-type TPA^+ polyimide had the best thermal stability of the Ultem-type polyimides from water soluble polyamic amic acid salts.

Although the Ultem-type NH_4^+ polyimide and the Ultem-type TMA^+ polyimide initially had molecular weights believed to be below the critical entanglement level, an increase in melt viscosity during a simulated processing thermal cycle and a measured gel fraction after a simulated processing thermal cycle both indicate that crosslinking occurs at temperatures above 350°C. After a simulated composite consolidation isothermal hold at 380°C for 30 minutes, the Ultem-type NH_4^+ polyimide had a gel fraction of 21% and the Ultem-type TMA^+ polyimide had a gel fraction of 13%. During the simulated composite consolidation isothermal hold at 380°C for 30 minutes, the melt viscosity of the Ultem-type NH_4^+ polyimide increased by a factor of 57, the melt viscosity of the Ultem-type TMA^+ polyimide increased by a factor of 12 and the melt viscosity of the Ultem-type TPA^+ polyimide increased by a factor of 10.

Model Matrix Ultem-type Polyimide/PEEK Blends Made From Aqueous Suspension

Model matrix Ultem-type polyimide/PEEK blends were prepared according to identical conditions as for aqueous suspension prepregging. A statistical analysis of the tensile test results for model matrix Ultem-type polyimide/PEEK blends showed that the tensile yield strengths were similar for all blends. This is an important conclusion because it provides verification that differences in composite performance would not be attributed to differences in matrix properties and therefore would be a result of interphase modification.

The melt viscosities of the model matrix Ultem-type polyimide/PEEK blends were characterized. The blends with Ultem-type TMA^+ polyimide and Ultem-type NH_4^+ polyimide had higher melt viscosities than the Ultem-type TPA^+ polyimide/PEEK blend. The results

indicate that a complex microstructure exists due to the presence of chemically active polyimide species in the blend.

The miscibility of the Ultem-type polyimide and PEEK was verified by a single T_g for 5 wt% and also 50 wt% Ultem-type polyimide/PEEK blends. There was some correlation between the trends of temperature of maximum crystallization, T_x^{max}, and the blend melt viscosity.

Estimations of the diffusion time at 380°C for Ultem 1000 and PEEK indicate that a diffusion distance of 150 nm requires approximately thirty minutes. Although the interdiffusion of the Ultem-type NH_4^+ polyimide with PEEK and the Ultem-type TMA^+ polyimide with PEEK is expected to occur more rapidly than the predicted diffusion times due to lower initial molecular weights, any crosslinking which occurs will severely limit interdiffusion.

Fabrication and Characterization of Carbon Fiber PEEK matrix composites with Ultem-type Polyimide Interphases of Tailored Properties for Studying the Effect of Interphase Modifications

The interphase thickness was estimated to have an upper bound of 200 nm for a 5 wt% interphase/95% matrix component system based on a hexagonally packed array of cylindrical fibers with a diameter of 8 mm and a fiber volume fraction of 60%. This upper bound was based on assumptions that all of the interphase polymer is distributed evenly around each of the fibers and that no interdiffusion of the pure phases occurs.

A series of PEEK matrix Ultem-type polyimide interphase composites of high quality were fabricated using the aqueous suspension prepregging technique. The void volume content was measured to be no greater than 0.99% for any of the unidirectional composites.

Interactions between the Ultem-type polyimide and the fiber surface were probed with X-ray photoelectron spectroscopy (XPS) with sized and sized, then solvent washed fiber samples. The results showed possible interactions between the Ultem-type NH_4^+ polyimide and the fiber surface. It is possible that the interactions were due to hydrogen bonds or covalent bonds between the free amine functionalities of the Ultem-type NH_4^+ polyimide and oxygen containing species on the fiber surface. However, it is also possible that the Ultem-type NH_4^+ polyimide formed a uniform coating around the fibers which then crosslinked to form an insoluble sheath. The Ultem-type TMA^+ polyimide and the Ultem-type TPA^+ polyimide did not show any interactions with the fiber surface by XPS of the sized and the sized, then washed fibers indicating that the level of adhesion for the Ultem-type NH_4^+ polyimide and the carbon fiber surface was greatest.

Iosipescu shear testing was not shown to be sensitive to the changes of composite interphase for the Ultem-type NH_4^+ polyimide interphase and the Ultem-type TMA^+ polyimide interphase. The experimentally measured shear moduli of the polyimide interphase/PEEK matrix composites from this chapter and from Gonzalez [12] were modeled well by the Halpin-Tsai model for estimating shear moduli.

A direct correlation was shown for transverse flexure strength and interfacial shear strength using data from Chang et al. [5] and Madhukar and Drzal [3]. As the interfacial shear strength increases, the transverse flexure strength increases. This relationship was used to rank the relative level of interfacial shear strengths for the Ultem-type polyimide/PEEK matrix composites. Using this correlation the trends showed that the interfacial shear strength of the 10 series Ultem-type TMA^+ polyimide interphase composite was lowest and the 30 series Ultem-

type NH_4^+ polyimide interphase composite and the 50 series Ultem-type TPA^+ polyimide interphase composite were greater and comparable. Examination of the transverse flexure failure surfaces by VC-XPS provided a quantitative measurement showing that the failure for all Ultem-type polyimide interphase composites was mostly cohesive to fully cohesive in nature.

The notched fatigue experiments using R=1.0 were shown to be insensitive to the interphase differences for the Ultem-type NH_4^+ polyimide composites and the Ultem-type TMA+ polyimide composites.

The notched fatigue results from experiments using R=0.1 showed a strong sensitivity to interphase differences for the 10 series, 30 series and 50 series composites. The 10 series composites had the highest quasi-static ultimate tensile strengths (UTS) of the crossply panels amounting to a 35% increase in UTS over the 30 series composites and a 25% increase in UTS over the 50 series composites. The split lengths measured as a function of loading cycles were used to study the relief of the stress concentrations caused by the circular notch. The split growth rate was found by taking the derivative of a second order polynomial fit to the split length vs. loading cycle data. The 10 series composite showed the most rapid longitudinal split growth rate and the 30 series composite showed the slowest longitudinal split growth rate at both 80% UTS and 87.5% UTS. The 50 series composite had an intermediate split growth rate. The trends of split growth rate were shown to be consistent with the ranking of ISS from the transverse flexure strength results. As the relative ISS estimated from transverse flexure strength increased the initial split growth rate decreased.

The longitudinal tensile strength of the 10 series composite was 12% greater than the longitudinal tensile strength of the 30 series composite and 8% greater than the 50 series

composite. A plot of normalized transverse flexure strength vs. longitudinal tensile strength showed qualitative agreement to the hypothesis proposed by Subramanian et al. [4]. The estimates of composite strength using the rule of mixtures showed very good agreement to the experimental data indicating that the assumptions for the rule of mixtures were applicable to the Ultem-type polyimide interphase/PEEK matrix composites, specifically, the composite has fibers that are continuous, aligned parallel and uniform in properties, good bonding exists between the fibers and matrix and each component has a linear elastic response. The estimates of composite modulus from the rule of mixtures also showed good agreement to the experimental data.

The repeated loading scheme for longitudinal tensile testing was shown to yield different results than the single loading longitudinal tensile test. It was demonstrated that damage occurred in the Ultem-type polyimide interphase/PEEK matrix composites during the three initial loadings.

Structure-Property Relationships of Model Interphase BisP-BTDA Polyimides Made from Water Soluble Precursors

The purpose of this work was to prepare and characterize model interphase and model matrix samples to represent the polymeric material in BisP-BTDA polyimide interphase/PEEK matrix composites. For this work, BisP-BTDA polyimides were made from water soluble polyamic amic acid salts.

The BisP-BTDA NH_4^+ polyimide had a glass transition temperature of 201° and a gel fraction of 97%. The BisP-BTDA TMA^+ polyimide had a glass transition temperature of 240°C

and a gel fraction of 29%. The melt viscosity of the BisP-BTDA NH_4^+ polyimide was higher at all temperatures during the simulated consolidation thermal cycle than the BisP-BTDA TMA^+ polyimide. After a simulated consolidation thermal treatment of 380°C/30 minutes, the BisP-BTDA NH_4^+ polyimide had a gel fraction of 100% and the BisP-BTDA TMA^+ polyimide had a gel fraction of 91%. The increase in melt viscosity during a simulated thermal processing cycle and an increase in measured gel fraction after a simulated thermal processing cycle both indicate that crosslinking occurs at temperatures above 370°C.

The BisP-BTDA NH_4^+ polyimide had a 5% weight loss temperature of 489°C and the BisP-BTDA TMA^+ polyimide had a 5% weight loss temperature of 443°C. After a simulated pyrolysis temperature cycle of 325°C for two hours, 10 wt% of HPC remained.

Model Matrix BisP-BTDA Polyimide/PEEK Blends Made From Aqueous Suspension

Model matrix BisP-BTDA polyimide/PEEK blends were prepared according to identical conditions as for aqueous suspension prepregging. Tensile testing of model matrix blends showed that the tensile yield strengths were statistically similar for all blends. This is an important conclusion because it provides verification that even if all the BisP-BTDA polyimide diffused completely into the bulk matrix, the mechanical properties are similar. Therefore, any differences in composite performance can be attributed to differences in interphase properties.

The melt viscosities of the model matrix blends were characterized. The HPC/PEEK blend film was brown in color indicating the presence of charred HPC. The HPC/PEEK blend had the highest melt viscosity at low shear rates and the BisP-BTDA NH_4^+ polyimide/PEEK

blend had the second highest melt viscosity at low shear rates. The melt viscosity of the BisP-BTDA TMA^+ polyimide/PEEK blend was very similar to the melt viscosity of neat PEEK during the first half of the rheological test. After a 42 minute residence time in the viscometer oven at 380°C the melt viscosity of the BisP-BTDA TMA^+ polyimide/PEEK blend was much higher than the corresponding melt viscosity of neat PEEK. These results are indications that chemically active species attributed to the polyimide are present in the blend. The high melt viscosity of the HPC/PEEK blend compared to neat PEEK can be attributed to the presence of domains of charred HPC.

Miscibility of the BisP-BTDA polyimide and PEEK was suggested by a single T_g for 5 wt% BisP-BTDA polyimide/PEEK blends. The glass transition temperatures and calculated crystalline fraction of the PEEK component for the model matrix blends were all similar.

Fabrication and Characterization of Carbon Fiber PEEK matrix composites with BisP-BTDA Polyimide Interphases of Tailored Properties for Studying the Effect of Interphase Modifications

PEEK matrix composites with two different BisP-BTDA polyimide interphases have been fabricated, analyzed and compared to PEEK matrix composites with an HPC fugitive binder. A statistical analysis of the longitudinal flexure test results show that there is not a difference among the longitudinal flexure strengths for the 60 series HPC/PEEK composites, the 70 series BisP-BTDA TMA^+/PEEK composite and the 80 series BisP-BTDA NH_4^+/PEEK composite. Only the longitudinal flexure failure strain showed a statistical difference among all three composites. The longitudinal flexure test was not shown to provide information for

ranking the performance of the interphase composites.

A statistical analysis of the transverse flexure properties showed that the 60 series HPC/PEEK composites and the 70 series BisP-BTDA TMA^+/PEEK composite had comparable transverse flexure strengths which were greater than the transverse flexure strength of the 80 series BisP-BTDA NH_4^+/PEEK composite. The relationship shown from the data of Chang et. al [5] and Madhukar and Drzal [2] indicate direct correlation of interfacial shear strength with transverse flexure strength. Therefore, this correlation can be used to show qualitatively that the 60 series HPC/PEEK composites and the 70 series BisP-BTDA TMA^+/PEEK composite had comparable interfacial shear strengths which were greater than the interfacial shear strength of the 80 series BisP-BTDA NH_4^+/PEEK composite.

The longitudinal tensile strengths of the 60 series HPC/PEEK composite and the 80 series BisP-BTDA NH_4^+/PEEK composite were shown to be statistically similar, however this does not detract from the usefulness of the test.

The hypothesis proposed by Subramanian et. al [4] indicates that a maximum in tensile strength exists at an optimum interfacial shear strength. It is therefore possible that the tensile strengths of the 60 series HPC/PEEK composite and the 80 series BisP-BTDA NH_4^+/PEEK composite lie on either side of this maximum as shown in Figure 6-10.

The data from this chapter combined with the data from Chapter 4 for Ultem-type polyimide interphase PEEK matrix composites for longitudinal tensile strength vs. normalized transverse flexure strength show qualitative reinforcement of the trends predicted by the model of Subramanian et. al [4].

Fabrication and Characterization of Carbon Fiber PPS matrix composites with Ultem-type Polyimide Interphases of Tailored Properties for Studying the Effect of Interphase Modifications

A series of PPS matrix Ultem-type polyimide interphase composites of high quality were fabricated using the aqueous suspension prepregging technique. Three different Ultem-type polyamic acid salts were used to tailor the interphase properties of the PPS matrix composites using the aqueous suspension prepregging technique.

The interlaminar shear strength (ILSS) was measured using a short beam shear test. The ILSS of the 50 series Ultem-type TPA^+/PPS composite was greater than both the 10 series and 30 series composites.

The PPS matrix composites were tested using a longitudinal flexure test. All longitudinal flexure test samples failed in an interlaminar shear mode of failure. The 10 series Ultem-type TMA^+/PPS composite had the lowest longitudinal flexure strength. The longitudinal flexure strength of the 30 series and 50 series composites were shown to be statistically similar.

A direct correlation was shown for transverse flexure strength and interfacial shear strength using data from Chang et al.[5] and Madhukar and Drzal [2]. As the interfacial shear strength increases, the transverse flexure strength also increases. This relationship was used to rank the relative level of interfacial shear strengths for the Ultem-type polyimide/PPS matrix composites. Using this correlation the trends showed that the interfacial shear strength of the 10 series Ultem-type TMA^+ polyimide interphase composite was lowest and the interfacial shear strength of the 30 series Ultem-type NH_4^+ polyimide interphase composite was the greatest. The interfacial shear strength of the 50 series Ultem-type TPA^+ polyimide interphase composite was intermediate between the 10 series and 30 series composites.

The longitudinal tensile properties of the Ultem-type polyimide/PPS matrix composites were measured. Since the fiber volume fraction of the unidirectional tensile coupons varied significantly the longitudinal tensile strengths were corrected to 61% fiber volume fraction. The 30 series Ultem-type NH_4^+ polyimide interphase composite had the lowest corrected tensile strength, the 10 series Ultem-type TMA^+ polyimide interphase composite had the greatest corrected tensile strength and the 50 series Ultem-type TPA^+ polyimide interphase composite had an intermediate corrected tensile strength.

The hypothesis proposed by Subramanian et. al indicates that a maximum in tensile strength exists at an optimum interfacial shear strength [3]. The data for the Ultem-type polyimide interphase/PPS composites show qualitative reinforcement of the trends predicted by the model of Subramanian et. al.

The estimates of composite strength using the rule of mixtures showed very good agreement to the experimental data indicating that the assumptions for the rule of mixtures were applicable to the Ultem-type polyimide interphase/PPS matrix composites, specifically, the composite has fibers that are continuous, aligned parallel and uniform in properties, good bonding exists between the fibers and matrix and each component has a linear elastic response. The estimates of composite modulus from the rule of mixtures also showed good agreement to the experimental data.

Recommendations For Future Work
Polyimides From Water Soluble Polyamic Acid Salts

There are many possible applications for polyimides that would benefit from using a water soluble precursor. Further development of the understanding of water soluble polyamic acid salts with various polyamic acids is necessary. This could be accomplished following the procedures outlined in this thesis using novel polyamic acids or polyamic acid precursors of commercial polyimides. The development of a suitable water soluble polyamic acid salt for the TPER-BPDA polyimide described in Chapter 2 would be of special interest because of the extremely high temperature stability of this polymer. Processability of this polyimide is difficult because the melt viscosity of this polyimide with number average molecular weights greater than 20,000 g/mol is very high. If a TPER-BPDA water soluble polyamic acid salt was developed demonstrating control of molecular weight of the polyimide, the difficulties of melt processing this polyimide would be avoided.

The processability of water soluble polyamic acid salts facilitates the formation of thin films of polyimide. Since the polyimide made from the Ultem-type TPA^+ polyamic acid salt was shown to have properties very similar to the commercially available Ultem Polyimide, it is very desirable to demonstrate the use of this polyamic acid salt for typical thin film polyimide applications. Some of the possible applications are coatings for optical fibers, adhesives for high performance applications, and electronic circuit chip manufacture. It would also be very interesting to develop a dry-jet fiber spinning process using a water soluble polyimide precursor.

The possibility of electrodeposition of aqueous polyamic acid salts would allow the deposition of thin, uniform films of polymer on conductive parts with complex geometry. This

could include electrodeposition of polyamic acid salts on carbon fibers for applying sizings with precise thickness.

Polyimide/PEEK blends

Surprisingly little information was found during the literature review on the rheological behavior of PEEK/Ultem 1000 blends in the melt. Most of the work in the literature on PEEK/Ultem 1000 blends is focused on the crystallization behavior of the PEEK component. Two different molecular weights of PEEK are readily available with the 150 grade and 450 grade Victrex PEEK materials. By systematically varying the composition of the PEEK/Ultem 1000 blends and studying the melt rheology at low shear rates, more information could be learned about the behavior of this important blend. It would be useful to include measurements of thermal properties from DSC, mechanical properties from tensile testing, and thermomechanical properties below T_g of both components using DMA .

The interdiffusion of the Ultem-type polyimides from water soluble polyamic acid salts is not completely understood. The competing mechanisms of thermally induced crosslinking of the polyimide and interdiffusion of the polyimide and PEEK present a very complex problem. To study the competing mechanisms analytically, very thin films of PEEK could be coated with various polyamic acid salts which would then be thermally imidized. While heating the sample FTIR could be used to monitor the migration of the polyimide using the imide peaks as a marker.

Polyimide Interphase Composites

A quantitative measure of the interfacial shear strength of all the polyimide interphase composites from this thesis would be very useful. This could be accomplished using a meso-indentation technique or a nano-indentation technique. Appropriate samples for both of these techniques are presently available. An alternative method would be to prepare samples for a single fiber fragmentation test. Analysis of the SFFT samples would be difficult since PEEK and PPS form opaque films, thus an x-ray technique would be needed for measuring the fragmentation lengths.

The development of the PPS matrix composites for this thesis included the separation of PPS powder into a narrow particle size distribution using a custom built air classifier. After a procedure for operation of the air classifier was developed, approximately 8 kg of PPS powder with a median particle diameter of 50 mm was procured. The PPS composites fabricated for the work of Chapter 7 of this thesis required less than 1 kg of the PPS powder. Therefore, there is a large supply of readily available PPS powder that could be used for fabrication of composites using the aqueous suspension prepregging technique.

Using the PPS matrix powder with the aqueous suspension prepregging technique, several composite systems are suggested:

(I.) Ultem-type NH_4^+ polyimide interphase composites. Since the fiber volume fraction of the $[0]_4$ composites was much lower than all the other composites, another 30 series $[0]_4$ panel having a fiber volume fraction around 60% would provide a useful comparison of longitudinal tension data to the present 10 series and 50 series Ultem-type polyimde/PPS composites.

(ii.) PPS matrix composites with varied fiber volume fraction. A designed experiment

making use of the three different Ultem-type polyimides described in this thesis and four different fiber volume fractions from 40% to 70% would increase the understanding of the affect of fiber volume fraction on the interfacial shear strength in thermoplastic matrix composites. Many interesting discussions regarding the effect of fiber volume fraction on composite micromechanics were initiated because the 30 series PPS matrix composite fabricated in Chapter 7 had a much lower fiber volume fraction. The composite testing schedule should include indentation testing for interfacial shear strength measurements, transverse flexure testing, unidirectional tension testing and R=0.1 notched fatigue testing. The failure surfaces from the transverse flexure testing should be analyzed using voltage contrast x-ray spectroscopy (VC-XPS) so that a quantitative measure of the remaining polymer can be used to qualify the whether the failure was cohesive or adhesive in nature. The VC-XPS results might also be useful for determining whether failure occurred in the polyimide interphase region or the bulk PPS matrix. Using a design of experiment (DOE) method the array of systematic variances in fiber volume fraction and interphase polyimide would provide a powerful examination of the important experimental interactions.

(iii.) TPER-BPDA polyimide/PPS composites. Providing that a technique can be developed for making water soluble TPER-BPDA polyamic acid salts, it is recommended that the aqueous suspension prepregging technique be used to fabricate TPER-BPDA polyimide/PPS composites. The composite testing schedule should include indentation testing for interfacial shear strength measurements, transverse flexure testing, unidirectional tension testing and R=0.1 notched fatigue testing. The failure surfaces from the transverse flexure testing should be analyzed using voltage contrast x-ray spectroscopy (VC-XPS) so that a quantitative measure of

the remaining polymer can be used to qualify the whether the failure was cohesive or adhesive in nature. The VC-XPS results might also be useful for determining whether failure occurred in the polyimide interphase region or the bulk PPS matrix.

(iv.) Polyimide-siloxane copolymer/PPS composites. The synthesis of novel copolymers containing polyamic acid and polysiloxane repeat units present an interesting possible interphase polymer for PPS matrix composites. While the polyamic acid repeat units could be made water soluble with the addition of a base, the polysiloxane repeat units may provide compatibility with the PPS matrix polymer.

Since the entire supply of 11mm diameter PEEK powder was exhausted during this study, no future work is suggested for fabrication of PEEK matrix composites.

An important recommendation for future work regarding the effect of interphase properties on the overall composite performance is the use of higher modulus carbon fibers for composite fabrication. Almost all of the mathematical models developed for understanding the micromechanical behavior of interphase composites rely on the ratio of the fiber modulus to the interphase modulus as a very important parameter. It can be shown that the calculated composite ineffective length increases with increasing carbon fiber modulus, with all other factors remaining constant. An increase in ineffective length corresponds to a relative decrease in interfacial shear strength (ISS). The hypothesis of Reifsnider et al. discussed throughout this thesis proposes the existence of an optimum ISS which yields a maximum composite tensile strength. While the polyimide interphase/PEEK matrix composites and the polyimide interphase/PPS matrix composites discussed throughout this thesis qualitatively validate the

hypothesis of Reifsnider et al., the data all appear to be greater in ISS than the possible optimum values. It is hereby proposed that the use of higher modulus carbon fibers for fabrication of polyimide interphase, thermoplastic matrix composites would decrease the composite ineffective length which would effectively shift the relative ISS to lower values. In this manner it is intended that values of ISS which are less than the optimum value could be explored.

The value of voltage contrast x-ray spectroscopy (VC-XPS) was discovered during the stages of completion of this thesis. This technique is extremely valuable for quantitative analysis of the failure surface. Using VC-XPS, it is possible to quantitatively rank the level of cohesive failure for a series of composites. It could also be possible to identify the composition of the polymers at the failure surface, although this would require further development of the technique. At the very least, VC-XPS should be used to demonstrate that the off-axis failure surface has failed in a mostly cohesive manner for interphase composites. If the failure is adhesive in nature, then the benefits and the scientific value of tailoring the properties of an interphase region are lost.

Vita

Slade Havelock Gardner earned a Bachelor's of Science degree in Chemical Engineering from Lafayette College in 1992. While at Lafayette College, an interest in polymers and composites was developed which led to a search for the finest institution for a balanced education of theoretical and applied polymer and composite science. The result of the search led to enrollment at Virginia Polytechnic Institute and State University. The ideal research project funded by the National Science Foundation Science and Technology Center was presented by Dr. Richey Davis of the Chemical Engineering Department and Slade joined Dr. Davis' research group. The interactive scientific community at VPI fostered many collaborative studies for the author, which provided exposure to many scientific projects in addition to his own PhD studies. While at VPI, Slade benefited from being a member of the National Science Foundation Science and Technology Center for High Performance Adhesives and Composites, the Center for Adhesive and Sealant Science, the Center for Composite Materials and Structures, and the Polymeric Materials and Interfaces Laboratory. Slade was also the Graduate Student Member of the Center for Composite Materials and Structures advisory board for two years.

Slade earned a PhD in Chemical Engineering in 1998 from Virginia Polytechnic Institute and State University. He is presently employed by Amoco Chemicals, Polymers Business Group in Alpharetta, Georgia working as a Research Engineer in the Carbon Fibers Group.